COMPOSITIONAL EVOLUTION OF TOURMALINE IN GRANITIC PEGMATITES

BY

JULIE BERYL SELWAY

A Thesis

Submitted to the Faculty of Graduate Studies

in Partial Fulfilment of the Requirements

for the Degree of

DOCTOR OF PHILOSOPHY

Department of Geological Sciences

University of Manitoba

Winnipeg, Manitoba

THE UNIVERSITY OF MANITOBA

FACULTY OF GRADUATE STUDIES

*****

COPYRIGHT PERMISSION PAGE

Compositional Evolution of Tourmaline in Granitic Pegmatites

BY

Julie Beryl Selway

A Thesis/Practicum submitted to the Faculty of Graduate Studies of The University of Manitoba in partial fulfillment of the requirements of the degree of Doctor of Philosophy

Abstract

Tourmaline is the most common B-bearing mineral in rare-element granitic pegmatites. The extensive substitutions in its crystal structure, which relate directly to the composition of the host rock, makes it a useful petrological and geochemical indicator mineral. The compositional evolution of tourmaline was examined from three pegmatite subtypes: (1) lepidolite-subtype: Laštovičky, Dobrá Voda, Dolní Bory, Rožná and Radkovice pegmatites, Czech Republic, and lepidolite pegmatites at Red Cross Lake, Manitoba; (2) petalite-subtype: Tanco pegmatite, Manitoba, Utö pegmatite, Sweden, and Marko's and Pegmatite #5, Separation Rapids pegmatite group, Ontario; (3) elbaite-subtype: Belo Horizonte pegmatite, California, and Řečice, Pikárec, Ctidružice and Vlastějovice pegmatites, Czech Republic.

The composition of exocontact tourmaline depends on the composition of the host rock and the amount plus composition of fluid injected into the host rock from the pegmatite melt. There are two compositional groups of tourmaline in the exocontact: (1) feruvite-uvite-schorl-dravite (Ca- and Mg-rich); (2) intermediate ternary tourmaline: elbaite-schorl-dravite (Na-, Al-, and Li-rich).

When a pegmatite intrudes a metapelite or a marble, the composition of the endocontact tourmaline depends on the composition of the host rock regardless of the pegmatite subtype. When an elbaite-subtype pegmatite intrudes a mafic rock, the composition of the endocontact tourmaline is Ca- and Mg-rich, but when a lepidolite- or petalite-subtype pegmatite intrudes a mafic rock, the endocontact tourmaline is Mg-rich and Ca-poor.

Each genetic subtype has characteristic tourmaline compositions. Lepidolite-subtype pegmatites are characterized by common foitite and rossmanite, absence of Na-rich schorl, low Mn and no Ca in the primary tourmaline, and late-stage enrichment of Fe and Mn in elbaite. Petalite-subtype pegmatites are characterized by common Na-rich schorl, low Mn and Ca in tourmaline, and late-stage enrichment of Ca and F in elbaite. Elbaite-subtype pegmatites are characterized by common Na-rich schorl in the massive pegmatite, common Mn-rich elbaite and rare liddicoatite in pockets, and late-stage enrichment of Ca and F in elbaite and liddicoatite.

Influx of Fe-rich fluids from Fe-rich host rock produces rare Fe-bearing elbaite or foitite rims or terminations on late-stage tourmaline in lepidolite- and petalite-subtype pegmatites, and elbaite-schorl to Fe-bearing elbaite or foitite rims, terminations or zones in elbaite-subtype pegmatites.

Acknowledgements

I would like to thank my two supervisors, Drs. Frank Hawthorne and Petr Černý, for their advice and guidance. Having two supervisors provided me with a diverse education in mineralogy; Frank taught me crystallography and Petr taught me pegmatite mineralogy. The availability of excellent analytical equipment at the University of Manitoba, CAMECA SX-50 electron microprobe and Nicolet *R*3*m* four-circle diffractometer, made it easy to collect high-quality data. Ron Chapman fixed the electron microprobe when it crashed, and often did trouble-shooting over the phone after-hours.

I would like to thank Milan Novák, Moravian Museum, Brno, Czech Republic, for his donation of tourmaline samples and descriptions of general geology from lepidolite-subtype pegmatites (Laštovičky, Dobrá Voda, Dolní Bory, Rožná, Radkovice) and elbaite-subtype pegmatites (Řečice, Pikárec, Ctidružice, Vlastějovice). I enjoyed collaborating with him on the Tourmaline 1997 Field Trip Guidebook and our numerous joint papers.

I would also like thank Peter Vanstone of Tantalum Mining Corporation of Canada, now of Cabot Corporation, for donation of tourmaline samples from Tanco pegmatite and for leading several informative mine tours. Fred Breaks, Ontario Geological Survey, donated tourmaline samples from Separation Rapid pegmatite group and led a tour of these pegmatites. Sten-Anders Smeds, Uppsala University, Sweden, donated tourmaline samples from Utö pegmatite. Matt Taylor, California, donated tourmaline samples from and explained the general geology of the Belo Horizonte pegmatite. Matt Bloomfield, Leicester University, provided me with a copy of his M.Sc.

thesis on tourmaline from Stewart Lithia and Sahatany Valley. Dave London, University of Oklahoma, provided me with a pre-print of his paper on tourmaline from Little Three pegmatite, and gave me helpful comments on my thesis.

I also learned a lot from discussions with other pegmatology students: Dave Teertstra, Matt Taylor, Harvey Buck and Morgan Masau, crystallography colleagues: Peter Burns, Mark Cooper and Bob Finch, and fellow tourmaline enthusiast: Chris McCracken.

I would like to thank my husband, Jian Xiong, for his love and support throughout the thesis and his frequent nagging to finish my thesis. His skills with computer graphics were very useful in the making of posters for GAC/MAC, and final production of figures with page numbers for my thesis. I would also like to thank my parents, Arnold and Christine, for their continued love and support.

Table of Contents

Chapter 2 - Introduction to Pegmatites

Chapter 3 - Experimental Methods

Chapter 4 - Tourmaline in lepidolite-subtype pegmatites

List of Figures

Chapter 1

Chapter 2

Chapter 4

List of Tables

Chapter 1

Chapter 2

Chapter 3

Chapter 4

Chapter 5

Chapter 6

CHAPTER 1

Introduction to tourmaline

1.1. General formula of tourmaline

Tourmaline is a borosilicate mineral with the general formula

$$X\ Y_3\ Z_6\ (T_6O_{18})\ (BO_3)_3\ V_3\ W$$

where

X = Na, Ca, □ (vacancy), K;

Y = Mg, Fe^{2+}, Al, Li, Mn^{2+}, Ti, Fe^{3+}, Cr^{3+}, V^{3+};

Z = Al, Mg, Fe^{3+}, Cr^{3+};

T = Si, Al;

V = O(3) = OH, O;

W = O(1) = OH, F, O.

The tourmaline group contains end-members (Table 1.1) that can be divided into three groups based on the occupancy of the *X*-site: sodic, calcic and *X*-site vacant (Hawthorne & Henry 1999). The most common tourmaline end-members are schorl, dravite and elbaite.

1.2. Crystallography

1.2.1. Morphology

Tourmaline crystals range in habit from prismatic to pyramidal to equant to lenticular. Euhedral tourmaline crystals may be doubly terminated by rhombohedra *r*

TABLE 1.1. TOURMALINE END-MEMBER COMPOSITIONS.*

Species	X	Y_3	Z_6	$[O(3)]_3$	O(1)
		calcic tourmaline			
liddicoatite	Ca	Li_2Al	Al_6	$(OH)_3$	F
uvite	Ca	Mg_3	Al_5Mg	$(OH)_3$	F
hydroxy-feruvite**	Ca	Fe^{2+}_3	Al_5Mg	$(OH)_3$	OH
		sodic tourmaline			
elbaite	Na	$Li_{1.5}Al_{1.5}$	Al_6	$(OH)_3$	OH
dravite	Na	Mg_3	Al_6	$(OH)_3$	OH
chromdravite	Na	Mg_3	Cr^{3+}_6	$(OH)_3$	OH
schorl	Na	Fe^{2+}_3	Al_6	$(OH)_3$	OH
buergerite	Na	Fe^{3+}_3	Al_6	O_3	F
povondraite	Na	Fe^{3+}_3	$Fe^{3+}_4Mg_2$	$(OH)_3$	O
olenite	Na	Al_3	Al_6	O_3	OH
		vacancy tourmaline			
rossmanite	□	$LiAl_2$	Al_6	$(OH)_3$	OH
foitite	□	Fe^{2+}_2Al	Al_6	$(OH)_3$	OH
magnesiofoitite	□	Mg_2Al	Al_6	$(OH)_3$	OH

* Several end-members have been modified to reflect a fixed end-member composition, to maintain overall electroneutrality and to correspond to the composition of the type specimen, see Hawthorne & Henry (1999) for a complete discussion.

** This species was originally defined as feruvite, but it has (OH) at O(1), whereas uvite has F at O(1); hence the name feruvite needs to be modified to "hydroxy-feruvite".

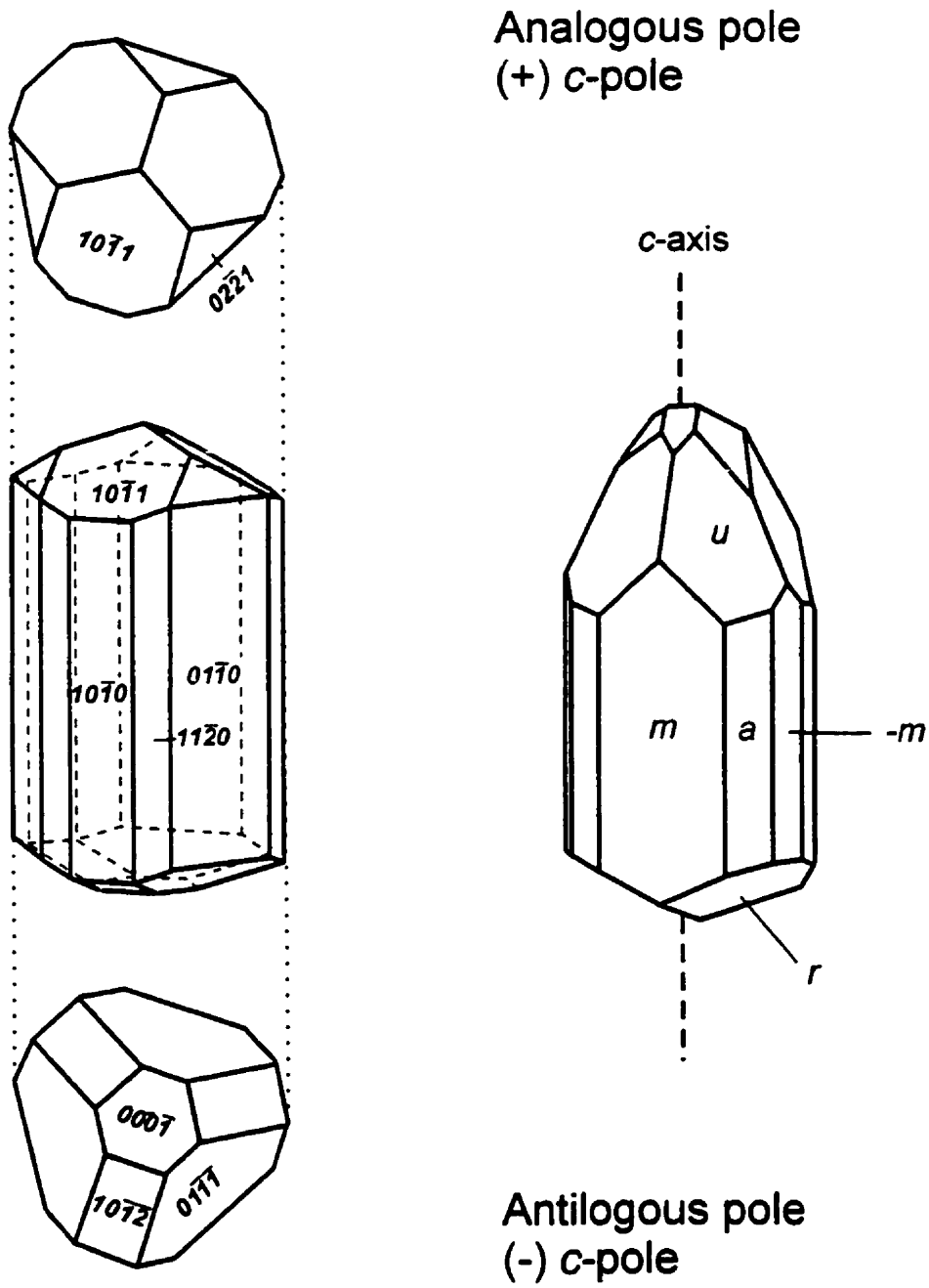

Figure 1.1. Examples of crystal morphologies (Tennyson 1979, Henry & Dutrow 1996).

{10$\bar{1}$1} and *o* {02$\bar{2}$1}, or by pedions *c* {0001} and {000$\bar{1}$} (Fig. 1.1). Tourmaline commonly shows a characteristic rounded triangular cross-section and vertically striated prisms of the forms *a* {11$\bar{2}$0} and *m* {10$\bar{1}$0}.

Tourmaline is noncentrosymmetric and has polar symmetry. The +*c* axis is the antilogous pole, and the -*c* axis is the analogous pole; all of the SiO_4 apices point toward the analogous pole and crystals show different forms at opposite ends of the *c*-axis (e.g., the pedions {0001} and {000$\bar{1}$}) (Fig. 1.1). Pyroelectricity and piezoelectricity in tourmaline are allowed by the polar symmetry.

1.2.2. Crystal structure

Tourmaline is a cyclosilicate in the hexagonal crystal system, trigonal/rhombohedral subsystem, crystal class 3*m* and has space-group symmetry *R*3*m*. The unit-cell dimensions for tourmaline are in the range *a* = 15.80-16.19, *c* = 7.09-7.44 Å and V = 1532-1689 $Å^3$ (Henry & Dutrow 1996) (Table 1.2). The tourmaline structure consists of 5 cation sites: *T*, *B*, *Z*, *Y* and *X*. The *T*-site is tetrahedrally coordinated, the *B*-site is triangularly coordinated, *Z*- and *Y*-sites are octahedrally coordinated, and *X*-site is coordinated by 9 or 10 anions.

The *T*-site is coordinated by four anions, O(4) to O(7), which form a tetrahedron with the T cation at the centre. The T-O bond-lengths vary from 1.602-1.626 Å. The TO_4 tetrahedra form a six-membered T_6O_{18} ring with all of the tetrahedra pointing toward the analogous (-*c*) pole. Each TO_4 tetrahedron links, by corner sharing, to two TO_4 tetrahedra, a Y octahedron and a Z octahedron (Fig. 1.2).

TABLE 1.2. CELL DIMENSIONS AND BOND LENGTHS OF TOURMALINE SPECIES

Species	*a*(Å)	*c*(Å)	V(Å^3)	*X*-O	*Y*-O	*Z*-O	ref.*
calcic tourmaline							
liddicoatite	15.875	7.126	1555	2.645	2.038	1.909	1
uvite	15.973	7.231	1594	2.651	2.050	1.928	2
feruvite	16.012	7.245	1607	2.654	2.055	1.944	3
sodic tourmaline							
elbaite	15.838	7.103	1543	2.670	2.002	1.905	2
dravite	15.941	7.201	1585	2.681	2.019	1.928	2
chromdravite	16.110	7.270	1634	-	-	-	4
schorl	15.990	7.195	1593	2.690	2.045	1.924	2
buergerite	15.874	7.196	1570	2.706	2.004	1.919	2
povondraite	16.186	7.444	1689	2.738	2.037	2.007	5
olenite	15.802	7.086	1532	2.728	1.969	1.898	6
X-site vacant tourmaline							
rossmanite	15.770	7.085	1526	2.737	1.966	1.904	7
foitite	15.967	7.126	1573	2.717	2.044	1.910	8
magnesiofoitite	15.884	7.178	1568	-	-	-	9

*references: (1) Nuber & Schmetzer 1981; (2) Grice & Ercit 1993; (3) Grice & Robinson 1989; (4) Rumantseva 1983; (5) Grice *et al.* 1993; (6) Gorskaya *et al.* 1982; (7) Selway *et al.* 1998a; (8) MacDonald *et al.* 1993; (9) Hawthorne *et al.* (submitted).

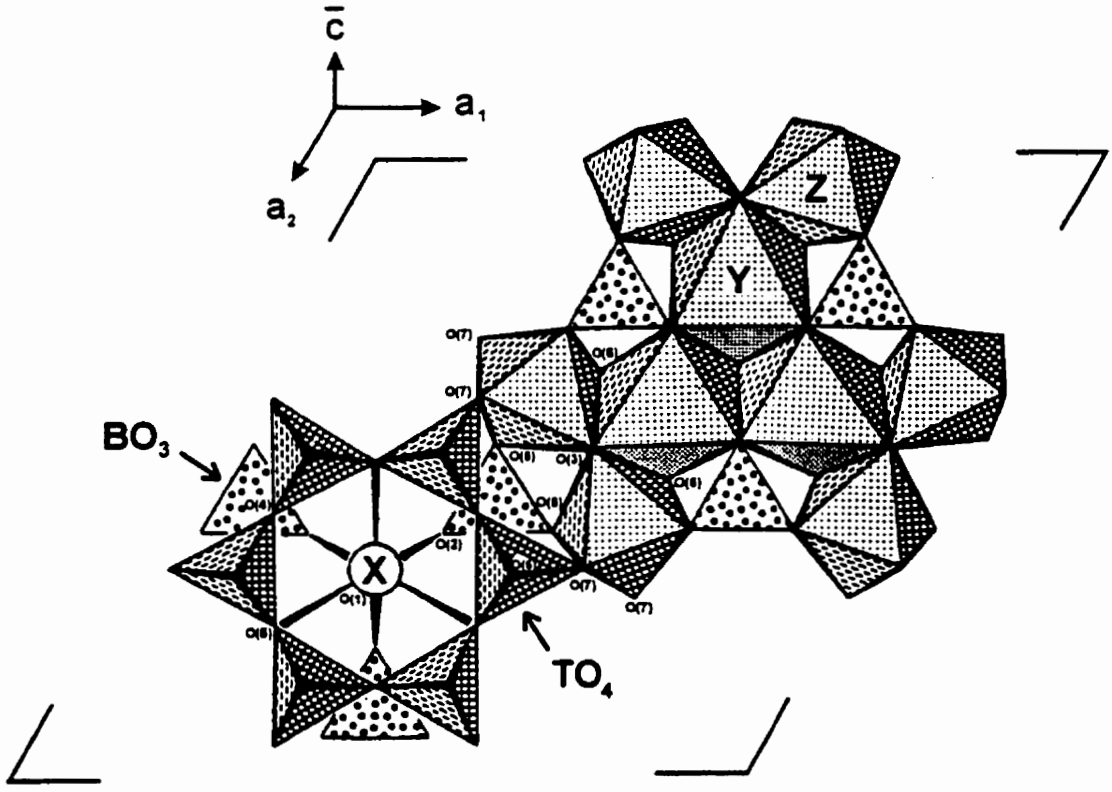

Figure 1.2. Tourmaline crystal structure projected onto (0001) (Jolliff et al. 1986).

The *B*-site is coordinated by three anions, O(2) and 2 x O(8), that form a triangle with B at the centre. The B-O bond-lengths vary in the range 1.36-1.38 Å, typical for [3]-coordinated B. The (BO_3) groups are parallel to (0001) and link, by corner sharing, to two Y octahedra and two Z octahedra (Fig. 1.2). Each BO_3 triangle may also link to the X cation.

The *Z*-site is octahedrally coordinated by six anions, O(3) [=OH,O], O(6), 2 x O(7) and 2 x O(8). The Z-O bond-lengths are in the range 1.898-2.007 Å (Table 1.2). The Z octahedra are smaller than the Y octahedra and are appreciably compressed along an axis approximately 70° to the *c*-axis (Foit 1989). Each Z octahedron links to three

T_6O_{18} rings to form a helix about the 3_1 screw axis (i.e., spiral up the trigonal screw axis). Each Z octahedron links by corner sharing to two BO_3 triangles from two different levels and three TO_4 tetrahedra from three different structural levels. Each Z octahedron also links to a Y octahedron by edge sharing (Fig. 1.2).

The *Y*-site is octahedrally coordinated by six anions, O(1) [=OH,F,O], 2 x O(2), 2 x O(6) and O(3) [=OH,O]. The Y-O bond-lengths are in the range 1.936-2.055 Å (Table 1.2). The Y octahedra are equidistant from the 3-fold axis and are located between the O(6) of the overlying TO_4 tetrahedra and the O(2) of the BO_3 triangles. Threc Y octahedra share edges to form a trimer with the O(1) anion common to all three octahedra (Fig. 1.2). Each Y octahedron links, by edge-sharing, to two adjacent Z octahedra, and may also link to the X cation.

The X cation is coordinated by 9 or 10 anions, ● O(1), 3 x O(2), 3 x O(4) and 3 x O(5), and the X-O bond-lengths are in the range 2.645-2.738 Å (Table 1.2). The X-site occurs on the 3-fold axis between three BO_3 triangles and six TO_4 tetrahedra of the six-membered ring (Fig. 1.2). The X cation links to three BO_3 triangles, three Y octahedra, six TO_4 tetrahedra, and to the O(1) anion.

There are eight anion sites, O(1) to O(8); O(1) and O(3) are occupied by monovalent (OH^-, F^-, Cl^-) or divalent (O^{2-}) anions, and the remaining sites are occupied by O^{2-} anions. The O(1) site occurs at the apex of the trimer of Y octahedra on the 3-fold axis, and is also bonded to the X cation (Fig. 1.2). When the O(1) site is occupied by OH, the H points toward the *X*-site and there is almost no hydrogen bonding with the surrounding oxygens (Robert *et al.* 1993). The O(3) site links one Y and two Z octahedra.

Hydroxyls at the O(3) site have significant hydrogen bonding with adjacent oxygens (Robert *et al.* 1993).

1.3. Substitution and solid solution

1.3.1. Representation of solid-solution relations

There are two ways of representing a solid-solution relation:

(1) equation notation (e.g., $2\ ^{[Y]}Fe^{2+} = {}^{[Y]}Li + {}^{[Y]}Al$); and

(2) vector notation of Burt (1989) (e.g., $LiAlFe_{-2}$).

The advantages of equation notation are that it is easy to understand, and the elements and crystallographic sites involved are explicitly expressed. The vector notation condenses all divalent cations as Mg, all trivalent cations as Al, and F as OH. The equation notation expresses the solid solution in both directions, whereas in vector notation, the substituion is only directional.

The composition of tourmaline is complicated by numerous isomorphous substitutions, particularly those involving the *Y*- and *Z*-sites (Gallagher 1988). There are two types of substitution schemes:

(1) homovalent substitutions (e.g., $Mg^{2+} = Fe^{2+}$, $(OH)^- = F^-$);

(2) heterovalent substitutions (e.g., $Mg^{2+} = Fe^{3+}$, $Li^+ = Mn^{2+}$, $O^{2-} = F^-$).

Hetrovalent susbtitutions of $M^{3+} \rightarrow M^{2+}$ at the *Y*- and *Z*-sites are charge-compensated by $Ca \rightarrow Na$ and $Na \rightarrow \square$ at the *X*-site, $O \rightarrow OH$ at the O(3) and O(1) sites, and $Si \rightarrow Al$ at the *T*-site. Common substitution schemes and corresponding exchange vectors in tourmaline are listed in Table 1.3.

Table 1.3. Important site substitutions and corresponding exchange vectors developed in tourmaline from metamorphic and igneous rocks.

Site substitution*	Exchange vector
$^{Y}Mg = {}^{Y}Fe^{2+}$	$FeMg_{-1}$
$^{Y}Mn = {}^{Y}Fe^{2+}$	$FeMn_{-1}$
$^{Z}Al = {}^{Z}Fe^{3+}$	$FeAl_{-1}$
$^{Z}Al = {}^{Z}Cr^{3+}$	$CrAl_{-1}$
$^{O(1)}OH = {}^{O(1)}F$	$F(OH)_{-1}$
$2\,{}^{Y}Fe^{2+} = {}^{Y}Li + {}^{Y}Al$	$LiAlFe_{-2}$
$^{X}Na + {}^{Y}Mg = {}^{X}\square + {}^{Y}Al$	$\square AlNa_{-1}Mg_{-1}$
$^{X}Na + 2\,{}^{Y}Mg + {}^{O(1)}OH = {}^{X}\square + 2\,{}^{Y}Al + {}^{O(1)}O^{2-}$	$\square Al_2ONa_{-1}Mg_{-2}(OH)_{-1}$ or $\square Al_2Na_{-1}Mg_{-2}H_{-1}$
$^{Y}Mg + {}^{O(3)}OH = {}^{Y}Al + {}^{O(3)}O^{2-}$	$AlOMg_{-1}(OH)_{-1}$
$^{Y}Fe^{2+} + {}^{O(3)}OH = {}^{Y}Fe^{3+} + {}^{O(3)}O^{2-}$	$Fe^{3+}OFe^{2+}_{-1}(OH)_{-1}$ or H_{-1}
$^{Y}Mg + {}^{T}Si = {}^{Y}Al + {}^{T}Al$	$Al_2Mg_{-1}Si_{-1}$
$2\,{}^{Y}Al = {}^{Y}Mg + {}^{Y}Ti$	$TiMgAl_{-2}$
$^{X}Na + {}^{Y}Al = {}^{X}Ca + {}^{Y}Mg$	$CaMgNa_{-1}Al_{-1}$
$^{X}\square + {}^{Y}Al + {}^{O(1)}OH = {}^{X}Ca + {}^{Y}Mg + {}^{O(1)}O^{2-}$	$CaMgO\square_{-1}Al_{-1}(OH)_{-1}$
$2\,{}^{Y}Mg + {}^{Z}Al + {}^{O(1)}OH = 2\,{}^{Y}Al + {}^{Z}Mg + {}^{O(1)}O^{2-}$	$Al_2MgOMg_{-2}Al_{-1}(OH)_{-1}$ or $AlMg_{-1}H_{-1}$

*Precursor superscripts designate specific sites (Henry & Dutrow 1996).

1.3.2. Dravite-schorl and schorl-elbaite solid solution series

The most common solid-solution series in tourmaline are dravite - schorl (Mg ⇌ Fe) and schorl - elbaite ($2Fe^{2+}$ ⇌ Li+Al) (Fig. 1.3). The extent of solid solution between dravite and schorl, and between schorl and elbaite is reflected in a plot of *c* vs. *a* cell-dimensions (Fig. 1.4).

Natural compositions between dravite and elbaite are rare. The only known locality of Mg-rich elbaite is the Bližná pegmatite, Czech Republic, an elbaite-subtype pegmatite intruding marble (Fig. 1.5) (Novák *et al.* 1999a). The rarity of natural

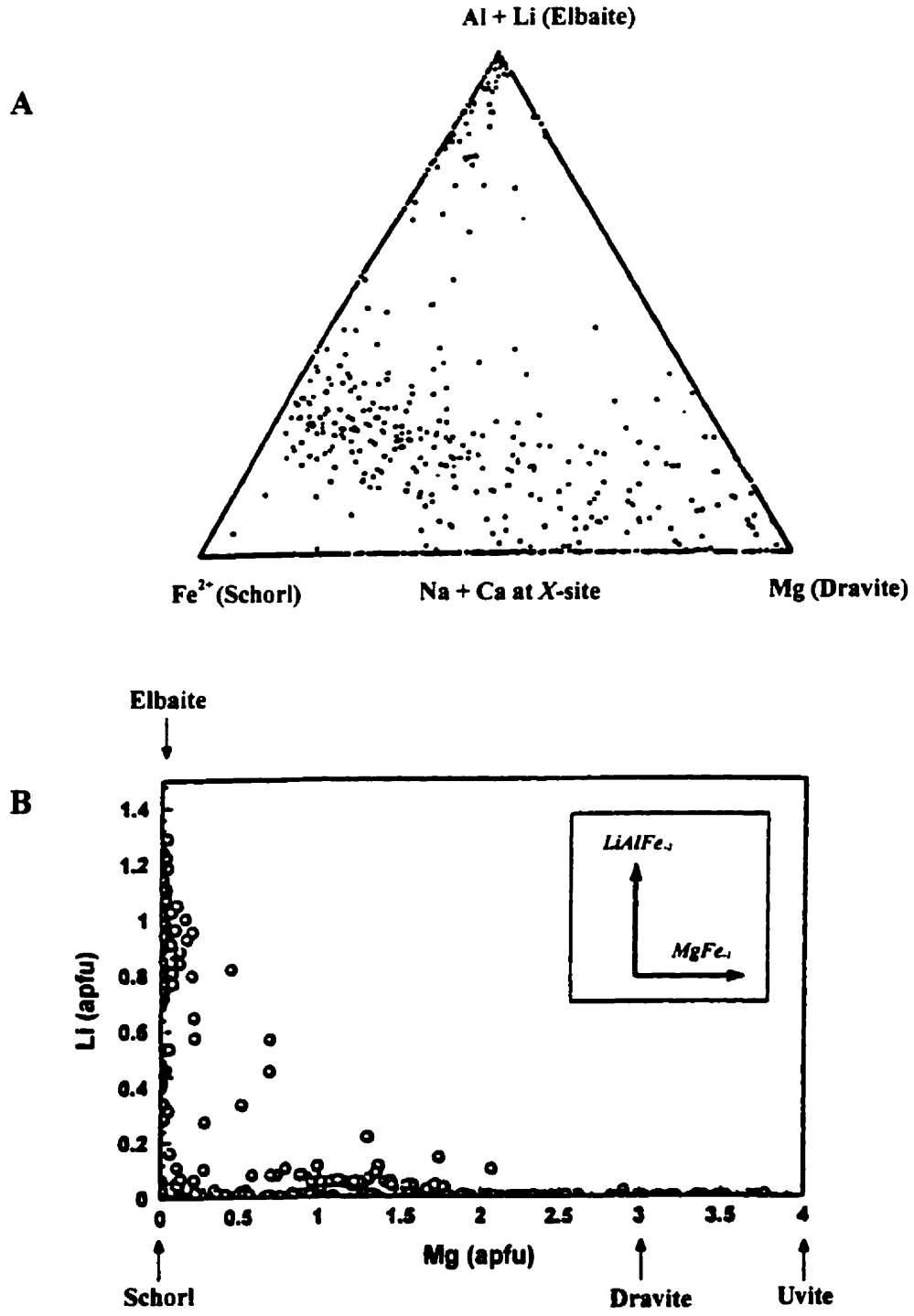

Figure 1.3. (a) Elbaite-schorl-dravite ternary diagram (Dietrich 1985a). (b) Li vs. Mg *(apfu)* for a variety of igneous and metamorphic tourmalines. The 307 compositions are taken from several references listed in Henry & Dutrow (1996).

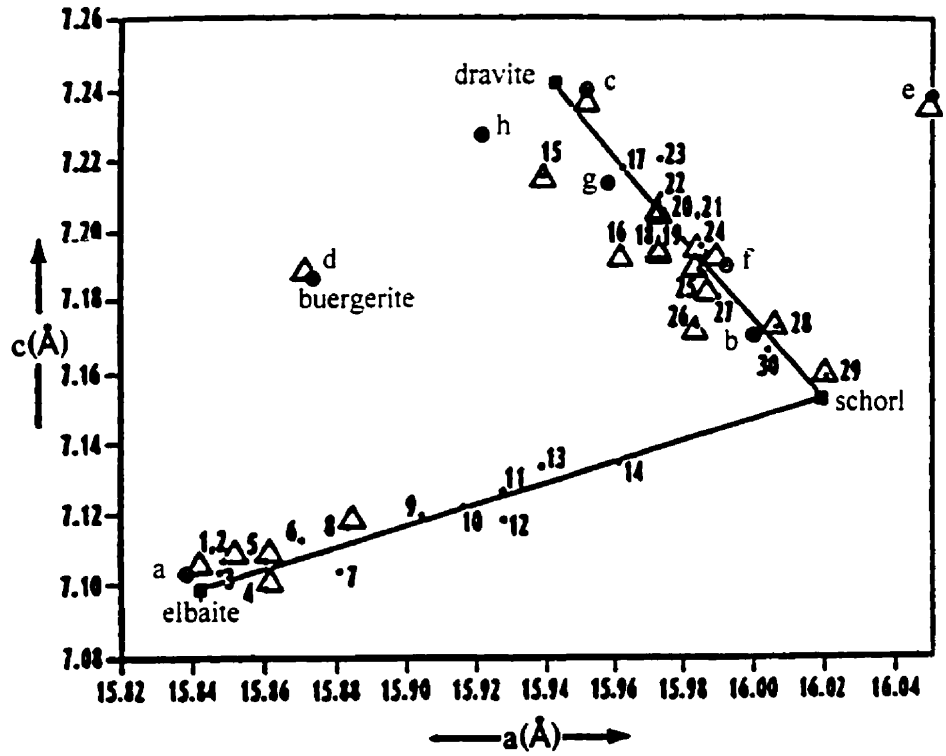

Figure 1.4. Cell dimensions for elbaite, schorl, dravite and buergerite. Data points with numbers are taken from Epprecht's collection of literature data (1953). Data points with letters are from several references listed in Donnay & Barton (1972).

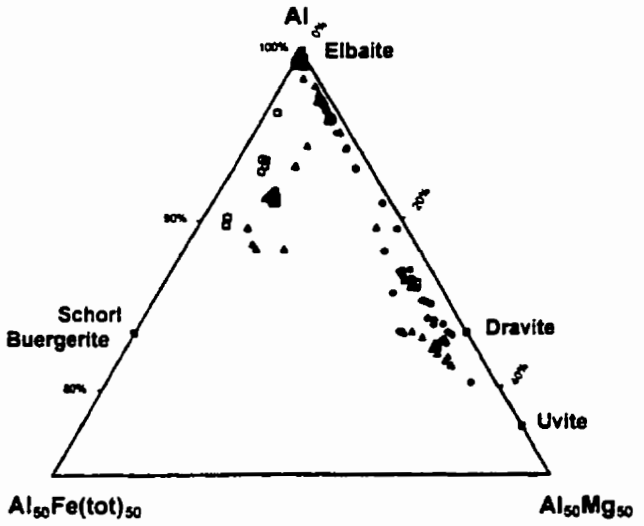

Figure 1.5. Al - Fe(tot) - Mg diagram for tourmaline from the Bližná pegmatite, Czech Republic: ■ end-members, □ pegmatite unit (A), △ pegmatite unit (B), ◇ exocontact, ○ fissure (Novák *et al.* 1997).

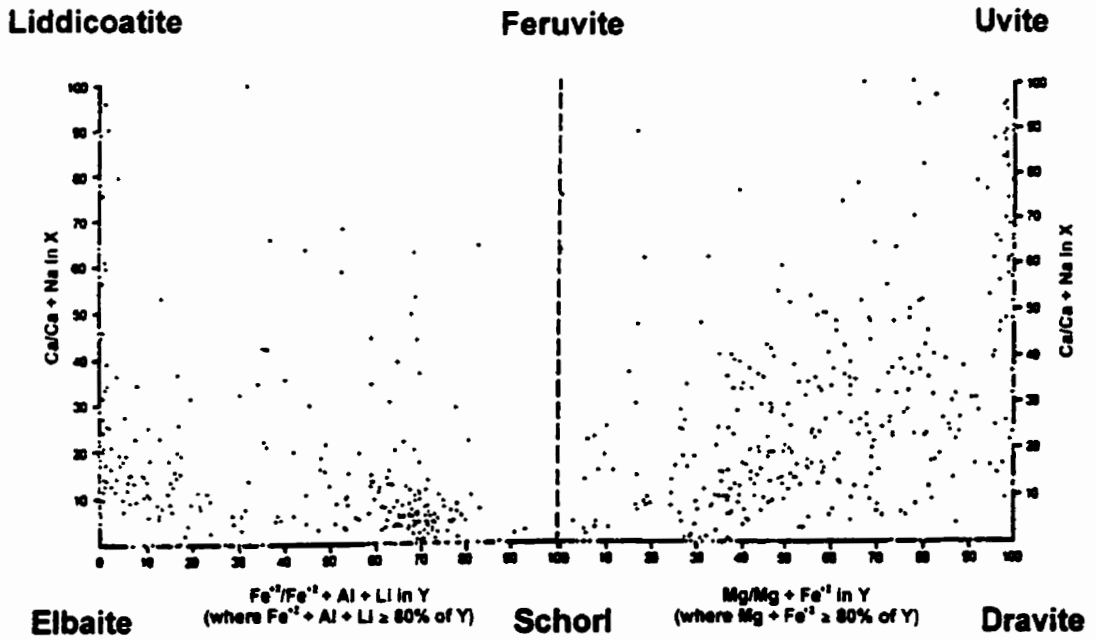

Figure 1.6. Liddicoatite-elbaite-schorl-feruvite and feruvite-schorl-dravite-uvite compositions (Dietrich 1985a).

compositions between dravite and elbaite was previously thought to be due to a miscibility gap (Foit & Rosenberg 1977). However, Foit & Rosenberg (1979) proposed that the rarity of dravite-elbaite solid-solution is due to the extreme fractionation between Mg and Li during crystallization. Staatz *et al.* (1955) noted that the first tourmaline grains to crystallize from a pegmatite melt are Mg- and Fe^{2+}-rich and the last are Li-rich. Thus, by the time Li-rich tourmaline crystallizes, the melt is depleted in Mg. Tourmalines with greater than 0.2 *apfu* Li (elbaite, schorl) occur almost entirely in Li-rich pegmatites; tourmaline with greater than 1.0 *apfu* Mg (dravite) contain < 0.2 *apfu* Li and are metamorphic in origin (Fig. 1.3b).

In dravite, the $^{[Y]}Al + O \rightarrow {}^{[Y]}Mg + OH$ [$AlO(MgOH)_{-1}$] substitution, and in elbaite, $2^{[Y]}Fe^{2+} \rightarrow {}^{[Y]}Al + {}^{[Y]}Li$ [$Fe^{2+}{}_2(LiAl)_{-1}$] substitution, are common. Thus, extensive subsitution of cations of different size takes place without difficulty, and there seems to be no structural reason why dravite-elbaite solid-solution should not be more extensive (Foit & Rosenberg 1977).

There is solid solution between elbaite and liddicoatite involving $2^{[X]}Na + {}^{[Y]}Al = 2^{[X]}Ca + {}^{[Y]}Li$ (Fig. 1.6). The Al:Li ratio is greater in elbaite (1:1) than in liddicoatite (1:2). There is solid solution between schorl and feruvite, and between dravite and uvite, due to $^{[X]}Na + {}^{[Z]}Al = {}^{[X]}Ca + {}^{[Z]}Mg$. There is no known solid solution between liddicoatite and uvite due to the extreme fractionation of Mg and Li during crystalliation. There is solid-solution between feruvite and uvite due to $^{[Y]}Fe^{2+} = {}^{[Y]}Mg$ (Selway *et al.* 1998b).

1.3.3. Anion substitution

Hydroxyl will preferentially partition at the O(3) site unless the *Y* and *Z* sites are completely occupied by trivalent cations (Grice & Ercit 1993, Hawthorne & Henry 1999). The ideal formulae for olenite and buergerite contain oxygen, rather than hydroxyl, at the O(3) site (Table 1.1).

Tourmaline can be divided into three subgroups based on the occupancy of the O(1) site: hydroxy-, fluor- and oxy-end-members (Hawthorne & Henry 1999). Buergerite, uvite and liddicoatite have F at the O(1) site, whereas O^{2-} is at the O(1) site in povondraite and the rest of the tourmaline end-members have OH at the O(1) site (Hawthorne & Henry 1999). Fluorine is ordered completely at the O(1) site (Grice & Ercit 1993). Elbaite tends to be more F-rich than schorl and dravite. Fluorine-rich schorl is found in Li-bearing pegmatites which also contain other F-rich minerals, as the F content in schorl depends only on the chemical activity of F present in the fluids from which the tourmaline crystallized (Němec 1969). Incorporation of O^{2-} at the O(1) site induces disorder of Al and Mg at the *Y*- and *Z*-sites: $2^{[Y]}Mg + {}^{[Z]}Al + {}^{O(1)}OH = 2^{[Y]}Al + {}^{[Z]}Mg + {}^{O(1)}O$ (Hawthorne 1996). The disordering of Al and Mg is required to satisfy local bond-valence requirements.

Only very small amounts of chlorine may substitute for F at the O(1)-site: 0.00-0.24 wt% Cl (Fuge & Power 1969). This limited Cl^- substitution is probably due its large ionic radius, $^{[6]}Cl = 1.81$ *verus* $^{[3]}OH = 1.34$ and $^{[3]}F = 1.30$ Å (Shannon 1976).

1.3.4. Effects of substitution on the crystal structure

Substitutions in the tourmaline structure produce systematic changes in the principal structural units (Foit 1989). Many chemical analyses indicate a Si content of less than 6 *apfu*, suggesting Al → Si substitution (Foit & Rosenberg 1977). Substitution of tetrahedral Si by Al occurs in other ring silicates, such as cordierite (Gallagher 1988). Barton (1969) suggested that excess B may substitute for Si at the *T*-site. However, appreciable substitution of B for Si has not been confirmed. Aluminum → silicon substitution increases the <*T*-O> distances (MacDonald & Hawthorne 1995). The unit-cell expansion produced by significant Al → Si substitution partially offsets the contraction due to simultaneous substitution of Al at the *Y*-site.

Substitution at the *Z*-site has little or no effect on the overall distortion of the Z octahedron. The distortion and compression of the Z octahedron is primarily influenced by the size of the Y cation (Foit 1989). The *Y*-site incorporates extensive substitutions which produce substantial variation in the <*Y*-O> bond-length (Table 1.2).

There is a high linear correlation between Na + □ and the <*X*-O> bond-length (Table 1.2) (Foit 1989). The <*X*-O> distance for calcic tourmaline ranges from 2.645-2.654 Å, for sodic tourmaline ranges from 2.670-2.738 Å, and for *X*-site-vacant tourmaline ranges from 2.717-2.737 Å.

The volume of the unit cell correlates with the weighted mean size of the Y and Z octahedra (Fig. 1.7) (Foit 1989).

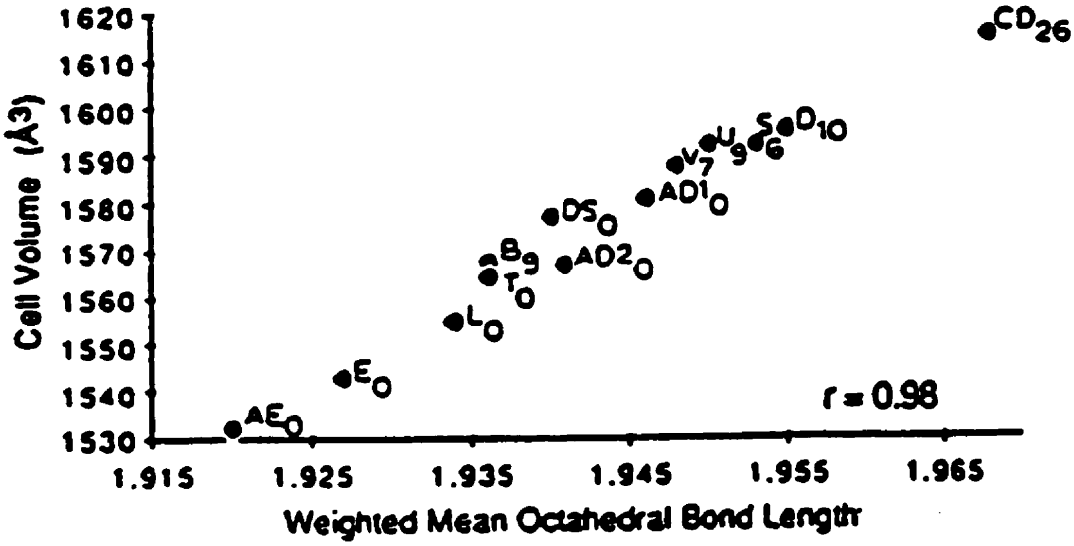

Figure 1.7. Cell volume (Å^3) vs. weighted mean octahedral bond-length (<<Y-, Z-O>>) (Foit 1989). AE - Al-rich elbaite, E - elbaite, L - liddicoatite, T - tsilaisite (Mn-rich elbaite), B - buergerite, AD1, AD2 - Al-rich dravite, D - dravite, S - schorl, V - V-bearing dravite, U - uvite and CD - Cr-bearing dravite.

1.3.5. Local order-disorder of anions and cations

The linear correlation between bond-length and the constituent-cation radius at the *Y*- and *Z*-sites in tourmaline can be used to determine cation order-disorder patterns and possible variations in valence states of the transition metals (e.g., Fe and Mn) (Fig. 1.8) (Burns *et al.* 1994). Factors which can affect these relations are:

(1) incorrect assignment of cations between the *Y*- and *Z*-sites (Fig. 1.8);

(2) variable OH and F contents and possible order-disorder over O(1) and O(3);

(3) incorrect assignment of valence states for the transition metals (e.g., Fe^{2+}/Fe^{3+}) (Fig. 1.8) (Hawthorne *et al.* 1993).

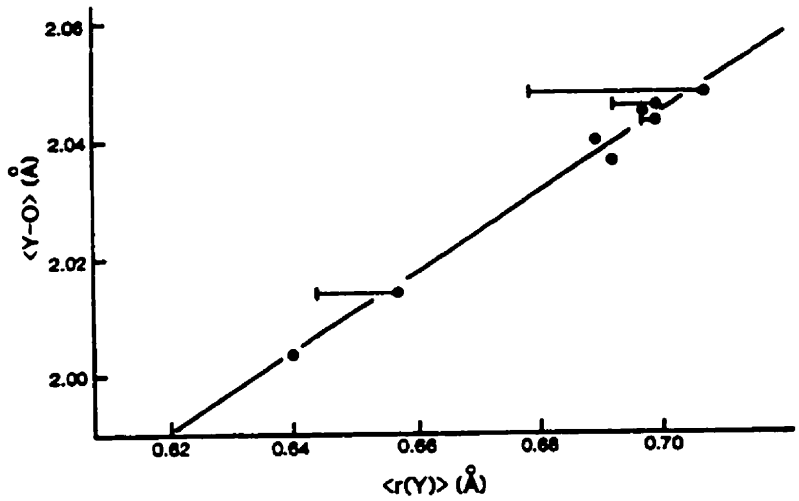

Figure 1.8. Relationship between <Y-0> and constituent Y-cation radius (curve from Hawthorne *et al.* 1993). Horizontal lines show the variation in constituent-cation radius as a function of the Fe^{3+}/Fe^{2+} ratio; symbols with no associated horizontal lines are Fe-free. Note that the curve is compatible with all Fe in the divalent state (Burns *et al.* 1994).

The weighted mean bond-length of the Y and Z octahedra (i.e., <*Y*-O> and <*Z*-O>) vs. the weighted mean radii of Y and Z cations (i.e., <r(Y)> and <r(Z)>) shows a linear correlation (Fig. 1.10). If the graphs of Y and Z cation sizes individually do not produce linear relations (Fig. 1.9), then there is incorrect assignment of cations between the *Y*- and *Z*-sites (Hawthorne *et al.* 1993).

There are significant differences in the radii of the three anions in tourmaline:

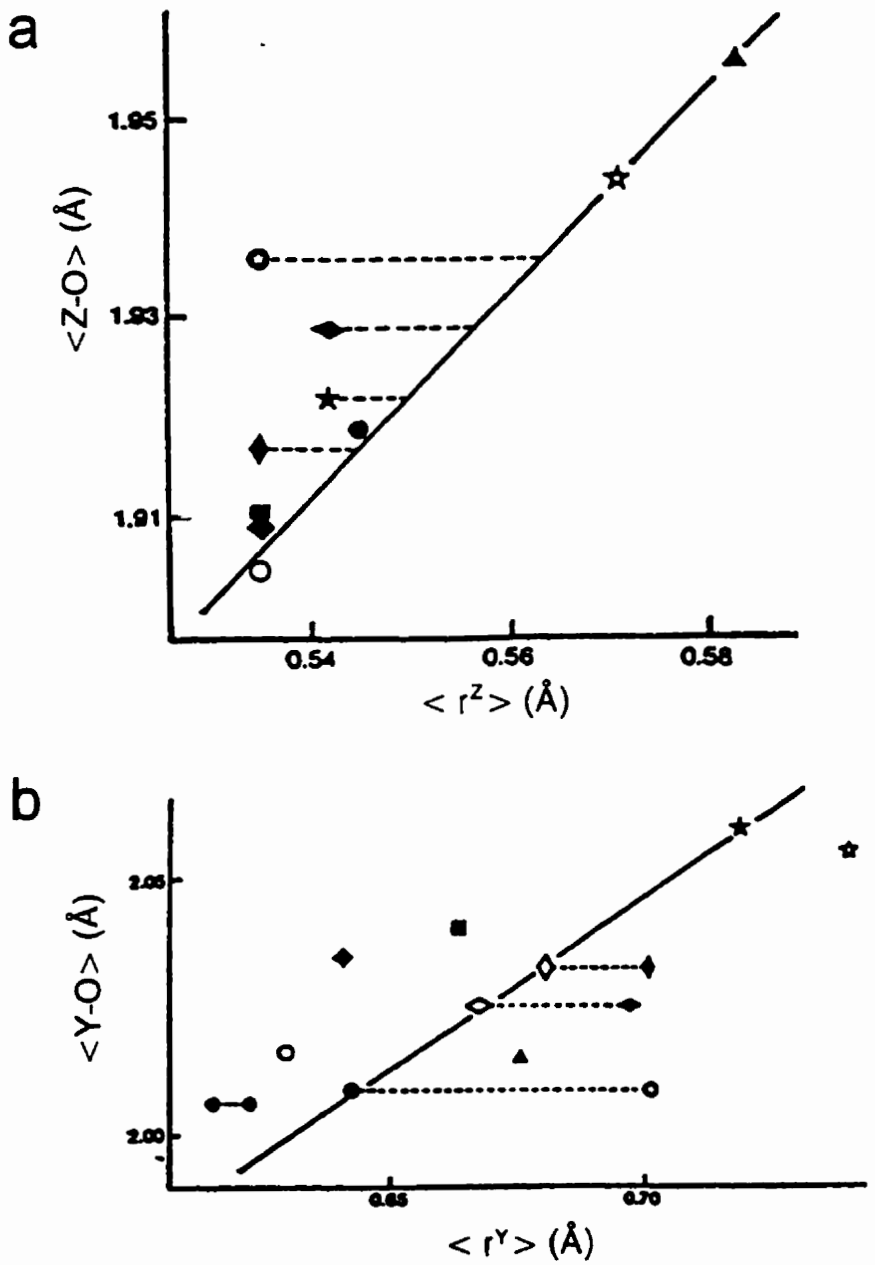

Figure 1.9. Relationships between mean bond length and constituent ionic radius in refined tourmaline structures: (a) the Z site; (b) the Y site. The horizontal dashed lines show the revised constituent cation radii for the reassigned populations. Buergerite: solid circle feruvite: open star; schorl; solid star; liddicoatite: inclined solid square; elbaite: open circle; tsilaisite: solid square: chromium tourmaline: triangle; vanadium dravite: horizontal solid diamond; □-schorl: vertical solid diamond; dravite: circled stars (Hawthorne *et al.* 1993).

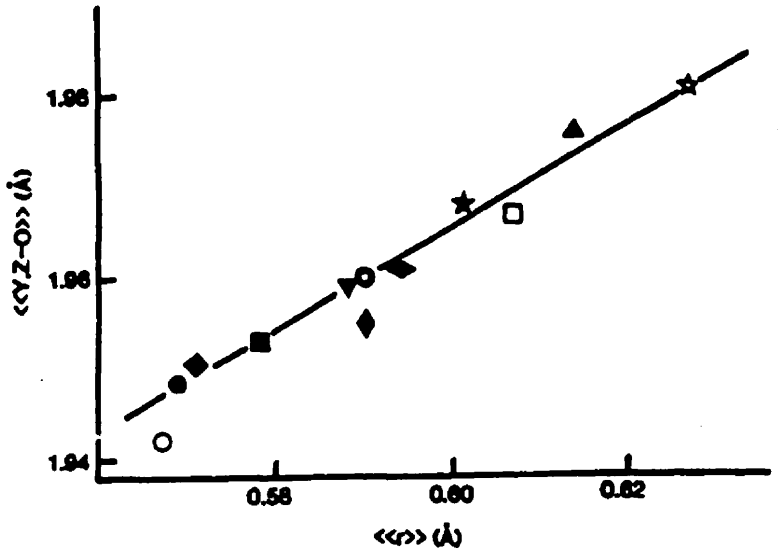

Figure. 1.10. Weighted-mean bond length of the Y and Z polyhedra as a function of constituent cation radius in tourmalines. The squares show the data points in three F-rich tourmalines corrected for their F content. Legend as in Fig.1.9 plus aluminum dravite: solid inverted triangle; uvite: open square (Hawthorne *et al.* 1993).

$^{[3]}$O = 1.36 Å, $^{[3]}$OH = 1.34 Å and $^{[3]}$F = 1.30 Å (Shannon 1976). This variation in radius can cause significant differences in mean bond-lengths around the cations to which they are coordinated (Hawthorne *et al.* 1993). The individual mean bond-lengths can be affected by monovalent-anion ordering over the O(1) and O(3) sites for fixed anion composition.

Large isotropic-displacement factors indicate local disorder at cation and anion sites (MacDonald *et al.* 1993). There is a wide range in bond-valence arrangements due to cation substitution at the *Y*-site. The anion locally adopts a position to satisfy its bond-valence requirements according to the specific local cation

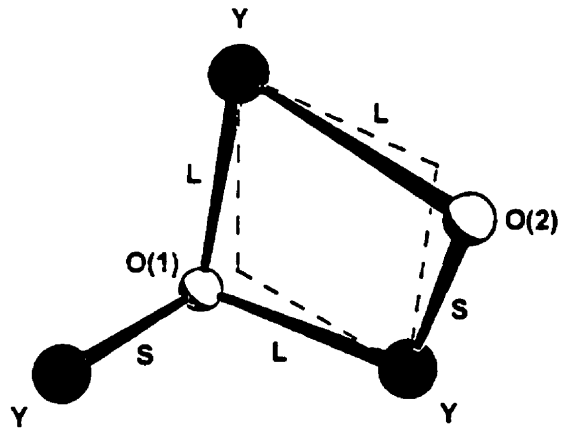

Figure 1.11. A sketch of a set of coupled displacements associated with local disorder at the O(1) and O(2) sites. The broken lines show the bonds from the *Y* cations to the ideal positions of the O(1) and O(2) anions. The displacements of the O(1) and O(2) anions from their ideal positions are exaggerated for clarity (Burns *et al.* 1994).

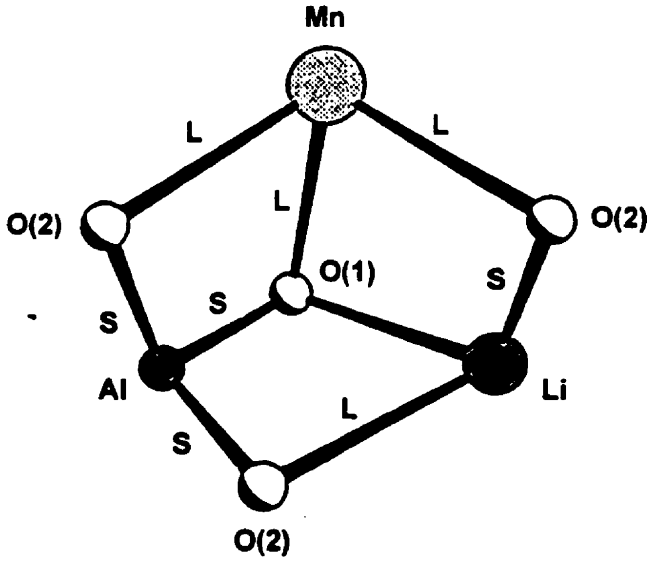

Figure. 1.12. Proposed dominant local arrangement in manganiferous elbaite; the letters "L" and "S" denote long and short bonds, respectively, relative to the bonds to O(1) and O(2) at their ideal positions. (Burns *et al.* 1994)

configuration to which it is coordinated (MacDonald *et al.* 1993). The O(1) anion can be locally displaced by about 0.5 Å, and the O(2) anion can be displaced by about 0.3 Å (Burns *et al.* 1994). It is notable that only the <*Y*-O> bond lengths are affected by O(1) and O(2) disorder, which suggests that the local disorder may be induced by occupancy of the *Y*-site by cations of significantly different size and charge. For example, in Mn-bearing elbaite, O(1) is displaced off the 3-fold axis toward one of the three surrounding *Y*-sites, resulting in one short *Y*-O(1) and two long *Y*-O(1) bonds (Fig. 1.11). The O(2) anion is displaced off the mirror plane toward one of the two neighboring Y cations, resulting in one short *Y*-O(2) and one long *Y*-O(2) bond; Li and Mn require long *Y*-O(1) bonds in order to satisfy bond-valence requirements (Fig. 1.12). The Mn site requires two long Mn-O(2) bonds, which forces short Li-O(2) and Al-O(2) bonds. The Li site requires one short and one long Li-O(2) bonds, which forces the second Al-O(2) bond to be short. This configuration produces an ordered Y trimer (Burns *et al.* 1994).

1.4. Zoning in tourmaline

Zoning in tourmaline can be identified by differences in colour and composition. There are four types of zoning in tourmaline:

(1) zoning parallel to the pedion faces {0001} and perpendicular to the *c*-axis (Fig. 1.13) (e.g., elbaite with pink at the antilogous end (c) of the prism, colourless in the intermediate zone, and green at the analogous end ($\bar{c}$)).

(2) concentric zoning parallel to the prism faces or *c*-axis (Figs 1.14, 1.15) (e.g.,

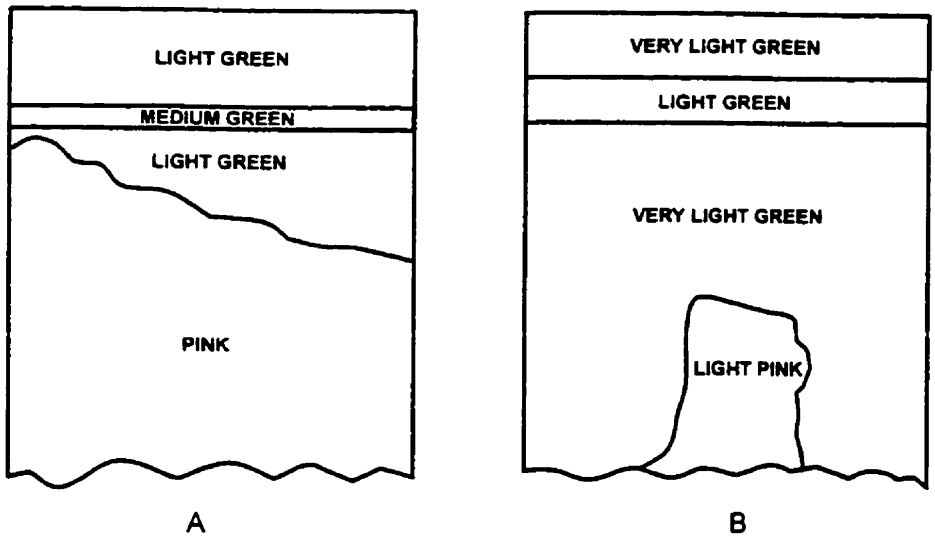

Figure 1.13. Zoning (a) parallel to the *c*-axis, and (b) irregular zoning in elbaite from Newry, Maine; both sections are cut parallel to *c* (Dietrich 1985b).

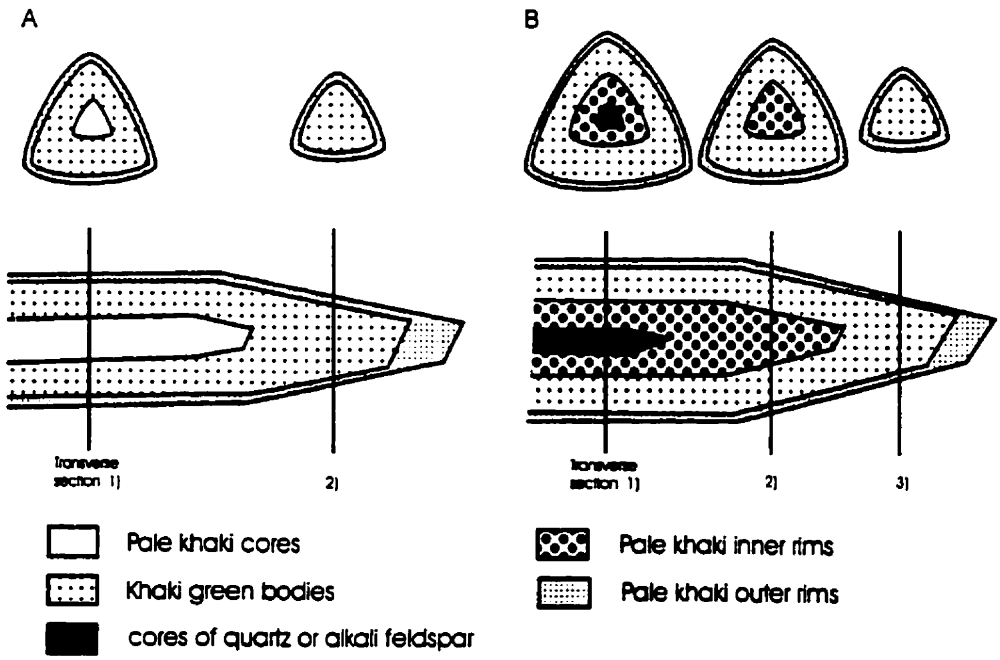

Figure 1.14. Three-dimensional concentric zoning in traverse and longitudinal sections of tourmaline from Hub Kapong. (A) non-skeletal, and (b) skeletal tourmaline crystals (Manning 1982).

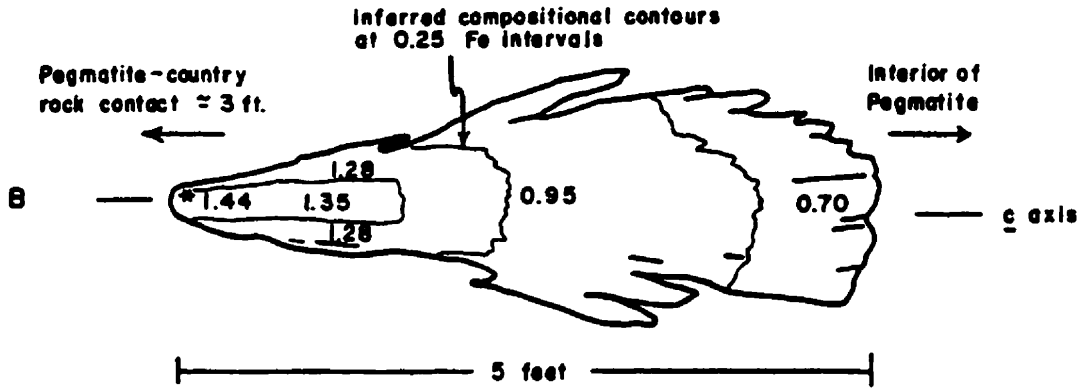

Figure 1.15. Longitudinal section of tourmaline compositionally zoned parallel to the *c*-axis. Numerical values are Fe *apfu* (Jolliff *et al.* 1986).

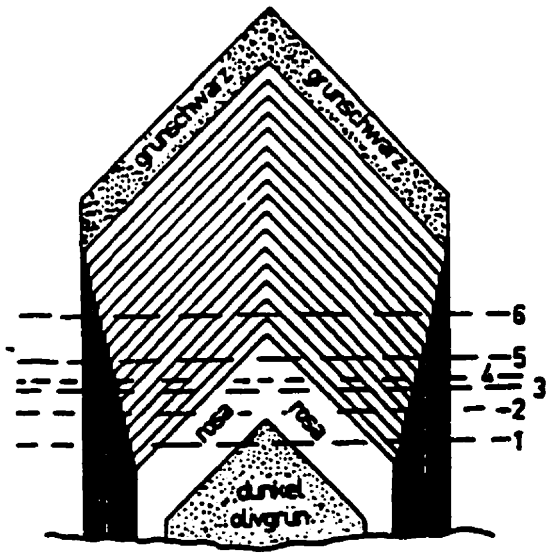

Figure 1.16. Longitudinal section of liddicoatite with 3-dimensional concentric zoning from Madagascar; grunschwarz = greenish black, rosa = pink, and dunkel oligrün = dark olive green (Althaus 1979).

elbaite with rose-red cores and green rims, known as "watermelon" tourmaline).
(3) zoning parallel to the pyramidal faces (Fig. 1.16) (e.g., sector zones in liddicoatite). The zoning parallel to the pedion, prism and pyramidal faces can combine to form a 3-dimension concentric pattern (Figs. 1.14, 1.16).
(4) patchy or irregular zoning (Fig. 1.13) due to fractures in the crystal, or hydrothermal alteration. The transitions between different-coloured zones can be sharp or gradational.

Zoning causes problems for experimental techniques that use bulk samples (e.g., wet chemistry, Mössbauer spectroscopy, bulk H_2O analysis and x-ray diffraction). Microbeam techniques and optical properties are important to distinguish chemical zones.

1.5. Geochemistry of boron

The crystallization of tourmaline depends on the presence of B. Boron is a relatively uncommon light lithophile element; the atomic number is 5, the atomic weight is 10.811, the formal valence is 3+, and the cation radius is 0.01 Å in triangular coordination and 0.11 Å in tetrahedral coordination (Shannon 1976). Boron forms covalent bonds with oxygen. The grand $\langle^{[3]}B\text{-}\varphi\rangle$ ($\varphi = O^{2-}$, OH^-) distance is 1.370 Å, the minimum and maximum $\langle^{[3]}B\text{-}\varphi\rangle$ distances are 1.351 and 1.403 Å, respectively, and the range of variation is 0.052 Å (Hawthorne *et al.* 1996). According to the bond-valence curve for B from Brown (1981), the range of variation in $^{[3]}B\text{-}\varphi$ bond valence is 1.19 to 0.86 *vu* (valence units).

The concentration of B in the continental crust is 10 ppm, in shale is 100 ppm and in deep-sea clay is 230 ppm (Faure 1991). Boron is relatively abundant in sediments and sedimentary rocks, residing mainly in (or on) phyllosilicates, borosilicates and borate minerals (Leeman & Sisson 1996). Boron concentrations in phyllosilicates decrease in the sequence muscovite > paragonite > biotite (Leeman & Sisson 1996). The B content of pelites and argillites (i.e., marine shales and clays) varies with their content of B-bearing minerals (e.g., clays and tourmaline) (Leeman & Sisson 1996). Boron is enriched in salt deposits and evaporites which contain borate minerals (Henry & Guidotti 1985). Boron is enriched in submarine volcanic exhalations (or fumarolic centres and hot springs) and subduction volcanic-arc rocks (Henry & Guidotti 1985). Boron is commonly enriched in oceanic crust and ultramafic rocks due to adsorption of B from seawater onto smectites, Fe hydroxides and other low-temperature- alteration phases (e.g., sericite) (Leeman & Sisson 1996). Illite can contain several thousand ppm of adsorbed or structurally bound B (Henry & Dutrow 1992).

Boron is readily soluble in moderate- to high-temperature ($\geq \sim 100°C$) aqueous fluids, making it susceptible to redistribution in geothermal, hydrothermal and ore-forming environments. With prograde metamorphism and devolatilization, B is gradually depleted in metamorphic rocks due to removal by aqueous fluids (Leeman & Sisson 1996). Boron may also be mobilized into tourmalinizing fluids during isochemical metamorphism of sedimentary rocks. Boron is an incompatible element which may be concentrated by fractional crystallization in a residual melt in igneous

systems. Therefore, B is enriched in magmatic felsic and silicic differentiates, i.e., granites and pegmatites.

1.6. Tourmaline as a petrogenetic indicator

Tourmaline is a minor mineral in many rock types: granitoids, pegmatites, metapelites, metacarbonates, metapsammites, graphite schists and veins. Tourmalinites are composed almost entirely of tourmaline (schorl and dravite) and quartz, and are formed by alteration of granitoid and metasedimentary rocks by B-rich hydrothermal fluids. Hydrothermal tourmaline is associated with Sn, Au, Pb-Zn, Mo and Cu ore-deposits.

Tourmaline is a useful petrogenetic indicator because it is a common mineral, chemically and mechanically stable, and has extensive compositional variations that typically reflect the environment in which it crystallized (Henry & Guidotti 1985). Changes in tourmaline composition can be related to the bulk composition of the host rock, the composition of co-existing minerals, and P-T-fO_2 conditions.

Henry and Guidotti (1985) plotted available tourmaline compositions in Al-Fe(tot)-Mg and Ca-Fe(tot)-Mg ternary diagrams and showed that composition correlates with host-rock type (Figs. 1.17a,b). Elbaite and Li-rich tourmaline occur in Li-rich granitoid pegmatites and aplites (field 1). Schorl occurs in Li-poor granitoids and their associated pegmatites and aplites (field 2), and buergerite occurs in Fe^{3+}-rich quartz-tourmaline rocks (tourmalinites) and hydrothermally altered granites (field 3). The presence of an Al-saturated phase (e.g., staurolite) increases the total Al content

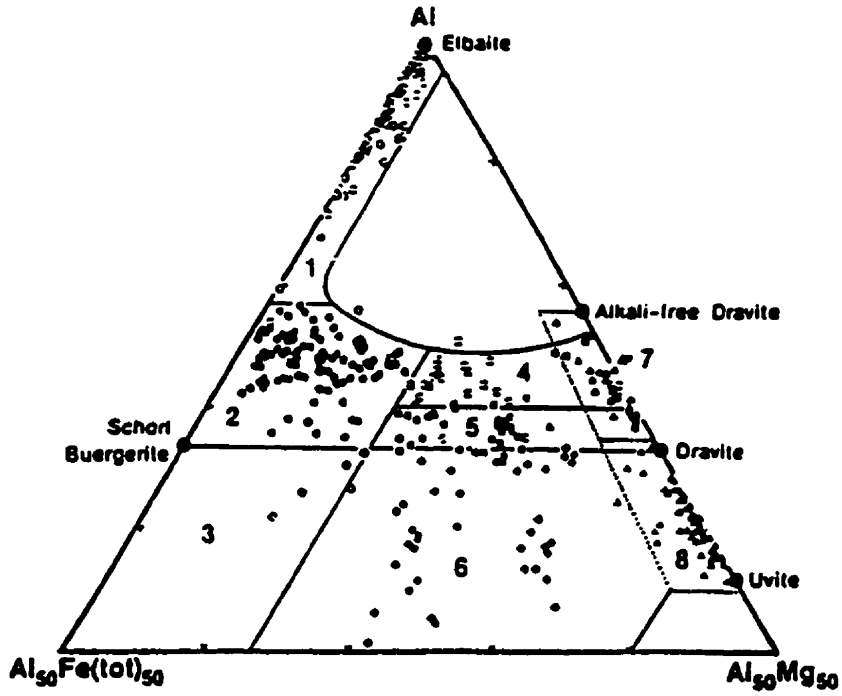

Figure 1.17a. Al-Fe(tot)-Mg ternary diagram; (1) Li-rich granitoid pegmatites and aplites, (2) Li-poor granitoids and their associated pegmatites and aplites, (3) Fe^{3+}-rich quartz-tourmaline rocks (hydrothermally altered granites), (4) metapelites and metapsammites not coexisting with an Al-saturating phase, (6) Fe^{3+}-rich quartz-tourmaline rocks, calc-silicate rocks and (Cr, V)-rich metasediments, and (8) metacarbonates and meta-pyroxenites (Henry & Guidotti 1985).

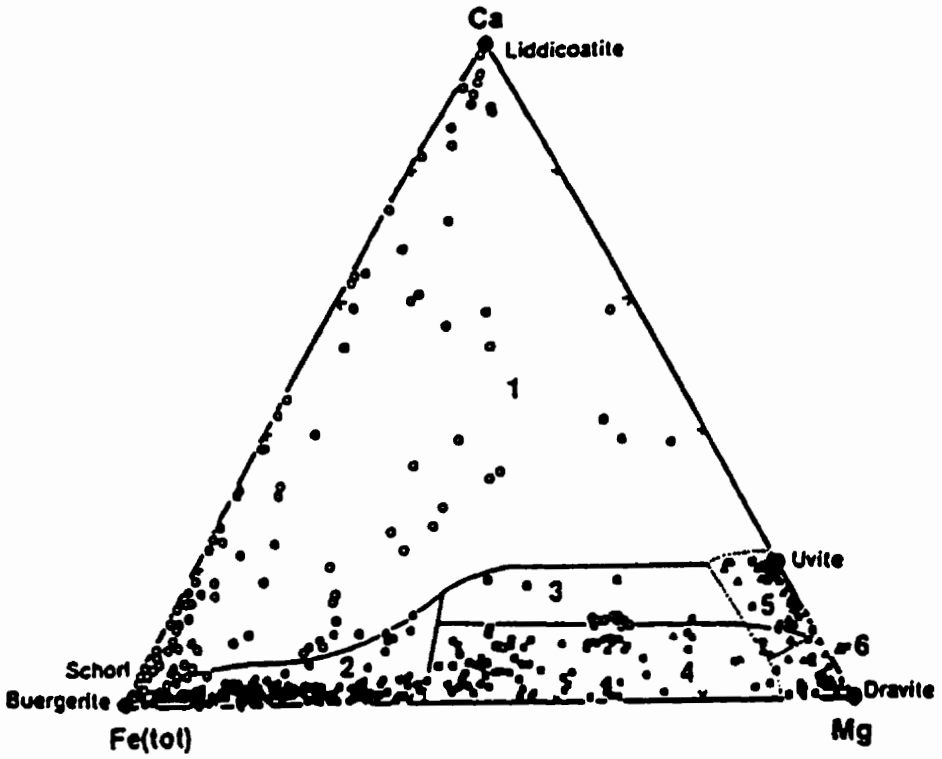

Figure. 1.17b. Ca-Fe(tot)-Mg ternary diagram; fields: (1) Li-rich granitoid pegmatites and aplites, (2) Li-poor granitoids and their associated pegmatites and aplites, (3) Ca-rich metapelites, metapsammites and calc-silicate rocks, (4) Ca-poor metapelites, metapsammites and quartz-tourmaline rocks, (5) metacarbonates, and (6) meta-ultramafics (Henry & Guidotti 1985).

in tourmaline, so that Al-rich dravite occurs in metapelites and metapsammites (field 4). Dravite occurs in three rock types: field 5 - metapelites and metapsammites not co-existing with an Al-saturating phase; field 6 - Fe^{3+}-rich quartz-tourmaline rocks, calc-silicate rocks and metapelites; and field 8 - metacarbonates and metapyroxenites. Uvite occurs in metacarbonates and metapyroxenites (field 8). Tourmalines occur in similar fields in the Ca-Fe(tot)-Mg diagram (Fig. 1.17b).

These discrimination diagrams are useful because

(1) the parameters are easily obtainable from electron-microprobe data;

(2) there is no reliance on one particular structural-formula calculation scheme;

(3) variations in the data represent the cumulative effect of several substitutions (e.g., Al (total) and Mg (total) are plotted, accounting for the total Al⇌Mg substitution at the *Y*- and *Z*-sites without partitioning Mg between these two sites);

(4) the most common tourmaline compositions plot in these diagrams;

(5) they distinguish uvite, dravite, schorl and elbaite compositions and solid solutions;

(6) inference can be made about cations which can not be analyzed by electron microprobe (e.g., elbaite contains high Al at the *Y*- and *Z*-sites and vacancies at the *Y*-site which indicates the presence of Li).

If the tourmaline composition falls below the schorl-dravite line, Mg or Fe^{3+} can be assumed to substitute for Al at the *Z*-site (Fig. 1.17, fields 3,6) (Henry & Guidotti 1985).

There are also several disadvantages to these types of diagrams:

(1) they do not account for V, Cr and Mn which can be found in significant quantities in tourmaline and can be used as a discriminating factor for certain rock types (e.g, V-,Cr-rich dravite occurs in mafic rocks and graphite schists);

(2) tourmaline formed by hydrothermal alteration of a pre-existing rock or

pegmatite (e.g., exocontact and border-zone tourmaline in pegmatites) may take on the chemical characteristics of the host-rock;

(3) zoned tourmaline grains that re-equilibrated with co-existing matrix minerals will not give an accurate corresponding rock type.

The Al-Fe(tot)-Mg diagram is better than the Ca-Fe(tot)-Mg diagram, as it accounts for major-element substitution at the *Y*-site above the schorl-dravite line and at the *Y*- and *Z*-sites below the schorl-dravite line. The Ca-Fe(tot)-Mg diagram combines one element from the *X*-site (Ca) and the Fe=Mg substitution at the *Y*-site, and ignores the common elements Na and Al. Also, the majority of the compositional space in the Ca-Fe(tot)-Mg diagram represents only field 1: Li-rich granitoid pegmatites and aplites, and hence the Ca-Fe(tot)-Mg diagram is a less effective discriminator than the Al-Fe(tot)-Mg diagram.

CHAPTER 2

Introduction to pegmatites

2.1. Characteristics of pegmatites

Granitic pegmatites resemble coarse-grained granites, and contain quartz, albite, microcline and mica. The characteristics that distinguish pegmatites from granites (London 1992) are as follows:

(1) extremely coarse grain-size: individual crystals are commonly from a few centimetres to a few metres in size.

(2) extremely variable grain-size: the grain size of the principal minerals (i.e., quartz and feldspars) is fine at the margin of the pegmatite and coarse-to-giant at the centre.

(3) pegmatitic textures:

(a) comb structure: carrot-shaped crystals (e.g., tourmaline, microcline, beryl and apatite)with the tapered end pointing toward the margin of the pegmatite and the flared end pointing toward the centre;

(b) layered structure: aplitic albite with a continuous layer of garnet, tourmaline or wodginite;

(c) graphic texture: quartz + microcline, quartz + muscovite, quartz + schorl intergrowths;

(d) radial crystal habit: micas and coarse-grained albite which radiate outward from a central core crystal;

(e) skeletal crystal habit: crystals of tourmaline or microcline which exhibit a

branching form that expands toward the centre of the pegmatite.

(4) chemical heterogeneity: zoning in individual crystals (e.g., feldspars, micas, beryl and tourmaline); different compositions of the same mineral for each pegmatite zone; different mineral assemblages for each pegmatite zone and a different modal composition of major minerals for each pegmatite zone.

(5) chemical fractionation within pegmatites: rare lithophile elements (e.g., Li, Rb, Cs, Be, Ga, B, P, F, Mn, Nb, Ta, Zr, Hf and Sn) are enriched in pegmatites. These elements can be fractionated within an individual pegmatite as the melt crystallizes, so that the core margin is enriched relative to the border zone. These elements can also be fractionated between pegmatites within a pegmatite field, so that the distal pegmatites in a cogenetic group surrounding a parent granite are enriched relative to the proximal pegmatites.

2.2. Classification of pegmatites

Pegmatites are classified according to their geological environment, mineral assemblage and geochemical signature. Ginsburg *et al.* (1979) defined four pegmatite classes according to their geological environment and genetic features: (1) abyssal, (2) muscovite, (3) rare-element and (4) miarolitic, which were modified by Černý (1991a) as shown in Table 2.1. Abyssal-class pegmatites occur in low- to high-pressure granulite facies (~7-9 kb; ~700-800°C) and crystallize from segregations of anatectic melt. Muscovite-class pegmatites occur in high-pressure kyanite-bearing amphibolite facies (~5-8 kb; ~650-580°C) and crystallize from anatectic melt or a melt slightly fractionated

Table 2.1. The four classes of granitic pegmatites (Černý 1991a).

Class	Family*	Typical Minor Elements	Metamorphic Environment	Relation to Granites	Structural Features	Examples
Abyssal	—	U,Th,Zr,Nb,Tl,Y, REE,Mo poor (to moderate) mineralization	(upper amphibolite to) low- to high-P granulite facies; ~4-9 kb, ~700-800°C	none (segregations of anatectic leucosome)	conformable to mobilized cross-cutting veins	Ree and Hearne Provinces, Sask. (Tremblay, 1978); Aldan and Anaber Shields, Siberia (Bushev and Koplus, 1960); Eastern Baltic Shield (Kalita, 1965)
Muscovite	—	Li,Be,Y,REE,Tl, U,Th,Nb>Ta poor (to moderate)** mineralization; micas and ceramic minerals	high-P, Barrovian amphibolite facies (kyanite-sillimanite); ~5-8 kb, ~650-580°C	none (anatectic bodies) to marginal and exterior	quasi-conformable to cross-cutting	White Sea region, USSR (Goriov, 1975); Appalachian Province (Jahns *et al.*, 1952); Rajahstan, India (Shmakin, 1976)
Rare-element	LCT	Li,Rb,Cs,Be,Ga,Sn, Hf,Nb≥Ta,B,P,F poor to abundant mineralization; gemstock; industrial minerals	low-P, Abukuma amphibolite (to upper greenschist) facies (andalusite-sillimanite); ~2-4 kb, ~650-500°C	(interior to marginal to) exterior	quasi-conformable to cross-cutting	Yellowknife field, NWT (Meintzer, 1987); Black Hills, South Dakota (Shearer *et al.*, 1987); Cat Lake-Winnipeg River field, Manitoba (Černý *et al.*, 1981)
	NYF	Y,REE,Tl,U,Th,Zr, Nb>Ta,F; poor to abundant mineralization; ceramic minerals	variable	interior to marginal	interior pods, conformable to cross-cutting exterior bodies	Llano Co., Texas (Landes, 1932); South Platte district, Colorado (Simmons *et al.*, 1987); Western Kelvy, Kola, USSR (Beus, 1960)
Miarolitic	NYF	Be,Y,REE,Tl,U,Th, Zr,Nb>Ta,F; poor mineralization; gemstock	shallow to sub-volcanic; ~1-2 kb	interior to marginal	interior pods and cross-cutting dykes	Pikes Peak, Colorado (Foord, 1982); Idaho (Boggs, 1986); Koroster pluton, Ukraine (Lazarenko *et al.*, 1973)

Notes
* See Table 4 for explanation; ** Some Soviet authors distinguish a rare-element-muscovite class, in all respects intermediate between the muscovite and rare-element classes proper

Table 2.2. The three petrogenetic families of rare-element pegmatites (Černý 1991a).

Family	Pegmatite types	Geochemical signature	Pegmatite bulk composition	Associated granites	Granite bulk composition	Source lithologies	Examples
LCT	beryl complex albite-spodumene albite	Li,Rb, Cs,Be,Sn,Ga, Ta>Nb(B,P,F)	peraluminous**	(synorogenic to) late orogenic (to anorogenic); largely heterogeneous	peraluminous S,I or mixed S+I types	undepleted upper- to middle-crust supracrustals and basement gneisses	Bikita field, Zimbabwe (Martin, 1964); Utö-Mysingen field, Sweden (Smeds and Černý, 1989); White Picacho field, New Mexico (London and Burt, 1982a)
NYF *	rare-earth	Nb>Ta,Ti, Y,Sc,REE, Zr,U,Th, F	subaluminous to metaluminous (to subalkaline)	(syn-, late, post-to) mainly anorogenic; largely homogeneous	(peraluminous to) subaluminous to metaluminous (rarely peralkaline); A and (I) types	depleted middle to lower crustal granulites, or undepleted juvenile granitoids	Shatford Lake group, Manitoba (Černý *et al.*, 1981); Sancroft-Renfrew field, Ontario-Quebec (Černý, 1990; Lentz, 1991); Stockholm area, Sweden (Nordenskjöld, 1910; Smeds, 1990)
Mixed	"cross-bred" LCT and NYF	mixed	(metaluminous to) moderately peraluminous	(postorogenic to) anorogenic; moderately heterogeneous	subaluminous to slightly peraluminous; mixed geochemical signature	mixed protoliths, or assimilation of supracrustals by NYF granites	Tørdal district, S. Norway (Juve and Bergstøl, 1988); Kimito, Finland (Pehrman, 1945); Evje-Iveland field, S. Norway (Bjørlykke, 1935; Frigstad, 1988).

Notes
* This family also includes pegmatites of the miarolitic class (*cf.* Table 2)
** Definitions: Peraluminous, A/CNK>1; subaluminous, A/CNK~1; metaluminous, A/CNK<1 at A/NK>1; subalkaline, A/NK~1; peralkaline, A/NK<1, where A = molecular Al_2O_3, CNK = CaO + Na_2O + K_2O, and NK = Na_2O + K_2O (Černý, 1991a)

Table 2.3. Classification of pegmatites of the rare-element class (Černý 1991a).

PEGMATITE TYPE [feldspar + mica content]	*Pegmatite subtype*, geochemical signature	Typical minerals	Economic potential	Typical examples
RARE-EARTH [Kf>plg to ab; bi≥msc]	*allanite-monazite* (L)REE,U,Th (P,Be,Nb>Ta)	allanite monazite	(REE)	Upper Tura River, Ural Mtns. (Fersman, 1940) West Portland, Quebec (Spence and Muench, 1935) Kobe, Japan (Tatekawa, 1955)
	gadolinite Y,(H)REE,Be,Nb>Ta F(U,Th,Ti,Zr)	gadolinite fergusonite euxenite (topaz) (beryl)	Y,REE,U (Be,Nb-Ta)	Shatford Lake group, Manitoba (Černý *et al.*, 1981) Ytterby, Sweden (Nordenskjöld, 1910) Evje-Iveland field, Norway (Bjørlykke, 1935) Barringer Hill, Texas (Landes, 1932) Pyörönmaa, Finland (Vorma *et al.*, 1966)
BERYL [Kf>ab; msc>bi]	*beryl-columbite* Be,Nb≥Ta (±Sn,B)	beryl columbite-tantalite	Be	Meyers Ranch, Colorado (Hanley *et al.*, 1950) Greer Lake group, Manitoba (Černý *et al.*, 1981) Donkerhoek, Namibia (Schneiderhöhn, 1961) Ural Mtns., USSR (Kuzmenko, 1976)
	beryl-columbite-phosphate Be,Nb≥Ta,P (Li,F,±Sn,B)	beryl, columbite-tantalite triplite triphylite	(Nb-Ta)	Hagendorf-Süd, Germany (Strunz *et al.*, 1975) Dan Patch, South Dakota (Norton *et al.*, 1964) Connecticut localities (Cameron and Shainin, 1947) Crystal Mtn. field, Colorado (Thurston, 1955)
COMPLEX [Kf≥ab; msc≥lep]	*spodumene* Li,Rb,Cs,Be,Ta≥Nb (Sn,P,F,±B)	spodumene beryl tantalite (amblygonite) (lepidolite) (pollucite)	Li,Rb, Cs,Be Ta, (Sn,Ga,Hf)	Harding, New Mexico (Jahns and Ewing, 1976) Hugo, South Dakota (Norton *et al.*, 1962) Mongolian Altai #3 (Wang *et al.*, 1981) Etta, South Dakota (Norton *et al.*, 1964) White Picacho, Arizona (London and Burt, 1982a) Manono, Zaire (Thoreau, 1950)
	petalite Li,Rb,Cs,Be,Ta>Nb (Sn,Ga,P,F,±B)	petalite beryl tantalite (amblygonite) (lepidolite)		Tanco, Manitoba (Černý, 1982c) Bikita, Zimbabwe (Cooper, 1964) Varutträsk, Sweden (Quensel, 1956) Luolamäki, Finland (Neuvonen and Vesasalo, 1960) Londonderry, Australia (McMath *et al.*, 1953) Hirvikallio, Finland (Vesasalo, 1959)
	lepidolite F,Li,Rb,Cs,Be Ta>Nb (Sn,P,±B)	lepidolite topaz beryl microlite (pollucite)	Li,Rb, Cs,Ta Be (Sn,Ga)	Brown Derby, Colorado (Heinrich, 1967) Pidlite, New Mexico (Jahns, 1953b) Himalaya district, California (Foord, 1976) Khukh-Del-Ula, Mongolia (Vladykin *et al.*, 1974) Wodgina, Australia (Blockley, 1980)
	amblygonite P,F,Li,Rb,Cs Be,Ta>Nb (Sn,±B)	amblygonite beryl tantalite (lepidolite) (pollucite)	Li,Rb Cs,Ta Be (Sn,Ga)	Viitaniemi, Finland (Lahti, 1981) Maleklalina, Madagascar (Varlamoff, 1972) Peerless, South Dakota (Sheridan *et al.*, 1957) Finnis River, Australia (Jutz, 1966)
ALBITE-SPODUMENE [ab>Kf; ((msc))]	Li (Sn,Be,Ta≥Nb, ±B)	spodumene (cassiterite) (beryl) (tantalite)	Li,Sn (Be,Ta)	Kings Mountain, North Carolina (Kesler, 1976) Preissac-Lacorne, Quebec (Mulligan, 1965) Peg Claims, Maine (Sundelius, 1963) Volta Grande, Brazil (Heinrich, 1964)
ALBITE [ab>>Kf; (ms,lep)]	Ta≥Nb,Be (Li,±Sn,B)	tantalite beryl (cassiterite)	Ta (Sn)	Hengshan, China (Černý, 1989a) USSR (Solodov, 1969) Tin Dyke, Manitoba (Checkowsky, 1987)

from primitive granites. Rare-element-class pegmatites occur in low-pressure andalusite-bearing amphibolite facies (~2-4 kb; ~650-500°C) as differentiation products of a parental granite. Miarolitic-class pegmatites are shallow to subvolcanic, and crystallize from residual melts fractionated from plutonic granite intrusions.

The rare-element class was further subdivided by Černý (1991a) into three petrogenetic families (Table 2.2) and ten paragenetic/geochemical types and subtypes (Table 2.3).

The petrogenetic families are: (1) LCT pegmatites are enriched in the elements Li, Cs, Ta and Li-bearing minerals; (2) NYF pegmatites are enriched in the elements Nb, Y, F and REE-bearing minerals; (3) mixed pegmatites display characteristics of both LCT and NYF. The LCT pegmatites are derived from peraluminous S- and I-type granites, whereas the NYF pegmatites are related to subaluminous A-type granites (Fig.2.1). The NYF-family is represented by the rare-earth type and its two subtypes: (1) allanite-monazite, and (2) gadolinite (Table 2.3). The allanite-monazite subtype pegmatites are enriched in LREE, U, Th and P, whereas the gadolinite-subtype pegmatites are enriched in HREE, Y, Be, Nb and F. The LCT-family consists of four types: (1) beryl; (2) complex; (3) albite-spodumene; (4) albite (Table 2.3). In terms of feldspars and micas, (1) the beryl type contains K-feldspar > albite and muscovite > biotite; (2) the complex type contains K-feldspar, albite, muscovite, and Li-rich minerals (*i.e.*, spodumene, petalite, lepidolite and/or amblygonite); (3) the albite-spodumene type contains albite > K-feldspar

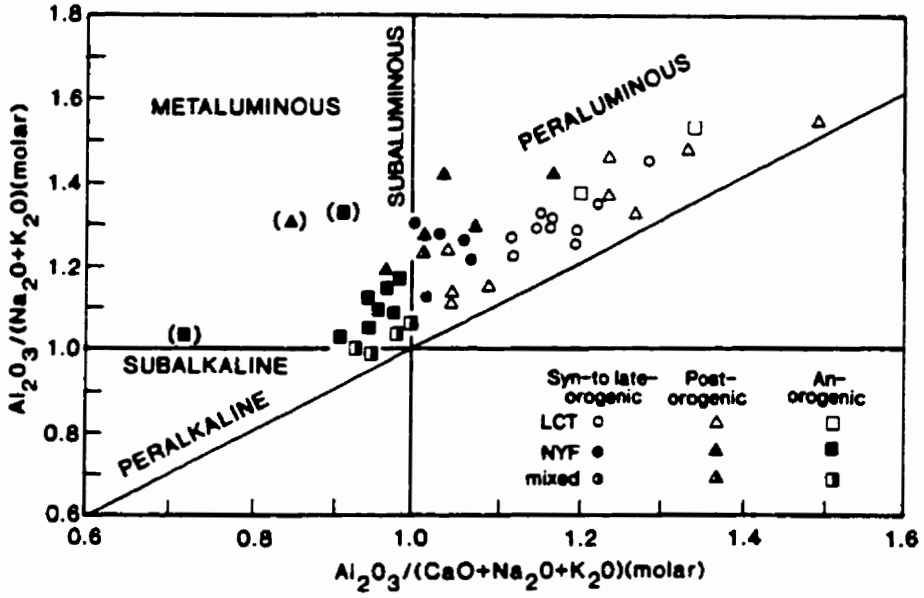

Figure. 2.1. Alumina saturation (Shand index) in the modified Maniar and Piccoli (1989) diagram; most individual granite systems discussed in the text are represented by several symbols covering their compositional range. The granites are coded for their tectonic affiliation and geochemical signature. Symbols in brackets denote compositions genetically related to, but not identical with, fertile granites proper (Černý 1991a).

and accessory muscovite; (4) the albite type contains albite >> K-feldspar, muscovite and lepidolite. The beryl type can be divided into two subtypes: (a) beryl-columbite and (b) beryl-columbite-phosphate. The albite-spodumene-type pegmatites have abundant spodumene, whereas the albite-type pegmatites may contain tantalite and beryl.

The complex type is divided into five subtypes according to the dominant Li-bearing mineral: (a) spodumene, (b) petalite, (c) lepidolite, (d) elbaite (Novák & Povondra 1995) and (e) amblygonite (Table 2.3). They differ by the dominant Li-bearing phase, as indicated by each name, and by the corresponding pressure, temperature and

geochemical conditions of formation. Otherwise, most of them may contain minerals such as beryl (Be), cassiterite (Sn), tantalite (Ta), columbite (Nb), pollucite (Cs), tourmaline (B) and apatite (P, F).

The pegmatites examined in this thesis belong to the LCT family, rare-element class and complex type.

2.3. Control of source lithology on the geochemistry of LCT and NYF pegmatites

The geochemistry of rare-element pegmatites is controlled by the source lithologies from which the melts of the parental fertile granites were derived (Černý 1991b). LCT pegmatites are enriched in Li, Rb, Cs, Be, Ga, Sn, Nb>Ta, B, P and F; NYF pegmatites are enriched in Nb>Ta, Y, REE, Sc, Ti, Zr, Be, Th, U and F.

Rare elements are extracted into the first melts derived from progressively metamorphosed lithologies under relatively hydrous conditions (Černý 1991b). LCT pegmatites are derived during the first anatectic event. Source rocks were not depleted by previous anatexis or granulite-grade metamorphism. There are two modes of origin for LCT granite and pegmatite melts:

(1) the first anatectic event in undepleted upper- to middle-crustal or supracrustal rocks;

(2) the same in juvenile igneous to metamorphic basement rocks.

The host rocks for LCT pegmatites are schists, gneisses, metasediments, metapelites, metaturbidites and metavolcanics mainly at lower amphibolite facies (Černý 1991b). LCT pegmatites may evolve during early to late orogenic events (e.g., synorogenic to mainly late orogenic), concentrating mobile components in relatively fluid-rich environments of

first- generation melts. LCT pegmatites are derived from post-orogenic to anorogenic plutons generated from undepleted sources.

The crystal chemistry and geochemical behaviour of Ti, Zr, Nb, Ta and F suggest that NYF pegmatites become enriched in these elements in the residual pegmatite melt after the first melting event and are preferentially mobilized during subsequent high-temperature anatexis (Černý 1991b). NYF pegmatites and their parent plutons are mainly post-orogenic to anorogenic. There are two modes of origin for NYF granite and pegmatite melts:

(1) melting of middle to lower crustal granulite-grade lithologies depleted by previous anatectic events;

(2) anatexis of juvenile igneous lithologies (e.g., granitoids) with short-lived crustal residence.

The NYF pegmatites commonly reside within or close to their plutonic parents (*e.g.*, A-type granites).

2.4. Regional zoning

Regional zoning is restricted to peraluminous granites and surrounding LCT pegmatites (Černý 1991c, 1992). Typical NYF pegmatites are clustered within, or in close proximity to, the parental granite and do not show significant compositional variations on a regional scale. Residual pegmatitic melts may accumulate mainly in two ways, but a third way is possible (Černý 1991c). (1) If filter pressing, fluid transport and/or gravitational convection-diffusion were the main mechanism generating the

residual melt, it would accumulate in the uppermost cupolas of parent granitic intrusions. This would produce a general sequence for zoning within fertile peraluminous granite from centre outerward: biotite granite → two-mica leucogranite → coarse-grained muscovite leucogranite → pegmatitic leucogranite → aureole of LCT pegmatites (Fig. 2.2a). With increasing fractionation, the granite increases in grain size. (2) If crystal-melt fractionation were dominant, promoted by the cooling effect of the metamorphic host rocks, the residual melt would concentrate in deeper central parts of fertile intrusions that solidified from the contacts inward (Fig. 2.2b). The LCT pegmatites occur interior to marginal of the inward-fractionated parent granite. (3) Buoyant rise of local segregations of pegmatite melts through incompletely solidified parent magma is rather uncommon (Fig. 2.2c).

The fertile parent granite is at the centre of and the surrounding pegmatite aureole consists of concentric zones of LCT pegmatite bodies. The general spatial sequence in zoned cogenetic LCT pegmatite groups from the peraluminous granite outward is as follows: (1) barren, (2) ±rare-earth type, (3) beryl-columbite subtype, (4) beryl-columbite-phosphate subtype, (5) spodumene and/or petalite + amblygonite subtypes, (6) lepidolite subtype, (7) albite-spodumene type, (8) albite type and (9) ±Be, Sn, Mo, W- to Au, Cu, Pb, Zn-bearing quartz veins (Fig. 2.3). This sequence represents increasing fractionation and volatile enrichment of the pegmatite melt, and increasing complexity of zoning and extent of replacement within individual pegmatite bodies. The number of pegmatite bodies of a particular type/subtype decreases with increasing complexity and fractionation. For example, complex pegmatites typically constitute <2% of any given

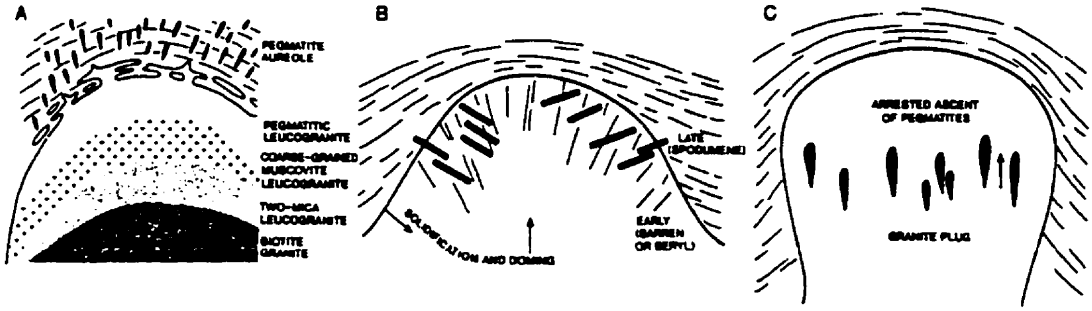

Figure 2.2. Schematic representation of granite-pegmatite relationships. (a) Zoned outward-fractionated fertile granite with an aureole of exterior LCT pegmatites, typical of many fields of Kenoran and Hudsonian age. (b) Interior to marginal LCT pegmatites in an inward-fractionated parent granite, located in fracture systems generated by upwarping of solidified upper crust of the intrusion. (c) Turnip-shaped NYF pegmatites trapped during ascent through the parent granitoid mush (Černý 1991a).

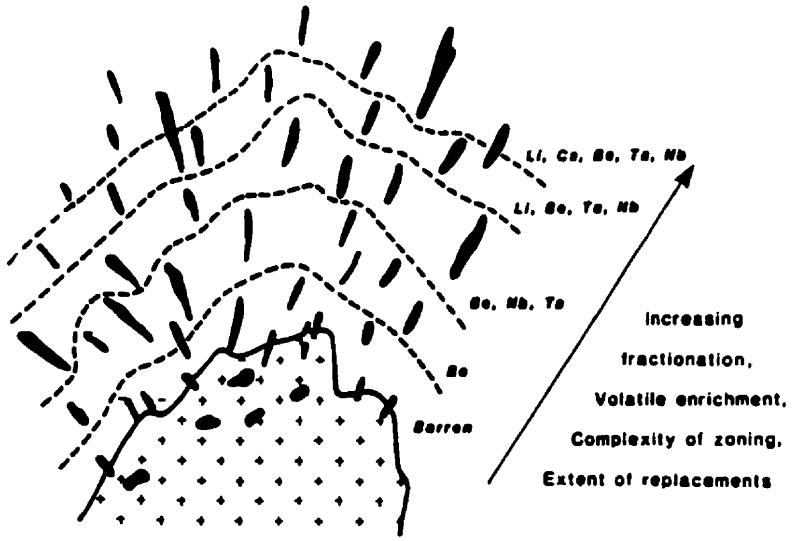

Figure 2.3. Schematic representation of regional zoning in a cogenetic granite+pegmatite group (Černý 1991a).

group of genetically related pegmatites.

Commonly, only parts of this sequence are seen. Typically, this sequence lacks the rare-earth-type pegmatites of zone (2) and the mineralized quartz veins of zone (9). There is variable representation of the complex-type pegmatites in zones (5) and (6), and of the albite-spodumene- and albite-type pegmatites in zones (7) and (8). Often only one of these four zones is developed in a given pegmatite group.

2.5. Internal Structure

The internal structure of rare-element pegmatites can be homogeneous, layered or zoned. Homogeneous coarse-grained pegmatites are uniform in their mineral assemblage and textures (Fig. 2.4). Homogeneous pegmatites are rare, except for the albite-spodumene type which consists of elongate megacrysts of spodumene and quartz embedded in a fine-grained matrix of albite and quartz (Černý 1991a). An example of homogeneous pegmatites is the lepidolite pegmatites at Red Cross Lake which consist dominantly of lepidolite, albite and quartz (Černý *et al.* 1994).

Layered pegmatites are asymmetrically zoned. They are subhorizontal with sodic-aplite units in the footwall and K-feldspar + quartz in the hangingwall (Fig. 2.5). Highly fractionated layered pegmatites may contain large vugs (e.g., elbaite-bearing pockets of the Pala district) (Černý 1991a). An example of a layered pegmatite is Belo Horizonte, which consists dominantly of sodic albite in the footwall, microcline-perthite in the hangingwall, and elbaite-bearing pockets in the centre (M.C. Taylor, pers. comm.).

Zoned pegmatites consist of zones characterized by their mineral assemblage and

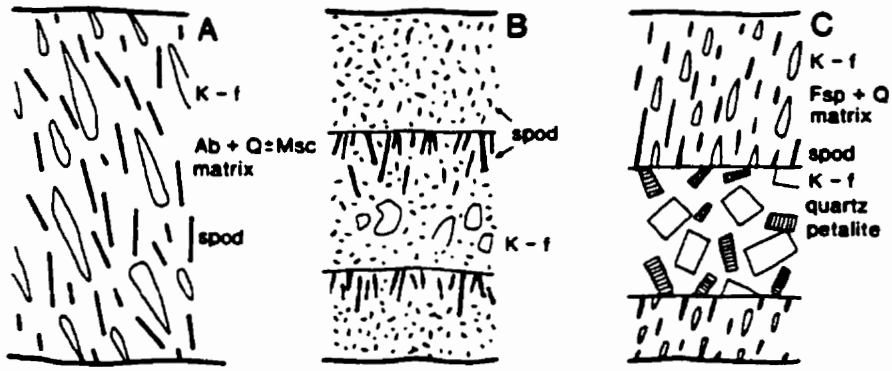

Figure 2.4. Internal structure of homogeneous pegmatites in cross-sections. (A) Preferred orientation of spodumene and K-feldspar in albite-spodumene type, Kings Mountain, North Carolina (*e.g.*, Kunasz, 1982); (B) Cockscomb texture of spodumene in multiple intrusions of parallel pegmatite dykes, Volta Grande, Brazil (after Heinrich, 1964); (C) Early spodumene-bearing pegmatite (as in A) penetrated by a parallel dyke with random orientation of K-feldspar and petalite, Järkvissle, Sweden (Černý 1991a).

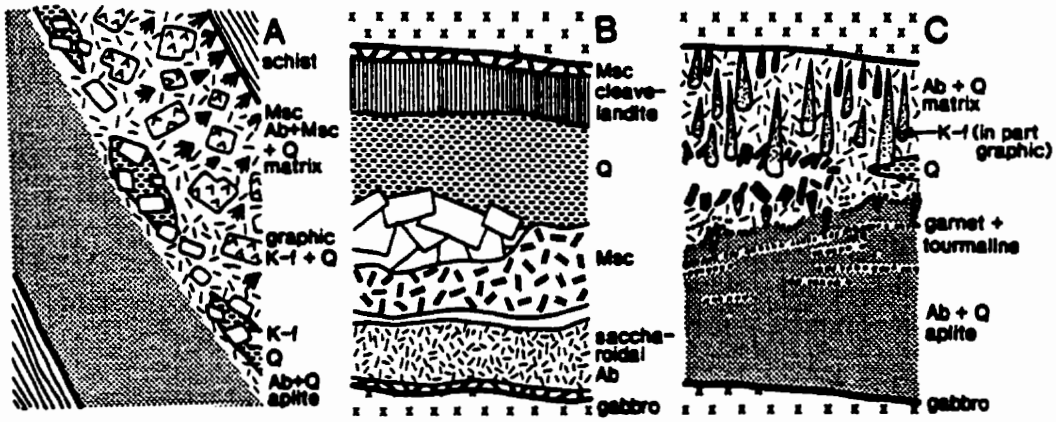

Figure 2.5. Vertical sections across three representatives of layered pegmatites. (A) A barren steeply dipping pegmatite, Buell Ranch, South Dakota (after Orville 1960); (B) An unnamed, subhorizontal beryl-bearing pegmatite (after Solodov, 1971); (C) A vug-bearing, subhorizontal pegmatite of the complex lepidolite subtype, Himalaya district, California (after Foord 1976 and Jahns 1982) (Černý 1991a).

texture. These zones may form by primary crystallization, replacement, or fracture filling. The primary zones form concentric envelopes from the pegmatite margin to the core: (1) border zone; (2) wall zone; (3) first, second and third intermediate zones; (4) core margin; (5) core (Fig. 2.6). The border zone is fine-grained, usually granitic in composition, and contains albite, biotite and muscovite; the wall zone is medium-grained, and contains albite, muscovite and graphic K-feldspar + quartz intergrowths; the intermediate zones are coarse-grained and contain blocky K-feldspar; the core-margin contains the most fractionated minerals (e.g., elbaite, beryl and spodumene); the core is commonly monomineralic quartz. Examples of other primary monomineralic zones are lepidolite and pollucite. With progressive crystallization from the margin to the core, the pegmatite zones show an increase in grain size, a decrease in number of rock-forming minerals, and textural changes from granitic or aplitic to graphic to blocky to coarse-grained monomineralic in the core (Černý 1991a). Tanco pegmatite is an example of a zoned pegmatite (Černý *et al.* 1998).

An exocontact (zone) surrounds homogeneous and zoned pegmatites, and is the part of the host rock that was metasomatically altered by infiltration of B, H_2O and other highly mobile components from the pegmatite melt (London *et al.* 1996). An amphibolite host rock, for example, alters to holmquistite or tourmaline + biotite in the exocontact.

Saccharoidal-albite units are considered by some to be replacement units and by others to be the result of primary crystallization (Černý 1991a). The most common form of fracture-filling units involves quartz rooted in the core and transecting intermediate zones (Černý 1991a).

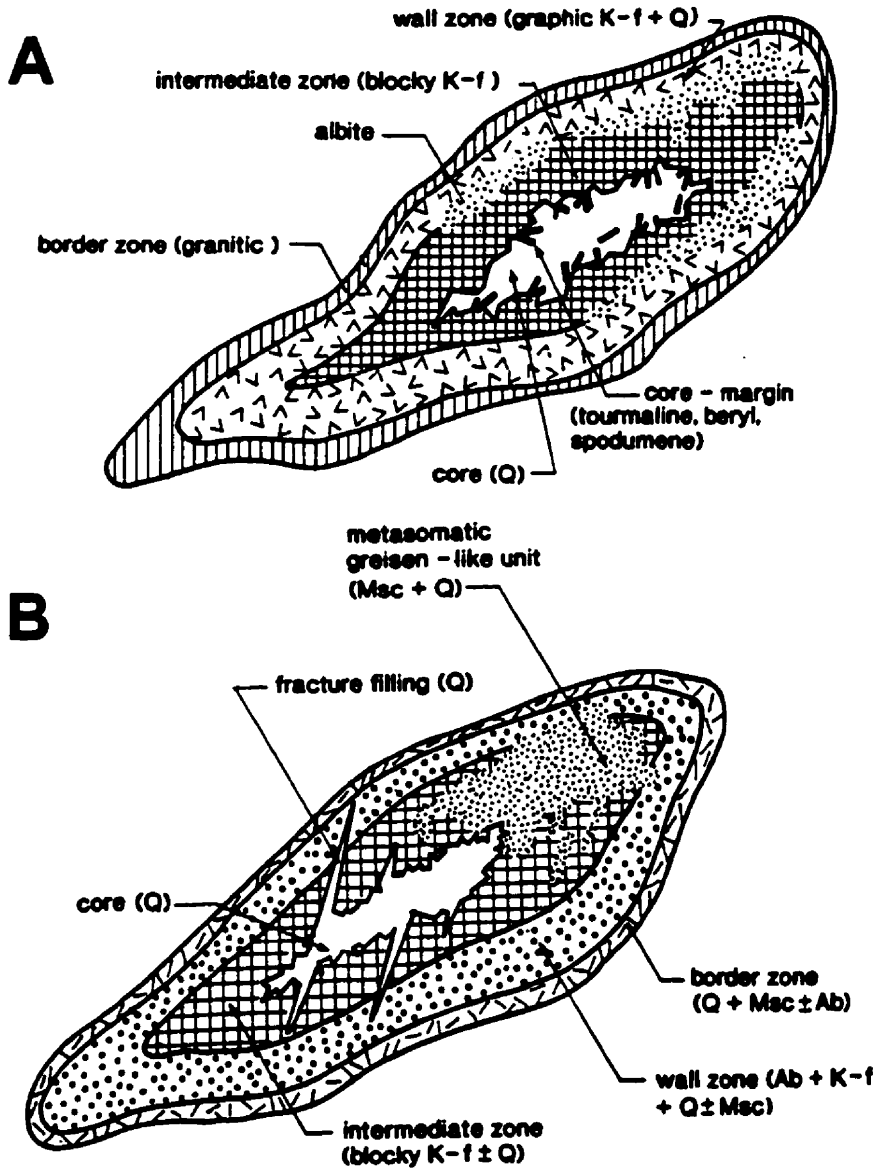

Figure 2.6. Internal structure of zoned pegmatites in schematic horizontal sections. (A) Concentric pattern of primary zones, with zonal control of the distribution of albite units, and core-margin mineralization; (B) Concentric pattern of primary zones cross-cut by fracture fillings, with a lithology-controlled, but, in part, fracture-related, metasomatic unit (Černý 1991a).

2.6. Internal Evolution

2.6.1. The Jahns and Burnham model of pegmatite crystallization

In the Jahns and Burnham model, the key to pegmatite crystallization is the presence of an aqueous fluid coexisting with silicate melt (Jahns & Burnham 1969, Jahns 1982, Burnham & Nekvasil 1986). Pegmatite crystallization consists of three stages:

(1) the silicate-melt stage: crystallization from a hydrous silicate melt yields anhydrous solid phases with a coarse-grained granitic texture. As crystallization progresses and the temperature decreases, the silicate melt becomes enriched in volatiles, especially water.

(2) two-fluid stage: this stage is essential to the formation of the pegmatite. The silicate melt becomes saturated in volatiles and an aqueous fluid exsolves. The silicate melt crystallizes to fine-grained aplite and sodium-bearing minerals, and giant-textured pegmatites and K- and Li-bearing minerals crystallize from the co-existing exsolved aqueous fluid. Quartz crystallizes simultaneously from both fluids. The partitioning of constituents between the two fluids, and rapid diffusion of materials through the aqueous phase, lead to segregation of the constituents into zones with different mineral assemblages. The silicate melt is completely used up at this stage.

(3) interaction between solid crystals and the aqueous fluid causes alteration of the solid phases. Late-stage minerals and pocket minerals crystallize from the aqueous fluid. The aqueous fluid also may metasomatically alter the country rocks.

2.6.2. The London model of pegmatite crystallization

2.6.2.1 Internal evolution of pegmatites

In the London model, the key to pegmatite crystallization is an increase in H_2O, B, P and F concentrations which leads to a decrease in crystal-nucleation density in a homogeneous, volatile-rich, but undersaturated, silicate melt (London *et al.* 1988, 1989, London 1990, 1992).

The parental granite and the outermost granitic border zone of pegmatites crystallize from an H_2O-undersaturated melt. Nominally dry, B-, P-, F-rich silicic magmas should form granites, as opposed to pegmatites, due to high nucleation densities. The pegmatite melt becomes enriched in Li, B, P and F as crystallization progresses, which increases the solubility of H_2O in the melt. Increasing B, P and F in the melt and increasing H_2O pressure lowers the temperature of minimum melting and causes expansion of the liquidus field of quartz at the expense of albite. The increasing B, P, F and H_2O contents of the melt decrease the number of crystal nuclei per unit volume (nucleation density), resulting in growth of a few giant crystals. The granitic to pegmatitic grain-size transition is due to a sharp decrease in nucleation density. The increase in B and P in the melt will delay H_2O-saturation until later stages of crystal fractionation.

The stability of tourmaline is a key factor in the accumulation of B in granitic melts. Equilibrium between tourmaline and other ferromagnesian silicates (e.g., biotite, cordierite and hornblende) buffers the B content of melt at concentrations well below 1 wt% B_2O_3. Once the buffer capacity of equilibria between tourmaline and biotite or hornblende is exhausted (i.e., tourmaline is the only ferromagnesian phase), then the B

content may increase by fractionation.

Most, if not all, pegmatite-forming magmas become H_2O-saturated and exsolve an aqueous vapour phase near the solidus as they approach complete crystallization. By combining phase relations of the lithium aluminosilicates (Fig. 2.7) with fluid-inclusion data, London (1986a, b) defined solidi for both the massive Tanco pegmatite and miarolitic rare-element pegmatites from Afghanistan and California as being near 475°C. Only B partitions preferentially into the aqueous vapour. The transition from magmatic to hydrothermal conditions may be continuous or may be abrupt due to loss of B, P and F to late-crystallizing minerals.

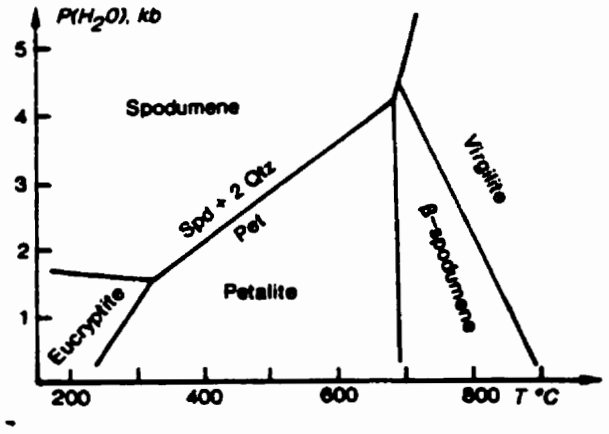

Figure 2.7. Phase diagram for the bulk composition 20 Ecr 80 Qtz (mole%) in the system $LiAlSiO_4$-SiO_2-HO_2 (modified by Černý 1991a, from London 1984).

Attainment of H_2O-saturation during late pegmatite consolidation is indicated by the presence of primary miarolitic cavities and metasomatic replacement of pre-existing minerals within the pegmatite (London 1992). The first stage of subsolidus metasomatic

alteration is usually alkaline in character due to excess alkaline components not conserved by crystallization of albite. The next stage involves weakly acidic potassic alteration in which feldspars, lithium aluminosilicates and montebrasite are replaced by sericite mica. Sericitic alteration of feldspars liberates phosphorus which crystallizes as secondary phosphates in fractures. Other subsolidus minerals are zeolites, sulphides and clay minerals.

Water-oversaturated conditions in the melt lead to external alteration. Wallrock alteration is restricted to evolved pegmatites. Metasomatic alteration assemblages in the host rock (e.g., metapelites, gneisses and amphibolites) and within the pegmatite normally indicate greenschist-to-zeolite metamorphic facies. The chemical composition of metasomatic assemblages in host rocks mirrors the composition of the innermost units of the adjacent pegmatite, indicating that fluids are expelled from pegmatites after they have fully crystallized. These fluids must have interacted with the outer zones (e.g., pegmatite wall and border zones) as they passed through the contact area (Morgan & London 1987), although many pegmatites lack evidence of fluid-induced wallrock alteration. Conversion of amphibolite host-rock to tourmaline-rich metasomatic aureole requires a pH below 5.5, low alkalinity, and high Fe, Mg and Al contents (Morgan & London 1987, 1989). Aluminum and B from the pegmatite infiltrate the Ca-, and Mg-rich amphibolite to produce uvite or dravite (Fig. 2.8). Almost 80% of the original B content of the Tanco pegmatite was lost to the host rocks, of which 60-70% was incorporated in tourmaline within the host rocks (Morgan & London 1989). In addition to (Ca, Mg)-rich tourmaline, the exocontact of Tanco consists of biotite, epidote, calcite, titanite, arsenopyrite and

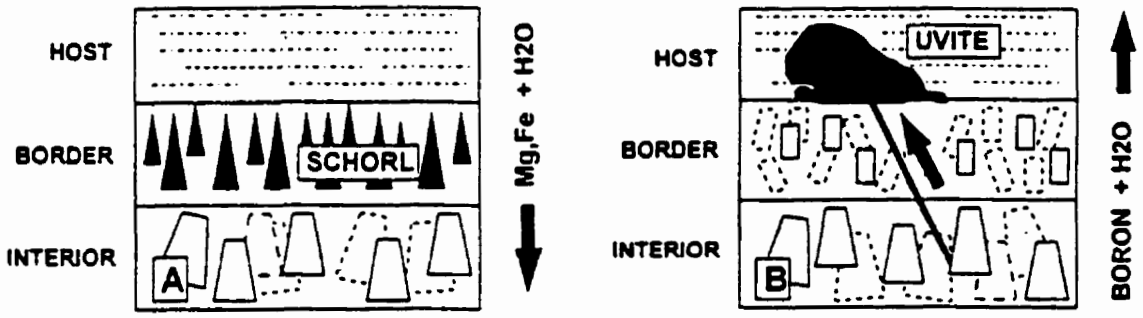

Figure 2.8. Schematic depiction of the mass transfer involved in two different styles of tourmalinization. (a) Mixing of externally derived FM-bearing fluid within B-rich granite-pegmatite precipitates a concentrated and oriented fringe of tourmaline within the igneous body with little or no tourmaline produced in the wallrock tourmaline composition starts as aluminous schorl. (b) Reaction of wallrock (*e.g.* amphibolite) with B-rich fluid derived from granite-pegmatite; wallrock chemistry controls tourmaline composition, and in replaced amphibolites the tourmaline composition approaches that of uvite (London *et al.* 1996).

holmquistite (London *et al.* 1996). Ca-rich tourmaline is rarer than Na-rich tourmaline due to the early fractionation of Ca-bearing minerals in magmatic processes; thus Ca-Fe and Ca-Mg silicates (e.g., hornblende, diopside, epidote) would probably crystallize long before Ca-Fe and Ca-Mg tourmaline (e.g., feruvite, uvite) (Grice & Robinson 1989).

Metasomatic exocontact tourmaline typically shows fine-scale zoning within individual crystals and reflects the Mg/(Fe+Mg) ratios of the host rocks. Conversely, Fe and Mg from the host rocks infiltrate the B-rich pegmatitic melt to produce Al-rich schorl in the border zone (Fig. 2.8).

2.6.2.2. Correlation between pegmatite textures and geochemical conditions

Pegmatites contain two forms of anisotropic fabric: (1) oriented crystals (e.g., comb-structure), and (2) layered structures (London 1992). The transition from isotropic granitic fabrics to anisotropic comb-structured pegmatite fabrics reflects change from internal nucleation to strongly heterogeneous nucleation. This transition correlates with an increasing degree of disequilibrium, low nucleation-density, and low growth-rate caused by increasingly large and rapid initial undercooling of melt due to increasing H_2O, B, P and F concentrations.

Quartz and K-feldspar graphic intergrowths, skeletal crystals and radial or plumous aggregates are common pegmatitic textures. Graphic quartz + K-feldspar intergrowths result from saturation of quartz on a cellular (skeletal) growth-surface of K-feldspar due to rapid growth of K-feldspar relative to the diffusion rate of silica through the melt. Graphic quartz + K-feldspar intergrowths are generated in H_2O-undersaturated melts, which explains why graphic textures occur in the outermost pegmatite zones. Skeletal, branching and radial habits of crystals indicate rapid disequilibrium-induced growth in silicate melts due to increasing degrees of undercooling.

Layered structures consist of aplitic albite with layers of garnet, tourmaline or (Nb, Ta)- oxide minerals. The layers may be only centimetres thick and up to one kilometre long. Webber *et al.* (1997) state that layered aplite is a diffusion-controlled process of oscillatory nucleation and in-situ crystallization. Strong undercooling may initiate rapid heterogeneous nucleation and oscillatory crystal growth which leads to the development of a layer of excluded components in front of the crystallization front, and

the formation of line rock.

The formation of mineral zones in zoned pegmatites is due to two mechanisms: (1) disequilibrium fractional crystallization of silicate melt by sequential inward crystallization from the margins; (2) eutectic equilibrium crystallization in which the pegmatite zones develop simultaneously but separately because of incongruency in the solubilities of alkalis, Al and Si between silicate melt and aqueous vapour. During sequential fractionation, there are large variations in the composition of the residual melt which result in chemical zonation within individual crystals and changes in the composition of a mineral during different stages of crystallization. The sequential evolution of grain size from fine-grained granitic borders to coarse-grained K-feldspar intermediate zones to megacrystic quartz cores is also promoted by fractional crystallization. The greater the degree of disequilibrium between the melt and a crystalline assemblage, the greater the tendency for oriented (comb-structure) surface nucleation over internal nucleation. Habits of individual crystals evolve to more graphic and skeletal forms with increasing disequilibrium.

2.7. Element trends in tourmaline in pegmatites

The most common occurrence of tourmaline is as an accessory mineral in pegmatites. The composition of tourmaline varies according to the pegmatite zone in which it occurs. The general element trends in tourmaline as a function of paragenesis are as follows (Jolliff *et al.* 1986; Staatz *et al.* 1955):

(1) tourmaline in the exocontact is enriched in Ca, Mg, Ti and Fe (uvite and

dravite-schorl);

(2) Mg (dravite), Ti and Ca decrease abruptly from the country rock through the border zone to the wall zone (Figs. 2.9,2.10);

(3) Fe (schorl) decreases and (Li+Al) (elbaite) increases from the wall zone to the core, reflecting the dominant substitution $Li+Al \rightleftharpoons 2Fe^{2+}$ at the *Y*-site (Fig. 2.9);

(4) Na decreases and *X*-site vacancies increase toward the core of the pegmatite;

(5) Mn generally increases toward the core of the pegmatite (Fig. 2.10);

(6) Zn initially increases from the border zone, reaches a maximum in the inner wall zone and then decreases toward the core of the pegmatite (Fig.2.10);

(7) Rb and Cs are concentrated in pink elbaite within the core of the pegmatite, and Cr and V occur only in black tourmaline near the wall zone;

(8) The Li content of tourmaline is greater in albitized than in nonalbitized pegmatites.

The lack of systematic trends for other trace elements in tourmaline is due to the following factors:

(1) trace elements are strongly partitioned into mica and feldspar (Rb, Cs), apatite (REE) and (Nb, Ta)-oxides (Nb, Ta);

(2) trace elements occur in mineral inclusions, fluid inclusions and fracture fillings within tourmaline.

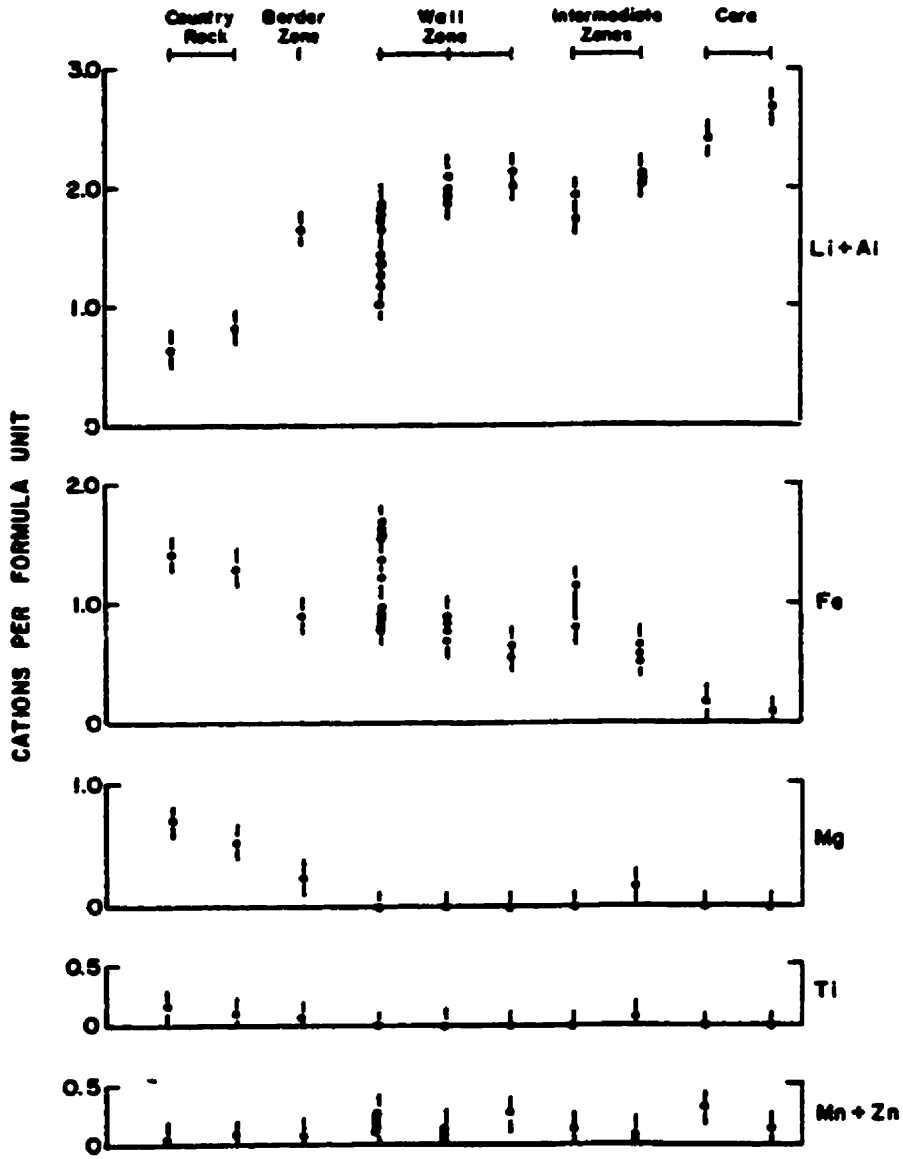

Figure 2.9. General compositional variations of the Y-site cations in tourmaline of the Bob Ingersoll No. 1 dike. Data points represent averages of multiple microprobe analyses (Jolliff *et al.* 1986).

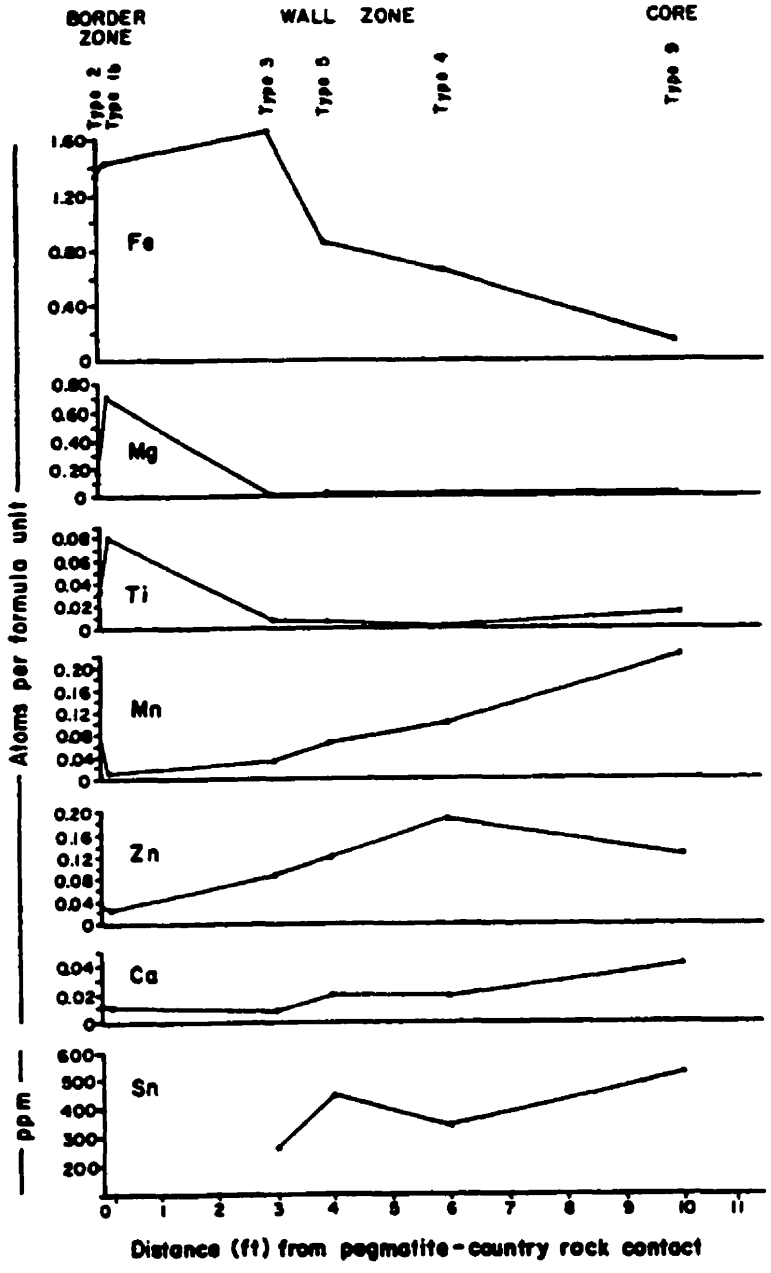

Figure 2.10. Compositional variation with respect to distance from country-rock contact. Representative samples from west-central part of Bob Ingersoll No. 1 dike as follows type 1b, country-rock inclusion (a); type 2, border zone (b); type 3, wall zone, coarse; type 5, wall zone, intergrown with muscovite; type 4, wall zone, fine E1b; type 9, core (First and second intermediate zones absent in this area; third intermediate zone is thin and contains no tourmaline (Jolliff *et al.* 1986).

Tourmaline composition, texture and habit may be used to interpret crystallization processes. There are three factors that affect the compositional variation of tourmaline:

(1) the bulk composition of the pegmatite melt-fluid system during fractional crystallization;

(2) the crystallization process and medium (i.e., metasomatism, crystallization from a silicate melt and crystallization from a silicate melt in the presence of an exsolving aqueous fluid). A mobile exsolving fluid differentially scavenges elements from the initial melt and enriches the residual melt;

(3) the crystal-chemical preferences of the tourmaline structure in response to changing pressure and temperature conditions.

These compositional trends in tourmaline may be used to indicate the fractionation trends and relative degree of evolution of the host pegmatite (Fig. 2.11a). Zoned pegmatites crystallize from the border zone inward to the core. The trend from relatively Mg-rich tourmaline (dravite) in early granitic rocks to Fe-rich tourmaline (schorl) in late differentiates is caused by magmatic differentiation (Manning 1982; Power 1968). Another major trend of decreasing dravite and schorl components and a corresponding increase in elbaite component indicates an increasing degree of fractionation or evolution (Jolliff *et al.* 1986). The compositional trends of the *Y*-site cations can be examined in a ternary plot of dravite-schorl-elbaite (Fig. 2.11b) or Al-Fe(tot)-Mg (Fig. 1.17).

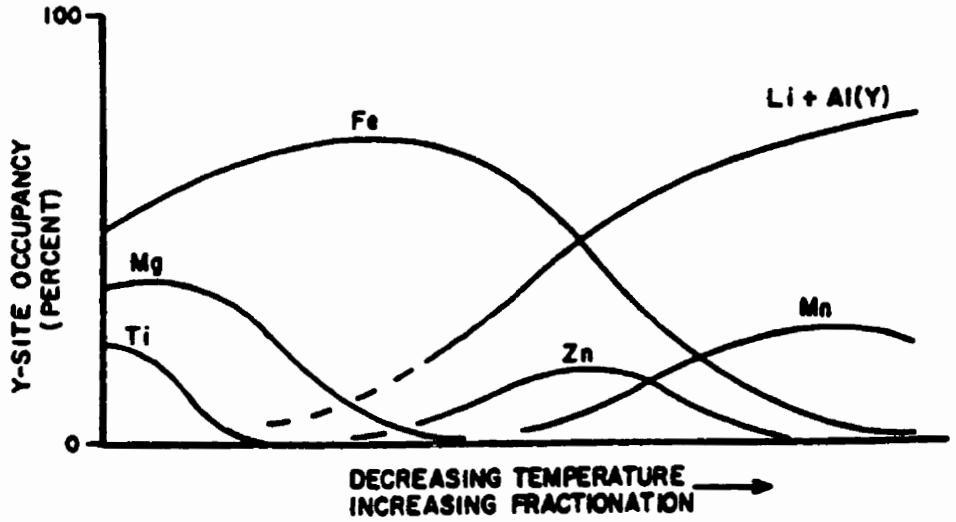

Figure 2.11a. Schematic illustration of ideal covariation of Y-site cations of tourmaline in response to decreasing temperature and increasing fractionation of melt (Jolliff *et al.* 1986).

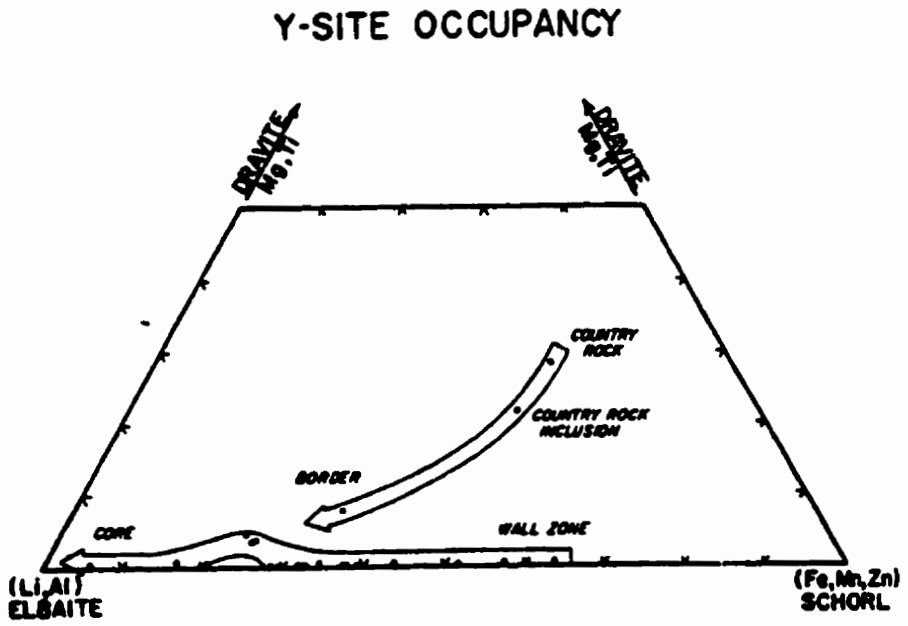

Figure 2.11b. End-member compositions of the Bob Ingersoll tourmaline plotted in terms of schorl (Fe + Mn + Zn), dravite (Mg + Ti), and elbaite (Li + Al) (Jolliff *et al.* 1986).

2.8. Interpretation of the physical properties of tourmaline in pegmatites

The colour of tourmaline reflects its composition. In the country rock, tourmaline is dark brown to black dravite-schorl; in the border and wall zones, tourmaline is black schorl; in the intermediate zone, tourmaline is green, pink, blue and colourless elbaite (Jolliff *et al.* 1986).

Compositional variations in individual zoned tourmaline crystals reflect compositional trends within the pegmatite. One common cause for compositional zoning is rapid crystal-growth during which the rate of crystallization is faster than the rate of diffusion in the melt (Jolliff *et al.* 1986). Zoning may also result from a change in the rate of crystallization. Other common causes of zoning are a change in water pressure, temperature or composition of the crystallizing melt during crystallization. A change in temperature due to rapid loss of volatiles from the melt (*i.e.*, pocket rupture) would provide an efficient removal of latent heat of crystallization and possibly a local pressure drop, causing rapid disequilibrium crystallization (Jolliff *et al.* 1986). The changing composition of the pegmatite melt-fluid system with progressive crystallization is closely related to the stability of a specific tourmaline composition at specific temperature-pressure conditions. Of the major Y cations, Mg would be preferred at higher temperature, Fe at intermediate and Li at lower temperatures. Crystal chemistry (e.g., charge balance and ionic radius) also controls compositional trends in tourmaline (Jolliff *et al.* 1986).

The texture of tourmaline crystals also reflects crystallization conditions. In the border zone, prismatic crystals may be fractured perpendicular to the *c*-axis and the

fractures are filled with fine-grained matrix minerals (Jolliff *et al.* 1986); this indicates that tourmaline crystallized before the fine-grained matrix minerals. In the wall zone, tourmaline may be oriented with its *c*-axis perpendicular to the outer contact of the pegmatite, giving rise to comb structure (Fig. 2.8a). The tourmaline prisms are tapered toward the country-rock/pegmatite contact and splayed toward the interior of the pegmatite (Fig. 1.15). The tapered end (closer to the contact) has high Fe content and the splayed end (closer to the interior of the pegmatite) has low Fe content (Jolliff *et al.* 1986). In the wall zone, tourmaline crystals are strongly zoned concentrically about the *c*-axis; however, they are not significantly zoned along their length.

Tourmaline crystals in the outermost zones of pegmatites are commonly skeletal with quartz cores, or occur as graphic intergrowths of schorl plus quartz (London *et al.* 1996; Jolliff *et al.* 1986). The conditions favouring skeletal crystal growth are (1) a high degree of supersaturation of the growth medium, (2) high crystal-growth rate, (3) low diffusion rate, (4) heterogeneous nucleation of crystals from a pegmatite fluid (Manning 1982). High crystal-growth rate and the high diffusion rate are caused by the low viscosity of pegmatitic fluids as compared with a silicate melt (Manning 1982). The skeletal crystals were probably formed by early heterogeneous nucleation and rapid crystal growth of euhedral tourmaline, followed by crystallization of quartz which filled in the open end of the tapered tourmaline crystals (Jolliff *et al.* 1986; Manning 1982).

In the innermost zones of pegmatites, disseminated tourmaline occurs as isolated prisms or interstitial grains. The tourmaline ranges in habit from euhedral (early crystallization) to anhedral and interstitial (late crystallization), and lacks fine-scale

compositional zoning (London *et al.* 1996).

In miarolitic cavities or pockets, elbaite is commonly zoned optically and chemically parallel to, or perpendicular to, the *c*-axis. Tourmaline projects from the massive pegmatite into the cavities, if present, and represents a continuity from magmatic to hydrothermal crystallization in pegmatites (London *et al.* 1996).

CHAPTER 3

Experimental Methods

3.1. Sample preparation for electron-microprobe analysis

Tourmaline samples were selected to represent each pegmatite zone. Euhedral tourmaline crystals > 0.5 cm were cut perpendicular to the *c*-axis to examine core-to-rim zoning. Tourmaline crystals were put into probe mounts or ring mounts for microprobe analysis. Back-scattered electron (BSE) images of tourmaline crystals that were optically zoned were taken using a Kontron IBAS image-analysis system attached to either a CAMECA SX-50 electron microprobe or a Cambridge Stereoscan 120 scanning electron microscope. The most important advantage of the SEM over the electron microprobe for image analysis is that the lowest magnification of the SEM is 14x, whereas the lowest magnification of the microprobe is 62x. The low magnification allows grains 1 cm in diameter to be photographed in one picture rather than several pictures.

The BSE images were used as maps when selecting points for analysis. For zoned tourmaline grains, each BSE zone in a tourmaline grain was analyzed three times. For homogeneous tourmaline grains, the rim, core and opposite rim were analyzed.

3.2. Electron-microprobe analysis

Electron-microprobe analysis was done at the University of Manitoba on a CAMECA SX-50 instrument in wavelength-dispersive mode. The beam voltage for all elements was 15 kV and the spot diameter was 1 μm. The majority of the data were collected with a beam current of 20 nA for Na, Fe, Ca, Al, Si and Mg, and 30 nA for F,

Mn, Zn, K, Ti and P. Counting times for peak and background determinations for all elements were 20 and 10 s, respectively. Near the end of the life of the filament, a current of 30 nA could not be regulated, so the trace elements (F, Mn, Zn, K, Ti and P) were analyzed with a beam current of 20 nA and peak counting times of 40 s. The increased counting time compensates for the lower beam current. The compositions resulting from both sets of conditions are approximately equal. The standards and detection limits for wt% oxides are listed in Table 3.1.

Table 3.1. TOURMALINE ANALYSIS BY ELECTRON MICROPROBE

standard	element, line, crystal	oxide	beam current (nA)/ peak time	detection limit (wt%)	beam current (nA)/ peak time	detection limit (wt%)
apatite	P, K_α, PET	P_2O_5	20 / 40	0.067	30 / 20	0.073
diopside	Si, K_α, PET	SiO_2	20 / 20	0.085	-	-
titanite	Ti, K_α, PET	TiO_2	20 / 40	0.044	30 / 20	0.050
kyanite	Al, K_α, TAP	Al_2O_3	20 / 20	0.038	-	-
olivine	Mg, K_α, TAP	MgO	20 / 20	0.005	-	-
diopside	Ca, K_α, PET	CaO	20 / 20	0.042	-	-
spessartine	Mn, K_α, LiF	MnO	20 / 20	0.083	-	-
fayalite	Fe, K_α, LiF	FeO	20 / 20	0.103	-	-
gahnite	Zn, K_α, LiF	ZnO	20 / 40	0.132	30 / 20	0.148
albite	Na, K_α, TAP	Na_2O	20 / 20	0.037	-	-
orthoclase	K, K_α, PET	K_2O	20 / 20	0.027	-	-
fluor-riebeckite	F, K_α, TAP	F	20 / 40	0.154	30 / 20	0.141

Detection limits are calculated using: L.D. = $[3(\text{wt\%oxide})(R_b/t_b)^{1/2}] / (R_p-R_b)$ where R_b = background count rate (counts/s), t_b = background count time (s), R_p = peak count rate (counts/s).

The analytical data were reduced using the φ(ρz) method (Pouchou & Pichoir 1984, 1985). Diopside, kyanite, fayalite, albite, olivine and spessartine standards were each analyzed twice at the beginning of a run, followed by analysis of approximately 40 unknowns, and two determinations of each standard. This sequence was repeated and the run ended with analysis of the standards. The K-values (intensity of unknown/intensity of standard) for the specific element for each of the standards (e.g., the K-value of Al in kyanite) were averaged over the entire run. The ideal K-value is 1.0. If the average K-value for each element was <0.99 or >1.01, the data for the entire run were corrected to a K-value of 1.0 for that particular element.

3.3. Structural-formula calculation

Structural formulae were calculated on the basis of 31 anions, assuming stoichiometric amounts of H_2O as $(OH)^-$ (*i.e.*, OH + F = 4 *apfu*), B_2O_3 [as (BO_3)], and Li_2O (as Li) (MacDonald *et al.* 1993, Burns *et al.* 1994). All Mn and Fe were assumed to be divalent (Burns *et al.* 1994). Crystal-structure refinement and bond-valence calculations indicate that B=3 *apfu* in all tourmalines structurally analyzed to date (Hawthorne 1996).

In the absence of an H_2O analysis, OH+F is assumed to be equal to 4 *apfu*. If the tourmaline contained significant amounts of O^{2-} substitution for OH, (*i.e.*, OH + F < 4.0 *apfu*) then the number of all cations, including Si and Li, would be underestimated (Taylor *et al.* 1995, Henry & Dutrow 1996). The tourmaline compositions have close to 6.0 *apfu* Si, so the assumption of OH + F = 4 *apfu* seems reasonable.

Lithium is assumed to be present, as structural-formula calculation for a Li-free composition produces vacancies at the *Y*-site, and the pegmatites discussed in this thesis are rich in Li. The amount of Li assigned to the *Y*-site is taken to be equal to the ideal sum of the *T* + *Z* + *Y*-sites minus the amount of other cations occupying those sites [Li = 15 - (Si + Al + Ti + Mg + Fe + Mn)], and the calculation was iterated to self-consistency (Burns *et al.* 1994). Standards were analyzed and K-values were corrected before and after 40 analyses of tourmaline to minimize errors in the analyzed elements which may affect the Li calculation. Lithium values are best estimates; they not plotted directly in the figures and are not used to name the tourmaline. The dominance of Al at the *Y*-site is used to indicate that the tourmaline is elbaite.

3.4. Tourmaline nomenclature

In order to describe the tourmaline composition in more detail, a combination of end-member names and adjectives is used following the method of Selway & Novák (1997) and Selway *et al.* (1999).

(i) Usually, the tourmaline is named according to the dominant end-member.

(ii) If the ratio of two end-members, within an individual tourmaline composition, is between 4:6 and 6:4 *apfu* (i.e., the composition is close to the 50:50 dividing line), both end-member names are used (e.g., schorl-dravite) with the first name designating the dominant component.

(iii) If an element (A) occupies 20 - 40 % of the *X* or *Y*-site, the adjective A-rich is used (e.g., Ca-rich dravite and Fe-rich dravite).

(iv) If an element (A) occupies 10 - 20 % of the *X* or *Y*-site, the adjective A-bearing is used (e.g., Ca-bearing schorl and Mg-bearing schorl).

3.5. X-ray crystallography

The crystal structure of rossmanite was determined using powder diffraction and single-crystal structure refinement (Selway *et al.* 1998a).

Powder diffraction

Powder-diffraction data for bulk samples were recorded on a Philips PW 1710 diffractometer with graphite-monochromatized Cu K_α X-radiation. Peak positions were measured by fitting a five-point parabolic curve to the top of the diffraction peaks, followed by correction for α_1-α_2 splitting; NBS Si was used as a standard. Cell dimensions were refined from the corrected *d*-values using the program CELREF (Appleman & Evans 1973).

Single-crystal diffraction

A fragment of rossmanite was ground to a sphere and mounted on a Nicolet *R*3*m* four-circle diffractometer. Twenty-five reflections over the range $6 < 2\theta < 28°$ were centered using graphite-monochromated Mo Kα X-radiation. The cell dimensions were derived from the setting angles of the automatically aligned reflections by least-squares refinement. Data were collected using the θ-2θ scan-method with a scan range of 2.1 °. A variable scan-rate inversely proportional to the peak intensity was used, with maximum

and minimum scan-rates of 29.3°/min and 4.0°/min, respectively. A total of 1135 reflections was measured over the range $4° \leq 2\theta \leq 60°$, with index ranges $0 \leq h \leq 23$, $0 \leq k \leq 23$ and $-10 \leq l \leq 10$. Two standard reflections were measured every eighty reflections; there was no significant change in their intensities during data collection. A psi-scan absorption-correction based on 36 psi-scans of each 11 reflections over a range $10 \leq 2\theta \leq 60°$ was applied, with the crystal modelled as an ellipsoid. The absorption correction reduced R(azimuthal) from 1.18 to 1.09%. The data were merged and corrected for Lorentz and polarization effects, and background. Structure refinement was initiated with the atom coordinates of foitite (MacDonald *et al.* 1993), and rapidly converged to an R index of ~1.8% for an anisotropic-displacement model. The crystal used in the collection of the X-ray intensity data was subsequently analyzed by electron microprobe techniques (see above), and the most appropriate X-ray scattering factors were used at the final stages of refinement, which converged to an R index of 1.7% for 1094 observed (5σ) reflections.

3.6. Determination of specific gravity

The specific gravity of rossmanite was determined using heavy liquids and a pycnometer bottle (Selway *et al.* 1998a).

The best method to determine the specific gravity of small grains (1-2 mm in diameter) is to use heavy liquids and a pycnometer. Specific gravity (SG) is defined as the ratio of the mass of a substance (e.g., a mineral or a heavy liquid) to the mass of an equal volume of water at 4 °C. Density (D) is defined as the mass of a unit of volume of a

substance, usually as g/cm^3. If the unit-cell dimensions and composition of the mineral are known, then the density can be calculated:

D = (Z*molecular weight) / (Avogadro's number * volume of unit cell Å * 10^{-24})

where Z = the number of formula units in a unit cell; the molecular weight is measured in grams; and volume of the unit cell * 10^{-24} converts Å to cm^3. The specific gravity is usually measured to confirm the calculated density; ideally, they should be equal.

First, one chooses a heavy liquid whose specific gravity is slightly higher than that of the mineral. Three heavy liquids are commonly used: Clerici solution, methylene iodide and bromoform.

liquid	specific gravity at	diluent
Clerici solution	4.280	water
methylene iodide (CH_2I_2)	3.325	*n*-butyl alcohol or acetone
bromoform ($CHBr_3$)	2.890	*n*-butyl alcohol or acetone
water at 4 °C	1.000	
n-butyl alcohol (C_4H_9OH)	0.810	
acetone (CH_3COCH_3)	0.790	

The two organic heavy liquids, methylene iodide and bromoform, are light-sensitive, and the break-down products produce a marked discoloration. All of these heavy liquids are toxic, so the experiment should be done in a fume hood. *n*-Butyl alcohol is a preferable diluent to acetone because of a much lower vapour pressure and hence a slower rate of evaporation.

Sodium polytungstate ($3Na_2WO_4 \cdot 9WO_3 \cdot H_2O$; S.G. 2.89) with water as a diluent is

preferable to the above heavy liquids, as it is non-toxic.

The empty pycnometer with capillary stopper is weighed to 0.000X g (W1). Then the pycnometer is filled with distilled water and the stopper inserted. The water should reach the top of the capillary tube and any overflow should be carefully removed. The pycnometer with water should be weighed as fast as possible to reduce evaporation of water from the capillary tube (W2). The weight of the water will be (W2-W1) in g, which is equal to the volume of the water in the pycnometer bottle in ml.

The mineral grain to be used in this experiment should be homogeneous and without inclusions of other minerals. Two homogeneous tourmaline grains were put into a 50 ml Erlenmeyer flask (a cylinder can also be used) with about 30 ml of methylene iodide. As it was difficult to see the small colourless mineral grains in the heavy liquid, a light was shone through the liquid from behind, making the grains clearly visible. The heavy liquid should have a higher specific gravity than the tourmaline grains, so they will float to the top of the liquid. Acetone was added (using a pipet) to dilute the methylene iodide. The flask was covered with a watch glass and the two liquids were thoroughly mixed using a vigorous circular motion. This was repeated until the tourmaline grains neither floated or sank; the SG of the heavy liquid is then equal to that of the tourmaline grains.

After hydrostatic balance was achieved, the tourmaline grains were removed from the heavy liquid and put in a breaker of acetone to clean them. The heavy liquid was poured into the empty pycnometer bottle using a tiny funnel until it reached the bottle's neck. Additional heavy liquid was added using the pipet until it reached half-way up the

bottle neck and then the stopper was inserted. The heavy liquid should just reach the top of the capillary tube. The pycnometer with heavy liquid was then weighed (W3) as fast as possible to minimize the effect of evaporation of the volatile acetone.

The specific gravity of the heavy liquid and hence of the tourmaline grains was then calculated as SG = (W3-W1) / (W2-W1) where W1 = weight of empty pycnometer; W2 = weight of pycnometer and water; (W2-W1) = weight of water = volume of water; W3 = weight of pycnometer, methylene iodide and acetone; (W3-W1) = weight of heavy liquid = weight of tourmaline grains.

3.7. Proton-induced x-ray-emission analysis

The trace-element contents of tourmaline from Tanco were analyzed for 23 elements with atomic number ≥ 26 (Fe) using proton-induced X-ray emission (PIXE) at the University of Guelph Van de Graaff accelerator facility. A 5 x 5 μm 3 MeV proton beam was used, with a range in beam-current of 4.598-6.289 nA and an average of 5.517 nA; counting time ranged from 318-435 s. The resulting X-ray spectra were recorded with a Si(Li) detector. The time-integrated charge for each analysis was 2 μC. A 0.125 mm mylar filter was used to suppress low-energy background radiation. Spectra were processed using the Guelph PIXE software package GUPIX (Maxwell *et al.* 1989). Elemental concentrations are derived from the intensities of various X-ray peaks through established mathematical and physical relations involving X-ray generation and associated matrix effects (including secondary fluorescence); this approach (Campbell *et al.* 1990) resembles the better-known methodology of electron-probe microanalysis.

Backscattered- electron images were used to correlate microprobe-analyzed spots and PIXE-analyzed spots. Only Ga, Ge, Sr and rare Pb and Nb were above the limit of detection (LOD) in tourmaline from Tanco: Ga 4.0, Ge 2.8, Sr 2.4, Pb 8.3 and Nb 3.2 ppm LOD.

CHAPTER 4

Tourmaline in lepidolite-subtype pegmatites

4.1. Lepidolite-subtype pegmatites

Lepidolite-subtype pegmatites are defined as pegmatites with lepidolite as the dominant Li-bearing mineral (Černy 1991a). They are commonly zoned and consist of, from outermost to innermost zone: (1) granitic zone, (2) graphic zone, (3) blocky K-feldspar, (4) albite, (5) lepidolite zones, (6) quartz core and (7) rare-to-absent small pockets (miarolitic cavities). In the lepidolite zone, lepidolite (trilithionite to polylithionite) is dominant, elbaite is commonly subordinate to accessory, and petalite and amblygonite-montebrasite are rare (Němec 1981; Černy *et al.* 1995; Novák & Povondra 1995). Other typical minor-to-accessory minerals of the lepidolite zone include quartz, albite, K-feldspar, garnet (spessartine-almandine), beryl, cassiterite, manganocolumbite, stibiotantalite, manganotantalite, apatite, zircon, microlite and topaz (Novák & Povondra 1995). Examples of lepidolite-subtype pegmatites which will be discussed in detail include Laštovičky, Dobrá Voda, Dolní Bory, Rožná and Radkovice pegmatites of the Czech Republic, and Red Cross Lake, Manitoba (Selway *et al.* 1998b). Previously, the tourmaline compositions from only two lepidolite-subtype pegmatites have been discussed in the literature: the Brown Derby (Staatz *et al.* 1955) and Stewart Lithia (Bloomfield 1997) pegmatites of the United States, but the lack of correlation with detailed paragenesis has prevented any general conclusions on tourmaline crystallization in this subtype.

4.2. The Laštovičky pegmatite

4.2.1. General geology

The Laštovičky pegmatite is a zoned lepidolite-subtype pegmatite located in the district of Žďár n. Sáz., 4.5 km north of the Dolní Bory pegmatite and 7 km NNW of the Dobrá Voda pegmatite, Czech Republic. Laštovičky, Dolní Bory and Dobrá Voda pegmatites have similar mineral assemblages and textures. Laštovičky is 1 m thick and intrudes biotite-sillimanite gneiss. It consists of (i) granitic zone, (ii) graphic zone, (iii) coarse-grained albite, (iv) blocky K-feldspar zones and a (v) lepidolite core with (vi) pockets (M. Novák, pers. comm., Staněk 1973). The major minerals are K-feldspar = albite = quartz > muscovite > lepidolite, and the minor to accessory minerals are tourmaline, biotite, cookeite, apatite, topaz, cassiterite, manganocolumbite, stibiotantalite and tapiolite (M. Novák, pers. comm.). The graphic zone consists of graphic pink orthoclase + quartz. The inner coarse-grained albite zone consists of albite, quartz, abundant blue and green tourmaline, muscovite, and minor cassiterite and manganocolumbite. The blocky K-feldspar zone consists of pink or brown orthoclase and orange microcline. The pockets reach a maximum size of 20 by 15 by 10 cm and are lined with abundant smoky quartz, microcline, albite, pale pink-violet coarse-grained lepidolite rosettes (polytype 1M), pink tourmaline, Mn-bearing fluorapatite, stibiotantalite, tapiolite, and minor topaz and cookeite.

Tourmaline occurs in the coarse-grained albite zone and in the pockets of the lepidolite zone (Staněk 1973). The outer part of the coarse-grained albite zone contains black columnar tourmaline (5 cm long and 1 cm wide), and the inner part, adjacent to the

lepidolite zone, contains green and blue tourmaline associated with silver-white Li-poor muscovite. Blue tourmaline is the rarest tourmaline at Laštovičky; it occurs as 1-2 mm rounded grains or rarely as 2 mm long acicular crystals. Pale or dark green tourmaline occurs as parallel growths of needles or columns (1-4 cm long and up to 7 mm wide). Zoned tourmalines with blue cores and green rims occur in the inner coarse-grained albite zone. The pockets in the lepidolite zone contain pink fine-grained zoned euhedral columnar-to-fibrous tourmaline. It also forms divergently arranged needles up to 1 cm long and with a silky luster. Pink tourmaline is the most common colour in crystals 1-2 cm long and 1-3 mm wide. Pink-violet (Fe, Mg)-bearing lepidolite occurs in the lepidolite core, associated with pink tourmaline. Rare cookeite is an alteration product of lepidolite and is one of the last minerals to crystallize.

Staněk (1973) examined the optical properties of tourmaline from Laštovičky. Most varieties of tourmaline are pleochroic: black tourmaline is brownish green to pale rose, blue tourmaline is bluish green to pale rose, green tourmaline is pale green to colourless, and pink tourmaline is non-pleochroic colourless in plane-polarized light. The refractive indices and birefringence in tourmaline range from high in black tourmaline through blue and green tourmaline to low in pink tourmaline.

4.2.2. Composition of tourmaline from Laštovičky

Figure 4.1 shows the two dominant substitutions in these tourmalines: Na ⇔ □ at the *X*-site and Al ⇔ Fe at *Y*-site. Tourmaline compositions with Mg > 0.1 *apfu* are not plotted in this diagram. The ideal end-member compositions are shown as solid squares,

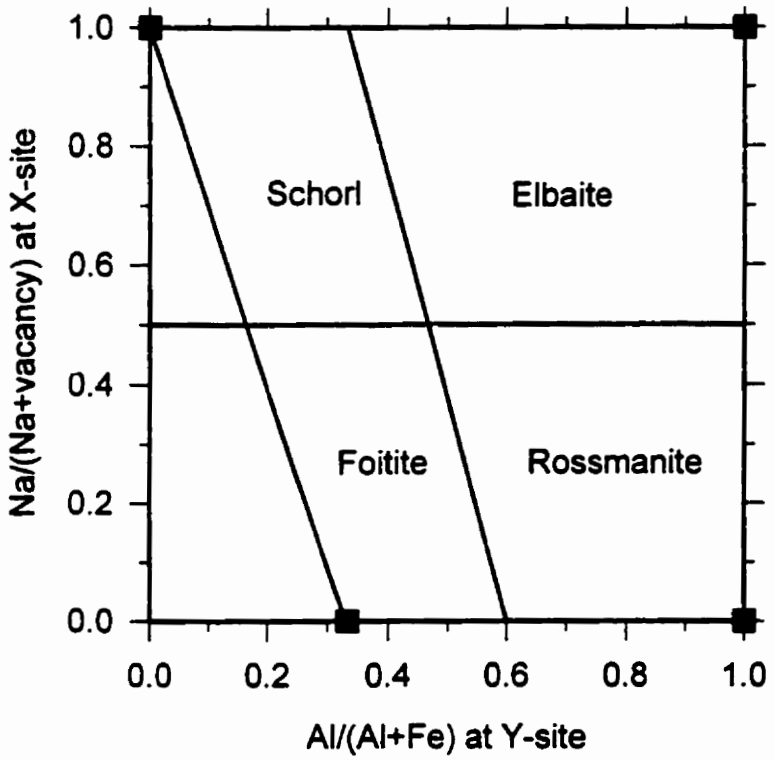

Figure 4.1. General Na/(Na+vacancy) at X-site vs. Al/(Al+Fe) at Y-site diagram; solid squares represent end-member compositions.

and the diagram can be divided into four compositional fields: foitite, schorl, elbaite and rossmanite. The border between foitite and schorl, and elbaite and rossmanite is defined as Na/(Na+□) = 0.50. The midpoint between end-member schorl ($Y = Fe_3$) and end-member elbaite ($Y = Al_{1.5}Li_{1.5}$) is defined as $Y = Fe_{1.5}Al_{0.75}Li_{0.75}$ for which Al/(Al+Fe) =

0.33; similarly, the midpoint between end-member foitite ($Y = Fe_2Al$) and end-member rossmanite ($Y = Al_2Li$) is $Y = FeAl_{1.5}Li_{0.5}$ for which Al/(Al+Fe) = 0.60. The slope of this border line is negative, as this diagram does not include variation in Li which is a significant component at the *Y*-site in elbaite and rossmanite, but not in schorl and foitite. Compositions to the left of the schorl-foitite line require $Ti^{4+} \rightleftharpoons Al^{3+}$ substitution at the *Y*-site or $Ca^{2+} \rightleftharpoons Na^{+}$ substitution at the *X*-site to maintain electroneutrality. Compositions to the left of the line may also indicate analytical problems, especially with Al.

The tourmaline composition at Laštovičky evolves following the crystallization sequence from the outermost to the innermost zone: schorl-foitite → elbaite-schorl → elbaite → elbaite-rossmanite → rossmanite-elbaite → elbaite-rossmanite (Fig. 4.2a, Table 4.1). Dark brown to black schorl-foitite occurs in the outer coarse-grained albite zone. Blue-green, green, pale-green and colourless elbaite-schorl, Fe-rich elbaite and elbaite occur in the inner coarse-grained albite zone. Pink elbaite-rossmanite and rossmanite-elbaite occur as needles and columns in pockets in the lepidolite zone. The columnar crystals consist of a pale-pink rossmanite-elbaite core, a colourless elbaite-rossmanite intermediate zone and a pink elbaite-rossmanite rim. This crystallization sequence results in a negative correlation between Fe and (Al+Li) at the *Y*-site (Fig. 4.3a). Tourmaline is enriched in Fe in the outer coarse-grained albite zone and enriched in (Al+Li) in the lepidolite zone.

There is a negative correlation between Fe and Mn as the composition evolves over the sequence schorl-foitite → elbaite-schorl → elbaite, with a maximum Mn content of 0.26 *apfu* for pale-green elbaite in the inner coarse-grained albite zone (Fig. 4.2b,

TABLE 4.1. REPRESENTATIVE COMPOSITIONS OF TOURMALINE (WT%) AT LAŠTOVIČKY

	1	2	3	4	5	6	7	8	9
SiO_2	34.80	34.80	34.99	36.70	36.30	37.40	37.40	38.24	38.37
TiO_2	0.36	0.55	0.00	0.00	0.04	0.00	0.00	0.00	0.00
B_2O_3*	10.26	10.31	10.29	10.62	10.68	10.84	10.82	11.00	11.32
Al_2O_3	33.90	34.10	34.04	36.70	38.20	38.40	38.90	41.60	44.01
MgO	0.51	1.23	0.04	0.01	0.00	0.00	0.00	0.03	0.00
CaO	0.08	0.10	0.00	0.08	0.00	0.00	0.00	0.15	0.00
MnO	0.19	0.10	0.25	0.75	0.88	1.30	1.92	0.24	0.00
FeO	13.80	12.40	14.80	6.17	4.20	3.54	1.84	0.24	0.00
ZnO	0.00	0.00	0.20	0.20	0.35	0.75	0.23	0.00	0.00
Li_2O*	0.26	0.33	0.23	1.44	1.56	1.56	1.71	1.90	1.86
Na_2O	1.53	1.67	1.75	2.63	2.75	2.44	2.32	1.73	1.38
K_2O	0.00	0.00	0.00	0.00	0.00	0.00	0.00	0.09	0.00
H_2O*	3.31	3.39	3.31	2.96	3.00	3.25	3.13	3.53	3.80
F	0.48	0.35	0.51	1.48	1.45	1.03	1.28	0.46	0.23
O=F	-0.20	-0.15	-0.21	-0.62	-0.61	-0.43	-0.54	-0.19	-0.10
total	99.28	99.18	100.20	99.12	98.80	100.08	99.01	99.02	100.87
Formulae contents normalized to 31 anions									
T -Si	5.90	5.86	5.91	6.00	5.91	6.00	6.00	6.01	5.89
Al	0.10	0.14	0.09	0.00	0.09	0.00	0.00	0.00	0.11
B	3.00	3.00	3.00	3.00	3.00	3.00	3.00	2.99	3.00
Z -Al	6.00	6.00	6.00	6.00	6.00	6.00	6.00	6.00	6.00
Y -Al	0.66	0.64	0.68	1.08	1.24	1.25	1.36	1.71	1.85
Ti	0.05	0.07	0.00	0.00	0.01	0.00	0.00	0.00	0.00
Mg	0.13	0.31	0.01	0.00	0.00	0.00	0.00	0.01	0.00
Mn	0.03	0.01	0.04	0.10	0.12	0.18	0.26	0.03	0.00
Fe^{2+}	1.95	1.75	2.09	0.85	0.57	0.47	0.25	0.03	0.00
Zn	0.00	0.00	0.02	0.02	0.04	0.09	0.03	0.00	0.00
Li	0.18	0.22	0.16	0.95	1.02	1.01	1.10	1.20	1.15
$\sum Y$	3.00	3.00	3.00	3.00	3.00	3.00	3.00	2.98	3.00
X -Ca	0.02	0.02	0.00	0.01	0.00	0.00	0.00	0.03	0.00
Na	0.50	0.55	0.57	0.83	0.87	0.76	0.72	0.53	0.41
K	0.00	0.00	0.00	0.00	0.00	0.00	0.00	0.02	0.00
□	0.48	0.43	0.43	0.16	0.13	0.24	0.28	0.42	0.59
OH	3.74	3.81	3.73	3.23	3.25	3.48	3.35	3.70	3.89
F	0.26	0.19	0.27	0.77	0.75	0.52	0.65	0.23	0.11

*B_2O_3, Li_2O and H_2O calculated by stoichiometry; B = 3 *apfu*, Li = 15 - $\sum T + Z + Y$ and OH+F = 4 *apfu*.

(1) dark brown schorl-foitite from outer coarse-grained albite zone, sample LA1-2-3; (2) dark brown Mg-bearing schorl-foitite from outer albite zone, sample LA1-1-1; (3) black schorl-foitite from outer albite zone, sample 202; (4) blue-green elbaite-schorl from inner albite zone, sample LA4-1-1; (5) blue-green Fe-bearing elbaite from inner albite zone, sample LA3-2-3; (6) green-blue Fe-bearing elbaite from inner albite zone, sample LA3-2-2; (7) pale green elbaite from inner albite zone, sample LA3-2-1; (8) light pink elbaite-rossmanite from pockets, sample 5/75, B_2O_3, Li_2O and H_2O determined by wet chemistry (Povondra *et al.* 1985); (9) pink rossmanite-elbaite from pockets in lepidolite zone, sample 620.

Table 4.1, composition 7). This negative correlation is followed by a decrease in Mn in elbaite → elbaite-rossmanite → rossmanite-elbaite. In rossmanite-elbaite, Fe and Mn are below detection limits (Table 4.1, composition 9). The most primitive tourmaline is Fe-rich and (Mn, Al+Li)-poor (schorl-foitite) with increasing fractionation the Fe decreases and the Mn and Al+Li increases (elbaite) and the most fractionated tourmaline is (Al+Li)-rich and (Mn, Fe)-free (elbaite-rossmanite).

Figures 4.2c and 4.2d show a stong positive correlation between Na and F and a weak positive correlation between Mn and F in tourmaline: (1) The most primitive schorl-foitite compositions have low Na, Mn and F; (2) elbaite-schorl and Fe-rich elbaite have high Na, Mn and F contents ($\leq$ 0.87 *apfu* Na and $\leq$ 0.77 *apfu* F) (Table 4.1, composition 4 and 5). (3) Rossmanite-elbaite has low Na, Mn and F ($\leq$ 0.50 *apfu* Na, $\leq$ 0.03 *apfu* Mn and $\leq$ 0.31 *apfu* F). The overall positive correlation between Na, F and Mn is shown in Figure 4.3b.

Most tourmaline at Laštovičky contains no Mg or Ti, except for the most primitive schorl-foitite with $\leq$ 0.31 *apfu* Mg and 0.07 *apfu* Ti (Table 4.1, composition 2).

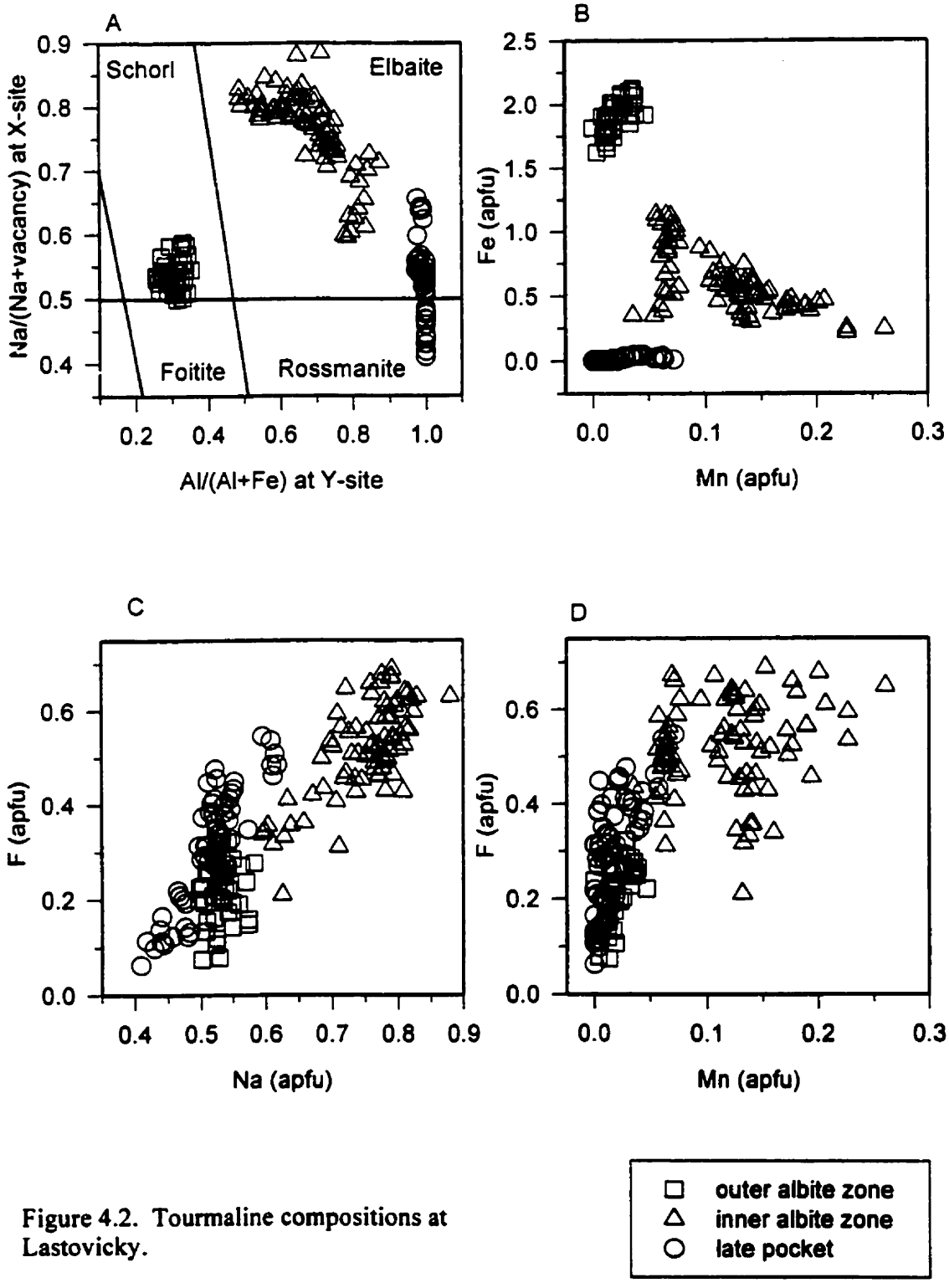

Figure 4.2. Tourmaline compositions at Lastovicky.

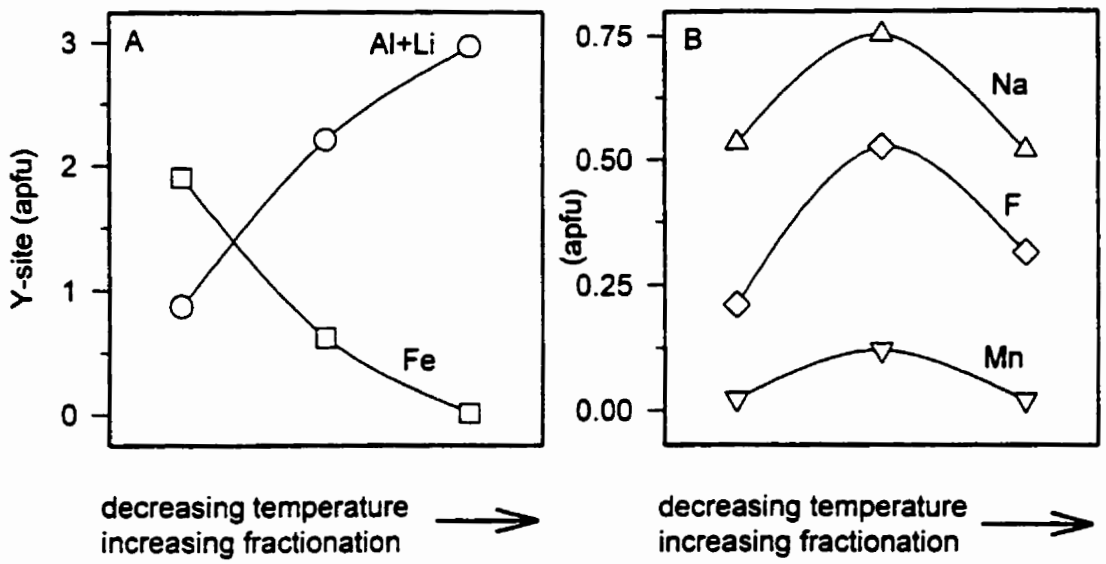

Figure 4.3. Idealized trends of tourmaline composition based on the average tourmaline composition for each pegmatite zone at Lastovicky.

Most tourmaline contains no Zn, except for Fe-bearing elbaite with ≤ 0.09 *apfu* Zn, and no Ca, except for the pink elbaite from the pockets with ≤ 0.06 *apfu* Ca.

4.3. The Dobrá Voda pegmatite

4.3.1. General geology

The Dobrá Voda pegmatite is a zoned, 100 m long and 7-8 m wide, lepidolite-subtype pegmatite which intrudes hornblende-biotite gneiss and amphibolite in the Czech Republic (Staněk 1963, 1965, Černý *et al.* 1995). From outermost to innermost zone, it

consists of (i) granitic aplite, (ii) medium-grained granitic zone, (iii) graphic zone, (iv) coarse-grained zone, (v) blocky K-feldspar zone, (vi) albitic zone and (vii) lepidolite zone with (viii) late pockets. The granitic aplite (i) contains abundant K-feldspar, plagioclase, quartz, black tourmaline, biotite > muscovite, and accessory dumortierite and andalusite. The medium-grained granitic zone (ii) consists of abundant K-feldspar, plagioclase, quartz and muscovite, and minor brownish-black biotite; graphic zone (iii) consists of graphic microcline + quartz, and minor biotite and albite. The coarse-grained zone (iv) consists of albite, quartz, black tourmaline and K-feldspar which encloses the blocky K-feldspar zone (v). The albitic zone (vi) consists of albite, quartz, black, green, blue and pink tourmaline, pale-greenish-yellow muscovite > purple lepidolite, columbite and cassiterite. The lepidolite zone (vii) occurs in the centre of the dyke and contains lepidolite, quartz, albite, pink and minor colourless tourmaline, topaz, zircon, cassiterite, manganotantalite, stibiotantalite, microlite and cesstibtantite. The lepidolite in the outer lepidolite zone is pale purple; in the inner lepidolite zone, it is pale pink and pale grey to greenish. The late pockets (viii) are commonly elongate or rarely equidimensional (M. Novák, pers. comm.). The equidimensional pockets, up to 10 cm in size, occur close to the contact with the lepidolite zone, and are lined with crystals of smoky quartz, pink tourmaline and lepidolite. The elongate fissure-like pockets, up to 20 cm long and 5 cm thick, occur within the lepidolite zone and are lined with quartz, albite, zoned pink, green, violet and black tourmaline, and late apatite and cookeite. The crystallization sequence of minerals in the pockets is albite, tourmaline, botryoidal crusts of cookeite and apatite (Staněk 1963, Černý *et al.* 1971).

Black tourmaline occurs as rounded aggregates with biotite > muscovite in the granitic aplite zone (i), and as columnar and graphic intergrowths in the coarse-grained zone (iv). Fine-grained (<1 cm long) needles of green and blue tourmaline associated with pale-greenish-yellow muscovite, and thin late-stage blue tourmaline rims on amblygonite occur in the albitic zone (vi). Pink tourmaline in zones (vi) and (vii) ranges from columns a few cm long to radiating needles. Pink tourmaline is associated with purple lepidolite in the inner albite zone (vi), pale-purple lepidolite in the outer lepidolite zone (vii), and pale-pink and pale-grey to greenish lepidolite in the inner lepidolite zone (vii). In late pockets, doubly terminated 5-15 mm-long zoned crystals of pink-to-colourless, pale-green and violet tourmaline are terminated by dark-violet to black tourmaline (Povondra *et al.* 1985, Novák & Taylor 1996). The crystallization sequence of minerals in the pockets is albite, tourmaline, and botryoidal crusts of cookeite and apatite (Staněk 1963, Černý *et al.* 1971).

4.3.2. Composition of tourmaline from Dobrá Voda

The tourmaline composition at Dobrá Voda follows the crystallization sequence from the outermost to the innermost zone: foitite-schorl → schorl-foitite → elbaite-schorl → elbaite-rossmanite → rossmanite-elbaite → elbaite-rossmanite → Fe-bearing elbaite → foitite (Fig. 4.4a, Table 4.2). Black foitite-schorl and schorl-foitite occur in the coarse-grained zone. Green and blue elbaite-schorl occurs in the outer albite zone, and pink elbaite-rossmanite and rossmanite-elbaite needles occur in the inner albite zone. Pink and minor colourless elbaite-rossmanite occur in the lepidolite zone and in early pockets. The

TABLE 4.2. REPRESENTATIVE COMPOSITIONS OF TOURMALINE (WT%) AT DOBRÁ VODA

	1	2	3	4	5	6	7	8	9	10
SiO_2	35.55	36.10	36.32	37.15	38.82	39.11	39.12	38.29	37.74	37.20
TiO_2	0.10	0.30	0.16	0.00	0.00	0.00	0.00	0.00	0.00	0.00
B_2O_3*	10.38	10.42	10.46	10.64	11.31	11.18	11.13	10.94	10.81	10.68
Al_2O_3	34.04	33.89	34.26	35.67	43.30	41.28	40.16	37.94	36.95	36.00
Fe_2O_3	0.00	1.31	0.00	0.00	0.00	0.00	0.00	0.00	0.00	0.00
MgO	0.17	0.41	0.12	0.00	0.00	0.00	0.00	0.00	0.00	0.00
CaO	0.05	0.20	0.00	0.08	0.00	0.00	0.06	0.53	0.47	0.00
MnO	0.35	0.28	0.22	0.29	0.00	0.15	0.79	1.55	1.96	0.58
FeO*	14.55	12.00	11.12	7.90	0.00	0.00	0.65	2.61	3.52	11.10
Li_2O*	0.27	0.16	1.00	1.54	1.94	2.26	2.26	2.10	1.93	0.77
Na_2O	1.58	1.67	2.43	2.61	1.45	1.72	1.93	2.41	2.57	1.25
K_2O	0.00	0.09	0.00	0.00	0.00	0.00	0.00	0.00	0.00	0.00
H_2O*	3.40	2.88	3.13	3.06	3.72	3.55	3.64	3.11	3.13	3.69
F	0.39	0.28	1.02	1.29	0.39	0.64	0.43	1.41	1.26	0.00
O=F	-0.16	-0.12	-0.43	-0.54	-0.16	-0.27	-0.18	-0.59	-0.53	0.00
total	100.67	99.87	99.81	99.69	100.77	99.62	99.99	100.30	99.81	101.27
Formulae contents normalized to 31 anions										
T -Si	5.95	6.08	6.03	6.07	5.96	6.08	6.11	6.08	6.07	6.05
Al	0.05	0.00	0.00	0.00	0.04	0.00	0.00	0.00	0.00	0.00
B	3.00	3.03	3.00	3.00	3.00	3.00	3.00	3.00	3.00	3.00
Z -Al	6.00	6.00	6.00	6.00	6.00	6.00	6.00	6.00	6.00	6.00
Y -Al	0.67	0.72	0.71	0.87	1.80	1.57	1.39	1.10	1.00	0.90
Ti	0.02	0.04	0.02	0.00	0.00	0.00	0.00	0.00	0.00	0.00
Mg	0.04	0.10	0.03	0.00	0.00	0.00	0.00	0.00	0.00	0.00
Mn	0.05	0.04	0.03	0.04	0.00	0.02	0.10	0.21	0.27	0.08
Fe^{2+}	2.04	1.69	1.54	1.08	0.00	0.00	0.09	0.35	0.47	1.51
Fe^{3+}	0.00	0.17	0.00	0.00	0.00	0.00	0.00	0.00	0.00	0.00
Li	0.18	0.11	0.67	1.01	1.20	1.41	1.42	1.34	1.26	0.51
$\sum Y$	3.00	2.87	3.00	3.00	3.00	3.00	3.00	3.00	3.00	3.00
X -Ca	0.01	0.04	0.00	0.01	0.00	0.00	0.01	0.09	0.08	0.00
Na	0.51	0.55	0.78	0.83	0.43	0.52	0.58	0.74	0.80	0.39
K	0.00	0.02	0.00	0.00	0.00	0.00	0.00	0.00	0.00	0.00
□	0.48	0.39	0.22	0.16	0.57	0.48	0.41	0.17	0.12	0.61
OH	3.79	3.23	3.46	3.33	3.81	3.69	3.79	3.29	3.36	4.00
F	0.21	0.15	0.54	0.67	0.19	0.31	0.21	0.71	0.64	0.00

*B_2O_3, Li_2O and H_2O calculated by stoichiometry; B = 3 *apfu*, Li = 15 - $\sum T + Z + Y$ and OH+F = 4 *apfu*. All Fe is assumed to be Fe^{2+}, except for (2).

(1) black schorl-foitite from coarse-grained zone, sample 1392; (2) black schorl-foitite from coarse-grained zone, sample 64, Fe_2O_3, B_2O_3, Li_2O and H_2O determined by wet chemistry (Povondra 1981); (3) black schorl-elbaite from coarse-grained zone, sample 1394; (4) blue elbaite-schorl which rims amblygonite from outer albite zone, sample 1503; (5) pink rossmanite-elbaite needles from inner albite zone, sample 1609; (6) pink elbaite-rossmanite from lepidolite zone, sample 1721; (7) pink elbaite-rossmanite from lepidolite zone, sample y664; (8) green Fe-bearing elbaite from late pockets, sample 1017; (9) green (Fe, Mn)-bearing elbaite from late pockets, sample 1015; (10) violet foitite terminations from late pockets, sample DV509.

sequence of crystallization of the zoned tourmaline in late pockets is as follows: pink-to-colourless elbaite-rossmanite, pale-green to violet Fe-bearing elbaite, and dark-violet to black foitite. The foitite terminations have up to 0.78 *apfu* vacancies at the *X*-site (Table 4.2, composition 10). They crystallized from late Fe-rich hydrothermal fluids and may represent the completion of the cycle of tourmaline at Dobrá Voda from foitite to elbaite to rossmanite to elbaite and back to foitite. This crystallization sequence results in an overall negative correlation between Fe and (Al+Li) at the *Y*-site (Figure 4.5a).

There is a negative correlation between Fe and Mn in tourmaline as the composition evolves over the sequence foitite-schorl → schorl-foitite → elbaite-schorl (Fig. 4.4b). Manganese and Fe are absent in elbaite-rossmanite and rossmanite-elbaite. The Fe-bearing elbaite in late pockets is enriched in Mn, with up to 0.30 *apfu* Mn (Table 4.2, composition 8 and 9), whereas late foitite terminations contain < 0.09 *apfu* Mn. The most primitive tourmaline is Fe-rich and (Mn, Al+Li)-poor (foitite-schorl) with increasing fractionation the Fe decreases and the Mn and Al+Li increases (elbaite-schorl), Fe and Mn decreases to nil and Al+Li increases (elbaite-rossmanite) and the most

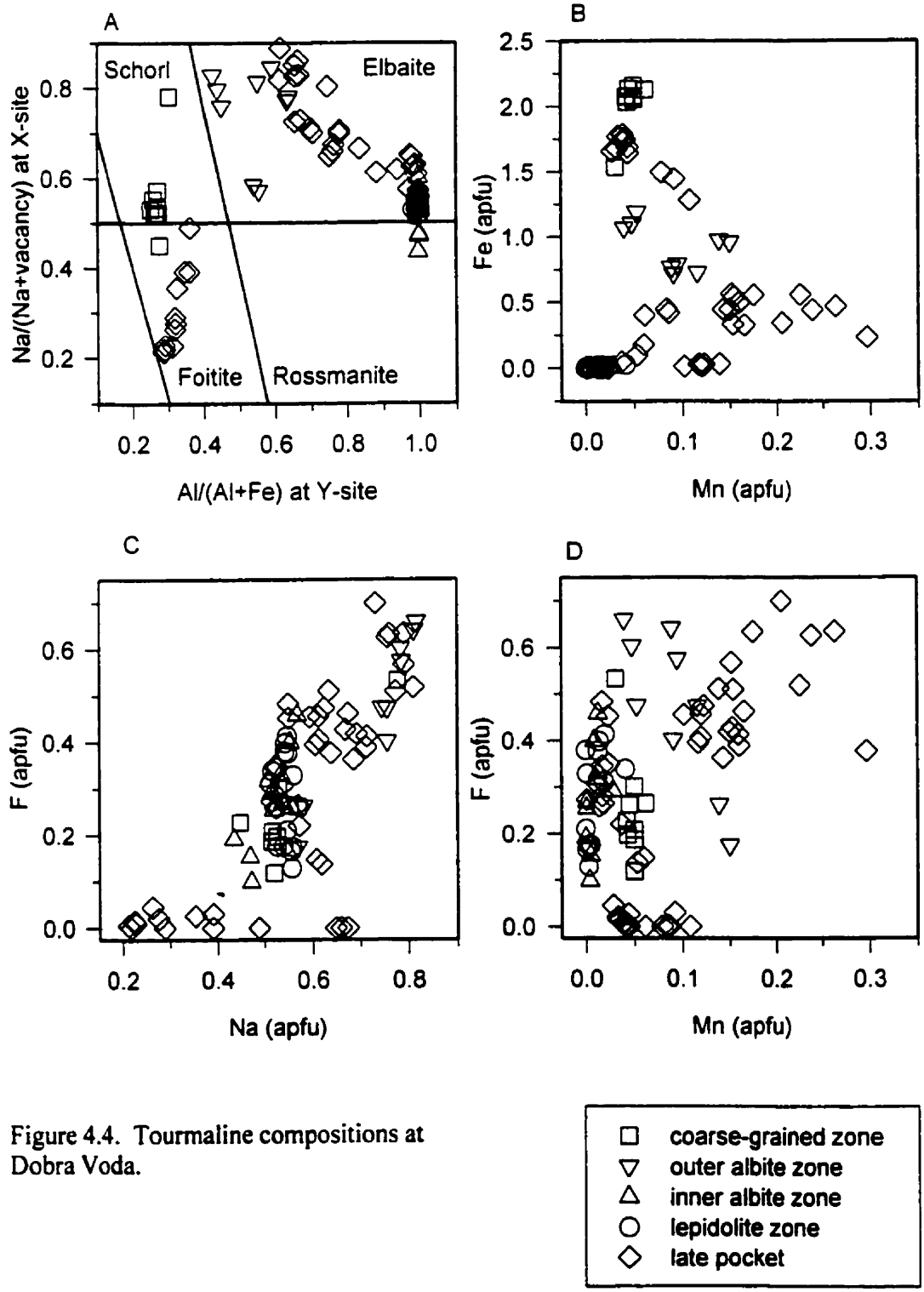

Figure 4.4. Tourmaline compositions at Dobra Voda.

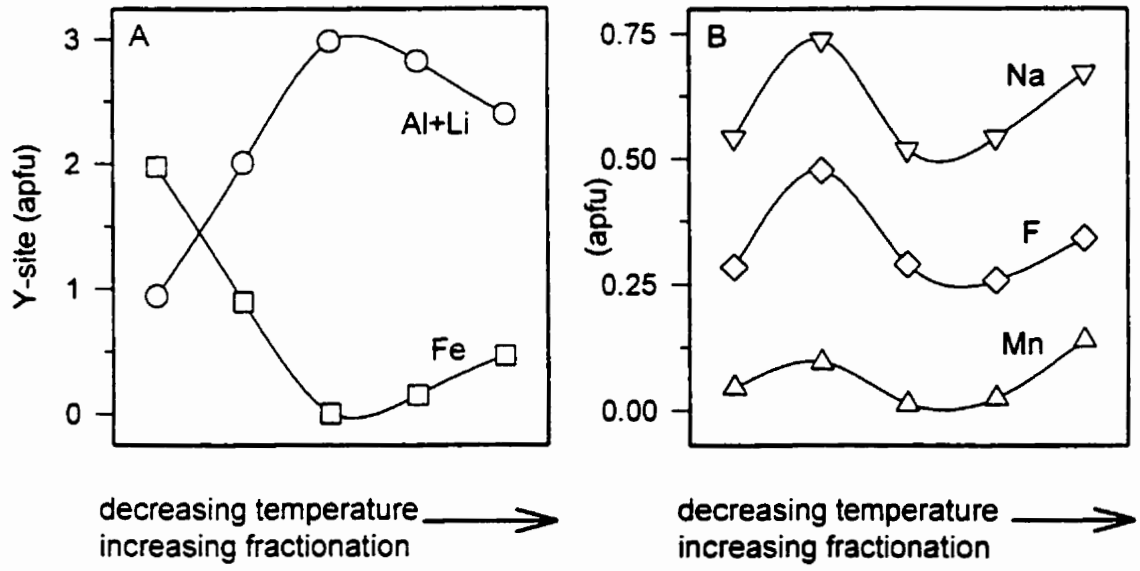

Figure 4.5. Idealized trends of tourmaline composition based on the average tourmaline composition for each pegmatite zone at Dobra Voda.

fractionated tourmaline is (Al+Li)-rich and (Mn, Fe)-poor (Fe-bearing elbaite). The last tourmaline to crystallize (foitite) is Fe-rich.

Figures 4.4c and 4.4d show a strong positive correlation between Na and F and weak positive correlation between Mn and F in tourmaline. The Na, Mn and F contents in tourmaline alternate between low and high: (1) the most primitive schorl-foitite compositions have low Na, Mn and F; (2) elbaite-schorl has high Na and F (≤ 0.83 *apfu* Na) (Table 4.2, composition 4) and moderate Mn; (3) elbaite-rossmanite has low Na, Mn and F; (4) Fe-bearing elbaite has high Na, Mn and F (≤ 0.71 *apfu* F) (Table 4.2,

composition 8); (5) late foitite has the lowest Na and F and low Mn. The overall positive correlation between Na, Mn and F is shown in Figure 4.5b.

Most tourmaline at Dobrá Voda contains no Mg, Ti or Zn, except for the most primitive black schorl-foitite with up to 0.10 *apfu* Mg and 0.04 *apfu* Ti from the coarse-grained zone (Table 4.2, composition 2). Most tourmaline contains no Ca, except for green Fe-bearing elbaite with up to 0.09 *apfu* Ca from late pockets (Table 4.2, composition 8).

4.3.3. Composition of micas from Dobrá Voda

Compositional variation in tourmaline is closely related to that of the micas at Dobrá Voda (Černý *et al.* 1971, 1995). The evolution of Fe and (Al+Li) in tourmaline and mica are similar (Figs. 4.6a,b,c). Biotite in the medium-grained granitic zone and schorl-foitite in the coarse-grained zone have high Fe content which decrease inward. Evolution of (Al+Li) is the inverse of the Fe trend; elbaite-rossmanite and lepidolite in the lepidolite zone have high (Al+Li) contents which decreases outward. In the late pockets, the presence of Fe-bearing elbaite and foitite reflects an increase in Fe, whereas the presence of cookeite reflects an increase in (Al+Li).

The evolution of Na in tourmaline and mica is similar (Fig. 4.6d). Sodium is preferentially partitioned into tourmaline relative to mica. Tourmaline and mica in the medium-grained granitic zone both have low Na which increases through the outer albite zone and then decreases in the lepidolite zone. There is an increase in Na in Fe-bearing elbaite, but not in cookeite, in the late pockets.

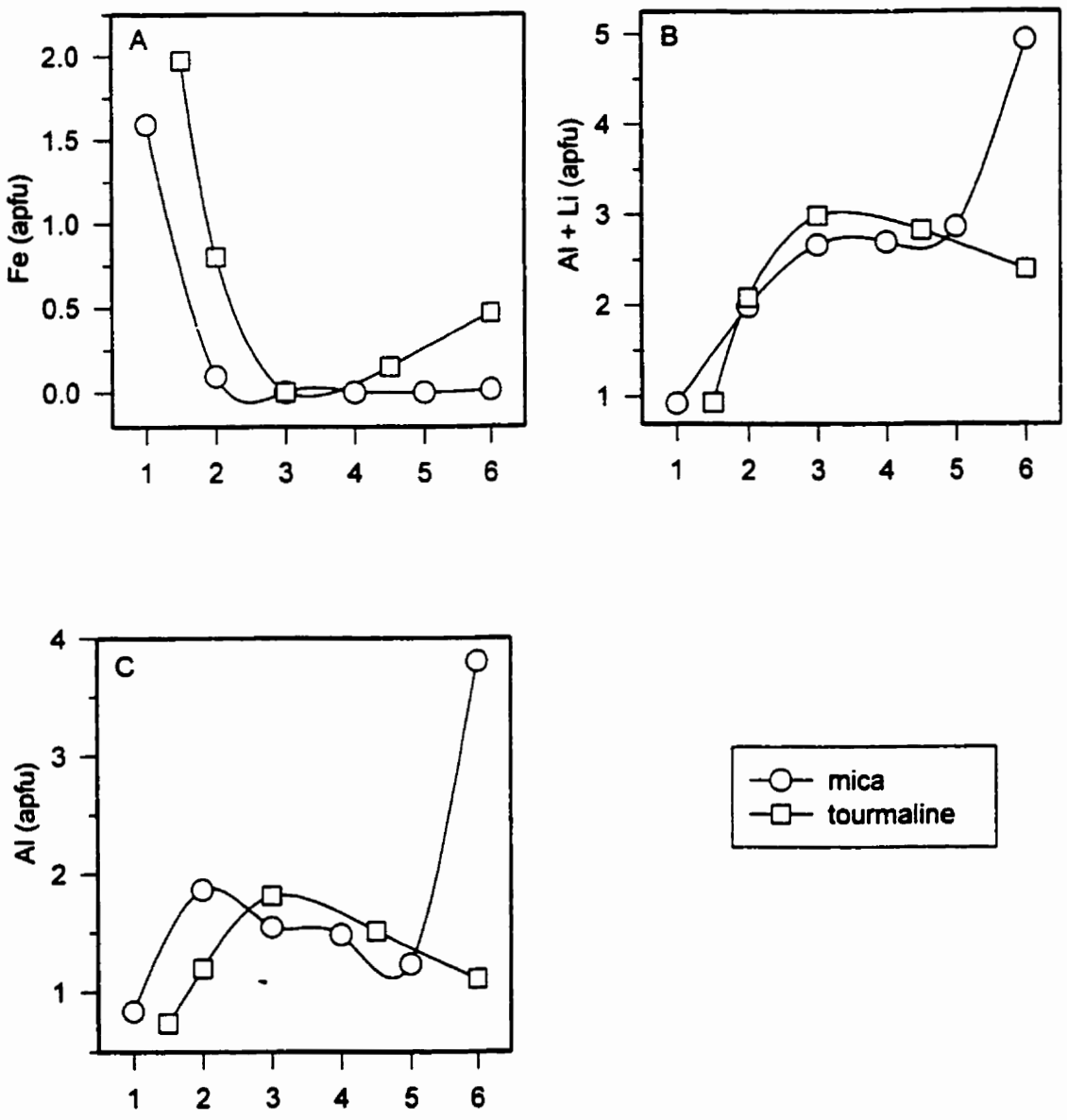

Figure 4.6. Comparison of tourmaline and mica element trends for selected pegmatite zones at Dobra Voda. Pegmatite zones: (1) medium-grained granitic zone with biotite, (1.5) coarse-grained zone, (2) outer albite zone with muscovite, (3) inner albite zone with lepidolite, (4) outer lepidolite zone, (4.5) lepidolite zone, (5) inner lepidolite zone and (6) late pockets with cookeite. Mica data is from Cerny et al. (1971, 1995).

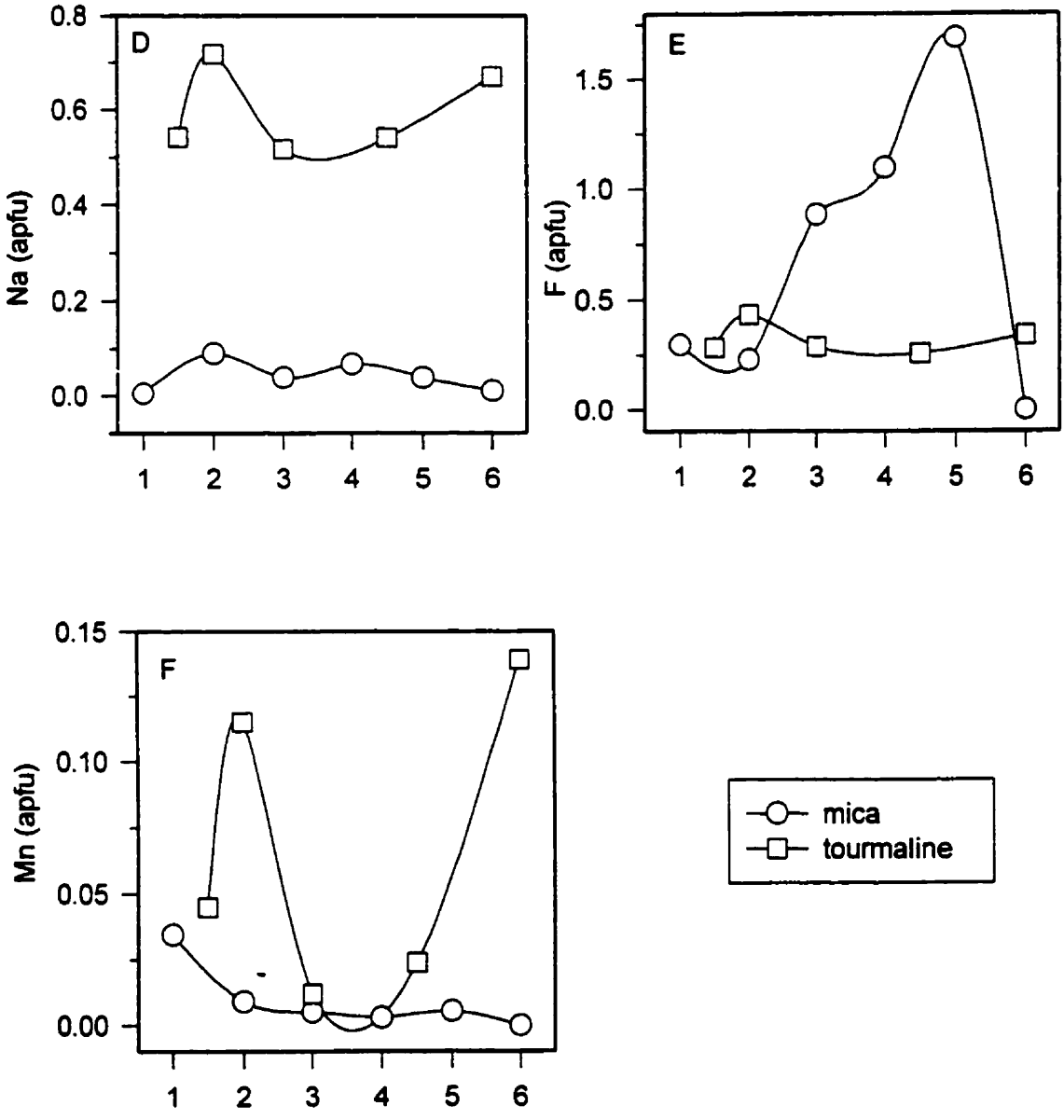

Figure 4.6. (continued)

The evolution of F in tourmaline and mica shows different trends (Fig. 4.6e). The F content of tourmaline has two maxima, whereas mica shows a gradual increase followed by a sharp decrease during crystallization in the late pockets. Fluorine-rich elbaite-schorl is associated with F-poor muscovite in the outer albite zones; F-poor rossmanite-elbaite is associated with F-rich lepidolite, and F-rich Fe-bearing elbaite is coated by F-free cookeite in late pockets. Fluorine is preferentially partitioned into lepidolite over elbaite-rossmanite and rossmanite-elbaite in the inner albite and lepidolite zones. Fluorine is low in biotite and muscovite, high in lepidolite and nil in cookeite, reflecting the positive correlation between F and Li in micas (Robert *et al.* 1993).

The evolution of Mn in tourmaline and mica shows different trends (Fig. 4.6f). Manganese is preferentially partitioned into tourmaline over mica. The Mn content of tourmaline shows the same trend as the Na content: Mn is high in biotite, and low in muscovite, lepidolite and cookeite.

4.4. The Dolní Bory pegmatite No.21

4.4.1 General geology

The Dolní Bory pegmatite dyke No. 21 is a zoned lepidolite-subtype pegmatite, 100 m long and 4 m thick, which intrudes leucocratic peraluminous biotite-, kyanite- and sillimanite-bearing granulite in the Czech Republic (Němec 1981, Staněk 1981a and b). It consists of (i) an outermost medium-grained aplite zone, (ii) coarse-grained granitic zone, (iii) blocky K-feldspar zone, (iv) albite zone, (v) lepidolite zone and (vi) late-stage pockets. The medium-grained aplite zone (i) contains abundant quartz (32.7 vol%),

perthitic microcline (45.3%), oligoclase (21.3%), minor biotite (0.7%) and accessory muscovite, black tourmaline, dumortierite, garnet (almandine-spessartine) and apatite. The coarse-grained granitic zone (ii) contains abundant graphic albite + quartz intergrowths and muscovite, and minor microcline and biotite. The blocky K-feldspar (iii) is up to 10 cm^3 in size and is graphically intergrown with quartz. The coarse-grained albite zone (iv) contains abundant albite, quartz, muscovite and black tourmaline, and minor microcline and green, blue and grey tourmaline (M. Novák pers. comm.). The lepidolite zone (v) contains abundant lepidolite, quartz, cleavelandite and pink tourmaline, minor pale-green tourmaline and amblygonite, and accessory topaz and cassiterite. The late-stage pockets (vi) contains abundant quartz, pink and green tourmaline, lepidolite and albite, and minor apatite and late cookeite coatings.

Tourmaline occurs in the albite zone, lepidolite zone and late-stage pockets (Němec 1981). The albite zone contains dominant black tourmaline and rare green, blue and grey tourmaline. Black tourmaline occurs as several-cm-long graphic intergrowths with quartz and as up to 10 cm-long isolated columnar crystals. Green tourmaline (<1 vol%) occurs as columns along the cleavage planes of muscovite. Blue tourmaline occurs as a late-stage replacement of amblygonite, and is similar to the blue tourmaline at Dobrá Voda. The lepidolite zone contains radiating pink needles of tourmaline with rare fine-grained muscovite inclusions in the core. Rare pink tourmaline with green rims or terminations, up to 1 cm thick, occurs in the lepidolite zone and late-stage pockets. The pockets also contain green tourmaline as isolated crystals that are coated with abundant cookeite.

4.4.2. Composition of tourmaline from Dolní Bory No. 21

Tourmaline composition at Dolní Bory evolves following the crystallization sequence from the outermost to the innermost zone: schorl-foitite → elbaite-schorl → elbaite → elbaite-rossmanite → (Fe, Mn)-bearing elbaite (Fig. 4.7a, Table 4.3). The albite zone contains black schorl-foitite, grey elbaite-schorl and green elbaite crystals, and blue elbaite-schorl rims around amblygonite (Table 4.3, compositions 2-5). Pink elbaite-rossmanite needles occur in the lepidolite zone (Table 4.3, composition 6). The lepidolite zone and late-stage pockets contain rare pink elbaite with green Fe-rich elbaite rims or terminations. The pockets also contain green Fe-bearing elbaite and pale-green (Fe, Mn)-bearing elbaite (Table 4.3, compositions 7-9). Figure 4.8a shows the overall negative correlation between Fe and (Al+Li).

There is a negative correlation between Fe and Mn as the tourmaline composition evolves from schorl-foitite → elbaite-schorl → elbaite which is followed by elbaite-rossmanite with no Fe or Mn and an increase in Fe and Mn in (Fe, Mn)-bearing elbaite in the pockets (Fig. 4.7b). The maximum content of 0.48 *apfu* Mn occurs in pale-green (Fe,Mn)-bearing elbaite in pockets (Table 4.3, composition 8). The most primitive tourmaline is Fe-rich and (Mn, Al+Li)-poor (schorl-foitite) with increasing fractionation, Fe and Mn decreases and Al+Li increases (elbaite-rossmanite) and the most fractionated tourmaline is (Al+Li)-rich with moderate Fe and Mn ((Fe, Mn)-bearing elbaite).

Figures 4.7c and 4.7d show a strong positive correlation between Na and F and a weak positive correlation between Mn and F in tourmaline: (1) The most primitive schorl-foitite compositions have low Na, Mn and F contents; (2) elbaite-schorl has high

TABLE 4.3. REPRESENTATIVE COMPOSITIONS OF TOURMALINE (WT%) AT DOLNÍ BORY

	1	2	3	4	5	6	7	8	9
SiO_2	35.35	34.82	36.14	36.68	38.15	38.18	38.64	37.85	37.60
TiO_2	0.60	0.12	0.00	0.08	0.00	0.00	0.00	0.00	0.00
B_2O_3*	10.48	10.23	10.42	10.60	10.95	11.18	11.02	10.79	10.75
Al_2O_3	34.23	33.63	34.61	35.96	39.34	42.76	39.21	36.60	36.81
Fe_2O_3	1.60	0.00	0.00	0.00	0.00	0.00	0.00	0.00	0.00
MgO	1.61	0.06	0.00	0.01	0.00	0.00	0.00	0.00	0.00
CaO	0.45	0.00	0.00	0.05	0.12	0.00	0.51	0.14	0.18
MnO	0.10	0.33	0.79	0.34	0.58	0.00	1.21	3.00	2.51
FeO*	10.94	15.32	10.52	8.09	2.12	0.00	0.60	2.83	2.84
ZnO	0.00	0.00	0.00	0.00	0.00	0.00	0.00	0.18	0.00
Li_2O*	0.01	0.15	0.92	1.34	2.01	1.96	2.32	1.91	1.93
Na_2O	1.75	1.56	2.20	2.66	2.20	1.71	2.14	2.70	2.76
K_2O	0.16	0.00	0.00	0.00	0.00	0.00	0.00	0.00	0.00
H_2O*	2.88	3.38	3.04	3.09	3.32	3.63	3.31	3.07	3.10
F	0.13	0.31	1.17	1.20	0.97	0.47	1.04	1.38	1.29
O=F	-0.05	-0.13	-0.49	-0.51	-0.41	-0.20	-0.44	-0.58	-0.54
total	100.24	99.78	99.32	99.59	99.35	99.69	99.56	99.87	99.23
Formulae contents normalized to 31 anions									
T -Si	5.93	5.91	6.03	6.01	6.05	5.94	6.09	6.10	6.08
Al	0.07	0.09	0.00	0.00	0.00	0.06	0.00	0.00	0.00
B	3.03	3.00	3.00	3.00	3.00	3.00	3.00	3.00	3.00
Z -Al	6.00	6.00	6.00	6.00	6.00	6.00	6.00	6.00	6.00
Y -Al	0.70	0.64	0.80	0.95	1.36	1.77	1.29	0.95	1.02
Ti	0.07	0.02	0.00	0.01	0.00	0.00	0.00	0.00	0.00
Mg	0.40	0.01	0.00	0.00	0.00	0.00	0.00	0.00	0.00
Zn	0.00	0.00	0.00	0.00	0.00	0.00	0.00	0.02	0.00
Mn	0.01	0.05	0.11	0.05	0.08	0.00	0.16	0.41	0.34
Fe^{2+}	1.54	2.18	1.47	1.11	0.28	0.00	0.08	0.38	0.38
Fe^{3+}	0.20	0.00	0.00	0.00	0.00	0.00	0.00	0.00	0.00
Li	0.01	0.10	0.62	0.88	1.28	1.23	1.47	1.24	1.26
$\sum Y$	2.93	3.00	3.00	3.00	3.00	3.00	3.00	3.00	3.00
X -Ca	0.08	0.00	0.00	0.01	0.02	0.00	0.09	0.02	0.03
Na	0.57	0.51	0.71	0.84	0.68	0.52	0.65	0.84	0.87
K	0.03	0.00	0.00	0.00	0.00	0.00	0.00	0.00	0.00
□	0.32	0.49	0.29	0.15	0.30	0.48	0.26	0.14	0.10
OH	3.22	3.83	3.38	3.38	3.51	3.77	3.48	3.30	3.34
F	0.07	0.17	0.62	0.62	0.49	0.23	0.52	0.70	0.66

*B_2O_3, Li_2O and H_2O calculated by stoichiometry; B = 3 *apfu*, Li = 15 - $\sum T + Z + Y$ and OH+F = 4 *apfu*. All Fe is assumed to be Fe^{2+}, except for (1).

(1) black Mg-bearing schorl from medium-grained aplite zone, sample 55, Fe_2O_3, B_2O_3, Li_2O and H_2O determined by wet chemistry (Povondra 1981); (2) black schorl-foitite from albite zone, sample 8047; (3) blue elbaite-schorl rims amblygonite from albite zone, sample 9058; (4) grey elbaite-schorl from albite zone, sample 8051; (5) green elbaite from albite zone, sample 8055; (6) pink elbaite-rossmanite from lepidolite zone, sample 1181; (7) pale-green elbaite from pockets, sample 7015; (8) pale-green (Mn, Fe)-bearing elbaite from pockets, sample 7012; (9) pale-green (Fe, Mn)-bearing elbaite from pockets, sample 7013.

Na and F, and low Mn contents; (3) elbaite-rossmanite has low Na, Mn, F contents; (4) (Fe,Mn)-bearing elbaite has high Na, Mn and F contents (≤ 0.87 *apfu* Na, ≤ 0.70 *apfu* F) (Table 4.3, compositions 8,9). Figure 4.8b shows the overall positive correlation between Na, Mn and F.

Tourmaline at Dolní Bory No. 21 contains no Mg, Ti or Zn, and most of the tourmaline contains no Ca except for ≤ 0.40 *apfu* Mg, ≤ 0.07 *apfu* Ti and ≤ 0.08 *apfu* Ca in Mg-bearing schorl from the medium-grained aplite zone (Table 4.3, composition 1) and ≤ 0.09 *apfu* Ca in pale-green pocket elbaite (Table 4.3, composition 7).

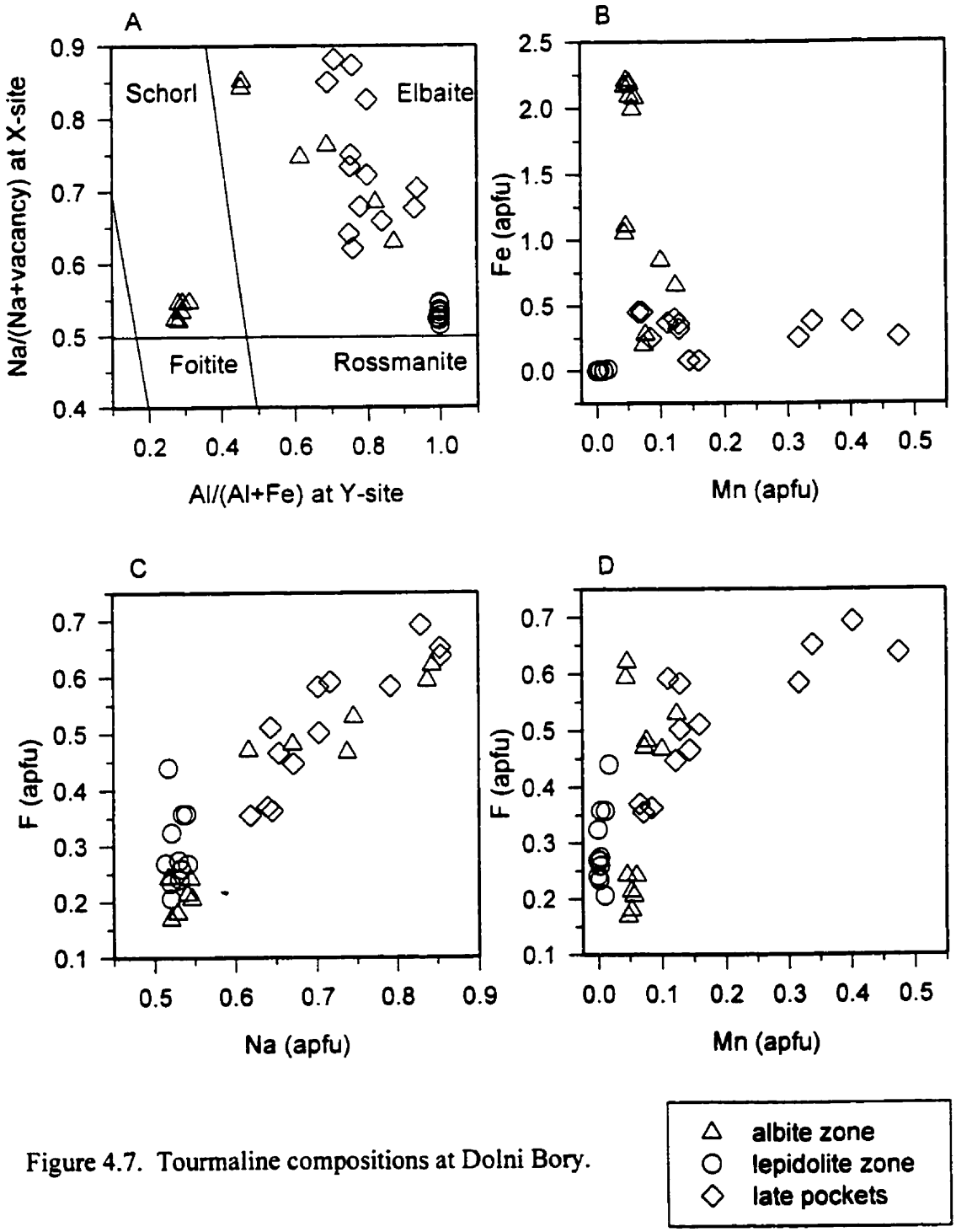

Figure 4.7. Tourmaline compositions at Dolni Bory.

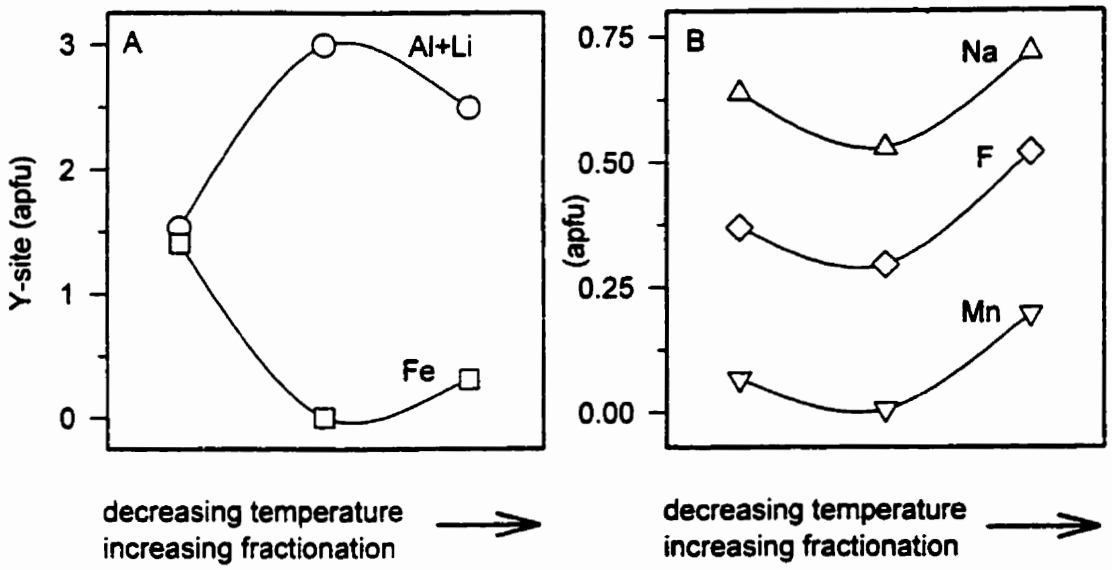

Figure 4.8. Idealized trends of tourmaline composition based on the average tourmaline composition for each pegmatite zone at Dolni Bory.

4.5. The Rožná pegmatite

4.5.1. General geology

The Rožná pegmatite is a zoned lepidolite-subtype pegmatite located near the town of Rožná, Czech Republic. It is 1 km long and 35 m wide, and intrudes biotite gneiss (Novák 1992, Černý *et al.* 1995, Novák & Selway 1997). The Rožná pegmatite was mined in two quarries on Hradisko and Borovina hills, which are separated by a small fault along the Sušírna valley (Novák 1992). The Hradisko quarry displays the most differentiated and fractionated central part of the dyke, with famous massive

aggregates of lepidolite and a quartz core. The Borovina quarry displays the less-fractionated albite subunit with weak Li mineralization. The samples discussed in this thesis are from the Hradisko quarry.

The Rožná pegmatite consists of (i) coarse-grained biotite-bearing wall zone, (ii) coarse-grained schorl-bearing intermediate zone, (iii) graphic zone, (iv) fine- to medium-grained granitic zone, (v) blocky core-margin zone, (vi) albite subunit, (vi) lepidolite subunit and (vii) quartz core (Novák 1992, Černý *et al.* 1995, Novák & Selway 1997). The coarse-grained biotite-bearing wall zone (i) consists of quartz, K-feldspar, plagioclase and biotite; the coarse-grained schorl-bearing intermediate zone (ii) consists of quartz, K-feldspar, plagioclase, black tourmaline and muscovite; the graphic zone (iii) consists of K-feldspar, albite, quartz, black tourmaline and plumose muscovite with veins or streaks of fine- to medium-grained granitic zone (iv) which consists of quartz, K-feldspar, albite, black tourmaline and minor silvery muscovite. The blocky core-margin zone (v) consists of abundant K-feldspar and quartz, and minor amblygonite. The albite subunit (vi) consists of dominant albite with abundant black, green and blue tourmaline, pale greenish-yellow to colourless muscovite, and accessory apatite, cassiterite, amblygonite-montebrasite, pale-pink to purple lepidolite, hydroxyl-herderite, zircon and beryl. The lepidolite subunit (vi) consists of dominant purple lepidolite, abundant pink tourmaline, quartz and albite with accessory green, grey, blue and colourless tourmaline, apatite, manganocolumbite, cassiterite, amblygonite-montebrasite, beryl and topaz. The quartz core (vii) consists of dominant quartz with accessory late greenish mica and green, colourless, blue and pink tourmaline. The albite and lepidolite subunits and outer part of

the quartz core contain rare small pockets with crystals of quartz, pink and green tourmaline, lepidolite and apatite. Late hydrothermal and weathering processes produced hydromicas, apatite, cookeite and clay minerals.

Tourmaline occurs in all pegmatite zones except the coarse-grained biotite-bearing wall zone (i) and the blocky core-margin zone (v). Black tourmaline in zones (ii), (iii) and (iv) forms isolated columnar crystals, radial aggregates and fine- to medium-grained masses associated with silvery muscovite. Black tourmaline is common in the outer part of the albite subunit (vi), and is usually rimmed by dark-green or dark-blue and pale-green tourmaline associated with greenish Li-rich muscovite. The lepidolite subunit (vi) and the outer parts of the quartz core (vii) contain zoned crystals and fine- to coarse-grained radial aggregates of tourmaline. In the outer part of the lepidolite subunit, brownish-to-purple lepidolite is associated with pink and blue tourmaline. In the central lepidolite subunit, purple-to-violet lepidolite is associated with columnar pink and minor greyish tourmaline. In the inner part of lepidolite subunit, close to the quartz core, green lepidolite is associated with pink and blue tourmaline. In the quartz core, zoned tourmaline with green to almost colourless rims and pink cores is associated with late greenish mica.

Based on a study of zoned crystals, the overall colour sequence of primary tourmaline in Rožná pegmatite is as follows: black → dark green (dark blue) → green → pink, blue → colourless → green. Terminals of zoned crystals are mostly green, and are the last tourmaline composition to crystallize.

4.5.2. Composition of tourmaline from Rožná

Table 4.4 is a summary of tourmaline colour and composition from each pegmatite zone at Rožná. The primary tourmaline from the pegmatite zones will be discussed separately from the hydrothermal tourmaline in fissures and enclaves.

4.5.2.1. Primary tourmaline from the pegmatite

The tourmaline composition at Rožná evolves following the crystallization sequence from the outermost to the innermost zone: foitite-schorl → schorl-foitite → elbaite-schorl → elbaite + Mn-bearing elbaite → elbaite-rossmanite → rossmanite-elbaite → elbaite-rossmanite → Fe-bearing elbaite + Mn-bearing elbaite (Fig. 4.9a, Tables 4.5, 4.6). Black foitite-schorl and schorl-foitite occur in the outermost (ii), (iii) and (iv) granitic zones. Black schorl-foitite is typical of the outer parts of the albite zone, but it is commonly rimmed by dark-green or dark-blue elbaite-schorl and pale-green Mn-bearing elbaite. Pink elbaite and blue Mn-bearing elbaite occur in the outer lepidolite zone; pink and grey elbaite-rossmanite and rossmanite-elbaite occur in the central lepidolite zone; pink elbaite-rossmanite and blue Fe-rich elbaite occur in the inner lepidolite zone, close to the quartz core. Zoned tourmaline with pink elbaite-rossmanite cores and colourless to pale-green elbaite rims occurs in the quartz core. The quartz core also contains green to almost colourless Fe-bearing elbaite and pink Mn-bearing elbaite crystals. The overall negative correlation between Fe and (Al+Li) at the *Y*-site is shown in Figure 4.10a.

There is a negative correlation between Fe and Mn as the composition of tourmaline evolves from foitite-schorl → schorl-foitite → elbaite-schorl → Mn-bearing

TABLE 4.4. TOURMALINE COLOUR AND COMPOSITION AT ROŽNÁ

Paragenesis	Colour	Composition
(i) coarse-grained biotite-bearing wall zone		no tourmaline present
(ii) coarse-grained schorl-bearing intermediate zone	black	foitite-schorl
(iii) graphic zone	black	foitite-schorl, schorl-foitite
(iv) fine- to medium-grained granitic zone	black	schorl-foitite
(v) blocky core-margin zone		no tourmaline present
(vi) albite subunit	black	schorl-foitite
	dark green, dark blue	elbaite-schorl
	green	Mn-bearing elbaite
(vi) lepidolite subunit		
- outer	pink	elbaite-rossmanite
	blue	Mn-bearing elbaite
- central	pink	elbaite-rossmanite, rossmanite-elbaite
	grey	elbaite-rossmanite
- inner	pink	elbaite-rossmanite
	blue	Fe-rich elbaite
(vii) quartz core	pink	elbaite-rossmanite, Mn-bearing elbaite
	green to colourless	elbaite-rossmanite, Fe-bearing elbaite
fracture-filling veins:		
- in zones (ii), (iii), (iv)	black, blue	Al-rich schorl, elbaite-schorl, foitite-schorl
	black, bluish-black	Mg-rich schorl
- in zone (vi)	deep blue, brownish	Mg,Fe-rich elbaite
	green	schorl-elbaite
	pink	elbaite
- in quartz core		
metapelite enclaves	brown	Mg-bearing elbaite-schorl, Mg, Fe-rich elbaite, dravite-schorl
	green	Mg, Fe-rich elbaite, foitite-schorl, schorl-dravite, schorl-elbaite, elbaite-schorl

TABLE 4.5. REPRESENTATIVE COMPOSITIONS OF TOURMALINE (WT%) FROM ZONES (iii) TO (vi) AT ROŽNÁ

	1	2	3	4	5	6
SiO_2	35.80	34.90	35.26	36.08	36.85	37.47
TiO_2	0.00	0.00	0.13	0.09	0.00	0.00
B_2O_3*	10.41	10.24	10.35	10.56	10.69	10.91
Al_2O_3	34.70	33.70	34.09	36.03	36.43	39.05
MgO	0.02	0.03	0.73	0.00	0.00	0.00
CaO	0.00	0.04	0.07	0.00	0.00	0.16
MnO	0.44	0.38	0.30	1.65	0.61	2.99
FeO*	13.80	14.80	13.80	10.39	9.00	1.71
ZnO	0.12	0.00	0.00	0.20	0.00	0.00
Li_2O*	0.25	0.24	0.22	0.57	1.11	1.67
Na_2O	1.24	1.72	1.54	1.52	2.37	2.33
K_2O	0.02	0.04	0.04	0.00	0.00	0.00
H_2O*	3.46	3.32	3.49	3.40	3.20	3.29
F	0.28	0.46	0.18	0.52	1.04	1.01
O=F	-0.12	-0.19	-0.08	-0.22	-0.44	-0.43
total	100.42	99.68	100.12	100.79	100.86	100.16
Formulae contents normalized to 31 anions						
T -Si	5.98	5.92	5.92	5.94	5.99	5.97
Al	0.02	0.08	0.08	0.06	0.01	0.02
B	3.00	3.00	3.00	3.00	3.00	3.00
Z -Al	6.00	6.00	6.00	6.00	6.00	6.00
Y -Al	0.81	0.66	0.67	0.93	0.97	1.30
Ti	0.00	0.00	0.02	0.01	0.00	0.01
Mg	0.01	0.01	0.18	0.00	0.00	0.00
Zn	0.02	0.00	0.00	0.02	0.00	0.00
Mn	0.06	0.06	0.04	0.23	0.08	0.41
Fe^{2+}	1.93	2.10	1.94	1.43	1.22	0.22
Li	0.17	0.17	0.15	0.38	0.73	1.06
∑Y	3.00	3.00	3.00	3.00	3.00	3.00
X -Ca	0.00	0.01	0.01	0.00	0.00	0.02
Na	0.40	0.57	0.50	0.49	0.75	0.70
K	0.00	0.01	0.01	0.00	0.00	0.00
□	0.60	0.41	0.48	0.51	0.25	0.28
OH	3.85	3.75	3.90	3.73	3.47	3.57
F	0.15	0.25	0.10	0.27	0.54	0.43

*B_2O_3, Li_2O and H_2O calculated by stoichiometry; B = 3 *apfu*, Li = 15 - $\sum T + Z + Y$ and OH+F = 4 *apfu*. All Fe is assumed to be Fe^{2+}.

(1) black foitite from graphic zone, sample 142; (2) black schorl-foitite from graphic zone, sample 1704; (3) black schorl-foitite from granitic zone, sample 332; (4) black foitite-schorl from albite subunit, sample 520; (5) dark green elbaite-schorl from albite subunit, sample 619; and (6) green Mn-bearing elbaite from albite subunit, sample 522.

TABLE 4.6. REPRESENTATIVE COMPOSITIONS OF TOURMALINE (WT%) FROM ZONES (vi) AND (vii) AT ROŽNÁ

	1	2	3	4	5	6	7	8
SiO_2	37.35	37.57	38.65	38.33	37.00	38.57	38.01	38.18
TiO_2	0.00	0.00	0.00	0.00	0.06	0.00	0.14	0.00
B_2O_3*	11.06	10.84	11.41	11.22	10.87	11.05	10.97	11.11
Al_2O_3	42.22	38.06	44.32	42.87	38.70	39.40	38.97	41.15
MgO	0.00	0.00	0.00	0.00	0.00	0.00	0.02	0.07
CaO	0.16	0.05	0.00	0.00	0.17	0.26	0.11	0.00
MnO	0.92	4.14	0.04	0.16	1.00	2.70	1.18	0.79
FeO*	0.15	1.28	0.00	0.00	5.07	0.00	3.29	1.75
ZnO	0.00	0.00	0.00	0.00	0.00	0.00	0.00	0.00
Li_2O*	1.84	1.68	1.86	1.95	1.49	2.11	1.74	1.73
Na_2O	1.83	2.46	1.41	1.70	2.46	2.21	2.16	1.83
H_2O*	3.49	3.22	3.81	3.54	3.11	3.30	3.40	3.66
F	0.69	1.10	0.26	0.70	1.34	1.09	0.82	0.37
O=F	-0.29	-0.46	-0.11	-0.29	-0.56	-0.46	-0.35	-0.16
total	99.42	99.94	101.65	100.18	100.71	100.23	100.46	100.48
Formulae contents normalized to 31 anions								
T -Si	5.87	6.02	5.89	5.94	5.92	6.07	6.02	5.97
Al	0.13	0.00	0.11	0.06	0.08	0.00	0.00	0.03
B	3.00	3.00	3.00	3.00	3.00	3.00	3.00	3.00
Z -Al	6.00	6.00	6.00	6.00	6.00	6.00	6.00	6.00
Y -Al	1.69	1.19	1.85	1.77	1.22	1.31	1.28	1.56
Ti	0.00	0.00	0.00	0.00	0.01	0.00	0.02	0.00
Mg	0.00	0.00	0.00	0.00	0.00	0.00	0.00	0.02
Mn	0.12	0.56	0.01	0.02	0.14	0.36	0.16	0.10
Fe^{2+}	0.02	0.17	0.00	0.00	0.68	0.00	0.43	0.23
Zn	0.00	0.00	0.00	0.00	0.00	0.00	0.00	0.00
Li	1.17	1.08	1.14	1.21	0.95	1.33	1.11	1.09
$\sum Y$	3.00	3.00	3.00	3.00	3.00	3.00	3.00	3.00
X -Ca	0.03	0.01	0.00	0.00	0.03	0.04	0.02	0.00
Na	0.56	0.76	0.42	0.51	0.76	0.67	0.66	0.56
□	0.41	0.23	0.58	0.49	0.21	0.29	0.32	0.44
OH	3.66	3.44	3.87	3.66	3.32	3.46	3.59	3.82
F	0.34	0.56	0.13	0.34	0.68	0.54	0.41	0.18

*B_2O_3, Li_2O and H_2O calculated by stoichiometry; B = 3 *apfu*, Li = 15 - $\sum T$ + *Z* + *Y* and OH+F = 4 *apfu*. All Fe is assumed to be Fe^{2+}.

(1) pink elbaite-rossmanite from outer purple lepidolite subunit, sample 886; (2) blue Mn-bearing elbaite from outer purple lepidolite subunit, sample 987; (3) pink rossmanite-elbaite from central purple lepidolite subunit, sample 1091; (4) grey elbaite-rossmanite from central purple lepidolite subunit, sample 1195; (5) blue Fe-rich elbaite from inner green lepidolite, sample 1805; (6) pink Mn-bearing elbaite from quartz core, sample 1419; (7) green Fe-bearing elbaite from quartz core, sample 1311 and (8) green elbaite-rossmanite from quartz core, sample 1208.

elbaite, with a maximum Mn content of 0.56 *apfu* Mn in blue Mn-bearing elbaite in the outer lepidolite zone (Fig. 4.9b, Table 4.6, composition 2). This negative correlation is followed by a decrease in Mn from elbaite → elbaite-rossmanite → rossmanite-elbaite which contains no Fe or Mn. There is an increase in Fe and Mn in green Fe-bearing elbaite and pink Mn-bearing elbaite with ≤ 0.40 *apfu* Mn in the quartz core (Table 4.6, compositions 6, 7). The most primitive tourmaline is Fe-rich and (Mn, Al+Li)-poor (foitite-schorl) with increasing fractionation Fe decreases and (Mn, Al+Li) increases (Mn-bearing elbaite), Fe and Mn decreases and Al+Li increases (elbaite-rossmanite), and Mn, Fe and Al+Li increases ((Fe, Mn)-bearing elbaite.

Figures 4.9c and 4.9d show a strong positive correlation between Na and F and a weak positive correlation between Mn and F in tourmaline: (1) foitite-schorl and schorl-foitite have low Na, Mn and F; (2) elbaite-schorl has high Na and F and moderate Mn; (3) elbaite and Mn-bearing elbaite have high Na, Mn and F; (4) rossmanite-elbaite and elbaite-rossmanite have low Na and Mn and F; (5) Fe-rich elbaite, Fe-bearing elbaite and Mn-bearing elbaite have high Na, Mn and F. Blue Fe-rich elbaite contains ≤ 0.77 *apfu* Na and ≤ 0.69 *apfu* F in the inner lepidolite zone (Table 4.6, composition 5). The overall

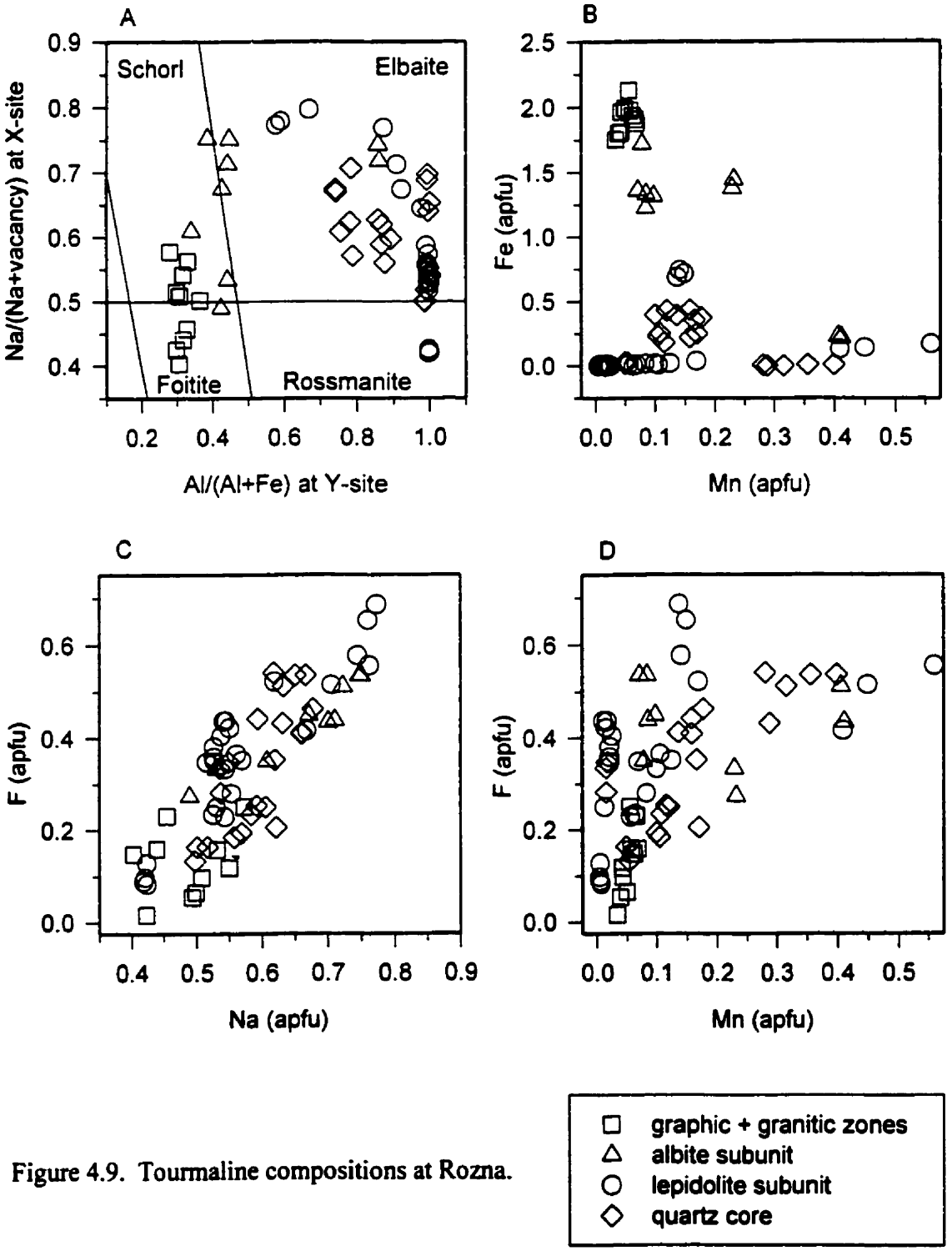

Figure 4.9. Tourmaline compositions at Rozna.

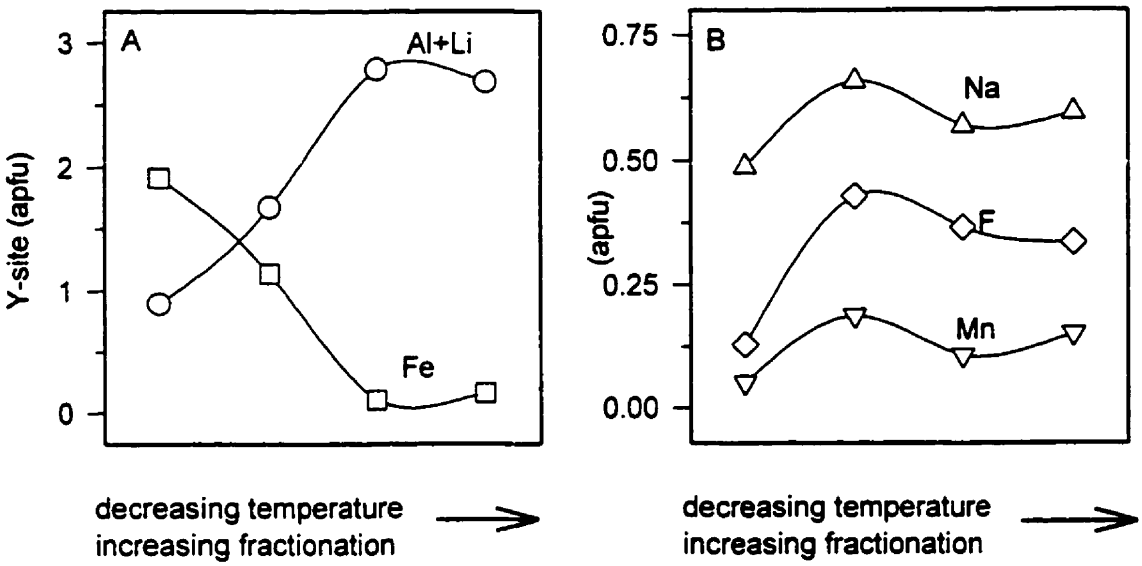

Figure 4.10. Idealized trends of tourmaline composition based on the average tourmaline composition for each pegmatite zone at Rozna.

positive correlation between Na, Mn and F is shown in Figure 4.10b.

Most tourmaline in the Rožná pegmatite contains no Mg, Ti and Zn except for ≤ 0.30 *apfu* Mg in black schorl-foitite in the graphic zone, ≤ 0.03 *apfu* Ti in black schorl-foitite in the fine- to medium-grained granitic zone, and ≤ 0.05 *apfu* Zn in black foitite-schorl in the graphic zone. Most tourmaline contains no Ca except for ≤ 0.05 *apfu* Ca in pink Mn-bearing elbaite in the quartz core.

4.5.2.2. Hydrothermal tourmaline from fissures and enclaves

Late fracture-filling veins, up to 2 cm thick and intruding zones (ii), (iii), (iv), (vi) and (vii), consist of albite, quartz, apatite and abundant zoned tourmaline. Veins in zones (ii), (iii) and (iv) commonly contain black to blue Al-rich schorl and elbaite-schorl, and rare foitite-schorl (Fig. 4.11, Table 4.7). Veins in the albite-lepidolite zone (vi) commonly contains zoned black, bluish-black, deep-blue, brown and green Mg-rich schorl, (Mg, Fe)-rich elbaite and schorl-elbaite which forms radial aggregates, fine- to medium-grained masses, and isolated, columnar crystals up to 5 mm in size. Rare thin veins of pink elbaite cut the quartz core (vii).

Enclaves of metapelites are very rare at this locality, and small fragments occur only in old dumps. Hydrothermally altered metapelite enclaves, up to 1 m in size, occur in the upper part of the dyke (Sekanina 1946). Feldspars and micas in the enclaves are replaced by a mixture of fine-grained micaceous minerals and metasomatic tourmaline. Abundant radial aggregates of hydrothermal tourmaline, up to 1 cm in size, are developed particularly along fissures. The tourmaline is zoned and displays a wide variety of colours, dark brown, greenish brown, green to yellowish green, and compositions (dravite-schorl, schorl-dravite), ((Mg, Fe)-rich elbaite, Mg-bearing elbaite-schorl), foitite-schorl, and (schorl-elbaite and elbaite-schorl) (Fig. 4.11, Table 4.7).

The (Mg, Fe)-rich elbaite in the fissures intruding zone (vi) and the metapelite enclaves has intermediate elbaite-dravite-schorl compositions and falls in the "compositional gap" noted by previous authors (*e.g.*, Dietrich 1985a, b, Henry & Guidotti 1985). Recently, Novák *et al.* (1999a) showed that tourmaline compositions do span this

TABLE 4.7. REPRESENTATIVE COMPOSITIONS OF TOURMALINE (WT%) FROM FISSURES AND METAPELITE ENCLAVES AT ROŽNÁ

	1	2	3	4	5	6	7	8	9
SiO_2	35.40	34.67	35.08	35.53	36.45	36.40	36.10	34.80	36.20
TiO_2	0.01	0.10	0.37	0.28	0.16	0.72	0.30	0.23	0.14
B_2O_3*	10.45	10.63	10.25	10.37	10.67	10.55	10.76	10.45	10.57
Al_2O_3	36.14	38.40	33.72	31.80	37.82	31.50	37.30	35.30	35.80
Fe_2O_3	0.00	0.00	1.47	0.00	0.00	0.00	0.00	0.00	0.00
MgO	0.21	0.07	0.86	3.51	2.21	5.65	2.67	1.47	1.01
CaO	0.12	0.36	0.23	0.20	0.59	0.70	0.48	0.29	0.06
MnO	0.10	0.33	0.48	0.08	0.77	0.14	0.48	0.47	0.29
FeO*	12.85	10.05	12.25	12.03	4.34	8.09	4.41	10.60	10.90
ZnO	0.00	0.00	0.00	0.00	0.00	0.00	0.00	0.00	0.00
Li_2O*	0.41	0.74	0.09	0.65	1.19	0.40	1.11	0.53	0.47
Na_2O	1.37	1.92	1.92	2.00	2.26	2.27	2.32	2.15	1.33
K_2O	0.00	0.00	0.07	0.09	0.00	0.00	0.00	0.00	0.00
H_2O*	3.39	3.40	3.10	3.49	3.30	3.05	3.14	3.14	3.49
F	0.49	0.57	0.46	0.19	0.92	1.25	1.20	0.99	0.34
O=F	-0.21	-0.24	-0.19	-0.08	-0.39	-0.53	-0.51	-0.42	-0.14
total	100.73	101.00	100.16	100.14	100.29	100.19	99.76	100.00	100.46
Formulae contents normalized to 31 anions									
T -Si	5.85	5.67	5.92	5.95	5.84	6.00	5.83	5.79	5.95
Al	0.15	0.33	0.08	0.05	0.16	0.00	0.17	0.21	0.05
B	3.00	3.00	2.98	3.00	3.00	3.00	3.00	3.00	3.00
Z -Al	6.00	6.00	6.00	6.00	6.00	6.00	6.00	6.00	6.00
Y -Al	0.89	1.06	0.62	0.23	0.99	0.12	0.93	0.71	0.88
Ti	0.00	0.01	0.05	0.04	0.02	0.09	0.04	0.03	0.02
Mg	0.05	0.02	0.22	0.88	0.53	1.39	0.64	0.36	0.25
Mn	0.01	0.05	0.07	0.01	0.11	0.02	0.07	0.07	0.04
Fe^{2+}	1.78	1.37	1.73	1.69	0.58	1.12	0.59	1.47	1.50
Fe^{3+}	0.00	0.00	0.19	0.00	0.00	0.00	0.00	0.00	0.00
Zn	0.00	0.00	0.00	0.00	0.00	0.00	0.00	0.00	0.00
Li	0.27	0.49	0.06	0.15	0.77	0.26	0.73	0.36	0.31
∑Y	3.00	3.00	2.94	3.00	3.00	3.00	3.00	3.00	3.00
X -Ca	0.02	0.06	0.04	0.12	0.10	0.12	0.08	0.05	0.01
Na	0.44	0.61	0.63	0.65	0.70	0.73	0.73	0.69	0.42
K	0.00	0.00	0.02	0.02	0.00	0.00	0.00	0.00	0.00
□	0.54	0.33	0.31	0.21	0.20	0.15	0.19	0.26	0.57
OH	3.74	3.70	3.49	3.90	3.53	3.35	3.39	3.48	3.82
F	0.26	0.30	0.25	0.10	0.47	0.65	0.61	0.52	0.18

*B_2O_3, Li_2O and H_2O calculated by stoichiometry; B = 3 *apfu*, Li = 15 - $\sum T + Z + Y$ and OH+F = 4 *apfu*. All Fe is assumed to be Fe^{2+}, except for (17).

(1) blue foitite-schorl in fissure in zone (iii), sample 239; (2) blue elbaite-schorl from fissure in zone (iii), sample 238; (3) blue Al-rich schorl from fissure in zone (iv), sample 70, B_2O_3, Li_2O and H_2O determined by wet chemistry (Povondra 1981); (4) green Mg-rich schorl in fissure in zone (iv), sample 6015; (5) green (Fe, Mg)-bearing elbaite in fissure in zone (vi), sample 6009; (6) brown dravite-schorl from enclave, sample T2; (7) brown (Mg, Fe)-rich elbaite from enclave, sample T1; (8) green Mg-bearing schorl-elbaite from enclave, sample T1; and (9) green foitite-schorl from enclave, sample T1.

gap, specifically intermediate elbaite-schorl-dravite and elbaite-dravite compositions from the elbaite-subtype Bližná pegmatite which intrudes marble.

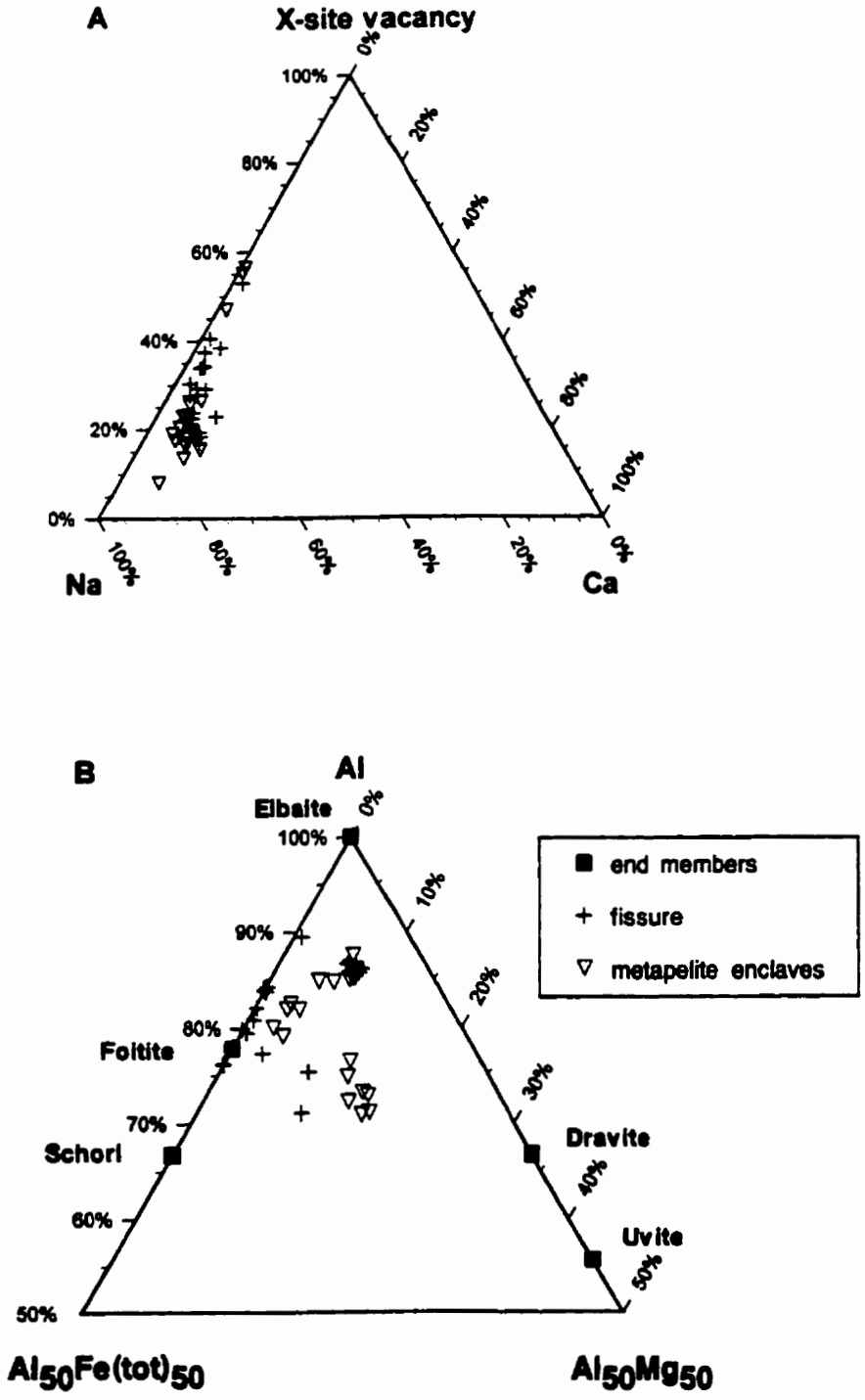

Figure 4.11. Tourmaline compositions from fissures and metapelite enclaves at Rožná (a) X-site vacancy-Na-Ca and (b) Al-Fe(tot)-Mg ternary diagrams.

4.5.3. Composition of micas from Rožná

The compositional variation of tourmaline is closely related to that in the micas at Rožná (Černý *et al.* 1995). The evolution of Fe and (Al+Li) in tourmaline is similar to that of mica (Figs. 4.12a, b). In the outer granitic-pegmatite zones, tourmaline and mica have high Fe content which decreases inward toward the core, except for slight Fe-enrichment in (Fe, Mn)-bearing elbaite in the quartz core. Biotite in the coarse-grained biotite-bearing wall zone (i) is not shown in Figure 4.12 because compositional data is not available. The (Al+Li) trend is the inverse of the Fe trend; tourmaline and mica in the outer granitic zones have low (Al+Li) content, but the latter increases inward. The Al content of mica decreases from muscovite to lepidolite, whereas the Al content increases from foitite-schorl to rossmanite-elbaite and decreases during crystallization of (Fe, Mn)-bearing elbaite (Fig. 4.12c).

Sodium variation in tourmaline and mica is similar (Fig. 4.12d): Na is preferentially partitioned into tourmaline relative to mica. Tourmaline and mica in the outer granitic-pegmatite zones have low Na content, increasing to the outer albite subunit, and decreasing to the lepidolite subunit. There is an increase of Na in tourmaline, but not in mica, in the inner lepidolite subunit and the quartz core as (Fe, Mn)-bearing elbaite starts to crystallize.

Fluorine variation in tourmaline and mica show different trends (Fig. 4.12e). The F content of tourmaline has two maxima during crystallization of (Fe, Mn)-bearing elbaite, whereas mica shows a gradual increase from muscovite to lepidolite, reflecting the positive correlation between F and Li in micas (Robert *et al.* 1993). Fluorine is

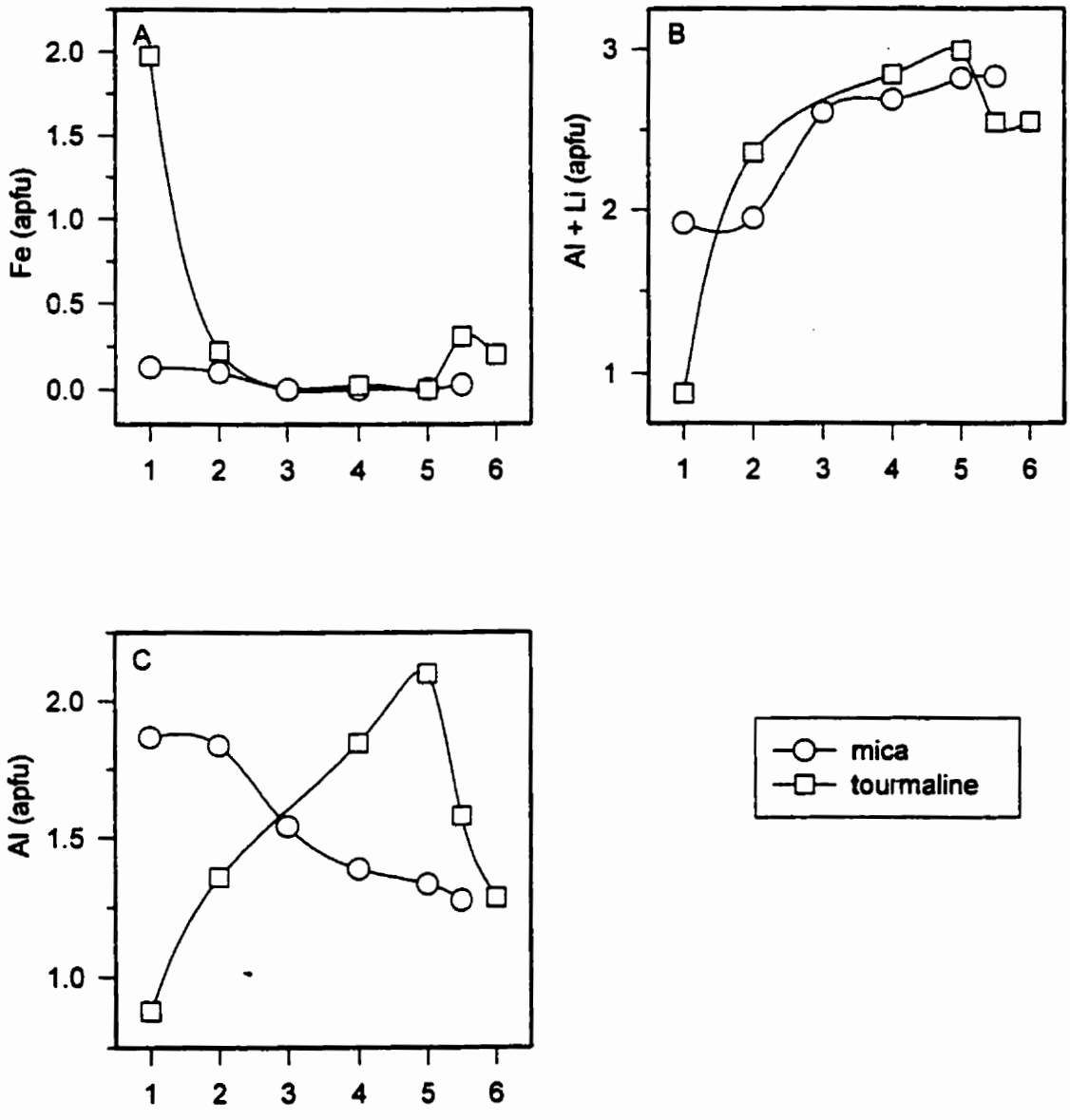

Figure 4.12. Comparison of tourmaline and mica element trends for selected pegmatite zones at Rozna. Pegmatite zones: (1) fine- to medium-grained granitic zone with muscovite, (3) central albite zone with lepidolite, (4) outer lepidolite zone, (5) lepidolite zone, (5.5) inner lepidolite zone, and (6) quartz core. Mica data is from Cerny et al. (1995).

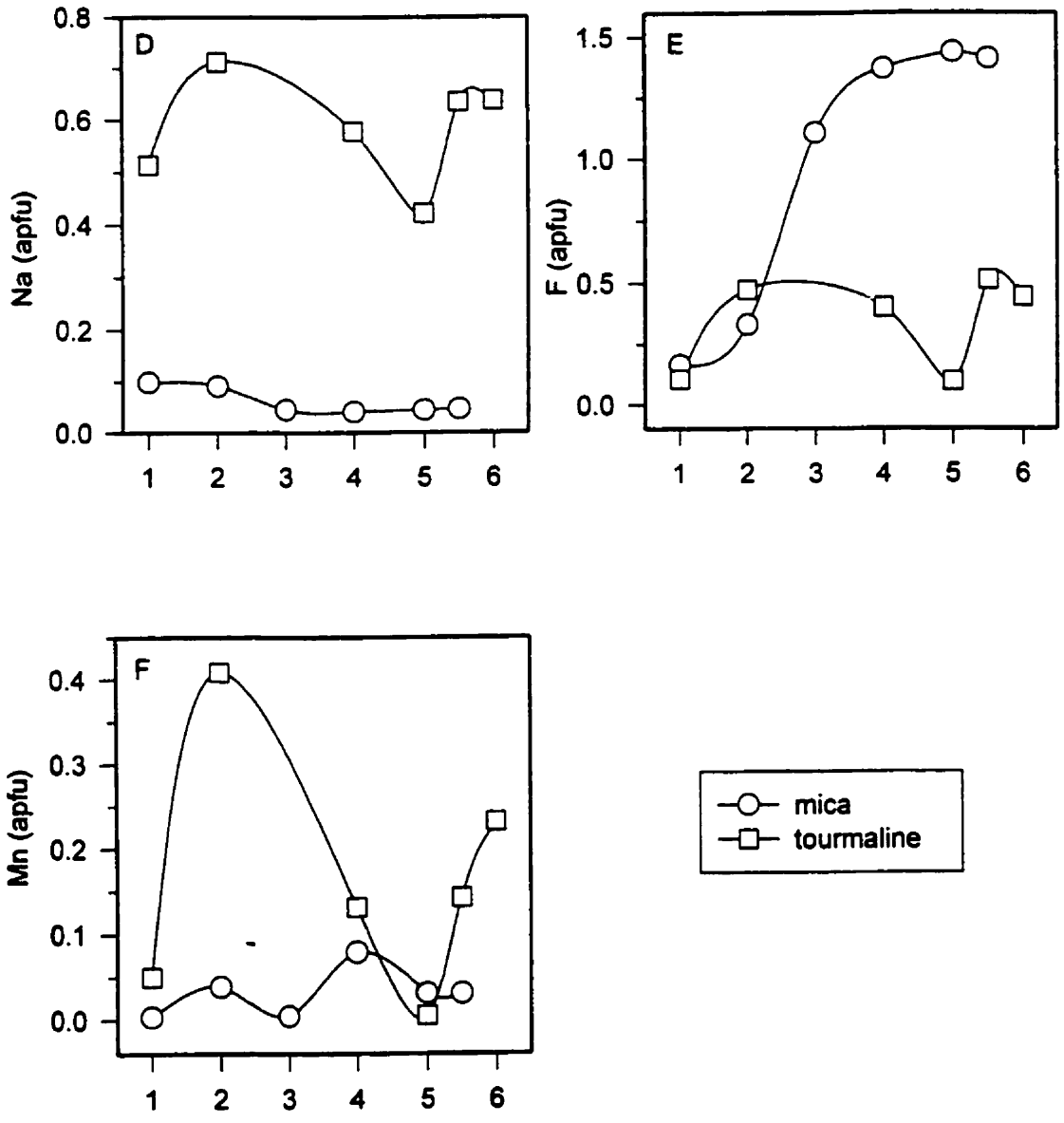

Figure 4.12. (continued)

preferentially partitioned into lepidolite relative to tourmaline.

Manganese variations in tourmaline and mica show different trends (Fig. 4.12f). The Mn content of tourmaline shows the same trend as the Na content. The Mn content in mica has two maxima, one in muscovite of the outer albite zone, and the other in lepidolite of the outer lepidolite zone. Manganese is preferentially partitioned into tourmaline relative to mica.

4.6. The Radkovice pegmatite

4.6.1 General geology

The Radkovice pegmatite is a 2.5 m thick lepidolite-subtype pegmatite which intrudes serpentinized garnetiferous peridotite 48 km WSW of Brno, Czech Republic (Černý *et al.* 1970; 1971). It consists of (i) graphic zone, (ii) blocky K-feldspar zone, (iii) albite zone, and (iv) lepidolite core. The graphic and blocky K-feldspar zones contain black tourmaline, the albite zone contains green tourmaline associated with muscovite, and the lepidolite core contains fine-grained pink needles of tourmaline associated with dark purplish-red lepidolite. The lepidolite zone consists of abundant fine- to medium-grained albite, lepidolite and quartz with accessory topaz, beryl and pink tourmaline. The fine-grained (1-10 mm) flakes of lepidolite are close to trilithionite in composition. Metasomatic B-rich cookeite, associated with adularia, replaces F-rich lepidolite in the lepidolite core. The quartz "core" was almost completely dissolved by late alkaline fluids from the Ca-rich host rock.

4.6.2. Composition of tourmaline from Radkovice

The composition of tourmaline at Radkovice evolves following the crystallization sequence from the outermost to the innermost zone: Mg-rich schorl → Mg-rich schorl-foitite → schorl-foitite → schorl-elbaite → Fe-rich, Mn-bearing elbaite → elbaite → elbaite-rossmanite → rossmanite-elbaite (Figs. 4.13a, 4.14, Table 4.8). Black Mg-rich schorl and Mg-rich schorl-foitite occur in the graphic zone; black schorl-foitite, schorl-elbaite and Fe-rich, Mn-bearing elbaite occur in the blocky K-feldspar zone; green elbaite occurs in the albite zone; pink fine-grained needles of elbaite-rossmanite and rossmanite-elbaite occur in the lepidolite core. The Mg content ($\leq$ 0.60 *apfu* Mg) of the Mg-rich schorl (Table 4.8, composition 1) and Mg-rich schorl-foitite in the graphic zone (Fig. 4.14b) are much higher that than in tourmaline from other lepidolite-subtype pegmatites due to an influx of Mg from the serpentinized garnetiferous-peridotite host-rock.

There is a negative correlation between Fe and Mn as the composition of tourmaline evolves from schorl-foitite and schorl-elbaite to Fe-rich, Mn-bearing elbaite with a maximum Mn content of 0.33 *apfu* in the blocky K-feldspar zone (Fig. 4.13b, Table 4.8, composition 4). This negative correlation is followed by a positive correlation of decreasing Mn and Fe from elbaite → elbaite-rossmanite → rossmanite-elbaite.

Figures 4.13 c and 4.13d show a strong positive correlation between Na and F and a weak positive correlation between Mn and F in tourmaline: (1) The schorl-foitite compositions have low Na, Mn and F contents; (2) schorl-elbaite and Fe-rich, Mn-bearing elbaite have high-to- moderate Na, Mn and F contents; (3) elbaite-rossmanite and rossmanite-elbaite have low Na, Mn and F contents. Most tourmaline at Radkovice

TABLE 4.8. REPRESENTATIVE COMPOSITIONS OF TOURMALINE (WT%) AT RADKOVICE

	1	2	3	4	5	6	7
SiO_2	35.96	35.57	36.70	36.26	37.38	38.14	38.70
TiO_2	0.29	0.11	0.12	0.00	0.09	0.00	0.00
B_2O_3*	10.47	10.46	10.57	10.64	10.94	11.19	11.32
Al_2O_3	33.41	35.33	34.78	37.77	40.40	42.66	43.31
MgO	2.44	0.00	0.00	0.00	0.00	0.00	0.00
CaO	0.10	0.00	0.00	0.00	0.09	0.00	0.00
MnO	0.00	1.19	0.96	2.40	1.01	0.43	0.12
FeO	11.93	12.30	10.56	5.00	1.78	0.00	0.00
ZnO	0.00	0.15	0.00	0.49	0.00	0.00	0.00
Li_2O*	0.30	0.40	1.00	1.11	1.75	1.93	1.95
Na_2O	1.92	1.58	2.39	1.94	2.05	1.83	1.62
H_2O*	3.56	3.39	3.23	3.37	3.44	3.58	3.69
F	0.12	0.46	0.89	0.64	0.71	0.59	0.46
O=F	-0.05	-0.19	-0.37	-0.27	-0.30	-0.25	-0.19
total	100.45	100.75	100.83	99.35	99.34	100.10	100.98
Formulae contents normalized to 31 anions							
T -Si	5.97	5.91	6.03	5.92	5.94	5.92	5.94
Al	0.03	0.09	0.00	0.08	0.06	0.08	0.06
B	3.00	3.00	3.00	3.00	3.00	3.00	3.00
Z -Al	6.00	6.00	6.00	6.00	6.00	6.00	6.00
Y -Al	0.50	0.82	0.74	1.20	1.50	1.73	1.78
Ti	0.04	0.01	0.02	0.00	0.01	0.00	0.00
Mg	0.60	0.00	0.00	0.00	0.00	0.00	0.00
Mn	0.00	0.17	0.13	0.33	0.13	0.06	0.02
Fe^{2+}	1.66	1.71	1.45	0.68	0.24	0.00	0.00
Zn	0.00	0.02	0.00	0.06	0.00	0.00	0.00
Li	0.20	0.27	0.66	0.73	1.12	1.21	1.20
$\sum$Y	3.00	3.00	3.00	3.00	3.00	3.00	3.00
X -Ca	0.02	0.00	0.00	0.00	0.02	0.00	0.00
Na	0.62	0.51	0.76	0.61	0.63	0.55	0.48
□	0.36	0.49	0.24	0.39	0.35	0.45	0.52
OH	3.94	3.76	3.54	3.67	3.64	3.71	3.78
F	0.06	0.24	0.46	0.33	0.36	0.29	0.22

*B_2O_3, Li_2O and H_2O calculated by stoichiometry; B = 3 *apfu*, Li = 15 - $\sum T + Z + Y$ and OH+F = 4 *apfu*.

(1) black Mg-rich schorl from graphic zone, sample 151; (2) black schorl-foitite from blocky K-feldspar zone, sample 253; (3) black schorl-elbaite from blocky K-feldspar zone, sample 254; (4) black Fe-rich, Mn-bearing elbaite from blocky K-feldspar zone, sample 358; (5) green elbaite from albite zone, sample 461; (6) pink needles of elbaite-rossmanite from lepidolite core, sample 562; and (7) pink needles of rossmanite-elbaite from lepidolite core, sample 561.

contains no Ti, Ca or Zn, except for Mg-rich schorl with ≤ 0.05 *apfu* Ti and ≤ 0.02 *apfu* Ca, and Fe-rich Mn-bearing elbaite with ≤ 0.06 *apfu* Zn.

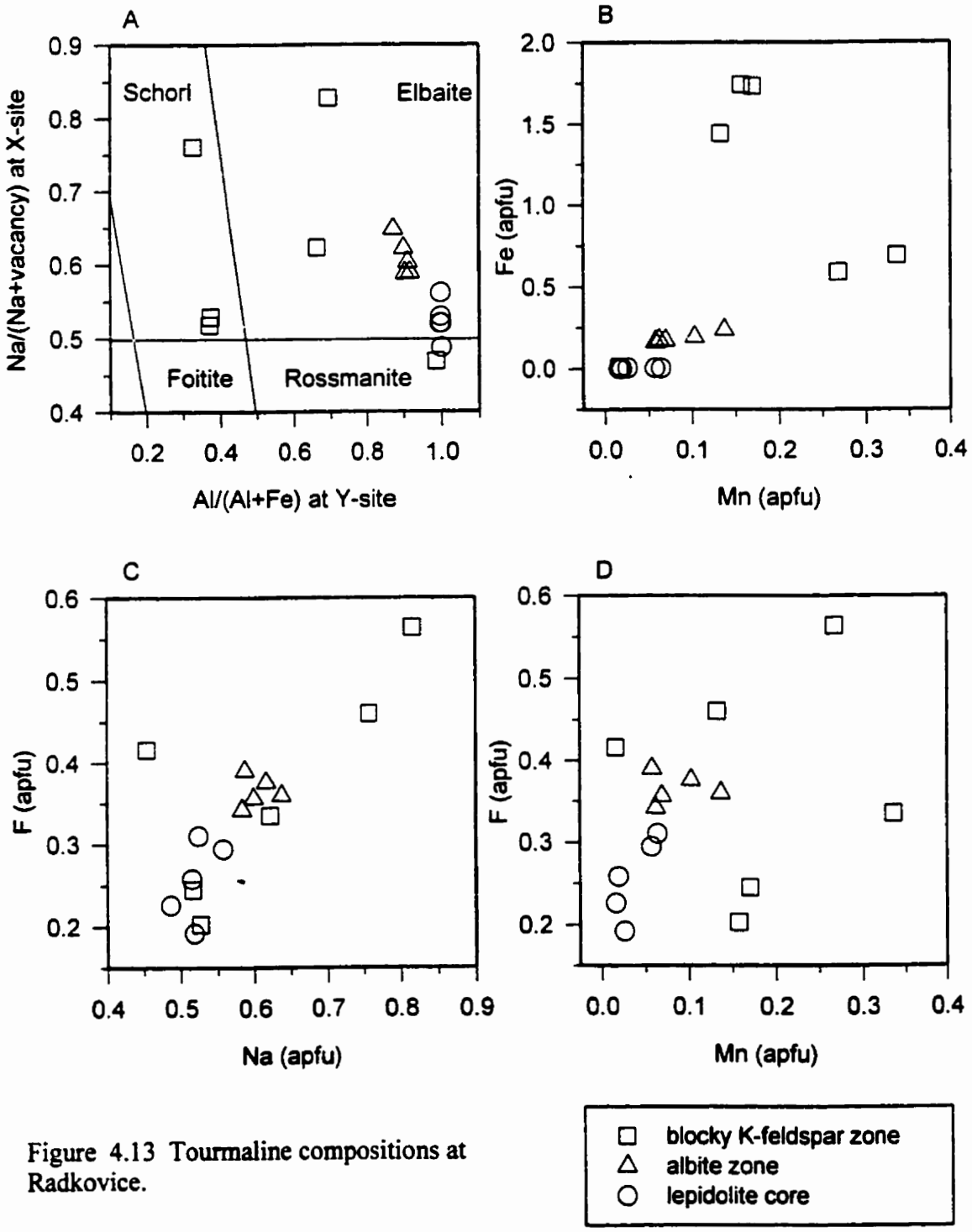

Figure 4.13 Tourmaline compositions at Radkovice.

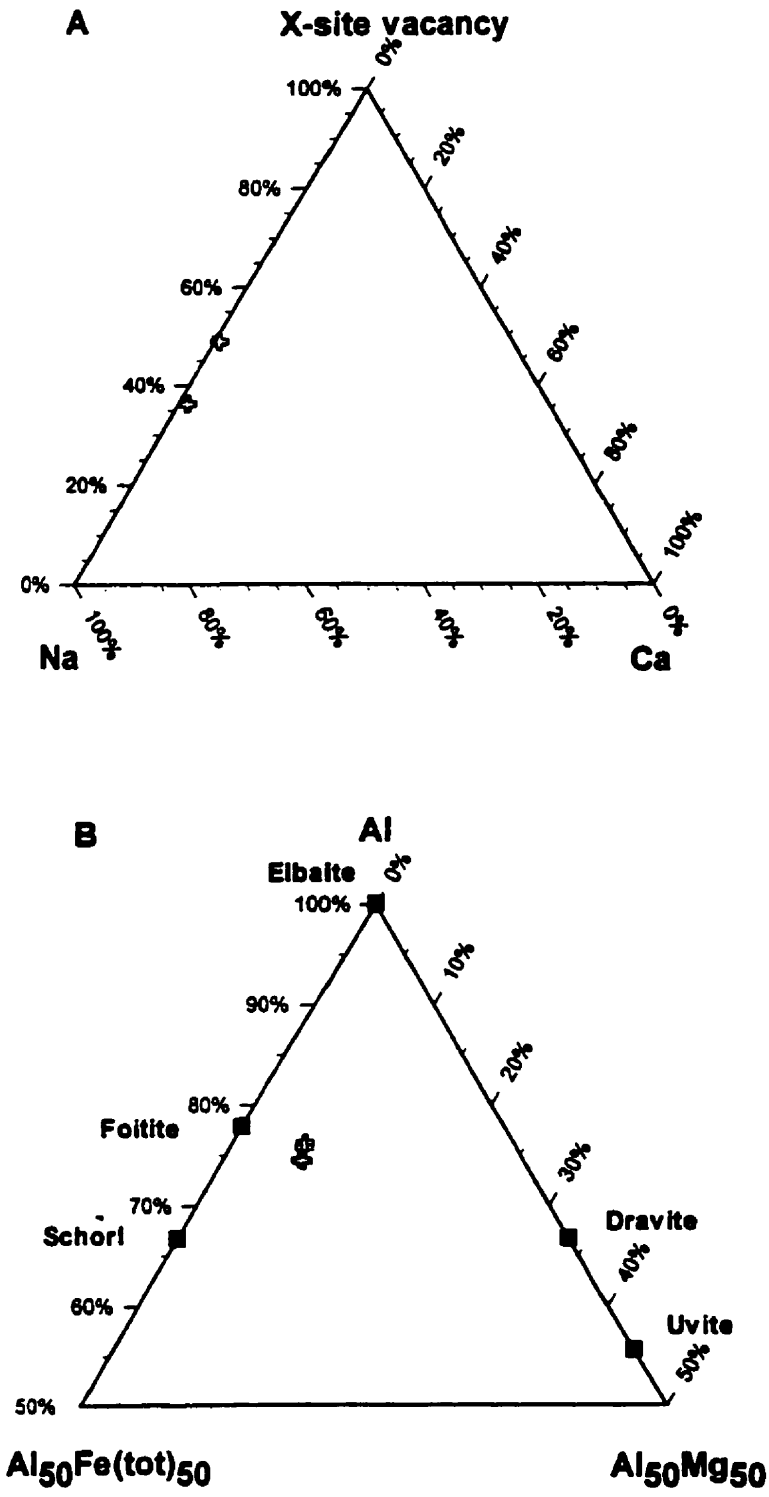

Figure 4.14. Tourmaline compositions at the graphic unit at Radkovice (a) X-site vacancy- Na-Ca and (b) Al-Fe(tot)-Mg ternary diagrams.

4.7. The lepidolite pegmatites at Red Cross Lake

4.7.1. General geology

The Red Cross Lake pegmatite field is located in the Oxford Lake greenstone belt of the Archean Superior province, northeastern Manitoba (Potter 1962, Jambor & Potter 1967, Trueman 1982, Chackowsky *et al.* 1985). The field consists of highly evolved pegmatitic leucogranites and a progressively fractionated suite of tourmaline-, spodumene-, and lepidolite-bearing pegmatite dikes intruding meta-andesitic to metabasaltic host-rock. All pegmatitic rocks are mylonitized, but the primary compositional features of virtually all minerals are well preserved (Eby 1986); in particular, the exocontacts are surprisingly well-preserved and are not mylonitized.

The swarm of 17 parallel homogenous lepidolite pegmatite dikes, up to 4 m wide, occur along the shore of the northeastern part of Red Cross Lake (Trueman 1982, Chackowsky *et al.* 1985). These lepidolite-subtype dikes are the most fractionated pegmatites known (Černý *et al.* 1994). The lepidolite pegmatites consist dominantly of alternating bands of purple fine-grained Rb-rich lepidolite and white quartz + albite + K-feldspar (Chackowsky *et al.* 1985). In addition, the pegmatites may carry subordinate spodumene + quartz pseudomorphs after petalite, and accessory pink tourmaline, pollucite, Cs-rich beryl, amblygonite, apatite, cassiterite, manganotantalite, wodginite, microlite, monazite, and hafnian zircon.

The pale-pink to almost colourless tourmaline is prismatic with crystals averaging 0.2 x 1.0 mm, and rarely up to 0.8 x 2.5 mm (Selway *et al.* 1998b). The tourmaline is broken and the separated segments are cemented by quartz, albite and mica mortar. The

primary composition of the tourmaline is preserved in the mylonitized pegmatite dykes. The exocontacts consist dominantly of Cs- and Rb-rich biotite and black tourmaline with subordinate-to-minor ferruginous muscovite, epidote, apatite, garnet, titanite, calcite, quartz and arsenopyrite (Selway *et al.* 1998b). The black exocontact tourmaline is fine-grained, ranges in habit from euhedral to subhedral, and contains minor inclusions of primary apatite, quartz, titanite and garnet.

4.7.2. Composition of tourmaline from lepidolite pegmatites at Red Cross Lake

Pink tourmaline in the lepidolite pegmatites ranges from rossmanite-elbaite to elbaite-rossmanite, as is the case in the lepidolite zones of the pegmatites discussed above (Fig. 4.15a, Table 4.9). Zoned grains have rossmanite-elbaite or elbaite-rossmanite cores and elbaite-rossmanite rims. The tourmaline contains no Fe, and the Mn content ranges from 0.27 *apfu* in elbaite-rossmanite to 0.02 *apfu* in rossmanite-elbaite (Fig. 4.15b). There is a positive correlation between Na, Mn and F (Figs. 4.15c, d), with the F content ranging from 0.71 *apfu* in elbaite-rossmanite to 0.20 *apfu* in rossmanite-elbaite. Most tourmaline contains no Mg, Ti, Zn or Ca, except for $\leq$ 0.11 *apfu* Ca in elbaite-rossmanite rims (Table 4.9, composition 3).

Black tourmaline in the exocontacts is commonly zoned, with feruvite cores surrounded by schorl or dravite, and rimmed by uvite (Selway *et al.* 1998b) (Fig. 4.16). This is the first recognized occurrence of feruvite in association with rare-element granitic pegmatites. There are negative correlations between Ca and Na at the *X*-site and between Mg and Al at the *Z*-site which indicate that the coupled substitution between

TABLE 4.9. REPRESENTATIVE COMPOSITIONS OF TOURMALINE (WT%) IN LEPIDOLITE PEGMATITES AT RED CROSS LAKE

	1	2	3	4	5	6	7	8
SiO_2	38.00	38.40	38.40	38.40	35.30	34.90	35.70	34.90
TiO_2	0.00	0.00	0.00	0.00	0.35	0.44	0.27	0.07
B_2O_3*	11.14	11.29	11.09	11.10	10.11	10.09	10.26	10.08
Al_2O_3	42.90	43.40	40.70	40.60	26.20	27.10	27.60	27.00
MgO	0.00	0.00	0.00	0.00	5.84	5.27	5.89	6.20
CaO	0.00	0.00	0.65	0.48	3.01	2.76	2.80	2.88
MnO	0.13	0.22	1.35	1.83	0.09	0.10	0.07	0.05
FeO	0.00	0.00	0.00	0.00	13.60	13.60	12.30	12.90
Li_2O*	1.87	1.91	2.07	2.01	0.26	0.16	0.31	0.07
Na_2O	1.43	1.64	1.70	1.87	1.18	1.25	1.29	1.25
H_2O*	3.46	3.71	3.23	3.22	3.06	3.12	3.06	3.20
F	0.81	0.40	1.27	1.28	0.90	0.76	1.02	0.58
O=F	-0.34	-0.17	-0.53	-0.54	-0.38	-0.32	-0.43	-0.24
total	99.40	100.80	99.93	100.25	99.52	99.23	100.14	98.94
Formulae contents normalized to 31 anions								
T -Si	5.93	5.91	6.02	6.01	6.07	6.01	6.05	6.02
Al	0.07	0.09	0.00	0.00	0.00	0.00	0.00	0.00
B	3.00	3.00	3.00	3.00	3.00	3.00	3.00	3.00
Z -Al	6.00	6.00	6.00	6.00	5.31	5.50	5.51	5.49
Mg	0.00	0.00	0.00	0.00	0.69	0.50	0.49	0.51
Y -Al	1.81	1.79	1.51	1.49	0.00	0.00	0.00	0.00
Ti	0.00	0.00	0.00	0.00	0.04	0.06	0.03	0.01
Mg	0.00	0.00	0.00	0.00	0.81	0.86	1.00	1.08
Mn	0.02	0.03	0.18	0.24	0.01	0.01	0.01	0.00
Fe	0.00	0.00	0.00	0.00	1.96	1.96	1.75	1.86
Li	1.17	1.18	1.31	1.27	0.18	0.11	0.21	0.05
$\sum Y$	3.00	3.00	3.00	3.00	3.00	3.00	3.00	3.00
X -Ca	0.00	0.00	0.11	0.08	0.56	0.51	0.51	0.53
Na	0.43	0.49	0.52	0.57	0.39	0.42	0.42	0.42
□	0.57	0.51	0.37	0.35	0.05	0.07	0.07	0.05
OH	3.60	3.81	3.37	3.37	3.51	3.59	3.45	3.68
F	0.40	0.19	0.63	0.63	0.49	0.41	0.55	0.32

*B_2O_3, Li_2O and H_2O calculated by stoichiometry; B = 3 *apfu*, Li = 15 - $\sum T + Z + Y$ and OH+F = 4 *apfu*.

Compositions 1-4 from lepidolite pegmatites, and 5-8 from exocontact. (1) pink elbaite-rosmanite, sample 9-1= A4; (2) pink elbaite-rossmanite, sample RC-2-115 = A16; (3) pink Ca-bearing rossmanite-elbaite, sample RCL9-3; (4) pink rossmanite-elbaite, sample 7-2b = AM15B; (5) black feruvite-schorl, sample 14-2T; (6) black feruvite-schorl, sample 14-2T; (7) black feruvite-schorl, sample 8-19T; (8) black feruvite-schorl, sample A4.

feruvite and schorl is $^{X}Ca + {}^{Z}Mg = {}^{X}Na + {}^{Z}Al$. There is a negative correlation between Fe and Mg at the *Y*-site which indicates that the solid solution between feruvite and uvite is $^{Y}Fe^{2+} = {}^{Y}Mg$. The maximum Ti content of 0.20 *apfu* Ti occurs in Ca-rich dravite-schorl and Ca-rich schorl-dravite. The exocontact tourmaline crystallized as a result of infiltration of the Ca-, Mg-, Fe-rich meta-andesitic and metabasaltic host-rocks by Na-, Al-, B-, H_2O-rich pegmatitic fluids.

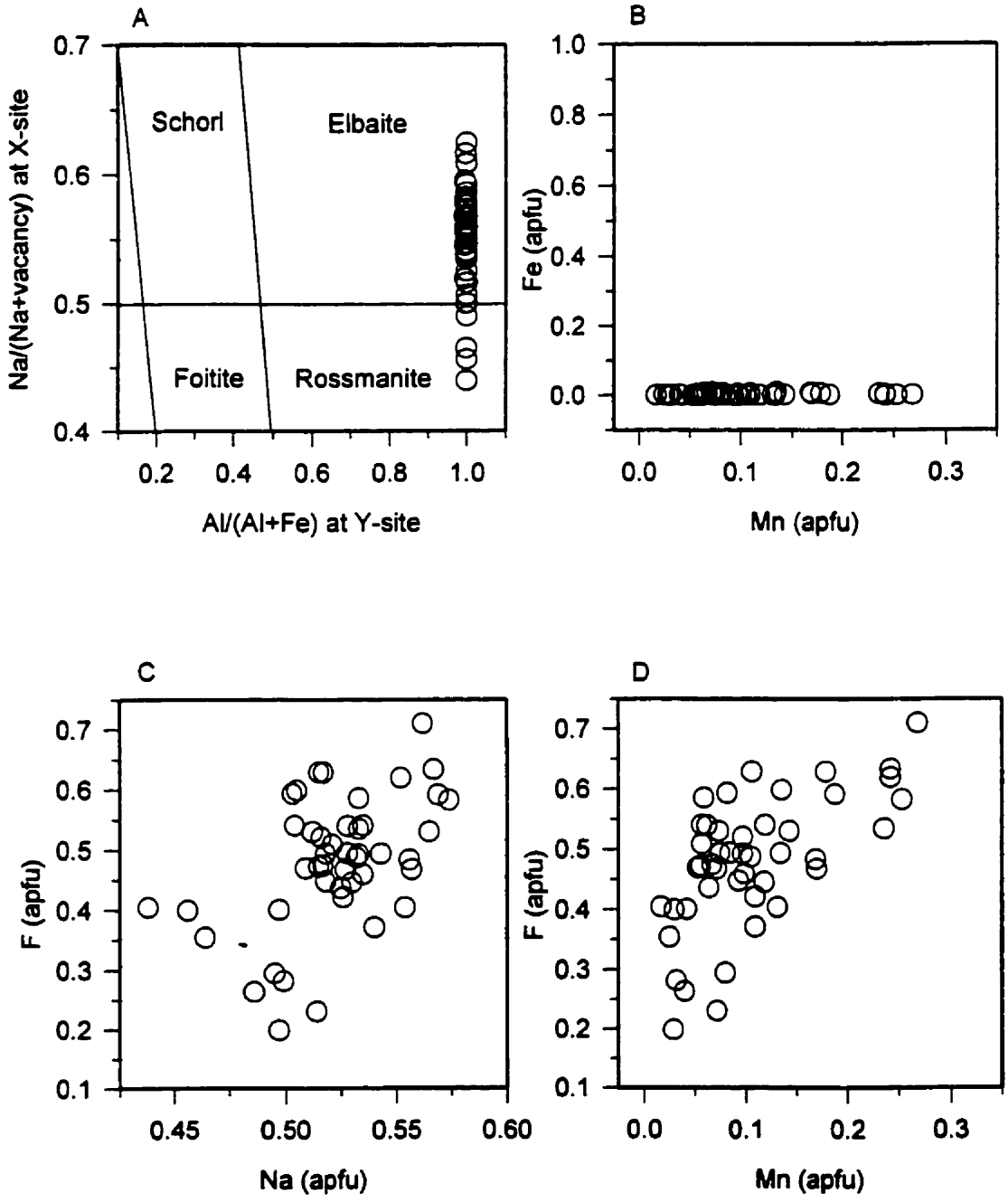

Figure 4.15. Tourmaline compositions in lepidolite pegmatites at Red Cross Lake.

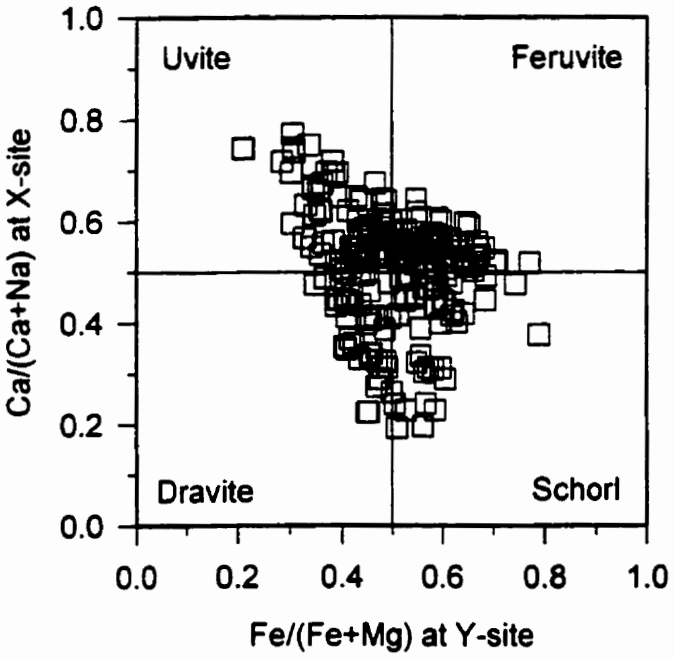

Figure 4.16. Tourmaline compositions in the exocontact of lepidolite pegmatites at Red Cross Lake.

CHAPTER 5

Tourmaline in petalite-subtype pegmatites

5.1. Petalite-subtype pegmatites

Petalite is a high-temperature low-pressure lithium aluminosilicate which breaks down to an intergrowth of spodumene + quartz (squi) at lower temperature (see Fig. 2.7) (London 1984). Petalite-subtype pegmatites are defined as pegmatites with petalite as the dominant Li-bearing mineral (Černý 1991a). They are commonly zoned with the petalite-bearing zone in the highly fractionated core or core margin. Miarolitic cavities are commonly absent in petalite-subtype pegmatites. The geology of the mines of the Tanco, Manitoba and Bikita, Zimbabwe pegmatites have been discussed in detail by Černý *et al.* (1998) and Cooper (1964), respectively. There are several similarities between them: the presence of aplitic albite zones with associated beryl, squi-rich zones and monomineralic lepidolite, pollucite and quartz zones. The pegmatites of the Separation Rapids pegmatite field and the Bikita pegmatite contain similar megacrystic petalite + microcline zones.

In the petalite-bearing zones of petalite-subtype pegmatites, megacrysts (10 cm - 13 m long) of petalite or spodumene + quartz pseudomorphs and blocky microcline-perthite, quartz, amblygonite and primary spodumene are dominant; albite, elbaite, blue fluorapatite, lithian muscovite, pollucite, beryl, lepidolite and triphylite-lithiophilite are subordinate; manganotantalite, microlite, cassiterite and wodginite are accessory (Smeds & Černý 1989, Černý & Lenton 1995, Černý *et al.* 1998). Petalite-subtype pegmatites, *e.g.* Tanco, Big Whopper, Separation Rapids pegmatite field, and Bikita, may contain

economic quantities of ceramic-grade petalite, spodumene and amblygonite-montebrasite, Ta (wodginite and tantalite), Cs (pollucite), Sn (cassiterite) and Rb (lepidolite and feldspar).

Examples of petalite-subtype pegmatites to be discussed in detail include Tanco, southeastern Manitoba, Utö, Sweden, and Marko's Pegmatite and Pegmatite #5 of the Separation Rapids pegmatite field, northwestern Ontario. Previously, tourmaline compositions from only one petalite-subtype pegmatite have been briefly discussed in the literature: Urubu, Brazil (Quéméneur *et al.* 1993, Marchetti 1997).

5.2. The Tanco pegmatite

5.2.1. General geology

The Tanco pegmatite is a zoned petalite-subtype pegmatite intruding amphibolite, and is located about 180 km east-northeast of Winnipeg, close to the Manitoba-Ontario boundary on the northwestern shore of Bernic Lake. The Tanco pegmatite is a member of the Bernic Lake pegmatite group, and is located in the Bird River Greenstone Belt of the Superior Province. The geology of the Tanco pegmatite has been described in detail by Černý *et al.* (1998) and references cited therein. The peak of regional metamorphism which predated emplacement of the pegmatite reached lower-amphibolite grade in the rocks immediately surrounding the pegmatite (Černý 1982). The Tanco pegmatite consists of an exomorphic halo and nine pegmatite zones: (10) border zone, (20) wall zone, (30) aplitic albite zone, (40) lower intermediate zone, (50) upper intermediate zone, (60) central intermediate zone, (70) quartz zone, (80) pollucite zone, and (90) lepidolite

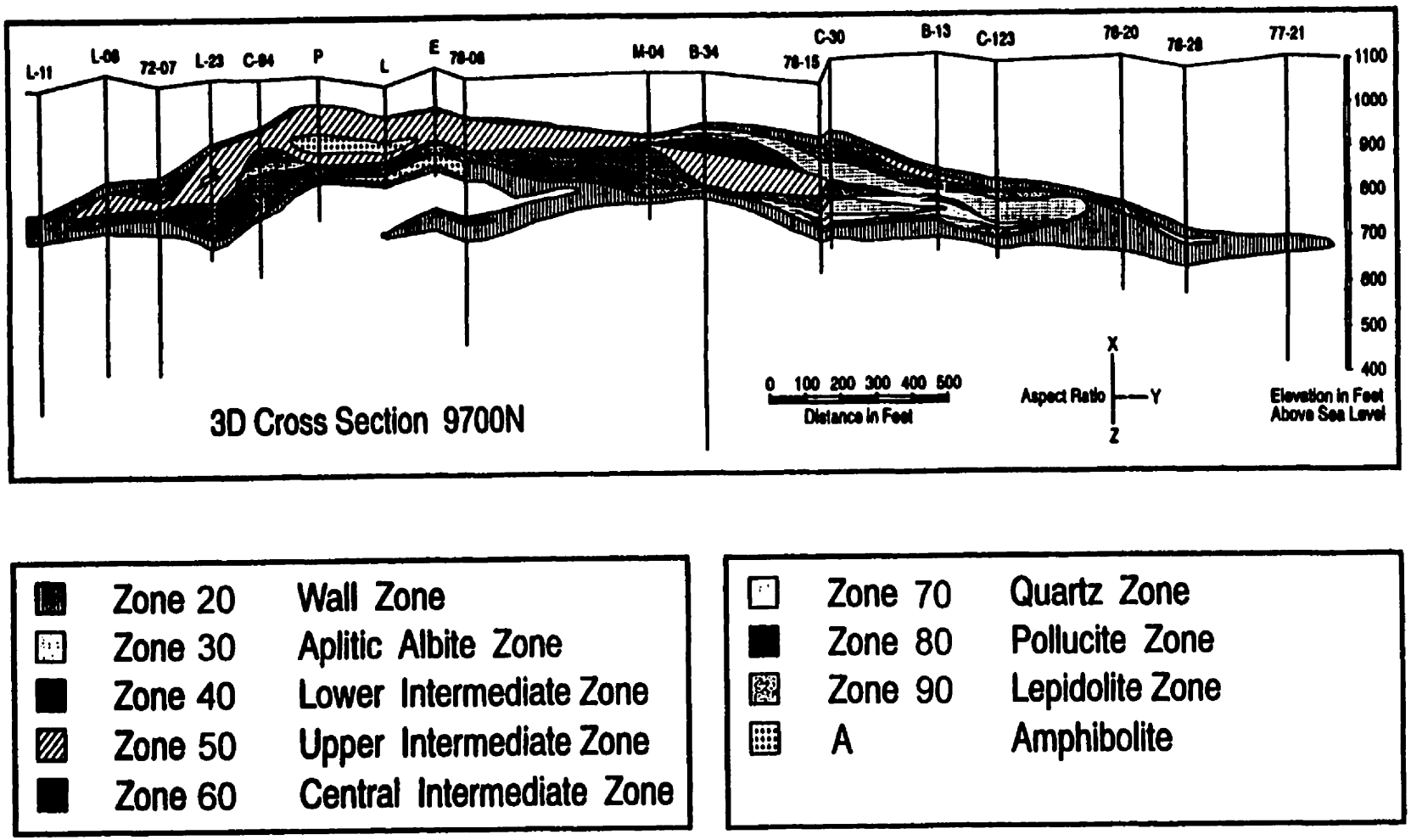

Figure 5.1. An east-west fence diagram through the Tanco pegmatite (modified from Stilling 1998).

Table 5.1. Zoning of the Tanco Pegmatite (modified from Černý *et al.* 1998).

Zone	Main constituents	Characteristic subordinate (accessory), and ((rare)) minerals	Textural and structural characteristics	Geochemically important major & (minor) elements
Exomorphic unit	biotite, tourmaline, holmquistite	(arsenopyrite)	fine-grained reaction rims and diffuse veins	K, Li, B (P,F)
(10) border zone	albite, quartz	tourmaline, apatite, (biotite) ((beryl, triphylite))	fine-grained layers	Na, (B,P,Be,Li)
(20) wall zone	albite, quartz, muscovite, Li-muscovite, microcline-perthite	beryl (tourmaline)	medium-grained, with giant K-feldspar crystals	K, Na(Li,Be,F)
(30) aplitic albite zone	albite, quartz (muscovite)	muscovite, Ta-oxide minerals*, beryl, (apatite, tourmaline, cassiterite) ((ilmentie, zircon, sulfides))	fine-grained undulating layers, fracture fillings, rounded blebs, diffuse veins	Na (Be,Ta,Sn,Zr,Hf,Ti)
(40) lower intermediate zone	microcline-perthite, albite, quartz, spodumene, amblygonite	Li-muscovite, lithiophilite ((lepidolite, petalite, Ta-oxide minerals))	medium- to coarse-grained inhomogeneous	K, Na, Li, P, F ((Ta))
(50) upper intermediate zone	spodumene, quartz, amblygonite	microcline-perthite, pollucite, lithiophilite (albite, Li-Muscovite), ((petalite, eucryptite, Ta-oxide minerals))	giant crystal size of major and most of the subordinate minerals	Li, P, F (K,Na,Cs,Ta)
(60) central intermediate zone	microcline-perthite quartz, albite, muscovite	beryl (Ta-oxide minerals), ((zircon, ilmenite, spodumene, sulfides lithiophilite, apatite, cassiterite))	medium- to coarse-grained	K(Na,Be,Ta,Sn,Zr,Hf,Ti)
(70) quartz zone	quartz	((spodumene, amblygonite))	monomineralic	Si (Li)
(80) pollucite zone	pollucite	quartz, spodumene ((petalite, muscovite, lepidolite, albite, microcline, apatite))	almost monomineralic	Cs (Li)
(90) lepidolite zone	Li-muscovite, lepidolite, microcline-perthite	albite, quartz, beryl, (Ta-oxide minerals, cassiterite), ((zircon))	fine-grained	Li,K,Rb,F (Na,Be,Ta,Sn, Zr,Hf,Ga)

*Underlined minerals occur in economic quantities in the zones indicated.

zone (Fig. 5.1, Table 5.1). The quartz, pollucite and lepidolite zones are monomineralic.

5.2.1.1. Primary crystallization of the Tanco pegmatite

Textural evidence indicates that the consolidation of the pegmatite proceeded from border zone (10) and wall zone (20) to lower and upper intermediate zones (40) and (50) (Černý *et al.* 1998). Zones (40) and (50) crystallized inward in their footwall and hangingwall segments, forming a shell-like concentric zone. The central intermediate zone (60), aplitic albite zone (30), lepidolite zone (90) and most of the quartz bodies (70) crystallized within this innermost concentric shell, the upper parts of which contain the pollucite zones (80) as a late but integral part. The pressure and temperature conditions of solidification, based on experimental petrology of Li-aluminosilicates (London 1984, 1986a) and on studies of fluid inclusions (London 1986a, Morgan & London 1987, Thomas & Spooner 1988a,b, Thomas *et al.* 1988, 1990) indicate a similar crystallization sequence (Fig. 5.2, Table 5.2).

Thomas *et al.* (1988, 1990) favour a near-isobaric process, whereas London (1984, 1986a) proposes a ~ 0.5 kbar decline in pressure during the main course of consolidation from the initial value of 3 kbar (Černý *et al.* 1998). Differences in interpretation of primary vs. secondary inclusions and other considerations lead the two groups of authors to different interpretations of the thermal regime. Thomas *et al.* (1988, 1990) propose a relatively rapid decrease in temperature during the main stages of consolidation (680 - ~300°C), and the temperature decreased to quite low levels in the near-final stages (265 °C). In contrast, London *et al.* (1984, 1986a) advocate a smaller

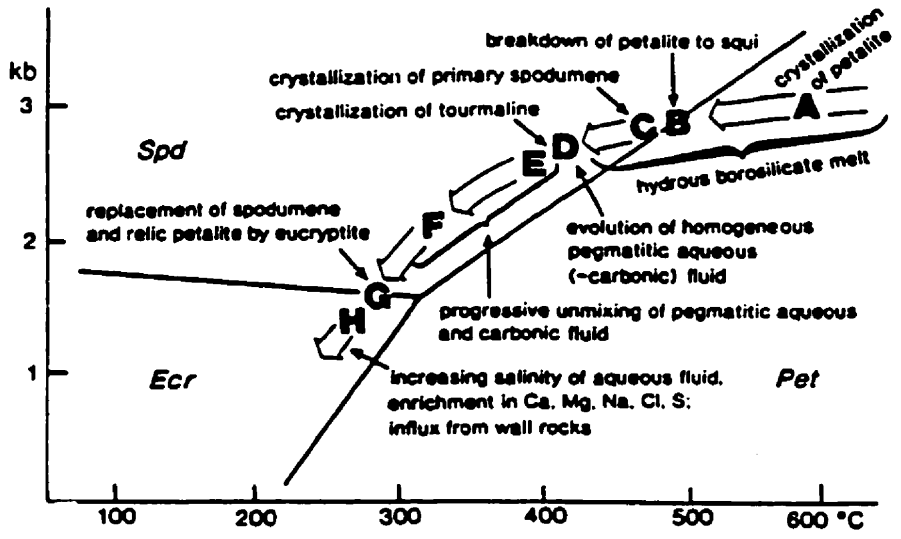

Figure 5.2. Evolution of the Tanco pegmatite melt, fluids and solid phases, based on stabilities of Li-aluminosilicates and studies of fluid inclusions (modified by Černý *et al.* 1998, from London 1986a, 1990).

Table 5.2. Crystallization history of the Tanco pegmatite (modified from Černý *et al.* 1998).

	Thomas *et al.* (1988, 90)		London (1986), Morgan & London (1987)	
(10) Border zone	680°C	2.9-2.7 kbar	700-600°C	~ 3 kbar
(20) Wall zone	600-500			
(40) Lower intermediate zone	475		600-500	3-2.8
(50) Upper intermediate zone	475		600-500	
(80) Pollucite zone	475		~ 500	~2.5
Pet → Spd + Qz inversion			475	~2.8
(60) Central intermediate zone	~320			
(30) Aplitic zone	316-291		470-420	
(70) Quartz zone	475-265			
(90) Lepidolite zone			~ 450	~2
Spd → Ecr + Qz inversion			~ 275	~1.5

temperature range for the main stages, including some of the late zones (~ 700 - 450 °C).

The presence of petalite, amblygonite, Rb-rich and Cs-bearing lepidolite, pink elbaite, manganotantalite and lithiophilite (81 - 92 mol % lithiophilite) in lower and upper intermediate zones (40) and (50) indicate that these zones are Li-rich and highly fractionated (Černý *et al.* 1998). There is a conspicuous lack of Li-bearing minerals in central intermediate zone (60) which is enclosed in the concentric shell of zones (40) and (50). The presence of greenish (Rb, Cs, Li)-poor muscovite, black tourmaline, ferrotapiolite and lithiophilite (77 mol % lithiophilite) in zone (60) indicates that zone (60) is Fe-enriched and, in some respects, less fractionated than zones (40) and (50).

In the eastern lobe of the pegmatite, aplitic albite zone (30) either forms sheet-like layers along the contacts of the wall zone (20) with overlying zones (60) and (70), or grades into zone (60) (Černý *et al.* 1998). In the western lobe, zone (30) is dispersed as a network within zone (60) and its contacts with zones (20) and (40). Some of the minerals in zone (30) (*i.e.*, greenish muscovite, curvilamellar lithian muscovite to lepidolite, black and green tourmaline) are slightly more fractionated than those in zone (60), whereas the oxide minerals in zone (60) are more fractionated than those in zone (30). Rare apatite, cassiterite, ilmenite, zircon and sulfides occur in zones (30) and (60).

5.2.1.2. Metasomatism and subsolidus processes in the Tanco pegmatite

The metasomatism of the wallrocks at Tanco has been studied in detail by Morgan and London (1987). The unaltered amphibolite consists of 54 vol% hornblende, 37 vol% plagioclase (An_{38}), 4 vol% ilmenite, 1 vol% apatite, and 4 vol% quartz, biotite, epidote,

titanite, garnet and chlorite. The texture of the unaltered amphibolite varies from medium-grained and weakly-foliated to very fine-grained, strongly foliated and gneissically banded. There are four types of alteration of the host rocks surrounding the Tanco pegmatite, in chronological order: (1) textural recrystallization, (2) B (± Li) metasomatism, (3) K-Rb-Cs-F (± Li) metasomatism and (4) propylitic alteration with concomitant influx of Li and CO_2. Holmquistite is present in all three metasomatic assemblages and served as a sink for Li. All metasomatic alteration took place at greenschist-facies conditions ($T \leq 500\text{-}550°C$, $P \leq 3$ kbar) (Morgan & London 1987).

The textural recrystallization is characterized by coarsening of hornblende and plagioclase and loss of foliation (Morgan & London 1987). The overall similarity of the recrystallized and unaltered amphibolite suggests that the recrystallization occurred during regional metamorphism preceding the pegmatite emplacement.

Boron (± Li) metasomatism is characterized by the alteration of hornblende + plagioclase ± biotite → tourmaline + quartz ● titanite ± apatite ± calcite ± holmquistite (Morgan & London 1987). The tourmaline aureole is 7 to 10 mm wide at the pegmatite-amphibolite contact, but locally penetrates up to 3 m into the host rock along fractures or small granitic offshoots. It may completely digest, in conjunction with biotite, small rafts of amphibolite engulfed by the pegmatite. Tourmalization is the most pervasive in the footwall where the voluminous aplitic albite zone (30) occurs in the pegmatite near the lower wall zone (20) and in the hangingwall above the pollucite zone (80). The common coexistence of metasomatic biotite and tourmaline and the complex cross-cutting relationships between the two metasomatic assemblages indicate that B (± Li)

metasomatism and K-Rb-Cs-F (± Li) metasomatism may have been nearly coeval at approximately 450 °C (Morgan & London 1987).

K-Rb-Cs-F (± Li) metasomatism is characterized by the alteration of hornblende ± plagioclase → magnesian biotite ± apatite ± holmquistite (Morgan & London 1987). Arsenopyrite and monazite are common accessory minerals. The biotite aureole is commonly less than 3 m thick and locally pentrates 4.5 m into the host rock along fractures or foliation surfaces. Biotitization is most pervasive in host rock where the microcline-rich central intermediate zone (60) and lower intermediate zone (40) occur next to wall zone (20).

The propylitic alteration with concomitant influx of Li and CO_2 is characterized by the alteration of hornblende + plagioclase to epidote + chlorite + titanite + calcite + clay and forms an aureole 2 to 9 m wide (Morgan and London 1987). All major phases in the propylitic assemblage, including holmquisitite, are low in Na, K, Rb, Cs and F.

Endomorphism occurs in border zone (10) and wall zone (20), close to amphibolite in wallrock or xenoliths (Černý *et al.* 1998). The presence of accessory (magnesian) biotite, black Mg-bearing tourmaline, andesine close to contacts with wallrock, and dark-grey Mg-bearing lithiophilite (52-68 mol % lithiophilite) which rims bioititized xenoliths of amphibolite in zone (10), indicate an influx of Mg and Ca into the pegmatite from the mafic wallrock. Modest contents of Ti in biotite, Ti and Sc in the (Nb, Ta)-oxide minerals, and minor Ti in black tourmaline, occur in zone (10), indicating contamination by fluids derived from the mafic wallrock.

Internal subsolidus processes caused petalite to break down to spodumene +

quartz and spodumene to eucryptite + quartz at Tanco (Fig. 5.2) (Černý *et al.* 1998). Subsolidus alteration produced secondary minerals, *e.g.*, K-feldspar to albite, muscovite and lepidolite; Li-aluminosilicates to muscovite, cookeite, adularia and calcite; elbaite to muscovite and lepidolite.

5.2.2. Tourmaline at Tanco

At Tanco, tourmaline occurs in the border zone (10), wall zone (20), lower and upper intermediate zones (40) and (50), central intermediate zone (60), aplitic albite zone (30), and the exocontact.

Zone (10): Fine tourmaline needles in border zone (10) range from black to brown to green, and are commonly zoned (but may be homogeneous). The tourmaline is enclosed in aplitic albite and quartz and may contain albite + quartz inclusions. Tourmaline and minor green prismatic beryl are perpendicular to the pegmatite contact.

Zone (20): Black to brown tourmaline occurs in 'leopard rock' (round brown quartz enclosed in pink cleavelandite network) and in granitic albite + K-feldspar + quartz in wall zone (20). The euhedral tourmaline has a wide range in size from medium (< 3 mm) to comb-textured and very coarse (≤ 24 cm x 4 cm), and is commonly zoned. The coarse to very coarse tourmaline may be crosscut by K-feldspar + quartz veinlets. Tourmaline commonly contains albite inclusions.

Green fine (< 1 mm) to coarse (< 5 mm) tourmaline needles occur in aplitic albite pods in zone (20), and may be zoned with a brown core and a green rim.

Zones (40) and (50): The lower and upper intermediate zones (40) and (50)

contain accessory euhedral zoned pink tourmaline and rare tourmaline with green cores and pink rims. Pink tourmaline ranges in size from coarse to very coarse columanr to fibrous (1 - 18 cm long) and is commonly zoned with cloudy pale-pink cores and clear pink rims. Rubellite (50 vol%) enclosed in albite forms parallel aggregates of very coarse columnar crystals (6 - 18 cm x 2 - 5 mm) surrounded by coarse (1 - 3 cm long) radiating needles and minor 1.5 cm pods of fine-grained lepidolite. Tourmaline enclosed in purple curvilamellar (Cs, Rb)-bearing lepidolite is dark pink to red. Zoned pink tourmaline enclosed in pollucite is columnar (6 cm x 1 cm) and contains K-feldspar + pollucite veinlets. Pink patchy-zoned tourmaline enclosed in amblygonite is associated with fine-grained F-rich topaz, to date the only occurrence of this mineral of this mineral recorded at Tanco.

Pink tourmaline in zones (40) and (50) is commonly altered to mica. Rubellite enclosed in fine-grained white mica is commonly completely pseudomorphed by medium-grained pale-purple lepidolite with the basal plane of the lepidolite perpendicular to the *c*-axis of the tourmaline. Some very coarse columns ($\leq$ 12 cm long) are zoned parallel to the *c*-axis and consist of pink tourmaline at one end, a narrow zone of very fine-grained green mica, a narrow zone (2 mm) of blue tourmaline and very fine-grained green mica at the other end.

Zone (60): Central intermediate zone (60) contains very coarse-grained (< 4 cm long) black to brown tourmaline with an occasional thin green rim.

Zone (30): Black-to-brown and green zoned tourmaline occurs in aplitic albite zone (30). It is enclosed in albite and forms medium (1-3 mm long) needles, whereas

tourmaline in contact with coarse-grained K-feldspar is coarser (5 mm long).

Black-to-brown euhedral tourmaline occurs in the biotitized amphibolite exocontact and xenoliths. In the exocontact, tourmaline ranges from fine- to coarse-grained (0.3-2.0 cm) and occurs as radiating needles perpendicular to the pegmatite contact. In xenoliths, the coarse-grained tourmaline (1.0-2.5 cm) occurs as columns perpendicular to the pegmatite contact and enclosed in very fine-grained brown biotite. Tourmaline may be homogeneous or zoned, and may be cross-cut by carbonate veinlets postdating the tourmaline. In xenoliths, tourmaline is commonly associated with rather abundant arsenopyrite and with minor calcite, K-feldspar, albite, quartz and apatite.

5.2.2.1. Composition of primary tourmaline at Tanco

Based on compositional zoning within individual tourmaline crystals (Table 5.3), tourmaline compositions at Tanco evolves through the following crystallization sequence from zone (10) to (20) to (40) and (50): (± foitite-schorl, schorl-foitite) → Al-rich schorl → schorl → schorl-elbaite → elbaite-schorl → Fe-rich elbaite → Mn-bearing elbaite → rossmanite-elbaite → elbaite-rossmanite → (± Ca-bearing elbaite, Ca-bearing elbaite-rossmanite) (Fig. 5.3) (Tables 5.4-5.7). A similar crystallization sequence occurs from zone (60) to zone (30): foitite-schorl → (± schorl-foitite) → schorl-elbaite → elbaite-schorl → Fe-rich elbaite (Fig. 5.3e) (Table 5.8).

This crystallization sequence can also be seen in the tourmaline compositions for each pegmatite zone (Fig. 5.3). Black-to-brown and green tourmalines in zones (10) and (20) have a similar compositional range, from foitite-schorl to Fe-rich elbaite (Fig. 5.3f).

TABLE 5.3. COMPOSITIONAL ZONING IN TOURMALINE AT TANCO

pegmatite zone	sample number	compositional zones
zone 10	TTC27-3	green schorl-foitite core, elbaite-schorl zone, Fe-rich elbaite rim
	TTC30-3	dark-green Al-rich schorl core, schorl zone, schorl-elbaite rim
	TTC31-3	brown Al-rich schorl core, schorl-elbaite zone, elbaite-schorl zone, Fe-rich elbaite rim
	TTC7-2	green schorl-elbaite core, elbaite-schorl zone, Fe-rich elbaite rim
	TTC36-1	brown primary Mg-bearing elbaite-schorl core, elbaite-schorl rim
zone 20	TTC24-2	brown Al-rich schorl core, schorl-elbaite zone, elbaite-schorl rim
	TTC11-1	brown schorl-elbaite core, green elbaite-schorl rim
	TTC21-1	green elbaite-schorl core, Fe-rich elbaite rim
	TTC8-2	dark brown Mg-bearing elbaite-schorl core, elbaite-schorl rim
zone 40 + 50	TTC40	green elbaite-schorl core, pink Mn-bearing elbaite rim
	TTC49	dark-green core Fe-rich elbaite, Mn-bearing elbaite rim
	common	cloudy pale-pink rossmanite-elbaite core, clear dark-pink elbaite-rossmanite rim
	common	pink rossmanite-elbaite core, Ca-bearing elbaite-rossmanite rim
	TTC41	pink-red Ca-bearing elbaite core, elbaite-rossmanite rim
	TTC50-3	patchy pink rossmanite-elbaite base, blue Fe-rich elbaite cap, above cap - tourmaline pseudomorphed by green fine-grained mica
zone 60	TTC 3-3	black foitite-schorl core, schorl-elbaite rim
zone 30	TTC19-2	brown primary Mg-bearing elbaite-schorl core, schorl-elbaite zone, elbaite-schorl rim
exocontact	TTC37-2	brown Ca-rich schorl-dravite core, feruvite-schorl zone, Ca-bearing schorl-dravite zone, Ca-bearing elbaite-schorl-dravite rim

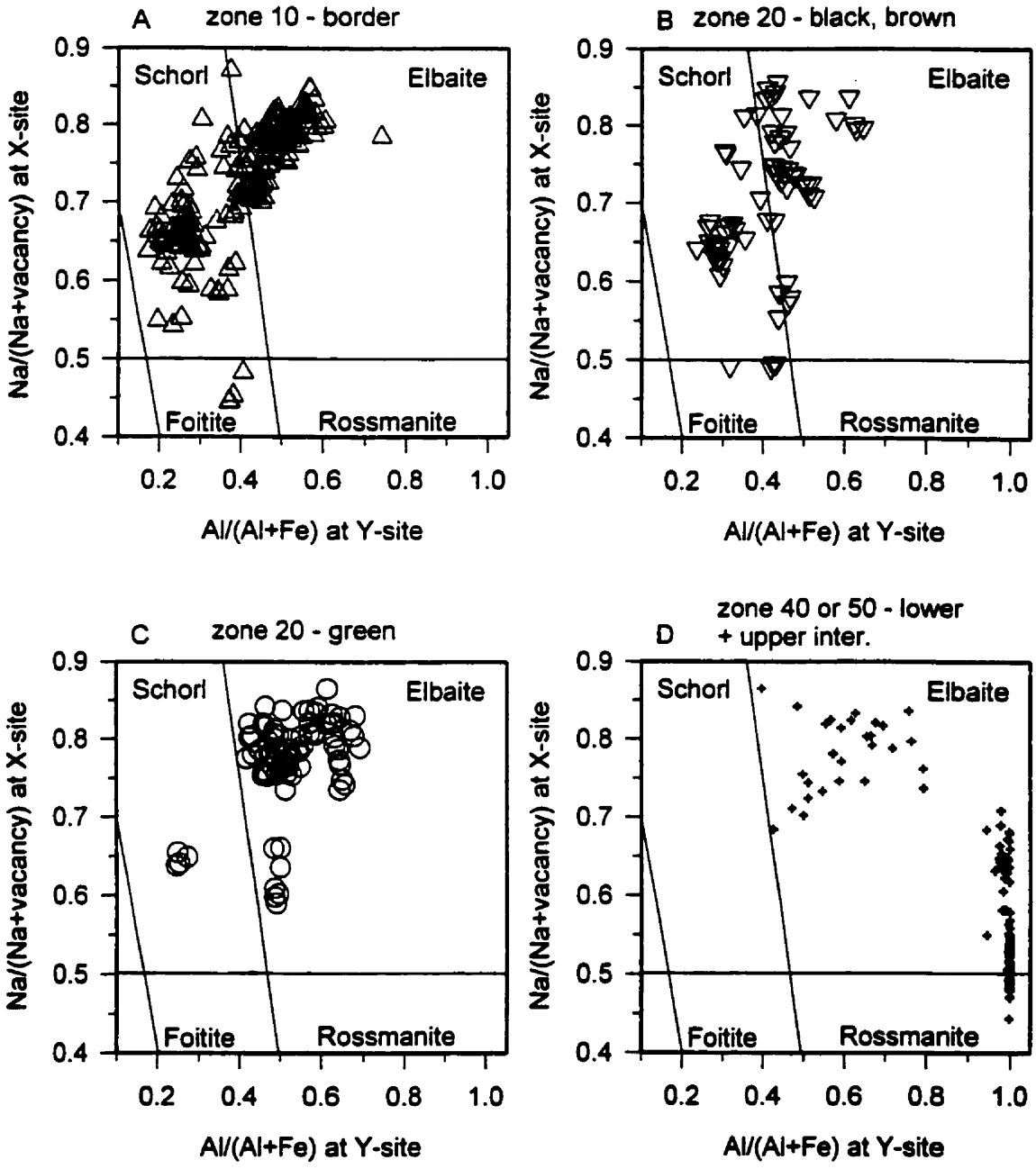

Figure 5.3. Tourmaline compositions from pegmatite zones (10), (20), (40) and (50) at Tanco.

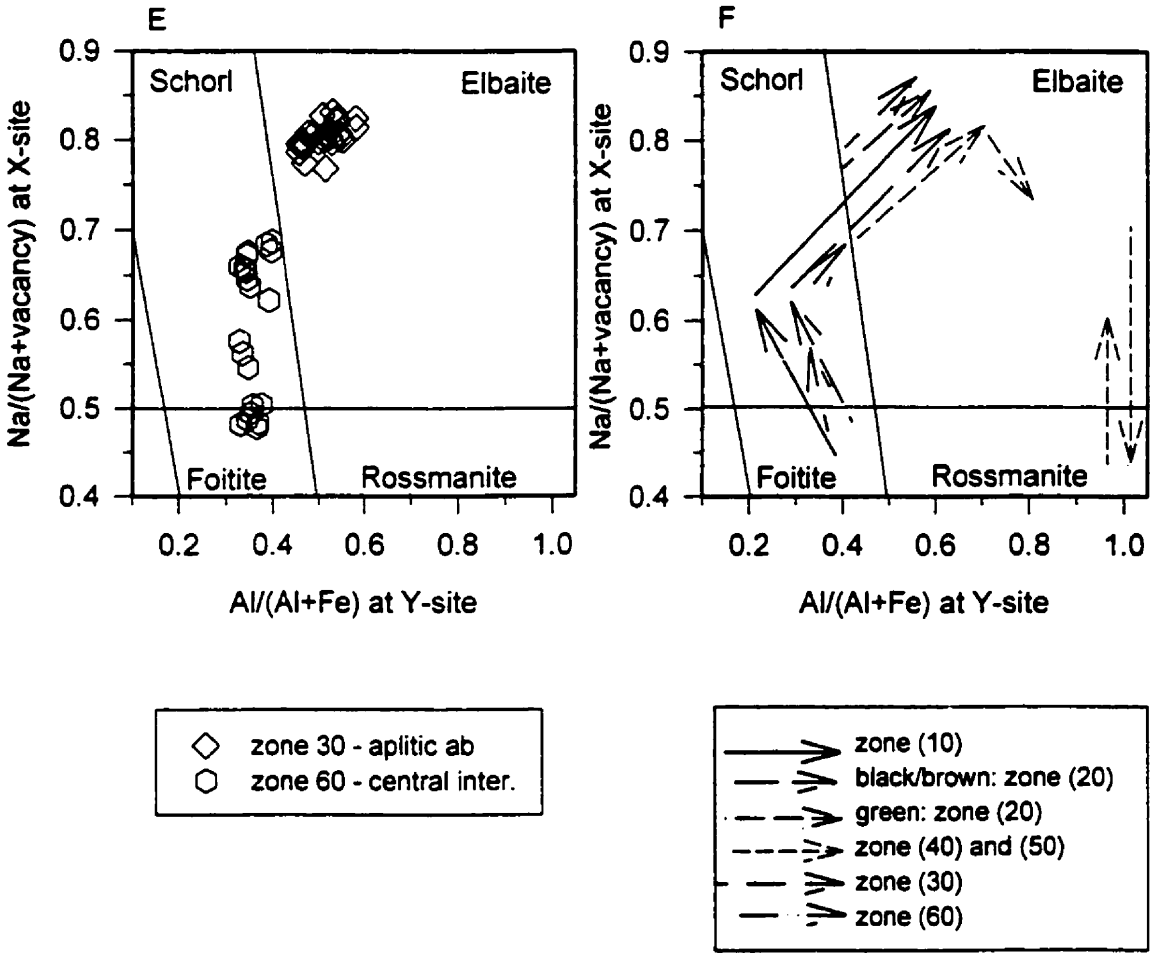

Figure 5.3. (E) Tourmaline compositions from pegmatite zones (30) and (60) at Tanco. (F) General compositional trend of tourmaline for each pegmatite zone.

TABLE 5.4. REPRESENTATIVE COMPOSITIONS OF TOURMALINE (WT%) IN ZONE (10) OF THE TANCO PEGMATITE

	1	2	3	4	5	6	7	8	9
SiO_2	35.60	35.60	34.80	35.60	35.00	37.20	36.50	34.30	36.70
TiO_2	0.17	0.27	0.40	0.73	0.43	0.31	0.14	0.75	0.68
B_2O_3*	10.40	10.30	10.21	10.30	10.34	10.62	10.61	10.16	10.62
Al_2O_3	35.20	33.20	33.20	32.30	34.50	35.00	36.60	32.10	34.30
MgO	0.04	0.37	0.24	0.45	0.62	0.20	0.18	1.73	1.55
CaO	0.00	0.00	0.05	0.06	0.08	0.00	0.06	0.13	0.08
MnO	0.55	0.31	0.35	0.28	0.29	0.11	0.74	0.18	0.36
FeO	11.80	13.80	13.60	14.10	11.50	8.03	6.03	13.40	8.94
ZnO	0.50	0.30	0.39	0.31	0.34	0.00	0.33	0.20	0.24
Li_2O*	0.45	0.36	0.38	0.44	0.56	1.60	1.40	0.23	0.94
Na_2O	1.36	1.65	1.91	1.93	1.99	2.78	2.63	2.17	2.43
H_2O*	3.45	3.37	3.26	3.35	3.22	3.18	3.04	3.25	3.24
F	0.30	0.39	0.56	0.43	0.74	1.03	1.31	0.54	0.89
O=F	-0.13	-0.16	-0.24	-0.18	-0.31	-0.43	-0.55	-0.23	-0.37
Total	99.69	99.76	99.11	100.10	99.30	99.63	99.02	98.91	100.60
Formulae normalized to 31 anions									
T -Si	5.95	6.01	5.93	6.01	5.88	6.09	5.98	5.87	6.01
Al	0.05	0.00	0.07	0.00	0.12	0.00	0.02	0.13	0.00
B	3.00	3.00	3.00	3.00	3.00	3.00	3.00	3.00	3.00
Z -Al	6.00	6.00	6.00	6.00	6.00	6.00	6.00	6.00	6.00
Y -Al	0.88	0.60	0.59	0.43	0.71	0.75	1.05	0.34	0.62
Ti	0.02	0.03	0.05	0.09	0.05	0.04	0.02	0.10	0.08
Mg	0.01	0.09	0.06	0.11	0.16	0.05	0.04	0.44	0.38
Mn	0.08	0.04	0.05	0.04	0.04	0.01	0.10	0.02	0.05
Fe^{2+}	1.65	1.95	1.94	1.99	1.62	1.10	0.83	1.92	1.22
Zn	0.06	0.04	0.05	0.04	0.04	0.00	0.04	0.03	0.03
Li	0.30	0.25	0.26	0.30	0.38	1.05	0.92	0.15	0.62
$\sum Y$	3.00	3.00	3.00	3.00	3.00	3.00	3.00	3.00	3.00
X -Ca	0.00	0.00	0.01	0.01	0.01	0.00	0.01	0.02	0.01
Na	0.44	0.54	0.63	0.63	0.65	0.88	0.84	0.72	0.77
□	0.56	0.46	0.36	0.36	0.34	0.12	0.15	0.26	0.22
OH	3.84	3.79	3.70	3.77	3.61	3.47	3.32	3.71	3.54
F	0.16	0.21	0.30	0.23	0.39	0.53	0.68	0.29	0.46

*B_2O_3, Li_2O and H_2O calculated by stoichiometry; B = 3 *apfu*, Li = 15 - $\sum T + Z + Y$ and OH+F = 4 *apfu*.

(1) black foitite-schorl, sample TTC6-1; (2) dark green schorl-foitite, sample TTC30-2; (3) brown Al-rich schorl core, sample TTC31-3; (4) dark green schorl, sample TTC30-2; (5) brown schorl-elbaite, sample TTC34-3; (6) brown elbaite-schorl, sample TTC31-2; (7) brown Fe-rich elbaite, sample TTC36-2; (8) black Mg-bearing schorl, sample TTC26-1; and (9) brown Mg-bearing elbaite-schorl core, sample TTC36-1.

TABLE 5.5. REPRESENTATIVE COMPOSITIONS OF BLACK TO BROWN TOURMALINE (WT%) IN ZONE (20) AT TANCO

	1	2	3	4	5	6	7	8
SiO_2	36.10	35.90	34.60	35.30	36.70	37.20	35.10	36.70
TiO_2	0.20	0.25	0.22	0.16	0.28	0.11	0.72	0.78
B_2O_3*	10.56	10.53	10.26	10.35	10.57	10.75	10.19	10.54
Al_2O_3	36.10	36.10	34.10	34.60	35.50	37.10	31.40	33.90
MgO	0.01	0.02	0.17	0.19	0.03	0.13	1.45	1.44
CaO	0.00	0.00	0.09	0.07	0.00	0.25	0.08	0.00
MnO	0.56	0.44	0.31	0.29	0.10	1.38	0.21	0.14
FeO	10.60	10.20	13.50	11.90	7.97	4.96	14.00	8.54
ZnO	0.54	0.56	0.35	0.35	0.26	0.00	0.16	0.19
Li_2O*	0.64	0.72	0.38	0.60	1.42	1.58	0.29	1.12
Na_2O	1.52	1.70	1.95	1.96	2.69	2.56	2.14	2.42
H_2O*	3.48	3.38	3.25	3.25	3.11	3.10	3.32	3.23
F	0.35	0.54	0.62	0.67	1.14	1.29	0.41	0.86
O=F	-0.15	-0.23	-0.26	-0.28	-0.48	-0.54	-0.17	-0.36
total	100.51	100.11	99.54	99.41	99.29	99.87	99.30	99.50
Formulae normalized to 31 anions								
T -Si	5.94	5.93	5.86	5.93	6.03	6.01	5.98	6.05
Al	0.06	0.07	0.14	0.07	0.00	0.00	0.02	0.00
B	3.00	3.00	3.00	3.00	3.00	3.00	3.00	3.00
Z -Al	6.00	6.00	6.00	6.00	6.00	6.00	6.00	6.00
Y -Al	0.95	0.95	0.67	0.77	0.88	1.07	0.29	0.59
Ti	0.02	0.03	0.03	0.02	0.03	0.01	0.09	0.10
Mg	0.00	0.00	0.04	0.05	0.01	0.03	0.37	0.35
Mn	0.08	0.06	0.05	0.04	0.01	0.19	0.03	0.02
Fe^{2+}	1.46	1.41	1.91	1.67	1.10	0.67	2.00	1.18
Zn	0.07	0.07	0.04	0.04	0.03	0.00	0.02	0.02
Li	0.42	0.48	0.26	0.41	0.94	1.03	0.20	0.74
$\sum Y$	3.00	3.00	3.00	3.00	3.00	3.00	3.00	3.00
X -Ca	0.00	0.00	0.02	0.01	0.00	0.04	0.02	0.00
Na	0.49	0.54	0.64	0.64	0.86	0.80	0.71	0.77
□	0.51	0.46	0.34	0.35	0.14	0.16	0.27	0.23
OH	3.82	3.72	3.67	3.64	3.41	3.34	3.78	3.55
F	0.18	0.28	0.33	0.36	0.59	0.66	0.22	0.45

*B_2O_3, Li_2O and H_2O calculated by stoichiometry; B = 3 *apfu*, Li = 15 - $\sum T + Z + Y$ and OH+F = 4 *apfu*.

(1) brown foitite-schorl, sample TTC25-1; (2) brown schorl-foitite, sample TTC25-1; (3) brown Al-rich schorl core, sample TTC24-2; (4) brown schorl-elbaite core, sample TTC11-1; (5) brown elbaite-schorl, sample TTC24-3; (6) black Fe-rich elbaite, sample TTC10-2; (7) black Mg-bearing schorl, sample TTC16-1; and (8) dark brown Mg-bearing elbaite-schorl core, sample TTC8-2.

TABLE 5.6. REPRESENTATIVE COMPOSITIONS OF GREEN TOURMALINE (WT%) IN ZONE (20) AT TANCO

	1	2	3
SiO_2	35.20	37.30	36.20
TiO_2	0.33	0.23	0.37
B_2O_3*	10.26	10.74	10.69
Al_2O_3	33.10	36.40	37.40
MgO	0.20	0.18	0.00
CaO	0.08	0.00	0.15
MnO	0.35	0.58	1.01
FeO	13.90	7.07	5.92
ZnO	0.46	0.00	0.47
Li_2O*	0.39	1.46	1.38
Na_2O	1.90	2.55	2.62
H_2O*	3.29	3.20	3.18
F	0.53	1.06	1.08
O=F	-0.22	-0.45	-0.45
Total	99.77	100.32	100.02
Formulae normalized to 31 anions			
T -Si	5.96	6.04	5.89
Al	0.04	0.00	0.11
B	3.00	3.00	3.00
Z -Al	6.00	6.00	6.00
Y -Al	0.57	0.94	1.05
Ti	0.04	0.03	0.04
Mg	0.05	0.04	0.00
Mn	0.05	0.08	0.14
Fe^{2+}	1.97	0.96	0.81
Zn	0.06	0.00	0.06
Li	0.26	0.95	0.90
$\sum Y$	3.00	3.00	3.00
X -Ca	0.02	0.00	0.03
Na	0.62	0.80	0.83
□	0.36	0.20	0.14
OH	3.72	3.46	3.45
F	0.28	0.54	0.55

*B_2O_3, Li_2O and H_2O calculated by stoichiometry; B = 3 *apfu*, Li = 15 - $\sum T + Z + Y$ and OH+F = 4 *apfu*.

(1) Al-rich schorl, sample TTC24-1; (2) elbaite-schorl rim, sample TTC11-1; and (3) Fe-rich elbaite, sample TTC21-2.

TABLE 5.7. REPRESENTATIVE COMPOSITIONS OF TOURMALINE (WT%) IN ZONE (40) AND (50) AT TANCO

	1	2	3	4	5	6	7	8
	core	rim		core	rim	core	rim	
SiO_2	36.20	38.00	38.39	38.30	38.30	39.40	38.80	38.10
TiO_2	0.09	0.00	0.00	0.00	0.00	0.00	0.00	0.00
B_2O_3*	10.48	11.11	10.97	11.24	11.20	11.32	11.21	11.07
Al_2O_3	35.50	41.10	38.14	43.30	42.50	41.90	41.50	40.50
MgO	0.02	0.00	0.00	0.00	0.00	0.00	0.00	0.00
CaO	0.05	0.13	0.20	0.00	0.22	0.44	0.65	0.94
MnO	0.64	2.52	0.40	0.00	0.18	0.29	0.52	1.51
FeO	9.04	0.11	4.22	0.00	0.00	0.00	0.00	0.00
ZnO	0.41	0.00	0.00	0.00	0.00	0.00	0.00	0.00
Li_2O*	0.98	1.80	1.98	1.91	2.02	2.23	2.16	2.09
Na_2O	2.11	2.06	2.38	1.54	1.77	1.53	1.63	1.78
H_2O*	3.06	3.33	3.26	3.60	3.65	3.43	3.29	3.32
F	1.18	1.06	1.11	0.59	0.46	1.01	1.22	1.05
O=F	-0.50	-0.45	-0.47	-0.25	-0.19	-0.43	-0.51	-0.44
Total	99.26	100.77	100.58	100.23	100.11	101.12	100.47	99.92
Formulae normalized to 31 anions								
T -Si	6.00	5.94	6.09	5.92	5.94	6.05	6.02	5.98
Al	0.00	0.06	0.00	0.08	0.06	0.00	0.00	0.02
B	3.00	3.00	3.00	3.00	3.00	3.00	3.00	3.00
Z -Al	6.00	6.00	6.00	6.00	6.00	6.00	6.00	6.00
Y -Al	0.94	1.52	1.13	1.81	1.72	1.58	1.58	1.48
Ti	0.01	0.00	0.00	0.00	0.00	0.00	0.00	0.00
Mg	0.01	0.00	0.00	0.00	0.00	0.00	0.00	0.00
Mn	0.09	0.34	0.05	0.00	0.02	0.04	0.07	0.20
Fe^{2+}	1.25	0.01	0.56	0.00	0.00	0.00	0.00	0.00
Zn	0.05	0.00	0.00	0.00	0.00	0.00	0.00	0.00
Li	0.65	1.13	1.26	1.19	1.26	1.38	1.35	1.32
$\sum Y$	3.00	3.00	3.00	3.00	3.00	3.00	3.00	3.00
X -Ca	0.01	0.02	0.03	0.00	0.04	0.07	0.11	0.16
Na	0.68	0.63	0.73	0.46	0.53	0.46	0.49	0.54
□	0.31	0.35	0.24	0.54	0.43	0.47	0.40	0.30
OH	3.38	3.48	3.44	3.71	3.77	3.51	3.40	3.48
F	0.62	0.52	0.56	0.29	0.23	0.49	0.60	0.52

*B_2O_3, Li_2O and H_2O calculated by stoichiometry; B = 3 *apfu*, Li = 15 - $\sum T + Z + Y$ and OH+F = 4 *apfu*.

(1) green elbaite-schorl core, sample TTC40-2; (2) pink Mn-bearing elbaite rim, sample TTC40-1; (3) blue Fe-rich elbaite rim, sample TTC50-3; (4) cloudy pale pink rossmanite-elbaite core, sample TTC44; (5) clear dark pink elbaite-rossmanite rim, sample TTC44; (6) green rossmanite-elbaite core, sample TTC39-2; (7) pink Ca-bearing elbaite-rossmanite rim, sample TTC39-1; and (8) pink to purple Ca-bearing elbaite core, sample TTC41-3.

TABLE 5.8. REPRESENTATIVE COMPOSITIONS OF TOURMALINE (WT%) IN ZONE (60) AND (30) AT TANCO

	1	2	3	4	5	6	7
SiO_2	35.50	35.60	35.20	36.30	36.90	37.00	36.50
TiO_2	0.19	0.29	0.43	0.36	0.05	0.00	0.59
B_2O_3*	10.40	10.43	10.36	10.56	10.73	10.72	10.55
Al_2O_3	35.10	34.90	34.90	34.90	36.90	37.20	34.30
MgO	0.03	0.05	0.02	0.50	0.20	0.00	1.33
CaO	0.00	0.00	0.06	0.09	0.07	0.07	0.05
MnO	0.43	0.34	0.41	0.28	0.29	1.11	0.18
FeO	12.20	12.50	11.10	11.00	7.62	5.93	8.85
ZnO	0.53	0.30	0.51	0.27	0.12	0.00	0.14
Li_2O*	0.44	0.50	0.67	0.76	1.29	1.44	1.02
Na_2O	1.45	1.66	1.86	2.09	2.59	2.59	2.47
H_2O*	3.53	3.41	3.41	3.38	3.20	3.18	3.16
F	0.12	0.39	0.35	0.56	1.07	1.09	1.01
O=F	-0.05	-0.16	-0.15	-0.24	-0.45	-0.46	-0.43
Total	99.87	100.21	99.13	100.81	100.58	99.87	99.72
Formulae normalized to 31 anions							
T -Si	5.93	5.93	5.91	5.97	5.98	6.00	6.02
Al	0.07	0.07	0.09	0.03	0.02	0.00	0.00
B	3.00	3.00	3.00	3.00	3.00	3.00	3.00
Z -Al	6.00	6.00	6.00	6.00	6.00	6.00	6.00
Y -Al	0.84	0.79	0.81	0.74	1.02	1.11	0.66
Ti	0.02	0.04	0.05	0.05	0.01	0.00	0.07
Mg	0.01	0.01	0.01	0.12	0.05	0.00	0.33
Mn	0.06	0.05	0.06	0.04	0.04	0.15	0.02
Fe^{2+}	1.70	1.74	1.56	1.52	1.03	0.80	1.22
Zn	0.07	0.04	0.06	0.03	0.01	0.00	0.02
Li	0.30	0.33	0.45	0.50	0.84	0.94	0.68
∑Y	3.00	3.00	3.00	3.00	3.00	3.00	3.00
X -Ca	0.00	0.00	0.01	0.02	0.01	0.01	0.01
Na	0.47	0.54	0.61	0.67	0.81	0.81	0.79
□	0.53	0.46	0.38	0.31	0.18	0.18	0.20
OH	3.94	3.79	3.81	3.71	3.45	3.44	3.47
F	0.06	0.21	0.19	0.29	0.55	0.56	0.53

*B_2O_3, Li_2O and H_2O calculated by stoichiometry; B = 3 *apfu*, Li = 15 - $\sum T + Z + Y$ and OH+F = 4 *apfu*.

Compositions 1-3 are from zone (60) and 4-6 are from zone (30). (1) black foitite-schorl core, sample TTC3-3; (2) black schorl-foitite, sample TTC2-2; (3) black schorl-elbaite rim of (1), sample TTC3-3; (4) brown schorl-elbaite, sample TTC19-1; (5) black elbaite-schorl, sample TTC20-1; (6) green and brown Fe-rich elbaite, sample TTC1-2; (7) brown Mg-bearing elbaite-schorl core, sample TTC19-2.

Black-to-brown tourmaline in the granitic part of zone (20) is foitite-schorl to elbaite-schorl, whereas the green tourmaline in aplitic pods in zone (20) is slightly more fractionated: elbaite-schorl to Fe-rich elbaite. The pink and rare green tourmalines in zones (40) and (50) are more fractionated than those in the rest of the pegmatite, with a compositional range from Fe-rich elbaite to Ca-bearing elbaite-rossmanite. Tourmaline in zone (60) has a compositional range from black foitite-schorl to schorl-elbaite, and in zone (30) has a range from black-to-brown and green schorl-elbaite to Fe-rich elbaite, similar to the compositional range of foitite-schorl to Fe-rich elbaite in zones (10) and (20) (Fig. 5.3f).

In Tanco tourmaline, the dominant substitution at the *X*-site is Na ⇔ □ (Fig. 5.4). The tourmaline in zone (10) and black-to-brown tourmaline in zone (20) have a similar wide range in Na content (from 0.44 - 0.87 *apfu* Na at the *X*-site); green tourmaline in zone (20) is slightly more Na-enriched (with 0.60 - 0.84 *apfu* Na). In zones (40) and (50), □-rich tourmaline (elbaite-rossmanite and rossmanite-elbaite) is abundant, but there is still a wide range in Na content: 0.45 - 0.86 *apfu* Na. Most tourmaline at Tanco contains almost no Ca, except for that in zones (40) and (50) where late-stage elbaite-rossmanite and elbaite contain up to 0.16 *apfu* Ca at the *X*-site (Table 5.7, composition 8). The

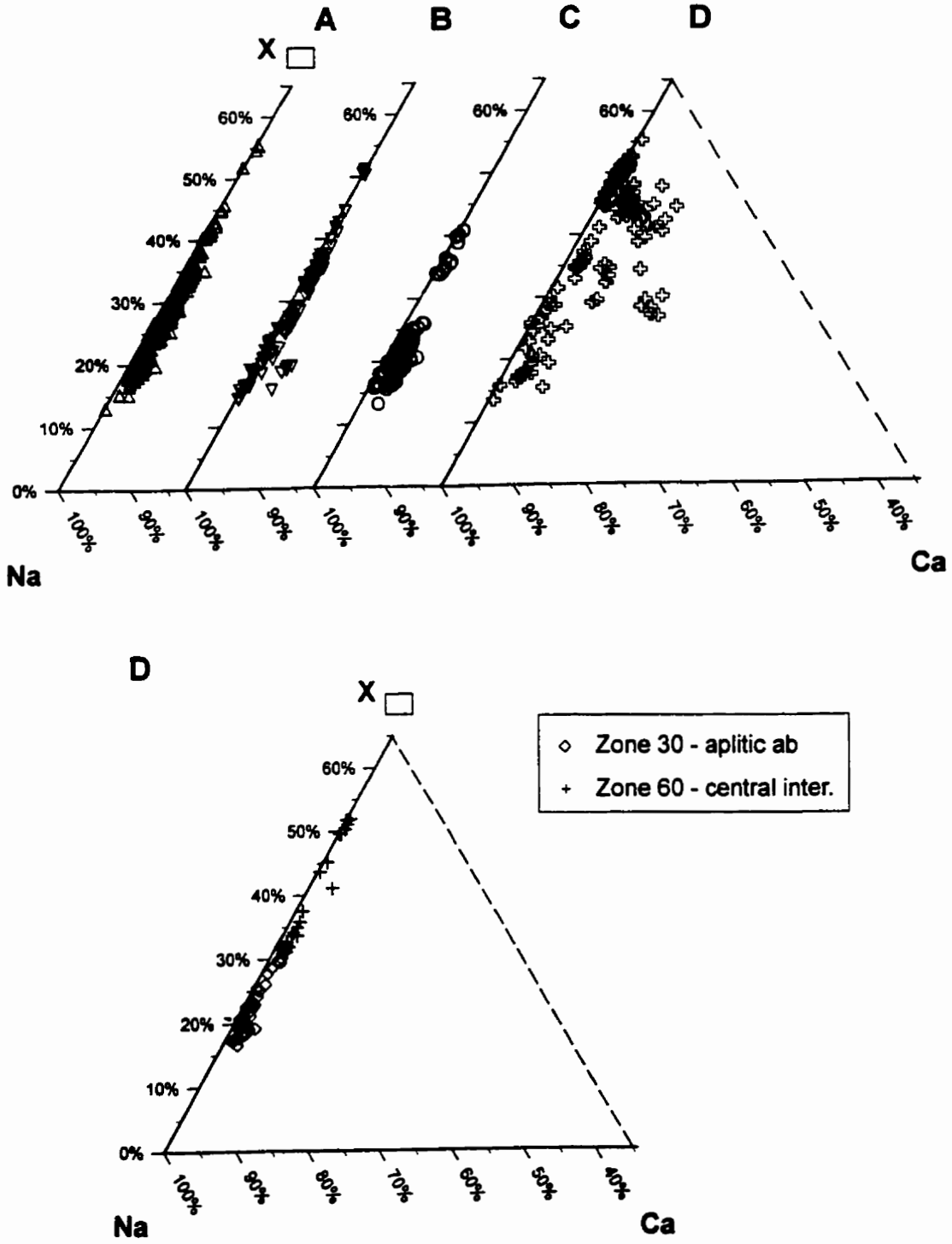

Figure 5.4. *X*-site contents in tourmaline at Tanco from (a) zone 10, (b) zone 20 - black, brown, (c) zone 20 - green, (d) zone 40 or 50, and (e) zone 30 and 60.

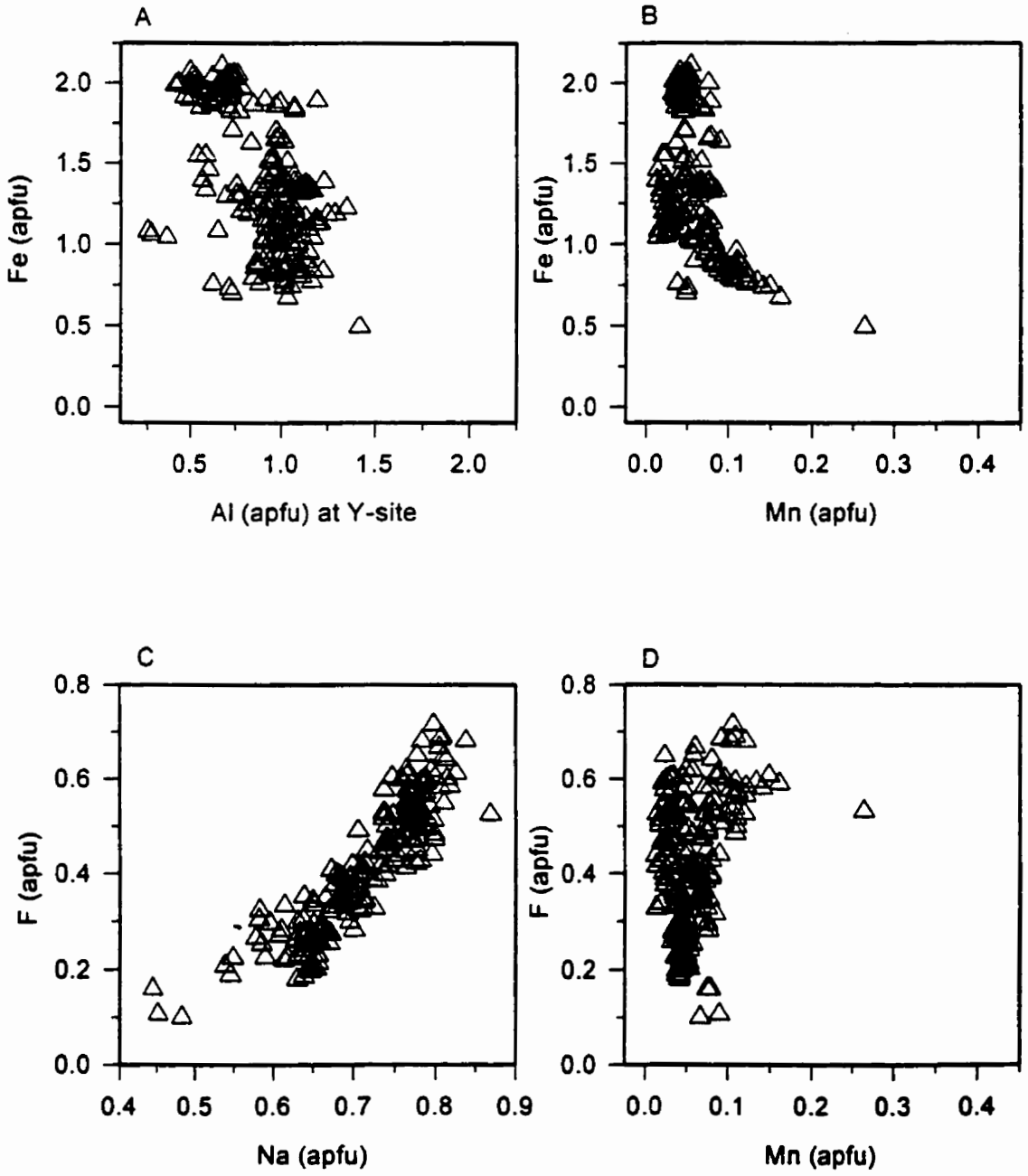

Figure 5.5. Tourmaline compositions from border zone (10) at Tanco.

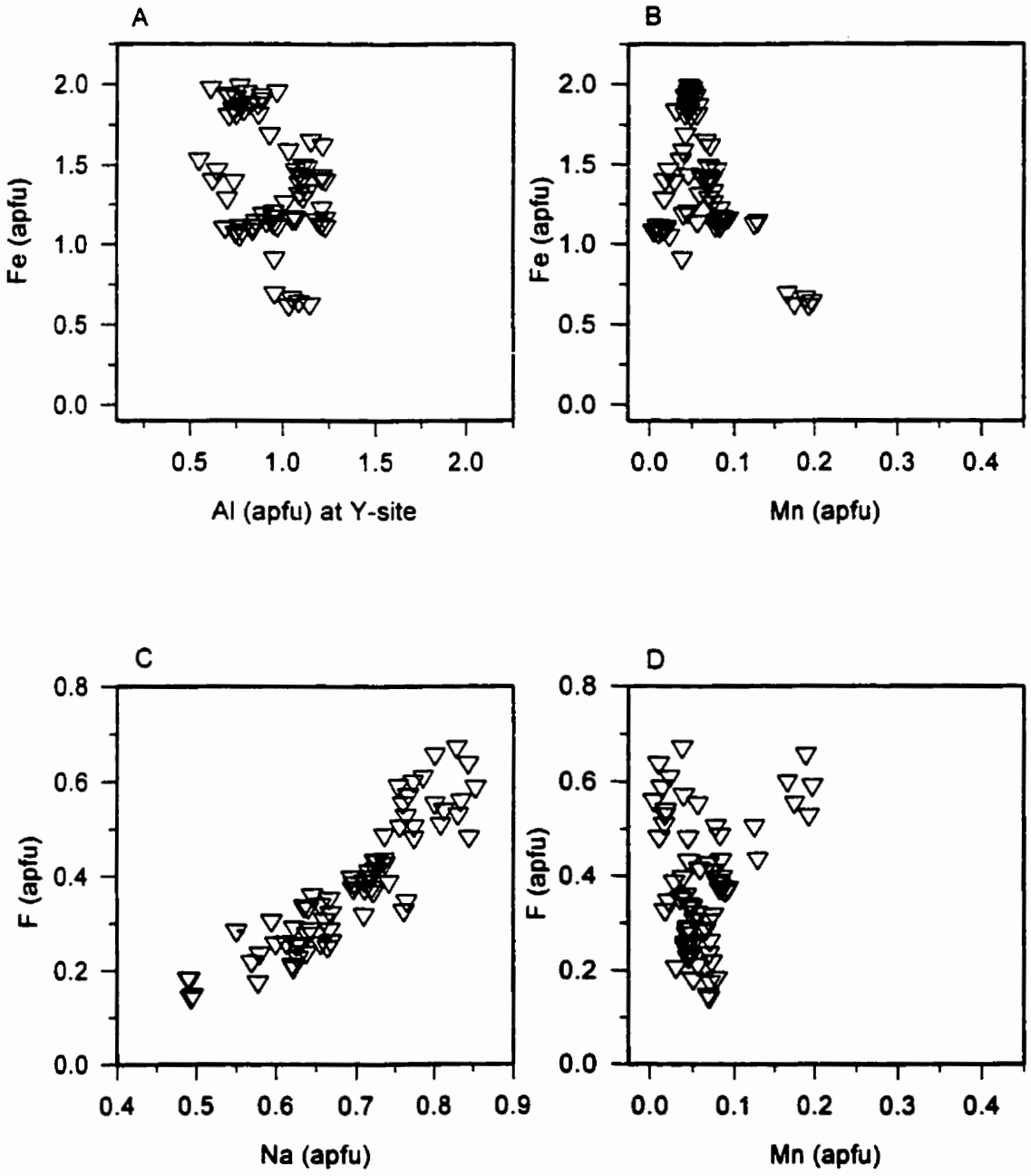

Figure 5.6. Black/brown tourmaline compositions from wall zone (20) at Tanco.

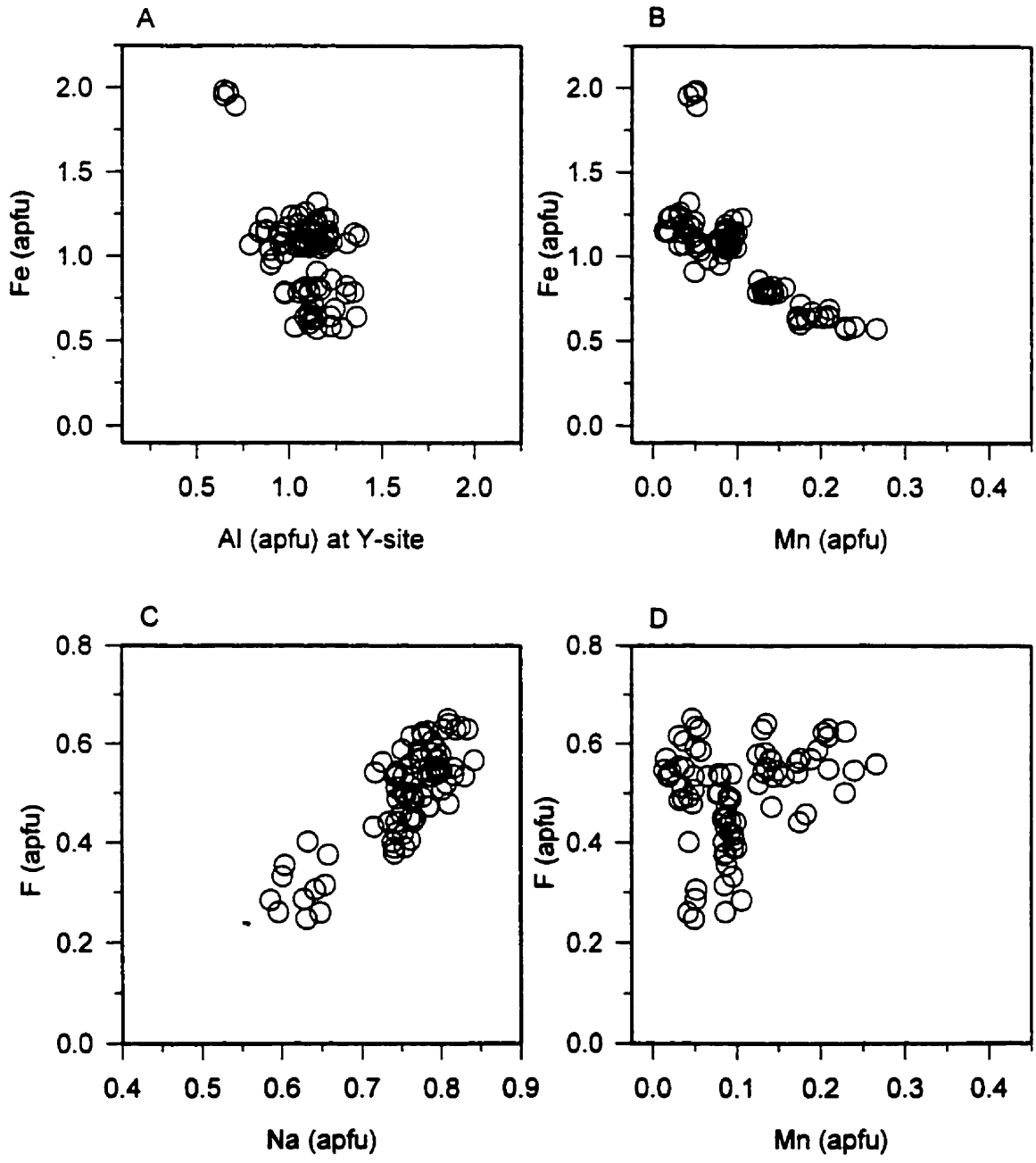

Figure 5.7. Green tourmaline compositions from wall zone (20) at Tanco.

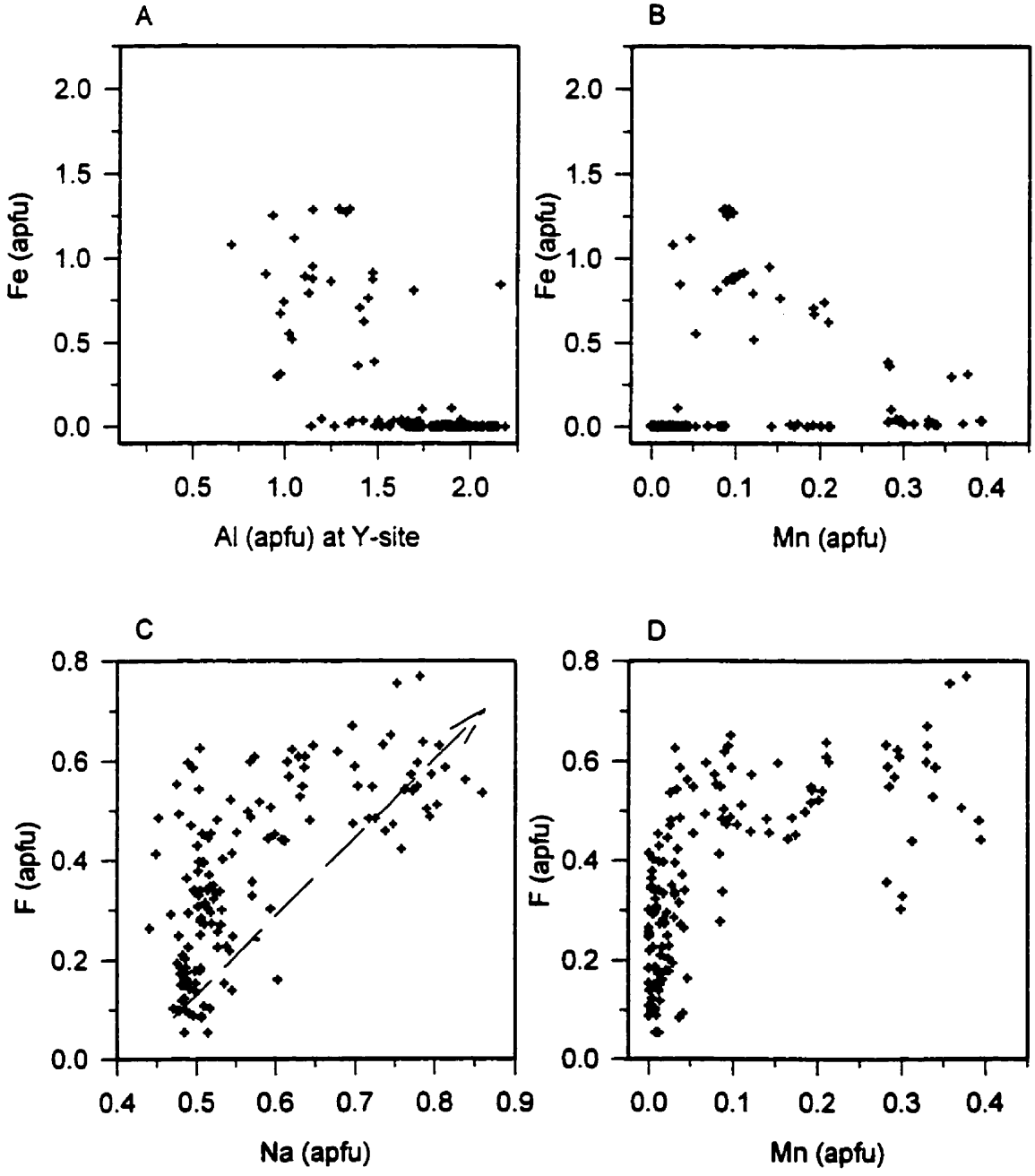

Figure 5.8. Tourmaline compositions at Tanco from lower + upper intermediate zone 40 or 50. (c) Arrow indicates the positive correlation which occurs in the other Tanco pegmatite zones.

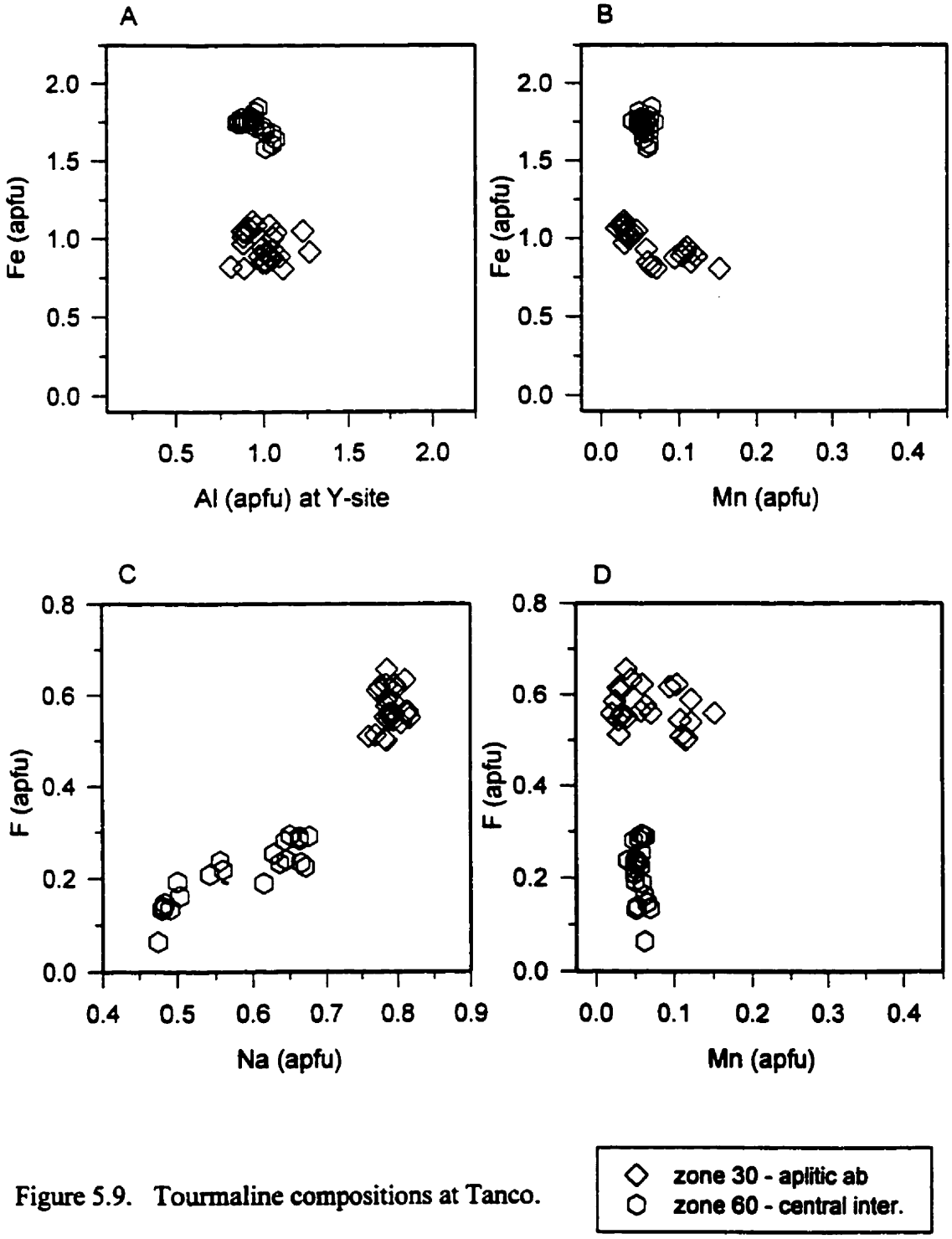

Figure 5.9. Tourmaline compositions at Tanco.

fractionation trend from zone (10) to (20) to (40) and (50) is from □-rich (foitite-schorl) to Na-rich (elbaite-schorl and Fe-rich elbaite) to □-rich (rossmanite-elbaite) to (Na, □)-rich (elbaite-rossmanite) and slight late-stage Ca-enrichment in Ca-bearing elbaite-rossmanite (Table 5.3, Fig. 5.4). Tourmaline in zones (60) and (30) has a narrow range in Na content, with 0.48 - 0.68 *apfu* Na in zone (60) and 0.67 - 0.82 *apfu* Na in zone (30). The fractionation trend from zone (60) to (30) is from □-rich (foitite-schorl) to Na-rich (elbaite-schorl and Fe-rich elbaite) (Table 5.3, Fig. 5.4e).

The negative correlation between Fe and Al at the *Y*-site indicates that the dominant substitution in tourmaline at Tanco is $3Fe^{2+} \rightleftharpoons 1.5Al + 1.5Li$ (Figs. 5.5a, 5.6a, 5.7a, 5.8a, 5.9a). Tourmaline in zone (10) and black-to-brown tourmaline in zone (20) have similar wide range in Fe and Al at the *Y*-site, but green tourmaline in zone (20) is slightly more Al-rich (Figs.5.5a, 5.6a, 5.7a). Most tourmaline in zones (40) and (50) contains no Fe. Tourmaline in zone (60) is more Fe-enriched than tourmaline in zone (30) (Fig. 5.9a). This negative correlation indicates that primitive tourmaline is Fe-rich and fractionated tourmaline is Al-rich at the *Y*-site (Table 5.3).

There is a negative correlation between Fe and Mn from schorl-foitite and schorl (Fe-rich, Mn-poor) to Fe-rich elbaite (moderate Fe and Mn) in zone (10) and black-to-brown tourmaline in zone (20) (Figs. 5.5b, 5.6b). Green tourmaline in zone (20) is slightly more Fe- and Mn-enriched with ≤ 0.27 *apfu* Mn in Fe-rich elbaite. Most tourmaline in zones (40) and (50) contains no Fe and has variable Mn content. The Mn content decreases from Mn-bearing elbaite with ≤ 0.39 *apfu* Mn (Table 5.7, composition 2) to no Mn in rossmanite-elbaite and elbaite-rossmanite, and increases to ≤ 0.07 *apfu* Mn

in Ca-bearing elbaite-rossmanite (Table 5.7, composition 7) and ≤ 0.20 *apfu* Mn in Ca-bearing elbaite (Table 5.7, composition 8). Foitite-schorl and schorl-elbaite in zone (60) contains high Fe and low Mn, whereas elbaite-schorl and Fe-rich elbaite in zone (30) contain moderate Fe and Mn (Fig. 5.9b).

The most primitive tourmaline is Fe-rich and (Mn, Al+Li)-poor (foitite-schorl) with increasing fractionation Fe decreases and Mn and Al+Li increases (Mn-bearing elbaite), Fe and Mn decreases to nil and Al+Li increases (elbaite-rossmanite).

There is a positive correlation between Na and F and a weak positive correlation between Mn and F in tourmaline in zones (10) and (20), from foitite-schorl (low Na , Mn and F) to elbaite0-schorl and Fe-rich elbaite (high Na and F) (Figs. 5.5c,d, 5.6c,d, 5.7c,d). The maximum F content occurs in Fe-rich elbaite in zone (10), with ≤ 0.72 *apfu* F and ≤ 0.80 *apfu* Na (Table 5.4, composition 7), and maximum Mn content occurs in green Fe-rich elbaite in zone (20). Most tourmaline in zones (40) and (50) lies above the positive correlation between Na and F in zone (10) and (20) because it contains high Ca and □ contents. The composition that plots furthest from the trend is Ca-bearing elbaite-rossmanite with ≤ 0.11 *apfu* Ca, ≤ 0.49 *apfu* Na and ≤ 0.60 *apfu* F (Table 5.7, composition 7). There is a positive correlation between Ca and F in late-stage tourmaline, as they increase from rossmanite-elbaite → Ca-bearing elbaite-rossmanite → Ca-bearing elbaite. Tourmaline in zones (40) and (50) shows a wide range in Mn and F contents, from Mn-bearing elbaite (high Mn and F) to rossmanite-elbaite (no Mn and very low F) to elbaite-rossmanite (no Mn and low F) to Ca-bearing elbaite-rossmanite (very low Mn and high F) and Ca-bearing elbaite (low Mn and high F) (Figs. 5.8c, d).

Tourmaline in zones (60) and (30) also shows a positive correlation between Na and F from foitite-schorl (low Na, Mn and F) in zone (60) to elbaite-schorl (high Na and F and low Mn) with ≤ 0.81 *apfu* Na, ≤ 0.66 *apfu* F and ≤ 0.04 *apfu* Mn (Table 5.8, composition 5) and Fe-rich elbaite (high Na and F, moderate Mn) in zone (30) (Figs. 5.9c, d).

Most tourmaline at Tanco contains no (or low) Zn content, except for ≤ 0.11 *apfu* Zn in dark green Fe-rich elbaite in zones (40) and (50) and ≤ 0.09 *apfu* Zn in green and dark brown elbaite-schorl in zone (20).

The overall fractionation sequence at Tanco is as follows: (± foitite-schorl, schorl-foitite) (□-, Fe-rich, Mn-, F-poor) → Al-rich schorl → schorl → schorl-elbaite → elbaite-schorl (Na-, F-rich) → Fe-rich elbaite (Na-, F-rich) → Mn-bearing elbaite (Mn-rich) → rossmanite-elbaite (□-, Al-, Li-rich, Mn, F-poor) → elbaite-rossmanite (Al-, Li-rich) → (± Ca-bearing elbaite, Ca-bearing elbaite-rossmanite) (Na-, □-rich, moderate F and Ca).

5.2.2.2. Metasomatic tourmaline and subsolidus alteration at Tanco

Tourmaline in the exocontact at Tanco is a result of B metasomatism and can be divided into two compositional groups: (a) feruvite-schorl-dravite ((Ca, Mg)-rich, Al-poor) and (b) elbaite-schorl-dravite ((Na, Al)-rich) (Table 5.9). The tourmalines of both groups are similar in appearance and texture. Commonly, tourmalines of group A and B occur in separate hand samples; however, only rarely do hand samples contain zoned tourmaline with group A cores and group B rims. Zoned tourmaline in sample TTC37 has feruvite-schorl-dravite compositions in the core and elbaite-schorl-dravite compositions

TABLE 5.9. REPRESENTATIVE COMPOSITIONS OF TOURMALINE (WT%) IN EXOCONTACT AT TANCO

	1	2	3	4	5	6	7	8	9
SiO_2	35.70	35.40	35.50	35.70	36.80	37.10	35.70	36.50	36.60
TiO_2	1.28	0.76	0.56	0.72	0.71	0.18	0.54	0.48	0.25
B_2O_3*	10.35	10.21	10.12	10.36	10.56	10.66	10.51	10.59	10.76
Al_2O_3	27.10	27.80	27.80	29.60	30.20	33.30	34.20	34.90	36.80
MgO	7.23	5.48	4.14	5.82	6.81	4.53	1.66	2.12	2.06
CaO	3.05	2.29	0.83	1.77	0.69	0.46	1.07	0.12	0.15
MnO	0.00	0.00	0.00	0.00	0.00	0.00	0.10	0.17	0.00
FeO	10.80	12.30	14.20	10.40	8.39	6.66	9.85	7.40	6.27
Li_2O*	0.22	0.27	0.29	0.23	0.35	0.87	0.88	0.97	1.09
Na_2O	1.15	1.48	2.24	1.58	2.31	2.43	1.89	2.38	2.47
H_2O*	3.35	3.31	3.14	3.04	3.18	3.05	3.27	3.28	3.19
F	0.47	0.45	0.75	1.13	0.97	1.33	0.76	0.79	1.10
O=F	-0.20	-0.19	-0.32	-0.48	-0.41	-0.56	-0.32	-0.33	-0.46
Total	100.50	99.56	99.25	99.87	100.56	100.01	100.11	99.37	100.28
Formulae normalized to 31 anions									
T -Si	6.00	6.02	6.10	5.99	6.06	6.05	5.90	5.99	5.91
Al	0.00	0.00	0.00	0.01	0.00	0.00	0.10	0.01	0.09
B	3.00	3.00	3.00	3.00	3.00	3.00	3.00	3.00	3.00
Z -Al	5.36	5.58	5.63	5.84	5.86	6.00	6.00	6.00	6.00
Mg	0.64	0.42	0.37	0.16	0.14	0.00	0.00	0.00	0.00
Y -Al	0.00	0.00	0.00	0.00	0.00	0.40	0.56	0.74	0.92
Ti	0.16	0.10	0.07	0.09	0.09	0.02	0.07	0.06	0.03
Mg	1.17	0.97	0.69	1.29	1.53	1.10	0.41	0.52	0.49
Mn	0.00	0.00	0.00	0.00	0.00	0.00	0.01	0.02	0.00
Fe^{2+}	1.52	1.75	2.04	1.46	1.15	0.91	1.36	1.02	0.85
Li	0.15	0.18	0.20	0.16	0.23	0.57	0.59	0.64	0.71
$\sum Y$	3.00	3.00	3.00	3.00	3.00	3.00	3.00	3.00	3.00
X -Ca	0.55	0.42	0.15	0.32	0.12	0.08	0.19	0.02	0.03
Na	0.37	0.49	0.75	0.51	0.74	0.77	0.61	0.76	0.77
□	0.08	0.09	0.10	0.17	0.14	0.15	0.20	0.22	0.20
OH	3.75	3.76	3.59	3.40	3.50	3.31	3.60	3.59	3.44
F	0.25	0.24	0.41	0.60	0.50	0.69	0.40	0.41	0.56

*B_2O_3, Li_2O and H_2O calculated by stoichiometry; B = 3 *apfu*, Li = 15 - $\sum T + Z + Y$ and OH+F = 4 *apfu*.

Compositions 1-5 are from group A and 6-9 are from group B. (1) black feruvite-schorl-uvite, sample TTC22-1; (2) black schorl-feruvite-dravite, sample TT2; (3) black Ca-bearing Mg-rich schorl, sample TT26; (4) brown Ca-rich schorl-dravite core, sample TTC37-2; (5) brown Ca-bearing dravite-schorl, sample TTC29-2; (6) brown dravite-elbaite-schorl, sample TT21; (7) brown (Ca, Mg)-bearing schorl-elbaite, sample TT23; (8) brown elbaite-schorl-dravite rim, sample TTC37-1; and (9) elbaite-schorl-dravite, sample TT24.

in the rim (Table 5.3).

Figure 5.10a indicates that tourmalines of the feruvite-schorl-dravite group (A) are Ca-rich with up to 0.57 *apfu* Ca at the *X*-site (Table 5.9, composition 1), significantly greater than ≤ 0.11 *apfu* Ca in the late-stage Ca-bearing elbaite-rossmanite from zones (40) and (50). Tourmalines of this group are Al-poor, commonly with < 6.0 *apfu* total Al (Fig. 5.10b), and up to 1.46 *apfu* Mg occurs at the *Z*-site in dravite-schorl and schorl-dravite. Figure 5.11a shows that schorl is the dominant component in these group A compositions, which range from feruvite-schorl to schorl-feruvite to Ca-rich schorl-dravite to Ca-bearing schorl-dravite to (Ca, Mg)-rich schorl to Ca-bearing dravite-schorl. The occurrence of feruvite is rare in nature, but it occurs in the amphibolite exocontact of the lepidolite pegmatites at Red Cross Lake (section 4.7.2) (Selway *et al.* 1998b). There is a positive correlation between Ca, Mg, and Ti, as they decrease from Ti-bearing feruvite-schorl (≤ 1.85 *apfu* total Mg and ≤ 0.18 *apfu* Ti) to Ca-bearing schorl-dravite (Figs. 5.11b, c). The source of Ca, Mg and Ti in these tourmalines is from the amphibolite host rock.

Figure 5.10a indicates that tourmaline of the elbaite-schorl-dravite group (B) is

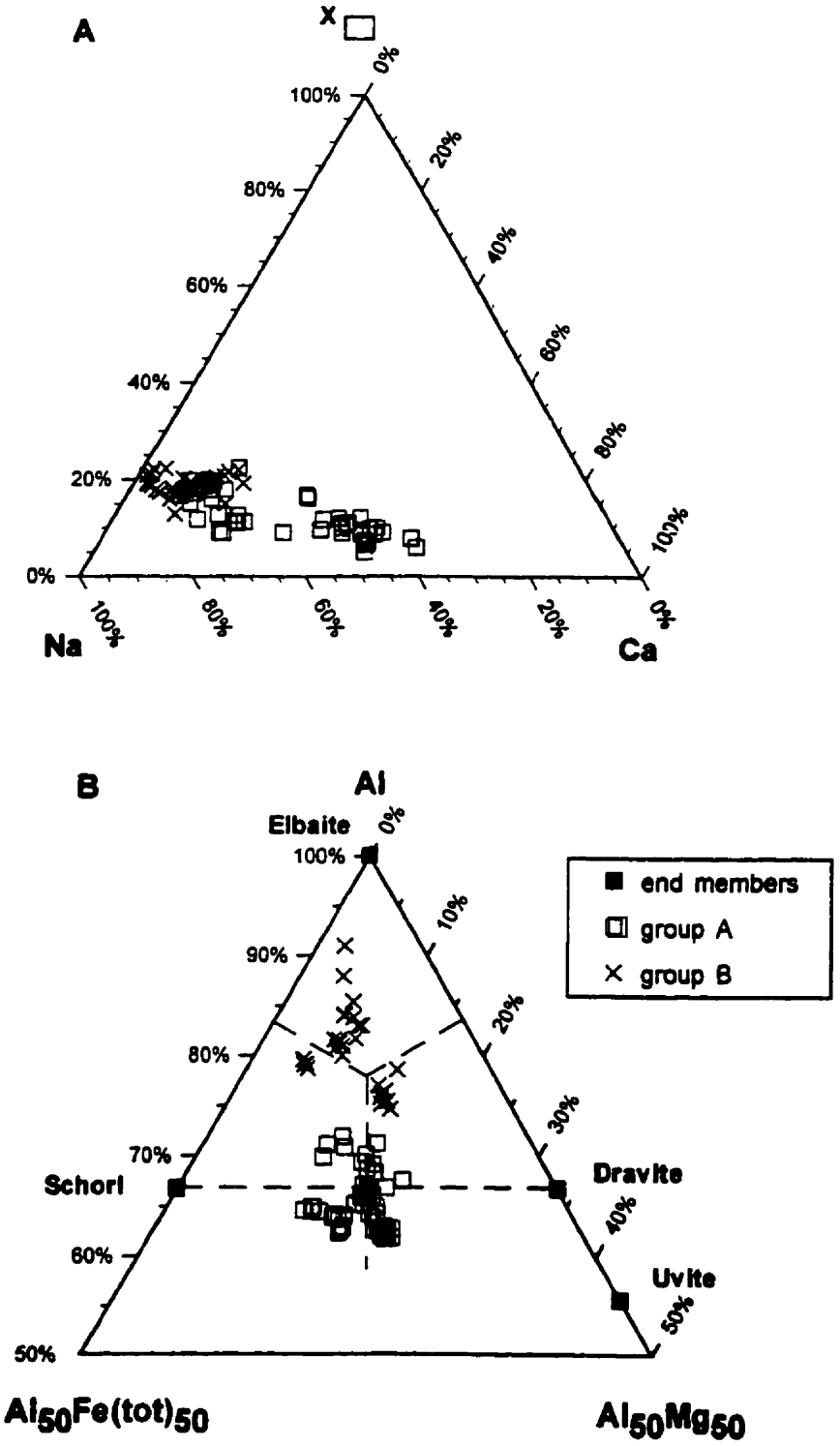

Figure 5.10. Tourmaline composition from the exocontact at Tanco; (a) ^{X} □-Na-Ca ternary diagram, and (b) Al-Fe-Mg ternary diagram.

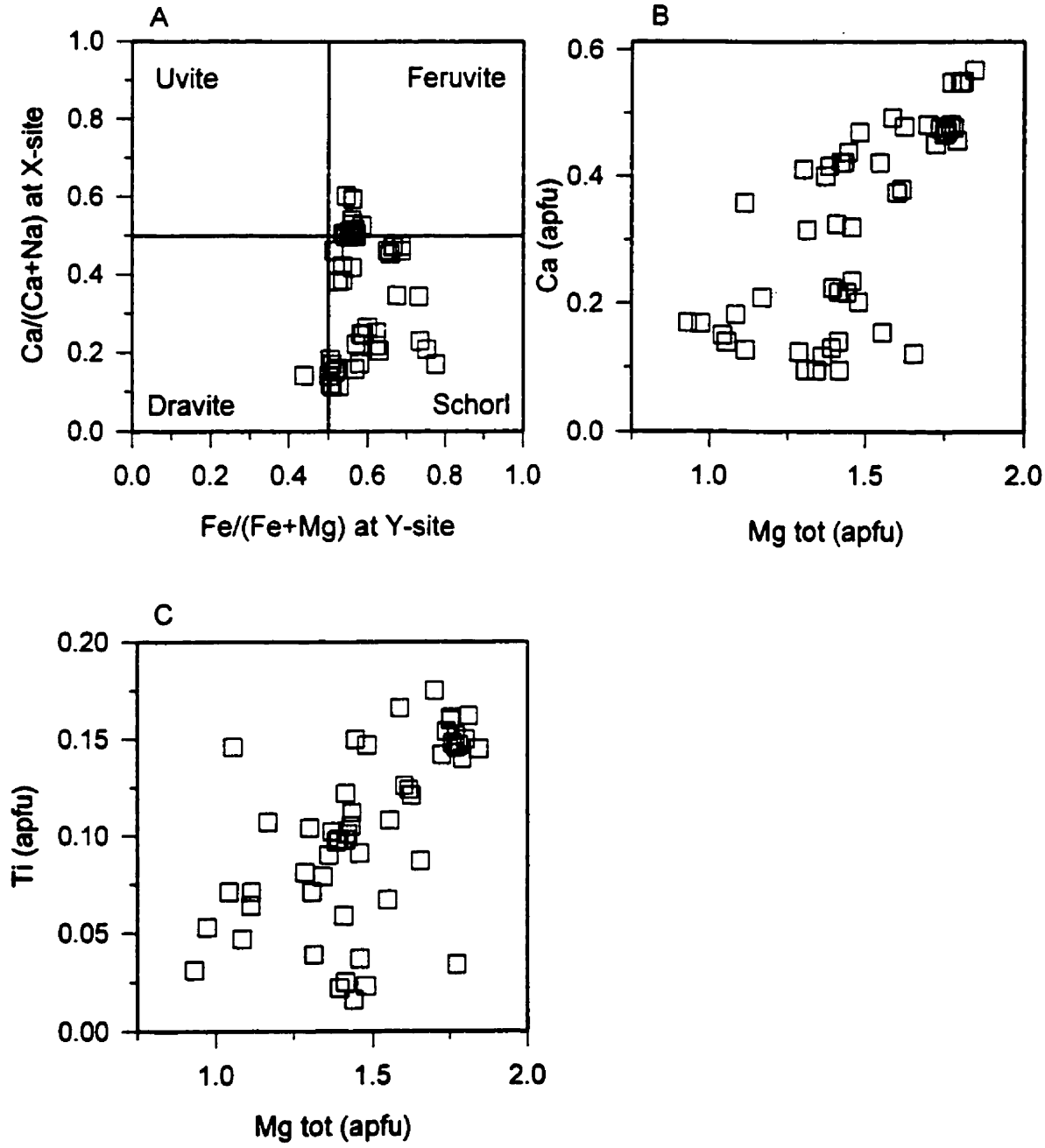

Figure 5.11. Group A tourmaline compositions from the exocontact at Tanco.

Na-rich (≤ 0.79 *apfu* Na) and Ca-poor (≤ 0.19 *apfu* Ca), and Al-rich with ≤7.43 *apfu* total Al (Fig. 5.10b). These tourmaline compositions plot close to the centre of elbaite-schorl-dravite compositional space, and range from intermediate dravite-schorl-elbaite to (Ca, Mg)-bearing schorl-elbaite to elbaite-schorl-dravite (Fig. 5.10b). All of these compositions plot in what was previously believed to be a compositional gap. The elbaite-schorl-dravite compositions are similar to those from the exocontact of elbaite-subtype Bližná pegmatite, which intrudes marble, and from metapelite xenoliths in the lepidolite-subtype Rožná pegmatite (section 4.5.2.2) (Novák *et al.* 1999). Novák *et al.* (1999) concluded that elbaite-schorl-dravite compositions occur in holmquistite-free amphibolite host rocks of LCT pegmatites. Holmquistite is rare in the tourmaline metasomatic aureole around Tanco pegmatite (Morgan & London 1987). The Na and Al for this tourmaline group comes from internal, melt-derived, pegmatitic fluid.

Endomorphic Mg-bearing tourmaline occurs in zones (10), (20) and (30), and ranges in composition from Mg-bearing schorl to Al-rich Mg-bearing schorl to Mg-bearing schorl-elbaite to Mg-bearing elbaite-schorl (Fig. 5.12). There is ≤ 0.44 *apfu* Mg and 0.10 *apfu* Ti in black Mg-bearing schorl in fine-grained albite in zone (10), close to a biotitized xenolith or the contact with the amphibolite host rock (Table 5.4, composition 8), ≤ 0.37 *apfu* Mg and ≤ 0.09 *apfu* Ti in black Mg-bearing schorl in the granitic parts of zone (20) (Table 5.5, composition 7), and ≤ 0.40 *apfu* Mg in green Mg-bearing schorl-elbaite in zone (30). Table 5.3 indicates that Mg-bearing elbaite-schorl occurs in the core and elbaite-schorl occurs in the rim of zoned tourmaline crystals in zones (10), (20) and (30). The source of Mg and Ti in the tourmaline is the host-rock amphibolite. Calcium

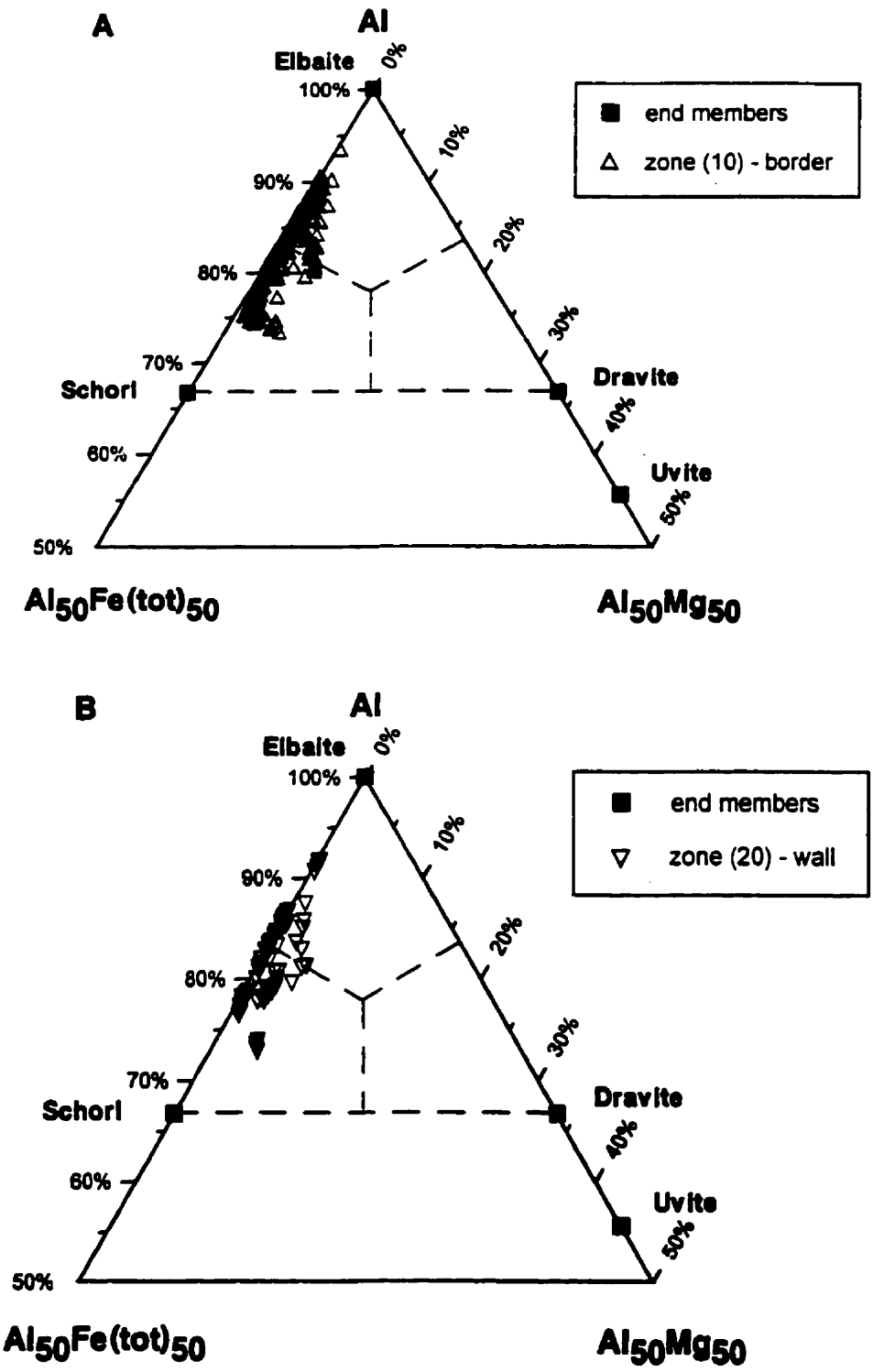

Figure 5.12. Black/brown tourmaline compositions at Tanco in (a) zone (10) and (b) zone (20).

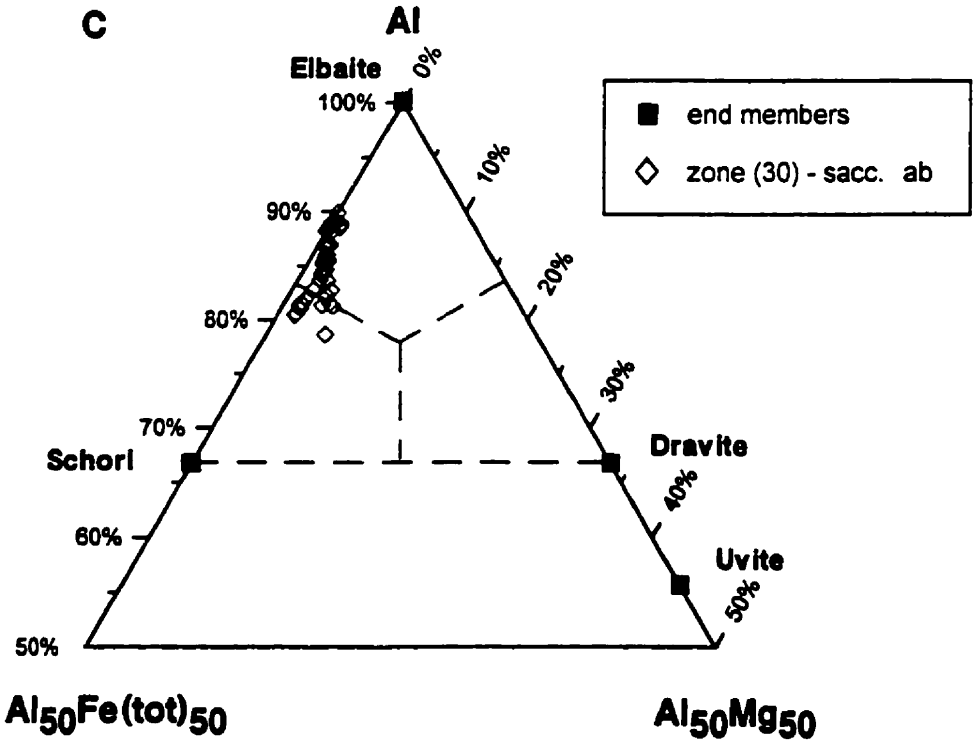

Figure 5.12. Tourmaline compositions at Tanco from (c) zone (30).

infiltrating from the host amphibolite was preferentially partitioned into plagioclase over tourmaline, and andesine occurs in border zone (10) (Černý *et al.* 1998).

In zones (20) and (30), orange lithiophilite is rimmed by blue tourmaline ranging in composition from elbaite-schorl to Fe-rich elbaite to Fe-bearing elbaite. In zone (20), green-to- brown (Fe, Mg)-rich lithiophilite (Černý *et al.* 1998) is rimmed by (Fe, Mg)-rich blue tourmaline which ranges in composition from schorl-elbaite, with up to 0.24 *apfu* Mg, to elbaite-schorl. This blue tourmaline may locally replace lithiophilite, but the tourmaline compositions are similar to those of primary tourmaline in the same pegmatite

zone.

Pink tourmalines in zones (40) and (50) are commonly altered along rims and cracks, or completely pseudomorphed by pink (Rb, Cs)-bearing lepidolite. Sample 50-3 is a 11 cm long zoned crystal of patchy pink rossmanite-elbaite at one end, a fine-grained green muscovite zone (about 1 cm long), narrow blue Fe-rich elbaite (Table 5.7, composition 3) + relic rossmanite-elbaite (2 mm long), and fine-grained green muscovite at the other end (about 5 cm long). The blue tourmaline zone is optically continuous with the pink rossmanite-elbaite zone, and the fine-grained green muscovite is a complete pseudomorph of the pink tourmaline. The fine-grained green muscovite and Fe-rich elbaite are subsolidus-alteration products of pink elbaite-rossmanite.

5.2.2.3. Trace-element content of tourmaline at Tanco

Representative tourmaline samples from zones (10), (20), (30) and a transition region from zones (20) to (40) were analyzed by proton-induced x-ray emission (PIXE) (see section 3.7). The PIXE work was completed before the discovery of pink tourmaline in zones (40) and (50), so they were not analyzed for trace elements. Each PIXE analysis (total of 49) involved 19 elements with $Z > 26$ (Fe), but only Ga, Ge, Sr and rare Pb and Nb were above the limit of detection; Co, Ni, Cu, As, Se, Br, Rb, Y, Zr, Mo, Sn, Cs, Ba and W were not detected.

Figure 5.13a shows that Ga is positively correlated with Al_2O_3 in tourmaline and that the Ga content increases with increasing fractionation. Gallium content ranges from 147 ppm in brown Ca-rich schorl-dravite core and 175 ppm in its elbaite-schorl-dravite

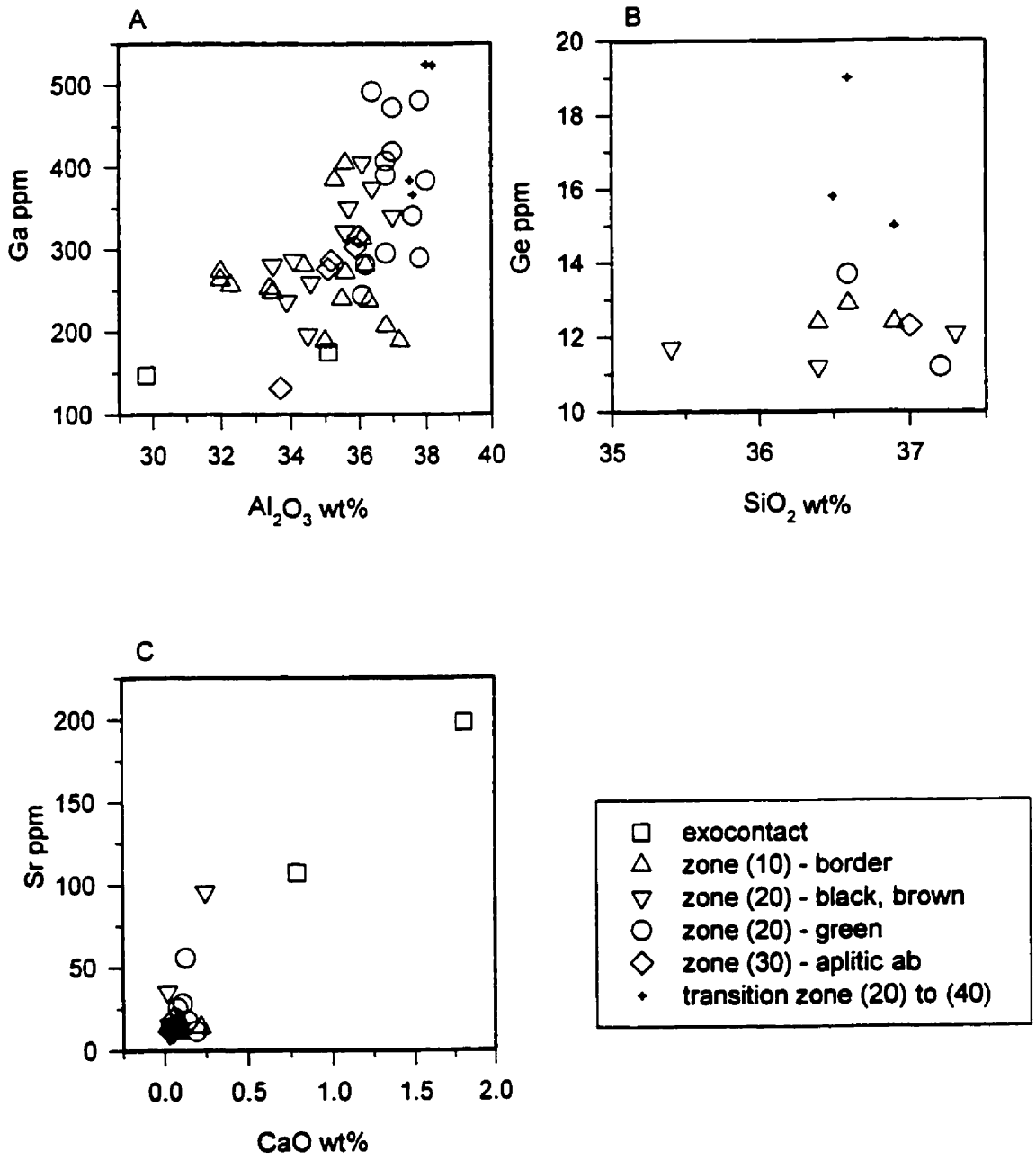

Figure 5.13. Trace element content in tourmaline at Tanco.

rim in the exocontact to 492 ppm in green elbaite-schorl in zone (20) to 525 ppm in pale-green Fe-bearing elbaite from the transition region between zones (20) and (40). The Al/Ga ratios range from 9677 in green Mg-bearing elbaite-schorl in zone (30) to 7640 in brown Ca-rich schorl-dravite in the exocontact to 2736 in pale-green Fe-bearing elbaite in the transition region between zones (20) and (40).

Figure 5.13b shows no correlation between Ge and SiO_2 in tourmaline, but Ge content increases with increasing fractionation. Germanium ranges from below the limit of detection in many samples (including the exocontact) to 11 ppm in black elbaite-schorl in zone (20) to 19 ppm in pale green Fe-bearing elbaite in transition between zones (20) and (40).

Lead is above detection limit in only five samples. It increases with increasing fractionation, and ranges from 15 ppm in brown Fe-rich elbaite in zone (10) to 44 ppm in black Fe-rich elbaite from zone (20) to 46 ppm in pale green Fe-bearing elbaite in the transition region between zones (20) and (40). Galena and other Pb-bearing sulfides and sulfosalts occur in late cavity- and fissure-filling aggregates in zones (40), (50), (60) and (30) (Černý *et al.* 1998).

Figure 5.13c shows that Sr is positively correlated with CaO and that the Sr content of tourmaline decreases with increasing fractionation. Strontium ranges from 198 ppm in brown Ca-rich schorl-dravite core to 107 ppm in its elbaite-schorl-dravite rim from the exocontact to 96 ppm in black Fe-rich elbaite from zone (20) to 56 ppm in green Fe-rich elbaite in zone (20) to 11 ppm in pale-green Fe-bearing elbaite in the transition region between zones (20) and (40).

Niobium is above the detection limit only in seven samples, most of which occur in zone (10). Niobium ranges from 13 in dark-green schorl to 75 ppm in green schorl-elbaite, both of which occur in zone (10) and are associated with columbite-tantalite. No real systematic correlation with fractionation was identified.

5.3. The Utö Pegmatites

5.3.1. General geology

Utö pegmatites are petalite-subtype pegmatites located on the northern part of Utö island, Sweden. The Utö pegmatites consist of three pegmatite bodies: Måsberget hill, Southern Nyköpingsgruvan pegmatite and Northern Nyköpingsgruvan pegmatite (Smeds & Černý 1989). The pegmatite at Måsberget hill is poorly exposed and is not discussed in this thesis. The samples examined here are from the genetically-related Southern (minor) and Northern (major) Nyköpingsgruvan pegmatite dykes. These two pegmatites intrude a previously mined iron formation. Minerals of these pegmatite dykes have been collected and studied since the late 1800's, and the dykes are the type locality of spodumene, petalite, manganotantalite and holmquistite (references cited by Smeds & Černý 1989). The paragenesis and chemical composition of tourmaline from the locality were first examined by Sjögren (1916).

The Southern Nyköpingsgruvan pegmatite is 5-7 m thick and consists of two zones: (1) an outer zone, and (2) an inner zone (Smeds & Černý 1989). The outer zone contains abundant greenish K-feldspar (1-5 cm), spodumene and dark-blue tourmaline,

subordinate fine-grained albite, quartz and grey mica, and accessory amblygonite. The inner zone contains abundant blocky petalite (10-30 cm), blocky greyish K-feldspar (10-30 cm) and amblygonite, subordinate fine-grained lepidolite, blue apatite and pink tourmaline.

The Northern Nyköpingsgruvan pegmatite is 18 m thick x 300 m long and intrudes iron formation, except for the western end (Grundberg outcrop) which intrudes dolomitic marble with small pods of iron formation (Smeds & Černý 1989). The pegmatite zones are: (i) spodumene, (ii) pink K-feldspar, (iii) lepidolite, (iv) coarse sugary albite (> 1 mm), (v) petalite, and (vi) fine sugary albite (< 1-2 mm). This sequence of crystallization of the pegmatite zones was determined based on their tourmaline compositions, as much of the outcrop is poorly exposed and has been reduced to rubble in dumps by iron mining (S.-A. Smeds, pers. comm.). The spodumene zone (i) contains abundant green spodumene, red K-feldspar and amazonite, subordinate black-to-blue tourmaline (2-3 cm long) and arsenopyrite, and accessory albite, brownish mica, quartz, microlite, cassiterite, sphalerite and galena. The spodumene zone is in contact with the magnetite- and galena-bearing iron formation and is 15-20 cm wide. Green spodumene crystallized due to an influx of Fe from the host rock which lowered the pressure of crystallization of spodumene and expanded its stability field. The dominant lithium aluminosilicate in the rest of the pegmatite is petalite. Amazonite and accessory galena crystallized due to an influx of Pb from the host rock. The pink K-feldspar zone (ii) contains abundant blocky pink K-feldspar (10's of cm), amazonite (5 cm) and petalite (10 cm), subordinate bluish-green apatite, amblygonite, blue tourmaline, white beryl and

accessory albite, quartz, lepidolite, muscovite, manganotantalite, microlite, zircon and cassiterite. The lepidolite zone (iii) contains abundant fine-grained lepidolite, subordinate muscovite, blue tourmaline and quartz, and accessory red and blue apatite, albite, petalite, amblygonite, microlite, manganotantalite, zircon and cassiterite. The coarse sugary albite (> 1 mm) zone (iv) contains abundant albite and quartz, subordinate corroded petalite, muscovite and blue tourmaline, and accessory K-feldspar, lepidolite, amblygonite, microlite and cassiterite. The petalite zone (v) contains abundant petalite (10-30 cm) and fine-grained lepidolite, subordinate pink, colourless and blue tourmaline and muscovite, and accessory quartz, K-feldspar, blue apatite, microlite, cassiterite and manganotantalite. The fine sugary albite (<1-2 mm) zone (vi) in the Grundberg outcrop contains dominant albite and quartz, abundant pink tourmaline (3-4 mm long), and accessory pollucite, microlite, tantalite, calciotantite and cesstibtantite (Smeds *et al.* 1999).

The sample labelled "GRB" from the Grundberg outcrop represents the fine sugary albite (<1-2 mm) zone affected by contamination from the host dolomitic marble (S.-A. Smeds pers. comm.). It contains abundant albite and quartz, subordinate blue tourmaline and apatite, and accessory pollucite, ferrocolumbite and calciotantite.

Holmquistite and biotite-phlogopite occur in the silicate exocontacts of these pegmatites (Smeds & Černý 1989). The banded iron formation was recrystallized and the magnetite ore altered to hematite by infiltrating oxidizing pegmatitic fluids.

5.3.2. Tourmaline at Utö

Tourmaline occurs in each of the pegmatite zones listed above. Black-to-navy-

blue tourmaline in the spodumene zone forms 1 cm long acicular crystals and may contain veinlets of cookeite, K-feldspar, quartz and minor galena and sphalerite. Black-to-navy-blue tourmaline in the pink K-feldspar zone forms 2-5 mm acicular crystals and may contain cookeite veinlets and K-feldspar and albite inclusions. Blue tourmaline (1-2 mm) in the lepidolite zone may contain cookeite veinlets and lepidolite and pollucite inclusions. Blue tourmaline in the coarse sugary-albite zone forms 1 cm long acicular crystals and may contain cookeite veinlets and lepidolite, Cs-bearing lepidolite, cassiterite and albite inclusions. Green to pink to colourless to minor blue tourmaline in the petalite zone forms 1-2 cm long columnar crystals that may be zoned with a colourless core and a pink rim, or with a green core and a pink rim. The pink and colourless tourmaline may contain veinlets of cookeite, apatite and K-feldspar, and inclusions of K-feldspar and quartz. Pink-to-colourless tourmaline forms 5-7 mm crystals in the fine sugary-albite zone in the Grundberg outcrop and may contain quartz and lepidolite inclusions.

Cookeite veinlets are common in tourmaline throughout the Utö pegmatites, but are rare in the other pegmatites discussed in this thesis. The cookeite veinlets may be due to weathering of tourmaline on the dumps (for over 100 years).

The metasomatic tourmaline can be divided into two groups, depending on the host rock composition; pegmatite in contact with (a) iron formation, and (b) dolomitic marble. Black-to-navy-blue exocontact tourmaline, which forms 2 mm - 1.5 cm long acicular crystals, occurs in mica schist in contact with the iron formation. The mica schist contains fine-grained albite, amazonite, cassiterite, biotite and magnetite. Colourless-to-blue endomorphic tourmaline (1-2 mm) occurs at the Grundberg outcrop in fine sugary

albite contaminated by dolomitic- marble host-rock.

5.3.3. Composition of tourmaline at Utö

The tourmaline composition at Utö evolves through the following crystallization sequence: Al-rich schorl → schorl-elbaite → elbaite-schorl → Fe-rich elbaite → Fe-bearing elbaite → elbaite → elbaite-rossmanite → rossmanite-elbaite → elbaite-rossmanite → Ca-bearing elbaite-rossmanite → Ca-bearing elbaite (Fig. 5.14, Table 5.10). Black to brown to blue Al-rich schorl, schorl-elbaite, ± Ca-bearing elbaite, ± Fe-rich elbaite and ± Fe-bearing elbaite occur in spodumene zone (i). Black to brown ± Ca-bearing schorl, ± Ca-bearing schorl-elbaite, ± elbaite-schorl and blue ± Fe-bearing elbaite and Fe-rich elbaite occur in the pink K-feldspar zone (ii). Blue Fe-rich elbaite, Fe-bearing elbaite and elbaite occur in the lepidolite zone (iii). Blue Fe-bearing elbaite and elbaite occur in coarse sugary-albite zone (iv). Minor blue Fe-rich elbaite, Fe-bearing elbaite and elbaite occur in the petalite zone (v). Dominant pink, colourless and rare green elbaite, elbaite-rossmanite, rossmanite-elbaite, ± Ca-bearing elbaite-rossmanite and ± Ca-bearing elbaite occur in the petalite zone (v). Pink-to-colourless elbaite-rossmanite, Ca-bearing elbaite-rossmanite and Ca-bearing elbaite occur in the fine sugary-albite zone in the Grundberg outcrop (vi).

In the Utö pegmatites, the dominant substitution at the *X*-site is Na = □ with minor Ca variation (Fig. 5.15). Tourmaline at Utö is more Ca-rich than tourmaline at Tanco. Tourmalines in the spodumene and K-feldspar zones of each pegmatite have a similar range in Na (0.61-0.80 *apfu* Na) and Ca (up to 0.12 *apfu* Ca). The maximum Na

TABLE 5.10. REPRESENTATIVE COMPOSITIONS OF TOURMALINE (WT%) FROM THE UTÖ PEGMATITE

	1	2	3	4	5	6	7	8	9	10
SiO_2	35.37	36.12	35.49	37.41	38.18	37.57	38.38	39.06	38.95	38.49
TiO_2	0.00	0.07	0.00	0.00	0.00	0.00	0.00	0.00	0.00	0.00
B_2O_3*	10.35	10.47	10.35	10.99	11.07	11.12	11.27	11.41	11.32	11.28
Al_2O_3	33.53	34.46	32.83	39.53	40.07	41.59	42.88	43.71	42.30	42.38
MgO	0.00	0.33	0.97	0.00	0.00	0.00	0.00	0.00	0.00	0.00
CaO	0.36	0.09	0.56	0.37	0.42	0.40	0.40	0.00	0.98	0.97
MnO	0.22	0.21	0.31	0.29	0.30	0.59	0.30	0.09	0.09	0.12
FeO	14.91	11.60	13.20	4.68	2.81	1.31	0.18	0.00	0.00	0.10
ZnO	0.13	0.17	0.23	0.30	0.19	0.79	0.00	0.00	0.00	0.00
Li_2O*	0.41	0.77	0.54	1.60	1.83	1.78	1.98	1.94	2.19	2.16
Na_2O	1.93	2.31	2.28	2.26	2.00	1.90	1.59	1.52	1.41	1.55
H_2O*	3.18	3.20	3.27	3.20	3.39	3.39	3.51	3.81	3.46	3.48
F	0.82	0.88	0.63	1.24	0.90	0.93	0.81	0.27	0.95	0.87
O=F	-0.35	-0.37	-0.27	-0.52	-0.38	-0.39	-0.34	-0.11	-0.40	-0.37
Total	100.86	100.31	100.39	101.35	100.78	100.98	100.96	101.70	101.25	101.03
Formulae normalized to 31 anions										
T -Si	5.94	5.99	5.96	5.92	6.00	5.87	5.92	5.95	5.98	5.93
Al	0.06	0.01	0.04	0.08	0.00	0.13	0.08	0.05	0.02	0.07
B	3.00	3.00	3.00	3.00	3.00	3.00	3.00	3.00	3.00	3.00
Z -Al	6.00	6.00	6.00	6.00	6.00	6.00	6.00	6.00	6.00	6.00
Y -Al	0.58	0.73	0.46	1.29	1.41	1.54	1.71	1.80	1.64	1.63
Ti	0.00	0.01	0.00	0.00	0.00	0.00	0.00	0.00	0.00	0.00
Mg	0.00	0.08	0.24	0.00	0.00	0.00	0.00	0.00	0.00	0.00
Mn	0.03	0.03	0.04	0.04	0.04	0.08	0.04	0.01	0.01	0.02
Fe^{2+}	2.09	1.61	1.86	0.62	0.37	0.17	0.02	0.00	0.00	0.01
Zn	0.02	0.02	0.03	0.03	0.02	0.09	0.00	0.00	0.00	0.00
Li	0.28	0.52	0.37	1.02	1.16	1.12	1.23	1.19	1.35	1.34
$\sum Y$	3.00	3.00	3.00	3.00	3.00	3.00	3.00	3.00	3.00	3.00
X -Ca	0.07	0.02	0.10	0.06	0.07	0.07	0.07	0.00	0.16	0.16
Na	0.63	0.74	0.74	0.69	0.61	0.58	0.48	0.45	0.42	0.46
□	0.30	0.24	0.16	0.25	0.32	0.35	0.45	0.55	0.42	0.38
OH	3.56	3.54	3.67	3.38	3.55	3.54	3.61	3.87	3.54	3.54
F	0.44	0.46	0.33	0.62	0.45	0.46	0.39	0.13	0.46	0.46

*B_2O_3, Li_2O and H_2O calculated by stoichiometry; B = 3 *apfu*, Li = 15 - $\sum T + Z + Y$; OH+F = 4 *apfu*.

(1) black Al-rich schorl, spod. zone, Uto3-2; (2) black schorl-elbaite, spod. zone, Uto3-2; (3) black Ca-bearing schorl-elbaite, K-feld. zone, Uto14-2; (4) blue Fe-rich elbaite, K-feld. zone, Uto1-1; (5) blue Fe-bearing elbaite, lep. zone, Uto7-3; (6) blue elbaite, coarse sugary-ab zone, Uto9-1; (7) colourless elbaite-rossmanite, pet. zone, Uto21-1; (8) colourless rossmanite-elbaite, pet. zone, Uto27; (9) colourless Ca-bearing elbaite-rossmanite, fine sugary-ab zone, Uto31-2; (10) colourless Ca-bearing elbaite, fine sugary ab zone, Uto11-1.

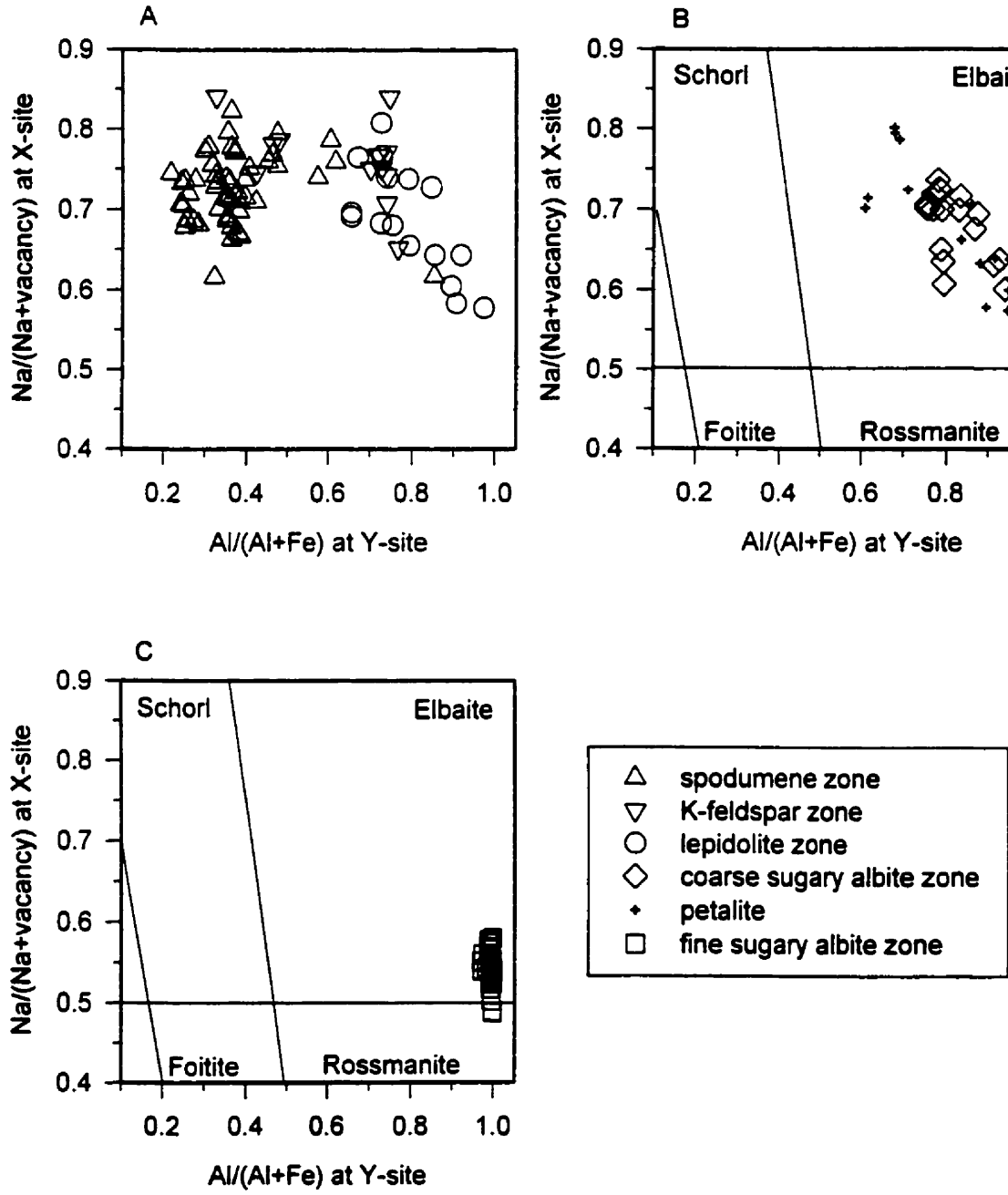

Figure 5.14. Tourmaline compositions at Uto.

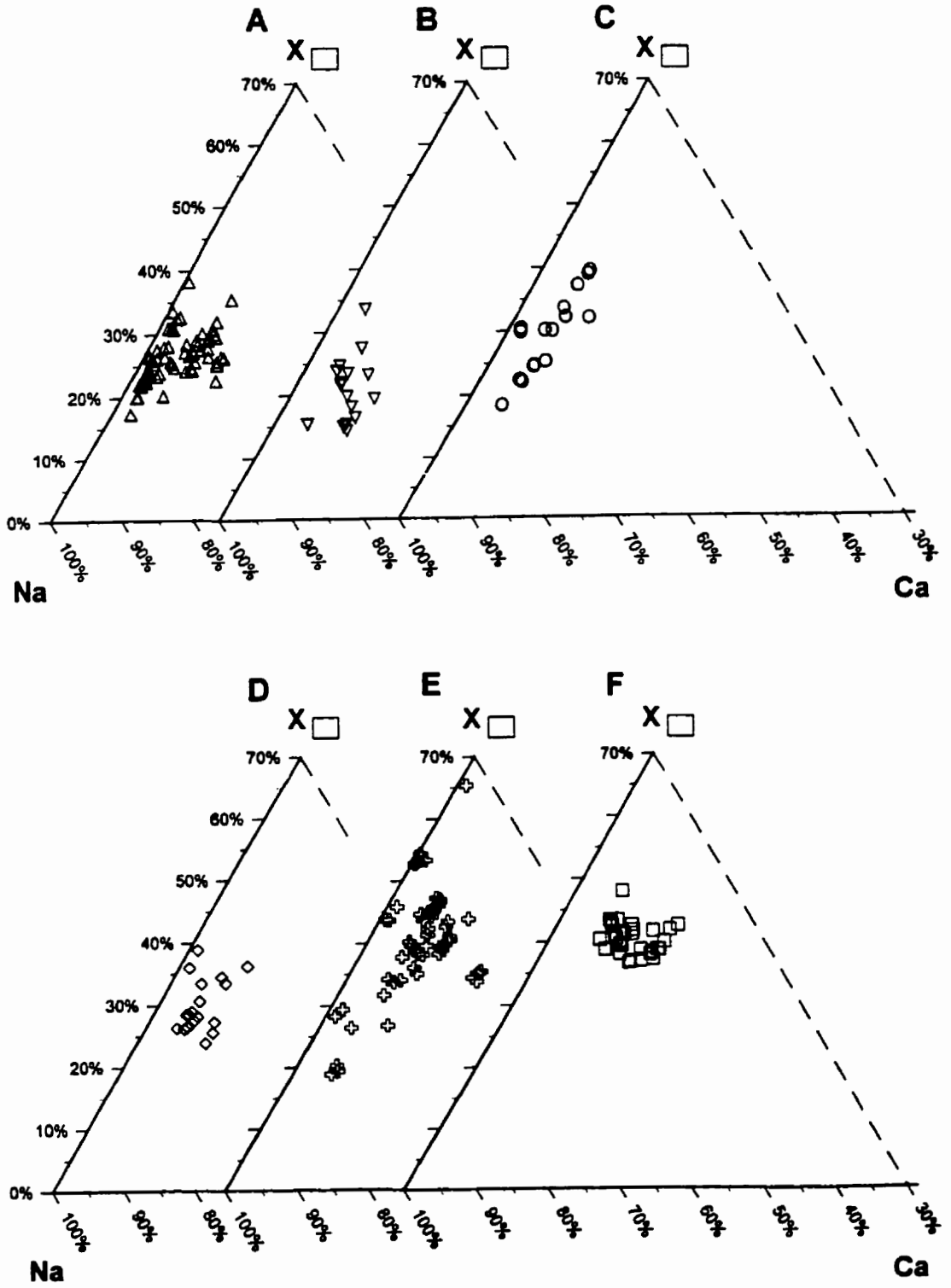

Figure 5.15. *X*-site content in tourmaline at Utö from (a) spodumene, (b) K-feldspar, (c) lepidolite, (d) coarse sugary-albite, (e) petalite and (f) fine sugary-albite zones.

content occurs in schorl-elbaite in the spodumene zone. Tourmaline in the lepidolite and coarse sugary-albite zones is more vacancy-rich and Ca-poor than tourmaline of the outermost pegmatite zones (with 0.54 - 0.77 *apfu* Na and up to 0.10 *apfu* Ca). Tourmaline in the petalite and fine sugary-albite zones is the most vacancy- and Ca-rich, with most of the data falling in the range 0.41 - 0.60 *apfu* Na and up to 0.18 *apfu* Ca (Table 5.10, compositions 9,10). The maximum □ content (0.65 *apfu* □) occurs in rossmanite-elbaite, and the maximum Ca content occurs in Ca-bearing elbaite of the petalite zone. The fractionation trend from the outermost to innermost pegmatite zones is from Na-rich to (□, Ca)-rich.

The dominant substitution in tourmaline at Utö is $3Fe^{2+} \rightleftharpoons 1.5Al + 1.5Li$ (Fig. 5.16a). The Fe content in tourmaline decreases from Al-rich schorl (with 2.1 *apfu* Fe) in the spodumene zone (Table 5.10, composition 1) to no Fe in tourmaline in most tourmalines of the petalite and fine sugary-albite zones. The negative correlation indicates that primitive tourmaline is Fe-rich and fractionated tourmaline is Al-rich.

There is a negative correlation between Fe and Mn from Al-rich schorl to schorl-elbaite in the spodumene zone to Fe-rich elbaite and Fe-bearing elbaite in the K-feldspar, lepidolite and coarse sugary-albite zones (Fig. 5.16b). The maximum of 0.11 *apfu* Mn occurs in Fe-bearing elbaite in the coarse sugary-albite zone. The Fe and Mn contents decrease to nil in elbaite, elbaite-rossmanite and rossmanite-elbaite in the petalite zone and in elbaite-rossmanite, Ca-bearing elbaite-rossmanite and Ca-bearing elbaite in fine sugary-albite zone. The most primitive tourmaline is Fe-rich and (Mn, Al+Li)-poor (Al-rich schorl) with increasing fractionation Fe decreases and Mn and Al+Li increases (Fe-

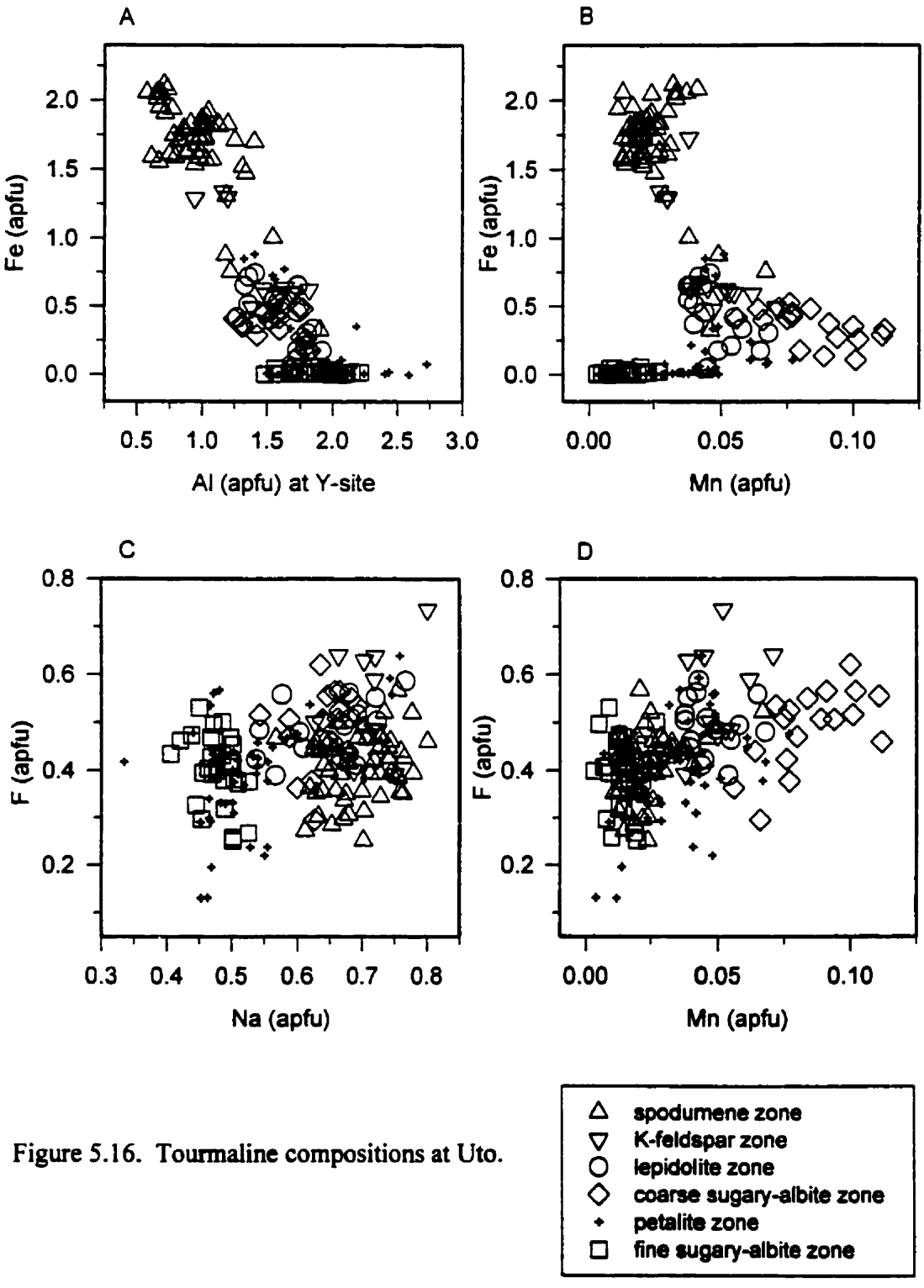

Figure 5.16. Tourmaline compositions at Uto.

bearing elbaite) and the most fractionated is (Fe, Mn)-free and (Al+Li)-rich (Ca-bearing elbaite-rossmanite).

There is a weak positive correlation between Na and F, and between Mn and F in tourmaline (Figs. 5.16c, d), and a strong positive correlation between Na and F in tourmaline from other pegmatites discussed in this thesis. The correlation between Na and F in tourmaline at Utö is slightly distorted due to the overall enrichment in Ca. The Al-rich schorl to Fe-bearing elbaite contains moderate-to-high Na, variable F and low Mn. The maximum Na and F contents of 0.80 *apfu* Na and 0.74 *apfu* F occur in Fe-rich elbaite in the K-feldspar zone. The Fe-bearing elbaite in the coarse sugary-albite zone contains high Mn and F. The Na, Mn and F contents decrease in tourmaline in the petalite and fine sugary-albite zones. The lowest Na and F contents of 0.42 *apfu* Na and 0.13 *apfu* F and no Mn occur in rossmanite-elbaite in the petalite zone.

Most tourmaline at Utö contains no Zn, except for ≤ 0.11 *apfu* Zn in Fe-bearing elbaite in the coarse sugary-albite zone. The Zn enrichment in Fe-bearing elbaite correlates with the Mn enrichment. Tourmaline at Utö contains no Ti. Most tourmaline contains no Mg, except for (Ca, Mg)-bearing Al-rich schorl with 0.34 *apfu* Mg in the K-feldspar zone and Ca-bearing schorl-elbaite in the spodumene zone.

The group-A exocontact tourmaline is in contact with the iron formation. Black tourmaline ranges in composition from uvite-feruvite to Ca-rich schorl-dravite to Ca-bearing schorl-dravite to Mg-rich schorl-feruvite to (Ca, Mg)-rich schorl to (Ca, Mg)-bearing schorl. The navy-blue-to-black tourmaline ranges in composition from elbaite-schorl to Fe-rich elbaite (Fig. 5.17, Table 5.11). Black tourmaline is enriched in Ca and

Mg relative to the tourmaline in the pegmatite, probably due to an influx of Ca and Mg from the host rock or the more distant dolomitic marbles in the area.

The group-B endomorphic blue tourmaline is in contact with dolomitic marbles at the Grundberg outcrop. Tourmaline grains range in composition from liddicoatite-elbaite to elbaite-liddicoatite to elbaite, with minor Fe in all compositions (Fig 5.17, Tables 5.11, 5.12). Tourmaline grains contain inclusions which range in composition from dravite to foitite to schorl-elbaite to elbaite-schorl-dravite, with significant Ca content in all compositions. The tourmaline inclusions may be metasomatic-replacement products due to an influx of Ca and Mg from the dolomitic host rock.

The group-A exocontact tourmaline is more (Na, Mg and Fe)-rich than group-B endomorphic tourmaline which is more Al-rich (Fig. 5.17).

TABLE 5.11. REPRESENTATIVE COMPOSITIONS OF METASOMATIC TOURMALINE (WT%) FROM THE UTÖ PEGMATITE

	1	2	3	4	5	6	7	8	9
SiO_2	35.78	35.57	35.02	34.65	37.26	38.00	37.41	36.83	35.40
TiO_2	0.06	0.00	0.00	0.00	0.00	0.00	0.00	0.00	0.00
$B_2O_3^*$	10.36	10.32	10.16	10.64	11.06	11.11	11.06	10.81	10.46
Al_2O_3	26.95	29.22	30.69	39.03	39.79	40.43	40.66	36.21	35.55
MgO	8.79	5.94	1.65	0.04	0.00	0.03	0.03	2.87	0.00
CaO	3.50	2.19	0.90	0.00	2.73	1.33	0.90	1.21	0.87
MnO	0.13	0.13	0.22	0.00	0.43	0.25	0.37	0.20	0.00
FeO	10.32	11.49	15.10	7.80	2.56	1.93	2.73	6.46	12.22
ZnO	0.16	0.00	0.00	0.00	0.00	0.00	0.00	0.00	0.00
Li_2O^*	0.00	0.13	0.31	1.14	2.19	2.07	1.85	0.99	0.69
Na_2O	1.05	1.61	2.18	2.87	1.29	1.69	1.89	1.68	1.36
H_2O^*	3.19	3.27	3.41	3.02	3.21	3.47	3.54	3.46	3.46
F	0.80	0.61	0.20	1.38	1.29	0.76	0.58	0.57	0.32
O=F	-0.34	-0.26	-0.08	-0.58	-0.54	-0.32	-0.24	-0.24	-0.13
Total	100.75	100.22	99.76	99.99	101.27	100.75	100.78	101.05	100.20
Formulae normalized to 31 anions									
T -Si	6.00	5.99	5.99	5.66	5.85	5.95	5.88	5.92	5.88
Al	0.00	0.01	0.01	0.34	0.15	0.05	0.12	0.08	0.12
B	3.00	3.00	3.00	3.00	3.00	3.00	3.00	3.00	3.00
Z -Al	5.33	5.79	6.00	6.00	6.00	6.00	6.00	6.00	6.00
Mg	0.67	0.21	0.00	0.00	0.00	0.00	0.00	0.00	0.00
Y -Al	0.00	0.00	0.18	1.18	1.22	1.40	1.41	0.78	0.84
Ti	0.01	0.00	0.00	0.00	0.00	0.00	0.00	0.00	0.00
Mg	1.53	1.27	0.42	0.01	0.00	0.01	0.01	0.69	0.00
Mn	0.02	0.02	0.03	0.00	0.06	0.03	0.05	0.02	0.00
Fe^{2+}	1.45	1.62	2.16	1.06	0.34	0.26	0.36	0.87	1.70
Zn	0.02	0.00	0.00	0.00	0.00	0.00	0.00	0.00	0.00
Li	0.00	0.09	0.21	0.75	1.38	1.30	1.17	0.64	0.46
$\sum Y$	3.03	3.00	3.00	3.00	3.00	3.00	3.00	3.00	3.00
X -Ca	0.63	0.40	0.17	0.00	0.46	0.22	0.15	0.21	0.16
Na	0.34	0.53	0.72	0.91	0.39	0.51	0.58	0.52	0.44
□	0.03	0.07	0.11	0.09	0.15	0.27	0.27	0.27	0.40
OH	3.58	3.68	3.89	3.29	3.36	3.62	3.71	3.71	3.83
F	0.42	0.32	0.11	0.71	0.64	0.38	0.29	0.29	0.17

*B_2O_3, Li_2O and H_2O calculated by stoichiometry; B = 3 *apfu*, Li = 15 - $\sum T + Z + Y$ and OH+F = 4 *apfu*.

Compositions 1-4 from exocontact next to iron formation and compositions 5-9 is endomorphic tourmaline in Grundberg outcrop; 5-7 - main tourmaline grains and 8 and 9 - inclusions. (1) black uvite-feruvite, sample Uto18-3; (2) black Mg-rich schorl-feruvite, sample Uto18-2; (3) black (Ca, Mg)-bearing schorl, sample 17-1; (4) blue elbaite-schorl, sample Uto32-1; (5) colourless Fe-bearing liddicoatite-elbaite, sample Uto 13-1; (6) colourless Ca-rich elbaite, sample Uto 13-1; (7) blue (Ca, Fe)-bearing elbaite, sample Uto 13-2; (8) colourless Ca-rich elbaite-schorl-dravite, sample Uto13-1; and (9) blue Ca-bearing schorl-elbaite, sample Uto13-2.

TABLE 5.12: TOURMALINE SPECIES FROM FOUR GRAINS FROM THE CONTAMINATED GRUNDBERG OUTCROP

	main grain	inclusions
1	Fe-bearing liddicoatite-elbaite Ca-rich elbaite Fe-bearing elbaite	(Ca,Fe)-rich dravite elbaite-schorl-dravite foitite
2	elbaite-liddicoatite (Ca,Fe)-bearing elbaite Ca-bearing elbaite	Fe-rich dravite-uvite Ca-bearing schorl-elbaite
3	Fe-bearing liddicoatite-elbaite Ca-rich Fe-bearing elbaite (Ca,Fe)-bearing elbaite	(Ca,Fe)-rich dravite Ca-bearing schorl-elbaite
4	liddicoatite-elbaite Fe-bearing elbaite-liddicoatite Ca-bearing elbaite Ca-rich Fe-bearing elbaite	Ca-bearing schorl-elbaite

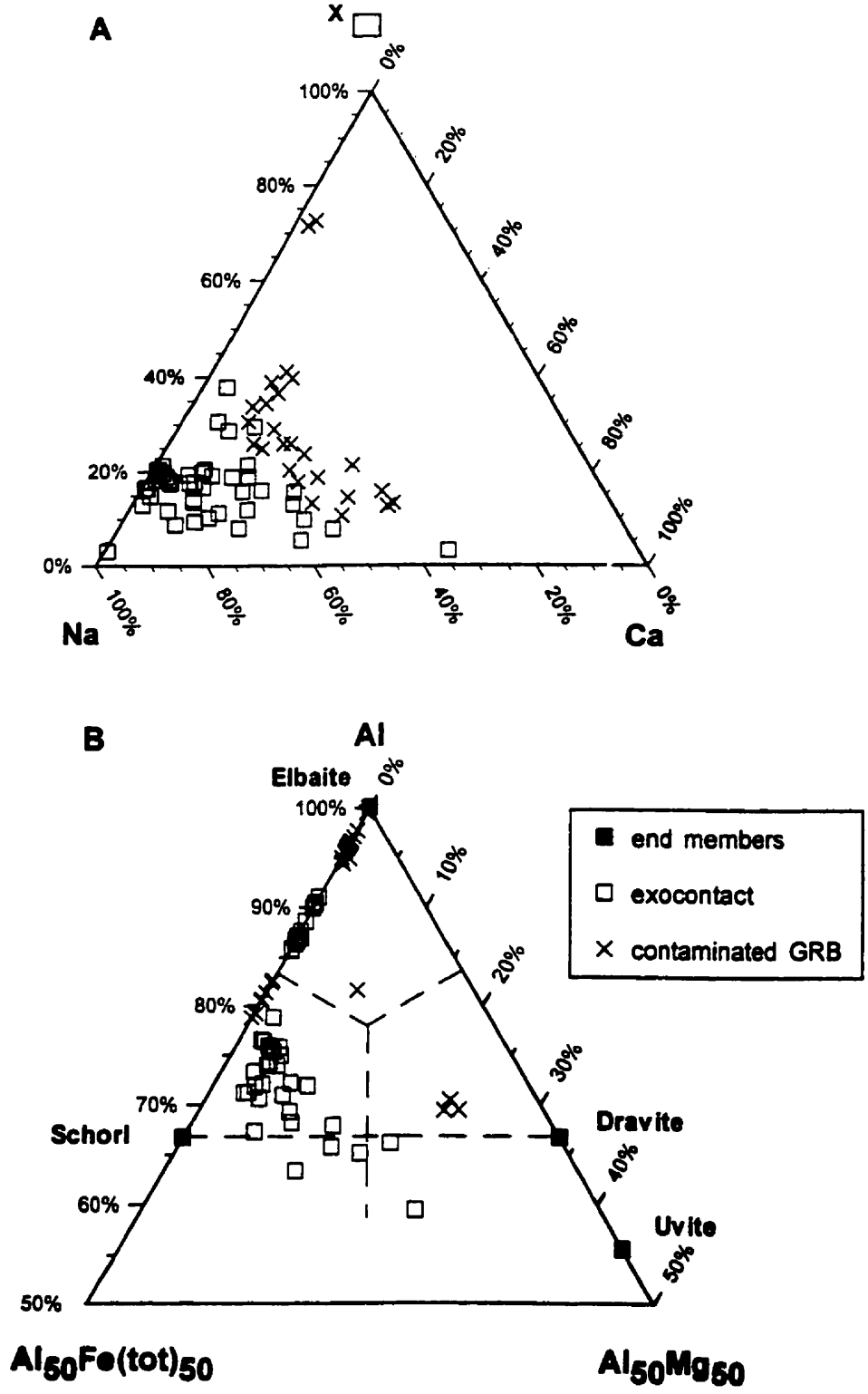

Figure 5.17. Tourmaline compositions at Utö from the exocontact and the contaminated GRB outcrop (a) ^{X}□-Na-Ca ternary diagram; (b) Al-Fe-Mg ternary diagram.

5.4. Marko's Pegmatite

5.4.1. General geology

Marko's Pegmatite is a petalite-subtype pegmatite located about 60 km north of Kenora, northwestern Ontario (Beakhouse *et al.* 1996, Pan & Breaks 1997). Marko's pegmatite is a member of the Separation Rapids pegmatite group within the Separation Lake greenstone belt of the Superior Province. All the supracrustal rocks of this greenstone belt have been subjected to lower-amphibolite grade metamorphism (500-550 °C and 3-4 kbar) (Pan *et al.* 1996).

Marko's pegmatite is 8 m wide x 130 m long and intrudes mafic metavolcanic rocks (amphibolite) at the southern contact, and banded iron formation at the northern contact (Beakhouse *et al.* 1996, Pan & Breaks 1997). It consists of a (i) wall zone, (ii) aplite zone, (iii) petalite zone, (iv) east-end pollucite-bearing zone, (v) replacement of wall zone and (vi) replacement pods overprinting the petalite zone. The wall zone (i) is 0.5-1.0 m thick and contains dominant quartz, subordinate coarse blocky pink-to-orange albite, muscovite and white beryl, and accessory cassiterite, Ti-rich wodginite, (Fe, Ti)-rich wodginite, dark-green tourmaline (sample 93-44A), apatite, and rare stibiomicrolite. The layered aplite (ii) in the western part of the pegmatite contains dominant quartz, albite, muscovite and beryl with a layer of quartz (30 vol%), orange garnet (60 vol%) and biotite (10 vol%), and an albite-rich layer with fine-grained black cassiterite, manganocolumbite and wodginite. The petalite zone (iii) is 0.5-6.0 m thick and contains dominant very coarse-grained white petalite (30-50 cm in diameter) (80-95 vol%) and subordinate coarse blocky microcline (up to 2 m long), interstitial quartz and accessory

manganotantalite. The east-end pollucite-bearing zone (iv), close to the wall zone, occurs at the very eastern end of the pegmatite and seems to be the most fractionated part of the pegmatite (F.W. Breaks, pers. comm.). The east-end zone contains dominant cream-coloured cleavelandite, pink quartz and light yellow-brown altered pollucite, and subordinate dark-blue tourmaline (sample 94-44C) and brown cassiterite (up to 0.5 cm wide).

Tourmaline does not occur in the exocontact (F.W. Breaks, pers. comm.). The replacement unit (v), which overprints the wall zone, contains dominant biotite and garnet, and subordinate black tourmaline (sample 94-44B) and albite (Beakhouse *et al.* 1996). This replacement unit formed by metasomatic influx of Fe from the banded iron formation host rock.

About 5-10 vol% of the petalite zone has been affected by albitization of petalite, break down of petalite to squi and alteration of petalite + K-feldspar to albite + muscovite pods (Beakhouse *et al.* 1996). The replacement pods (vi) contain dominant radial albite (70-80 vol%) and Li-muscovite (10-20 vol%), subordinate quartz, K-feldspar, white beryl, fluorapatite and dark-green primary tourmaline (sample 94-44D), and accessory petalite, pollucite, topaz, cassiterite, tantalite, microlite, wodginite, zircon and monazite. The dark-green tourmaline only occurs associated with the replacement pods, not in the unaltered petalite + K-feldspar assemblage (F.W. Breaks, pers. comm.). The dark-green tourmaline is assumed to be primary as (1) it has an euhedral contact with petalite; (2) it has the same composition as the tourmaline of the wall zone (see below); and (3) the only external source of B would be a narrow unit of pelitic metasediments close to pegmatites

#4 - 10, but far from Marko's pegmatite. One possible explanation is that (Na, B)-rich fluids from the wall zone caused late metasomatism of the solid petalite zone, as the wall zone and replacement pods contain similar mineral assemblages (quartz, albite and muscovite).

Dark-green tourmaline (5 mm) with Cs-muscovite inclusions occurs in wall zone (i), dark-green tourmaline needles (1 cm wide x 3.5 cm long) with pollucite inclusions occurs in albite-Li-muscovite pods (vi), and blue tourmaline columns (2.5 cm long) occur in the east-end pollucite-bearing zone (iv). Black endomorphic tourmaline (3-7 mm long) contains Cs-bearing biotite inclusions and is associated with biotite in the wall-zone replacement unit (v).

5.4.2. Tourmaline at Marko's pegmatite

The primary tourmaline composition at Marko's pegmatite evolves through the following crystallization sequence: (± elbaite-schorl), Ca-bearing elbaite-schorl, (± Ca-rich elbaite-schorl) (in wall and petalite zones) → (Ca, Fe, Mn)-bearing elbaite [± Ca-rich (Fe, Mn)-bearing elbaite] (in the east-end pollucite-bearing zone) (Fig. 5.18a, Table 5.13). The *X*-site contents in tourmaline form a tight cluster in Figure 5.11b for all three pegmatite zones, except for two compositions of elbaite-schorl from the petalite zone which are enriched in vacancies (Table 5.13, composition 2). A maximum of 0.20 *apfu* Ca occurs in Ca-rich elbaite-schorl in the wall zone, 0.21 *apfu* Ca occurs in Ca-rich elbaite-schorl in the petalite core, and in Ca-rich (Fe, Mn)-bearing elbaite in the east-end pollucite-bearing zone (Table 5.13, compositions 1, 4 and 6).

TABLE 5.13: REPRESENTATIVE COMPOSITIONS OF TOURMALINE (WT%) AT MARKO'S PEGMATITE, SEPARATION RAPIDS PEGMATITE GROUP

	1	2	3	4	5	6	7	8
SiO_2	34.40	36.20	36.30	35.30	36.30	35.80	33.70	34.20
TiO_2	0.14	0.05	0.15	0.08	0.05	0.00	0.05	0.05
B_2O_3*	10.58	10.57	10.74	10.71	10.75	10.77	10.24	10.15
Al_2O_3	38.40	36.30	37.40	38.30	38.20	39.20	35.20	33.50
MgO	0.08	0.04	0.06	0.02	0.00	0.00	0.02	0.01
CaO	1.14	0.21	0.86	1.23	1.00	1.20	0.59	0.48
MnO	1.12	1.11	1.07	1.20	2.52	2.79	0.36	0.25
FeO	6.80	9.02	7.10	7.04	3.68	2.56	13.60	15.10
Li_2O*	1.19	0.88	1.31	1.25	1.54	1.60	0.36	0.26
Na_2O	1.92	1.75	2.02	1.91	2.01	1.94	1.65	1.59
H_2O*	3.16	3.16	3.15	3.23	3.10	3.20	3.11	3.15
F	1.04	1.02	1.18	0.99	1.28	1.08	0.89	0.74
O=F	-0.44	-0.43	-0.50	-0.42	-0.54	-0.45	-0.37	-0.31
Total	99.53	99.88	100.84	100.84	99.89	99.69	99.40	99.17
Formulae normalized to 31 anions								
T -Si	5.65	5.95	5.88	5.73	5.87	5.78	5.72	5.85
Al	0.35	0.05	0.12	0.27	0.13	0.22	0.28	0.15
B	3.00	3.00	3.00	3.00	3.00	3.00	3.00	3.00
Z -Al	6.00	6.00	6.00	6.00	6.00	6.00	6.00	6.00
Y -Al	1.09	0.99	1.01	1.05	1.15	1.23	0.76	0.61
Ti	0.02	0.01	0.02	0.00	0.01	0.00	0.01	0.01
Mg	0.02	0.01	0.01	0.01	0.00	0.00	0.00	0.00
Mn	0.16	0.16	0.15	0.16	0.34	0.38	0.05	0.04
Fe^{2+}	0.93	1.24	0.96	0.96	0.50	0.35	1.93	2.16
Li	0.78	0.59	0.85	0.82	1.00	1.04	0.25	0.18
$\sum Y$	3.00	3.00	3.00	3.00	3.00	3.00	3.00	3.00
X -Ca	0.20	0.04	0.15	0.21	0.17	0.21	0.11	0.09
Na	0.61	0.56	0.63	0.60	0.63	0.61	0.54	0.53
□	0.19	0.40	0.22	0.19	0.20	0.18	0.35	0.38
OH	3.46	3.47	3.40	3.49	3.35	3.45	3.52	3.60
F	0.54	0.53	0.60	0.51	0.64	0.55	0.48	0.40

*B_2O_3, Li_2O and H_2O calculated by stoichiometry; B = 3 *apfu*, Li = 15 - $\sum T + Z + Y$ and OH+F = 4 *apfu*.

(1) dark-green Ca-rich elbaite-schorl, wall zone, sample 93-44A-3; (2) dark-green elbaite-schorl rim, petalite zone, sample 94-44D-1; (3) black Ca-bearing elbaite-schorl core, petalite zone, sample 94-44D-4; (4) black Ca-rich elbaite-schorl rim of (3), petalite zone, sample 94-44D-4; (5) blue (Ca, Fe, Mn)-bearing elbaite core, east- end zone, sample 94-44C; (6) blue Ca-rich (Mn, Fe)-bearing elbaite rim of (5), east- end zone, sample 94-44C; (7) dark-green Ca-bearing Al-rich schorl, wall-zone replacement, sample 94-44B-1; (8) dark-green Al-rich schorl, wall-zone replacement, sample 94-44B-3.

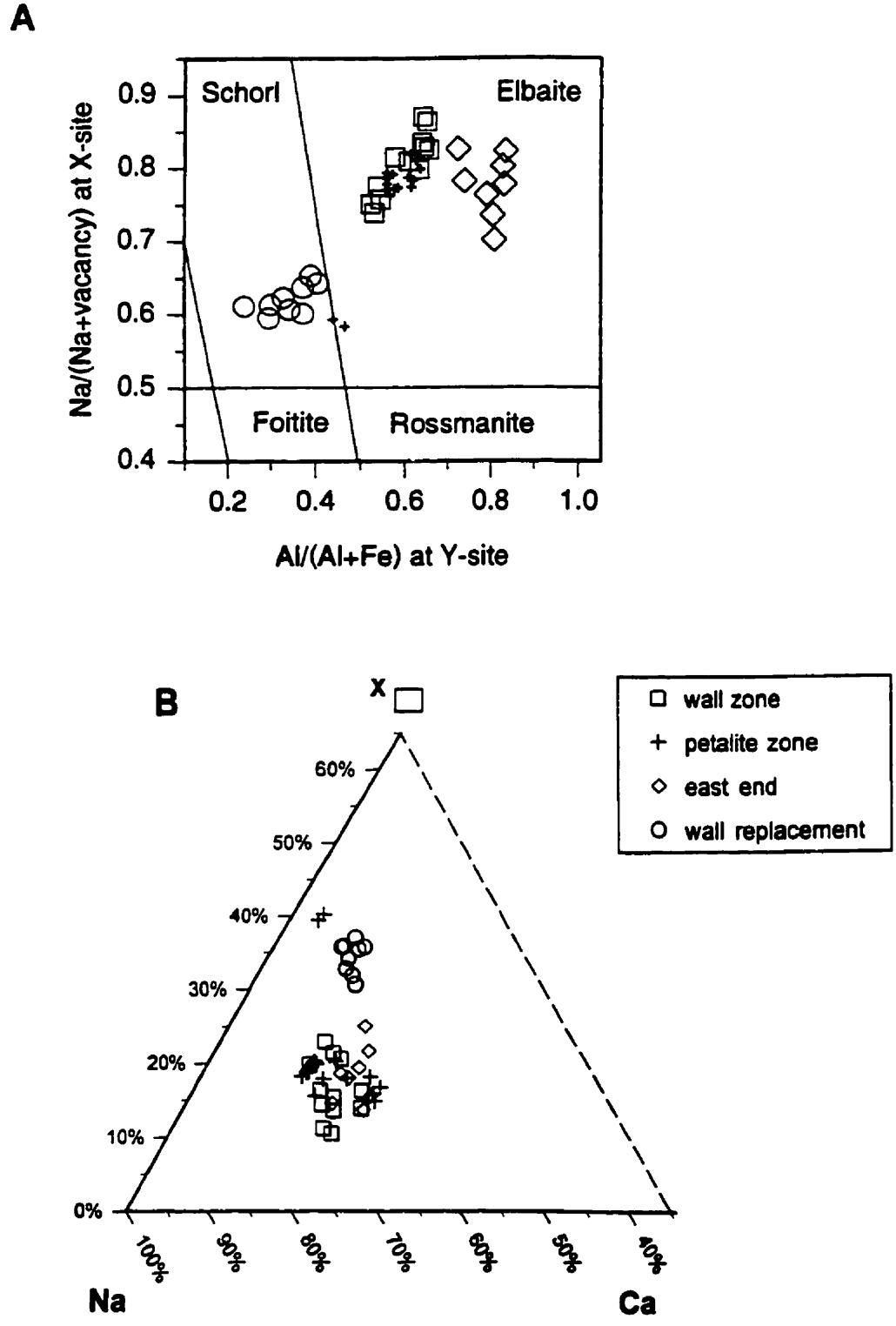

Figure 5.18. Tourmaline compositions at Marko's pegmatite, Separation Rapids pegmatite group.

Figures 5.19a and 5.19b show that Ca-bearing elbaite-schorl from the wall and petalite zones have similar high Fe and low Mn contents, and variable Al content at the *Y*-site; (Ca, Fe, Mn)-bearing elbaite from the east-end pollucite-bearing zone has much lower Fe and higher Mn contents, but similar variable Al content at the *Y*-site. The maximum Mn content of 0.38 *apfu* Mn occurs in blue Ca-rich (Mn, Fe)-bearing elbaite in the east-end pollucite-bearing zone (Table 5.13, composition 6). Figure 5.19b also shows a negative correlation between Fe and Mn. The most primitive tourmaline has moderate Fe and Al+Li and low Mn (elbaite-schorl) with increasing fractionation Fe decreases and Mn and Al+Li increases ((Ca, Fe, Mn)-bearing elbaite).

Figures 5.19c and 5.19d show that the ranges in F content for tourmaline in all three pegmatite zones are similar. There is a positive correlation between Na and F, with a maximum F content of 0.76 *apfu* F and Na content of 0.71 *apfu* Na in green Ca-bearing elbaite-schorl in the wall zone (Figure 5.19c).

Most tourmaline at Marko's pegmatite contains no Mg or Zn (< 0.02 *apfu* Mg and Zn). Lack of Mg in tourmaline indicates that the pegmatitic melt did not interact with the host amphibolite at the southern contact. The maximum Ti content is 0.05 *apfu* Ti in Ca-bearing elbaite-schorl which is associated with Ti-rich wodginite in the wall zone.

The dark-green tourmaline in the endomorphic replacement of the wall zone is Ca-bearing Al-rich schorl and Al-rich schorl. This tourmaline is more □- and Fe-rich and more Ca, Na, Mn- and F-poor than the primary tourmaline (Figs. 5.18a, b). The Fe-enrichment is due to the influx of Fe from the banded iron-formation host-rock.

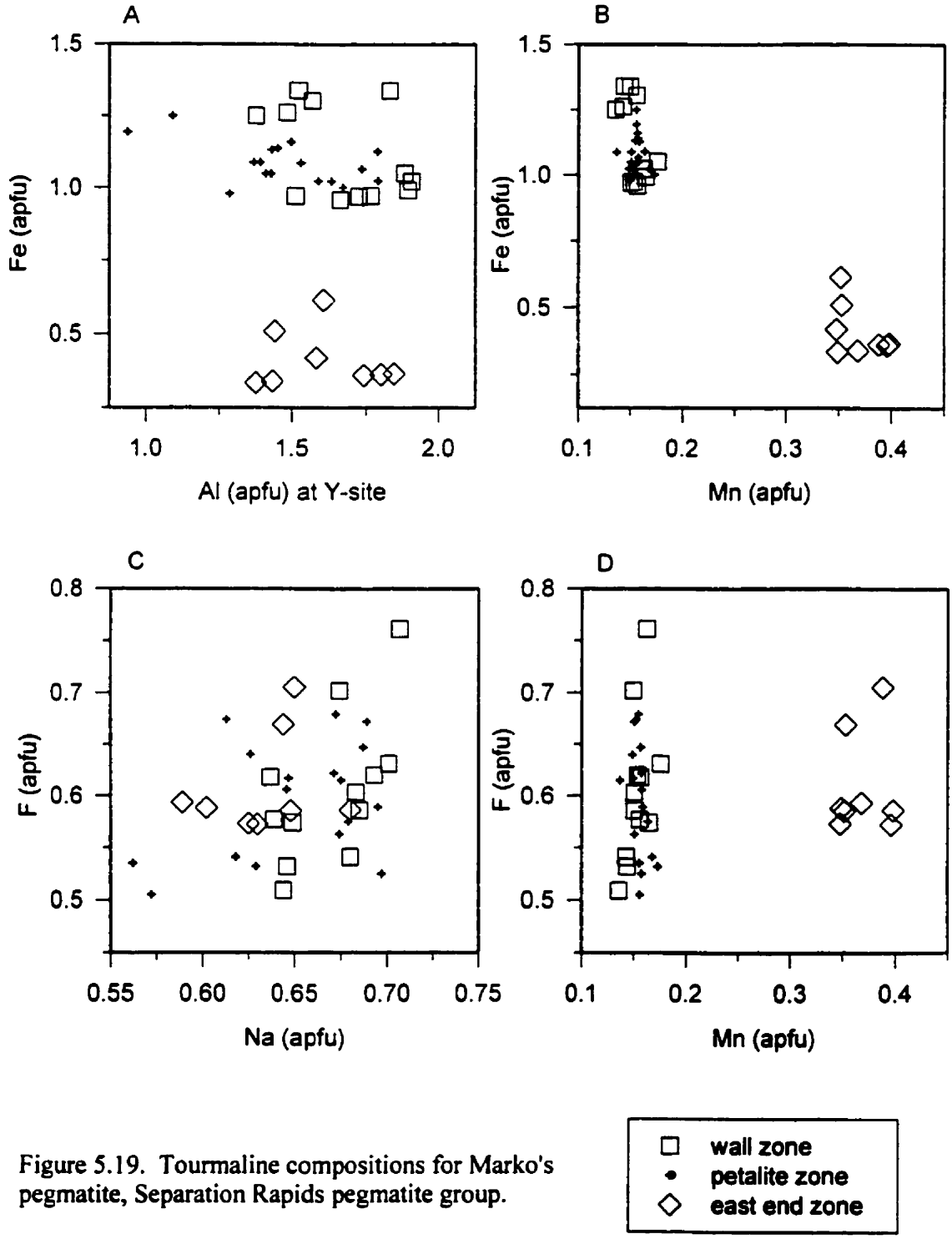

Figure 5.19. Tourmaline compositions for Marko's pegmatite, Separation Rapids pegmatite group.

5.5. Pegmatite #5, Separation Rapids pegmatite group

5.5.1. General geology

Pegmatite #5 is located within the Separation Rapids pegmatite group about 1.5 km northeast of Marko's pegmatite. Pegmatite #5 is a small petalite-subtype pegmatite dyke which intrudes mafic metavolcanic rocks (amphibolite). The geology of pegmatite #5 is very similar to that of Marko's pegmatite. Pegmatite #5 consists of (i) wall zone, (ii) K-feldspar-rich zone, (iii) petalite core, and (iv) replacement pods overprinting the petalite core (F.W. Breaks, pers. comm.; Pan & Breaks 1997). The wall zone (i) contains dominant albite, quartz and muscovite, and subordinate black tourmaline, K-feldspar, green beryl and fluorapatite. The K-feldspar-rich zone (ii) contains dominant pink blocky K-feldspar (with 2.06-3.50 wt% Rb_2O), quartz and albite, and subordinate black tourmaline and muscovite. The petalite core (iii) contains dominant petalite megacrysts (1-1.5 m diameter), subordinate K-feldspar, muscovite and black tourmaline, and accessory tungstenian wodginite, ferrowodginite, cassiterite and microlite. The replacement pods (iv) of the petalite core consist of dominant albite and muscovite, and subordinate fluorapatite and garnet.

Graphic intergrowths of black tourmaline + quartz (1-2 cm long) occur in wall zone (i), black tourmaline (1-0.5 cm long) with quartz inclusions occurs in K-feldspar-rich zone (ii), and black tourmaline occurs in the petalite core (iii).

5.5.2. Tourmaline at Pegmatite #5

The tourmaline composition at pegmatite #5 evolves through the following

sequence: schorl-dravite, Mg-rich schorl (in wall zone and K-feldspar zone) → Mg-rich schorl, schorl-elbaite (in petalite core) (Fig. 5.20a, Table 5.14). The *Y*-site contents form a tight cluster in Figure 5.20a for Mg-rich tourmaline (schorl-dravite and Mg-rich schorl), except for the Mg-poor, Al-rich compositions (schorl-elbaite).The Ti content in tourmaline ranges from 0.09 *apfu* in schorl-dravite from the wall and K-feldspar zones to 0.01 *apfu* in schorl-elbaite from the petalite core. The dominant substitution at the *X*-site is Na ▫ ▫with a maximum of 0.49 *apfu* vacancies in rare Mg-rich schorl-foitite in the K-feldspar zone (Fig. 5.20b, Table 5.14, composition 4). The maximum Ca content of 0.21 *apfu* occurs in one composition of Ca-rich schorl-dravite in the wall zone 0.5 cm from the contact with the host amphibolite (Table 5.14, composition 1). There is a positive correlation between Ca and Mg in most schorl-dravite and Mg-rich schorl (Fig. 5.21a).

There is a positive correlation between Na, Mn and F contents (Figs. 5.21b, c), with ≤ 0.69 *apfu* Na in schorl-dravite and Mg-rich schorl in the wall zone and K-feldspar zone, and ≤ 0.08 *apfu* Mn and ≤ 0.45 *apfu* F in schorl-elbaite in the petalite core (Table 5.14, composition 6).

The tourmaline compositions in pegmatite #5 are significantly more Mg-rich and (Al+Li)-poor than tourmaline from other petalite-subtype pegmatites discussed in this chapter, but are similar to tourmaline compositions from other pegmatite dykes in the Separation Rapids pegmatite group. The source of Ca, Mg and Ti in tourmaline is assumed to be fluids derived from the host amphibolite, as tourmaline in the miarolitic cavities in the genetically-related S-type peraluminous granites of the Treelined Lake complex is (Ca, Mg)-poor schorl-elbaite. Pan and Breaks (1997) showed that the REE

characteristics of fluorapatite in the sodic wall zones of the Separation Rapids rare-element pegmatites are similar to those of the host amphibolites, indicating significant fluid infiltration from the country rocks during formation of the pegmatites.

TABLE 5.14. REPRESENTATIVE COMPOSITIONS OF TOURMALINE (WT%) AT PEGMATITE #5, SEPARATION RAPIDS PEGMATITE GROUP

	1	2	3	4	5	6
SiO_2	35.60	35.65	35.70	36.27	35.91	35.57
TiO_2	0.56	0.52	0.62	0.15	0.12	0.10
B_2O_3*	10.33	10.50	10.54	10.54	10.54	10.52
Al_2O_3	30.90	33.04	33.11	34.24	35.07	35.67
MgO	4.14	3.42	4.16	3.14	0.94	0.89
CaO	1.17	0.38	0.49	0.16	0.13	0.16
MnO	0.18	0.46	0.25	0.29	0.41	0.58
FeO	10.90	10.73	9.75	9.68	11.70	10.36
Li_2O*	0.32	0.28	0.31	0.29	0.51	0.66
Na_2O	1.67	2.10	2.11	1.51	1.88	2.05
H_2O*	3.44	3.36	3.39	3.56	3.38	3.22
F	0.27	0.56	0.53	0.16	0.53	0.86
O=F	-0.11	-0.24	-0.22	-0.07	-0.22	-0.36
Total	99.37	100.76	100.74	99.92	100.90	100.28
Formulae normalized to 31 anions						
T -Si	5.99	5.90	5.89	5.98	5.92	5.88
Al	0.01	0.10	0.11	0.02	0.08	0.12
B	3.00	3.00	3.00	3.00	3.00	3.00
Z -Al	6.00	6.00	6.00	6.00	6.00	6.00
Y -Al	0.11	0.35	0.32	0.64	0.74	0.82
Ti	0.07	0.07	0.08	0.02	0.02	0.01
Mg	1.04	0.84	1.02	0.77	0.23	0.22
Mn	0.03	0.06	0.03	0.04	0.06	0.08
Fe^{2+}	1.53	1.49	1.34	1.34	1.61	1.43
Li	0.22	0.19	0.21	0.19	0.34	0.44
$\sum Y$	3.00	3.00	3.00	3.00	3.00	3.00
X -Ca	0.21	0.07	0.09	0.03	0.02	0.03
Na	0.55	0.67	0.67	0.48	0.60	0.66
□	0.24	0.26	0.24	0.49	0.38	0.31
OH	3.86	3.71	3.72	3.92	3.72	3.55
F	0.14	0.29	0.28	0.08	0.28	0.45

*B_2O_3, Li_2O and H_2O calculated by stoichiometry; B = 3 *apfu*, Li = 15 - $\sum T + Z + Y$ and OH+F = 4 *apfu*.

(1) black Ca-rich schorl-dravite 0.5 cm from the host rock, sample 94-80A-3; (2) black Mg-rich schorl from the wall zone, sample SPL1; (3) schorl-dravite from the K-feldspar zone, sample SPL3-4; (4) green Mg-rich schorl-foitite from the K-feldspar zone, sample SPL3-3; (5) brown schorl-elbaite from the petalite core, sample SPL2-1; and (6) black schorl-elbaite from the petalite core, sample SPL2-4.

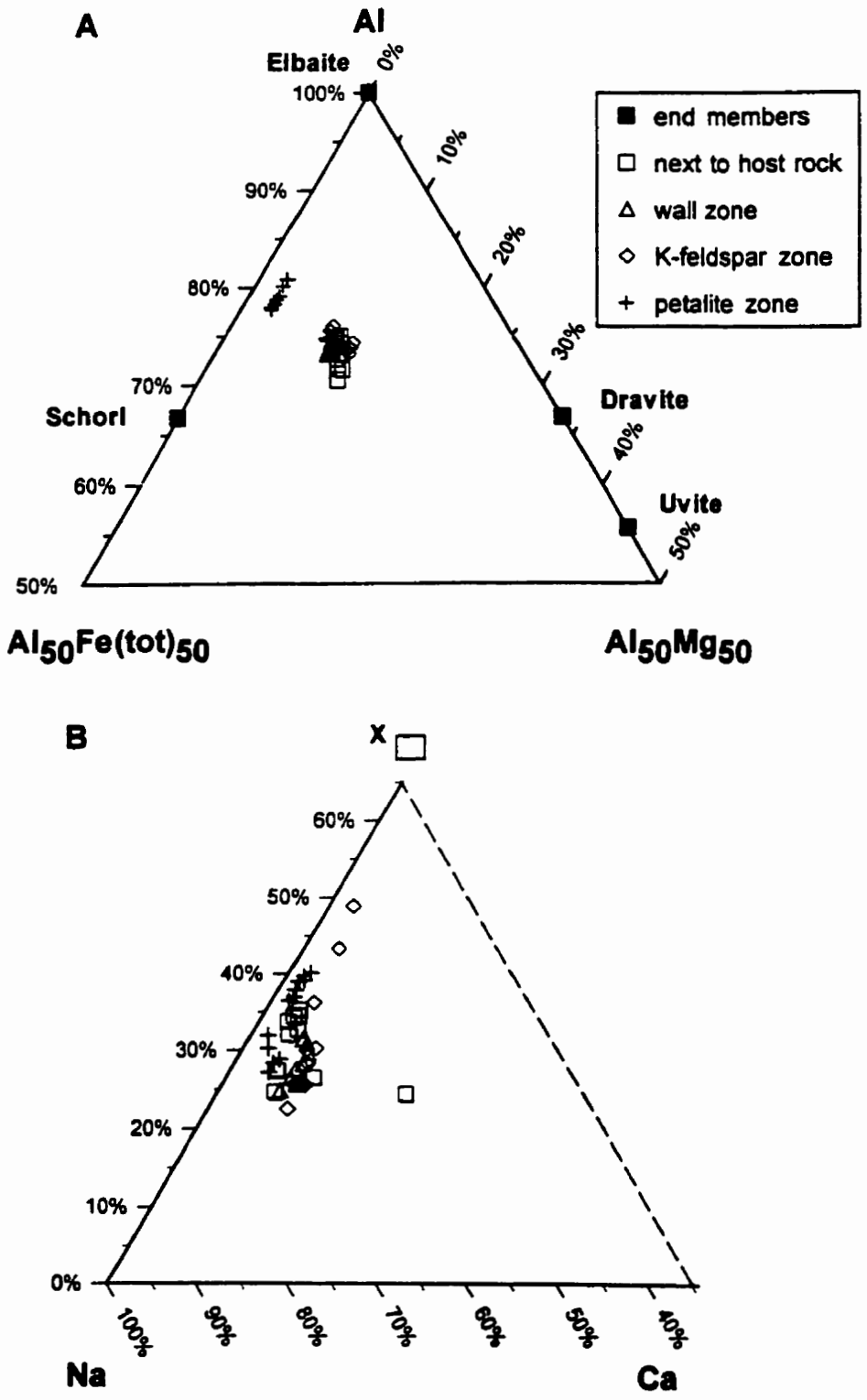

Figure 5.20. Tourmaline compositions in Pegmatite #5, Separation Rapids pegmatite group.

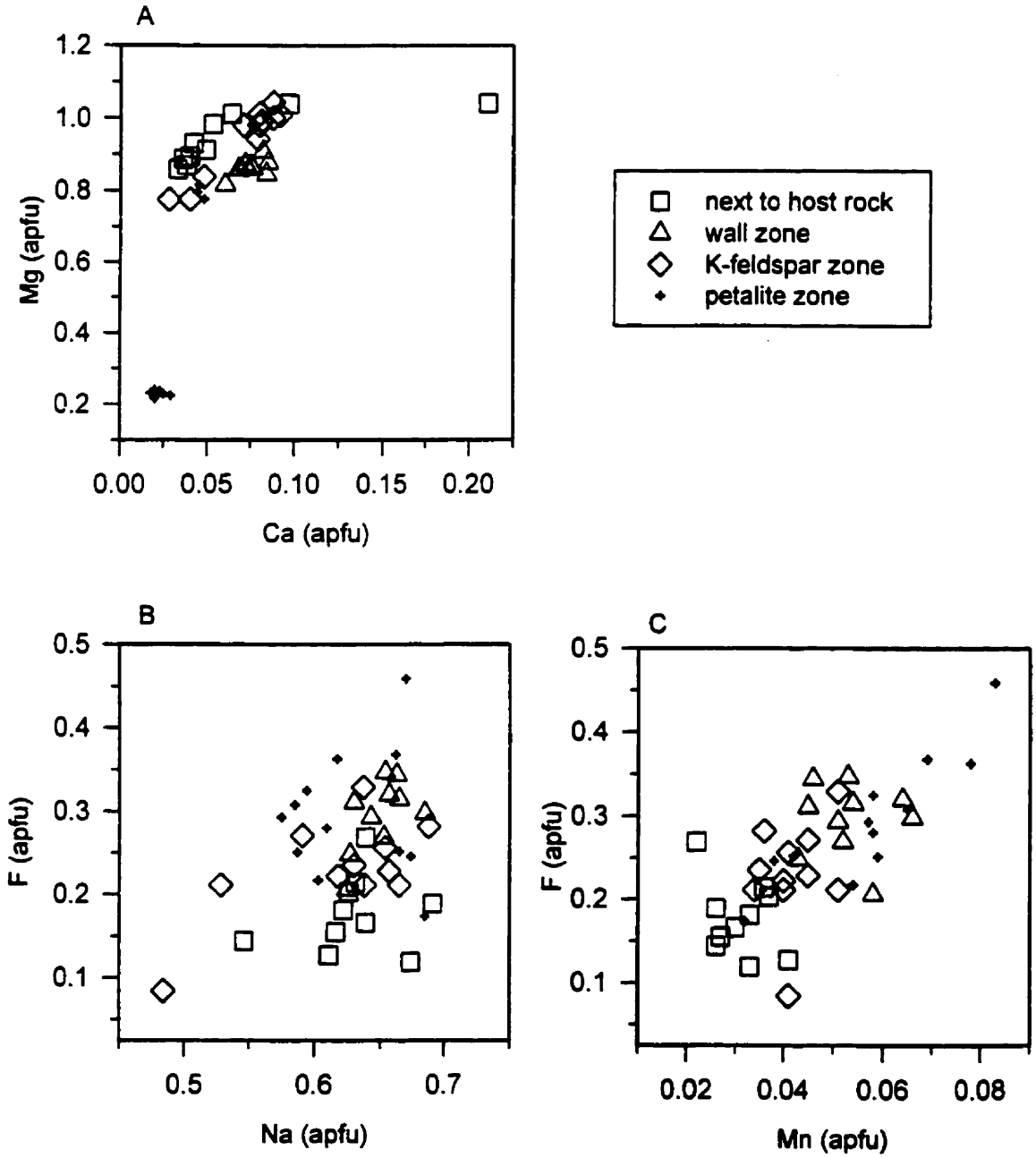

Figure 5.21. Tourmaline compositions in Pegmatite #5, Separation Rapids pegmatite group.

CHAPTER 6

Tourmaline in elbaite-subtype pegmatites

6.1. Elbaite-subtype pegmatites

Elbaite-subtype pegmatites are defined as pegmatites with elbaite as the dominant (and sometimes the only) Li-bearing mineral (Novák & Povondra 1995). The geology of the Moldanubian (Czech Republic) elbaite-subtype pegmatites is summarized by Novák & Povondra (1995).These pegmatites are commonly symmetrically zoned with a (1) fine- to coarse-grained granitic border zone (quartz + plagioclase + K-feldspar + biotite) which grades into a (2) graphic zone (K-feldspar + quartz) and (3) isolated pods of blocky K-feldspar. A (4) coarse-grained schorl-enriched zone (quartz + albite + schorl + K-feldspar ± garnet) is present in some dykes, forming local pods or even independent zones. Patches of an albite zone (5) which consists of medium- to coarse-grained bluish-greenish cleavelandite occur in the central parts of the dykes. (6) Pockets (*i.e.*, miarolitic cavities) occur in the central parts of the dyke. Note that quartz cores are absent in elbaite-subtype pegmatites.

The pockets contain very coarse-grained K-feldspar, smoky quartz and gem-quality multicoloured elbaite. Elbaite-subtype pegmatites may be mined for their economic quantities of elbaite (*e.g.*, Stak Nala, Pakistan; Little Three pegmatite, California; the Elba pegmatites). The pockets also contain minor albite, rare cassiterite, zircon, lepidolite, late Be-rich minerals (bertrandite and bavenite) and B-rich minerals (hambergite, danburite, datolite and boromuscovite).

Table 6.1. Mineral parageneses of some elbaite pegmatites.

	Řeč	Pik	Cti	Bis	JcII	Vla
quartz	A	A	A	A	A	A
K-feldspar	A	A	A	A	A	A
albite	C	C	A	C	A	M
biotite	R	VR	M	R	M	R
muscovite	–	–	R	R	–	–
lepidolite	R	VR	R	R	–	–
masutomilite	–	–	VR	–	–	–
schorl	C	M	C	M	M	M
dravite	–	–	–	R	–	–
elbaite	M	R	R	R	R	R
garnet	R	M	M	–	M	–
cordierite	–	–	–	R	–	–
andalusite	–	–	–	VR	–	–
beryl	–	VR	VR	–	R	–
cassiterite	R	VR	VR	VR	VR	–
columbite	VR	–	VR	VR	VR	VR
pyrochlor	VR	–	–	–	–	VR
niobian rutile	–	–	–	VR	–	–
loellingite	R	VR	–	–	–	–
zircon	VR	–	VR	VR	VR	VR
apatite	–	–	R	–	VR	–
hambergite	–	–	R	–	R	–
danburite	–	–	–	–	–	VR
datolite	–	–	–	–	–	VR
boromuscovite	VR	–	–	–	–	–
bertrandite	VR	–	VR	–	–	–
bavenite	–	–	–	–	VR	VR
stokesite	–	–	VR	–	–	–
fluorite	–	–	–	–	–	R
magnetite	–	–	–	–	–	R
scheelite	–	–	–	–	–	VR

Additional minor to accessory phases observed in the elbaite pegmatites (Sušice III, Bližná) including secondary minerals (As) from Řečice: liddicoatite, pollucite, analcime, helvite, ilmenite, titanite, diopside, tremolite, calcite, bastnaesite, scorodite, arseniosiderite, pharmacosiderite. **Řeč** Řečice; **Pik** Pikárec; **Cti** Ctidružice; **Bis** Biskupice; **JcII** Jeclov II; **Vla** Vlastějovice. **A** abundant, **C** common, **M** minor, **R** rare, **VR** very rare (Novák & Povondra 1995).

The characteristics of elbaite-subtype pegmatites that distinguish them from lepidolite-, petalite-, amblygonite- and spodumene-subtypes are as follows: (1) elbaite is the only substantial Li-bearing mineral present; (2) lepidolite, muscovite and topaz (F-poor) are absent or very rare; (3) the presence of B-rich minerals other than tourmaline; (4) the abundance of garnet (almandine and spessartine); (5) the presence of Mn-rich elbaite; (6) modal dominance of K-feldspar over albite (Novák & Povondra 1995) (Table 6.1).

Examples of elbaite-subtype pegmatites which will be discussed in detail include Belo Horizonte, California, and Řečice, Pikárec, Ctidružice, Vlastějovice, Czech Republic. The tourmalines from Stak Nala, Pakistan (Laurs *et al.* 1998), Little Three, California (Stern *et al.* 1986, Foord *et al.* 1989, Morgan & London, in press) and Sahatany Valley, Madagascar (Bloomfield 1997) pegmatites have been studied in detail, and work on tourmaline in the Elba pegmatites is in progress (Pezzotta *et al.* 1996; Aurisicchio & Pezzotta 1997; Tonarini *et al.* 1998; Aurisicchio *et al.* 1999).

6.2. The Belo Horizonte #1 pegmatite

6.2.1. General Geology

Belo Horizonte #1 pegmatite is a zoned miarolitic elbaite-subtype pegmatite located in the San Jacinto district of the Peninsular range, southwestern California. Belo Horizonte has an average thickness of 2 m, a depth of 6 m down dip, an exposed length of 30 m, and it strikes N56°E with a dip of 65°SE (M.C. Taylor, per. comm.). It crystallized from a highly evolved hydrous granitic melt 94.4±2 Ma ago, after intruding

and extensively altering a 101 Ma calcic olivine-gabbro (Taylor 1997).

The unaltered (Ca, Mg)-rich Thomas Mountain olivine-gabbro host-rock contains fosterite, orthopyroxene, clinopyroxene, cummingtonite-hornblende and bytownite-anorthite (An_{92-97}) (M.C. Taylor, pers. comm.). This gabbro has been hydrothermally altered up to 10 m from the contact with the Belo Horizonte pegmatite. In addition to metasomatic tourmaline, the following pseudomorphs have been noted: (a) F-bearing ferrian montmorillonite after forsteritic olivine; (b) F-bearing hydrobiotite after orthopyroxene, clinopyroxene and cummingtonite-hornblende; (c) halloysite after calcic plagioclase. This argillaceous alteration was caused by an influx of Si, Al, B, K, Na and F from the pegmatite into the host rock.

The pegmatite has a sodic-plagioclase-rich lower part and microcline-perthite-rich upper part. The symmetrically zoned pegmatite consists of (1) a border zone, (2) a lower wall zone, (3) an upper wall zone, (4) a lower first-intermediate zone, (5) an upper first-intermediate zone, (6) a lower second-intermediate zone, (7) an upper second-intermediate zone and (8) a pocket zone (Fig. 6.1, Table 6.2) (M.C. Taylor, pers. comm.).

The major minerals are quartz, sodic plagioclase and microcline-perthite, and the minor minerals are biotite, tourmaline, almandine-spessartine and cassiterite. Elbaite is the only Li-bearing mineral present at Belo Horizonte. The pegmatite is characterized by abundant graphic microcline-perthite+quartz and schorl+quartz intergrowths, minor almandine-spessartine, and accessory B-rich minerals (F-rich hambergite, danburite, manganoan hellandite and tusionite) and Be-rich minerals (hambergite and helvite-danalite) in the pockets (Taylor 1997). Late-stage Mn-enrichment is suggested by the

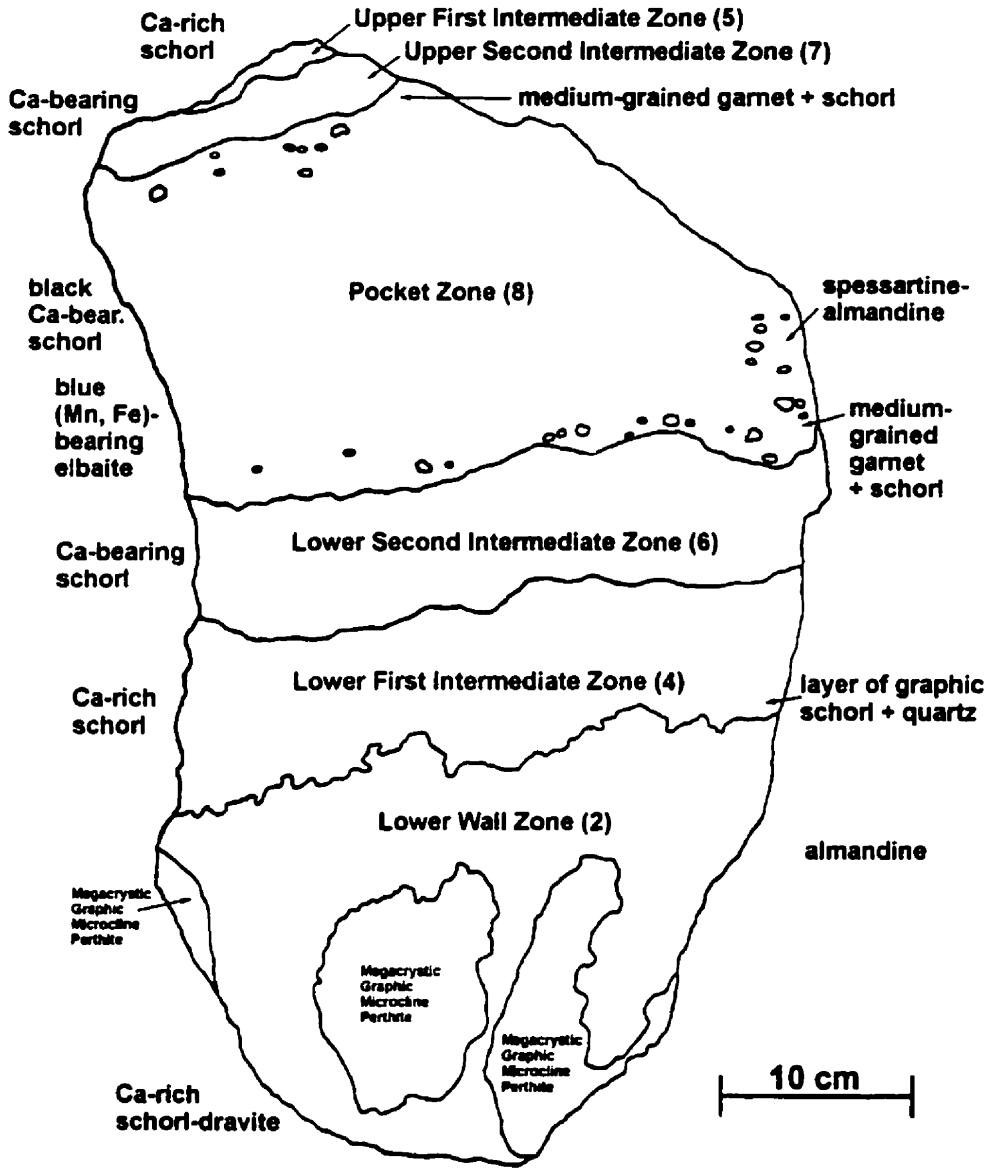

Figure 6.1. Cross-section of Belo Horizonte No. 1 pegmatite (M.C. Taylor, pers. comm. and data of author).

TABLE 6.2. INTERNAL ZONING IN THE ELBAITE-SUBTYPE BELO HORIZONTE #1 PEGMATITE, CALIFORNIA

pegmatite zone	mineral assemblage and texture
border zone (1)	fine- to medium-grained sodic plagioclase, quartz, microcline-perthite, megacrystic biotite up to 4 cm
upper wall zone (3)	graphic microcline-perthite+quartz (medium-grained graphic schorl+quartz), [almandine-spessartine]
upper first-intermediate zone (5)	medium-grained graphic microcline-perthite+quartz (medium-grained graphic schorl+quartz)
upper second-intermediate zone (7)	sodic plagioclase, quartz, microcline aplite (fine-grained graphic schorl+quartz)
pocket zone (8)	border layer of medium-grained euhedral garnet and schorl up to 5 mm with blue elbaite rims around garnet blocky microcline-perthite, cleavelandite, quartz (almandine-spessartine, elbaite, cassiterite)
pockets (8)	quartz, feldspars, multicoloured elbaite, cassiterite, Be-rich danalite, B-rich (danburite, hellandite and tusionite), stilbite, beidellite, Cu_2Se
lower second-intermediate zone (6)	same as upper second-intermediate zone (7)
lower first-intermediate zone (4)	medium-grained sodic plagioclase and quartz (graphic microcline-perthite+quartz) basal layer of graphic schorl+quartz, (euhedral monazite up to 1.6 cm)
lower wall zone (2)	fine-grained sodic plagioclase and quartz, megacrystic graphic microcline-perthite+quartz (almandine-spessartine, medium-grained graphic schorl+quartz)
border zone (1)	same as above

( ) - minor mineral, [ ] - accessory mineral, (M.C. Taylor, pers. comm.)

presence of Mn-rich elbaite, manganoan hellandite, tusionite, helvite and manganocolumbite in the pockets. Fluorine is limited to elbaite and F-rich hambergite in the pockets.

The only micas in the pegmatite are minor biotite in the border zone (1) and rare late muscovite in the pocket zone (8). The abundance of B-rich minerals and lack of

primary micas indicate that the crystallizing pegmatite melt was B-rich, F-poor and alkaline.

Tourmaline occurs in each pegmatite zone, including the exocontact (M.C. Taylor, pers. comm.). The tourmaline is black in all pegmatite zones except the pocket zone. It is very minor in the border zone, and occurs as medium-grained (2-5 mm) graphic schorl+quartz intergrowths and as euhedral grains in wall zones (2) and (3) and first intermediate zones (4) and (5). The graphic and euhedral schorl decreases in size to fine-grained (0.5-1.0 mm) in second intermediate zones (6) and (7). In the pocket zone (8), reaction rims of blue tourmaline occur surrounding garnet. The pockets contain multicoloured zoned tourmalines which commonly have a black core surrounded by pink, purple, blue and colourless intermediate zones and green rims.

6.2.2. Composition of exocontact and endomorphic tourmaline at Belo Horizonte

The (Ca, Mg, Ti)-rich nature of the host gabbro (forsterite- and bytownite-anorthite-bearing) is reflected in the composition of the exocontact tourmaline which is dominantly feruvite-uvite with minor uvite-feruvite, dravite-uvite and Ca-rich schorl-dravite (Fig. 6.2, Table 6.3, compositions 1, 2). The exocontact tourmaline is enriched in Ti (0.27-0.22 *apfu* Ti) relative to tourmaline in the pegmatite. The source of the Ca, Mg, Fe and Ti in the tourmaline is the gabbro host rock.

Tourmaline in the outermost pegmatite zones is affected by exomorphism in which Ca-, Mg-and Ti-rich fluids infiltrated the pegmatite from the host gabbro. In the lower border zone (1), tourmaline ranges in composition from Ti-bearing feruvite-schorl

TABLE 6.3. REPRESENTATIVE COMPOSITIONS OF EXOCONTACT AND ENDOMORPHIC TOURMALINE (WT%) IN ZONES (1), (2) AND (4) OF THE BELO HORIZONTE PEGMATITE

	1	2	3	4	5	6	7	8	9	10
SiO_2	35.40	34.80	34.20	35.00	33.90	35.10	34.70	33.90	34.00	34.80
TiO_2	2.01	1.82	2.82	1.25	1.16	0.91	1.66	1.25	0.97	0.29
B_2O_3*	10.33	10.29	10.05	10.24	9.96	10.35	10.22	10.00	9.95	10.08
Al_2O_3	27.00	28.00	25.20	27.90	28.50	30.20	29.40	28.90	28.70	30.20
MgO	6.96	7.35	4.06	4.58	1.43	4.63	3.14	1.69	0.92	0.63
CaO	3.00	2.28	2.68	2.00	1.44	1.68	1.25	1.25	1.21	0.81
MnO	0.09	0.00	0.28	0.25	0.42	0.08	0.12	0.20	0.20	0.28
FeO	10.30	9.55	16.10	14.40	17.10	12.20	14.30	17.10	18.20	17.10
Li_2O*	0.33	0.16	0.23	0.11	0.19	0.19	0.22	0.10	0.14	0.22
Na_2O	1.14	1.50	1.37	1.72	1.76	1.66	1.78	1.71	1.80	1.89
H_2O*	3.56	3.55	3.39	3.45	3.32	3.51	3.48	3.45	3.43	3.33
F	0.00	0.00	0.16	0.18	0.25	0.13	0.11	0.00	0.00	0.31
O=F	0.00	0.00	-0.07	-0.08	-0.11	-0.05	-0.05	0.00	0.00	-0.13
total	100.12	99.30	100.47	101.00	99.32	100.59	100.33	99.55	99.52	99.81
Formulae normalized to 31 anions										
T: Si	5.96	5.88	5.92	5.94	5.92	5.89	5.90	5.89	5.94	6.00
Al	0.04	0.12	0.08	0.06	0.08	0.11	0.10	0.11	0.06	0.00
B	3.00	3.00	3.00	3.00	3.00	3.00	3.00	3.00	3.00	3.00
Z: Al	5.31	5.46	5.06	5.52	5.78	5.87	5.79	5.81	5.85	6.00
Mg	0.69	0.54	0.94	0.48	0.22	0.13	0.21	0.19	0.15	0.00
Y: Al	0.00	0.00	0.00	0.00	0.00	0.00	0.00	0.00	0.00	0.14
Ti	0.26	0.23	0.37	0.16	0.15	0.12	0.21	0.16	0.13	0.04
Mg	1.06	1.31	0.10	0.68	0.16	1.03	0.59	0.25	0.08	0.16
Mn	0.01	0.00	0.04	0.04	0.06	0.01	0.02	0.03	0.03	0.04
Fe^{2+}	1.45	1.35	2.33	2.04	2.50	1.71	2.03	2.49	2.66	2.47
Li	0.22	0.11	0.16	0.08	0.13	0.13	0.15	0.07	0.10	0.15
$\sum Y$	3.00	3.00	3.00	3.00	3.00	3.00	3.00	3.00	3.00	3.00
X: Ca	0.54	0.41	0.50	0.36	0.27	0.30	0.23	0.23	0.23	0.15
Na	0.37	0.49	0.46	0.57	0.60	0.54	0.59	0.58	0.61	0.63
□	0.09	0.10	0.04	0.07	0.13	0.16	0.18	0.19	0.16	0.22
OH	4.00	4.00	3.91	3.90	3.86	3.93	3.94	4.00	4.00	3.83
F	0.00	0.00	0.09	0.10	0.14	0.07	0.06	0.00	0.00	0.17

*B_2O_3, Li_2O and H_2O calculated by stoichiometry; B = 3 *apfu*, Li = 15 - $\sum T + Z + Y$ and OH+F = 4 *apfu*.

(1) black feruvite-uvite from exocontact, sample BH26A-3; (2) black Ca-rich schorl-dravite from exocontact, sample BH26F-16; (3) black Ti-bearing feruvite-schorl from zone 1, sample BH22-1-8; (4) black (Ca,Mg)-rich schorl from zone 1, sample BH22-1-3; (5) black Ca-rich Mg-bearing schorl from zone 1, sample BH22-1-3; (6) black Ca-rich schorl-dravite from zone 2, sample BH1-3-2; (7) black (Ca, Mg)-rich schorl from zone 2, sample BH1-2-4; (8) black Ca-rich Mg-bearing schorl from zone 4, sample BH2-1-5; (9) black Ca-rich schorl from zone 4, sample BH3-2-3; (10) black Ca-bearing schorl from zone 4, sample BH3-5.

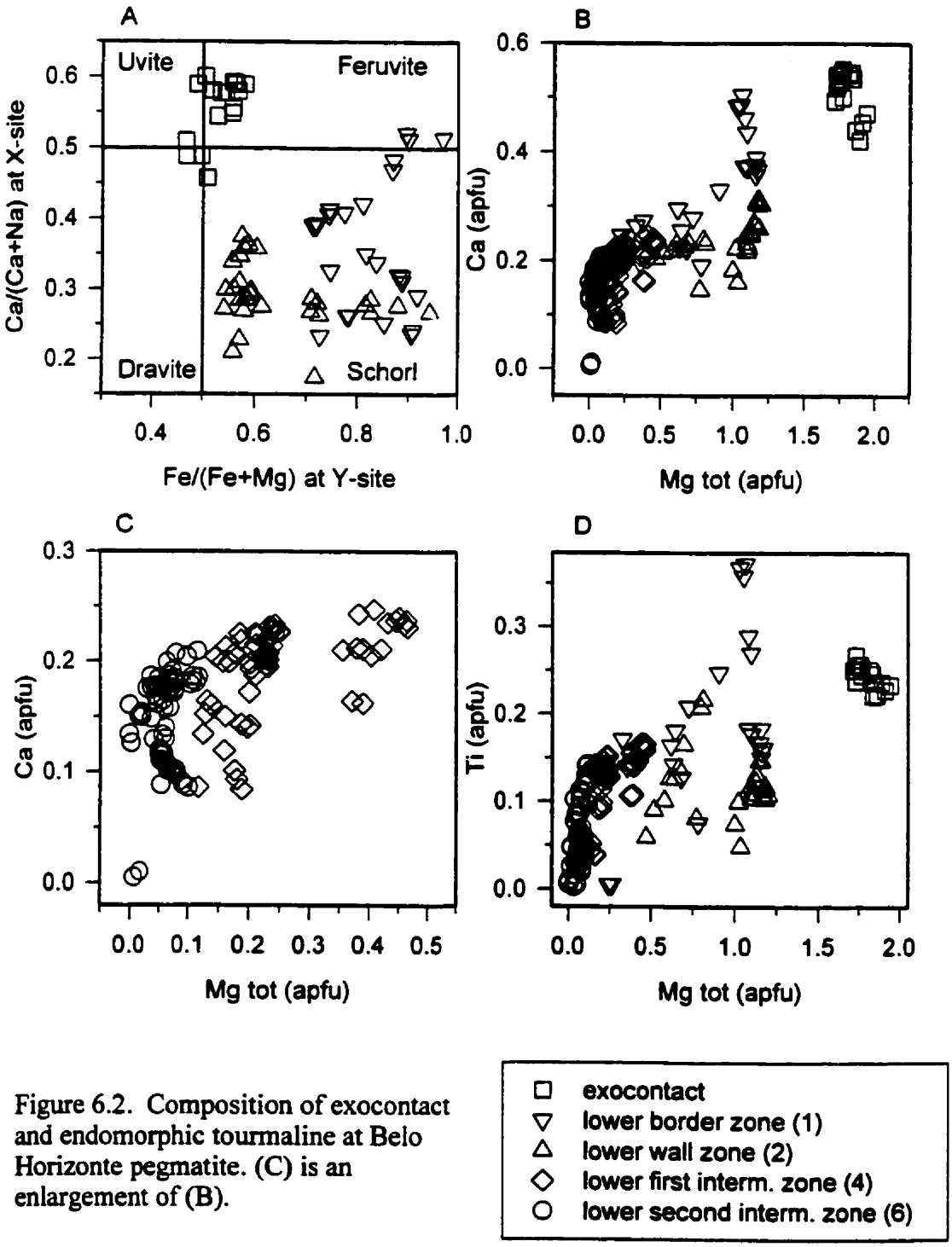

Figure 6.2. Composition of exocontact and endomorphic tourmaline at Belo Horizonte pegmatite. (C) is an enlargement of (B).

to (Ca, Mg)-rich schorl to Ca-rich Mg-bearing schorl (Fig. 6.2, Table 6.3, compositions 3-5). Zone (1) tourmaline is enriched in Ti (0.37-0.13 *apfu* Ti) relative to tourmaline in the pegmatite. Further evidence for infiltration of Ca, Mg and Ti from the host rock is the presence of abundant oligoclase (An_{17-29}) and Fe-rich Ti-bearing biotite in zone (1). Calcium is preferentially partitioned into tourmaline over plagioclase, as the Ca/Na ratio for tourmaline is 0.60 (n = 25) and for plagioclase is 0.33 (n = 9). Magnesium is preferentially partitioned into tourmaline over biotite, as the Mg/Fe ratio for tourmaline is 0.37 (n = 25) and for Fe-rich biotite is 0.24 (n = 5).

The composition of tourmaline in the lower wall zone (2) is also affected by endomorphism. Tourmaline in zone (2) is dominantly Ca-rich schorl-dravite with minor (Ca, Mg)-rich schorl (Fig. 6.2, Table 6.3, compositions 6, 7); the (Ca, Mg)-rich schorl is moderately enriched in Ti (0.22-0.06 *apfu* Ti). Garnet is subordinate in the lower wall zone (2); the average composition is $Alm_{63}Sps_{29}Grs_{7}Prp_{1}$ (Table 6.4, compositions 1-3). In contrast to the tourmaline composition, garnet compositions are Fe- and Mn-rich, and the minor Mg content is due to endomorphism. Iron is preferentially partitioned into tourmaline over garnet, and Mn is preferentially partitioned into garnet over tourmaline; the Fe/Mn ratio for tourmaline is 139 (n = 28) and for garnet is 2 (n = 13). Garnet has (Fe, Mg)-rich cores and (Mn, Ca)-rich rims.

In the lower first-intermediate zone (4), the dominant tourmaline is Ca-rich schorl with minor Ca-rich Mg-bearing schorl and Ca-bearing schorl, and rare schorl-elbaite (Fig.6.3, Table 6.3, compositions 8-10). Ca-rich Mg-bearing schorl has the highest Ti content ($\leq$ 0.17 *apfu* Ti) in the lower first-intermediate zone (4). Rarely, tourmaline

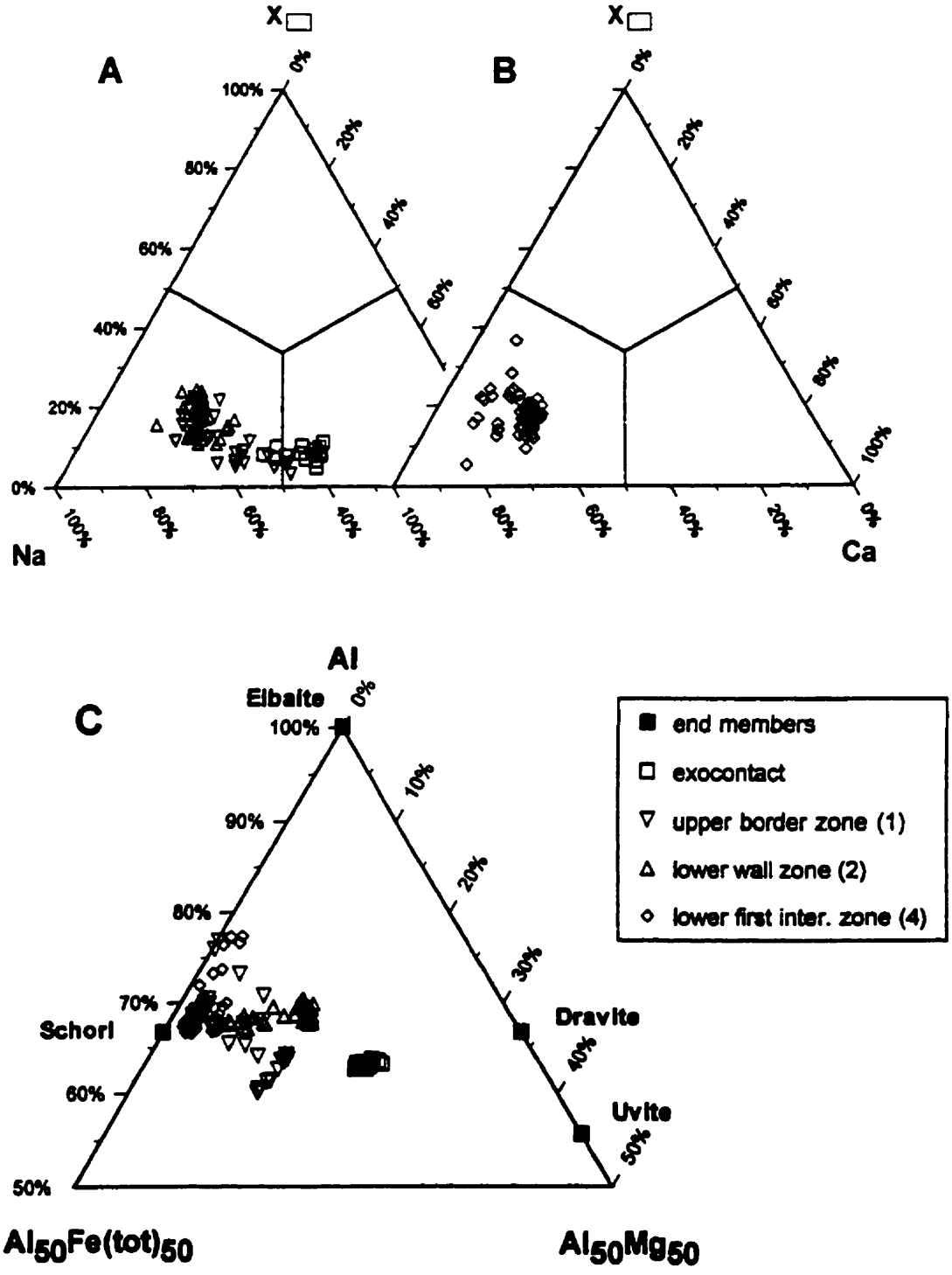

Figure 6.3. Compositions of exocontact and endomorphic tourmaline in Belo Horizonte pegmatite.

TABLE 6.4. REPRESENTATIVE COMPOSITIONS OF GARNET (WT%) IN ZONES (2) AND (8) OF THE BELO HORIZONTE PEGMATITE

	1	2	3	4	5	6
SiO_2	36.00	36.50	36.20	36.30	35.40	36.20
TiO_2	0.01	0.00	0.03	0.01	0.11	0.00
Al_2O_3	20.80	20.90	20.40	20.40	20.40	20.50
Fe_2O_3*	1.26	0.16	1.04	0.00	1.46	0.58
Y_2O_3	0.11	0.10	0.11	0.50	0.40	0.52
MgO	0.78	0.36	0.21	0.00	0.00	0.00
CaO	1.89	2.16	2.29	2.33	2.30	2.35
MnO	10.10	11.30	13.90	18.90	20.70	24.50
FeO	28.97	28.66	25.86	20.90	18.29	15.18
total	99.92	100.14	100.04	99.34	99.06	99.83
Formulae normalized to 12 anions and 8 cations						
T: Si	2.95	2.99	2.98	3.00	2.94	2.98
B: Ti	0.00	0.00	0.00	0.00	0.01	0.00
Al	2.01	2.02	1.98	1.99	2.00	1.99
Y	0.01	0.00	0.01	0.02	0.02	0.02
∑ B	2.02	2.02	1.99	2.01	2.03	2.01
A: Mg	0.09	0.04	0.03	0.00	0.00	0.00
Ca	0.17	0.19	0.20	0.21	0.21	0.21
Mn	0.70	0.78	0.97	1.32	1.46	1.71
Fe^{2+}	1.99	1.96	1.78	1.45	1.27	1.05
Fe^{3+}	0.08	0.01	0.06	0.00	0.09	0.04
∑ A	3.03	2.98	3.04	2.98	3.03	3.01
Alm	67.4	65.9	59.8	48.6	43.3	35.3
Sps	23.8	26.3	32.5	44.5	49.7	57.7
Grs	5.6	6.3	6.8	6.9	7.0	7.0
Prp	3.2	1.5	0.9	0.0	0.0	0.0

Analytical conditions: 15kV, 20 nA; standards: pyrope (Si, Mg), spessartine (Al, Mn), fayalite (Fe), anorthite (Ca), $SrTiO_3$ (Ti), and YAG (Y); not detected: Na, F, Sc, Zn, V, P, Sr, Zr, Cr, and Sn.*Fe_2O_3 calculated by adjusting the valence of Fe for 12 anions and 8 cations.

(1) orange almandine from zone 2, sample BHG1-3-2; (2) orange almandine core from zone 2, sample BHG1-2-4; (3) orange almandine rim of (2) from zone 2, sample BHG1-2-6; (4) yellow almandine-spessartine core from zone 8, sample BHG2-3-2; (5) yellow spessartine-almandine rim of (4) from zone 8, sample BHG2-3-1; (6) yellow spessartine from zone 8, sample BHG2-2-2.

grains have Ca-rich schorl cores and schorl-elbaite rims. The schorl-elbaite rims have high Al, Mn, Na and F contents, and represent the most fractionated tourmaline composition in zone (4). Tourmaline is the only (Mg, Fe, Mn)-bearing mineral in the lower and upper first-intermediate zones (4) and (5).

The Mg content of tourmaline decreases significantly to ≤ 0.12 *apfu* Mg and the Ti content decreases to ≤ 0.14 *apfu* Ti in Ca-rich schorl in the lower second-intermediate zone (6). The majority of the tourmaline in zone (6) is unaffected by endomorphism, and is discussed in the following section. Tourmaline is the only (Mg, Fe, Mn)-bearing mineral in zone (6).

Exocontact and endomorphic tourmalines evolve from feruvite-uvite → feruvite-schorl → Ca-rich schorl-dravite → (Ca, Mg)-rich schorl → Ca-rich schorl → Ca-bearing schorl → ± schorl-elbaite (Fig. 6.2a). The dominant solid-solution series in the outermost pegmatite zones is between dravite and schorl (Fig. 6.3c). Tourmaline in the exocontact is Ca-rich and tourmaline in the outermost pegmatite zones is Na-rich (Figs. 6.3a, b), and there is a positive correlation between Ca and Mg, and between Ti and Mg from the exocontact feruvite-uvite to the lower second- intermediate zone (6) Ca-bearing schorl (Figs. 6.2b, c, d). As crystallization proceeds from the exocontact to zone (6), tourmaline increases in Na and Fe, and decreases in Ca, Mg and Ti.

6.2.3. Composition of innermost pegmatitic tourmaline at Belo Horizonte

Tourmaline compositions for lower- and upper-intermediate zones (6) and (7) and the pocket zone (8) cover a similar compositional range (Ca-bearing schorl), except for

schorl-elbaite and elbaite in zone (8), and can be grouped together in graphs. Many tourmaline compositions plot on, or to the left of, the schorl-foitite border (Fig. 6.4a). Compositions plotted on this graph assume that all Fe is Fe^{2+}. Data that plot to the left of the schorl-foitite border indicate that some Fe is actually Fe^{3+} in Ca-bearing schorl. Further evidence for the presence of Fe^{3+} is shown in Table 6.5, in which Fe is present at the *Z*-site (compositions 4 and 5).

The dominant tourmaline composition in the lower and upper second-intermediate zones (6) and (7) and the pocket zone (8) is Ca-bearing schorl (Fig. 6.4a). The lower second-intermediate zone (6) also contains minor Ca-rich schorl, Ca-bearing schorl-elbaite, (Ca, Mn)-bearing schorl-elbaite and elbaite-schorl. Some tourmaline crystals in zone (6) are zoned, with Ca-rich schorl cores and Ca-bearing schorl rims, Ca-rich schorl cores and Ca-bearing schorl-elbaite rims, and Ca-bearing schorl cores and Ca-bearing schorl-elbaite rims. In addition to dominant Ca-bearing schorl, the upper second-intermediate zone (7) contains rare Ca-rich schorl. Tourmaline in zones (6) and (7) is only weakly affected by endomorphism; Ti ≤ 0.14 *apfu* and Mg ≤ 0.12 *apfu* in Ca-rich schorl in zone (6), and Ti ≤ 0.11 *apfu* and Mg ≤ 0.07 *apfu* in Ca-bearing schorl in zone (7). Tourmaline is the only (Mg, Fe, Mn)-bearing mineral in zones (6) and (7).

In addition to abundant Ca-bearing schorl, pocket zone (8) also contains minor schorl, schorl-elbaite and blue (Mn, Fe)-bearing elbaite (Fig. 6.4a). The (Mn, Fe)-bearing elbaite is the most Na- and F-rich tourmaline in the Belo Horizonte pegmatite with ≤ 0.82 *apfu* Na and ≤ 0.71 *apfu* F. Tourmaline in zone (8) is not affected by endomorphism, as most tourmaline has no Ti or Mg. The maximum Ti and Mg contents occur in Ca-bearing

TABLE 6.5. REPRESENTATIVE COMPOSITIONS OF TOURMALINE (WT%) IN ZONES (6), (7) AND (8) OF THE BELO HORIZONTE PEGMATITE

	1	2	3	4	5	6	7
SiO_2	34.70	35.50	35.00	34.30	34.00	35.70	37.90
TiO_2	0.86	0.12	0.06	0.34	0.43	0.11	0.00
B_2O_3*	10.06	10.55	10.35	9.91	9.89	10.41	10.89
Al_2O_3	29.20	35.60	34.00	28.70	28.60	33.90	37.30
MgO	0.27	0.15	0.00	0.13	0.04	0.00	0.00
CaO	0.97	0.82	0.73	0.90	0.93	0.23	0.40
MnO	0.31	1.32	2.53	0.34	0.51	1.46	3.53
FeO	18.40	10.80	11.60	19.40	20.00	11.80	2.59
ZnO	0.00	0.00	0.00	0.00	0.00	0.15	0.00
Li_2O*	0.24	0.77	0.58	0.11	0.03	0.72	1.81
Na_2O	1.92	1.83	1.91	2.04	2.01	2.42	2.64
H_2O*	3.47	3.35	3.24	3.32	3.25	3.14	3.09
F	0.00	0.61	0.69	0.21	0.35	0.96	1.40
O=F	0.00	-0.26	-0.29	-0.09	-0.15	-0.40	-0.59
total	100.40	101.16	100.40	99.61	99.89	100.60	100.96
Formulae normalized to 31 anions							
T: Si	6.00	5.85	5.88	6.02	5.97	5.96	6.05
Al	0.00	0.15	0.12	0.00	0.03	0.04	0.00
B	3.00	3.00	3.00	3.00	3.00	3.00	3.00
Z: Al	5.95	6.00	6.00	5.93	5.90	6.00	6.00
Mg	0.05	0.00	0.00	0.03	0.01	0.00	0.00
Fe	0.00	0.00	0.00	0.03	0.09	0.00	0.00
Y: Al	0.00	0.76	0.61	0.00	0.00	0.63	1.01
Ti	0.11	0.02	0.01	0.05	0.06	0.01	0.00
Mg	0.01	0.04	0.00	0.00	0.00	0.00	0.00
Mn	0.05	0.18	0.36	0.05	0.07	0.21	0.48
Fe^{2+}	2.66	1.49	1.63	2.82	2.85	1.65	0.35
Zn	0.00	0.00	0.00	0.00	0.00	0.02	0.00
Li	0.17	0.51	0.39	0.08	0.02	0.48	1.16
$\sum Y$	3.00	3.00	3.00	3.00	3.00	3.00	3.00
X: Ca	0.18	0.15	0.13	0.17	0.18	0.04	0.07
Na	0.64	0.58	0.62	0.69	0.68	0.78	0.82
□	0.18	0.27	0.25	0.14	0.14	0.18	0.11
OH	4.00	3.68	3.63	3.88	3.81	3.49	3.29
F	0.00	0.32	0.37	0.12	0.19	0.51	0.71

*B_2O_3, Li_2O and H_2O calculated by stoichiometry; B = 3 *apfu*, Li = 15 - $\sum T + Z + Y$ and OH+F = 4 *apfu*.

(1) black Ca-bearing schorl from zone 6, samp. BH5-4-1; (2) black Ca-bearing schorl-elbaite rim from zone 6, samp. BH4-2-1; (3) black (Ca, Mn)-bearing schorl-elbaite from zone 6, samp. BH5-1-7; (4) black Ca-bearing schorl from zone 7, samp. BH8-2-2; (5) black Ca-bearing schorl from zone 8, samp. BH6-2-4; (6) black schorl-elbaite from zone 8, samp. BH24-1-5; (7) pale blue (Mn, Fe)-bearing elbaite from zone 8, samp. BH24-3-4.

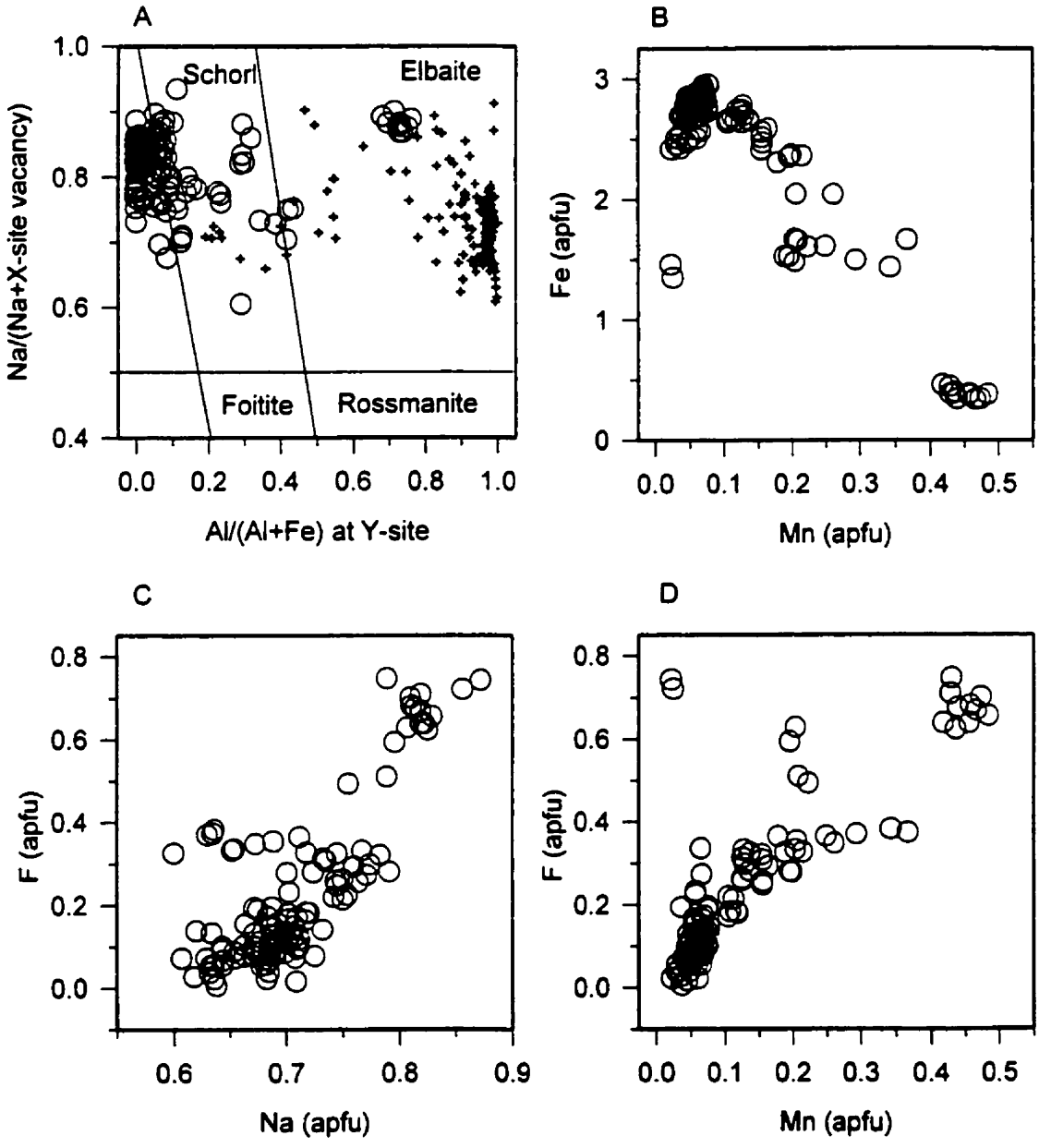

Figure 6.4. Tourmaline compositions at Belo Horizonte. All compositions plotted have Mg < 0.1 apfu.

schorl with Ti ≤ 0.08 *apfu* and Mg ≤ 0.02 *apfu*.

There is a negative correlation between Fe and Mn as Fe decreases and Mn increases from Ca-bearing schorl to (Mn, Fe)-bearing elbaite (Fig. 6.4b). There is a positive correlation between Na, Mn and F (Figs. 6.4c, d) with ≤ 0.82 *apfu* Na, ≤ 0.48 *apfu* Mn and ≤ 0.71 *apfu* F contents in (Mn, Fe)-bearing elbaite in the pocket zone (8) (Table 6.5, composition 7). Tourmaline in zones (6), (7) and (8) is Na-rich and the dominant solid-solution is between schorl and elbaite (Fig. 6.5).

The overall crystallization sequence for the innermost pegmatitic tourmaline is as follows: Ca-rich schorl → Ca-bearing schorl → Ca-bearing schorl-elbaite → (Ca, Mn)-bearing schorl-elbaite → schorl-elbaite → elbaite-schorl → (Mn, Fe)-bearing elbaite. As crystallization proceeds, tourmaline decreases in Ca and Ti, and increases in Na and Fe, followed by a final increase in Al, Li, Mn and F.

Pocket zone (8) has a layer of euhedral schorl and garnet along the lower and upper contacts with the second-intermediate zone. The average composition of the garnet in the pocket zone is $Alm_{48}Sps_{45}Grs_{7}$. Garnet frequently exhibits reaction rims of blue tourmaline. Iron is preferentially partitioned into tourmaline over garnet, and Mn is preferentially partitioned into garnet over tourmaline. Two almandine-spessartine grains (Fe/Mn = 1.2) are surrounded by Ca-rich schorl rims (Fe/Mn = 14.3 and 25.4); a spessartine-almandine grain (Fe/Mn = 0.9) is surrounded by Ca-bearing schorl rim (Fe/Mn = 11.2); another spessartine-almandine grain (Fe/Mn = 0.3) is surrounded by (Ca, Mn)-bearing schorl-elbaite rim (Fe/Mn = 3.7). Garnet in the pocket zone (8) is more Mn rich, and more Fe and Mg poor, than garnet in the lower wall zone (2).

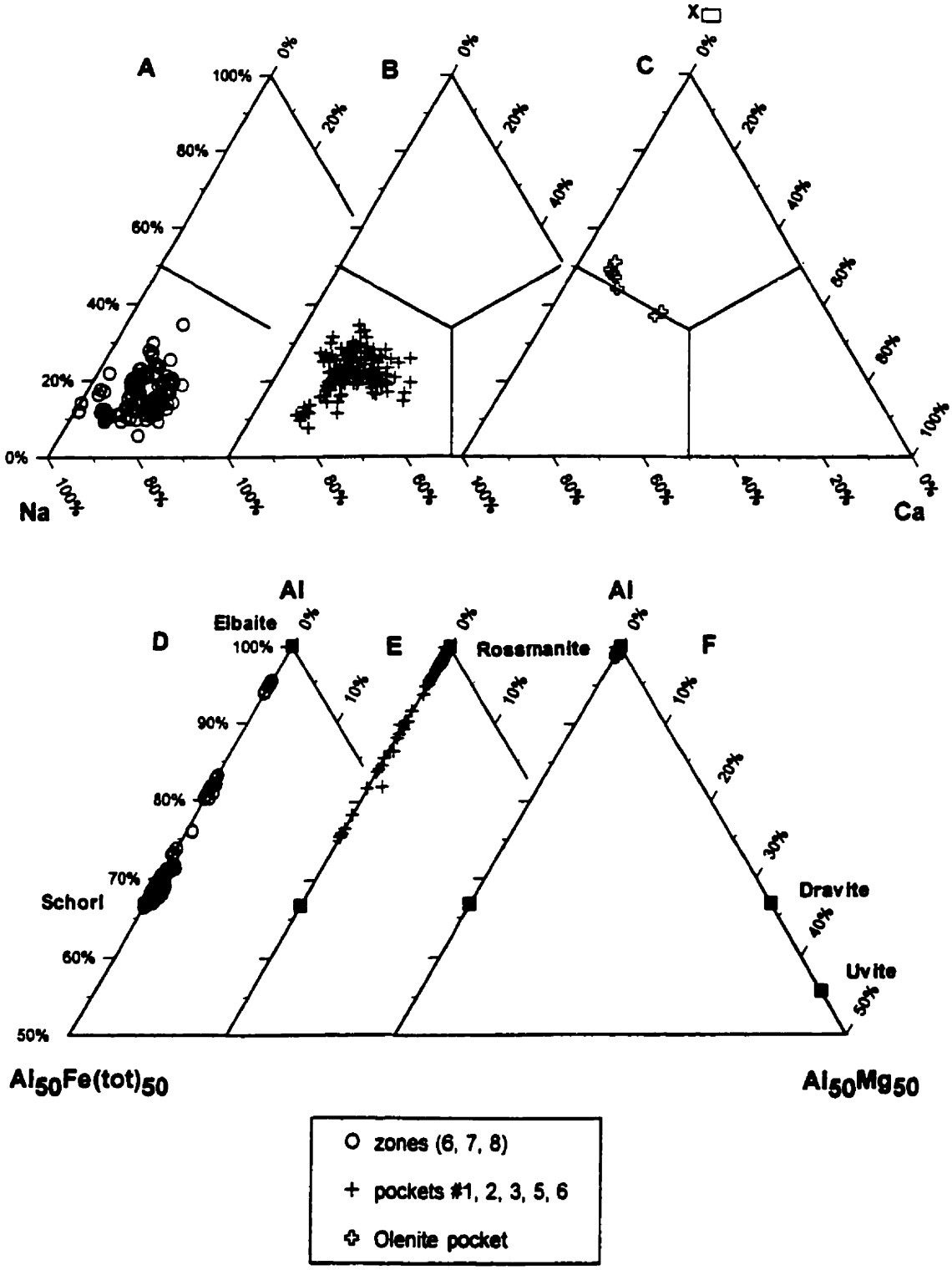

Figure 6.5. Tourmaline compositions at Belo Horizonte pegmatite.

6.2.4. Composition of pocket tourmaline at Belo Horizonte

Primary pocket tourmaline compositions:

The multicoloured tourmaline in the pockets is zoned parallel to the c-axis. Generally, this tourmaline has a black Fe-rich core surrounded by pink, purple or blue Mn-rich zones and green Al-rich rims. The dominant solid-solution is between schorl and elbaite (Figs. 6.4a, 6.5e) and the *X*-site is dominated by Na with significant Ca and □ contents (Fig. 6.5b).

Crystal BH9 from pocket #1 consists of a black (Ca, Mn)-bearing schorl (2.0 *apfu* Fe) core surrounded by pink Mn-rich Ca-bearing elbaite (1.0 *apfu* Mn), colourless (Ca, Mn)-bearing elbaite and green Ca-bearing elbaite (1.7 *apfu* Al at *Y*-site) (Table 6.6). Figures 6.6a and 6.6b indicate that Fe is enriched in the core, Mn and F are enriched in the pink intermediate zone, and Ca and Al are enriched in the rim. Crystal BH18 from pocket #5 has a similar crystallization sequence to crystal BH 9. Crystal BH18 consists of black Ca-bearing schorl (~ 2.1 *apfu* Fe) core surrounded by pink Mn-rich Ca-bearing elbaite (~ 1.0 *apfu* Mn), pink Ca-bearing elbaite (1.7 *apfu* Al at *Y*-site) (Table 6.7, composition 2) and a green Ca-bearing elbaite rim. Figures 6.6c and 6.6d show that Fe is enriched in the core, Mn and F are enriched in intermediate-zone Mn-rich Ca-bearing elbaite, Ca and Al are enriched in intermediate-zone Ca-bearing elbaite, and Ca and F are enriched in the rim.

Crystal BH11A from pocket #2 consists of a purple Mn-rich Ca-bearing elbaite (~ 1.0 *apfu* Mn) core surrounded by pink (Ca, Mn)-bearing elbaite and a green Ca-bearing rim. Figures 6.7a and 6.7b show that Na, Ca and Mn are enriched in the core, Al is

TABLE 6.6. REPRESENTATIVE COMPOSITIONS OF ZONED TOURMALINE (WT%) IN POCKET #1 OF THE BELO HORIZONTE PEGMATITE

	1-core	2	3	4-rim	5-core	6	7	8-rim
SiO_2	34.70	35.40	35.70	36.10	36.50	36.10	35.50	37.30
TiO_2	0.08	0.00	0.00	0.00	0.00	0.00	0.21	0.00
B_2O_3*	10.18	10.69	10.91	11.07	10.67	10.64	10.45	11.00
Al_2O_3	32.40	38.50	41.40	43.30	36.50	36.90	34.60	39.90
MgO	0.02	0.00	0.00	0.00	0.00	0.00	0.02	0.05
CaO	0.54	0.85	1.03	1.01	0.67	0.71	0.73	1.87
MnO	2.04	7.60	3.36	0.21	7.04	7.91	2.96	0.59
FeO	14.00	0.00	0.21	0.48	1.43	0.00	9.44	1.51
ZnO	0.14	0.00	0.00	0.00	0.00	0.00	0.15	0.00
Li_2O*	0.33	1.24	1.66	1.94	1.35	1.37	0.79	2.17
Na_2O	1.92	1.98	1.85	1.74	2.40	2.36	1.92	1.71
H_2O*	3.35	3.45	3.52	3.61	3.19	3.20	3.31	3.29
F	0.35	0.50	0.52	0.43	1.04	0.99	0.62	1.06
O=F	-0.15	-0.21	-0.22	-0.18	-0.44	-0.42	-0.26	-0.45
total	99.90	100.00	99.94	99.71	100.35	99.76	100.44	100.00
Formulae normalized to 31 anions								
T: Si	5.93	5.76	5.69	5.67	5.94	5.90	5.91	5.90
Al	0.07	0.24	0.31	0.33	0.06	0.10	0.09	0.10
B	3.00	3.00	3.00	3.00	3.00	3.00	3.00	3.00
Z: Al	6.00	6.00	6.00	6.00	6.00	6.00	6.00	6.00
Y: Al	0.45	1.14	1.46	1.69	0.95	1.01	0.69	1.33
Ti	0.01	0.00	0.00	0.00	0.00	0.00	0.03	0.00
Mg	0.00	0.00	0.00	0.00	0.00	0.00	0.00	0.01
Mn	0.29	1.05	0.45	0.03	0.97	1.09	0.42	0.08
Fe^{2+}	2.00	0.00	0.03	0.06	0.20	0.00	1.31	0.20
Zn	0.02	0.00	0.00	0.00	0.00	0.00	0.02	0.00
Li	0.23	0.81	1.06	1.22	0.88	0.90	0.53	1.38
$\sum Y$	3.00	3.00	3.00	3.00	3.00	3.00	3.00	3.00
X: Ca	0.10	0.15	0.18	0.17	0.12	0.12	0.13	0.32
Na	0.64	0.62	0.57	0.53	0.76	0.75	0.62	0.52
□	0.26	0.23	0.25	0.30	0.12	0.13	0.25	0.16
OH	3.81	3.74	3.74	3.79	3.46	3.49	3.67	3.47
F	0.19	0.26	0.26	0.21	0.54	0.51	0.33	0.53

*B_2O_3, Li_2O and H_2O calculated by stoichiometry; B = 3 *apfu*, Li = 15 - $\sum T + Z + Y$ and OH+F = 4 *apfu*.

Compositions 1-4 are from one crystal (sample BH9) and 5-8 are from another crystal (sample BH10). (1) black (Ca, Mn)-bearing schorl core, composition 12; (2) pink Mn-rich Ca-bearing elbaite zone, composition 8; (3) colourless (Ca, Mn)-bearing elbaite zone, composition 6; (4) green Ca-bearing elbaite rim, composition 2; (5) blue Mn-rich Ca-bearing elbaite core, composition 12; (6) purple Mn-rich Ca-bearing elbaite zone, composition 10; (7) black (Ca, Mn)-bearing elbaite-schorl zone, composition 7; (8) green Ca-rich elbaite rim, composition 3.

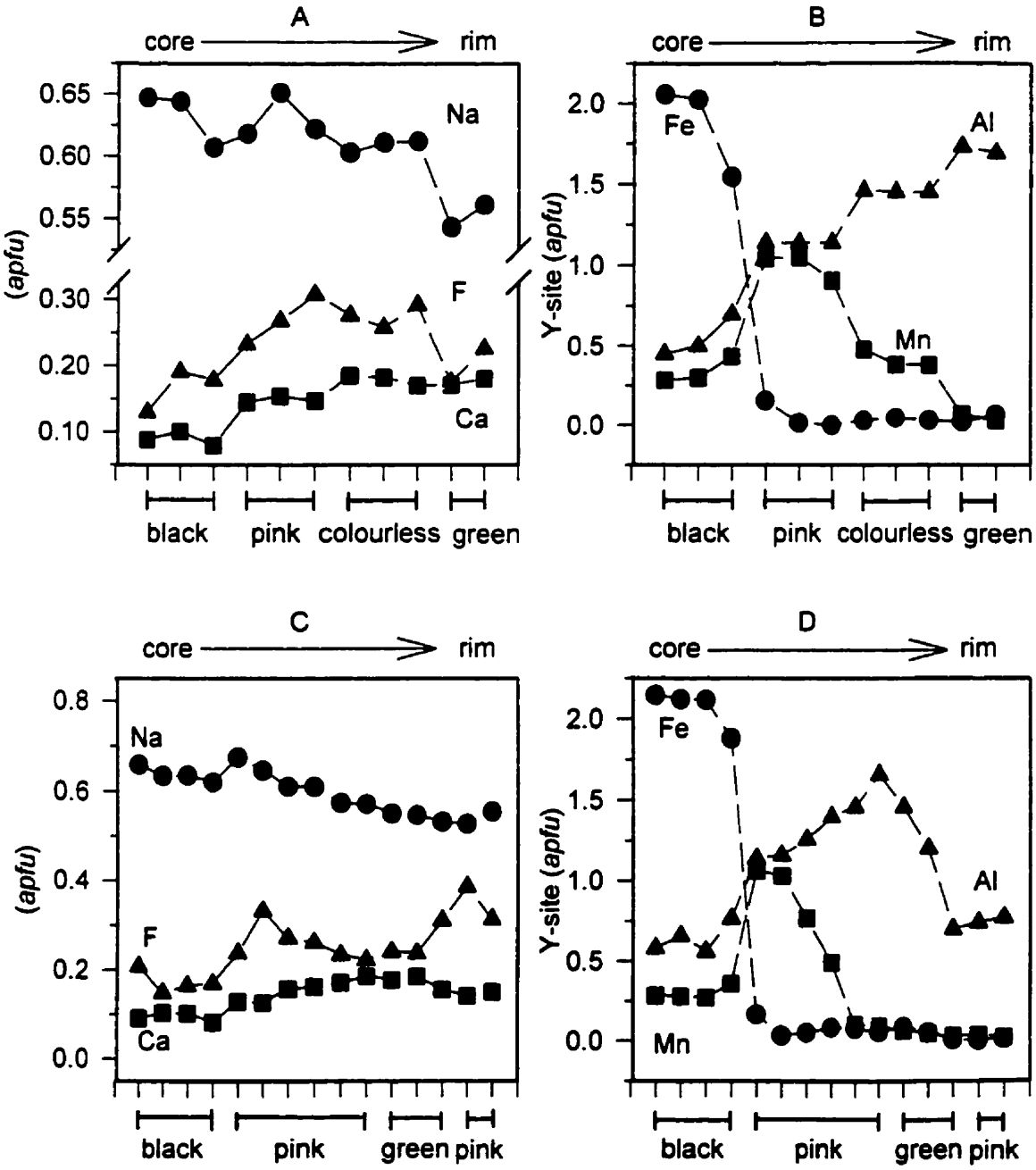

Figure 6.6. Compositional evolution of elbaite in pockets, Belo Horizonte pegmatite. (a), (b) sample BH9, pocket #1; (c), (d) sample BH18, pocket #5.

enriched in the intermediate zone and Al and F are enriched in the rim. Crystal BH16 from pocket #5 has a crystallization sequence similar to that of crystal BH11A; it consists of a purple Mn-bearing elbaite core surrounded by pink and colourless Ca-rich elbaite (1.7 *apfu* Al at *Y*-site) (Table 6.7, composition 3), pink Ca-bearing elbaite and a pink Ca-rich elbaite rim. Figures 6.7c and 6.7d show that Na and Mn are enriched in the core and intermediate zone, Ca and Al are enriched in Ca-rich elbaite intermediate zone, and F is enriched in Ca-bearing elbaite and the Ca-rich elbaite rim.

The overall crystallization sequence of these tourmaline crystals in the pockets is as follows: Ca-bearing schorl, (Ca, Mn)-bearing schorl → Mn-rich Ca-bearing elbaite → (Ca, Mn)-bearing elbaite → Ca-bearing elbaite, Ca-rich elbaite → Ca-bearing elbaite. Pink or purple Mn-rich Ca-bearing elbaite with ~ 1.0 *apfu* Mn is common in the pockets. As crystallization proceeds, tourmaline composition changes from Fe-rich → (Na, Mn, F)-rich → (Ca, Al)-rich → (Ca, F)-rich.

Tourmaline compositions affected by pocket rupture:

The previously mentioned tourmaline crystals in pockets (in the SW limb) contain Fe-rich tourmaline in the core, but crystals BH10 and BH12 (NW limb pockets) contain Fe-rich tourmaline in the intermediate zones. The crystallization sequence is the same as above, but it is interrupted by an Fe-rich zone. The source of the Fe is probably from hydrothermal fluids within the pegmatite which entered the pocket during pocket rupture. These hydrothermal fluids also produced schorl rims around spessartine-almandine cores in pocket-zone garnets. Crystal BH10 from pocket #1 consists of a blue Mn-rich Ca-

TABLE 6.7. REPRESENTATIVE COMPOSITIONS OF TOURMALINE (WT%) IN POCKETS OF THE BELO HORIZONTE PEGMATITE

	1	2	3	4	5	6	7	8	9	10
SiO_2	35.90	35.80	36.20	35.88	33.68	35.84	34.91	35.70	36.70	36.40
B_2O_3*	11.04	11.02	11.11	11.14	11.04	11.10	11.10	11.10	11.19	11.16
Al_2O_3	43.10	43.10	43.50	44.73	46.13	44.31	45.15	45.00	44.40	44.70
MgO	0.03	0.00	0.00	0.05	0.04	0.00	0.00	0.00	0.00	0.00
CaO	1.05	1.04	1.21	0.63	1.42	0.69	1.46	0.50	0.56	0.48
MnO	0.19	0.65	0.55	0.13	0.11	0.37	0.23	0.14	0.19	0.17
FeO	1.16	0.40	0.10	0.78	0.68	0.63	0.31	0.18	0.00	0.00
Li_2O*	1.83	1.89	1.95	1.67	1.62	1.71	1.79	1.70	1.83	1.77
Na_2O	1.64	1.76	1.57	1.41	1.29	1.46	1.22	1.40	1.41	1.37
H_2O*	3.72	3.60	3.65	3.84	3.73	3.83	3.78	3.83	3.86	3.85
F	0.18	0.42	0.39	0.00	0.17	0.00	0.11	0.00	0.00	0.00
O=F	-0.08	-0.18	-0.16	0.00	-0.07	0.00	-0.05	0.00	0.00	0.00
total	99.76	99.50	100.07	100.26	99.84	99.94	100.01	99.55	100.14	99.90
Formulae normalized to 31 anions										
T: Si	5.65	5.65	5.66	5.60	5.30	5.61	5.47	5.59	5.70	5.67
Al	0.35	0.35	0.34	0.40	0.70	0.39	0.53	0.41	0.30	0.33
B	3.00	3.00	3.00	3.00	3.00	3.00	3.00	3.00	3.00	3.00
Z: Al	6.00	6.00	6.00	6.00	6.00	6.00	6.00	6.00	6.00	6.00
Y: Al	1.65	1.66	1.69	1.82	1.86	1.79	1.80	1.89	1.83	1.87
Mg	0.01	0.00	0.00	0.01	0.01	0.00	0.00	0.00	0.00	0.00
Mn	0.03	0.09	0.07	0.02	0.01	0.05	0.03	0.02	0.03	0.02
Fe^{2+}	0.15	0.05	0.01	0.10	0.09	0.08	0.04	0.02	0.00	0.00
Li	1.16	1.20	1.23	1.05	1.03	1.08	1.13	1.07	1.14	1.11
$\sum Y$	3.00	3.00	3.00	3.00	3.00	3.00	3.00	3.00	3.00	3.00
X: Ca	0.18	0.18	0.20	0.10	0.24	0.12	0.25	0.08	0.09	0.08
Na	0.50	0.54	0.48	0.43	0.39	0.44	0.37	0.43	0.43	0.41
□	0.32	0.29	0.32	0.47	0.37	0.44	0.38	0.49	0.48	0.51
OH	3.91	3.79	3.81	4.00	3.92	4.00	3.95	4.00	4.00	4.00
F	0.09	0.21	0.19	0.00	0.08	0.00	0.05	0.00	0.00	0.00

*B_2O_3, Li_2O and H_2O calculated by stoichiometry; B = 3 *apfu*, Li = 15 - $\sum T + Z + Y$ and OH+F = 4 *apfu*.

Compositions 4-10 from the "olenite pocket". (1) green Ca-bearing elbaite rim from pocket #3, sample BH14-2; (2) pink Ca-bearing elbaite zone from pocket # 5, sample BH18-11; (3) pink Ca-rich elbaite zone from pocket #5, sample BH16-6; (4) pale yellow-green Ca-bearing rossmanite-elbaite core, sample 2C; (5) pale-yellow-green Ca-rich elbaite-rossmanite rim of (4), sample 2R1; (6) pale-green Ca-bearing elbaite-rossmanite, sample 3M; (7) pale-yellow-green Ca-rich rossmanite-elbaite rim, sample 6R; (8) colourless rossmanite-elbaite rim, sample BH17-1; (9) colourless rossmanite-elbaite core of (8), sample BH17-4; (10) pale-blue rossmanite-elbaite rim of (8), sample BH17-8.

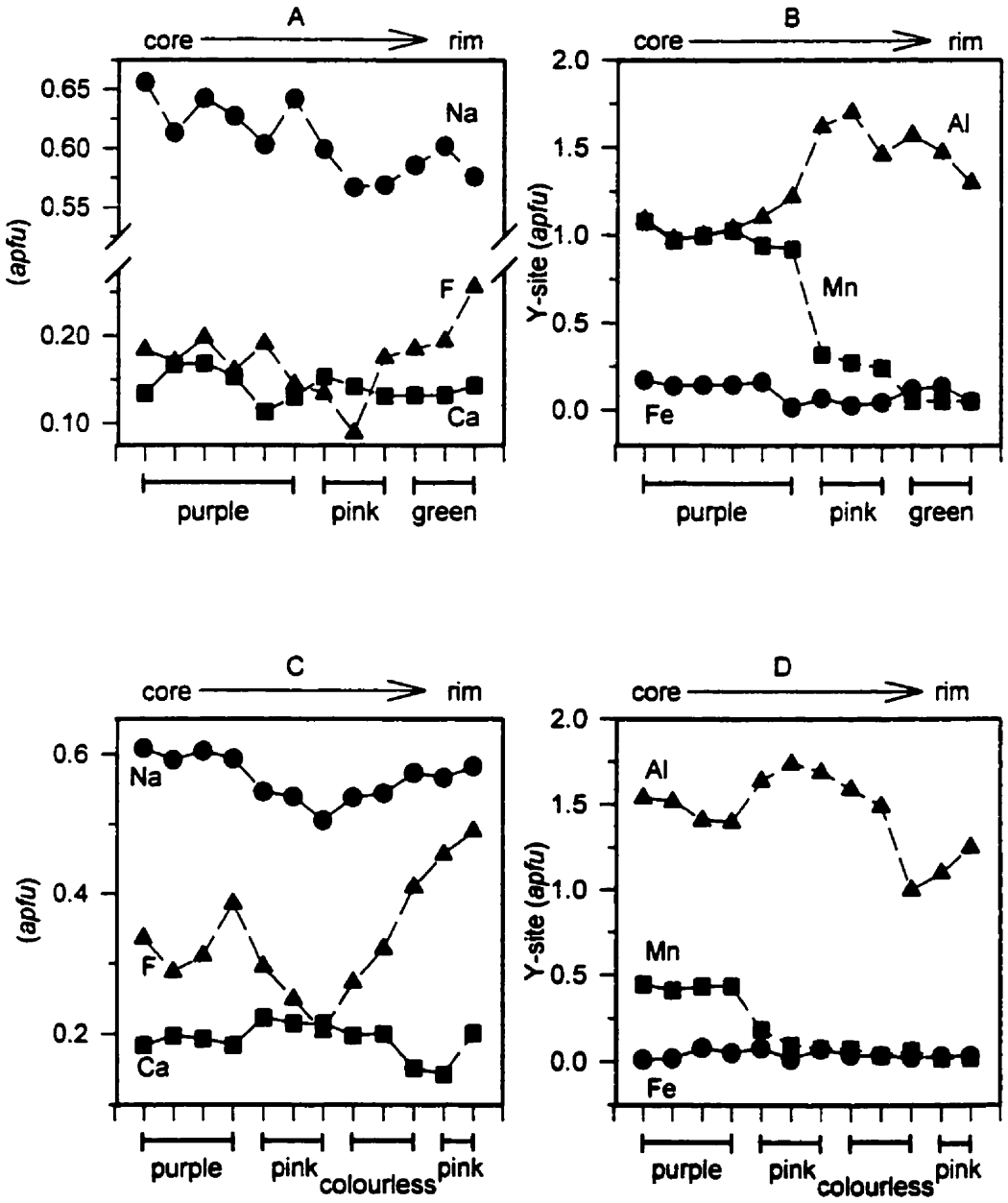

Figure 6.7. Compositional evolution of elbaite in pockets, Belo Horizonte pegmatite. (a), (b) sample BH11A, pocket #2; (c), (d) sample BH16, pocket #5.

bearing elbaite (0.8 *apfu* Na, 1.0 *apfu* Mn, 0.5 *apfu* F) core surrounded by purple Mn-rich Ca-bearing elbaite (0.8 *apfu* Na, 1.1 *apfu* Mn, 0.5 *apfu* F), black (Ca, Mn)-bearing elbaite-schorl (1.3 *apfu* Fe) and a green Ca-rich elbaite (0.3 *apfu* Ca) rim (Table 6.6, compositions 5-8). The core and first-intermediate zone are enriched in Na, Mn and F, the second-intermediate zone is enriched in Fe, and the rim is enriched in Ca and Al (Figs. 6.8a, b).

Crystal BH12 from pocket #2 consists of a black (Fe, Mn)-rich Ca-bearing elbaite core surrounded by black Mn-rich (Ca, Fe)-bearing elbaite (~ 0.9 *apfu* Mn), purple, blue and green (Ca, Mn)-bearing elbaite, brown Fe-rich Ca-bearing elbaite (~ 0.8 *apfu* Na, 0.9 *apfu* Fe, 0.5 *apfu* F), green Ca-rich elbaite, green (Ca, Fe)-bearing elbaite and a green Ca-rich Fe-bearing elbaite rim. The black core is enriched in Mn and Fe, the intermediate zones are Fe-poor, the brown zone is Na-, Fe- and F-rich, and the green rim is Ca and Al enriched (Figs. 6.8c, d).

Tourmaline compositions from the "olenite pocket":

Tourmaline in the "olenite pocket" is dominantly colourless with subordinate very pale- pink, pale-yellow-green and pale-blue crystals. This pocket was originally named the "olenite pocket" because the tourmaline has a high total-Al content; however 0.3-0.7 *apfu* Al occupies the *T*-site and 1.8-1.9 *apfu* Al occupies the *Y*-site and □ > Na, so the tourmaline is actually rossmanite (Table 6.7, compositions 5-10). The good correlation between the refined single-crystal site-scattering values and the electron-microprobe-determined site contents of this tourmaline verifies that it is rossmanite (unpub. data of

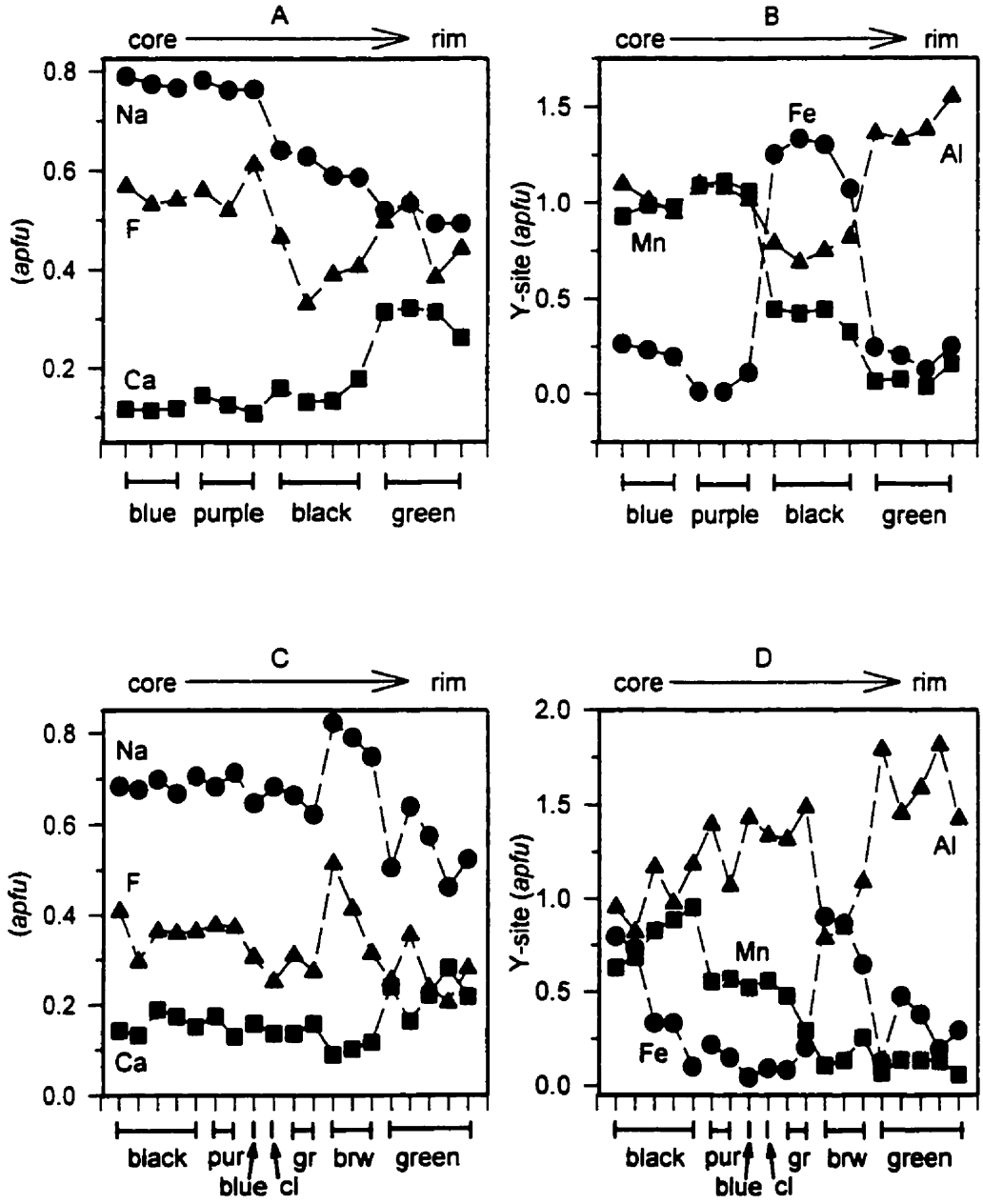

Figure 6.8. Compositional evolution of elbaite in pockets, Belo Horizonte pegmatite. (a), (b) sample BH10, pocket #1; (c), (d) sample BH12, pocket #2. pur - purple, cl - colourless, gr - green, bwn - brown.

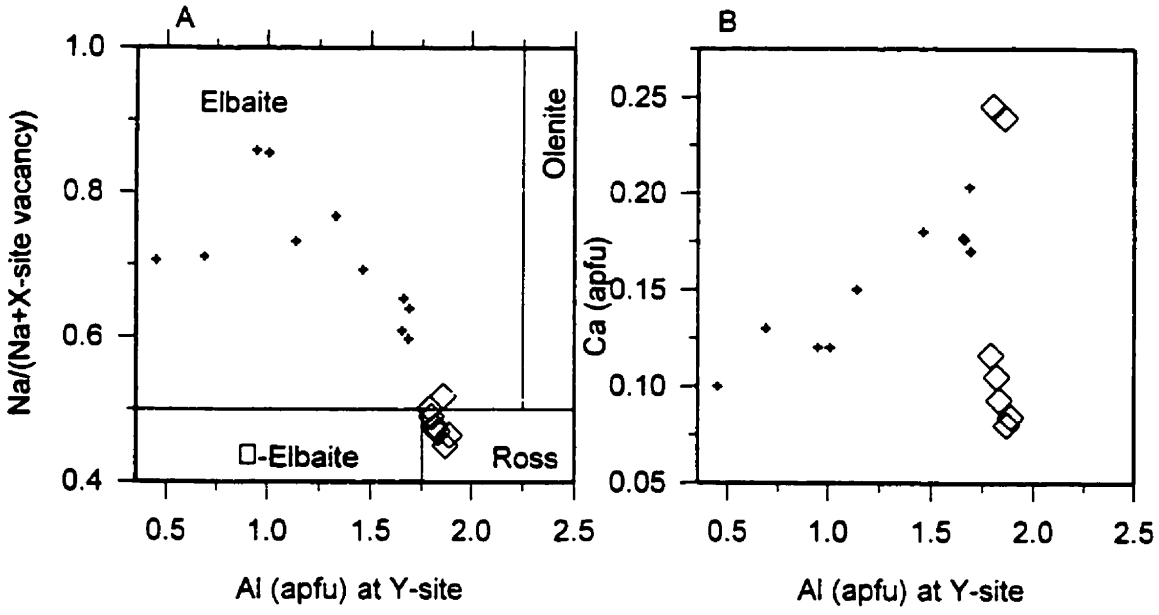

Figure 6.9. Composition of tourmaline in Belo Horizonte pegmatite. Only compositions from Tables 6 and 7 are plotted.

J.B. Selway). The rossmanite is more □-and Al-rich than tourmaline in the other pockets (Fig. 6.9). Only compositions from Tables 6.6 and 6.7 with calculated Li content are plotted in Figure 6.9, as compositions without calculated Li contents have misleadingly high total-Al contents. Tourmaline from the "olenite pocket" has a narrow range in composition and the compositions in Table 6.7 are truly representative of the 57 compositions microprobed. Cores tend to be Ca-bearing rossmanite-elbaite, and rarely the

rims tend to be Ca-rich elbaite-rossmanite. Most of the rossmanite is Ca-bearing (0.08 - 0.12 *apfu* Ca), but rarely the rims are Ca-rich (0.25 *apfu* Ca) (Fig. 6.9b). The Mn and Fe contents are very low (≤ 0.05 *apfu* Mn, ≤ 0.10 *apfu* Fe), and the majority of the rossmanite contains no F except for 0.08 *apfu* F in a Ca-rich elbaite-rossmanite rim. The overall crystallization sequence in the "olenite pocket" is from Ca-bearing rossmanite-elbaite to Ca-rich elbaite-rossmanite.

6.2.5. Summary of tourmaline compositions in the Belo Horizonte pegmatite

The most primitive tourmaline composition is the feruvite-uvite in the exocontact. The overall tourmaline compositional evolution in the massive pegmatite is as follows: feruvite-schorl → Ca-rich schorl-dravite → (Ca, Mg)-rich schorl → Ca-rich schorl → Ca-bearing schorl → Ca-bearing schorl-elbaite → (Ca, Mn)-bearing schorl-elbaite → schorl-elbaite → elbaite-schorl → (Mn, Fe)-bearing elbaite. Figures 6.10 and 6.11 show that this crystallization sequence represents a decrease in Ca, Mg and Ti, and an increase in Na and Fe, followed by an increase in Al, Li, Mn and F.

The overall compositional evolution of tourmaline in the pockets is as follows: black Ca-bearing schorl, (Ca, Mn)-bearing schorl → pink, purple or blue Mn-rich Ca-bearing elbaite → pink, purple or colourless (Ca, Mn)-bearing elbaite → green or pink Ca-bearing elbaite, Ca-rich elbaite. Pocket rupture may cause this crystallization sequence to be interrupted by a black (Ca, Mn)-bearing elbaite-schorl or a brown Fe-rich Ca-bearing elbaite zone just before the final green Ca-rich elbaite zone, but the overall crystallization sequence remains the same. The "olenite pocket" contains only a narrow

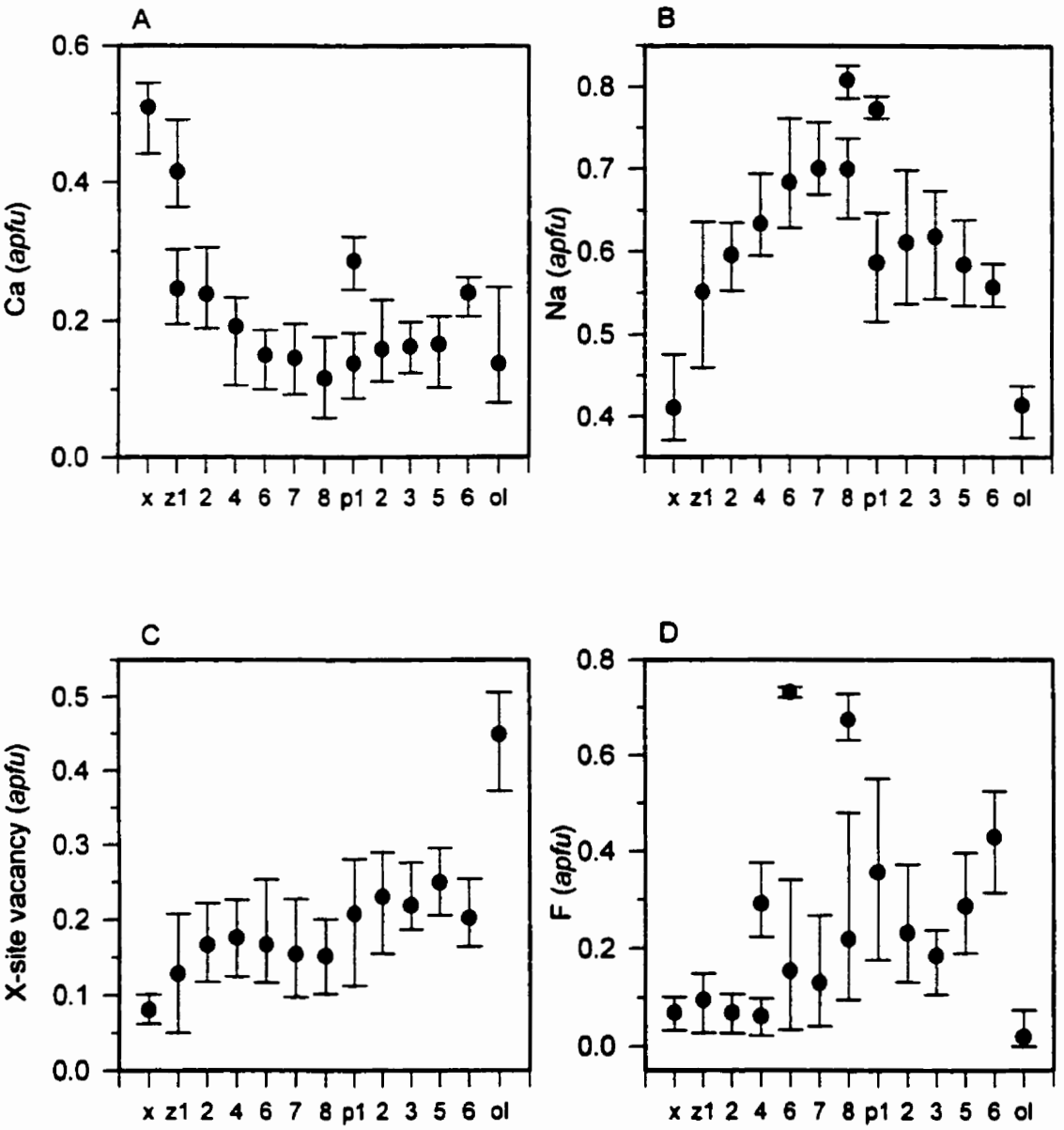

Figure 6.10. Dots represent the average and bars represent the range in Ca, Na, X-site-vacancy and F contents in tourmaline for each pegmatite zone at the Belo Horizonte pegmatite. x: exocontact, z: zone, p: pocket, ol: olenite pocket.

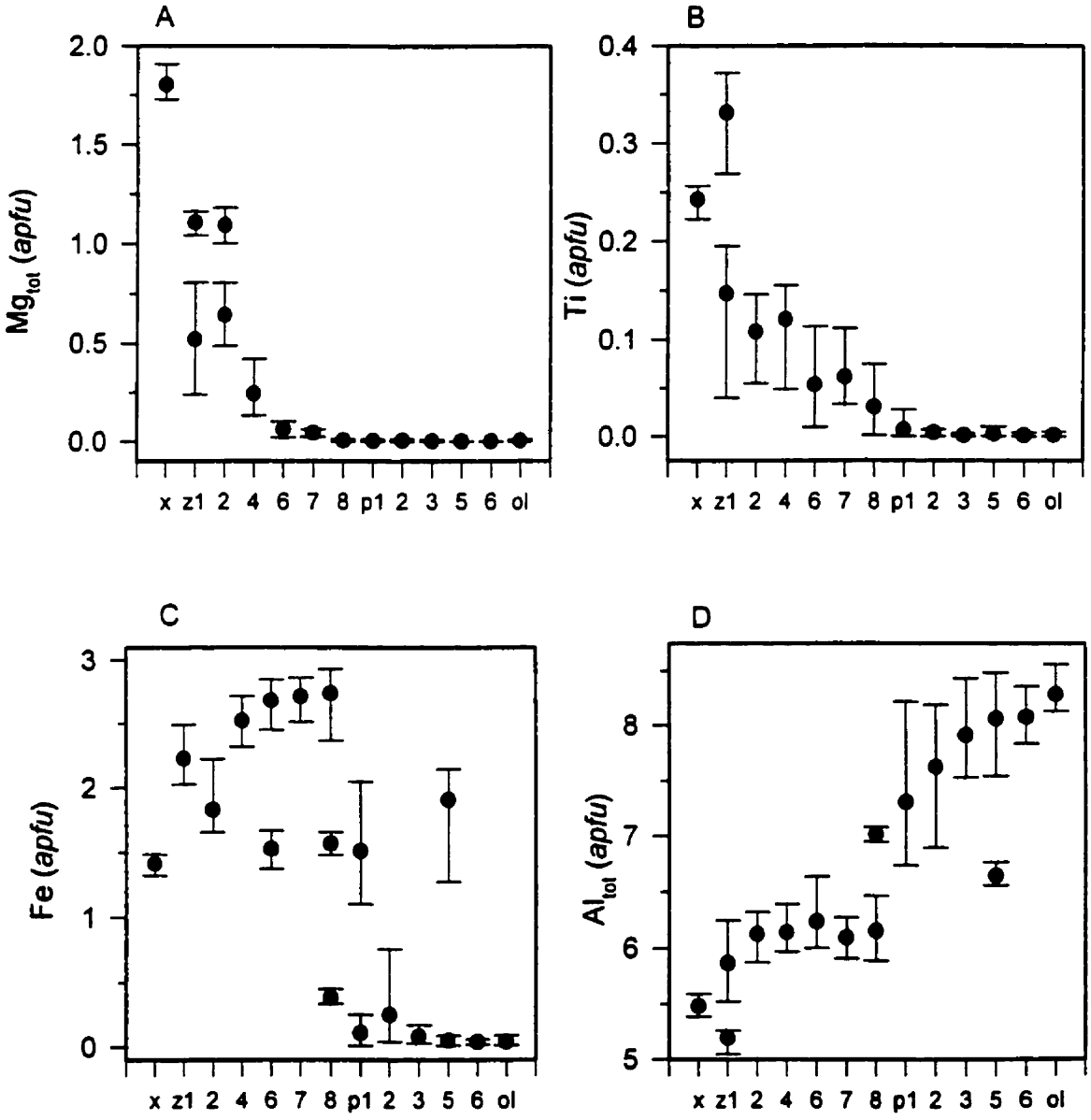

Figure 6.11. Dots represent the average and bars represent the range in Mg, Ti, Fe, Mn and total Al contents in tourmaline for each pegmatite zone at the Belo Horizonte pegmatite. x: exocontact, z: zone, p: pocket, ol: olenite pocket.

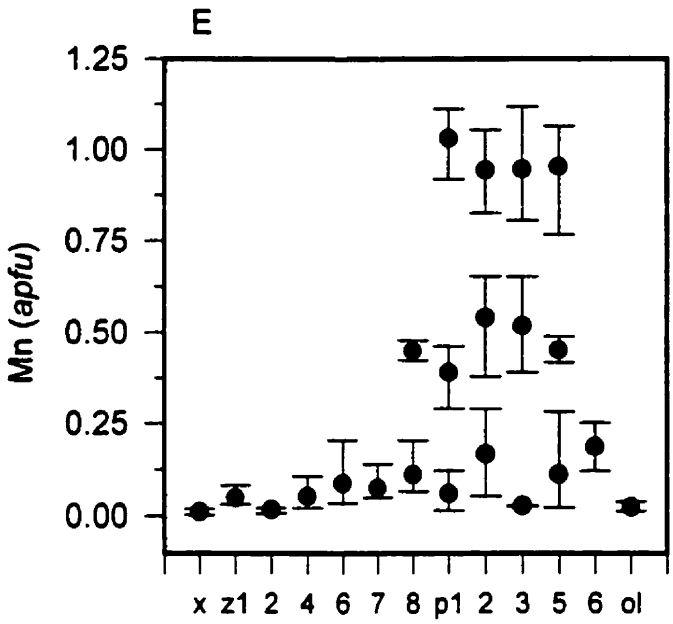

Figure 6.11. continued.

range in tourmaline composition: colourless Ca-bearing rossmanite-elbaite → Ca-rich elbaite-rossmanite. As elbaite does not occur in the "olenite pockets", where rossmanite fits into the above sequence (using zoned crystals) cannot be directly determined. However, the fact that rossmanite contains almost no Fe and Mn and is rich in Ca and Al implies that rossmanite crystallized at the same time as late-stage Ca-bearing elbaite and Ca-rich elbaite. Figures 6.10 and 6.11 show that pocket tourmaline is enriched in Ca, □, Al, Mn and F, and depleted in Na, Mg, Ti and Fe. Examination of zoned crystals shows

that tourmaline compositions progress from Fe-rich to Mn-rich to (Ca, Al)-rich to (Ca, F)-rich (Figs. 6.6, 6.7 and 6.8). The progression from Fe-rich (Ca-bearing schorl) to Mn-rich (elbaite) tourmaline is achieved by the "tsilaisite substitution", $3Fe \rightarrow Mn + Al + Li$.

6.3. The Řečice Pegmatite

6.3.1. General Geology

The Řečice pegmatite is located in the easternmost part of the Moldanubian region, western Moravia, Czech Republic. It is 1.5 m thick and 20 m long, and intrudes a strongly weathered pyroxene gneiss (Novák *et al.* in press). The Řečice pegmatite is a relatively homogeneous pegmatite with a minor medium-grained granitic zone, a dominant coarse-grained zone and randomly scattered pockets. Locally along the contact, there is a medium-grained granitic zone which consists of albite + quartz > K-feldspar + black tourmaline. The dominant massive coarse-grained pegmatite, which comprises of most of the pegmatite, consists of dominant K-feldspar > quartz > albite + black tourmaline, accessory cassiterite, löllingite, tusionite and garnet, and rare manganocolumbite, pyrochlore and zircon (Fig. 6.12). Tusionite is locally replaced by fine-grained pink tourmaline.

Numerous equidimensional pockets are randomly distributed within the pegmatite (Novák *et al.* in press). These pockets contain dominant euhedral reddish-pink orthoclase ($\leq$ 25 cm), smoky quartz, dark-violet to raspberry-red tourmaline type I ($\leq$ 15 cm long and $\leq$ 8 cm thick) and subordinate albite. The pockets also contain minor fine-grained pink tourmaline and boromuscovite and rare cassiterite ($\leq$ 1 cm), arseniosiderite and

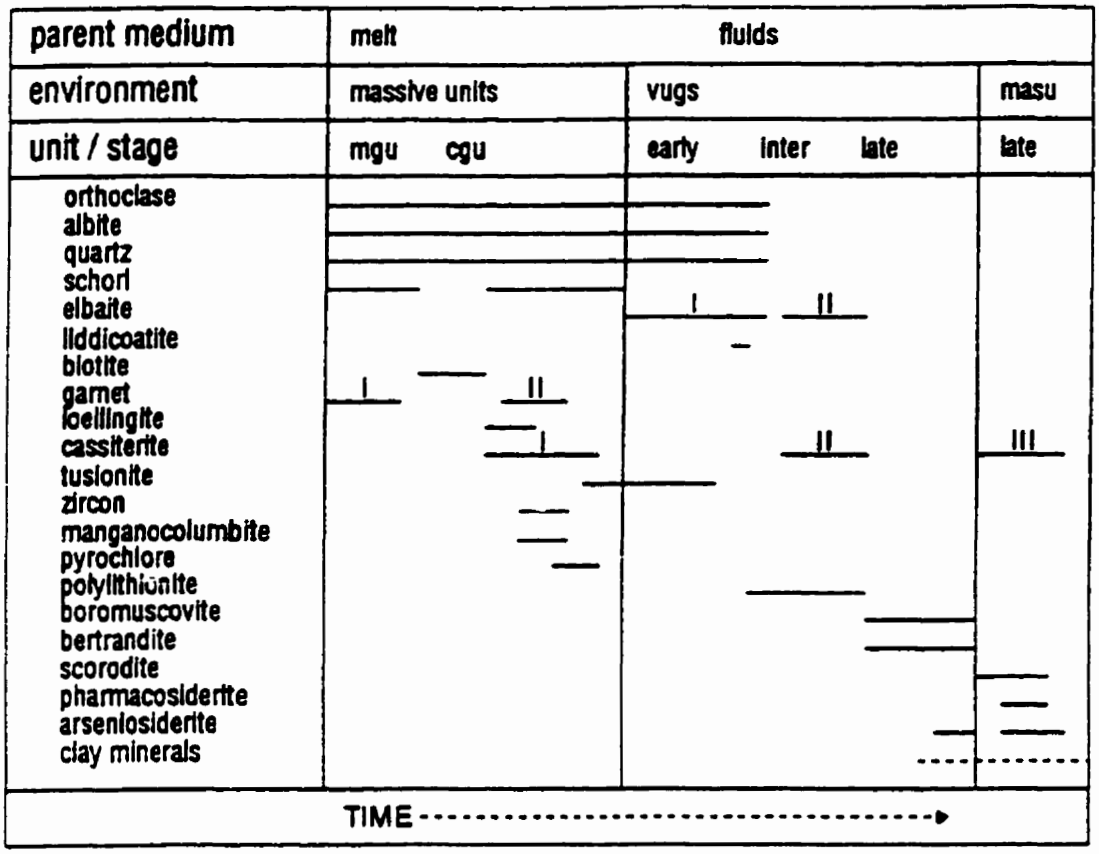

Figure 6.12. Paragenetic sequence of minerals in the Řečice pegmatite. mgu - medium-grained zone; cgu - coarse-grained zone; masu - massive zones; inter - intermediate. (Novák *et al.* in press).

crusts of bertrandite.

Two types of tourmaline occur in the pockets: early zoned dark-violet to raspberry-red columnar crystals of tourmaline type I (≤ 15 cm long), and late-stage fine-grained pink tourmaline type II (≤ 5 mm) (Staněk & Povondra 1987, Novák *et al.* in press). The coarse-grained tourmaline may be zoned with black cores and red to brown-

red rims. The fine-grained pink tourmaline typically occurs on large orthoclase crystals, between coarse flakes of polylithionite, or combines with cassiterite as a replacement of tusionite. In addition to common pink tourmaline, the tourmaline is rarely green, blue and colourless (Staněk & Povondra 1987). Columnar green tourmaline is about 7 mm long and 3 mm wide and occurs in the pegmatite. Fine-grained blue and colourless tourmaline occurs in the pockets.

Micas are rare to absent in the Řečice pegmatite. Rare biotite (≤ 2 cm) occurs in the coarse-grained zone and rare B-bearing polylithionite or boromuscovite aggregates form overgrowths on coarse-grained pink tourmaline I in pockets (Novák *et al.* in press). Rare spessartine-almandine occurs in the medium-grained and coarse-grained zones. Řečice also contains abundant B-rich minerals: dominant tourmaline, and subordinate tusionite, B-bearing polylithionite and boromuscovite. The high activity of B is maintained from magmatic to hydrothermal stage, as indicated by abundant early black tourmaline to late (Li, F)-poor boromuscovite. The paragenetic sequence of minerals in the Řečice pegmatite is summarized in Figure 6.12.

6.3.2. Tourmaline composition in the Řečice pegmatite

Black tourmaline in the medium-grained granitic zone has been affected by endomorphism, as fluids from the strongly weathered pyroxene-gneiss host-rock enriched tourmaline in Ca, Mg and Ti. The dominant tourmalines are Ca-rich schorl-dravite and Ca-bearing schorl-elbaite-dravite with minor Ca-bearing schorl-dravite-elbaite and Ca-bearing elbaite-schorl-dravite (Figs. 6.13a, 6.16a, Table 6.8). The maximum Ti content

TABLE 6.8. REPRESENTATIVE COMPOSITIONS OF BLACK PEGMATITIC TOURMALINE (WT%) FROM ŘEČICE PEGMATITE

	1	2	3	4	5	6	7
SiO_2	35.30	36.20	35.70	35.09	35.38	34.90	34.90
TiO_2	1.03	0.75	1.29	1.63	1.24	0.93	0.48
B_2O_3*	10.21	10.48	10.14	9.95	10.18	10.07	10.10
Al_2O_3	28.40	32.00	25.38	24.45	27.78	28.50	30.30
MgO	4.62	3.63	7.11	4.89	4.58	2.69	0.21
CaO	1.68	0.85	1.90	2.10	1.45	1.32	0.68
MnO	0.35	0.75	0.51	0.48	0.32	0.42	1.15
FeO	12.30	8.75	10.98	14.54	12.80	14.40	16.20
ZnO	0.00	0.00	0.00	0.00	0.00	0.00	0.19
Li_2O*	0.29	0.65	0.35	0.41	0.31	0.35	0.31
Na_2O	1.82	2.09	1.87	1.59	1.89	1.83	2.01
H_2O*	3.30	3.15	3.07	3.17	3.44	3.34	3.29
F	0.48	0.98	0.90	0.56	0.15	0.28	0.41
O=F	-0.20	-0.41	-0.38	-0.24	-0.06	-0.12	-0.17
total	99.58	99.87	98.82	98.62	99.46	98.91	100.06
Formulae normalized to 31 anions							
T: Si	6.01	6.00	6.12	6.13	6.04	6.03	6.01
B	3.00	3.00	3.00	3.00	3.00	3.00	3.00
Z: Al	5.70	6.00	5.13	5.03	5.59	5.80	6.00
Mg	0.30	0.00	0.87	0.97	0.41	0.20	0.00
Y: Al	0.00	0.26	0.00	0.00	0.00	0.00	0.15
Ti	0.13	0.09	0.17	0.21	0.16	0.12	0.06
Mg	0.87	0.90	0.94	0.31	0.75	0.49	0.05
Mn	0.05	0.11	0.07	0.07	0.05	0.06	0.17
Fe^{2+}	1.75	1.21	1.58	2.12	1.83	2.08	2.33
Zn	0.00	0.00	0.00	0.00	0.00	0.00	0.02
Li	0.20	0.43	0.24	0.29	0.21	0.25	0.22
$\sum Y$	3.00	3.00	3.00	3.00	3.00	3.00	3.00
X: Ca	0.31	0.15	0.35	0.39	0.27	0.24	0.13
Na	0.60	0.67	0.62	0.54	0.62	0.61	0.67
□	0.09	0.18	0.03	0.07	0.11	0.14	0.20
OH	3.74	3.49	3.51	3.69	3.92	3.85	3.78
F	0.26	0.51	0.49	0.31	0.08	0.15	0.22

*B_2O_3, Li_2O and H_2O calculated by stoichiometry; B = 3 *apfu*, Li = 15 - $\sum T + Z + Y$ and OH+F = 4 *apfu*.

Compositions 1 and 2 are from the medium-grained zone and compositions 3-7 are from the coarse-grained zone. (1) Ca-rich schorl-dravite, sample R1505; (2) Ca-bearing schorl-dravite-elbaite, sample R1507; (3) Ca-rich schorl-dravite, sample 660; (4) Mg-bearing schorl-feruvite, sample 662; (5) Ca-rich schorl-dravite, sample 759; (6) Ca-rich Mg-bearing schorl, sample R1303; (7) Ca-bearing schorl, sample R1606.

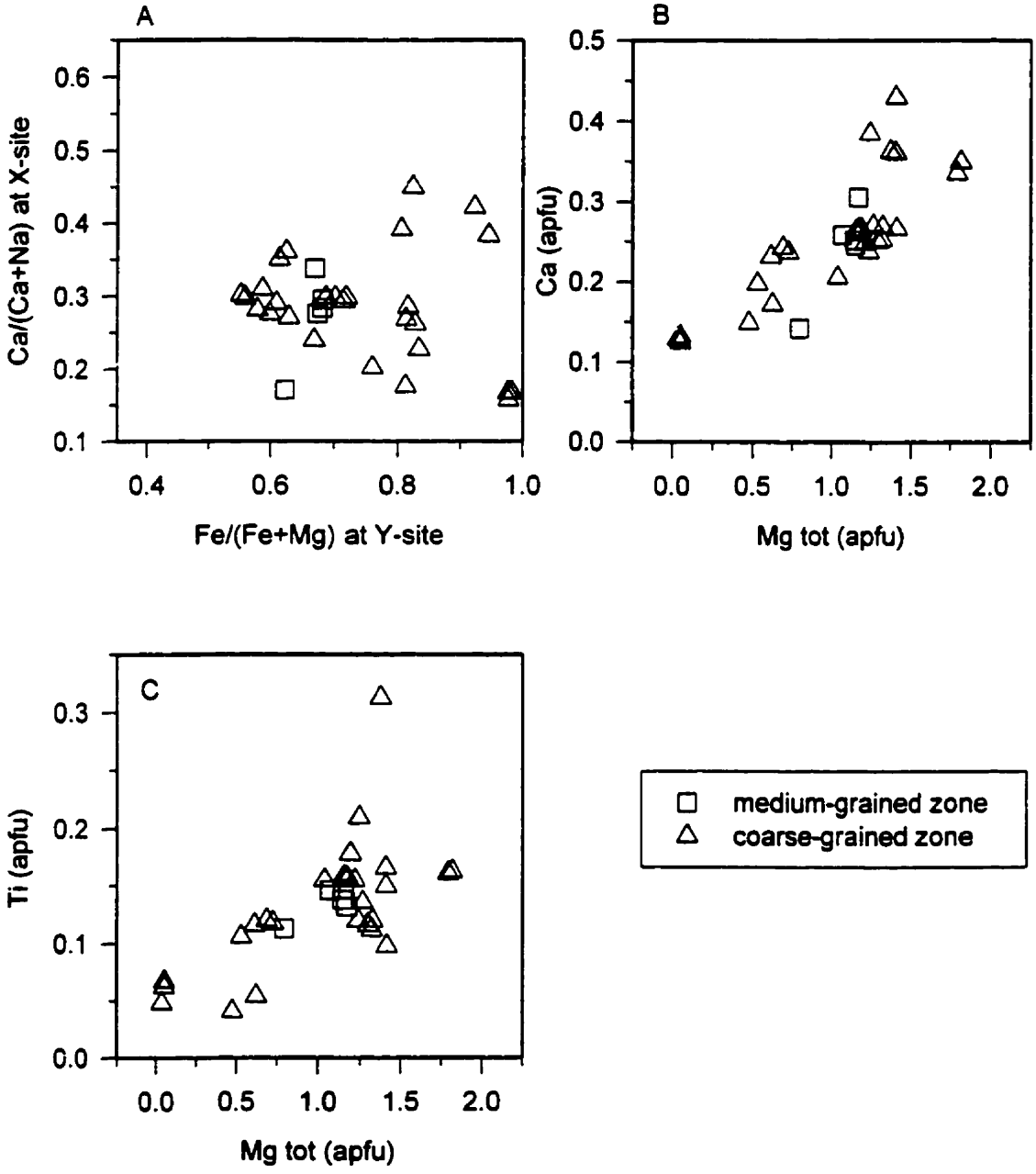

Figure 6.13. Composition of tourmaline in the Recice pegmatite. Only tourmaline compositions with Al at Y-site < 0.1 apfu are plotted.

(0.15 *apfu*) occurs in Ca-rich schorl-dravite.

Black tourmaline in the coarse-grained zone has also been affected by endomorphism. The dominant tourmaline is Ca-rich schorl-dravite with minor Mg-bearing schorl-feruvite, Ca-rich Mg-bearing schorl, Ca-bearing Mg-rich schorl, Ca-bearing schorl and Ca-bearing schorl-elbaite (Figs. 6.13a, 6.16a, Table 6.8). Both Ca-rich schorl-dravite and Mg-bearing schorl-feruvite have high Mg contents at the *Z*-site (≤ 1.07 *apfu* Mg) which represents a minor feruvite component.

The dominant tourmaline in the medium-grained and coarse-grained zones is schorl with minor dravite and elbaite components (Fig. 6.16a); Na is the dominant cation at the *X*-site, with minor Ca (Fig. 6.15a). There is a positive correlation between Ca, Mg and Ti; they decrease from Ca-rich schorl-dravite (≤ 1.82 *apfu* total Mg and ≤ 0.31 *apfu* Ti) to Ca-bearing schorl (0.04 *apfu* total Mg) and Ca-bearing schorl-elbaite (0.03 *apfu* Ti) (Fig. 6.13).

Tourmaline in the pockets has a wide range in composition from schorl-dravite to schorl to elbaite to liddicoatite (Figs. 6.14a, 6.16b). The most primitive compositions are affected by endomorphism, as shown by enrichment in Mg and Ti. The most primitive pocket- tourmaline compositions range from Ca-rich schorl-dravite (≤ 1.22 *apfu* total Mg and ≤ 0.16 *apfu* Ti) to (Ca, Mg)-rich schorl to Ca-bearing schorl-elbaite-dravite (Fig. 6.16b, Table 6.9, composition 1). The tourmaline compositions with schorl as the dominant component include Ca-rich schorl, Ca-bearing schorl (Table 6.9, composition 2) and (Ca, Mn)-bearing schorl-elbaite. Tourmaline compositions with elbaite as the dominant component and schorl as a minor component are numerous: (Ca, Mn)-bearing

TABLE 6.9. REPRESENTATIVE COMPOSITIONS OF TOURMALINE (WT%) IN POCKETS FROM ŘEČICE PEGMATITE

	1	2	3	4	5	6	7	8	9
SiO_2	35.90	34.81	35.57	36.90	36.00	37.94	38.50	38.39	37.89
TiO_2	0.53	0.34	0.26	0.00	0.08	0.00	0.00	0.00	0.00
B_2O_3*	10.41	10.07	10.39	10.79	10.75	10.95	11.30	11.09	11.03
Al_2O_3	32.90	30.28	33.51	38.00	37.90	38.61	42.40	39.72	39.44
MgO	1.63	0.14	0.02	0.00	0.04	0.00	0.00	0.02	0.00
CaO	0.59	0.64	0.81	0.74	1.48	1.86	1.37	2.23	2.54
MnO	2.01	1.39	2.96	1.39	4.58	1.94	0.00	0.44	1.06
FeO	9.19	16.08	10.09	4.47	2.29	0.15	0.00	0.10	0.14
ZnO	0.00	0.18	0.28	0.00	0.00	0.00	0.00	0.00	0.00
Li_2O*	0.74	0.30	0.79	1.62	1.54	2.35	2.25	2.52	2.43
Na_2O	2.14	2.05	2.05	2.22	1.93	1.82	1.39	1.44	1.37
H_2O*	3.19	3.34	3.28	3.45	3.27	3.17	3.66	3.34	3.33
F	0.84	0.28	0.65	0.58	0.93	1.28	0.51	1.02	1.01
O=F	-0.35	-0.12	-0.27	-0.24	-0.39	-0.54	-0.21	-0.43	-0.43
total	99.72	99.78	100.39	99.92	100.40	99.53	101.17	99.88	99.81
Formulae normalized to 31 anions									
T: Si	5.99	6.01	5.95	5.94	5.82	6.02	5.92	6.02	5.97
Al	0.01	0.00	0.05	0.06	0.18	0.00	0.08	0.00	0.03
B	3.00	3.00	3.00	3.00	3.00	3.00	3.00	3.00	3.00
Z: Al	6.00	6.00	6.00	6.00	6.00	6.00	6.00	6.00	6.00
Y: Al	0.47	0.16	0.56	1.16	1.04	1.22	1.61	1.34	1.30
Ti	0.07	0.05	0.03	0.00	0.01	0.00	0.00	0.00	0.00
Mg	0.40	0.04	0.01	0.00	0.01	0.00	0.00	0.00	0.00
Mn	0.28	0.20	0.42	0.19	0.63	0.26	0.00	0.06	0.14
Fe^{2+}	1.28	2.32	1.41	0.60	0.31	0.02	0.00	0.01	0.02
Zn	0.00	0.02	0.04	0.00	0.00	0.00	0.00	0.00	0.00
Li	0.50	0.21	0.53	1.05	1.00	1.50	1.39	1.59	1.54
$\sum Y$	3.00	3.00	3.00	3.00	3.00	3.00	3.00	3.00	3.00
X: Ca	0.11	0.12	0.15	0.13	0.26	0.32	0.23	0.37	0.43
Na	0.69	0.69	0.67	0.69	0.60	0.56	0.41	0.44	0.42
□	0.20	0.19	0.18	0.18	0.14	0.12	0.36	0.19	0.15
OH	3.56	3.85	3.65	3.71	3.52	3.36	3.75	3.49	3.50
F	0.44	0.15	0.35	0.29	0.48	0.64	0.25	0.51	0.50

*B_2O_3, Li_2O and H_2O calculated by stoichiometry; B = 3 *apfu*, Li = 15 - $\sum T + Z + Y$ and OH+F = 4 *apfu*.

(1) Ca-bearing schorl-elbaite-dravite, sample R1405; (2) Ca-bearing schorl, sample 1115; (3) (Ca, Mn)-bearing elbaite-schorl, sample 969; (4) Fe-rich Ca-bearing elbaite, sample R1709; (5) (Ca, Mn)-rich Fe-bearing elbaite, sample R1411; (6) Ca-rich elbaite, sample 920; (7) Ca-rich elbaite-rossmanite, sample R1704; (8) elbaite-liddicoatite, sample 924; (9) liddicoatite-elbaite, sample 923.

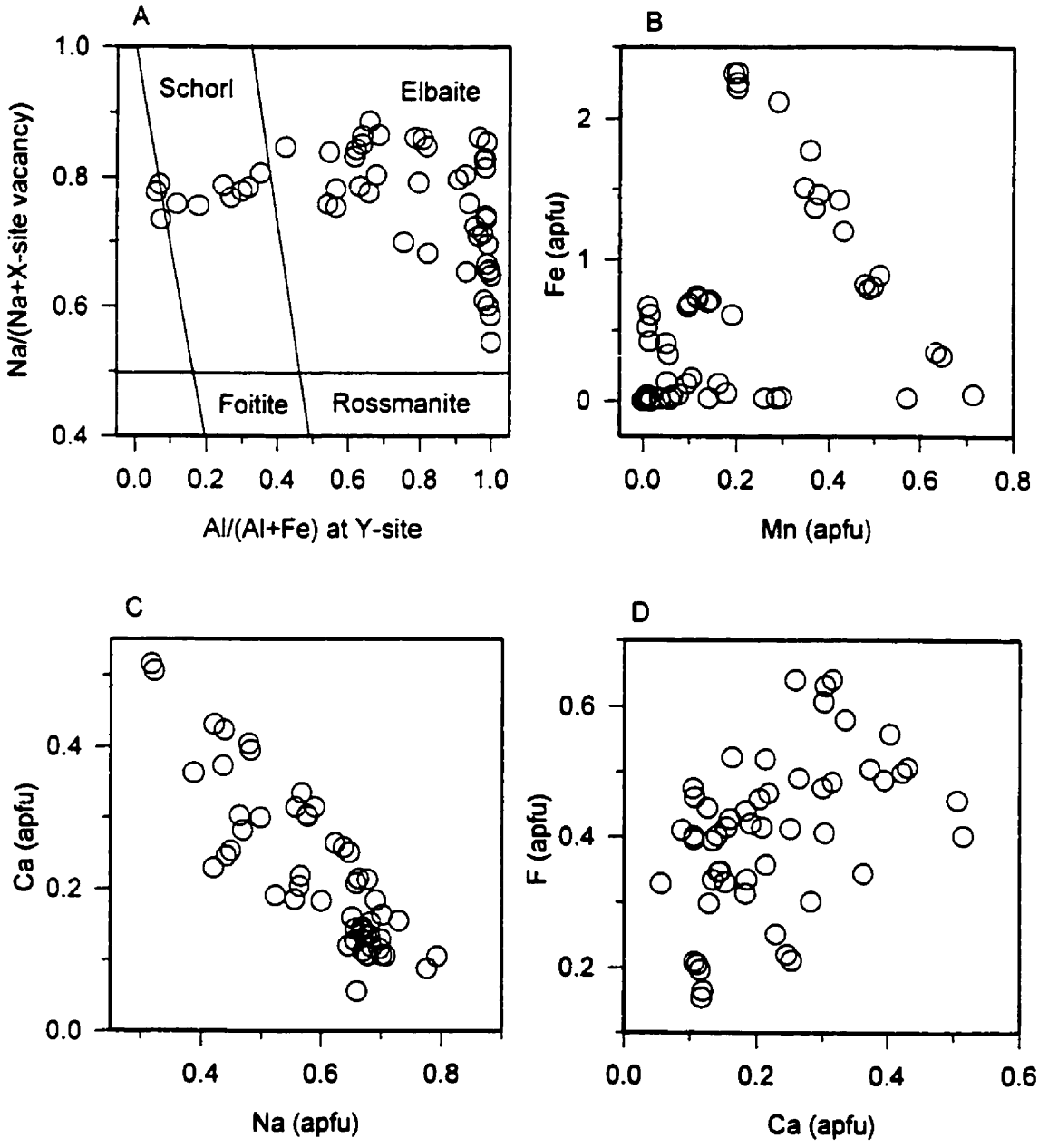

Figure 6.14. Tourmaline compositions from pockets in the Recice pegmatite. Only tourmaline compositions with < 0.1 apfu Mg are plotted.

elbaite-schorl, (Ca, Fe)-rich elbaite, (Ca, Fe)-bearing elbaite, Fe-rich Ca-bearing elbaite, Fe-rich (Ca, Mn)-bearing elbaite, (Ca, Mn)-rich Fe-bearing elbaite, and Fe-bearing elbaite (Fig. 6.14a, 6.16b) (Table 6.9, compositions 3-5). Iron-free elbaite is the most fractionated tourmaline and its variation in composition includes (Ca, Mn)-rich elbaite, Ca-rich Mn-bearing elbaite, Ca-rich elbaite, elbaite-liddicoatite, liddicoatite-elbaite and Ca-bearing elbaite-rossmanite (Table 6.9, compositions 6-9).

There is a negative correlation between Fe and Mn, as Fe decreases and Mn increases from Ca-bearing schorl (~ 0.20 *apfu* Mn) to (Ca, Mn)-rich Fe-bearing elbaite (≤ 0.64 *apfu* Mn) and (Ca, Mn)-rich elbaite (≤ 0.71 *apfu* Mn), followed by a decrease in Mn to Ca-rich elbaite, elbaite-liddicoatite, liddicoatite-elbaite and Ca-bearing elbaite-rossmanite with no Fe or Mn (Fig. 6.14b). There is a positive correlation between Mn and F; they increase from Ca-bearing schorl (~ 0.15 *apfu* F) to (Ca, Mn)-rich Fe-bearing elbaite (≤ 0.64 *apfu* F) and (Ca, Mn)-rich elbaite (≤ 0.64 *apfu* F).

There is a negative correlation between Ca and Na: Na decreases and Ca increases from Fe-rich Ca-bearing elbaite (≤ 0.79 *apfu* Na and 0.11 *apfu* Ca) to liddicoatite-elbaite (0.32 *apfu* Na and ≤ 0.52 *apfu* Ca). There is a positive correlation between Ca and F, as they increase from Ca-rich elbaite (≤ 0.46 *apfu* F) to elbaite-liddicoatite to liddicoatite-elbaite (≤ 0.51 *apfu* F) and they decrease to Ca-rich elbaite-rossmanite (≤ 0.25 *apfu* F) (Fig. 6.14d).

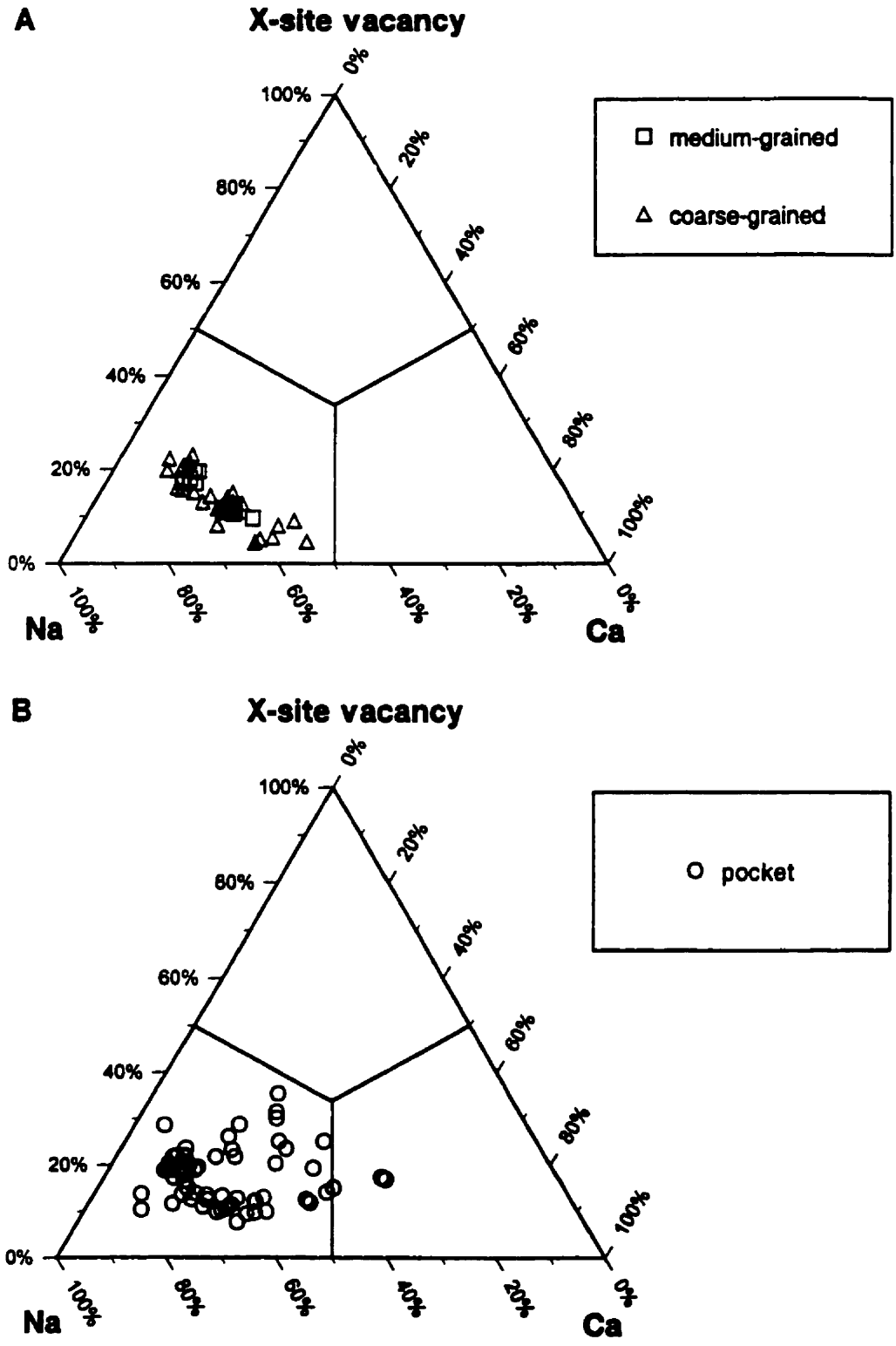

Figure 6.15. Tourmaline compositions at Řečice pegmatite.

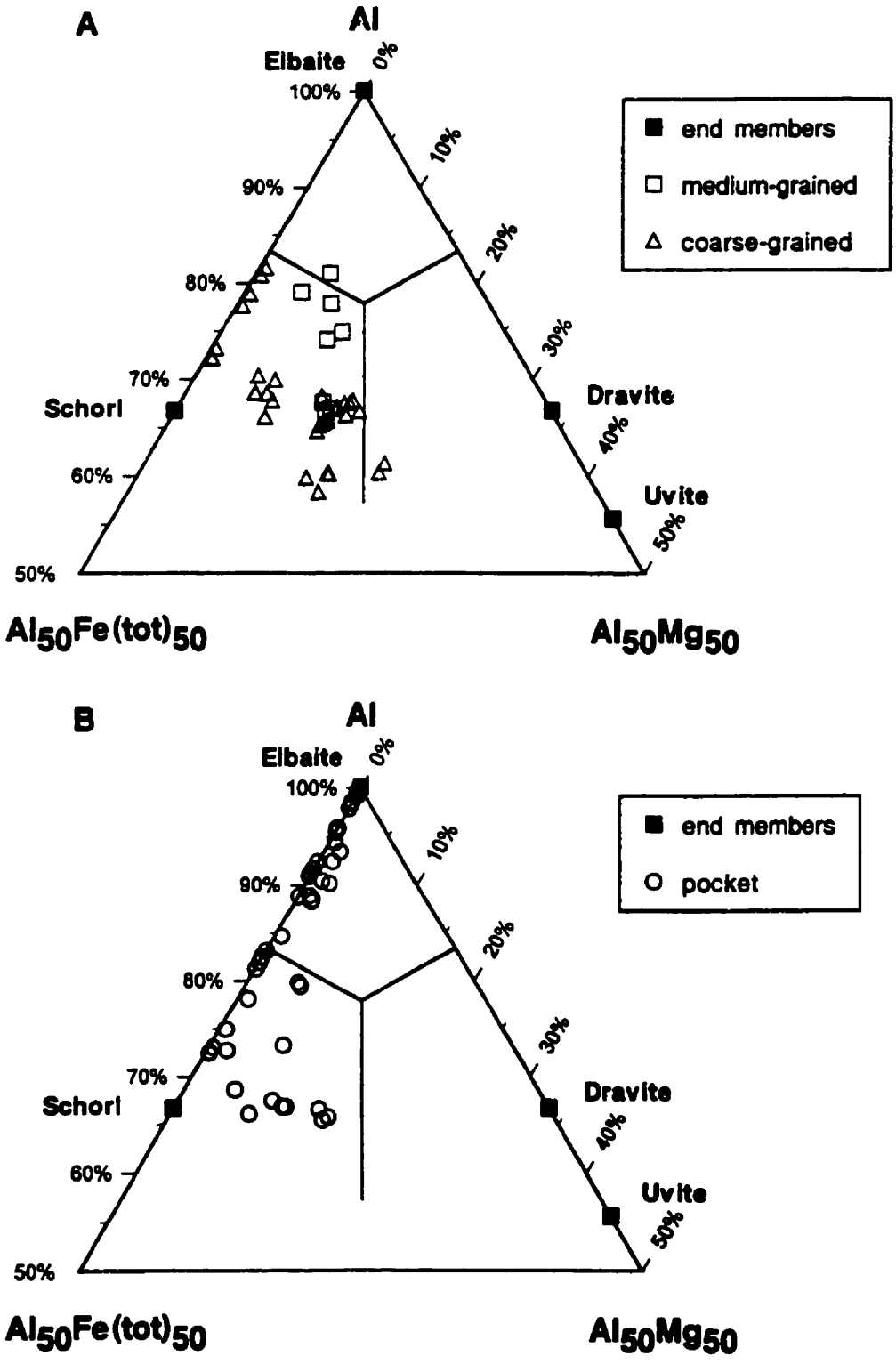

Figure 6.16. Tourmaline compositions at Řečice pegmatite.

6.4. The Pikárec Pegmatite

6.4.1. General Geology

The Pikárec pegmatite is located in the easternmost part of the Moldanubian region, western Moravia, Czech Republic. It is 3-4 m thick and intrudes migmatized biotite-sillimanite gneiss (M. Novák, per. comm.). It is zoned, with a simple internal structure which consists of a volumetrically dominant graphic zone and rare blocky K-feldspar with cleavelandite close to rare pockets. The graphic zone has abundant graphic intergrowths of black tourmaline + quartz and locally abundant spessartine-almandine + quartz. Elbaite occurs only in the most fractionated zones with blocky K-feldspar, cleavelandite and pockets. Zoned dark-grey tourmaline occurs close to the pocket, and tourmaline with smoky-grey cores and pink-to-colourless rims occurs in the pockets. Biotite is rare in the outer zones and polylithionite with inclusions of muscovite is extremely rare in the pockets.

6.4.2. Tourmaline composition in the Pikárec Pegmatite

According to Povondra (1981), the most primitive tourmaline at Pikárec is black schorl-dravite which contains 0.12 *apfu* Fe^{3+} as determined by wet chemistry (Table 6.10, composition 1). This Mg-rich tourmaline is probably associated with biotite, and the source of the Mg is fluids from the host biotite-sillimanite gneiss. The outer graphic zone contains black schorl-foitite (Fig. 6.17a). Tourmaline in the central graphic zone ranges from black schorl-foitite to Mn-bearing schorl-foitite to Fe-rich Mn-bearing elbaite and (Fe, Mn)-rich elbaite. Tourmaline in the inner graphic zone ranges from black Mn-

TABLE 6.10. REPRESENTATIVE COMPOSITIONS OF TOURMALINE (WT%) IN PIKÁREC PEGMATITE

	1	2	3	4	5	6-core	7-rim	8-core	9-rim
SiO_2	35.69	35.30	34.44	34.80	34.80	35.20	36.94	35.53	37.05
TiO_2	0.75	0.15	0.06	0.11	0.00	0.08	0.10	0.00	0.05
B_2O_3*	10.30	10.29	10.32	10.48	10.47	10.50	10.79	10.70	10.77
Al_2O_3	33.76	33.70	35.94	36.80	36.90	36.07	37.79	39.19	37.94
Fe_2O_3	0.96	0.00	0.00	0.00	0.00	0.00	0.00	0.00	0.00
MgO	3.82	0.02	0.00	0.08	0.00	0.00	0.00	0.00	0.00
CaO	0.43	0.04	0.00	0.15	0.05	0.04	0.06	0.06	0.04
MnO	0.05	0.95	3.52	1.54	5.04	3.15	6.42	7.93	5.45
FeO	9.08	13.60	9.28	10.30	6.46	8.82	0.20	0.67	0.00
ZnO	0.00	0.18	0.42	0.00	0.26	0.32	0.00	0.00	0.00
Li_2O*	0.00	0.33	0.29	0.53	0.54	0.63	1.47	0.84	1.63
Na_2O	2.09	1.65	1.40	1.66	1.74	2.15	2.67	1.58	2.78
K_2O	0.06	0.00	0.00	0.00	0.00	0.00	0.00	0.00	0.00
H_2O*	3.21	3.46	3.56	3.44	3.47	3.38	3.32	3.63	3.34
F	0.13	0.20	0.00	0.37	0.30	0.50	0.85	0.13	0.79
O=F	-0.11	-0.08	0.00	-0.16	-0.13	-0.21	-0.36	-0.05	-0.33
total	100.22	99.79	99.23	100.10	99.90	100.63	100.25	100.21	99.51
Formulae normalized to 31 anions									
T: Si	5.92	5.96	5.80	5.77	5.78	5.83	5.95	5.77	5.98
Al	0.08	0.04	0.20	0.23	0.22	0.17	0.05	0.23	0.02
B	2.94	3.00	3.00	3.00	3.00	3.00	3.00	3.00	3.00
Z: Al	6.00	6.00	6.00	6.00	6.00	6.00	6.00	6.00	6.00
Y: Al	0.52	0.67	0.93	0.97	1.00	0.87	1.13	1.27	1.19
Ti	0.09	0.02	0.01	0.01	0.00	0.01	0.01	0.00	0.01
Fe^{3+}	0.12	0.00	0.00	0.00	0.00	0.00	0.00	0.00	0.00
Mg	0.95	0.01	0.00	0.02	0.00	0.00	0.00	0.00	0.00
Mn	0.01	0.14	0.50	0.22	0.71	0.44	0.88	1.09	0.75
Fe^{2+}	1.26	1.92	1.31	1.43	0.90	1.22	0.03	0.09	0.00
Zn	0.00	0.02	0.05	0.00	0.03	0.04	0.00	0.00	0.00
Li	0.00	0.22	0.20	0.35	0.36	0.42	0.95	0.55	1.05
∑Y	2.95	3.00	3.00	3.00	3.00	3.00	3.00	3.00	3.00
X: Ca	0.07	0.01	0.00	0.03	0.01	0.01	0.01	0.01	0.01
Na	0.67	0.54	0.46	0.53	0.56	0.69	0.83	0.50	0.87
K	0.01	0.00	0.00	0.00	0.00	0.00	0.00	0.00	0.00
□	0.25	0.45	0.54	0.44	0.43	0.30	0.16	0.49	0.12
OH	3.55	3.89	4.00	3.81	3.84	3.74	3.57	3.93	3.60
F	0.13	0.11	0.00	0.19	0.16	0.26	0.43	0.07	0.40

*B_2O_3, Li_2O and H_2O calculated by stoichiometry; B = 3 *apfu*, Li = 15 - $\sum T + Z + Y$ and OH+F = 4 *apfu*.

(1) schorl-dravite analyzed by wet chemistry (Povondra *et al.* 1981); (2) schorl-foitite from outer graphic zone, sample PI105; (3) Mn-bearing foitite-schorl from inner graphic zone, sample 350; (4) schorl-foitite from outer graphic zone, sample PI103; (5) (Fe, Mn)-rich elbaite from central graphic zone, sample P203; (6) dark grey Mn-bearing elbaite-schorl core close to pockets, sample 454; (7) dirty grey Mn-rich elbaite rim of (6) close to pockets, sample 555; (8) smoky grey Mn-rich elbaite-rossmanite core from pockets, sample 661; (9) pink to colourless Mn-rich elbaite rim of (8) from pockets, sample 766.

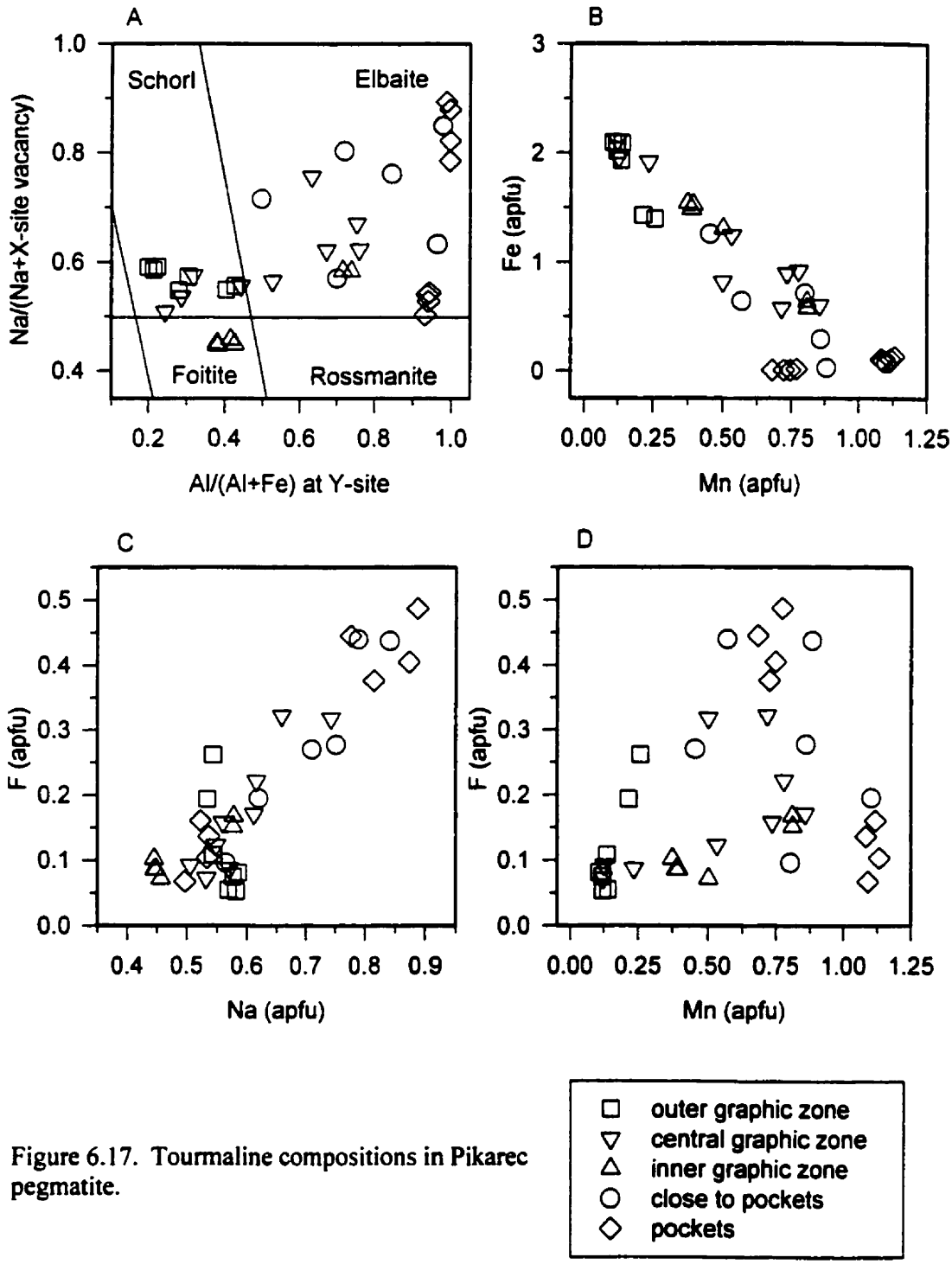

Figure 6.17. Tourmaline compositions in Pikarec pegmatite.

bearing foitite-schorl to (Mn, Fe)-rich elbaite. Tourmaline in the graphic zones contains rare to no Ca, reflecting the Ca-poor nature of the host gneiss (M. Novák, per. comm.). The dominant solid-solution in tourmaline in the graphic zones is between foitite and elbaite, and *X*-site vacancies range from 0.32-0.55 *apfu* (Figs. 6.18a, 6.19a).

Tourmaline close to the pockets is zoned with a dark-grey Mn-bearing elbaite-schorl and (Fe, Mn)-rich core and a dirty-grey (Mn, Fe)-rich elbaite and Mn-rich elbaite rim (Fig. 6.17a, Table 6.10, compositions 6, 7). This crystallization sequence indicates that Fe decreases and Mn increases with increasing fractionation (Fig. 6.17b). Tourmaline in the pockets is also zoned, with smoky-grey Mn-rich elbaite-rossmanite cores and pink-to-colourless Mn-rich elbaite rims (Table 6.10, compositions 8, 9). This crystallization sequence indicates that *X*-site vacancies, Mn and Al decrease and Na, Li and F increase with increasing fractionation (Figs. 6.17a, b, c). The dominant end-member component for tourmaline close to, or in, the pockets is elbaite and the *X*-site vacancies range from 0.11-0.47 *apfu* (Figs. 6.18b, 6.19b).

The overall crystallization sequence for black tourmaline in the Pikárec pegmatite is as follows: schorl-dravite → schorl-foitite → Mn-bearing schorl-foitite, Mn-bearing foitite-schorl → Mn-bearing elbaite-schorl → Fe-rich Mn-bearing elbaite → (Fe, Mn)-rich elbaite → (Mn, Fe)-rich elbaite. The crystallization sequence of pink-to-colourless tourmaline in pockets is as follows: Mn-rich elbaite-rossmanite → Mn-rich elbaite. There is a negative correlation between Fe and (Mn, Al+Li), as Fe decreases and Mn and Al+Li increase from schorl-foitite to Mn-rich elbaite-rossmanite, and then Mn decreases in Mn-rich elbaite (Fig. 6.17b). The progression from Fe-rich to Mn-rich tourmaline is caused by

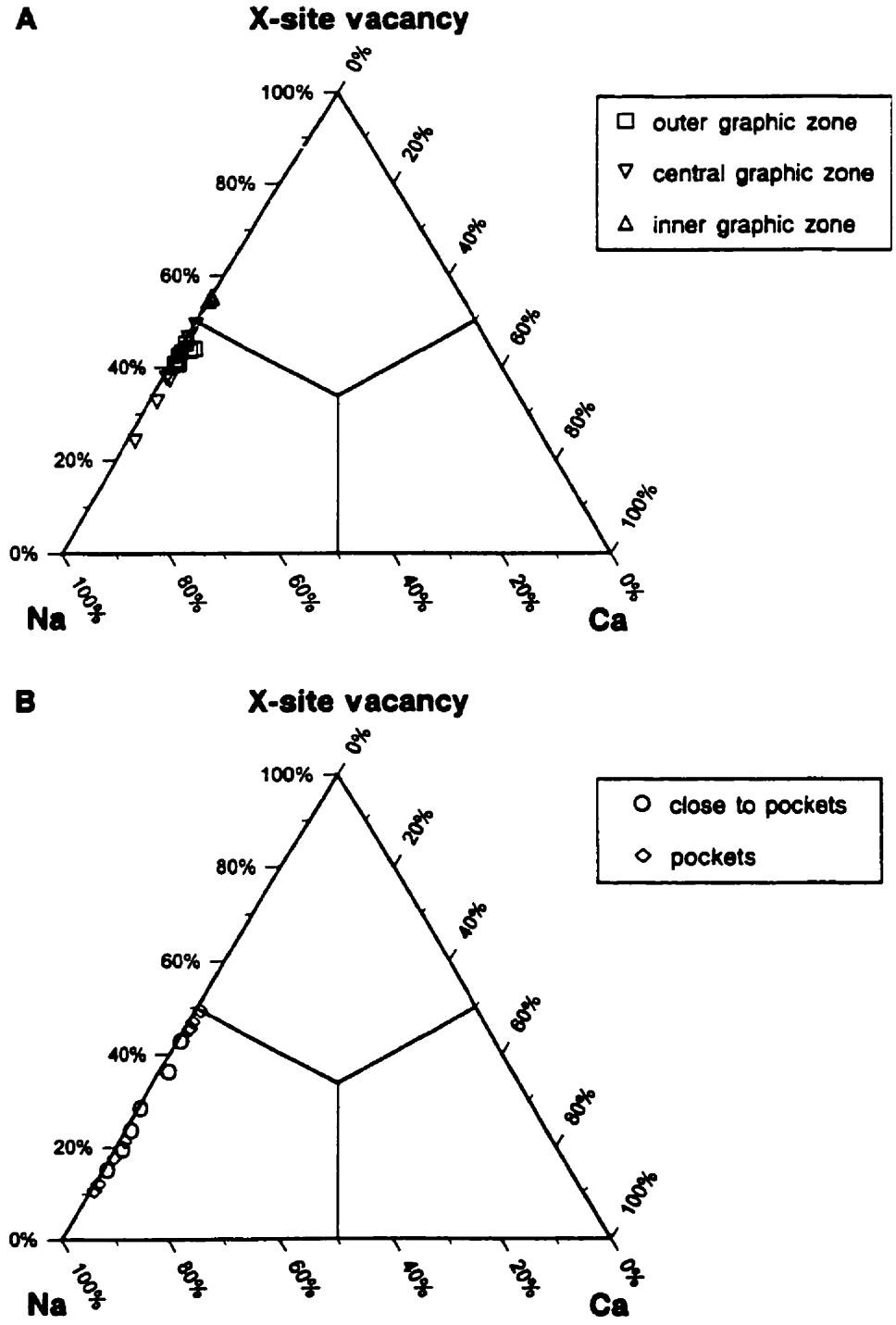

Figure 6.18. *X*-site contents for tourmaline in the Pikárec pegmatite.

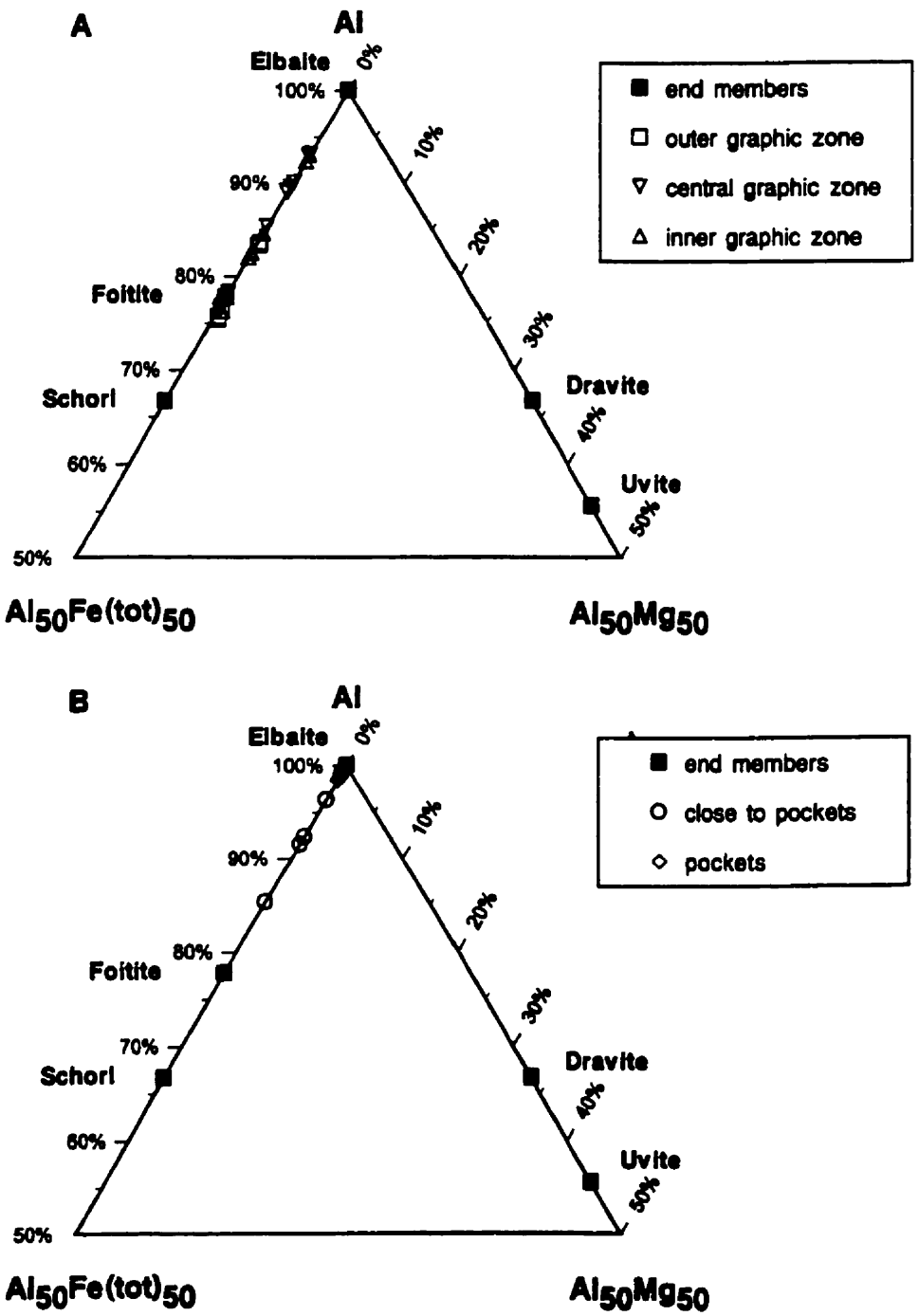

Figure 6.19. Ternary diagram of Al(tot) - $Al_{50}Fe_{50}$ - $Al_{50}Mg_{50}$ tourmaline in the Pikárec pegmatite.

the "tsilaisite substitution", 3Fe → Mn + Al + Li. There is a positive correlation between Na and F, together with low F content in tourmaline in the graphic zones and elevated Na and F in Mn-rich elbaite (Fig. 6.17c). There is no correlation between Mn and F (Fig. 6.17d).

6.5. The Ctidružice Pegmatite

6.5.1. General Geology

The Ctidružice Pegmatite is located in the easternmost part of the Moldanubian region, western Moravia, Czech Republic. It is up to 2 m thick and intrudes graphite-bearing biotite gneiss (M. Novák, per. comm.). The zoned pegmatite consists of the following (outermost to innermost) zones: coarse-grained granitic zone, graphic zone, coarse-grained albite zone, blocky K-feldspar (≤ 7 cm) with saccharoidal albite and albite-lepidolite zone as the most fractionated zone. Pockets are extremely rare. Colourless hambergite occurs in the blocky K-feldspar zone, and bertrandite replaces both beryl and hambergite (Čech 1957; Novák *et al.* 1998). Black tourmaline occurs in the graphic and saccharoidal-albite zones. Pink, green and grey tourmaline occurs in the albite-lepidolite zone.

The presence of subordinate biotite in the coarse-grained granitic zone and rare lepidolite indicates that Ctidružice is not a typical elbaite-subtype pegmatite. The Mn-rich lepidolite is rose-violet and is classified as polylithionite due to its high Si and Li and low Al contents (Němec 1983). The albite-lepidolite zone is rich in Mn, as indicated by the presence of very rare light-brownish-violet masutomilite (Mn-rich zinnwaldite) as rims

around garnet and as isolated flakes, and rare blue Mn-rich elbaite (Němec 1983). The spessartine-almandine grains are rimmed by ~1 mm thick blue tourmaline and scarce masutomilite flakes.

6.5.2. Tourmaline compositions in the Ctidružice pegmatite

Black tourmaline in the graphic zone is Mg-rich schorl and Mg-bearing schorl with 0.24 *apfu* Fe^{3+} as determined by wet chemistry (Povondra 1981) (Fig. 6.21b, Table 6.11, composition 1, 2). The source of Mg in this tourmaline is fluids from the biotite-gneiss host-rock. The tourmaline has almost no Ca which reflects the Ca-poor nature of the host gneiss.

The black tourmaline in the saccharoidal-albite zone ranges in composition from schorl-foitite to schorl to ± Mn-bearing elbaite-schorl (Fig. 6.20a, Table 6.11, compositions 3, 4). The pink, green and grey tourmaline in the albite-lepidolite zone ranges in composition from Mn-rich Fe-bearing elbaite to Mn-rich elbaite (Fig. 6.20a, Table 6.11, compositions 5, 6). The dominant solid- solution for tourmaline in the saccharoidal-albite and albite-lepidolite zones is between schorl and elbaite. Tourmaline in the saccharoidal-albite zone is *X*-site vacancy- and Fe-rich, and the tourmaline in the albite-lepidolite zone is Na-, Al-, Li-, Mn- and F-rich (Figs. 6.20, 6.21). This indicates that the "tsilaisite substitution", $3Fe \rightarrow Mn + Al + Li$, is dominant in the tourmaline and the change in composition is due to increasing fractionation of the pegmatite melt. There is a negative correlation between Fe and Mn, and a positive correlation between Na, Mn and F, with ≤ 0.88 *apfu* Na, ≤ 0.95 *apfu* Mn and ≤ 0.96 *apfu* F in Mn-rich elbaite (Figs.

TABLE 6.11. REPRESENTATIVE COMPOSITIONS OF TOURMALINE (WT%) IN THE CTIDRUŽICE PEGMATITE

	1	2	3	4	5	6
SiO_2	35.70	36.00	35.50	34.40	37.20	37.50
TiO_2	0.19	0.52	0.00	0.00	0.10	0.00
B_2O_3*	10.34	10.39	10.28	10.14	10.72	10.75
Al_2O_3	32.40	31.80	33.30	33.30	36.10	36.30
Fe_2O_3	0.00	1.88	0.00	0.00	0.00	0.00
MgO	2.77	1.45	0.00	0.00	0.00	0.00
CaO	0.31	0.34	0.00	0.06	0.20	0.18
MnO	0.20	0.70	0.97	1.83	4.76	7.03
FeO	11.80	11.61	14.50	13.40	3.55	0.31
ZnO	0.00	0.00	0.20	0.15	0.00	0.00
Li_2O*	0.26	0.02	0.22	0.25	1.46	1.66
Na_2O	1.86	1.95	1.56	1.91	2.68	2.76
K_2O	0.00	0.21	0.00	0.00	0.00	0.00
H_2O*	3.43	3.08	3.48	3.25	3.08	2.91
F	0.30	0.21	0.14	0.53	1.31	1.68
O=F	-0.13	-0.17	-0.06	-0.22	-0.55	-0.71
total	99.43	99.99	100.09	99.00	100.61	100.37
Formulae normalized to 31 anions						
T: Si	6.00	6.07	6.00	5.90	6.03	6.06
Al	0.00	0.00	0.00	0.10	0.00	0.00
B	3.00	3.02	3.00	3.00	3.00	3.00
Z: Al	6.00	6.00	6.00	6.00	6.00	6.00
Y: Al	0.42	0.32	0.64	0.62	0.90	0.92
Ti	0.02	0.07	0.00	0.00	0.01	0.00
Fe^{3+}	0.00	0.24	0.00	0.00	0.00	0.00
Mg	0.69	0.37	0.00	0.00	0.00	0.00
Mn	0.03	0.10	0.14	0.27	0.66	0.96
Fe^{2+}	1.66	1.64	2.05	1.92	0.48	0.04
Zn	0.00	0.00	0.02	0.02	0.00	0.00
Li	0.18	0.01	0.15	0.17	0.95	1.08
∑Y	3.00	2.75	3.00	3.00	3.00	3.00
X: Ca	0.06	0.06	0.00	0.01	0.04	0.03
Na	0.61	0.69	0.51	0.64	0.84	0.87
K	0.00	0.05	0.00	0.00	0.00	0.00
□	0.34	0.20	0.49	0.35	0.12	0.10
OH	3.84	3.46	3.93	3.71	3.33	3.14
F	0.16	0.22	0.07	0.29	0.67	0.86

*B_2O_3, Li_2O and H_2O calculated by stoichiometry; B = 3 *apfu*, Li = 15 - $\sum T + Z + Y$ and OH+F = 4 *apfu*.

(1) Mg-rich schorl from graphic zone, sample CT114; (2) Mg-bearing schorl, sample 67, determined by wet chemistry (Povondra 1981); (3) schorl-foitite from saccharoidal albite zone, sample CT225; (4) schorl from saccharoidal albite zone, sample CT203; (5) Mn-rich Fe-bearing elbaite from albite-lepidolite zone, sample CT332; (6) Mn-rich elbaite from albite-lepidolite zone, sample CT444.

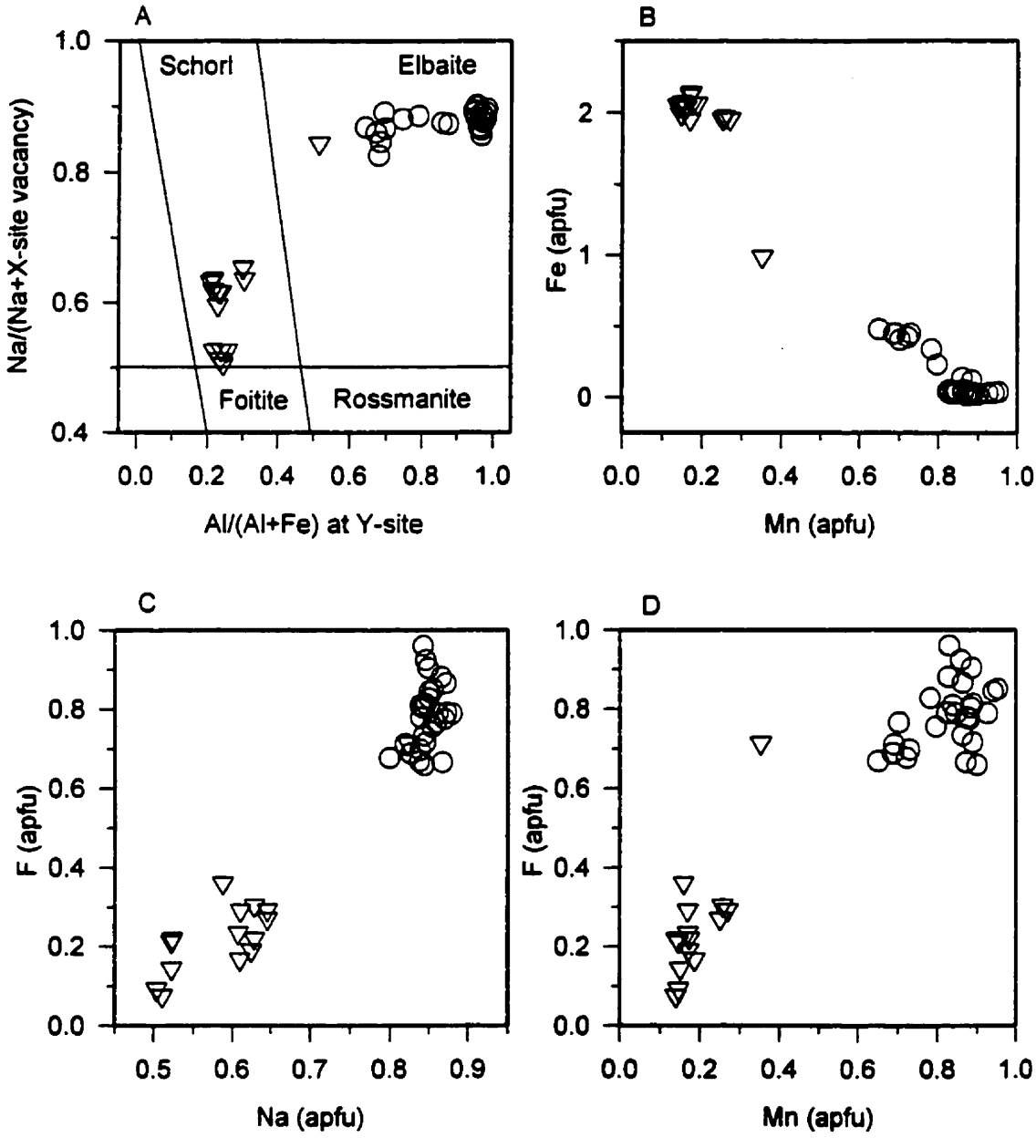

Figure 6.20. Tourmaline compositions in the Ctidruzice pegmatite.

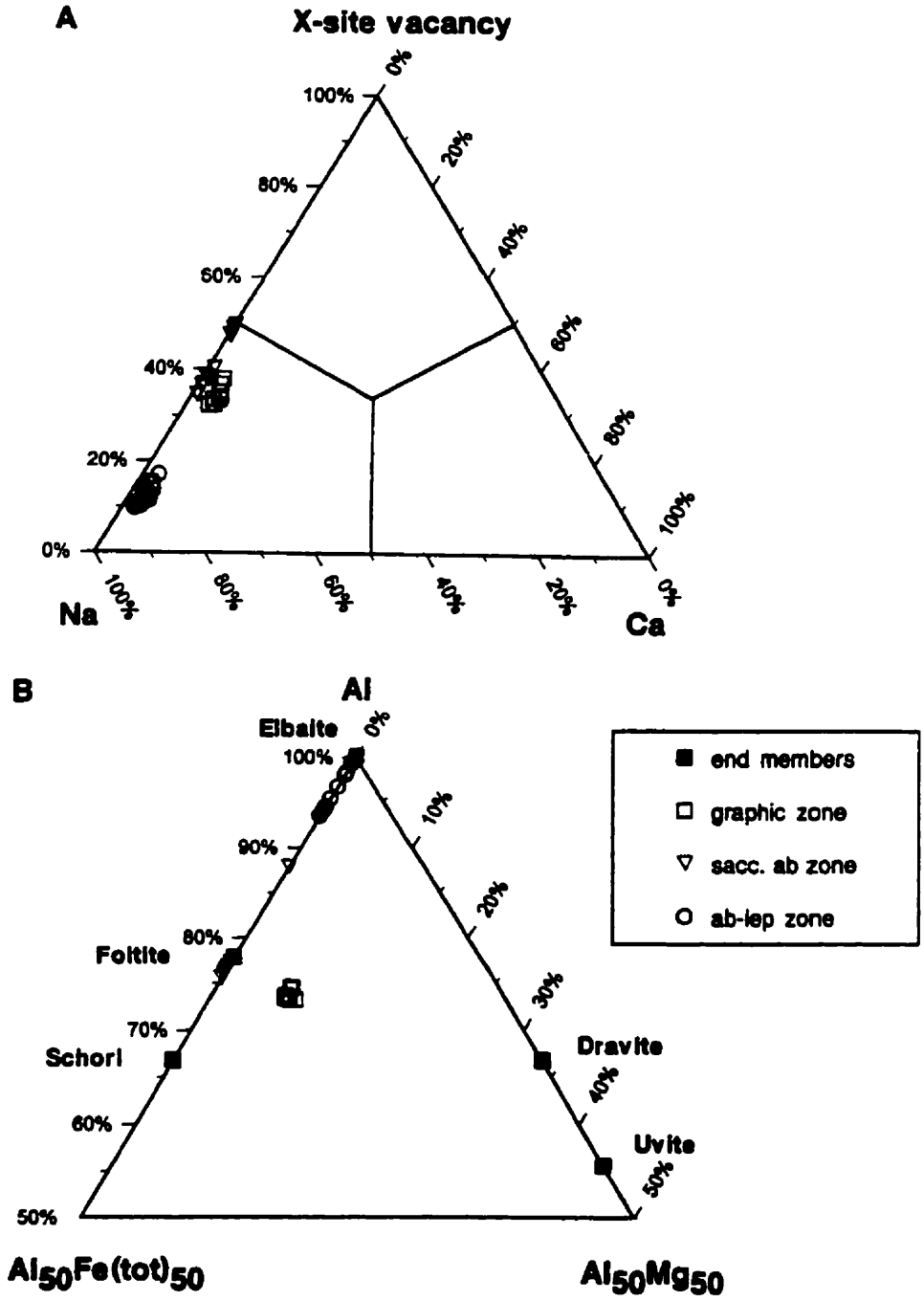

Figure 6.21. Ternary diagrams of tourmaline compositions from the Ctidružice pegmatite.

6.20b, c, d).

The overall crystallization sequence of tourmaline in the Ctidružice pegmatite is as follows: Mg-rich schorl → Mg-bearing schorl → schorl-foitite → schorl → Mn-bearing elbaite-schorl → Mn-rich Fe-bearing elbaite → Mn-rich elbaite.

6.6. The Vlastějovice Pegmatite

6.6.1. General Geology

The Vlastějovice pegmatite is located in the northern part of the Bohemian Moldanubicum at Vlastějovice. It consists of about 100 pegmatite dykes which range from several cm to 3 m thick and intrude a skarn (Novák & Hyršl 1992). The Ca- and Fe-rich skarn is medium- to coarse-grained, with dominant garnet (almandine, andradite-grossular) and hedenbergite-diopside, and locally with substantial amounts of hornblende, epidote, magnetite, quartz and calcite. The presence of andradite, epidote and magnetite indicates the abundance of Fe^{3+} and oxidizing conditions. Lenses of almost pure magnetite dispersed in the skarn were mined in the past.

The Vlastějovice pegmatite is quasi-homogeneous with a volumetrically dominant coarse-grained zone and a minor graphic zone, a blocky K-feldspar zone and pockets. The coarse-grained zone consists of dominant quartz and K-feldspar, subordinate albite and black tourmaline, and accessory biotite, pink tourmaline, fluorite, magnetite and manganocolumbite (Table 6.1) (Novák & Hyršl 1992). The pockets in the central part of the dyke contain K-feldspar, smoky quartz, pink tourmaline and rare albite overgrown by abundant late B-rich minerals (*i.e.*, danburite and datolite) and Be-rich bavenite. Black

schorl occurs with quartz as graphic intergrowths and may be rimmed by red elbaite in the coarse-grained zone. Most of the pink tourmaline occurs in the pockets.

6.6.2. Tourmaline compositions in the Vlastějovice pegmatite

In the outer coarse-grained zone, black tourmaline ranges in composition from Ca-rich schorl to Ca-bearing schorl to (Ca, Mn)-bearing schorl (Table 6.12, compositions 1-3). In the coarse-grained zone close to the pockets, black tourmaline ranges from Ca-rich schorl to Ca-bearing schorl (Table 6.12, compositions 4, 5). The source of Ca and Fe in schorl is fluids from the Ca- and Fe-rich skarn host-rock (Figs. 6.22a, b). The presence of Mg at the *Z*-site indicates a feruvite component in the schorl. The schorl probably contains Fe^{3+}, as Fe^{3+}-rich minerals are common in the skarn host-rock; and Povondra *et al.* (1985) determined 0.55 *apfu* Fe^{3+} in Ca-bearing schorl (Table 6.12, composition 5), Fe is present at the *Z*-site and Si at the *T*-site is overestimated in this schorl. Fe^{3+} can not be calculated from the electron-microprobe compositions because the OH content was not determined, and OH+F may be less than the assumed value of 4.0 *apfu*. Povondra *et al.* (1985) used wet chemistry to determine that OH+F = 2.88 *apfu* in the Ca-bearing schorl. The Fe^{3+}-bearing schorl is characterized by the presence of minor K at the *X*-site (0.02-0.03 *apfu* K).

Grey tourmaline in the coarse-grained zone close to the pockets ranges in composition from (Ca, Mn)-bearing schorl to Mn-rich elbaite-schorl to Mn-rich Fe-bearing elbaite (Fig. 6.22c, Table 6.12, compositions 7, 8). The purple-to-pink tourmaline in the pockets ranges from ± Ca-rich schorl to (Ca, Mn)-rich elbaite to elbaite-

TABLE 6.12. REPRESENTATIVE COMPOSITIONS OF TOURMALINE (WT%) IN THE VLASTĚJOVICE PEGMATITE

	1	2	3	4	5-	6-rim	7	8	9	10
SiO_2	34.05	34.74	34.58	33.94	34.52	36.22	35.38	35.70	36.10	35.96
TiO_2	1.18	0.24	0.14	0.43	0.29	0.02	0.08	0.05	0.00	0.00
B_2O_3*	9.67	9.94	10.07	9.76	10.00	10.49	10.41	10.54	10.67	11.03
Al_2O_3	23.14	27.57	31.05	26.09	29.16	39.39	34.23	36.02	37.43	42.15
Fe_2O_3	0.00	0.00	0.00	0.00	4.10	0.03	0.00	0.00	0.00	0.00
MgO	1.95	1.00	0.02	0.67	0.23	0.02	0.00	0.00	0.00	0.00
CaO	1.80	0.85	0.67	1.40	0.86	1.12	0.69	0.78	1.11	2.13
MnO	0.65	0.42	2.07	0.73	1.92	2.98	3.78	5.59	6.60	1.14
FeO	21.90	19.88	15.02	21.30	13.80	1.30	9.30	4.03	0.29	0.28
ZnO	0.00	0.00	0.00	0.07	0.00	0.00	0.15	0.00	0.00	0.00
Li_2O*	0.00	0.06	0.32	0.00	0.23	1.50	0.73	1.17	1.51	2.08
Na_2O	1.78	2.12	2.07	1.97	2.36	2.13	2.09	2.26	2.11	1.43
K_2O	0.11	0.08	0.00	0.08	0.09	0.13	0.00	0.00	0.00	0.00
H_2O*	3.12	3.17	3.16	3.14	2.03	2.71	3.24	3.19	3.27	3.48
F	0.45	0.56	0.67	0.48	0.44	0.78	0.75	0.94	0.87	0.68
O=F	-0.19	-0.24	-0.28	-0.20	-0.19	-0.33	-0.32	-0.40	-0.37	-0.29
total	99.61	100.3	99.56	99.86	99.84	98.49	100.5	99.87	99.59	100.0
Formulae normalized to 31 anions										
T: Si	6.12	6.07	5.97	6.04	6.10	5.96	5.91	5.88	5.88	5.67
Al	0.00	0.00	0.03	0.00	0.00	0.04	0.09	0.12	0.12	0.33
B	3.00	3.00	3.00	3.00	3.03	2.98	3.00	3.00	3.00	3.00
Z: Al	4.90	5.68	6.00	5.47	6.00	6.00	6.00	6.00	6.00	6.00
Mg	0.52	0.26	0.00	0.18	0.00	0.00	0.00	0.00	0.00	0.00
	0.58	0.06	0.00	0.35	0.00	0.00	0.00	0.00	0.00	0.00
Y: Al	0.00	0.00	0.28	0.00	0.07	1.60	0.65	0.88	1.06	1.49
Ti	0.16	0.03	0.02	0.06	0.04	0.00	0.01	0.01	0.00	0.00
	0.00	0.00	0.00	0.00	0.55	0.00	0.00	0.00	0.00	0.00
Mg	0.00	0.00	0.01	0.00	0.06	0.00	0.00	0.00	0.00	0.00
Mn	0.10	0.06	0.30	0.11	0.27	0.31	0.53	0.78	0.91	0.15
	2.72	2.85	2.17	2.82	2.04	0.18	1.30	0.55	0.04	0.04
Zn	0.00	0.00	0.00	0.01	0.00	0.00	0.02	0.00	0.00	0.00
Li	0.00	0.04	0.22	0.00	0.16	0.99	0.49	0.78	0.99	1.32
∑Y	2.98	2.98	3.00	3.00	3.19	3.08	3.00	3.00	3.00	3.00
X: Ca	0.35	0.16	0.12	0.27	0.15	0.14	0.12	0.14	0.19	0.36
Na	0.62	0.72	0.69	0.68	0.81	0.70	0.68	0.72	0.67	0.44
K	0.03	0.02	0.00	0.02	0.02	0.03	0.00	0.00	0.00	0.00
□	0.00	0.10	0.19	0.03	0.02	0.13	0.20	0.14	0.14	0.20
OH	3.74	3.69	3.63	3.73	2.39	2.98	3.60	3.51	3.55	3.66
F	0.26	0.31	0.37	0.27	0.49	0.81	0.40	0.49	0.45	0.34

*B_2O_3, Li_2O and H_2O calculated by stoichiometry; B = 3 *apfu*, Li = 15 - $\sum T + Z + Y$ and OH+F = 4 *apfu*.

(1) black Ca-rich schorl from the outer coarse-grained zone, sample x222; (2) black Ca-bearing schorl from the outer coarse-grained zone, sample 1029; (3) black (Ca, Mn)-bearing schorl from the outer coarse-grained zone, sample 116; (4) black Ca-rich schorl from the coarse-grained zone close to pockets, sample 2034; (5) black Ca-bearing schorl core from the coarse-grained zone close to pockets, sample 16/75 determined by wet chemistry by Povondra *et al.* (1985); (6) pink-red (Ca, Mn)-bearing elbaite rim from the coarse-grained zone close to pockets, sample 15/75 determined by wet chemistry by Povondra *et al.* (1985); (7) grey (Ca, Mn)-bearing elbaite-schorl from the coarse-grained zone close to pockets, sample 308; (8) grey Mn-rich Fe-bearing elbaite from the coarse-grained zone close to pockets, sample 307; (9) purple to pink (Ca, Mn)-rich elbaite from the pockets, sample 4006; (10) purple to pink elbaite-liddicoatite from the pockets, sample 401.

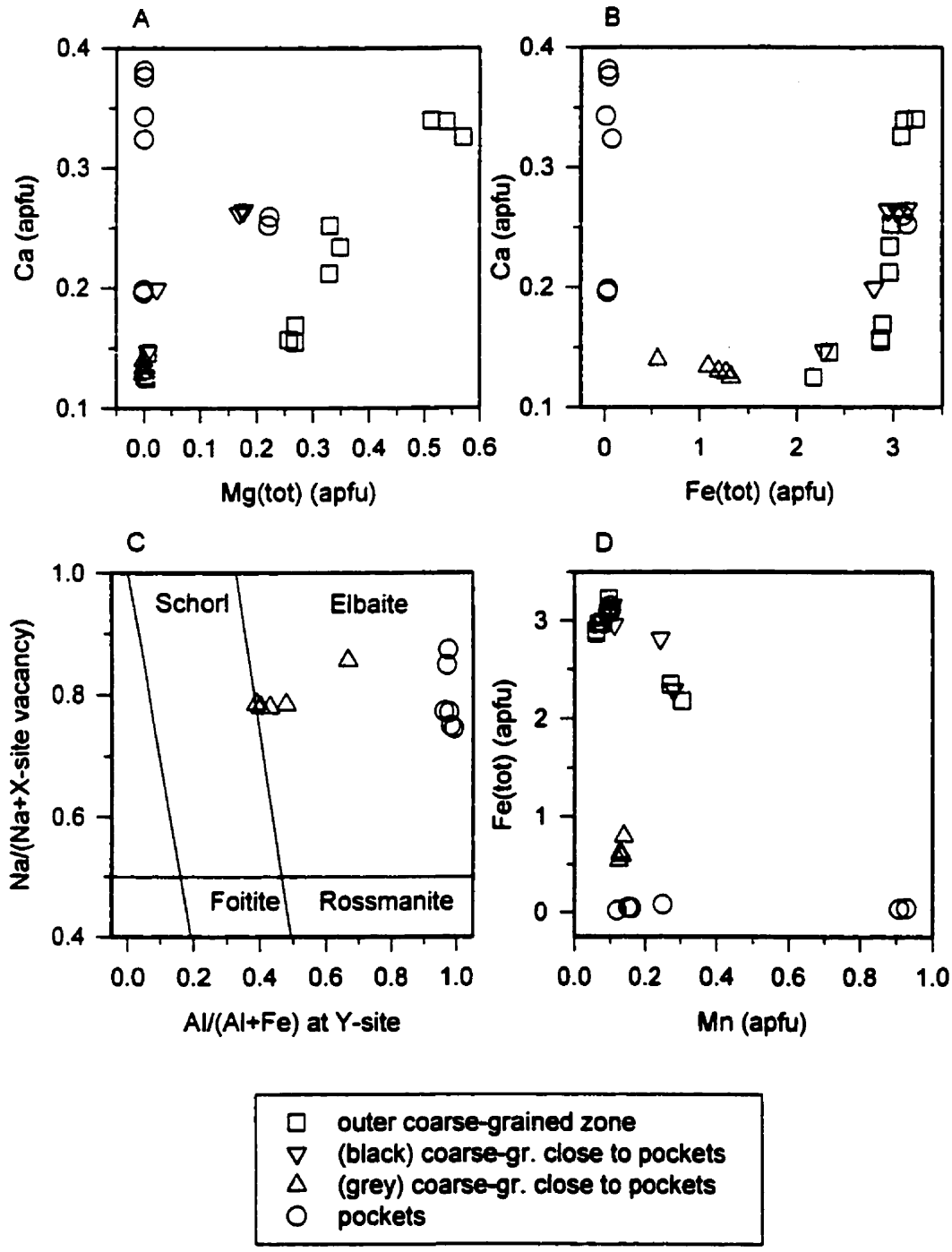

Figure 6.22. Tourmaline compositions in the Vlastejovice pegmatite.

liddicoatite (Table 6.12, compositions 9, 10). Evolved elbaite-schorl and elbaite is enriched in Ca and Mn.

The overall crystallization sequence of tourmaline in the Vlastějovice pegmatite is as follows: Ca-rich schorl → Ca-bearing schorl → (Ca, Mn)-bearing schorl → (Ca, Mn)-bearing elbaite-schorl → Mn-rich elbaite-schorl → Mn-rich Fe-bearing elbaite → (Ca, Mn)-rich elbaite → elbaite-liddicoatite. The dominant solid-solution series is between schorl and elbaite (Fig. 6.23b), and Na is the dominant *X*-site component, except for dominant Na and Ca in late purple-to-pink elbaite-liddicoatite in the pockets (Figs. 6.22a, 6.23a). Black schorl in the outer coarse-grained and inner coarse-grained zones, close to the pockets, has a positive correlation between Ca, Mg, Fe and Ti, as they decrease from Ca-rich schorl ($\leq$ 0.17 *apfu* Ti) to (Ca, Mn)-bearing elbaite-schorl ($\leq$ 0.01 *apfu* Ti) (Figs. 6.22a, b). There is a negative correlation between Fe and (Mn, Al +Li), as Fe decreases and Mn and Al+Li increase from Ca-rich schorl to (Ca, Mn)-rich elbaite, followed by decreases in Mn to elbaite-liddicoatite (Fig. 6.22d). The progression from Fe-rich to Mn-rich tourmaline is caused by the "tsilaisite substitution", 3Fe → Mn + Al + Li.

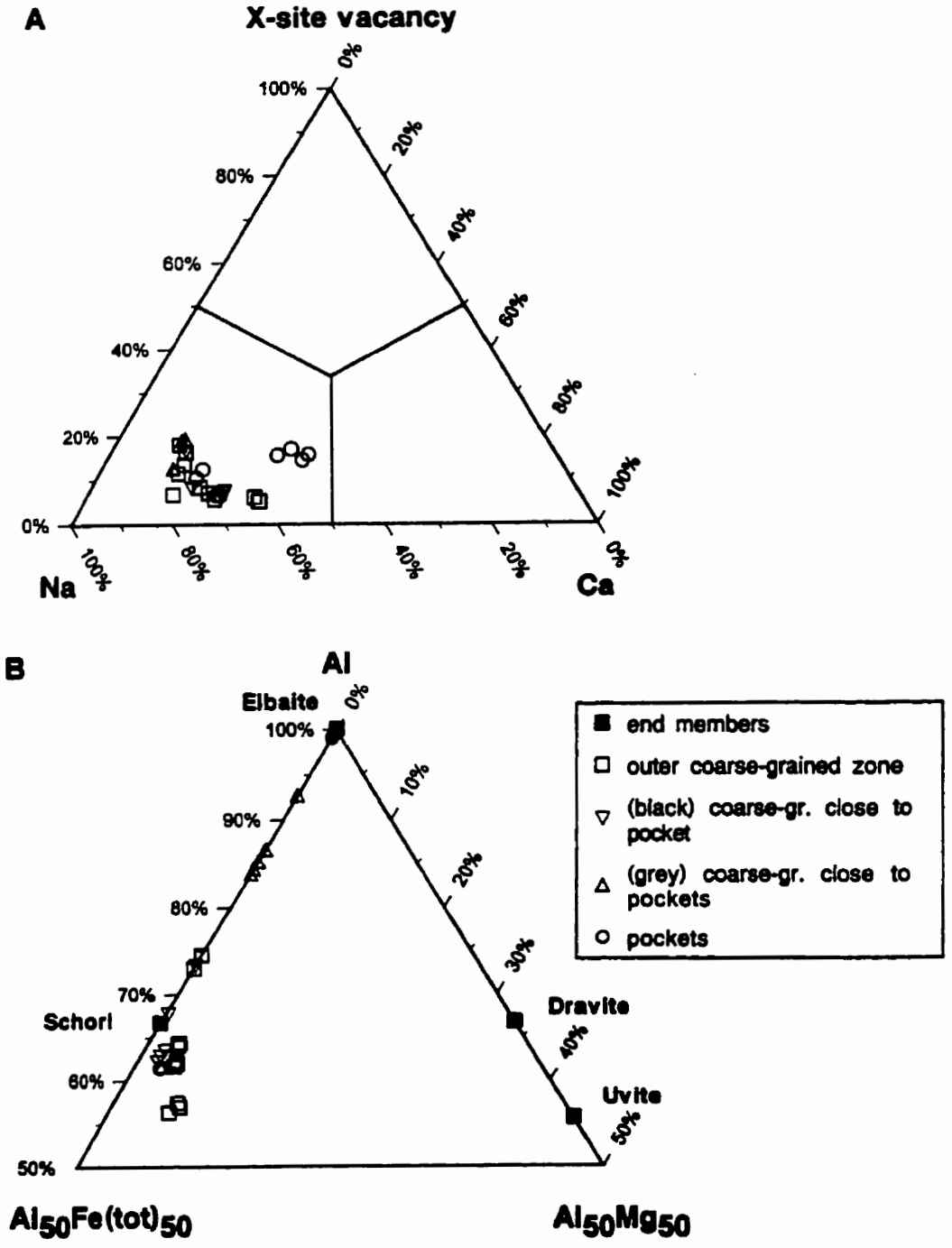

Figure 6.23. Ternary diagrams of tourmaline compositions from the Vlastějovice pegmatite.

CHAPTER 7

Discussion

7.1. Tourmaline from lepidolite-subtype pegmatites

The discussion of lepidolite-subtype pegmatites will begin with a review of tourmaline at the Stewart Litha pegmatite, California which will be followed by a summary of the compositional evolution of tourmaline from all of the lepidolite-subtype pegmatites discussed. The geology and compositional data of tourmaline from Stewart Lithia are directly from the literature, but the figures and interpretation are that of the author.

7.1.1. The Stewart Lithia pegmatite

The only lepidolite-subtype pegmatite in which the tourmaline composition has been previously studied in detail is Stewart Lithia pegmatite (M.Sc. thesis of Bloomfield 1997). Stewart Lithia pegmatite is located in the Pala district, San Diego County, southwestern California, and is > 1 km long and ≤ 25 m thick (Shigley & Brown 1985). It is a zoned lepidolite-subtype pegmatite which intrudes gabbro-norite, and was previously mined for Li, Cs and Rb in lepidolite and for gem-quality tourmaline, morganite, smoky quartz and kunzite (Bloomfield 1997). Much of the lepidolite zone has been removed and is only available in the dumps. The pegmatite was mapped extensively by Jahns & Wright (1951) and Jahns (1979). The upper pegmatite zones (above the core) are generally coarser-grained and rich in microcline, whereas the lower zones contain both coarse- and fine-grained minerals and are rich in albite (Shigley & Brown 1985). Gem-bearing

TABLE 7.1. GENERAL VERTICAL CROSS-SECTION OF THE STEWART LITHIA PEGMATITE •

	pegmatite zone	mineral assemblage	tourmaline composition
upper zones	graphic-granite wall- zone	medium- to coarse-grained microcline perthite + quartz (± muscovite, albite)	
	graphic-granite wall- zone	in parallel fracture-controlled veins: muscovite, cleavelandite, green tourmaline, quartz, lepidolite	black schorl-foitite, schorl, elbaite-schorl
	outer intermediate	blocky microcline-perthite (± quartz, muscovite, albite, tourmaline)	elbaite-rossmanite
	middle intermediate	blocky comb-texture microcline-perthite + quartz (± lithiophilite, secondary Mn-rich phosphates)	
	chimney structure	fine-grained albite + quartz + coarse-grained black tourmaline + pale-green muscovite	foitite-schorl, schorl-foitite, schorl, elbaite-schorl, Mn-bearing elbaite
	inner intermediate	massive quartz	
	core	quartz + spodumene (± pink tourmaline, amblygonite)	elbaite-rossmanite, rossmanite-elbaite
lower zones	pockets	coloured tourmaline, morganite, kunzite, smoky quartz, cleavelandite, perthite, muscovite, lepidolite, Ca, Na-rich clays and zeolites	elbaite-schorl, elbaite, Mn-bearing elbaite, elbaite-rossmanite
	lepidolite	lepidolite, pink tourmaline (± quartz, albite)	radiating elbaite-rossmanite
	inner intermediate	massive quartz, (± blocky perthite)	
	middle intermediate	coarse-grained albite + quartz + microcline, muscovite	
	aplitic wall zone	fine- to medium-grained albite + quartz + black tourmaline + muscovite (± perthite)	

• based on Jahns & Wright (1951), Jahns (1979), Shigley & Brown (1985), Foord *et al.* (1986), Bloomfield (1997).

pockets and massive lepidolite orebodies lie directly underneath the quartz core. The pegmatite zones, mineral assemblages and tourmaline compositions are summarized in Table 7.1.

Tourmaline composition at the Stewart Lithia pegmatite evolves over the crystallization sequence: foitite-schorl → schorl-foitite → schorl → elbaite-schorl → elbaite-rossmanite → rossmanite-elbaite → Mn-bearing elbaite → elbaite (Fig. 7.1a) (Bloomfield 1997). This overall sequence is similar to that in other lepidolite-subtype pegmatites, except for the presence of schorl with 0.60-0.70 *apfu* Na, which is absent in the other lepidolite-subtype pegmatites discussed in this thesis. Black foitite-schorl, schorl-foitite and schorl occur in fracture-controlled veins in the upper graphic-granite wall-zone and chimney structure in the middle intermediate- zone, both of which may be replacement in origin. Black to dark-blue/green elbaite-schorl occurs in veins in the upper graphic-granite wall-zone, chimney structure and pockets. Pink elbaite-rossmanite and rossmanite-elbaite occur in the outer intermediate zone, lepidolite zone, quartz + spodumene core, and pockets. Deep-blue/green, pale-green, clear, pink and blue Mn-bearing elbaite and elbaite occur in chimney structure and pockets. Pink Mn-bearing elbaite crystals (about 1.3 cm long) with green elbaite caps occur in the pockets; the green caps crystallized after pocket rupture.

There is a negative correlation between Fe and Mn as the composition evolves over the sequence: foitite-schorl → schorl-foitite → schorl → elbaite-schorl, followed by a decrease of Mn in elbaite-rossmanite and rossmanite-elbaite, and a late-stage increase of Mn in Mn-bearing elbaite and elbaite (Fig. 7.1b). The maximum Mn content of

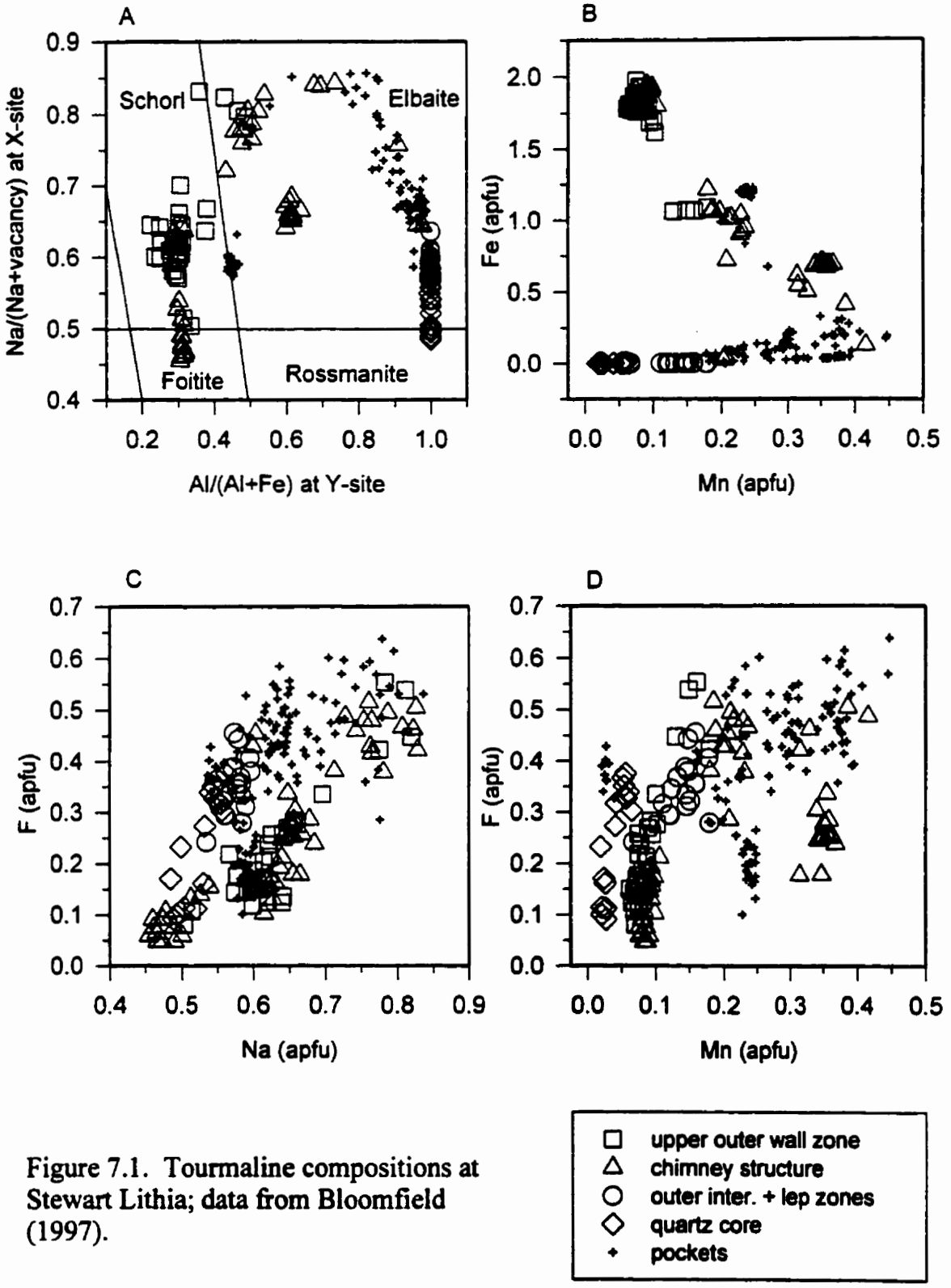

Figure 7.1. Tourmaline compositions at Stewart Lithia; data from Bloomfield (1997).

tourmaline is 0.45 *apfu* Mn in blue/green Mn-bearing elbaite in pockets.

Figures 7.1c and 7.1d show a strong positive correlation between Na and F and a weaker positive correlation between Mn and F in tourmaline: (1) foitite-schorl, schorl-foitite and schorl have low Na, Mn and F contents; (2) elbaite-schorl has high Na and F, and moderate Mn contents; (3) elbaite-rossmanite and rossmanite-elbaite have low Na and Mn, and moderate F contents; (4) Mn-bearing elbaite and elbaite have high Na, Mn and F contents.

Most of the tourmaline contains no Mg, except for 0.09-0.24 *apfu* Mg in schorl-foitite and schorl from veins in upper graphic-granite wall-zones, and foitite-schorl and schorl with ≤ 0.09 *apfu* Mg in the chimney structure. Most tourmaline contains no Ti, except for schorl in veins in upper graphic-granite wall-zones and chimney structure, which has ≤ 0.03 *apfu* Ti. Most tourmaline has no Ca, except for ≤ 0.10 *apfu* Ca in Mn-bearing elbaite in pockets.

7.1.2. Geochemical evolution in lepidolite-subtype pegmatites

The Fe-Mn substitution in minerals (*e.g.*, almandine-spessartine, columbite-tantalite) is commonly used to indicate the degree of fractionation in a pegmatite. The Fe-Mn fractionation trend in tourmaline is more complex than that in other pegmatite minerals (*i.e.*, decreasing Fe and increasing Mn with progressive fractionation). With increasing fractionation, there is an overall trend of decreasing Fe and increasing Mn and Al + Li from foitite-schorl to elbaite, followed by decreasing Mn to rossmanite-elbaite and late stage Fe and Mn enrichment in (Fe, Mn)-bearing elbaite (Fig. 7.2b).

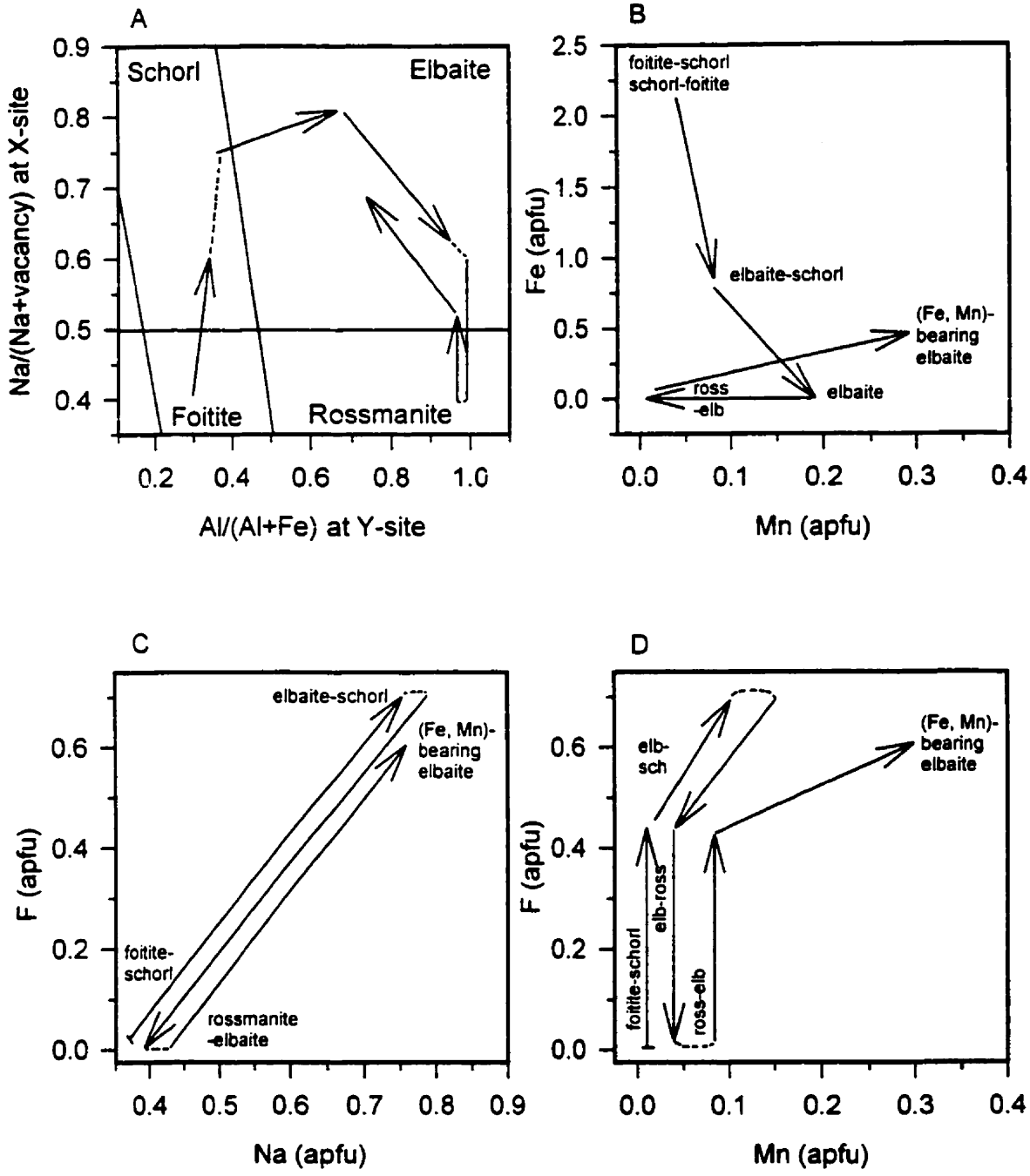

Figure 7.2. Idealized tourmaline compositional trends in lepidolite-subtype pegmatites.

The Fe, Li, Al, Mn and F contents in the abundant tourmaline and mica correlate with that in the pegmatite melt as it gradually evolves with progressive pegmatite consolidation. The pegmatite melt initially crystallizes foitite-schorl, schorl-foitite and biotite. With increasing fractionation, the melt crystallizes elbaite-schorl and muscovite to elbaite-rossmanite, rossmanite-elbaite and lepidolite. The final tourmaline to crystallize from a supercritical fluid is (Fe, Mn)-bearing elbaite that is subsequently coated by cookeite (Fig. 7.2a). Manganese is preferentially partitioned into tourmaline over mica, so the Mn content in mica does not show the same trend as the tourmaline.

There is a negative correlation between Fe and (Al+Li) at the *Y* site in tourmaline. Tourmaline is enriched in Fe in granitic zones, in (Al+Li) in the albite and lepidolite zones, and slightly enriched in Fe in late pockets. Late low-temperature enrichment of Fe occurs in tourmaline, mica and (Nb, Ta)-oxide minerals in lepidolite-subtype pegmatites (Ercit 1986, Černý 1991a, Černý *et al.* 1995, Novák & Taylor 1996, Aurisicchio *et al.* 1997). For example, in addition to tourmaline, late-stage Fe and Mn enrichment is also shown by the secondary Fe-enriched manganotantalite in veinlets crosscutting Fe-free stibiotantalite in the lepidolite zone (vii) (Novák & Černý 1998), and the pocket elbaite-rossmanite is capped by foitite at Dobrá Voda. For tourmalines in lepidolite-subtype pegmatites, this Fe enrichment in late hydrothermal fluids in pockets is not due to reaction with Fe-bearing primary phases within the pegmatite (as claimed by Aurisicchio *et al.* 1997) because the accessory Fe-bearing minerals in the pegmatites are not corroded. Late Fe-enrichment is more likely due to infiltration of country-rock fluids after thermal equilibration of the pegmatites with their host rocks (Černý 1991a, Černý *et al.* 1995).

However, increased contents of Mg and Ca in tourmaline is expected in this case.

There is a positive correlation between Na at the *X*-site and F at the O(1) site in tourmaline (Linnen & William-Jones 1993, Novák 1996, unpublished data of the author). The crystal-chemical explanation for this correlation (Gebert & Zemann 1965, Robert *et al.* 1997) is as follows: the OH group at the O(1) site is bonded to three *Y* cations and the O-H bond is directed along the threefold axis toward the *X*-site at the centre of the (T_6O_{18}) tetrahedral ring. The OH···O interactions between the H atom and the O atoms are weak when a cation occupies the *X* site, and this situation is favourable for F → OH substitution. When the *X* site is occupied by Na and the three *Y* sites are occupied by $3M^{2+}$ or $1.5M^{+}+ 1.5M^{3+}$ (*i.e.*, schorl and elbaite), F can replace OH in this environment. When *X* is empty and the three *Y* sites are occupied by $2M^{2+}+ 1M^{3+}$ or $1M^{+}+ 2M^{3+}$ (*i.e.*, foitite and rossmanite), F cannot enter the O(1) site. The positive correlation between Na and F in tourmaline from lepidolite-subtype pegmatites follows the trend of Robert *et al.* (1997), as foitite-schorl and rossmanite-elbaite are rich in *X*-site vacancies and contain no F, whereas elbaite-schorl is Na- and F-rich (Fig. 7.2c).

The Na and F contents in the tourmaline oscillates between (Na, F)-poor tourmaline and (Na, F)-rich tourmaline. The positive correlation between Na and F is caused by crystal chemical effects, but overall abundance of Na and F in the pegmatite melt is controlled by partition coefficients. The first tourmaline to crystallize is (Na, F)-poor foitite-schorl, as Na preferentially partitions into plagioclase over tourmaline. The pegmatite melt increases in F content with increasing fractionation. The presence of volatiles, such as B and F, drives the compositions of residual melts toward alkaline, Na-

rich compositions enriched in incompatible elements (London 1987). This promotes the crystallization of (Na, F)-rich elbaite-schorl associated with muscovite. The next tourmaline to crystallize is Na-poor rossmanite-elbaite, as F preferentially partitions into lepidolite and accessory topaz over tourmaline. The (Fe, Mn)-bearing elbaite which is rich in Na and F crystallizes with the F-free cookeite.

Minor topaz is associated with F-rich lepidolite in the lepidolite zone at Laštovičky, Dobrá Voda, Rožná, Dolní Bory and Radkovice, and in pockets at Laštovičky (Staněk 1973, Černý *et al.* 1970, Černý *et al.* 1995). A general trend of increasing acidity (μHF) during crystallization of micas is indicated by the change from muscovite to trilithionite, and the presence of topaz (London 1982, Černý *et al.* 1995). Subsequent shift from lepidolite toward polylithionite indicates decreasing pH of the pegmatite melt (Gordiyenko & Ponomareva 1988). The Mn-enrichment in elbaite is correlated with, and seems to be caused by increased acidity of the pegmatite melt.

Cookeite occurs as an alteration product of F-rich lepidolite in the lepidolite zones at Laštovičky and Radkovice, and as a coating on pocket walls at Dobrá Voda and Dolní Bory (Černý *et al.* 1971, Staněk 1973, Němec 1981). At all four localities, cookeite is one of the last minerals to crystallize. The presence of cookeite indicates decreasing salinity and low F-activity in the late low-temperature hydrothermal fluids (London 1982).

7.1.3. Summary of tourmaline and mica compositions in lepidolite-subtype pegmatites

In lepidolite-subtype pegmatites, tourmaline and mica evolve from the outermost zones to the innermost zones in the following sequence: (1) granitic and graphic zones contain foitite-schorl to schorl-foitite, minor biotite and abundant muscovite; (2) albite zones contain elbaite-schorl and muscovite; (3) inner albite and outer lepidolite zones contain elbaite and lepidolite (trilithionite); (4) lepidolite zones contain elbaite-rossmanite to rossmanite-elbaite; (5) quartz core and late pockets contain (Fe, Mn)-bearing elbaite and minor cookeite (Fig. 7.2a).

The crystallization sequence begins with vacancy-rich tourmaline (foitite), and evolves to Na-rich tourmaline (elbaite-schorl) to vacancy-rich tourmaline (rossmanite) and rarely to Na-rich tourmaline (elbaite) (Fig. 7.2a). There is a negative correlation between Fe and (Al+Li), and a positive correlation between Na, Mn and F in tourmaline. The Fe-Mn trend in tourmaline begins with high Fe, followed by moderate Fe and Mn, no Fe or Mn, and slight enrichment in Fe and Mn in the final tourmaline (Fig. 7.2b). Typically, the Mn content in tourmaline is < 0.30 *apfu*, except for ≤ 0.40 *apfu* Mn in Mn-bearing elbaite in the quartz core at Rožná, ≤ 0.45 *apfu* Mn in Mn-bearing elbaite in pockets at Stewart Lithia, and ≤ 0.48 *apfu* Mn in (Fe, Mn)-bearing elbaite in pockets at Dolní Bory.

Most tourmaline in lepidolite-subtype pegmatites contains no Mg or Ti, except for schorl-foitite in the most primitive outermost zones (*e.g.*, 0.32 *apfu* Mg and 0.08 *apfu* Ti in schorl-foitite from the outer coarse-grained albite zone at Laštovičky, and 0.61 *apfu*

Mg plus 0.05 *apfu* Ti in Mg-rich schorl from graphic zone at Radkovice). Most tourmaline contains no Zn, except for up to 0.06 *apfu* Zn in foitite-schorl from the most primitive graphic zone at Rožná, and schorl-foitite and Fe-rich elbaite from the intermediate zones at Radkovice and Laštovičky. Most tourmaline in lepidolite-subtype pegmatites contains ~ 0.01 *apfu* Ca, except for ≤ 0.09 *apfu* Ca in (Fe, Mn)-bearing elbaite from late pockets at Dobrá Voda and Dolní Bory, ≤ 0.10 *apfu* Ca in Mn-bearing elbaite in the pockets at Stewart Lithia, and ≤ 0.11 *apfu* Ca in elbaite-rossmanite rims at Red Cross Lake.

7.2. Tourmaline from petalite-subtype pegmatites

The discussion of petalite-subtype pegmatites will begin with a review of tourmaline at the Urubu pegmatite, Brazil which will be followed by a summary of the compositional evolution of tourmaline from all of the petalite-subtype pegmatites discussed. The geology and compositional data of tourmaline from Urubu are directly from the literature, but the figures and interpretation are that of the author.

7.2.1. The Urubu pegmatite

The only petalite-subtype pegmatite in the literature in which the tourmaline composition has been studied in detail is the Urubu pegmatite (Marchetti 1997). The Urubu pegmatite is located near the junction of the Piauí and Jequitinhonha rivers in the northern part of the state of Minas Gerais, Brazil. It is 180 m long x 60 m wide x 12 m thick and intrudes dark-grey biotite schist with beds of quartz. It was previously mined

for lepidolite and amblygonite, and is well known for pink and green tourmaline. The Urubu pegmatite consists of the following zones: (1) exocontact, (2) border zone, (3) wall zone, (4) intermediate zone, (5) pocket zone, and (6) quartz core (Cassedanne & Cassedanne 1981, Quéméneur *et al.* 1993, Marchetti 1997). The exocontact (1) is a tourmalinized biotite schist with dominant small black needles of tourmaline (30-40 vol%) and zinnwaldite (10-30 vol%). The border zone (2) contains abundant quartz and muscovite, subordinate green tourmaline and aplitic albite, and accessory biotite and lithiophilite. The wall zone (3) contains abundant muscovite, subordinate cleavelandite, quartz and green tourmaline, and accessory pyrolusite and beryl. The intermediate zone (4) (also called the albite unit) contains dominant cleavelandite, blocky K-feldspar, muscovite and green tourmaline, subordinate quartz, cassiterite and altered spodumene, and accessory beryl, columbite-tantalite and cookeite. The pocket zone (5) contains abundant pink and colourless tourmaline (up to 60 cm long) and lepidolite, subordinate cleavelandite, and accessory amblygonite, petalite (up to 10 cm long), pollucite and morganite. The quartz core (6) contains dominant quartz (90 vol%), subordinate apple-green gem-quality tourmaline (10-20 cm long), colourless, blue and pink tourmaline and aquamarine.

The tourmaline composition at the Urubu pegmatite evolves over the following crystallization sequence: elbaite-schorl → Fe-rich elbaite → Fe-bearing elbaite → elbaite → (± rossmanite-elbaite) → elbaite-rossmanite → elbaite → Fe-bearing elbaite (Fig. 7.3a) (Marchetti 1997 and data of the author). Schorl is not a primary tourmaline at this locality, but is common in other petalite-subtype pegmatites. Green tourmaline in the

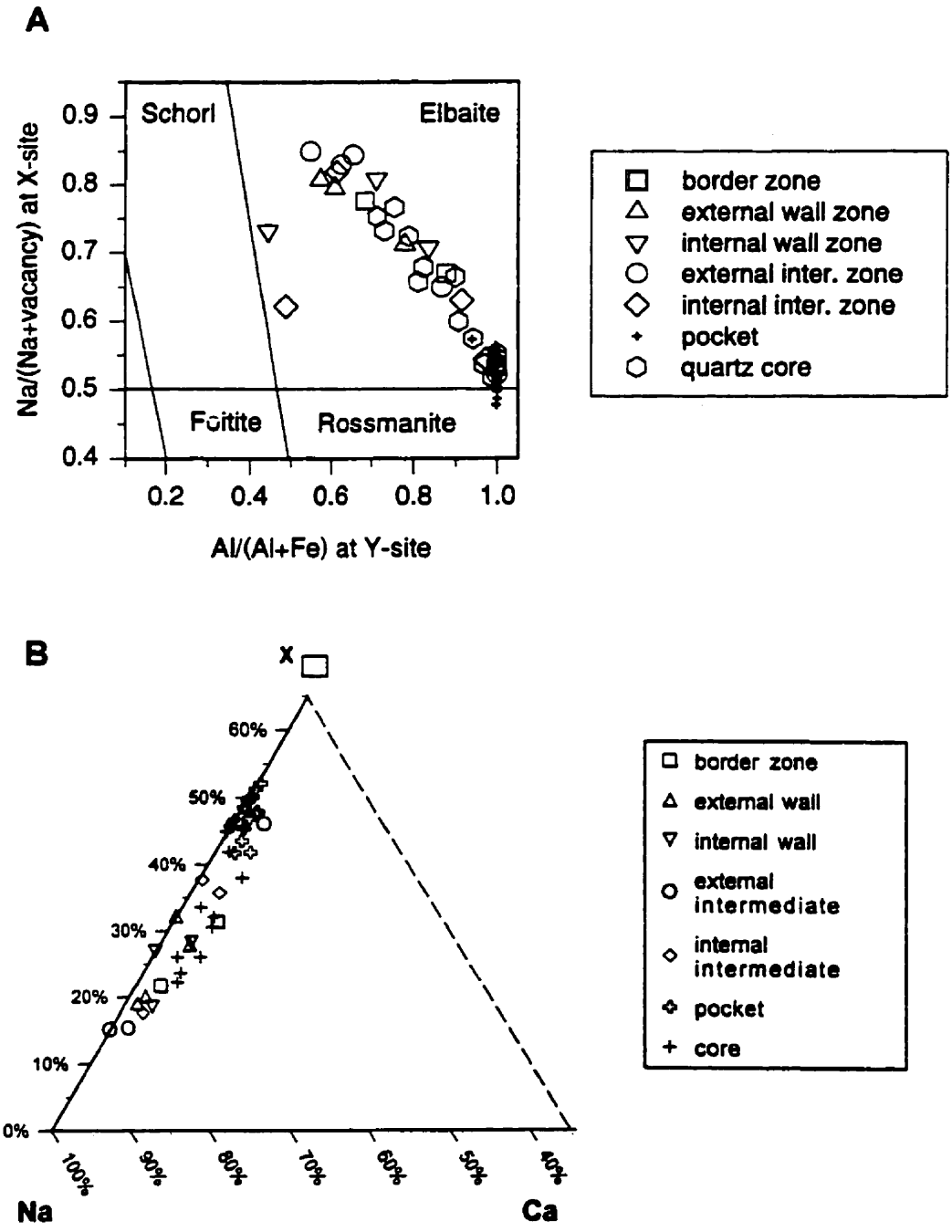

Figure 7.3. Tourmaline compositions at Urubu pegmatite. Data from Quéméneur *et al.* (1993), Marchetti (1997) and the author.

border, wall and intermediate zones has a similar wide range in composition from elbaite-schorl to elbaite. Pink tourmaline in the pocket zone has a cloudy pale-pink rossmanite-elbaite and elbaite-rossmanite core, and a clear pink elbaite-rossmanite rim. Tourmaline in the quartz core ranges from elbaite-rossmanite to Fe-bearing elbaite. Tourmaline with colourless elbaite-rossmanite cores and green Fe-bearing elbaite rims occurs in the quartz core; compositional zoning within individual crystals throughout the pegmatite is reversed relative the Fe-(Al+Li) zoning which commonly occurs in tourmaline with (Al+Li)-enriched cores and Fe-enriched rims (Marchetti 1997).

The dominant substitution at the *X* site is Na ⇔ □(Fig. 7.3b). Most of the □-rich tourmaline occurs in the petalite-bearing pocket zone. The maximum Ca content is 0.06 *apfu* in Fe-bearing elbaite in the quartz core. The negative correlation between Fe and Al at the *Y* site indicates that the dominant substitution is Fe ⇔ (Al+Li) (Fig. 7.4a). There is a positive correlation between Fe and Mn, which is the opposite of that in tourmaline in other petalite-subtype pegmatites (Fig. 7.4b). The maximum Mn content is 0.09 *apfu* in Fe-bearing elbaite in the internal wall zone and in Fe-rich elbaite in the external intermediate zone. Manganese is absent in rossmanite-elbaite and elbaite-rossmanite. Elbaite-schorl in the internal intermediate zone plots as an isolated point with high Fe and low Mn.

The positive correlation between Na, Mn and F is comprised of two trends, one for the border, wall and intermediate zones, and another for the pocket and quartz-core zones (Figs. 7.4c and d). Tourmaline in the pocket and quartz-core zones, and rarely in the external intermediate zone is enriched in F relative to that in the border, wall and

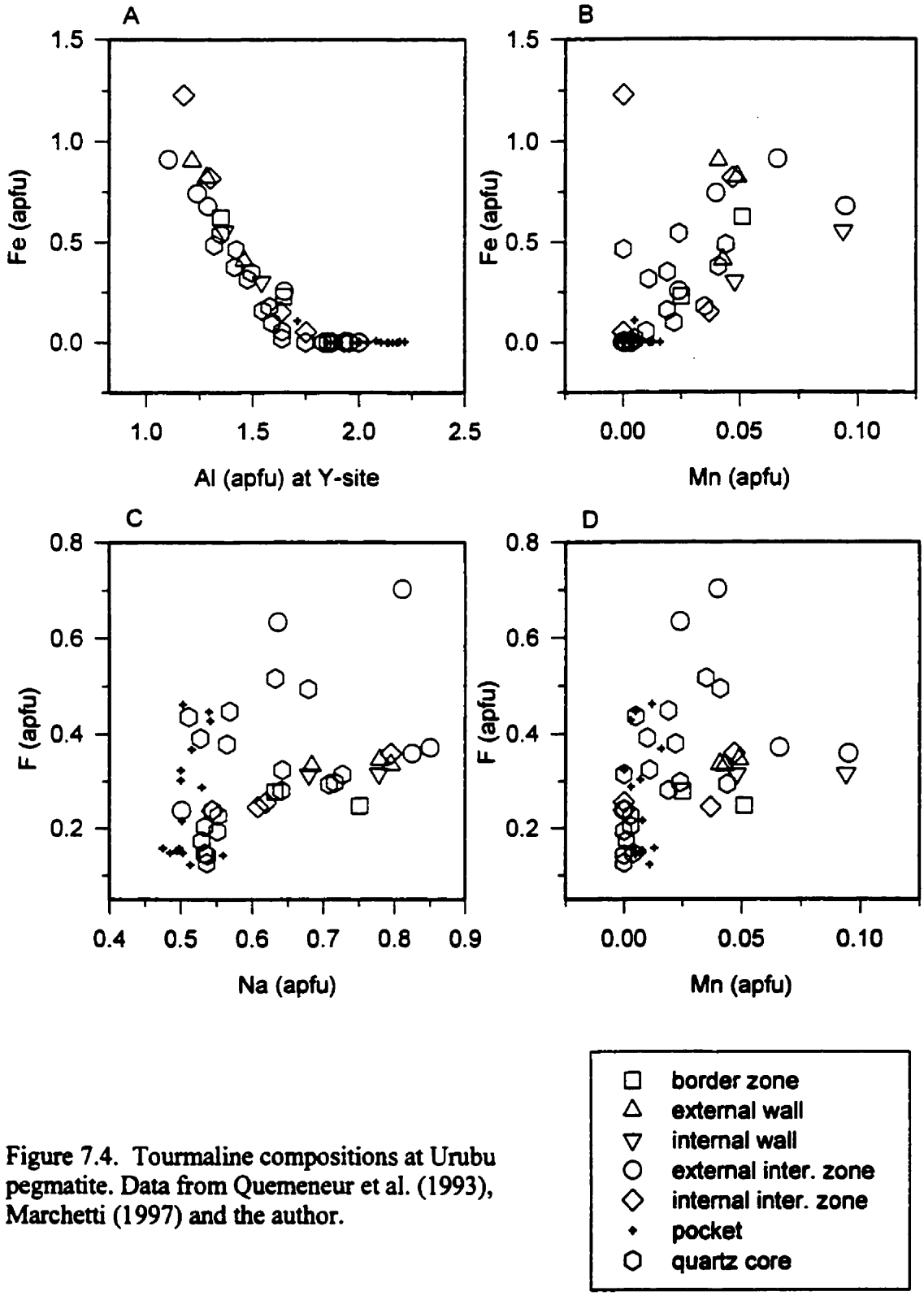

Figure 7.4. Tourmaline compositions at Urubu pegmatite. Data from Quemeneur et al. (1993), Marchetti (1997) and the author.

intermediate zones. The maximum Na content is 0.85 *apfu* in Fe-rich elbaite and the maximum F content is 0.70 *apfu* in Fe-bearing elbaite in the external intermediate zone.

Rare elbaite-schorl contains ≤ 0.20 *apfu* Mg and ≤ 0.04 *apfu* Ti in the external wall zone. The source of Mg and Ti in tourmaline is probably an influx of Mg and Ti from the host biotite schist. Black tourmaline in the exocontact is Ca-bearing schorl-dravite with minor Ti (0.12 *apfu*) and abundant F (0.47 *apfu*). The Na and F in exocontact tourmaline reflects an influx of Na- and F-rich pegmatitic fluids into the host rock.

7.2.2. Geochemical evolution in petalite-subtype pegmatites

The composition of tourmaline in pegmatites is controlled by fractionation of the pegmatitic melt (*i.e.*, Na-□, Fe-(Al+Li), Fe-Mn and Mn-F geochemical pairs). The dominant substitution at the *X* site is Na ⇌ □ for most tourmaline, except for the late-stage Ca-bearing elbaite-rossmanite in petalite-bearing zones (Figs. 7.5a, b). The most primitive tourmaline is □-rich (foitite) followed by Na-rich (elbaite) and □-rich (rossmanite). The most fractionated tourmaline is (Ca, □)-rich (Ca-bearing elbaite-rossmanite). This late-stage Ca-enrichment is not likely a result of Ca infiltration from the host rock, as the expected associated Mg-enrichment is not present in the tourmaline or in any other minerals within the petalite-bearing zones. The Ca-enrichment is not caused by reaction with Ca-bearing primary phases within the pegmatite, as the associated minor Ca-bearing phases are unaltered. The presence of other primary accessory (Ca, F)-bearing minerals in the petalite-bearing pegmatite zones associated with the Ca-bearing elbaite-rossmanite indicates that this is probably due to conservation of Ca through consolidation

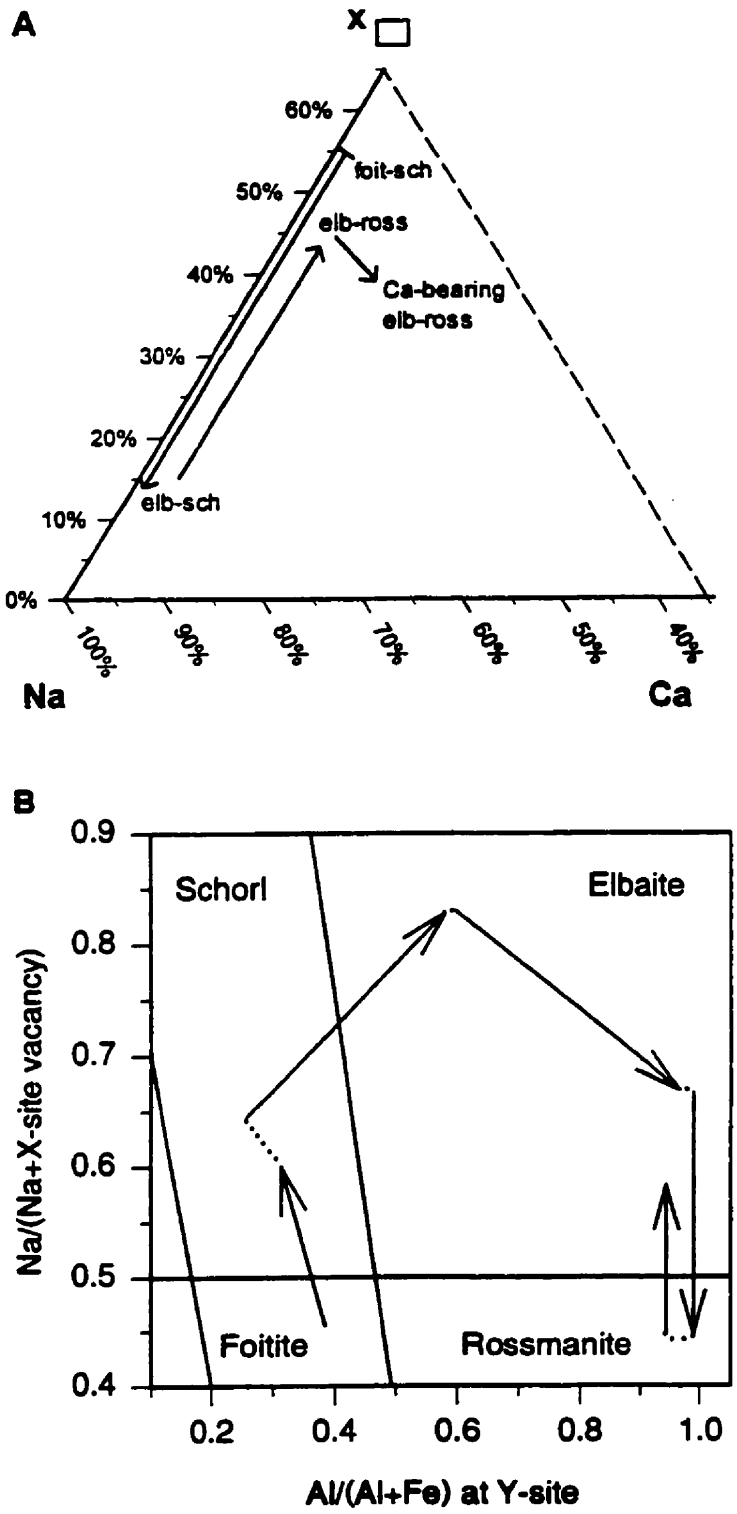

Figure 7.5. Idealized compositional trends for the dominant substitutions at the *X*- and Y-sites in tourmaline in petalite-subtype pegmatites.

of the pegmatite by sequestering Ca in the melt as fluoride complexes. At Tanco, in zones (4) and (5), the associated albite (An_{1-3}) is relatively pure, blocky amblygonite is subordinate, minor altered primary fluorapatite does not show any loss of Ca, F-rich microlite is rare (0.02 vol%) and F-rich topaz is very rare (Černý *et al.* 1998). At Utö, in the petalite zone and fine sugary-albite zone, Ca-bearing elbaite-rossmanite is associated with accessory apatite and microlite.

The dominant substitution at the *Y* site is $3Fe^{2+} \rightleftharpoons 1.5Al + 1.5Li$, as the most primitive tourmaline is Fe-rich (foitite and schorl) and the most fractionated tourmaline is (Al+Li)-rich (elbaite and rossmanite) (Figs. 7.5b, 7.6a). This fractionation trend is also shown by the micas, with rare biotite in the most primitive pegmatite zones, and lithian muscovite and lepidolite in the more fractionated zones.

The Fe-Mn substitution in minerals is also used to indicate the degree of fractionation in a pegmatite. The fractionation trend in tourmaline is ± foitite-schorl and schorl-foitite with high Fe and low Mn, Mn-bearing elbaite with maximum Mn content and no Fe, and Ca-bearing elbaite-rossmanite with no Fe and no Mn (Fig. 7.6b). Tourmaline with the maximum F content is Fe-rich elbaite and Mn-bearing elbaite (Figs. 7.6c, d).

At Tanco, most of the primary blue manganoan fluorapatite occurs in upper intermediate zone (5), pollucite zone (8) and as local accumulations in aplitic albite zone (3). The high Mn, F and Ca contents in fluorapatite are related to similarly high contents in Mn-bearing elbaite, Fe-rich elbaite and Ca-bearing elbaite-rossmanite, respectively, in zones (4) and (5).

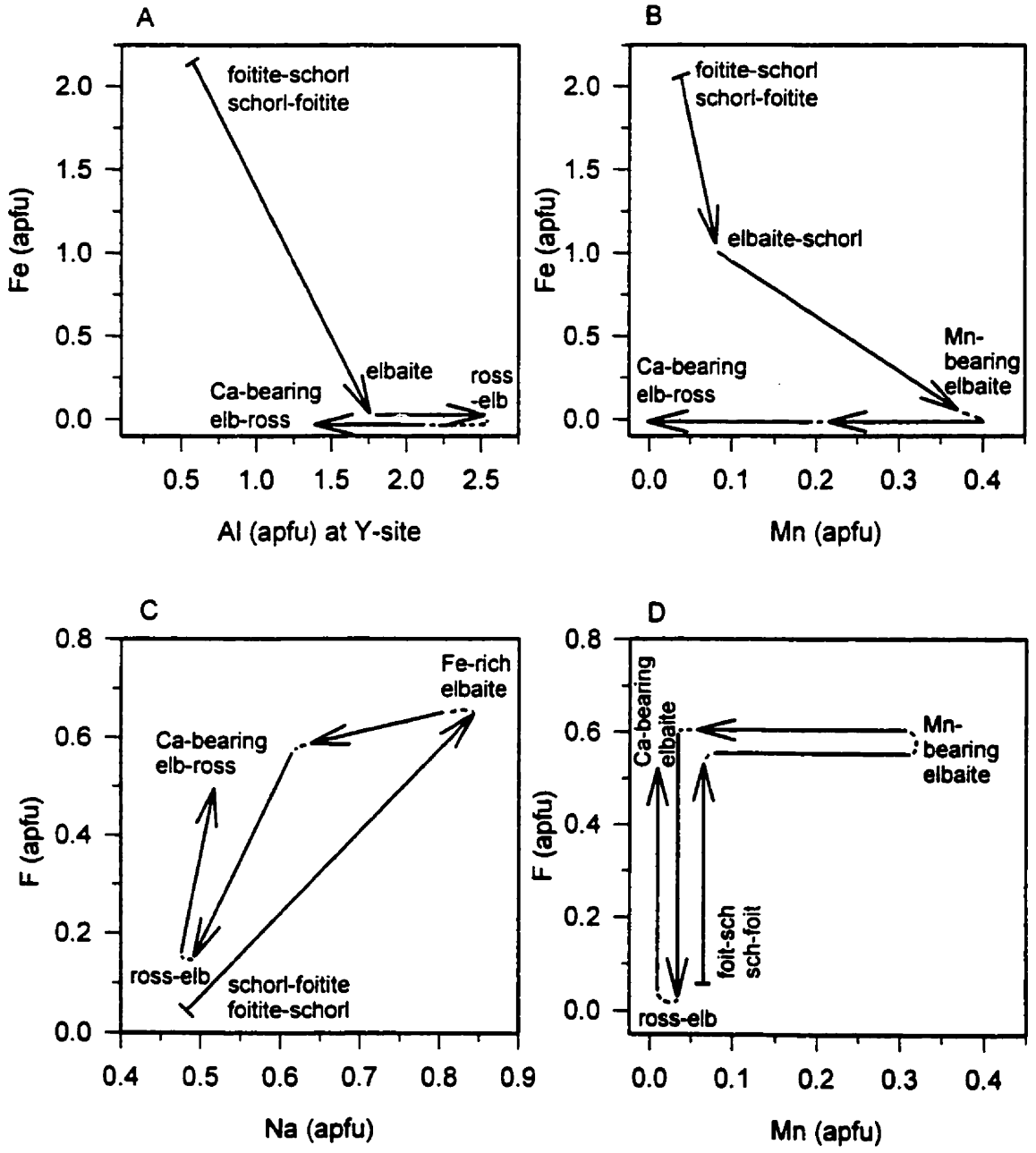

Figure 7.6. Idealized tourmaline compositional trends for petalite-subtype pegmatites.

The tourmaline composition may also be affected by crystal-chemical constraints, as shown by the correlation between Na at the *X* site and F at the O(1) site (Robert *et al.*, 1997). A positive correlation between Na and F is common in tourmaline, but in the petalite-subtype tourmaline, there is a positive correlation for foitite-schorl and schorl-foitite to Fe-rich elbaite with maximum Na and F (Fig. 7.6c) which is followed by decreasing Na and F to rossmanite-elbaite with low Na and no F. With increasing Ca content in the tourmaline, this positive correlation is distorted, with the most Ca-rich elbaite-rossmanite plotting furthest from the Na-F correlation.

The tourmaline composition is also a result of the crystallization conditions within the pegmatite melt. The petalite-bearing zone crystallized under conditions of high salinity (μKF), as indicated by the abundance of blocky microcline-perthite, especially at Tanco (24-25 vol% microcline) (Černý *et al.* 1998) and in the Separation Rapids pegmatite group (London 1982). The petalite-bearing zones in pegmatites also contain abundant to rare lepidolite (0.1-0.5 vol% at Tanco) (Černý *et al.* 1998) which indicates intermediate acidity (μHF) and high Li-activity (London 1982). Very rare topaz is associated with amblygonite in the most fractionated zones (4) and (5) at Tanco, and in the intermediate K-feldspar, lepidolite and coarse sugary albite zones at Utö (Smeds & Černý 1989), and may indicate a brief period of high acidity (London 1982).

7.2.3. Summary of tourmaline in petalite-subtype pegmatites

In petalite-subtype pegmatites, tourmaline evolves from the outermost zones to the innermost zones in the following sequence: (± foitite-schorl, schorl-foitite) → Al-rich

schorl → schorl → schorl-elbaite → elbaite-schorl → Fe-rich elbaite → Mn-bearing elbaite → elbaite-rossmanite → (± rossmanite-elbaite) → elbaite-rossmanite → Ca-bearing elbaite-rossmanite → Ca-bearing elbaite. Tourmaline compositions from Tanco cover the entire crystallization sequence, whereas tourmaline from Utö and Urubu cover sections of this sequence. Tourmaline at Utö lacks the primitive foitite-schorl and schorl-foitite, and intermediate Mn-bearing elbaite compositions. Tourmaline from Urubu only contains elbaite, elbaite-schorl, Fe-rich elbaite, elbaite-rossmanite and rare rossmanite-elbaite compositions. Iron-rich tourmaline did not crystallize in the Utö and Urubu pegmatites because these pegmatites crystallized in closed systems with no infiltration of Fe from the host rock and Utö is highly fractionated.

Tourmaline from the Separation Rapids pegmatite group is more primitive than that at the other localities. The primary tourmaline at Marko's pegmatite is more Ca-rich and covers the narrow range from Ca-bearing elbaite-schorl to (Ca, Fe, Mn)-bearing elbaite, which is a short segment of the crystallization sequence for tourmaline in petalite-subtype pegmatites. In pegmatite #5, the tourmaline is more Ca-rich in the outer pegmatite zones than in the petalite zone (Fig. 7.7a). It is also more Mg-rich than tourmaline in other petalite-subtype pegmatites, as it covers the narrow range from schorl-dravite and Mg-rich schorl in the outer pegmatite to schorl-elbaite in the petalite zone (Fig. 7.7b). Similar Mg-rich tourmaline occurs in other pegmatites in the Separation Rapids pegmatite group: Lou's pegmatite, James' pegmatite, pegmatite #6 and in the muscovite pegmatite hosted by migmatized metasedimentary terrain (unpublished data of author). Tourmaline in the Separation Rapids pegmatite group is more primitive than

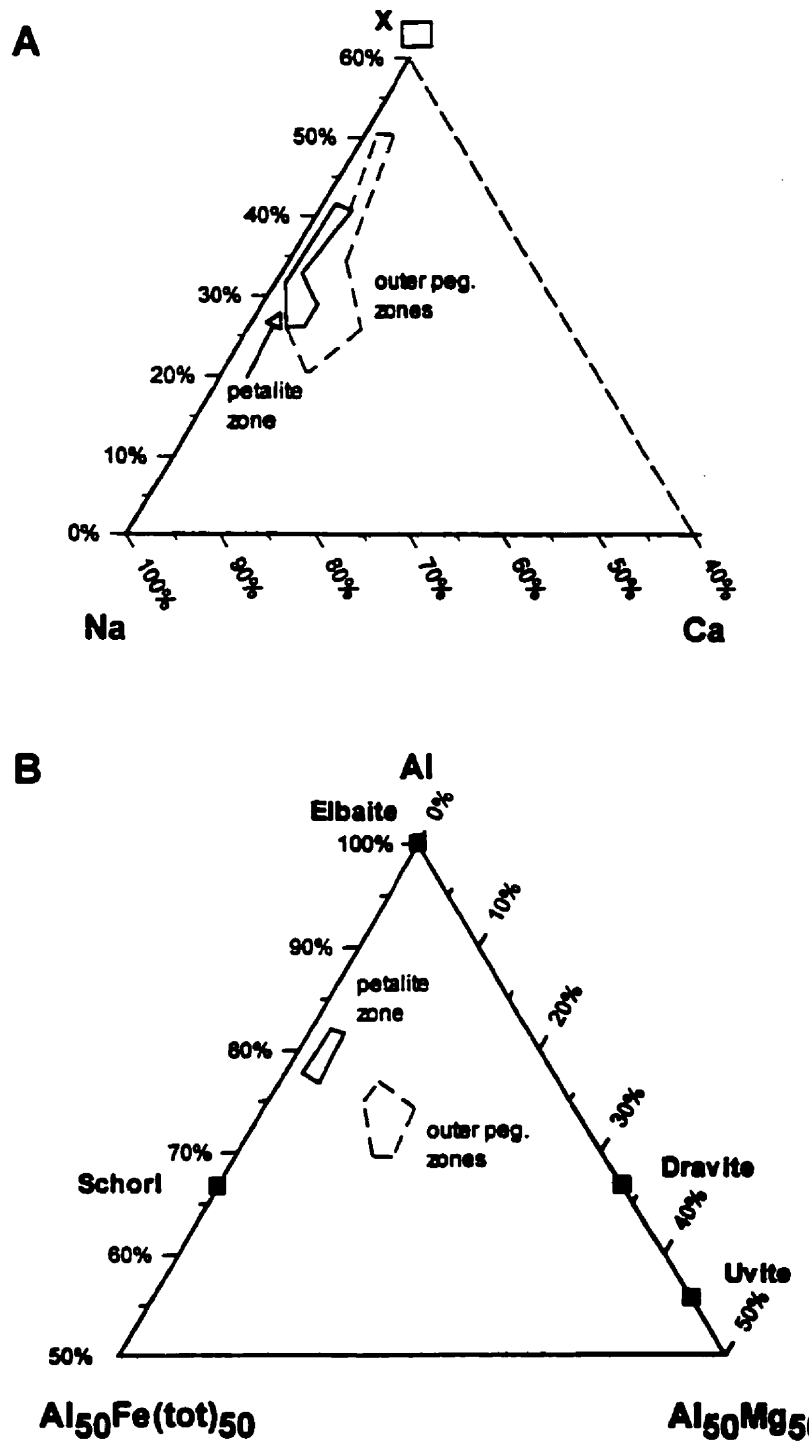

Figure 7.7. Tourmaline compositions from petalite-subtype Pegmatite #5, Separation Rapids pegmatite group.

tourmaline from other petalite-subtype pegmatites because its composition is influenced by Ca and Mg contamination from the amphibolite host-rock, and all B was consumed during crystallization of (Mg, Fe)-rich tourmaline, so that no B remained for crystallization of (Al+Li)-rich tourmaline. Tourmaline does not occur in the exocontacts of the Separation Rapids pegmatites and in the largest pegmatite within the group, the Big Whopper (F.W. Breaks, pers. comm.).

7.3. Tourmaline from elbaite-subtype pegmatites

The discussion of elbaite-subtype pegmatites will begin with a review of tourmaline at Stak Nala, Pakistan, Sahatany Valley, Madagscar, Little Three, California and Elba Island which will be followed by a summary of the compositional evolution of tourmaline from all of the elbaite-subtype pegmatites discussed. The geology and compositional data of tourmaline from Stak Nala, Sahatany Valley, Little Three and Elba are directly from the literature, but the figures and interpretation are that of the author.

7.3.1. The Stak Nala pegmatites

7.3.1.1 General geology

The Stak Nala pegmatites are located in the northeast part of the Nanga Parbat - Haramosh Massif in northern Pakistan. Laurs *et al.* (1998) described the geology and mineralogy of the main- and south-mine pegmatites at Stak Nala. These miarolitic granitic pegmatites are mined for crystals of bi- and tri-coloured tourmaline. The geology of the symmetrically zoned main- and south-mines is very similar and is summarized in

TABLE 7.2. GENERAL VERTICAL CROSS-SECTION OF THE MAIN-MINE PEGMATITE, STAK NALA*

	pegmatite zone	mineral assemblage	tourmaline composition
Hanging wall and footwall	unaltered flaser gneiss	K-feldspar >quartz, oligoclase, (muscovite, biotite), [alm-grs-prp]	Ca-bearing schorl-dravite
	altered gneiss (along contact)	K-feldspar >quartz, oligoclase, (muscovite > biotite, black tourmaline), [alm-grs-prp]	Mg-rich Ca-bearing schorl
	border zone	oligoclase > microcline-perthite > quartz, (black tourmaline), [sps-alm]	Mg-bearing schorl, ± schorl-foitite, schorl
	wall zone	blocky K-feldpar (3-25 cm), albite-oligoclase > quartz, (black tourmaline), [sps-alm, muscovite]	Mg-bearing schorl, schorl-foitite, schorl
centre	aplite pods (in core zone)	albite-oligoclase, black tourmaline, quartz, (sps-alm, fluorite)	schorl
	core zone	blocky K-feldpar (20-30 cm), albite-oligoclase > quartz, (black tourmaline, muscovite), [sps-alm, fluorite]	schorl-elbaite
	pockets (upper part of core zone)	albite, quartz (10 cm), microcline-perthite (<8 cm), green, colourless and pink tourmaline (1-10 cm), muscovite or F-rich lepidolite, fluorite, topaz, [hambergite, borian muscovite]	Mn-rich elbaite, elbaite-rossmanite, Ca-bearing elbaite, Ca-rich elbaite

*based on Laurs *et al.* (1998); ( ): subordinate minerals, 1-15 vol%, [ ]: accessory minerals, <1 vol%

TABLE 7.3. GENERAL VERTICAL CROSS-SECTION OF THE SOUTH-MINE PEGMATITE, STAK NALA*

	pegmatite zone	mineral assemblage	tourmaline composition
Hanging wall and footwall	unaltered biotite-granodiorite gneiss	oligoclase, quartz > bioitite, (K-feldspar > muscovite), [alm-grs-sps]	Ca-rich dravite-schorl, Ca-bearing dravite-schorl, Ca-rich schorl-dravite, Ca-bearing schorl-dravite
	altered gneiss (along contact)	albite-oligoclase, quartz, (K-feldspar, muscovite, black tourmaline > biotite), [alm-grs-sps]	Ca-bearing schorl-dravite, elbaite-dravite-schorl, Mg-bearing elbaite-schorl
	border zone	K-feldspar, albite-oligoclase > quartz, (muscovite), [sps-alm > black tourmaline]	Ca-bearing schorl-dravite, (Ca, Fe)-bearing elbaite, Ca-rich Fe-bearing elbaite
	wall zone	K-feldspar, albite > quartz, (black tourmaline > muscovite), [sps-alm]	schorl, Fe-rich Ca-bearing elbaite
centre	core zone	blocky K-feldspar (40 cm), albite > quartz, (muscovite), [black tourmaline, sps-alm, fluorite, topaz]	
	pockets (upper part of core zone)	fluorite, lepidolite, black, green and colourless tourmaline, muscovite	Mn-bearing elbaite-schorl, Fe-rich Mn-bearing elbaite, Ca-rich Mn-bearing elbaite, Mn-rich Ca-bearing elbaite, Mn-rich (Ca, Fe)-bearing elbaite, Ca-rich elbaite, Ca-bearing elbaite,

*based on Laurs *et al.* (1998); ( ): subordinate minerals, 1-15 vol%, [ ]: accessory minerals, <1 vol%

Tables 7.2 and 7.3. The main-mine pegmatite is 1 m thick and 120 m long, a sill which intrudes flaser gneiss. The south-mine pegmatite is 4 m thick and > 110 m long, a sill which intrudes biotite-granodiorite gneiss. The pegmatites seem to be transitional between elbaite- and lepidolite-subtypes, but tourmaline and garnet compositions are characteristic of elbaite-subtype pegmatites, and lepidolite + cleavelandite pods in the

core zone are late hydrothermal in origin. The pegmatites consist of K-feldspar, sodic plagioclase, quartz and black tourmaline, minor muscovite and traces of spessartine-almandine and löllingite. The Li-, B-, Mn- and F-rich core and pocket zones contain multicoloured tourmaline, fluorite, fluorapatite, topaz, F-rich lepidolite, and rare hambergite, borian muscovite and manganocolumbite.

7.3.1.2. Tourmaline compositions in the main-mine pegmatite, Stak Nala

Tourmaline compositions in the main-mine pegmatite are very similar to those in the south-mine pegmatite; representative compositions are given by Laurs *et al.* (1998). Tourmaline in the unaltered flaser gneiss at the main-mine is Ca-bearing schorl-dravite, and in the altered gneiss along the contact is Mg-rich Ca-bearing schorl (Fig. 7.8a). This Ca-, Mg- and Ti-rich exocontact tourmaline is associated with Ca-rich oligoclase, Ca- and Mg-bearing garnet ($Alm_{72-74}Grs_{11-12}Prp_{7-13}Sps_{2-10}$) and Mg- and Ti-rich biotite (Laurs *et al.* 1998). Tourmaline in the outermost pegmatite zones of the main-mine pegmatite has been affected by endomorphism due to influx of Mg from the host rock. Tourmaline in the border zone and wall zone ranges from Mg-bearing schorl to schorl-foitite to schorl, and the associated garnet has an average composition of $Sps_{52-74}Alm_{21-42}Grs_{4-7}$ (Figs. 7.8a, 7.9a). The Fe is preferentially partitioned into tourmaline and Mn is preferentially partitioned into garnet. Comparison of the bulk composition of unaltered flaser gneiss and altered flaser gneiss indicates that altered gneiss has had an influx of Si, Li, F, B and ± Mn and removal of H_2O, K and Ba by pegmatitic fluids. Some Fe and Mg released from conversion of biotite to muscovite in the altered gneiss is consumed by crystallization of

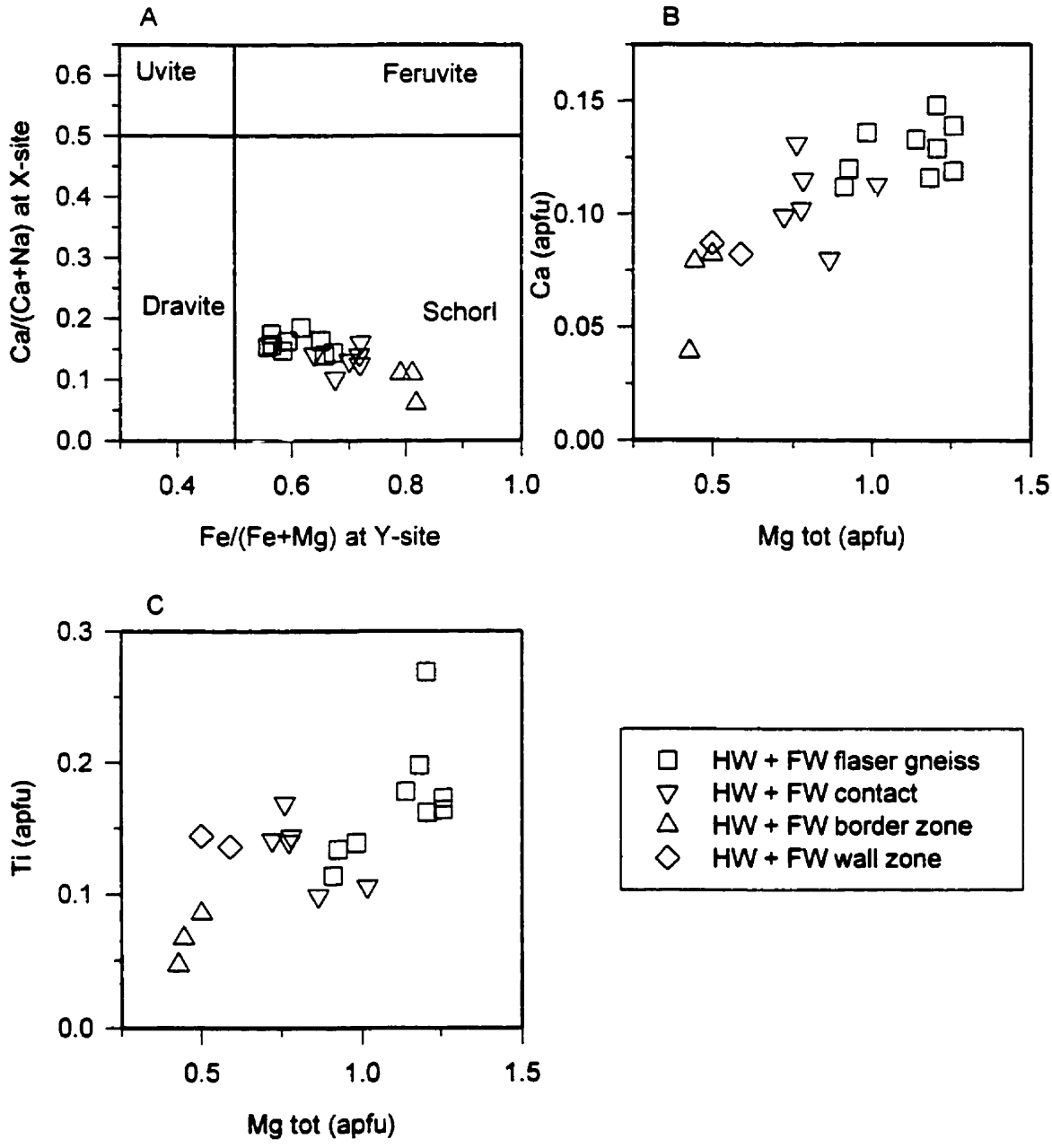

Figure 7.8. Tourmaline compositions from the exocontact and outermost pegmatite zones from the main-mine pegmatite, Stak Nala. HW: hanging wall; FW: footwall. Only compositions with > 0.1 apfu Mg are plotted.

Fe- and Mg-rich tourmaline in the gneiss and the pegmatite. In the exocontact and endomorphic tourmalines, there is a positive correlation between Ca, Mg and Ti, which decrease from Ca-bearing schorl-dravite (≤ 0.27 *apfu* Ti) to schorl-foitite (≤ 0.01 *apfu* Ti) (Figs. 7.8b, c).

Tourmaline in the innermost zones of the main-mine pegmatite has no (or almost no) Mg. Tourmaline in the aplite pods of the core zone is black schorl, and tourmaline in the rest of the core zone is black schorl-elbaite with thin (<1 mm) green overgrowths (Fig. 7.9a). Garnet in the aplite and core zones has an average composition $Sps_{48-65}Alm_{30-47}Grs_{3-7}$. Tourmaline in the pockets is zoned parallel to the c-axis. One crystal has an olive-green Mn-rich elbaite root (≤ 0.83 *apfu* Na, 0.92 *apfu* Mn, ≤ 0.77 *apfu* F), grass-green Mn-rich elbaite zone and a colourless elbaite-rossmanite overgrowth (≤ 0.42 *apfu* □) (Fig. 7.10b). Another crystal has a grass-green Ca-bearing elbaite root, a colourless Ca-rich elbaite zone and a very light-pink Ca-rich elbaite termination (≤ 0.31 *apfu* Ca, ≤ 0.81 *apfu* F) (Fig. 7.10a). Late colourless tourmaline in druses is Ca-rich elbaite The overall sequence of tourmaline crystallization in the pockets is as follows: Mn-rich elbaite → elbaite-rossmanite → Ca-bearing elbaite → Ca-rich elbaite, representing a change from (Na, Mn, F)-rich to □-rich to (Ca, F)-rich. There is a negative correlation between Fe and Mn, as Fe decreases and Mn increases from schorl in the aplite to Mn-rich elbaite in the pockets, followed by a decrease in Mn to elbaite-rossmanite and Ca-rich elbaite (Fig. 7.9b). There is a positive correlation between Na, Mn and F as they decrease from Mn-rich elbaite to elbaite-rossmanite, followed by an increase in Ca and F in Ca-rich elbaite (Figs. 7.9c, d). The presence of Ca in tourmaline distorts the positive correlation between

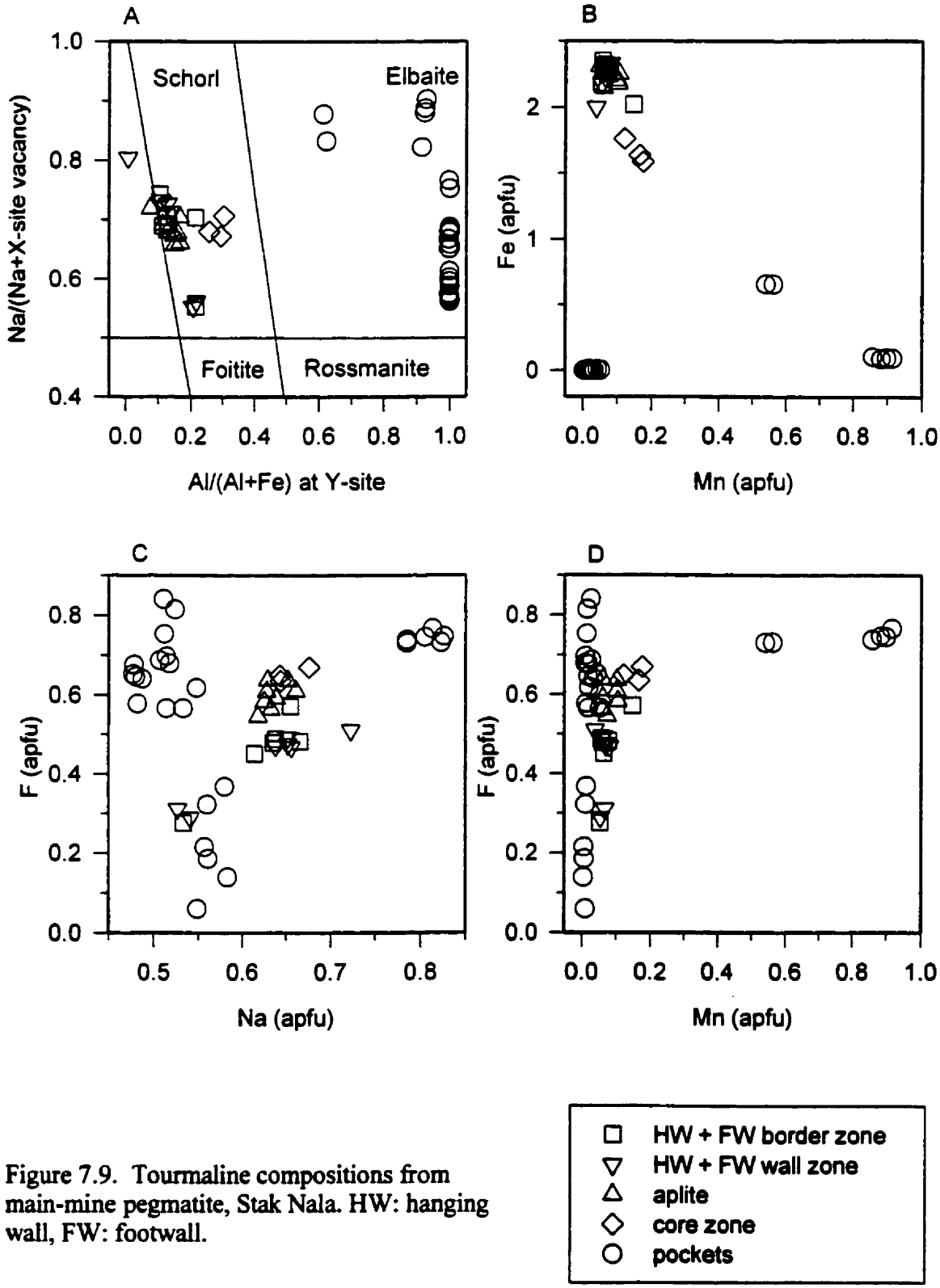

Figure 7.9. Tourmaline compositions from main-mine pegmatite, Stak Nala. HW: hanging wall, FW: footwall.

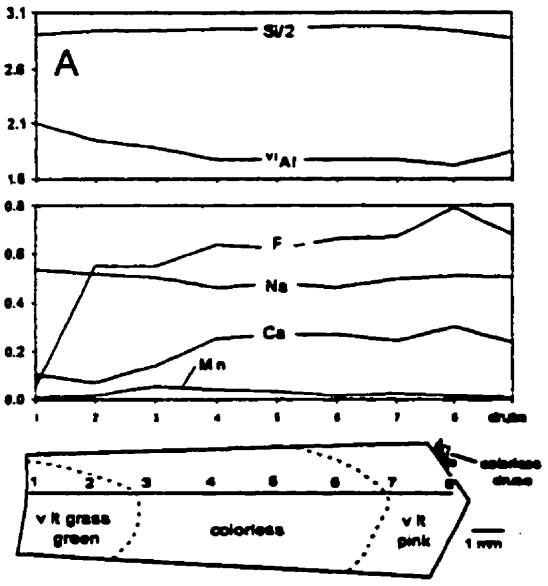

Ca-bearing elbaite – Ca-rich elbaite – Ca-rich elbaite

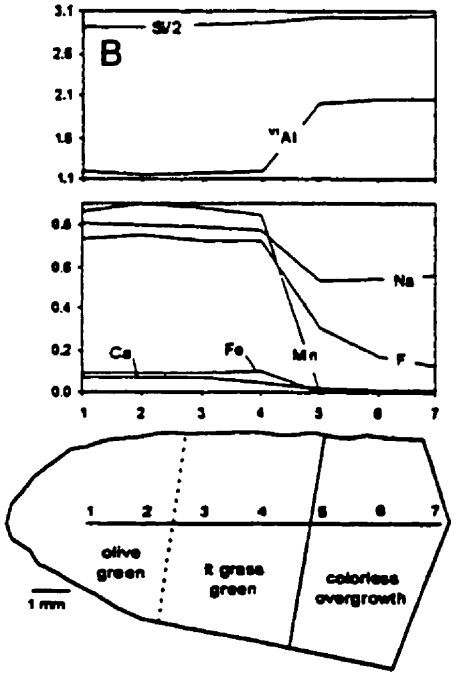

Mn-rich elbaite – Mn-rich elbaite – elbaite-rossmanite

Figure 7.10. Compositions of zoned tourmaline *(apfu)* from main-mine pegmatite, Stak Nala. (A) Pale tricoloured elbaite crystal cut parallel to the *c*-axis with drusy overgrowth of fine-grained elbaite and borian muscovite; Fe and Ti are below detection limit. (B) Tricoloured elbaite crystal cut parallel to *c*-axis; Ti is below detection limit. (Laurs *et al.* 1998)

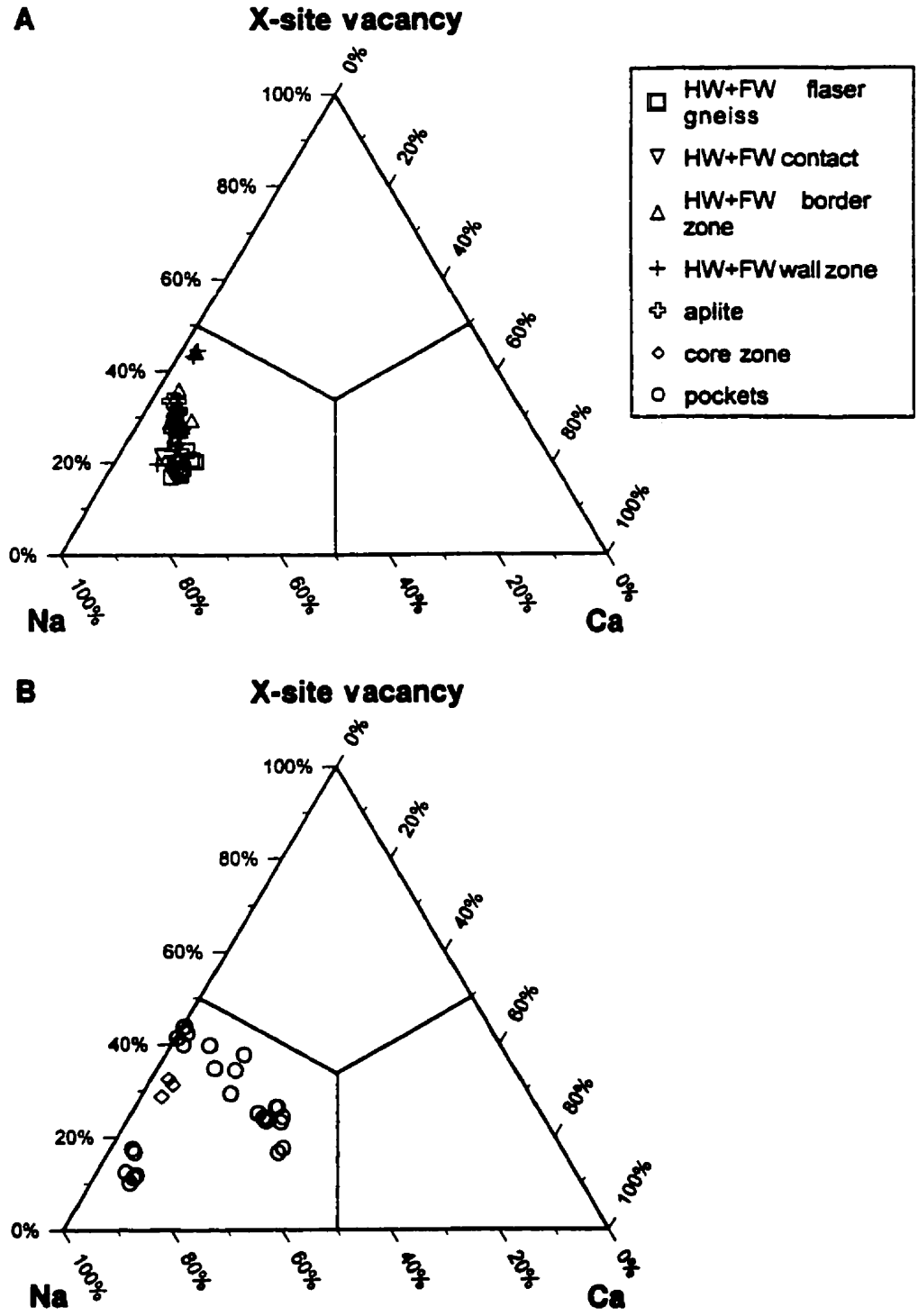

Figure 7.11. *X*-site contents for tourmaline from the main-mine pegmatite, Stak Nala.

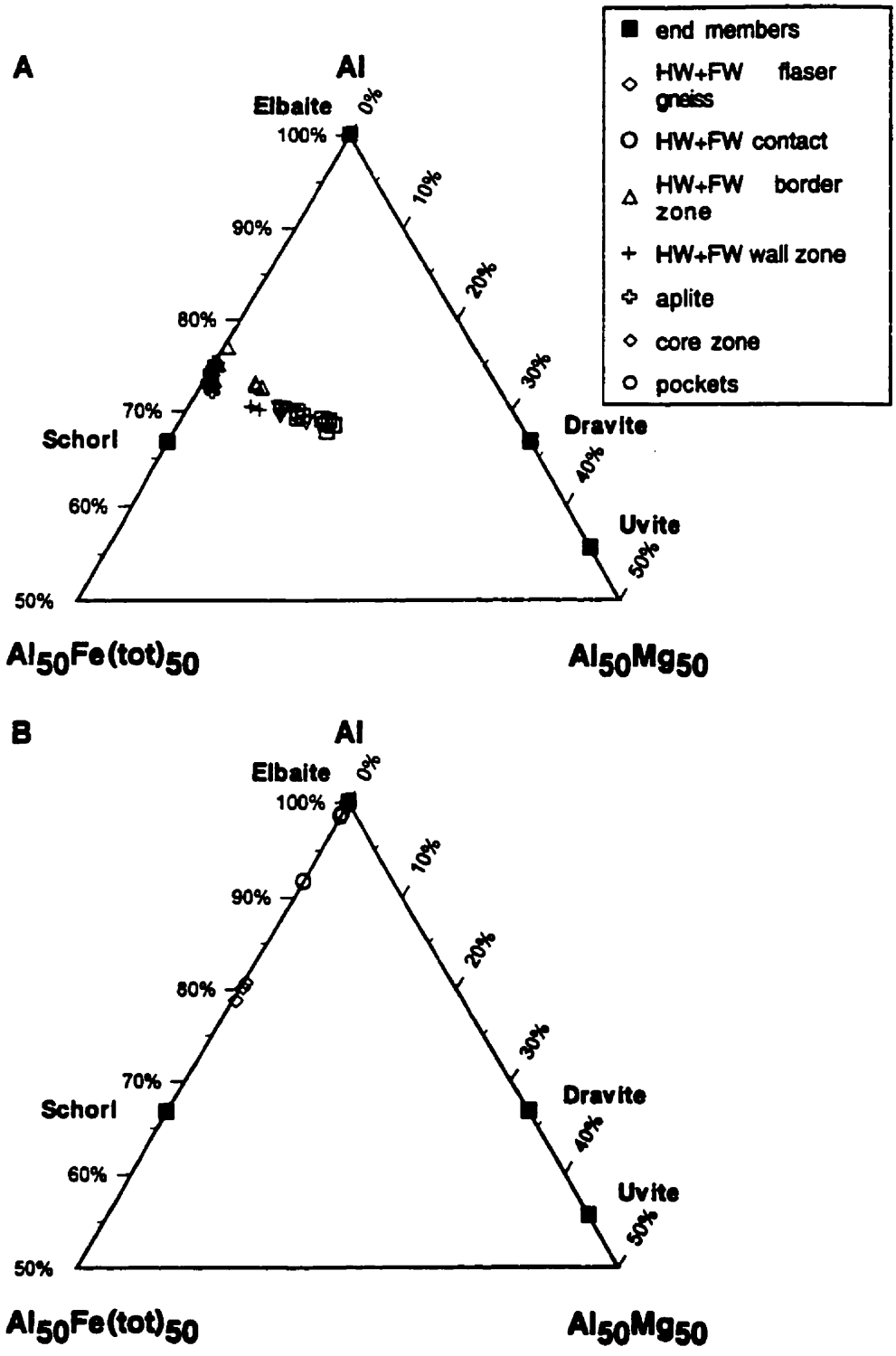

Figure 7.12. *Y*- and *Z*-site contents for tourmaline from the main-mine pegmatite, Stak Nala.

Na and F.

The overall crystallization sequence for black tourmaline in the main-mine pegmatite body, Stak Nala, is as follows: Ca-bearing schorl-dravite → Mg-rich Ca-bearing schorl → Mg-bearing schorl → schorl-foitite → schorl → schorl-elbaite; for the green, colourless and pink pocket tourmaline, crystallization is: Mn-rich elbaite → elbaite-rossmanite → Ca-bearing elbaite → Ca-rich elbaite. The dominant *X*-site cation for the pegmatitic tourmaline is Na with minor □ content; for the pocket tourmaline, it is Na with significant □ and Ca (Fig. 7.11). The dominant solid-solution series for pegmatitic tourmaline is between dravite and schorl, and the pocket tourmaline is elbaite (Fig. 7.12).

7.3.1.3. Tourmaline compositions in the south-mine pegmatite, Stak Nala

The Ca-, Mg- and Fe-rich tourmaline in the unaltered biotite granodiorite ranges in composition from ± Ca-rich dravite-schorl → Ca-bearing dravite-schorl → ± Ca-rich schorl-dravite → Ca-bearing schorl-dravite (Fig. 7.13a). The biotite-granodiorite gneiss along the south- mine pegmatite contact is more extensively tourmalinized and albitized than the gneiss exocontact for the north-mine pegmatite (Laurs *et al.* 1998). Late-stage tourmalinization is characterized by Li-rich overgrowths and replacement of Fe-rich tourmaline, both in the pegmatite and in the wallrock within 1 cm of the contact. Rare veinlets of olive-green elbaite-dravite-schorl locally infiltrate the hanging wall contact. In the hanging wall of the altered biotite granodiorite, tourmaline is Na-, Li- and Al-rich and ranges from elbaite-dravite-schorl to Mg-bearing elbaite-schorl; tourmaline in the

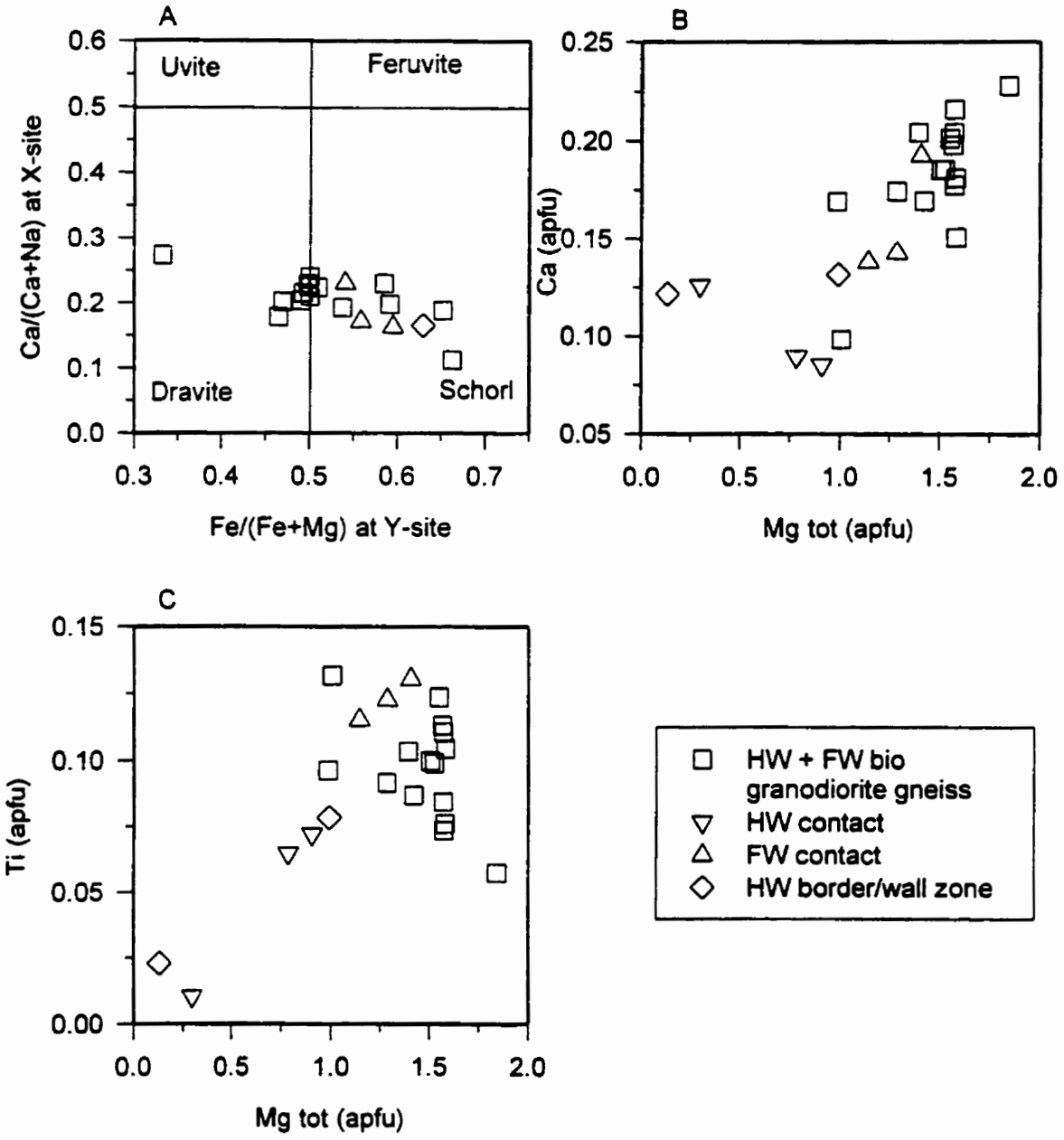

Figure 7.13. Tourmaline compositions from exocontact and outermost pegmatite zones from the south-mine pegmatite, Stak Nala. HW: hanging wall; FW: footwall. Only compostions with < 0.1 apfu Mg are plotted.

footwall is Ca-bearing schorl-dravite, similar to tourmaline in the unaltered gneiss (Fig. 7.13a, 7.17a). Tourmaline in the border/wall zone has a wide range in composition due to influx of Ca and Mg from the host gneiss into the pegmatite. This tourmaline ranges in composition from Ca-bearing schorl-dravite → schorl → Fe-rich Ca-bearing elbaite → (Ca, Fe)-bearing elbaite → Ca-rich Fe-bearing elbaite (Figs. 7.13a, 7.14a).

The overall crystallization sequence of the black pegmatitic tourmaline is as follows: ± Ca-rich dravite-schorl → Ca-bearing dravite-schorl → ● Ca-rich schorl-dravite → Ca-bearing schorl-dravite → ● elbaite-dravite-schorl → ± Mg-bearing elbaite-schorl → schorl → Fe-rich Ca-bearing elbaite → (Ca, Fe)-bearing elbaite → Ca-rich Fe-bearing elbaite. In the exocontact and endomorphic tourmaline, there is a positive correlation between Ca, Mg and Ti as they decrease from Ca-rich dravite-schorl and Ca-bearing schorl-dravite to elbaite-dravite-schorl (Fig. 7.13). The dominant component at the *X*-site is Na (Fig. 7.16a) and at the *Y*- and *Z*-sites is Mg and Fe for most of the tourmaline, but elbaite-dravite-schorl in the hanging-wall contact; (Ca, Fe)-bearing elbaite and Ca-rich Fe-bearing elbaite in the border/wall zone have Al as the dominant component (Fig. 7.17a).

Pocket tourmaline in the south-mine pegmatite is zoned. One crystal is zoned parallel to the *c*-axis, with a black Mn-bearing elbaite-schorl core, a black Fe-rich Mn-bearing elbaite zone, colourless Ca-rich elbaite and Ca-bearing elbaite rim (Fig. 7.15). Another crystal is zoned parallel to the *c*-axis with a light-green Ca-rich elbaite root, light-green Ca-rich Mn-bearing elbaite zone, olive-green Mn-rich Ca-bearing elbaite zone, olive-green Mn-rich (Ca, Fe)-bearing elbaite zone to dark olive-green Mn-rich (Ca,

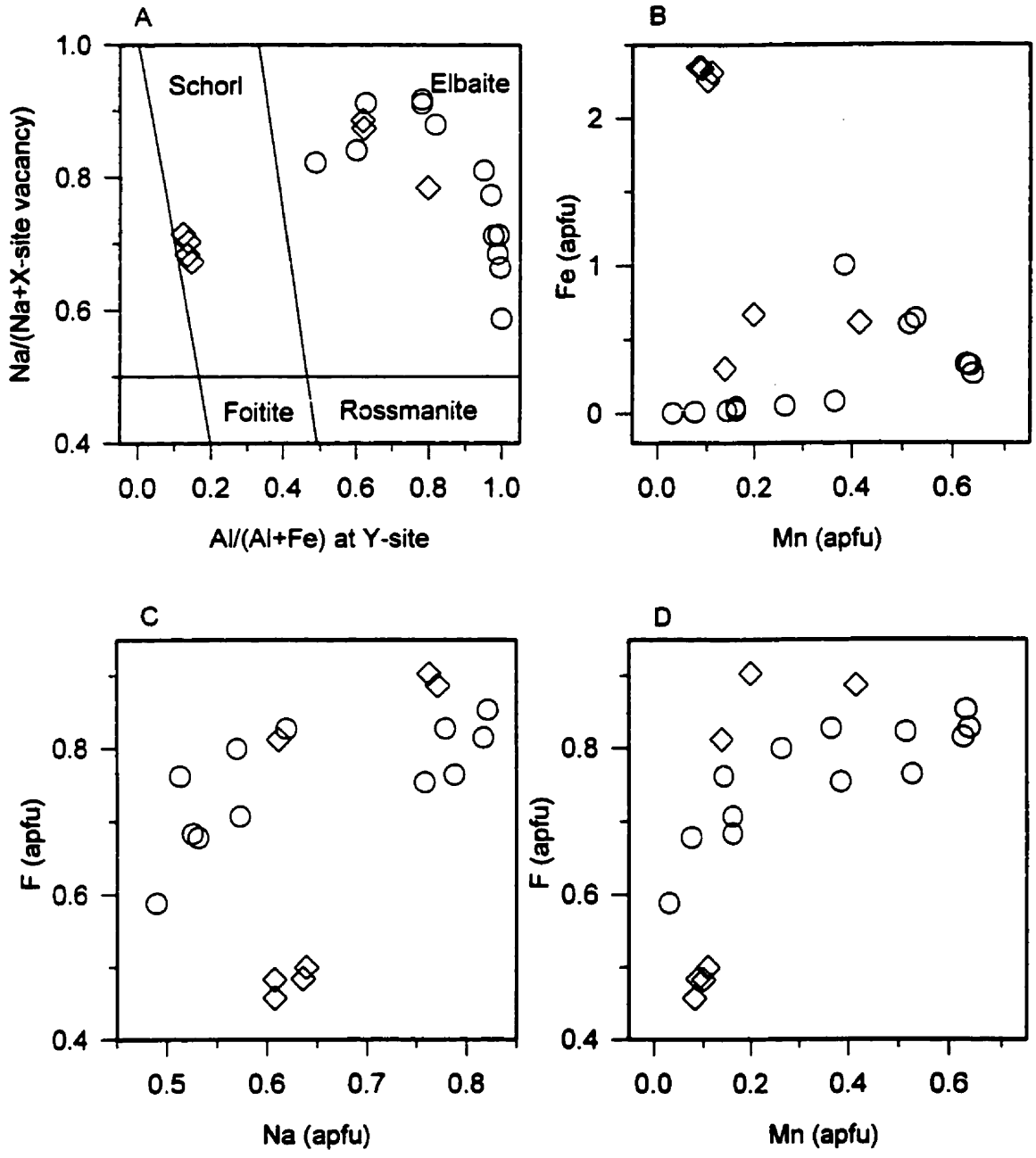

Figure 7.14. Tourmaline compositions from south -mine pegmatite, Stak Nala. HW: hanging wall.

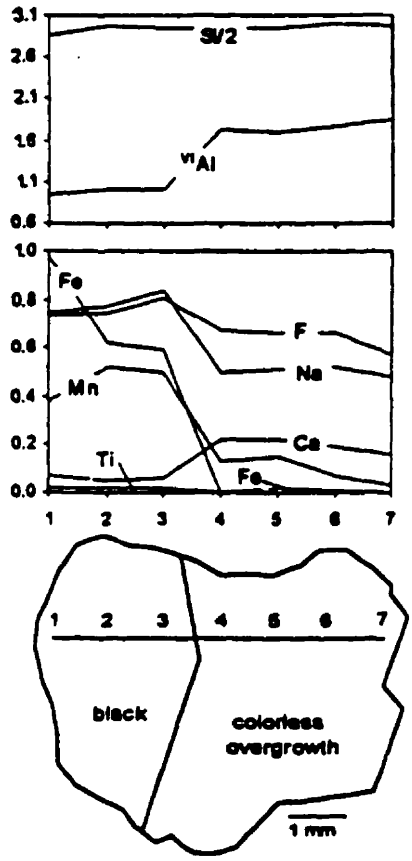

Mn-bearing → Fe-rich Mn-bearing → Ca-rich → Ca-bearing
elbaite-schorl elbaite elbaite elbaite

Figure 7.15. Compositions of zoned tourmaline *(apfu)* from the south-mine pegmatite, Stak Nala: concentrically zoned tourmaline cut perpendicular to the *c*-axis (Laurs *et al.* 1998).

Fe)-bearing elbaite termination. This crystal is cut by a late-stage Ca-rich elbaite vein.

The overall crystallization sequence for the pockets is as follows: Mn-bearing elbaite-schorl → Fe-rich Mn-bearing elbaite → Ca-rich Mn-bearing elbaite → Mn-rich Ca-bearing elbaite → Mn-rich (Ca, Fe)-bearing elbaite → Ca-rich elbaite → Ca-bearing elbaite. This sequence represents a change in tourmaline composition from Fe-rich to (Na, Mn, F)-rich to Ca-rich with influx of Fe during pocket rupture. There is a negative correlation between Fe and Mn, as Fe decreases and Mn increases from schorl in the border/wall zone to Mn-rich (Ca, Fe)-bearing elbaite in the pockets, followed by a decrease in Mn to Ca-bearing elbaite (Fig. 7.14b). There is a positive correlation between Na, Mn and F in the pockets, with a decrease from Mn-rich (Ca, Fe)-bearing elbaite (0.82 *apfu* Na, 0.63 *apfu* Mn and 0.85 *apfu* F) to Ca-bearing elbaite (0.49 *apfu* Na, 0.03 *apfu* Mn and 0.59 *apfu* F) (Figs. 7.14c, d). The dominant component at the *X* site in the pocket tourmaline is Na with significant Ca and □ contents (Fig. 7.16b); the dominant components at the *Y*- and *Z*-sites are Al and Li (Fig. 7.17b).

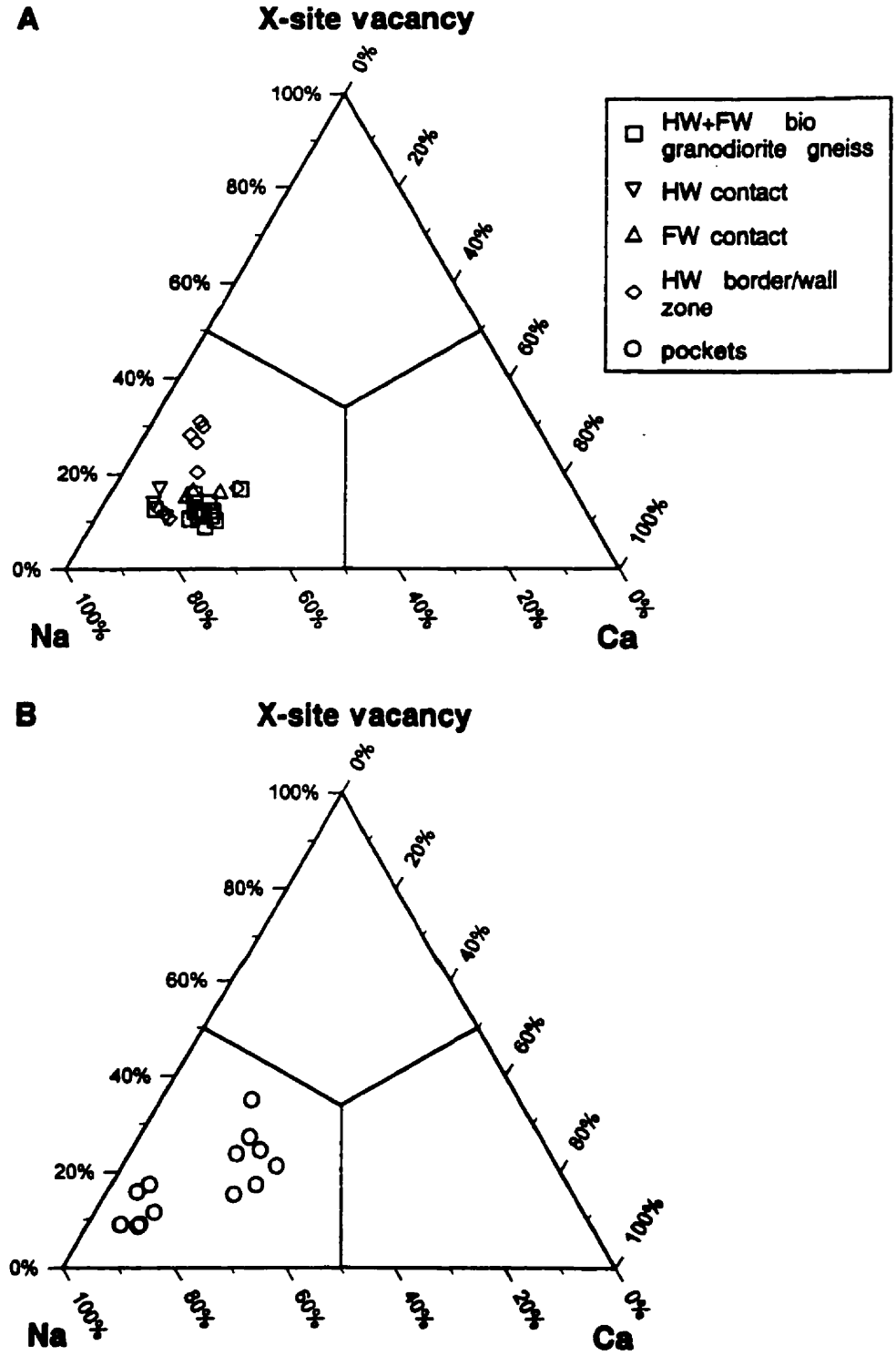

Figure 7.16. *X*-site contents for tourmaline from the south-mine pegmatite, Stak Nala.

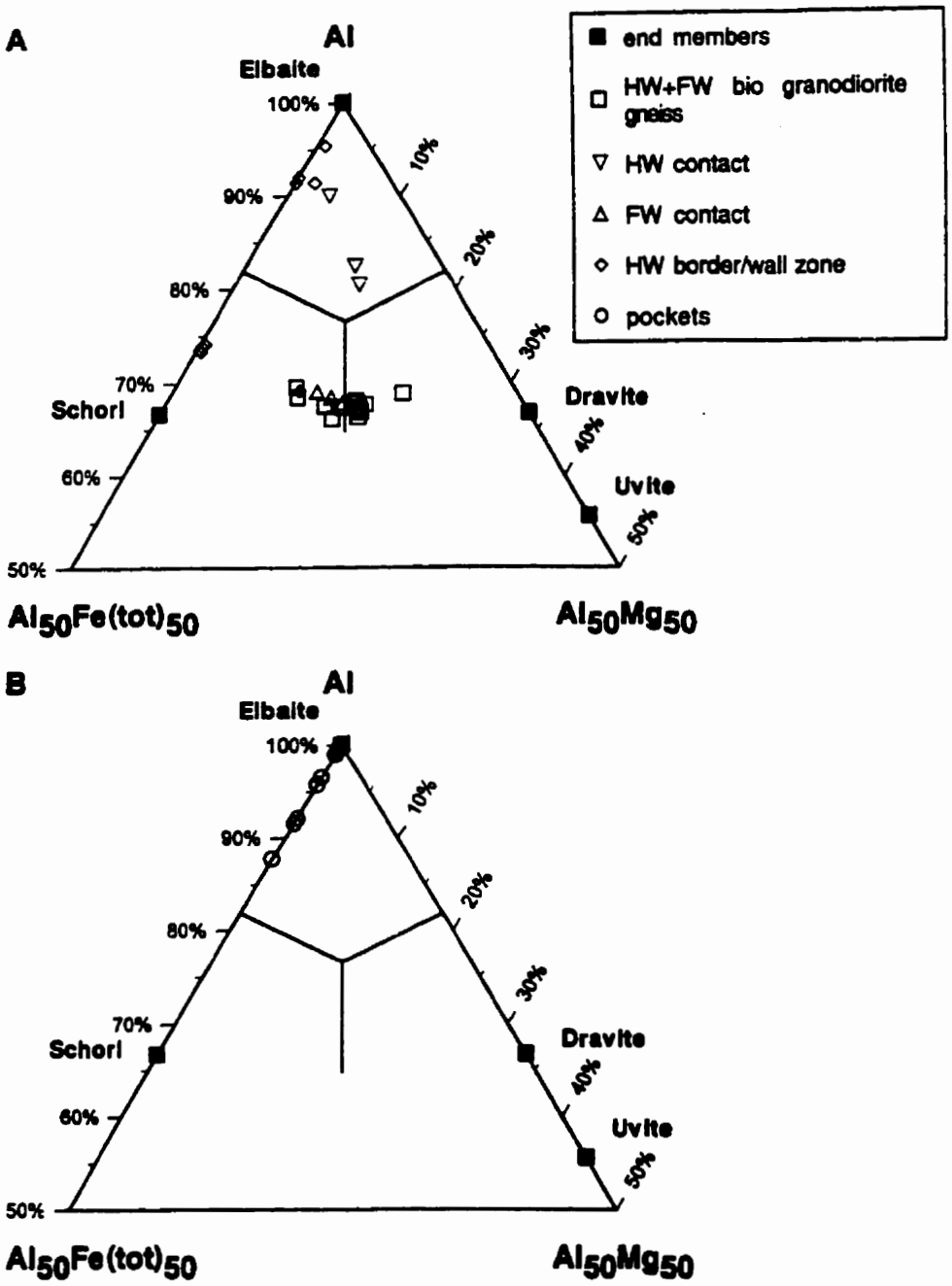

Figure 7.17. *Y*- and *Z*-site contents for tourmaline from the south-mine pegmatite, Stak Nala.

7.3.2. The Sahatany Valley pegmatite

Sahatany Valley is located 25 km southwest of Antsirabe in the central Manandona region of Madagascar Island; the type locality of liddicoatite is in this area (Dunn *et al.* 1977). Sahatany Valley pegmatites contain Mn-rich minerals (*i.e.*, spessartine and Mn-rich elbaite), minor spodumene, and B and Be-bearing minerals (*i.e.*, beryl, manandonite, danburite and rhodizite). The "pit 6" pegmatite intrudes impure dolomitic marble (Bloomfield 1997). The exocontact zone consists of pale-yellow calcite, quartz, and fine-grained brown uvite-dravite and dravite-uvite which grades into fine-grained calcite, quartz and dark-green Ca-rich amphibole. The border zone consists of fine-grained quartz, and black dravite-schorl and schorl-dravite which is aligned perpendicular to the contact. The outer intermediate zone is coarse-grained feldspar and quartz. The pockets contain pink and green tourmaline. The dominant minerals in the pegmatite are feldspar, perthite and quartz with minor spodumene.

The following discussion of tourmaline compositions is based on the data of Bloomfield (1997). Tourmaline in the "Pit 6" pegmatite is characterized by an overall Ca enrichment which may be due to an influx of exomorphic fluids from the dolomite-marble host rock into the pegmatitic melt or chemical reaction between the host marble and the pegmatite melt. The crystallization sequence of the Ca- and Mg-rich tourmaline in the contact to the border zone is as follows: Fe-bearing uvite-dravite → Fe-rich uvite-dravite → Fe-bearing dravite-uvite → Fe-rich dravite-uvite → Ca-rich dravite → Ca-rich dravite-schorl → Ca-rich schorl-dravite (Fig. 7.18a). The most primitive tourmaline compositions in the intermediate zone are Ca-rich schorl-dravite and Ca-rich Mg-bearing

schorl (Fig. 7.18a). There is a positive correlation between Ca and Mg and a negative correlation between Ti and Mg, as Ca and Mg decrease and Ti increases from Fe-bearing uvite-dravite (~ 0.07 *apfu* Ti) to Ca-rich Mg-bearing schorl (≤ 0.25 *apfu* Ti) (Figs. 7.18b, c). Tourmaline in the contact and border zone is □-poor at the *X* site (Fig. 7.20a) and Mg-rich at the *Y* site (Fig. 7.21a).

Tourmaline in the intermediate zone has a wide range in composition from Ca-rich schorl-dravite → Ca-rich Mg-bearing schorl → Ca-rich elbaite-schorl-dravite → Ca-rich (Fe, Mg)-bearing elbaite → Ca-rich Fe-bearing elbaite → Ca-rich elbaite (Figs. 7.18a, 7.19a, 7.21a). Zoned tourmaline crystals have black Ca-rich schorl-dravite cores, a black Ca-rich elbaite-schorl-dravite zone, a black Ca-rich Fe-bearing elbaite zone and green Ca-rich elbaite rims. Tourmaline compositions evolve from Ca-rich schorl-dravite [□-poor and (Fe, Mg, Ti)-rich] to Ca-rich elbaite [Ca and □-rich and (Al, Li)-rich] (Figs. 7.20b, 7.21a). The presence of Ca-rich elbaite-schorl-dravite and Ca-rich (Fe, Mg)-bearing elbaite in the intermediate zone indicates that this zone was also affected by exomorphic fluids from the marble or chemical reaction between the marble and the pegmatite melt.

The crystallization sequence of tourmaline in the core zone is as follows: (Ca, Mn)-bearing schorl-elbaite → (Ca, Mn)-bearing elbaite-schorl → (Ca, Mn)-bearing Fe-rich elbaite → Ca-bearing Mn-rich elbaite → Ca-rich Mn-bearing elbaite → Ca-rich elbaite → Ca-rich Fe-bearing elbaite → (Ca, Fe)-rich elbaite (Fig. 7.19a). Zoned tourmaline crystals have black (Ca, Mn)-bearing schorl-elbaite (≤ 1.57 *apfu* Fe and 0.18 *apfu* Mg) cores, pink Ca-bearing Mn-rich elbaite zones (≤ 0.78 *apfu* Mn) and green Ca-rich Fe-bearing elbaite rims (≤ 0.42 *apfu* Fe, 0.29 *apfu* Mg), with blue (Ca, Fe)-rich

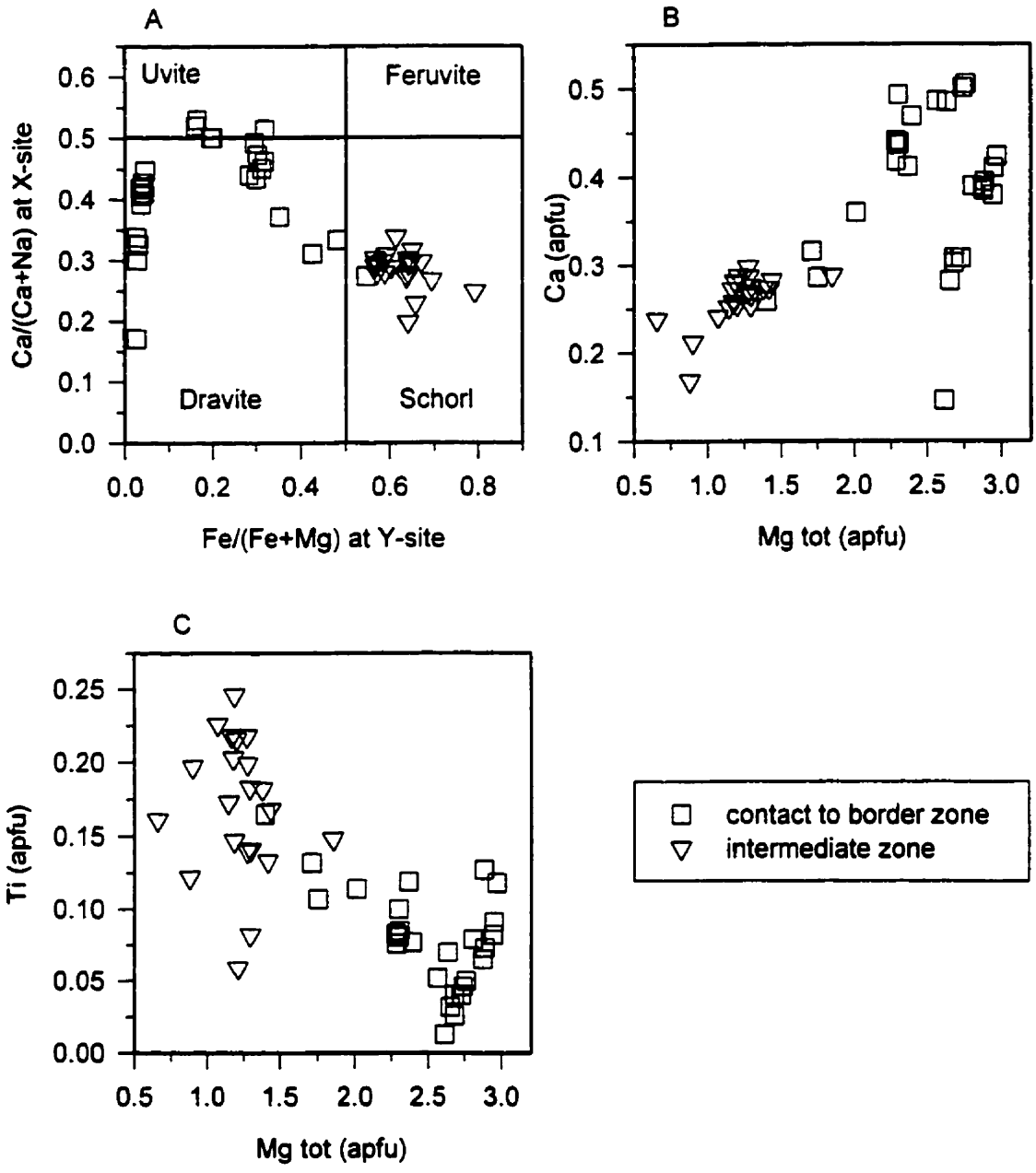

Figure 7.18. Tourmaline compositions from the outermost pegmatite zones from the Sahatany Valley pegmatite. Only compositions with < 0.1 apfu Al at Y site are plotted.

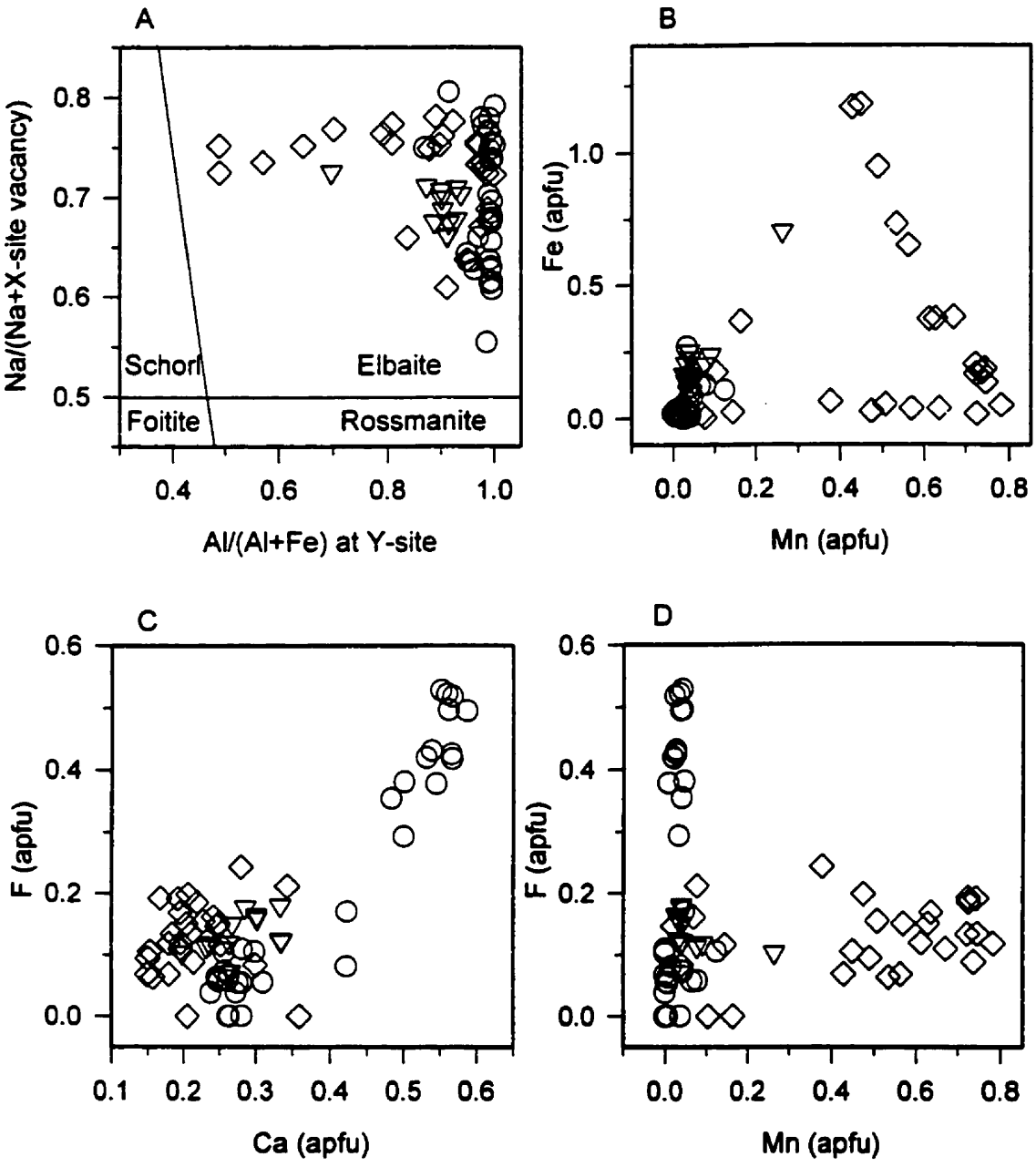

Figure 7.19. Tourmaline compositions at Sahatany the Valley pegmatite. All compositions plotted have Mg < 0.1 apfu.

elbaite infilling fractures. Tourmaline in the core zone is characterized by significant to minor Mn content. Tourmaline evolves from (Na, Fe)-rich to Mn-rich to (Ca, □, Al, Li)-rich (Figs. 7.19a, 7.19b, 7.20c, 7.21b). There is a negative correlation between Fe and Mn, as they decrease from (Ca, Mn)-bearing elbaite-schorl to Ca-bearing Mn-rich elbaite, followed by decrease in Mn in elbaite-liddicoatite and liddicoatite-elbaite (Fig. 7.19b). Tourmaline in the core zone is F-poor, with ≤ 0.24 *apfu* F in Ca-rich Mn-bearing elbaite (Fig. 7.19c). Late-stage Fe and Mg enrichment results from an influx of fluid from the host rock after pocket rupture.

Pink tourmaline in the pockets is elbaite-liddicoatite and liddicoatite-elbaite, with green rims of liddicoatite-elbaite with minor Fe and Mg contents (≤ 0.27 *apfu* Fe and 0.07 *apfu* Mg). Elbaite-liddicoatite is (Na, □, Al, Li)-rich and liddicoatite-elbaite is (Ca, Al, Li)-rich (Figs. 7.20d, 7.21b). The pink pocket tourmaline contains almost no Fe and Mn (Fig. 7.19b) and has a wide range in F content from ≤ 0.11 *apfu* in elbaite-liddicoatite to ≤ 0.53 *apfu* in liddicoatite-elbaite indicating a positive correlation between Ca and F (Figs. 7.19c, d). The minor Fe and Mg contents in the green rims result from pocket rupture.

The crystallization sequence of tourmaline in the outermost pegmatite zones is as follows: Fe-bearing uvite-dravite → Fe-rich uvite-dravite → Fe-bearing dravite-uvite → Fe-rich dravite-uvite → Ca-rich dravite → Ca-rich dravite-schorl → Ca-rich schorl-dravite → Ca-rich Mg-bearing schorl → Ca-rich elbaite-schorl-dravite → Ca-rich (Fe, Mg)-bearing elbaite → Ca-rich Fe-bearing elbaite → Ca-rich elbaite. This sequence evolves from Mg-rich to Fe-rich to (Al, Li)-rich tourmaline.

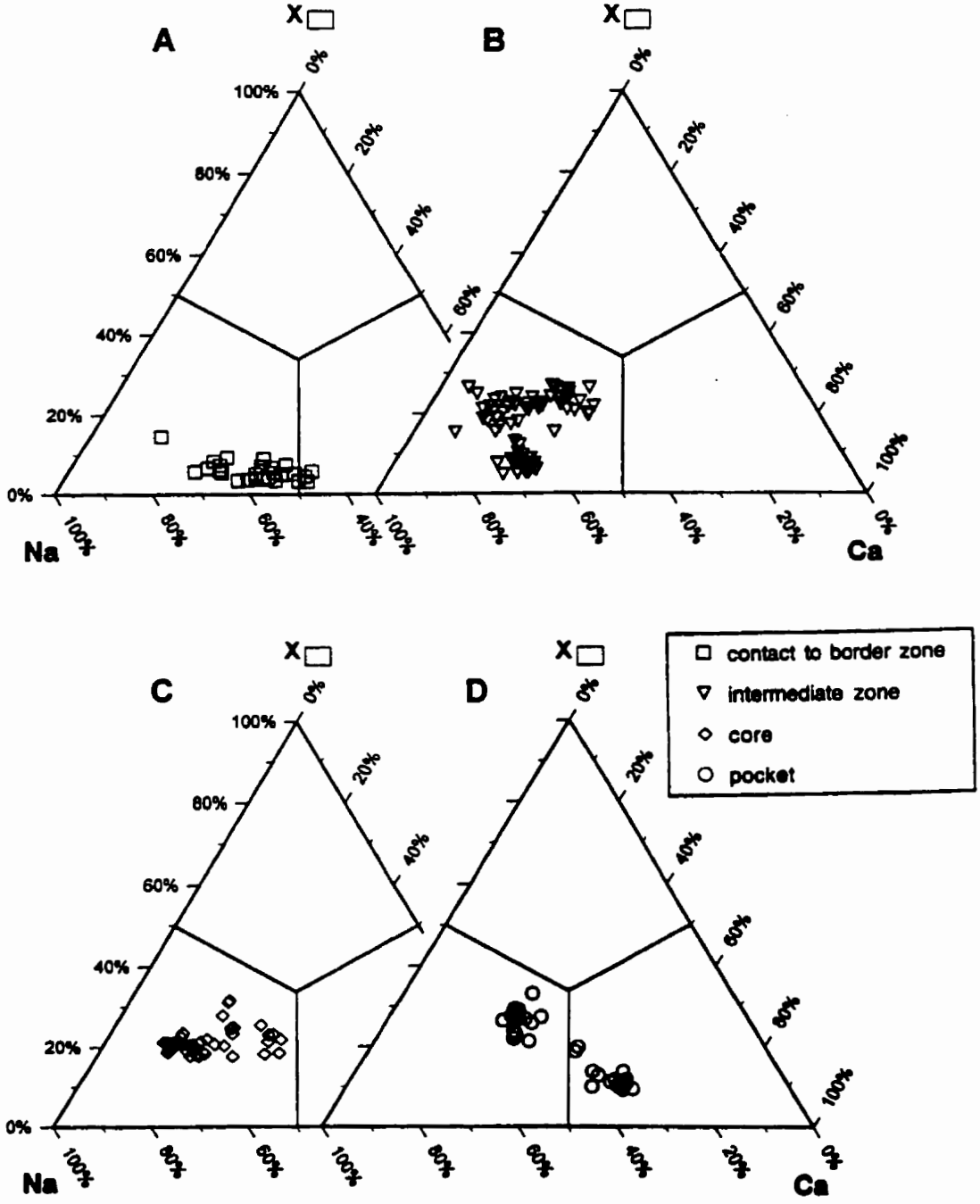

Figure 7.20. *X*-site contents tourmaline from the Sahatany Valley pegmatite.

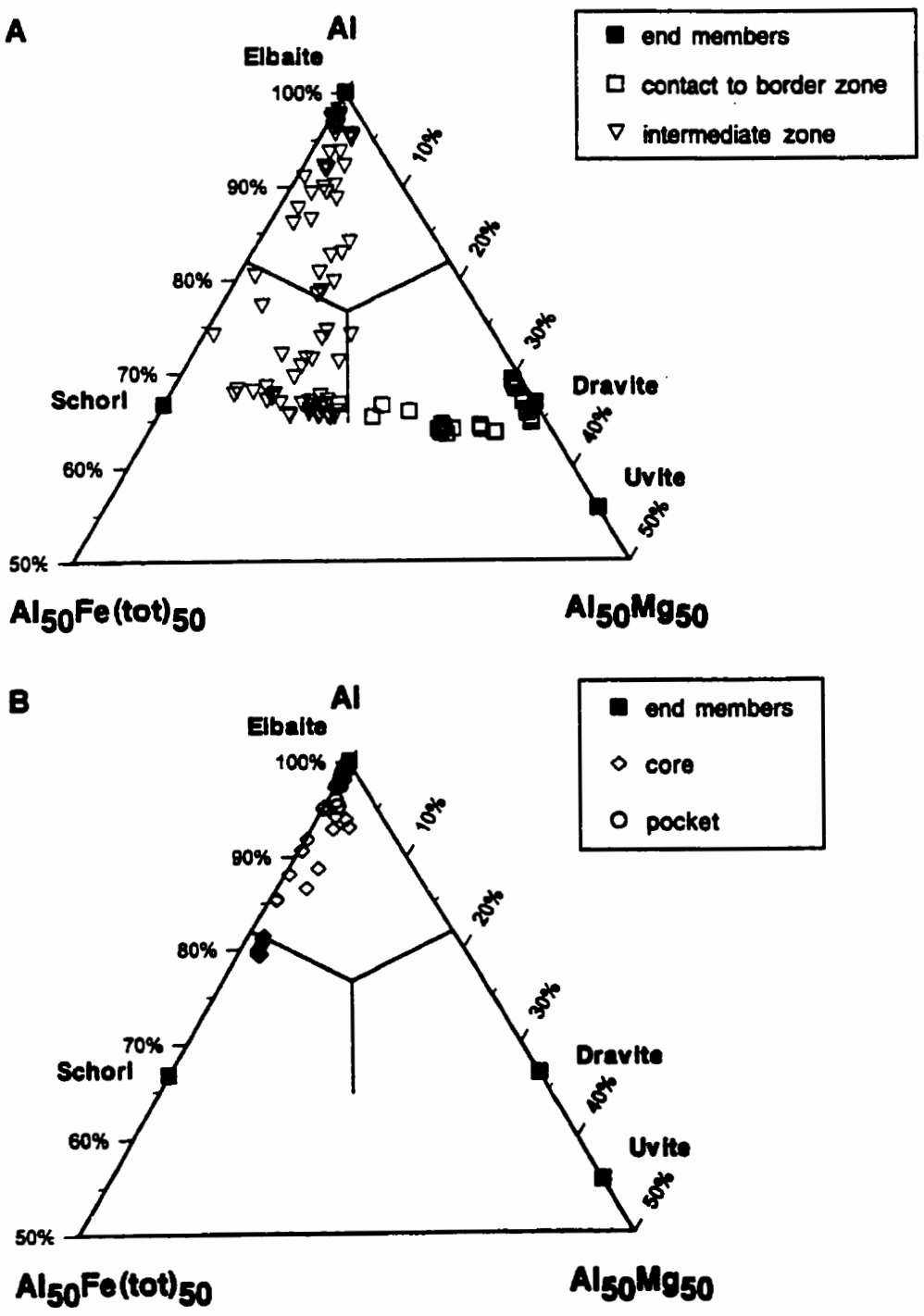

Figure 7.21: *Y*- and *Z*-site contents for tourmaline from the Sahatany Valley pegmatite.

The crystallization sequence of tourmaline in the core zone and pockets is as follows: (Ca, Mn)-bearing schorl-elbaite → (Ca, Mn)-bearing elbaite-schorl → (Ca, Mn)-bearing Fe-rich elbaite → Ca-bearing Mn-rich elbaite → Ca-rich Mn-bearing elbaite → Ca-rich elbaite → Ca-rich Fe-bearing elbaite → (Ca, Fe)-rich elbaite → elbaite-liddicoatite, liddicoatite-elbaite. This sequence evolves from Fe-rich to Mn-rich to (Al, Li)-rich tourmaline.

7.3.3. The Little Three Pegmatite

The Little Three dyke is one of five principal pegmatite dykes on the Little Three property, Ramona District, California: Little Three main, Hercules-Spessartine, Spaulding, Sinkankas and Hatfield Creek dykes. These dykes are genetically related, but are separate intrusions. The pegmatite dykes on the Little Three property are mined for gem-quality minerals: Hercules-Spessartine and Spaulding dykes for spessartine, Sinkankas dyke for abundant hambergite, and Hatfield Creek dyke for abundant axinite (Foord *et al.* 1989, Shigley *et al.* 1986, Stern *et al.* 1986, Morgan & London, in press).

The mineralogy of the Little Three main pegmatite dyke has been studied by Stern *et al.* (1986), Foord *et al.* (1989), and Morgan and London (in press). The Little Three dyke is a 1.5-2.0 m thick pegmatite which intrudes mafic biotite tonalite. It has a graphic K-rich upper portion and an aplite Na-rich lower portion, and is mined for gem-quality green tourmaline and blue F-rich topaz. The mineral assemblage at the roof of the pockets is (Si, Na, B)-rich (*i.e.*, quartz, cleavelandite and tourmaline), whereas at the floor of the pockets, it is (K, F)-rich (*i.e.*, microcline, F-rich lepidolite and F-rich topaz). The Little

Three main pegmatite can be classified as an elbaite-subtype pegmatite because elbaite is more abundant than lepidolite and topaz (D. London pers. comm.), garnet is abundant throughout the pegmatite, and hambergite is rare in the pockets. The geology and mineralogy of the Little Three pegmatite is schematized in Table 7.4.

The composition of tourmaline in this dyke has been studied in detail by Morgan and London (in press). Tourmaline in the outermost pegmatite zones is enriched in Mg due to influx of Mg from the biotite tonalite host-rock. Black tourmaline in the massive aplite is Mg-rich schorl associated with biotite with minor Mg and Ti contents. Black tourmaline in the line- rock aplite ranges from Mg-bearing schorl-foitite to schorl-foitite associated with almandine-spessartine with minor Mg and Ca contents (Fig. 7.22a). There is a sharp decrease in the Mg content of tourmaline at the transition from the biotite-bearing massive-aplite zone to the almandine-spessartine-bearing line-rock aplite. Black tourmaline in the upper graphic zone is Mg-bearing schorl.

Within about 10 cm of the pocket zones, there is a significant increase in Mn, Al and F in tourmaline. Tourmaline in the graphic zone below the pockets has foitite-schorl cores and Mn-rich Fe-bearing elbaite rims, and in the graphic zone above the pockets, it has black Mn-bearing rossmanite-foitite cores and pink or green Mn-rich elbaite jackets (Fig. 7.22a). This is the first reported occurrence of a solid solution between rossmanite and foitite, and it only occurs in one large zoned crystal. In the graphic zone above the pockets, Mn-rich elbaite is associated with F-bearing spessartine and (Mn, F)-rich lepidolite. The dark-green tourmaline in the pockets ranges from Mn-rich elbaite to Mn-bearing elbaite, the concentration of Mn decreasing from core to rim. Pocket tourmaline

TABLE 7.4. GENERAL VERTICAL CROSS-SECTION OF THE LITTLE THREE PEGMATITE*

	pegmatite zone	mineral assemblage	tourmaline composition
upper portion	border zone	fine-grained quartz, K-feldspar, albite, (biotite), [black tourmaline needles, mus]	
	graphic zone-quartz-perthite	coarse-grained quartz, graphic microcline- perthite > albite, muscovite, (radial sprays of black tourmaline 4-6 cm long), [sps-alm]	Mg-bearing schorl
	graphic zone-cleavelandite-bearing	coarse-grained quartz, cleavelandite > microcline-perthite, (Mn, F)-rich maustomilite-lepidolite, spessartine, tourmaline with black core and pink or green late jacket ≤ 10 cm long	Mn-bearing rossmanite-foitite core, Mn-rich elbaite rim
pockets	roof	giant-textured quartz, cleavelandite, (dark green tourmaline with pink-red jackets > 7 cm), [hambergite, beryl]	Mn-rich elbaite
	floor	giant-textured microcline, F-rich lepidolite, (blue F-rich topaz), [hambergite, beryl]	
	"snow on the roof" coating	fine-grained coating of K-feldspar, borian muscovite, [lepidolite]	
	late-stage	montmorillonite and kaolinite	
lower portion	graphic zone-quartz-perthite-albite	coarse-grained quartz, microcline-perthite megacrysts, cleavelandite, (black tourmaline), [sps-alm, muscovite]	Mn-rich Fe-bearing elbaite rim, foitite-schorl core
	line rock - aplite	alternating layers of fine-grained albite + quartz + [muscovite] and black tourmaline needles + orange almandine-spessartine	schorl-foitite, Mg-bearing schorl-foitite
	massive aplite	fine-grained albite, quartz, (microcline, black tourmaline needles), [almandine-spessartine, biotite, muscovite]	Mg-rich schorl

* based on (Stern *et al.* 1986, Shigley *et al.* 1986, Foord *et al.* 1989, Morgan & London in press). ( ): subordinate, [ ]: accessory minerals.

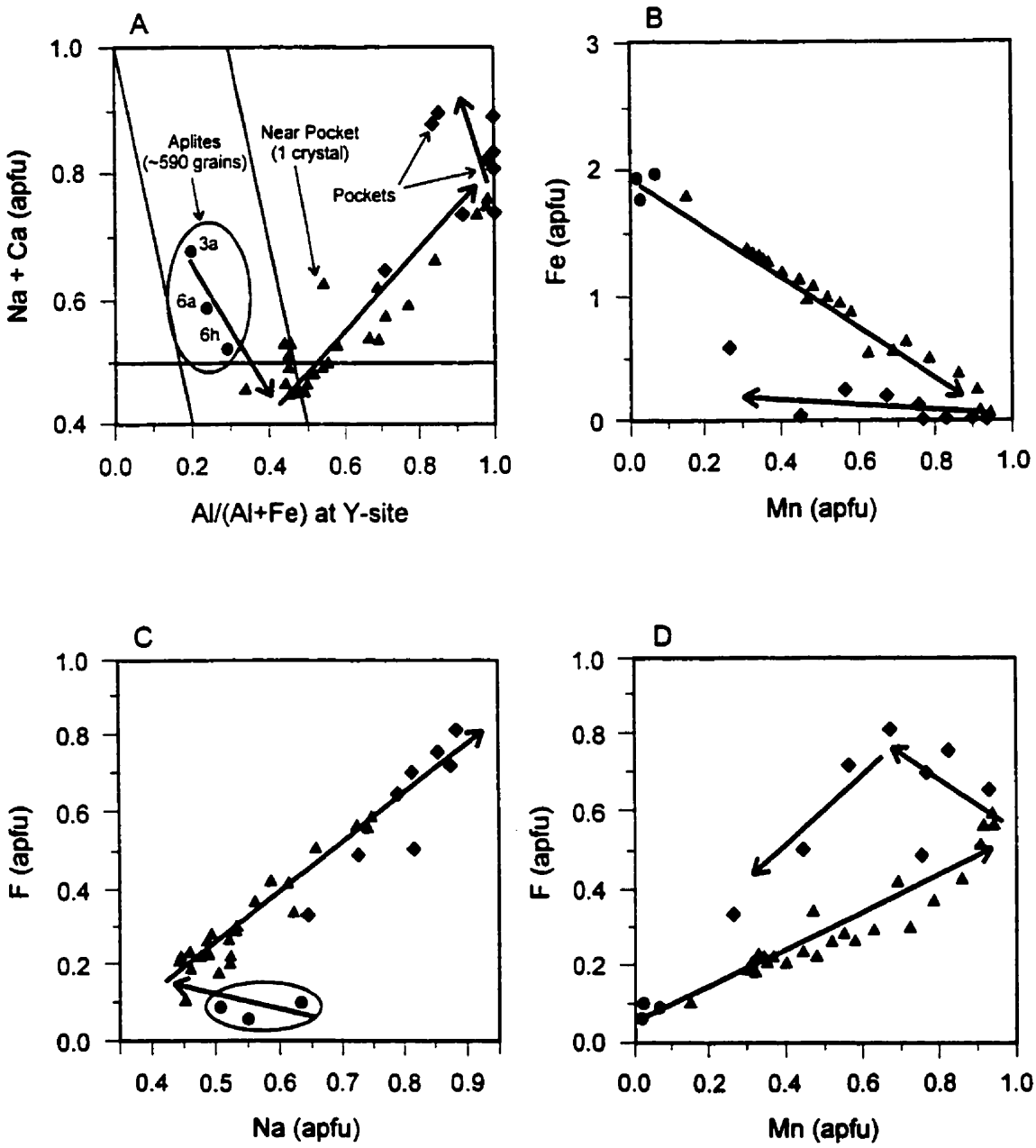

Figure 7.22. Crystallization sequence of tourmaline in the Little Three main pegmatite is indicated by arrows. Circles: aplites and upper graphic zone; triangles: a 10 cm long zoned crystal from the graphic zone above the pockets; diamonds: pockets (modified from G.B. Morgan VI pers. comm.).

has thin (usually < 1 mm) cranberry-red Fe-rich and F-poor caps on euhedrally terminated crystals which crystallized as a result of an influx of Fe-rich fluids from the biotite-tonalite host after pocket rupture.

The overall crystallization sequence of tourmaline in the Little Three main pegmatite is as follows: Mg-rich schorl → Mg-bearing schorl → Mg-bearing schorl-foitite → schorl-foitite → foitite-schorl → Mn-bearing rossmanite-foitite → Mn-rich Fe-bearing elbaite → Mn-rich elbaite → Mn-bearing elbaite (Fig. 7.22a). This sequence indicates that tourmaline evolves from Mg-rich → (□, Fe)-rich → (□, Al, Li)-rich → (Na, Mn, F)-rich (Fig. 7.23). Tourmaline in the Little Three pegmatite is Ca-poor with a wide range in Na and □ contents; the highest □ content occurs in foitite-schorl and rossmanite-foitite in the graphic zones above and below the pockets (Fig. 7.23a). There is a negative correlation between Fe and Mn, as Fe decreases and Mn increases from Mg-bearing schorl-foitite in the aplite to Mn-rich elbaite in the pockets, followed by a decrease Mn in Mn-bearing elbaite (Fig. 7.22b). As Mn preferentially partitions into garnet over tourmaline, Mn-rich elbaite is common in garnet-free pockets. There is a positive correlation between Na and F for tourmaline in the graphic zones and pockets, whereas there is a negative correlation between Na and F for tourmaline in the aplite (Fig. 7.22c). The Mn-rich elbaite in the pockets is the most Na-, Mn- and F-rich tourmaline in the pegmatite, indicating increasing alkalinity of the evolved pegmatite melt in the pockets.

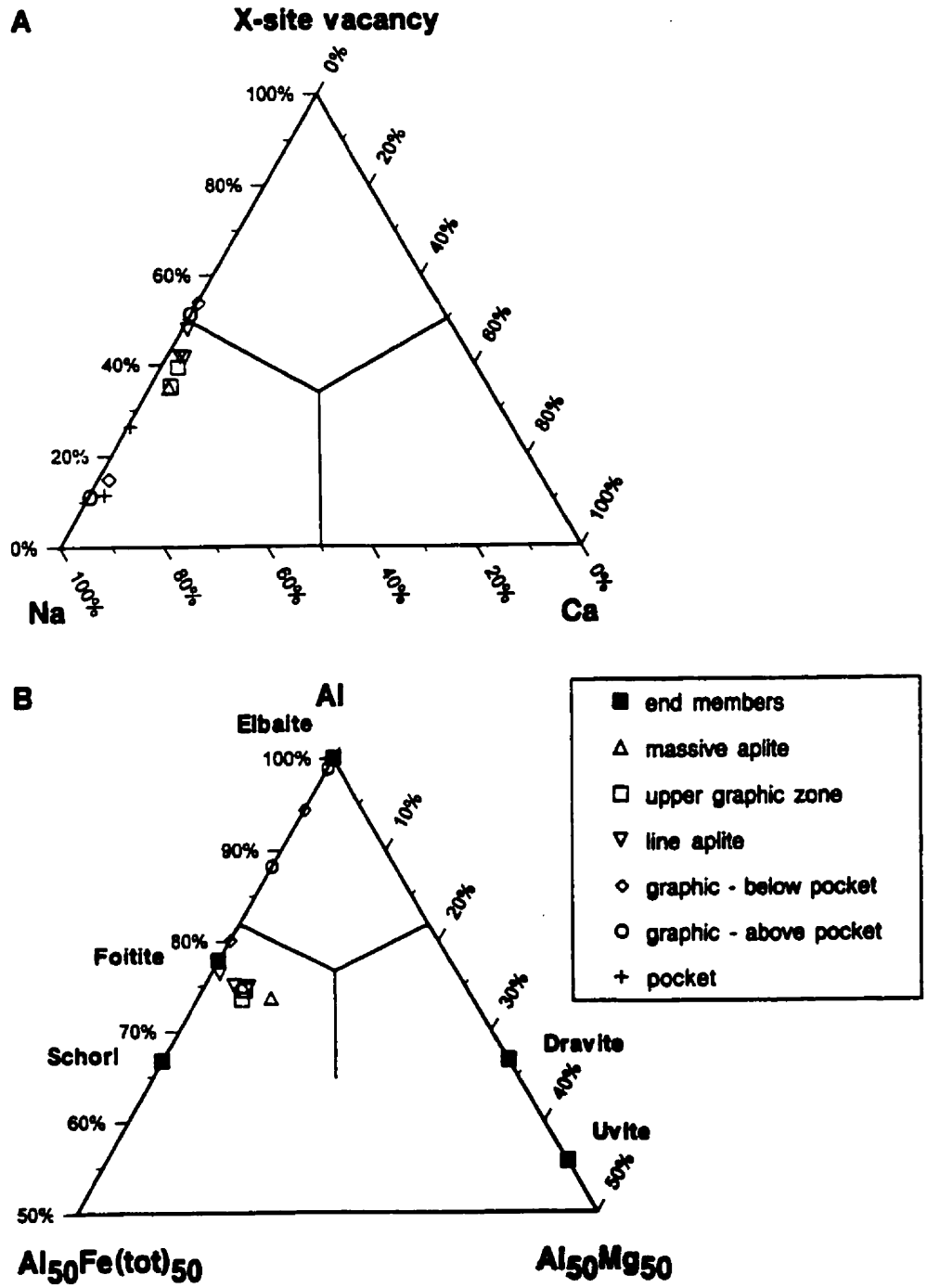

Figure 7.23. (a) *X*-site content and (b) *Y*- and *Z*-site contents of tourmaline in the Little Three main pegmatite (data from Morgan & London in press).

7.3.4. The Elba Island pegmatites

Miarolitic (shallow depth of intrusion) LCT aplite-pegmatite dykes occur along the eastern margin of the monzogranitic Mt. Capanne pluton (Tonarini *et al.* 1998). The aplites and pegmatites occur as swarms and networks of dykes, ranging in width from a few millimeters up to 2 m, and may be hosted by monzogranite, cordierite- and tourmaline-bearing leucocratic lenses, or hornfels (meta-serpentinite) of the metamorphic aureole (Ruggieri & Lattanzi 1992, Tonarini *et al.* 1998). Dykes may consist of alternating aplite and pegmatite layers, or aplitic Na-rich footwalls and coarse-grained pegmatite K-rich hanging walls (Pezzottta *et al.* 1996). In general, the aplitic-pegmatitic dykes consist of outer portions of aplite and a central graphic and/or massive pegmatite with miarolitic cavities. The aplite zones consist of quartz, K-feldspar, albite to oligoclase, tourmaline, muscovite, ± biotite and ● sekaninaite. The graphic zone consists of graphic intergrowths of K-feldspar + quartz, albite + quartz and tourmaline + quartz, and the massive pegmatite zone consists of coarse-grained perthitic K-feldspar, quartz and tourmaline. The central parts of the pegmatite zone contain miarolitic cavitites (~ 1 cm) and pockets lined with dominant coarse-grained euhedral multicoloured tourmaline, beryl (aquamarine and morganite) quartz, albite and K-feldspar, and minor lepidolite, petalite, pollucite, spessartine and topaz. Late-stage hydrothermal fluids also crystallized Ca- and Na-rich zeolites (*i.e.*, stilbite, heulandite, laumontite, mordenite and dachiardite) which coat the primary pocket minerals or form alteration products of K-feldspar (Aurisicchio *et al.* 1999).

An abstract of a detailed study of tourmaline in the Elba pegmatites was published

by Aurisicchio and Pezzotta (1997). Black tourmaline in the monzogranite, cordierite-bearing leucogranite, the exocontacts of the aplite-pegmatite dykes, and in hydrothermal veins is schorl-dravite. Black graphic and prismatic tourmaline in the fine-grained and coarse-grained zones is schorl with a minor dravite component and locally a moderate foitite component.

Tourmaline in the pockets is commonly multicoloured and zoned perpendicular to the *c*-axis, *e.g.*, black base, green zone and pink cap (Fig. 7.24c) (Aurisicchio & Pezzotta 1997). The zoned tourmaline has a black schorl base, a Mn-rich elbaite zone, an elbaite zone, an elbaite-rossmanite zone, a rossmanite-elbaite zone and a foitite overgrowth. The Mn-rich elbaite does not crystallize simultaneously with spessartine, as Mn preferentially partitions into garnet over tourmaline. The sharp decrease in Mn content in elbaite is associated with the beginning of spessartine crystallization. Foitite occurs as acicular and fibrous crystals and as black-violet, fibrous-to-prismatic overgrowths at the terminations of multicoloured elbaite (Fig. 7.24b) (Aurisicchio *et al.* 1999). Foitite overgrowths represent an influx of Fe and minor Mg ($\leq$ 0.23 *apfu* Mg), and they either crystallized (a) at the beginning of the hydrothermal stage which altered the primitive Fe-rich biotite and sekaninaite to white mica in the surrounding aplite-pegmatite zones, or (b) during circulation of hydrothermal fluids from the biotite-bearing monzogranite along fractures into the pegmatite dykes and pockets (Aurisicchio *et al.* 1999).

The overall crystallization sequence of tourmaline in the Elba pegmatites is as follows: schorl-dravite → Mg-rich schorl → schorl → Mn-rich elbaite → elbaite → elbaite-rossmanite → rossmanite-elbaite → foitite. Tourmaline evolves from (Na, Mg)-

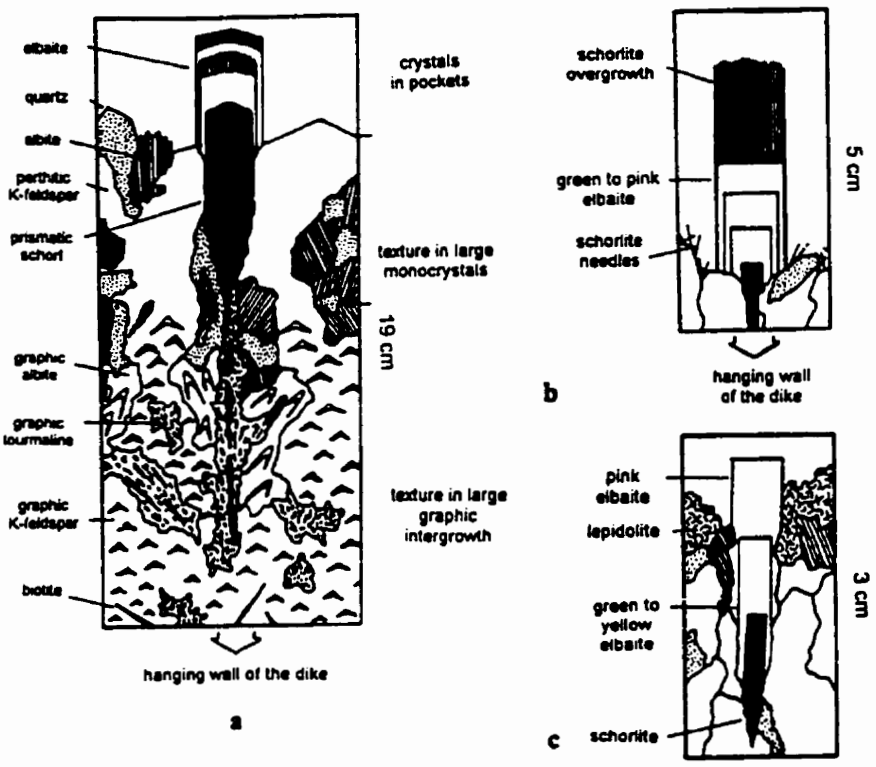

Figure 7.24. Textural relations between zoned tourmaline and the other minerals in the Elba pegmatite dykes: (a) sample 1; (b) sample 2; (c) sample 3 (Tonarini *et al.* 1998).

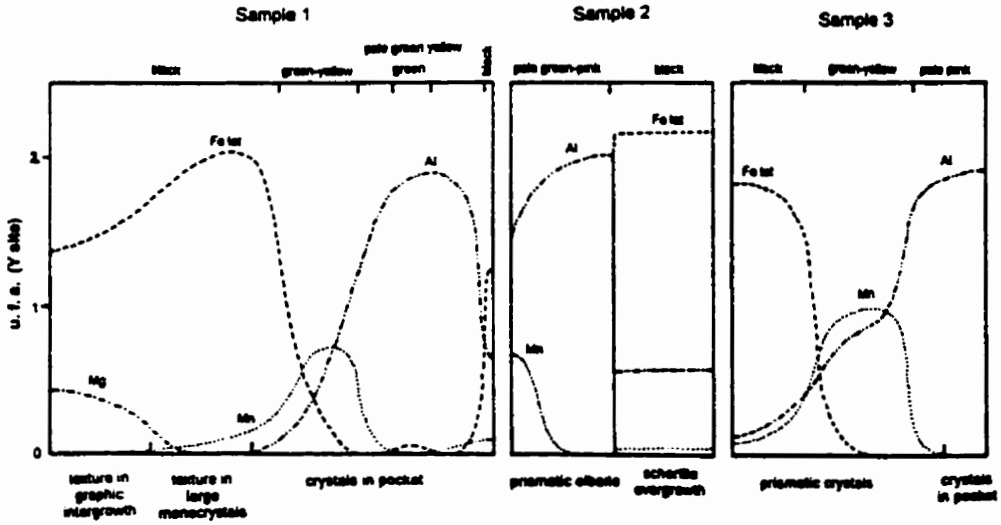

Figure 7.25. Compositional trend of *Y*-site contents *(apfu)* in tourmaline for the same samples as in Figure 7.24 (Tonarini *et al.* 1998).

rich → (Na, Fe)-rich → (Na, Mn, Al, Li)-rich → (□, Al, Li)-rich → (□, Fe)-rich (Fig. 7.25). The Ca content is negligible throughout crystallization of the aplite-pegmatite dykes.

7.3.5. Geochemical evolution of elbaite-subtype pegmatites

Compositional variation in primary tourmaline in pegmatites may be caused by fractionation of the pegmatite melt (*i.e.*, Na-□, Fe-(Al+Li), Fe-Mn and Mn-F geochemical pairs). The *X* site is dominated by Na in Ca-bearing schorl to Mn-bearing elbaite, except for late-stage □- and Ca-enrichment in Ca-rich elbaite-rossmanite in pockets, followed by Ca-enrichment in liddicoatite-elbaite.

The substitution $3Fe^{2+} \rightleftharpoons 1.5Al + 1.5Li$ in tourmaline is caused by increasing fractionation within pegmatites. The most primitive tourmaline is Ca-bearing schorl and the most fractionated is Ca-rich elbaite-rossmanite or liddicoatite-elbaite (Fig. 7.26a).

There is a negative correlation between Fe and Mn in tourmaline, from Ca-bearing schorl to Mn-rich elbaite, and in garnet, from almandine to spessartine (Fig. 7.26b). This positive correlation is followed by decrease in Mn from Mn-rich elbaite to liddicoatite. There is a sharp contrast between Fe-rich tourmaline and garnet in the pegmatite zones, and Mn-rich garnet in the pegmatite zones surrounding the pockets and Mn- and Li-rich tourmaline in the pockets. The sudden increase of Mn in tourmaline actually reflects variation of Li and B in the melt rather than that of Mn, as the surrounding pegmatite was saturated in Mn-rich spessartine throughout most of its crystallization (Morgan & London, in press). Spessartine-rich garnet occurs only associated with schorl or foitite,

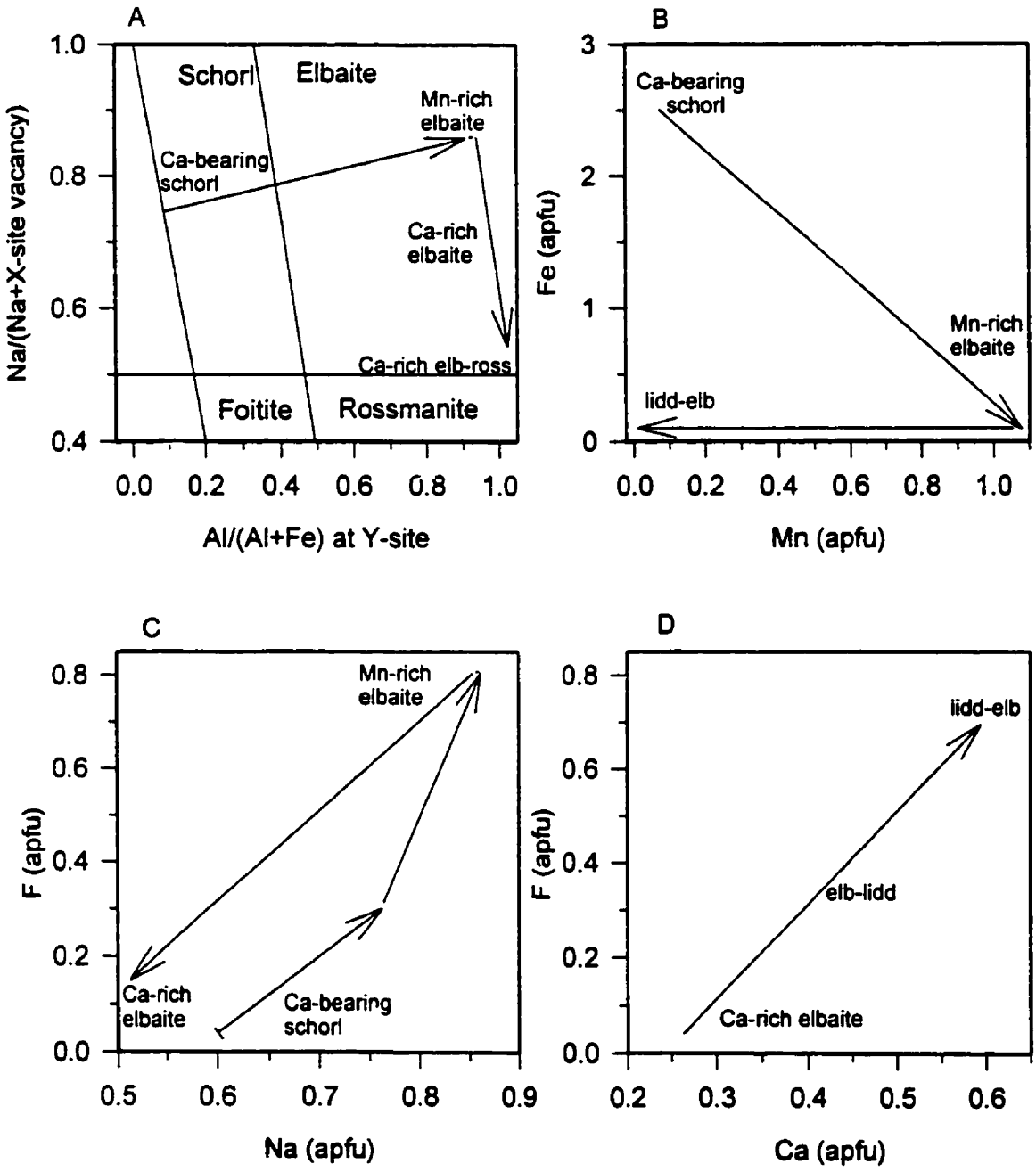

Figure 7.26. Idealized compositional trends of tourmaline in elbaite-subtype pegmatites. All compositions plotted have Mg < 0.1 apfu.

never with elbaite (Morgan & London, in press) and Mn-rich elbaite only occurs in garnet-free pockets. Therefore, increasing Li and B contents of the melt facilitates the tsilaisite substitution ($3Fe^{2+} \rightleftharpoons Li + Al + Mn$) that destabilizes spessartine + schorl or foitite relative to Mn-rich elbaite.

Tourmaline composition may also be affected by crystal-chemical constraints, as shown by the correlation between Na and Ca at the *X* site and F at the O(1) site (Robert *et al.* 1997). There is a positive correlation between Na and F, as they increase from Ca-bearing schorl to Mn-rich elbaite, and decrease to Ca-rich elbaite (Fig. 7.26c). There is also a positive correlation between Ca and F, increasing from Ca-rich elbaite to liddicoatite-elbaite (Fig. 7.26d).

Commonly, Ca-rich tourmaline and plagioclase crystallize early in the exocontact or endocontact of the pegmatite and Li-rich tourmaline crystallizes late in the core margin or pockets, so liddicoatite is rare in nature. Teertstra *et al.* (1999) suggested three possible origins for late liddicoatite:

(a) mobilization of Ca from early pegmatite minerals, *e.g.*, alteration of plagioclase to Ca-rich zeolites, or albitization of feldspar;

(b) mobilization of Ca from the host rocks, *i.e.*, exomorphic fluids flowing from the Ca-, Mg- and Fe-rich host rocks into the pegmatite melt to form Ca-rich schorl-dravite in the border zone;

(c) conservation of Ca through consolidation of the pegmatite, *e.g.*, the presence of rare primary Ca-rich pocket minerals: danburite and hellandite at Belo Horizonte; danburite and datolite in Vlastějovice pegmatite; fluorapatite and fluorite in Stak Nala and Little

Three pegmatites; microlite in Elba pegmatites. Calcium may be conserved through consolidation of the pegmatite by sequestering some Ca in the melt as fluoride complexes (Weidner & Martin 1987). Evidence of Ca conserved by fluoride complexes is suggested by the positive correlation between Ca and F in liddicoatite-elbaite, and the presence of rare fluorapatite and fluorite in pockets. Evidence that F is conserved through consolidation of the pegmatite is the presence of rare primary F-rich pocket minerals: fluorapatite, fluorite and topaz in Stak Nala and Little Three pegmatites; fluorapatite in Ctidružice; fluorite in Vlastějovice pegmatite; topaz in Elba pegmatites; F-rich hambergite in Belo Horizonte pegmatite

The presence of abundant K-feldspar and rare lepidolite and topaz in the pockets indicates that pocket minerals crystallized from an aqueous fluid with high acidity (μHF) and high salinity (μKF) (London 1982). Lepidolite in pockets is polylithionite, indicating decreasing pH of the pegmatite melt (Gordiyenko & Ponomareva, 1988). The presence of B-rich minerals (*i.e.*, hambergite, danburite, datolite and boromuscovite), the presence of rare polylithionite and the absence of muscovite indicate increasing alkalinity of the parent medium (Novák & Povondra 1995). The presence of volatiles, such as B and F, drives the compositions of residual melts toward alkaline, Na-rich compositions enriched in incompatible elements (London 1987).

Pocket rupture results in an influx of Fe-rich fluids into the pockets. The source of these Fe-rich fluids may be (a) alteration of primary Fe-rich minerals within the pegmatite, or (b) the host rock. At Belo Horizonte, the source of the Fe-rich fluids is the alteration of spessartine-almandine which produced blue Ca-rich schorl rims in the pocket

zone. At Little Three, the source of the Fe-rich fluids is the biotite-tonalite host-rock. At Elba, foitite overgrowths in the pockets represent an influx of Fe and minor Mg, and crystallized either (a) at the beginning of the hydrothermal stage which altered the primitive Fe-rich biotite to white mica in the surrounding aplite-pegmatite zones, or (b) during circulation of hydrothermal fluids from the biotite-bearing monzogranite along fractures into the pegmatite dykes and pockets (Aurisicchio *et al.* 1999).

After pocket rupture, primary pocket minerals may have been coated by hydrothermal clays, micas, zeolites or carbonates derived from alteration of primary pegmatite minerals or from the host rock (Foord *et al.* 1986). This is often referred to as "snow-on-the-roof" (*e.g.*, stilbite at the Belo Horizonte pegmatite). The source of Na- and Ca-rich alkaline fluids is the calcic olivine gabbro. Pocket minerals in Elba pegmatites are coated or replaced by hydrothermal Ca- and Na-rich zeolites (*i.e.*, stilbite, heulandite, laumontite, mordenite and dachiardite), and the source of the Ca- and Na-rich fluids is the monzogranite host-rock (Aurisicchio *et al.* 1999). The "snow-on-the-roof" coating consists of K-feldspar and boromuscovite in the Little Three pegmatite (Foord *et al.* 1989) which crystallized under high salinity, high alkalinity and low Li-activity (London 1982). Pocket minerals at the Stak Nala main- and south-mines are coated by a < 1 mm thick layer of fine-grained muscovite or borian muscovite (Laurs *et al.* 1998) which crystallized under moderate salinity and acidity, and low Li-activity (London 1982). The source of K may be the release of K following albitization of K-feldspar.

Elbaite-subtype pegmatites crystallized in an open system, as fluids flowed from the pegmatite into the host rock and from the host rock into the pegmatite or there was

chemical reaction between the host rock and the pegmatite melt. Belo Horizonte, Stak Nala and Elba pegmatites have (1) exocontact tourmaline as a result of addition of B and Na to the host rock; (2) endocontact tourmaline as a result of influx of Ca and Mg from the host rock; (3) Fe-rich tourmaline zones in pockets as a result of influx of Fe in the pockets; and (4) Ca- and Na-rich zeolite and mica coatings on primary pocket minerals as a result of an influx of Na, Ca and K into the pockets. The Little Three pegmatite does not have exocontact tourmaline, but does have endocontact tourmaline, Fe-rich tourmaline zones in pockets, and coatings of K-feldspar and boromuscovite on pocket minerals.

7.3.6. Summary of tourmaline and garnet in elbaite-subtype pegmatites

Tourmaline in elbaite-subtype pegmatites is black in most of the pegmatite and occurs as zoned multicoloured (*i.e.*, pink, green, colourless, blue and purple) crystals in pockets. Some elbaite-subtype pegmatites are mined for their gem-quality tourmalines (*e.g.*, Stak Nala and Elba Island pegmatites).

In elbaite-subtype pegmatites, the border zone is commonly affected by influx of Mg- and Ti-rich fluid from the host rocks or chemical reaction between the Mg- and Ti-rich host rock and the pegmatite melt to produce schorl-dravite, Mg-rich schorl and Mg-bearing schorl. Tourmaline composition evolves from the outermost to innermost pegmatite zones in the following sequence: (± schorl-foitite) → (± foitite-schorl) → schorl (± Ca, Mn) → schorl-elbaite (± Ca, Mn) → elbaite-schorl (± Ca, Mn) → Fe-rich elbaite (± Ca, Mn) → Fe-bearing elbaite (± Ca, Mn). Tourmaline composition in the pockets evolves from (± Fe-rich Mn-bearing elbaite) → Mn-rich Fe-bearing elbaite →

Mn-rich elbaite (± Ca) → Mn-bearing elbaite (± Ca) → Ca-rich elbaite → elbaite-rossmanite (± Ca, Mn), (± rossmanite-elbaite) → (± elbaite-liddicoatite, liddicoatite-elbaite).

If the host rock of the pegmatite is Ca-rich (*e.g.*, calcic olivine gabbro at Belo Horizonte, pyroxene gneiss at Řečice, Ca- and Fe^{3+}-rich skarn at Vlastějovice, dolomitic marble at Sahatany Valley), then tourmaline in the pegmatite will likely be Ca-rich due to influx of Ca-rich fluids from the host rock. On the other hand, if the host rock of the pegmatite is Ca-poor (*e.g.*, biotite- and sillimanite-bearing gneiss at Pikárec, graphite-bearing biotite gneiss at Ctidružice, biotite tonalite at Little Three, monzogranite at Elba pegmatites), then tourmaline in the pegmatite is Ca-poor. The absence of exocontact tourmaline in the host rock at Pikárec, Ctidružice and Little Three indicates a lack of B metasomatism. Elbaite-liddicoatite and liddicoatite-elbaite have been found only in elbaite-subtype pegmatites which intrude Ca-rich host rocks (*e.g.*, Řečice, Vlastějovice and Sahatany Valley pegmatites).

The crystallization sequence of dominant primary tourmaline in elbaite-subtype pegmatites may be condensed as follows: Ca-bearing schorl → Mn-rich elbaite → Ca-rich elbaite → Ca-rich elbaite-rossmanite → liddicoatite-elbaite (Fig. 7.26a). Pocket tourmaline is commonly zoned with a black Fe-rich core, a pink (Na, Mn, F)-rich zone, a (Ca, Al)-rich zone and a (Ca, F)-rich rim (Fig. 7.27). Tourmaline in the Pikárec and Little Three pegmatites have a slightly different crystallization sequence: schorl-foitite → foitite-schorl → (± Mn-bearing rossmanite-foitite) → Mn-rich elbaite. Pikárec, Ctidružice and Little Three pegmatites contain Mn-rich elbaite as the most fractionated tourmaline

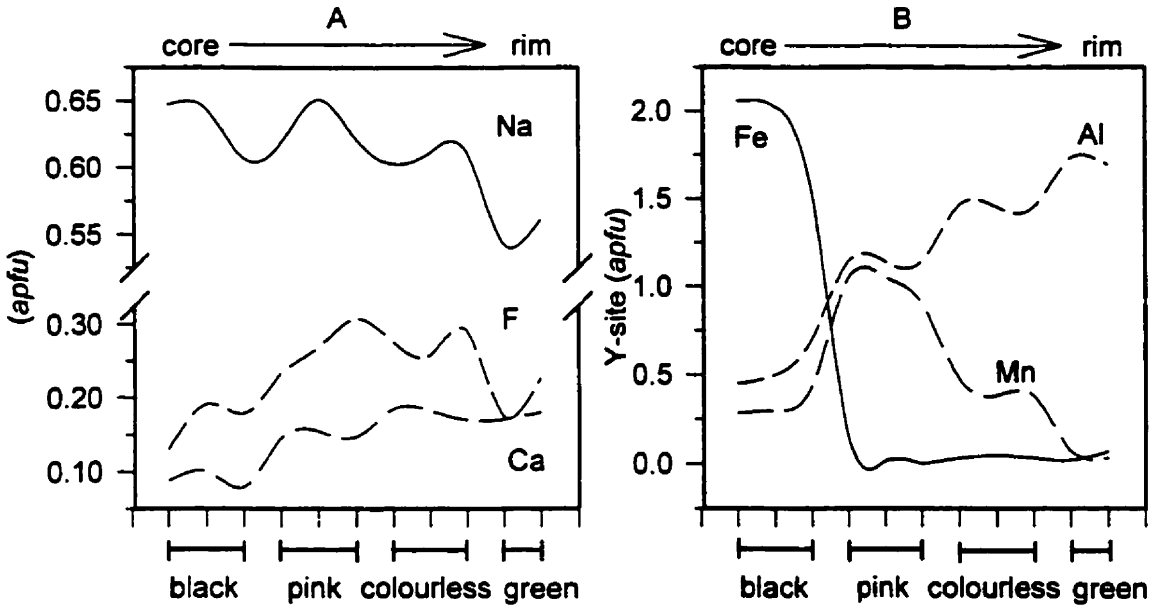

Figure 7.27. Compositional evolution of tourmaline in pockets at Belo Horizonte is very similar to that in the Elba and Stak Nala pegmatites.

composition. Belo Horizonte, Řečice, main mine Stak Nala and Elba pegmatites have Ca-rich elbaite-rossmanite as one of the most fractionated tourmaline compositions, whereas Řečice, Vlastějovice and Sahatany Valley pegmatites have elbaite-liddicoatite or liddicoatite-elbaite as the most fractionated tourmaline.

Schorl in elbaite-subtype pegmatites may be Mn-bearing (*i.e.*, Belo Horizonte, Pikárec, Vlastějovice, Little Three pegmatites), but the Mn content increases significantly in elbaite in the garnet-free pockets. In elbaite-subtype pegmatites, pink Mn-rich elbaite with up to 1.1 *apfu* Mn is the most characteristic tourmaline.

There is a negative correlation between Fe and Mn, as Fe decreases and Mn

increases from Ca-bearing schorl to Mn-rich elbaite, followed by a decrease in Mn in liddicoatite-elbaite (Fig. 7.26b). There is a positive correlation between Na and F, as they increase from Ca-bearing schorl to Mn-rich elbaite and decrease to Ca-rich elbaite and Ca-rich elbaite-rossmanite (Fig. 7.26b). There is a positive correlation between Na, Mn and F, all reaching a maximum in Mn-rich elbaite. There is a positive correlation between Ca and F, increasing from Ca-rich elbaite to elbaite-liddicoatite to liddicoatite-elbaite (Fig. 7.26c). Teertstra *et al.* (1999) also noted a positive correlation between Ca and F, as these elements increase from Ca-bearing elbaite-rossmanite cores to liddicoatite-elbaite rims in the High Grade pegmatite dyke, Manitoba. Due to limited outcrop exposure, the subtype of the High Grade Dyke is uncertain, but it is suspected to be either lepidolite- or petalite-subtype (P. Černý, pers. comm.).

Pocket rupture results in an influx of Fe-rich fluids and Fe-rich tourmaline overgrowths on pocket crystals. Bent and broken crystals, mineral shards and mineral overgrowths within the pockets are evidence of pocket rupture in the Stak Nala south-mine pegmatite (Laurs *et al.* 1998). The zoned pocket tourmaline at Belo Horizonte has brown Fe-rich Ca-bearing elbaite and black (Ca, Mn)-bearing elbaite-schorl zones which interrupt the crystallization sequence. In Little Three pockets, dark-green Mn-rich elbaite has cranberry-red Fe-rich F-poor jackets. The pockets in the Elba pegmatite contain multicoloured elbaite which is capped by foitite. Foitite occurs as acicular and fibrous crystals and as black-violet fibrous-to-prismatic overgrowths at the terminations of multicoloured elbaite.

Garnet is common in pegmatite zones in elbaite-subtype pegmatites, but is usually

absent from the pockets. Garnet composition evolves from almandine (with a subordinate spessartine component and minor Mg and Ca contents associated with schorl-dravite in the outermost pegmatite zones) → almandine-spessartine (with minor Ca contents associated with schorl) → spessartine-almandine (with minor Ca contents associated with schorl) → spessartine (with minor Fe and Ca contents associated with Mn-rich elbaite near the pockets). The Fe is preferentially partitioned into tourmaline and Mn is preferentially partitioned into garnet. The absence of garnet in the pockets allows crystallization of Mn-rich elbaite.

CHAPTER 8

Conclusions: Comparison of lepidolite-, petalite-, and elbaite-subtype pegmatites

8.1. Exocontact tourmaline

Exocontact tourmaline is typically black needles in the metasomatically-altered host rock, which are aligned perpendicular to the contact with the pegmatite. There are two compositional groups of tourmaline in the exocontact:

(1) feruvite-uvite-schorl-dravite (Ca- and Mg-rich);

(2) intermediate ternary tourmaline: elbaite-schorl-dravite (Na-, Al-, and Li-rich).

Group (1) tourmaline is common and group (2) tourmaline is rare in exocontacts. Both compositional groups occur in the tourmalinized and biotitized amphibolite surrounding the petalite-subtype Tanco pegmatite. At Tanco, group (1) tourmaline has a dominant schorl component with minor feruvite and dravite components, and group (2) tourmaline is dravite-schorl-elbaite, elbaite-schorl-dravite and (Ca, Mg)-bearing schorl-elbaite which plots in the centre of the elbaite-schorl-dravite ternary diagram. Zoned tourmaline in the Tanco exocontact has feruvite-schorl-dravite cores and elbaite-schorl-dravite rims.

There is a positive correlation between Ca, Mg and Ti in group (1) tourmaline, as the tourmaline far away from the contact with the pegmatite is Ca-, Mg- and Ti-rich and the tourmaline closest the contact is Ca-, Mg- and Ti-poor. In exocontact tourmaline at Tanco, Ca, Mg and Ti decrease from feruvite-schorl ($\leq$ 0.18 *apfu* Ti) to Ca-bearing schorl-dravite (> 0.02 *apfu* Ti).

The composition of exocontact tourmaline depends on the composition of the host

rock and the amount of fluid exchanged between the host rock and the pegmatite melt. Lepidolite pegmatites at Red Cross Lake intrude meta-andesite and metabasalt, and have uvite, feruvite, dravite and schorl in the exocontact. Petalite-subtype Tanco intrudes amphibolite and has dominant schorl (with minor feruvite and dravite components) in the exocontact. Elbaite-subtype Belo Horizonte pegmatite intrudes olivine gabbro and has dominant uvite (with minor feruvite and dravite components) in the exocontact. All three of these pegmatites intrude Ca-, Mg- and Fe-rich mafic rocks with similar bulk compositions and have similar group (1) exocontact tourmaline compositions. Petalite-subtype Utö pegmatite intrudes iron formation and marble, and has (Ca, Mg)-rich schorl in the exocontact.

Lepidolite-subtype Rožná pegmatite intrudes biotite-bearing metapelite and has dravite-schorl, Mg-bearing elbaite-schorl and (Mg, Fe)-rich elbaite in the exocontact. Metapelite at Rožná is Al-rich and thus has Al-rich group (2) exocontact tourmaline.

Group (1) feruvite-uvite-schorl-dravite is common in exocontacts. It crystallizes as a result of Na-, Al- and B-rich pegmatite fluids infiltrating Ca-, Mg- and Fe-rich host rocks or as a chemical reaction between pegmatite melt and host rock. Group (2) ternary elbaite-schorl-dravite tourmaline is rare in exocontacts. It crystallizes in Ca- and Mg-rich exocontacts at a high activity of B infiltrating from the pegmatite melt, which destabilizes holmquistite. Thus, holmquistite is not present in the tourmalinized aureoles.

8.2. Endocontact tourmaline

The composition of endocontact tourmaline in elbaite-subtype pegmatites depends

on the composition of the host rock. Elbaite-subtype Řečice pegmatite intrudes strongly weathered pyroxene gneiss and has Ca- and Mg-bearing endocontact tourmaline. The endocontact tourmaline consists of the same two compositional groups as the exocontact tourmaline. At Řečice, the outermost medium-grained granitic zone contains common Ca-rich schorl-dravite group (1) tourmaline, and common Ca-bearing schorl-elbaite-dravite and minor Ca-bearing schorl-dravite-elbaite and Ca-bearing elbaite-schorl-dravite group (2) tourmaline. Elbaite-subtype Belo Horizonte pegmatite intrudes calcic olivine gabbro, and the lower border zone contains Ti-bearing feruvite-schorl, (Ca, Mg)-rich schorl and Ca-rich Mg-bearing schorl group (1) tourmaline. Elbaite-subtype Sahatany Valley pegmatite intrudes dolomite marble; the endocontact tourmaline is Ca-rich Mg-bearing schorl group (1) tourmaline, and Ca-rich elbaite-schorl-dravite group (2) tourmaline. Elbaite-subtype Ctidružice pegmatite intrudes graphite-bearing biotite gneiss and contains Mg-rich schorl and Mg-bearing schorl as endocontact tourmaline.

There is a positive correlation between Ca, Mg and Ti in exocontact and endocontact tourmalines. At Řečice, Ca, Mg and Ti decrease from Ca-rich Ti-bearing schorl-dravite ($\leq$ 0.31 *apfu* Ti) to Ca-bearing schorl ($>$ 0.04 *apfu* Ti) in the coarse-grained zone. At Belo Horizonte, Ca, Mg and Ti decrease from Ti-bearing feruvite-schorl ($\leq$ 0.27 *apfu* Ti) in the exocontact to Ca-bearing schorl ($>$ 0.02 *apfu* Ti) in lower second-intermediate zone.

In addition to the above two compositional groups, primitive endocontact tourmaline may result from simple addition of Mg, especially in lepidolite- and petalite-subtype pegmatites. The Ca-poor nature of endocontact tourmaline may reflect the Ca-

poor nature of the host rock. For example, lepidolite-subtype Laštovičky pegmatite intrudes biotite-sillimanite gneiss and the outer albite zone contains rare Mg-bearing schorl-foitite. Calcium-poor endocontact tourmaline may occur despite a Ca-rich mafic host rock. For example, lepidolite-subtype Stewart Lithia pegmatite intrudes gabbro-norite, and the upper graphic-granite wall zone contains Mg-bearing schorl-foitite and Mg-bearing schorl. Petalite-subtype Tanco pegmatite intrudes amphibolite, and the outer pegmatite zones have Mg-bearing schorl group (1) tourmaline, and Al-rich Mg-bearing schorl, Mg-bearing schorl-elbaite and Mg-bearing elbaite-schorl group (2) tourmaline.

Petalite-subtype Utö pegmatite is the only exception to the Ca-rich host rock - Ca-poor endocontact tourmaline 'rule'. Utö pegmatite differs from the other petalite-subtype pegmatites in that it intrudes marble and iron formation, and contains Ca-rich dravite group (1) and Al-rich (Ca, Mg)-rich schorl and elbaite-schorl-dravite group (2) endocontact tourmaline.

Endocontact tourmaline is a result of fluids from the host rock infiltrating the pegmatite melt or a chemical reaction between the host rock and the pegmatite melt. When a pegmatite intrudes a biotite-bearing metapelite or marble, the composition of the endocontact tourmaline depends on the composition of the host rock regardless of the pegmatite subtype.

When an elbaite-subtype pegmatite intrudes a Ca- and Mg-rich mafic rock, the composition of the endocontact tourmaline is Ca- and Mg-rich. This reflects the overall Ca-rich nature of elbaite-subtype pegmatites in which Ca-bearing tourmaline occurs throughout the crystallization sequence. However, when a lepidolite- or petalite-subtype

pegmatite intrudes a Ca- and Mg-rich mafic rock, the endocontact tourmaline is Mg-rich and Ca-poor. This reflects the overall Ca-poor nature of lepidolite- and petalite-subtype pegmatites, and may indicate that all of the Ca is partitioned into plagioclase: thus the Ca-poor endocontact tourmaline in the border zone at Tanco is associated with andesine. The petalite-subtype endocontact tourmaline is Ca-poor when the pegmatite intrudes a mafic rock but Ca-rich when it intrudes a marble; this may merely reflect the fact that a marble has significantly more Ca than a mafic rock and that the Ca is not completely consumed by plagioclase.

8.3. Primary Tourmaline

This thesis deals with tourmaline in lepidolite-, petalite- and elbaite-subtype pegmatites. The major distinction between these three subtypes is the dominant Li-bearing mineral which is controlled by temperature, pressure and bulk composition of the pegmatite melt. Lithium-free minerals can also be used to differentiate between them (Table 8.1). Lepidolite-subtype pegmatites are characterized by abundant micas, accessory topaz and a quartz core. Petalite-subtype pegmatites commonly contain monomineralic quartz zones and accessory (Nb, Ta)-oxides. Elbaite-subtype pegmatites are characterized by abundant garnet throughout the massive pegmatite, and abundant multicoloured elbaite and accessory B- and Be-rich minerals in the pockets.

The compositional evolution of tourmaline is different in each pegmatite subtype: (1) *Lepidolite subtype*: black foitite-schorl → black schorl-foitite → dark-blue or green elbaite-schorl → green or pink elbaite → pink elbaite-rossmanite → pink rossmanite-

TABLE 8.1. COMPARISON OF MINERAL ASSEMBLAGES FOR LEPIDOLITE-, PETALITE- AND ELBAITE-SUBTYPES

Distinguishing Characteristics	Lepidolite-subtype	Petalite-subtype	Elbaite-subtype
micas	abundant, biotite-muscovite - lepidolite	common, biotite-muscovite - lepidolite	absent to rare
lepidolite composition	trilithionite to polylithionite	?	polylithionite
topaz	accessory	rare to absent	rare
quartz core	common	common	absent
petalite	rare	abundant, megacrystic	absent
(Nb, Ta)-oxides	accessory	accessory	rare
elbaite	accessory	accessory	abundant in pockets-multicoloured and gem quality
almandine-spessartine	accessory	subordinate	abundant
B-rich minerals	absent	absent	accessory in pockets: hambergite, danburite, datolite, boromuscovite
Be-rich minerals	accessory beryl	accesory beryl	accessory in pockets: beryl, bertrandite and bavenite, hambergite
pockets	rare to absent	rare to absent	minor to abundant

elbaite → green (Fe, Mn)-bearing elbaite (Fig. 8.1a). In the granitic and outer albite zones, foitite-schorl and schorl-foitite are associated with minor biotite and abundant Fe-bearing muscovite. In the albite zones, elbaite-schorl is associated with pale greenish-yellow Na-bearing muscovite. In the lepidolite zones, elbaite-rossmanite and rossmanite-elbaite occurs with purple lepidolite and minor pink and green lepidolite. The (Fe, Mn)-bearing elbaite occurs in the quartz core at Rožná and is associated with cookeite in late pockets at Dobrá Voda and Dolní Bory. The Fe, Li, Al, Mn and F contents of tourmaline

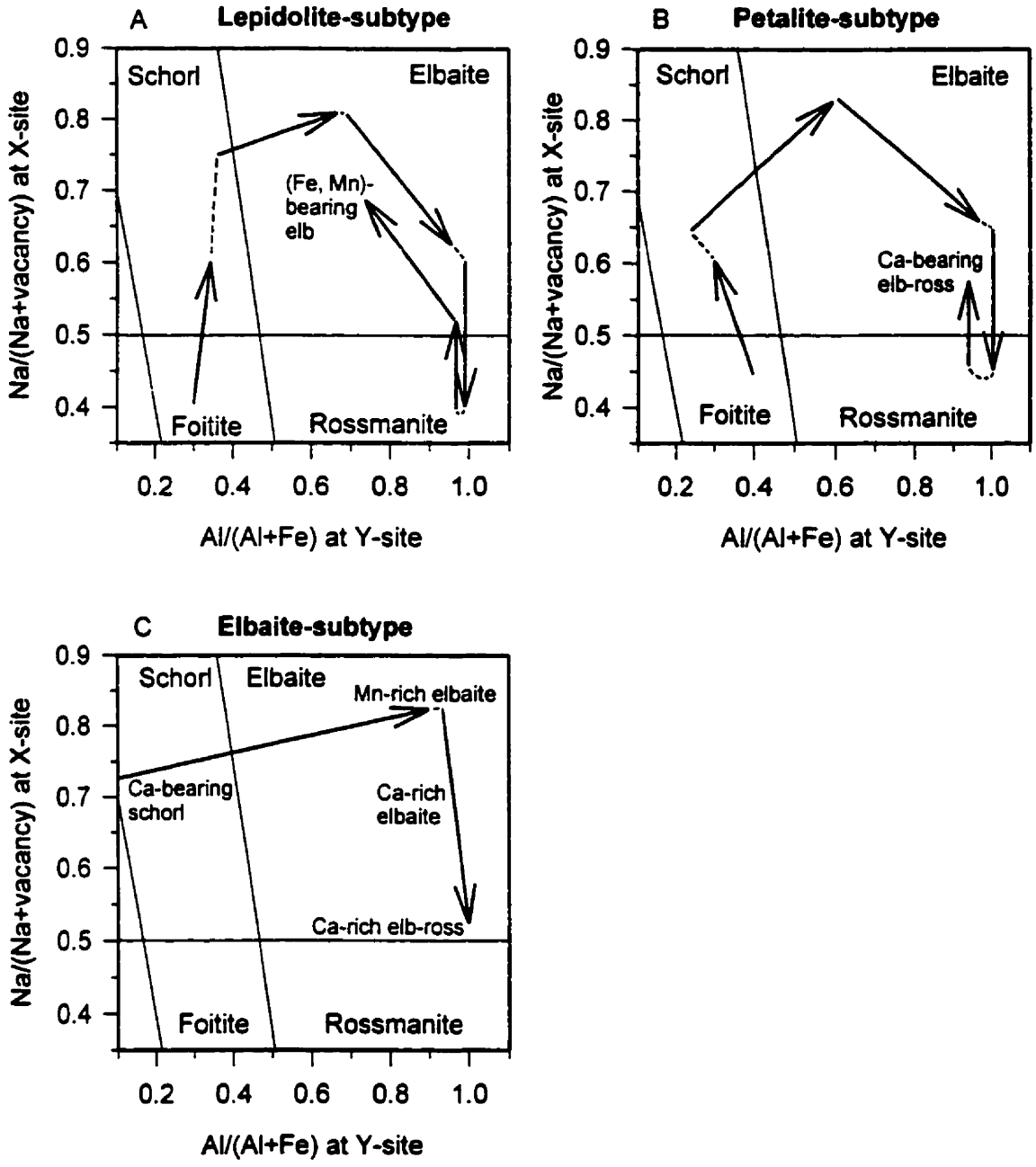

Figure 8.1. Idealized tourmaline compositional trends plotted in Na/(Na+ vacancy) at X-site vs. Al/(Al+Fe) at Y-site.

and mica correlate with that in the pegmatite melt as it gradually evolves with progressive pegmatite consolidation.

(2) *Petalite subtype*: (± black foitite-schorl, schorl-foitite) → black or brown Al-rich schorl → black or brown schorl → black or brown schorl-elbaite → green elbaite-schorl → green, blue or pink Fe-rich elbaite → blue Fe-bearing elbaite → (± pink Mn-bearing elbaite) → green or blue elbaite → pink elbaite-rossmanite → (± pink rossmanite-elbaite) → pink elbaite-rossmanite → pink Ca-bearing elbaite-rossmanite → pink Ca-bearing elbaite (Fig. 8.1b). Black foitite and schorl occur in the outermost pegmatite zones; pink elbaite-rossmanite, rossmanite-elbaite, Ca-bearing elbaite-rossmanite and Ca-bearing elbaite occur in the fractionated petalite-bearing zone.

(3) *Elbaite subtype*:

(a) black tourmaline in massive pegmatite: (± schorl-foitite) → (± foitite-schorl) → schorl (± Ca, Mn) → schorl-elbaite (± Ca, Mn) → elbaite-schorl (± Ca, Mn) → Fe-rich elbaite (± Ca, Mn) → Fe-bearing elbaite (± Ca, Mn) (Fig. 8.1c). In the outermost pegmatite zones, schorl is associated with almandine-spessartine and spessartine-almandine, both of which have minor Ca content. Near the pockets, Mn-bearing schorl-elbaite, Mn-bearing rossmanite-foitite and Mn-rich elbaite are associated with spessartine with minor Fe and Ca content. The Fe-Mn correlation between tourmaline and garnet represents increasing fractionation of the pegmatite melt.

(b) pink, green, colourless, blue or purple tourmaline in pockets: (± Fe-rich Mn-bearing

elbaite) → Mn-rich Fe-bearing elbaite → Mn-rich elbaite (± Ca) → Mn-bearing (± Ca) → Ca-rich elbaite → elbaite-rossmanite (± Ca, Mn) → (± rossmanite-elbaite) → (± elbaite-liddicoatite, liddicoatite-elbaite) (Fig. 8.1c). The absence of garnet in the pockets allows crystallization of Mn-rich elbaite (≤ 1.1 *apfu* Mn), as Mn is preferentially partitioned into garnet over tourmaline.

The overall tourmaline crystallization sequence may be condensed to: Ca-bearing schorl → Mn-rich elbaite → Ca-rich elbaite → Ca-rich elbaite-rossmanite → liddicoatite-elbaite.

Each genetic subtype has characteristic tourmaline compositions (Table 8.2):

- Lepidolite-subtype pegmatites are characterized by common foitite and rossmanite, absent Na-rich schorl, low Mn and no Ca in the primary tourmaline, and late-stage enrichment of Fe and Mn in elbaite.
- Petalite-subtype pegmatites are characterized by common Na-rich schorl, low Mn and Ca in tourmaline, and late-stage enrichment of Ca and F in elbaite.
- Elbaite-subtype pegmatites are characterized by common Na-rich schorl in the massive pegmatite, common Mn-rich elbaite and rare liddicoatite in pockets, and late-stage enrichment of Ca and F in elbaite and liddicoatite.

There is a negative correlation between Fe and Mn from foitite or schorl to elbaite, followed by a decrease in Mn to nil for rossmanite-elbaite, elbaite-rossmanite or liddicoaite-elbaite for all three subtypes (Fig. 8.2). This negative correlation between Fe and Mn is caused by increasing fractionation of the pegmatite melt. The distinguishing

TABLE 8.2. COMPARISON OF PRIMARY TOURMALINE FOR LEPIDOLITE-, PETALITE- AND ELBAITE-SUBTYPES

Distinguishing Characteristics	Lepidolite-subtype	Petalite-subtype	Elbaite-subtype
most primitive composition	foitite-schorl	Al-rich schorl	Ca-bearing schorl
foitite	common	rare	rare
Na-rich schorl	absent	common	common
Mn in schorl	≤ 0.10 *apfu*	≤ 0.07 *apfu*	≤ 0.40 *apfu*
Mn content in elbaite	≤ 0.30 *apfu* in elbaite	≤ 0.40 *apfu* in elbaite	≤ 1.10 *apfu* in elbaite
rossmanite	common	rare	rare
Ca content	~ 0.01 *apfu*	≤ 0.16 *apfu* in elbaite	≤ 0.60 *apfu* in liddicoatite
liddicoatite	absent	absent	rare
late-stage enrichment	□, Fe and Mn	□, Ca and F	□, Ca and F
most fractionated composition	elbaite-rossmanite, (Fe, Mn)-bearing elbaite	Ca-bearing elbaite-rossmanite, Ca-bearing elbaite	Ca-rich elbaite-rossmanite, liddicoatite-elbaite
negative correlation (Fe-Mn)	foitite to elbaite	foitite to Mn-bearing elbaite	Ca-bearing schorl to Mn-rich elbaite
no Fe, no Mn	rossmanite-elbaite	Ca-bearing elbaite-rossmanite	liddicoatite-elbaite
positive correlation (Na-Mn-F)	yes: maximum (Na, Mn, F) in elbaite-schorl and (Fe, Mn)-bearing elbaite	yes: maximum (Na, Mn, F) in Fe-rich elbaite and Mn-bearing elbaite	yes: maximum (Na, Mn, F) in Mn-rich elbaite
positive correlation (Ca-F)	no	yes: rossmanite-elbaite to Ca-bearing elbaite	yes: Ca-rich elbaite to elbaite-liddicoatite to liddicoatite-elbaite

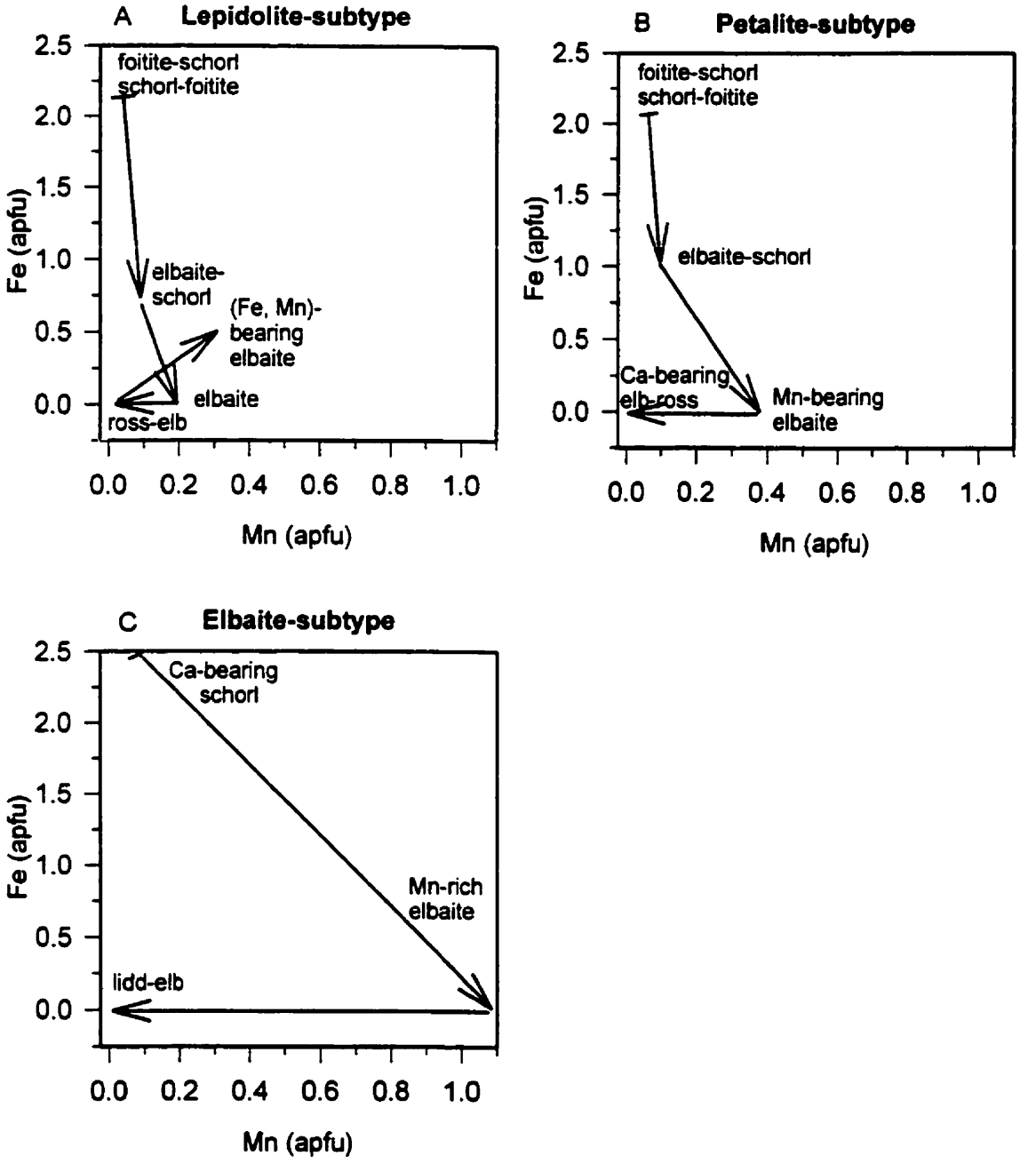

Figure 8.2. Idealized tourmaline compositional trends plotted in Fe vs. Mn graphs.

features of these three subtypes are:

- lepidolite-subtype tourmaline has late-stage Fe and Mn enrichment;
- petalite-subtype tourmaline has moderate intermediate-stage Mn enrichment;
- elbaite-subtype elbaite is significantly more Mn-rich than elbaite in other subtypes. In the elbaite-subtype pegmatites, the evolution of the tourmaline composition from schorl to Mn-rich elbaite is caused by the "tsilaisite substitution", $3Fe^{2+} \rightleftharpoons Mn + Al + Li$. The crystallization of Mn-rich elbaite is promoted by the absence of garnet, as Mn preferentially partitions into garnet and Fe preferentially partitions into tourmaline.

There is a positive correlation between Na and F for all three subtypes (Fig. 8.3) due to crystal-chemical constraints.

- In lepidolite-subtype pegmatites, tourmaline has a strong Na-F correlation and no Ca content. The tourmaline composition oscillates from (1) (Na, F)-poor foitite-schorl, as Na preferentially partitions into plagioclase, followed by (2) (Na, F)-rich elbaite-schorl, as an increase in volatiles, such as F, causes an increase in Na in the pegmatite melt, followed by (3) (Na, F)-poor rossmanite-lepidolite, as F preferentially partitions into lepidolite over tourmaline and (4) late-stage (Na, F)-rich (Fe, Mn)-rich elbaite associated with F-free cookeite.
- in petalite- and elbaite-subtype pegmatites, the Na-F correlation becomes distorted when Ca is added to the late-stage tourmaline, and a Ca-F correlation is developed. There is a positive correlation between Ca and F from rossmanite-elbaite to Ca-bearing elbaite in petalite-subtype pegmatites, and from Ca-bearing elbaite to liddicoatite-elbaite in elbaite-subtype pegmatites (Fig. 8.4).

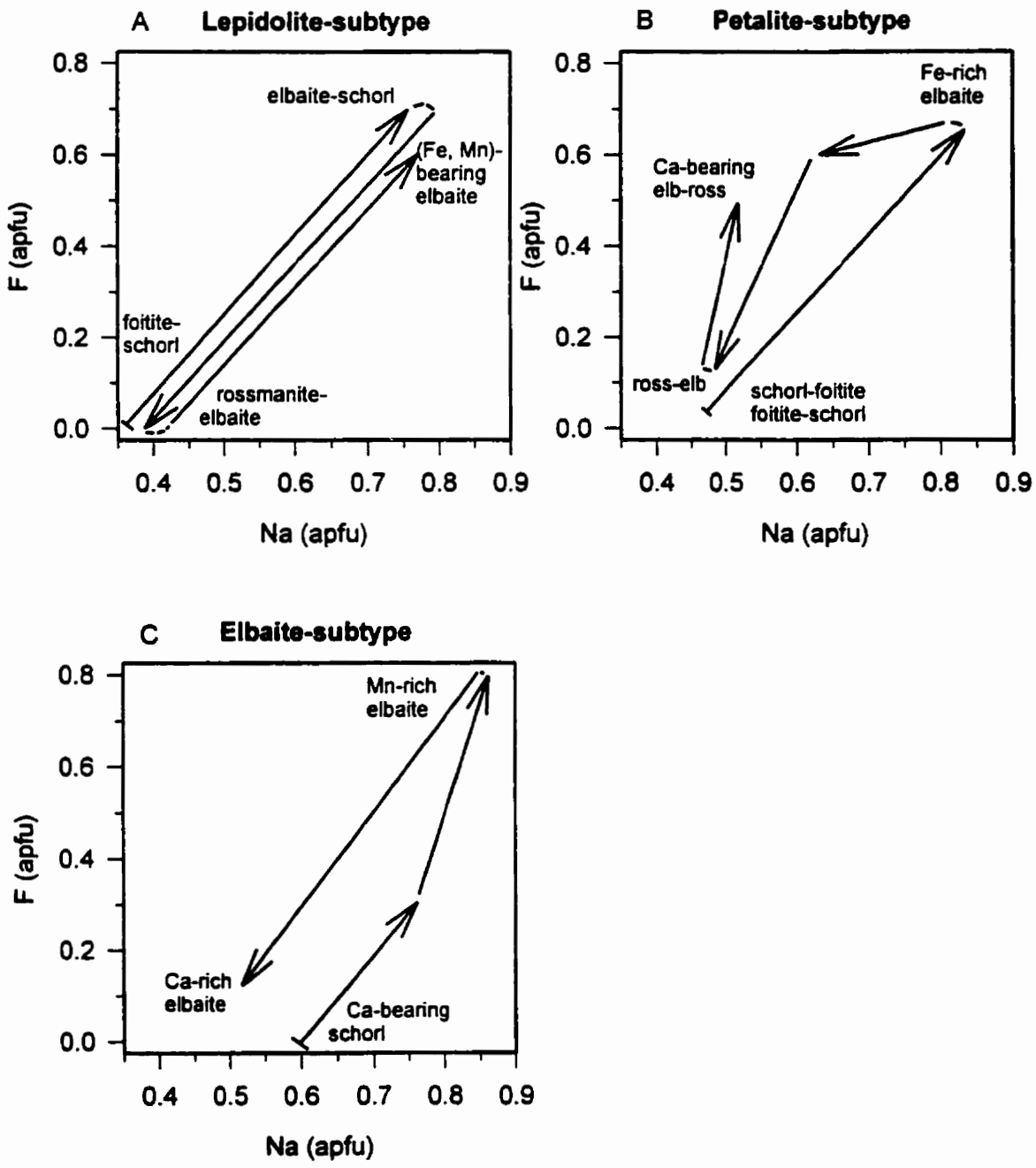

Figure 8.3. Idealized tourmaline compositional trends plotted in F vs. Na graphs.

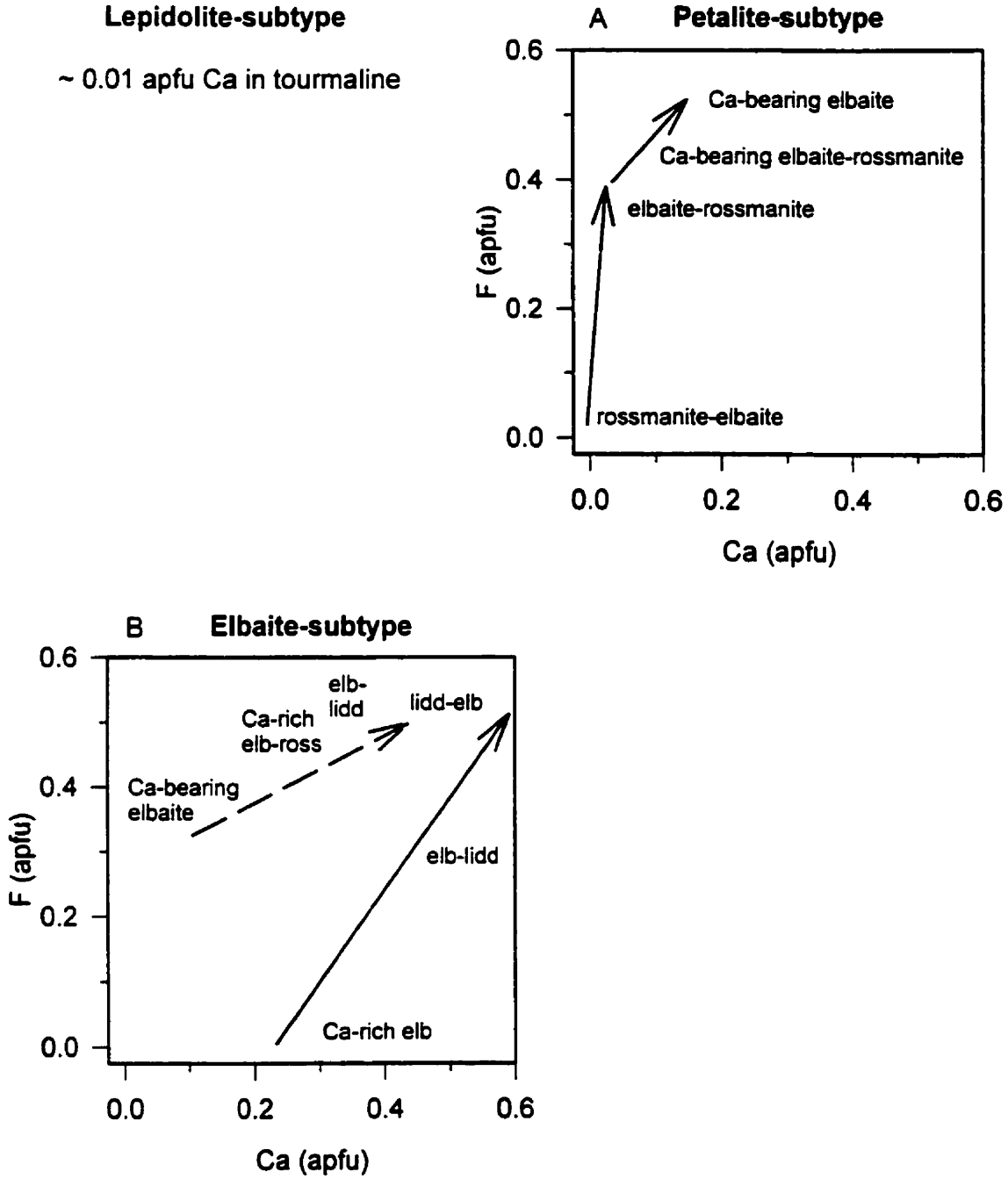

Figure 8.4. Idealized tourmaline compositional trends plotted in F vs. Ca graphs. (A) Tanco: petalite-bearing zone (4) and (5) (B) dashed line: Recice pockets; solid line: Sahatany Valley pockets.

The positive correlation between Na and F and between Ca and F is caused by crystal-chemical constraints. The OH group at the O(1) site is bonded to three *Y* cations and the O-H bond is directed along the threefold axis toward the *X*-site at the centre of the (T_6O_{18}) tetrahedral ring (Robert *et al.* 1997). The OH···O interactions between the H atom and the O atoms are weak when a cation occupies the *X* site, and this situation is favourable for F → OH substitution. When the *X* site is occupied by Na or Ca and the three *Y* sites are occupied by $3M^{2+}$ or $1.5M^{+}+1.5M^{3+}$, F can replace OH in this six-charge environment. When *X* site is empty and the three *Y* sites are occupied by $2M^{2+}+1M^{3+}$ or $1M^{+}+2M^{3+}$ to produce a seven-charge environment, F cannot enter the O(1) site.

There is a positive correlation between Na, Mn and F for all three subtypes (Figs. 8.3, 8.5).

- In lepidolite-subtype pegmatites, the maximum Na, Mn and F contents occur in elbaite-schorl and (Fe, Mn)-bearing elbaite;
- in petalite-subtype pegmatites, they occur in Mn-bearing elbaite;
- in elbaite-subtype pegmatites, they occur in Mn-rich elbaite.

The positive correlation between Na, Mn and F is caused by increasing fractionation in the pegmatite melt.

Each subtype has different geochemical conditions in the crystallizing pegmatite melt.

- In lepidolite-subtype pegmatites, the change from muscovite to trilithionite and the presence of accessory topaz associated with F-rich lepidolite indicate a general trend of increasing acidity (μHF) during pegmatite consolidation.

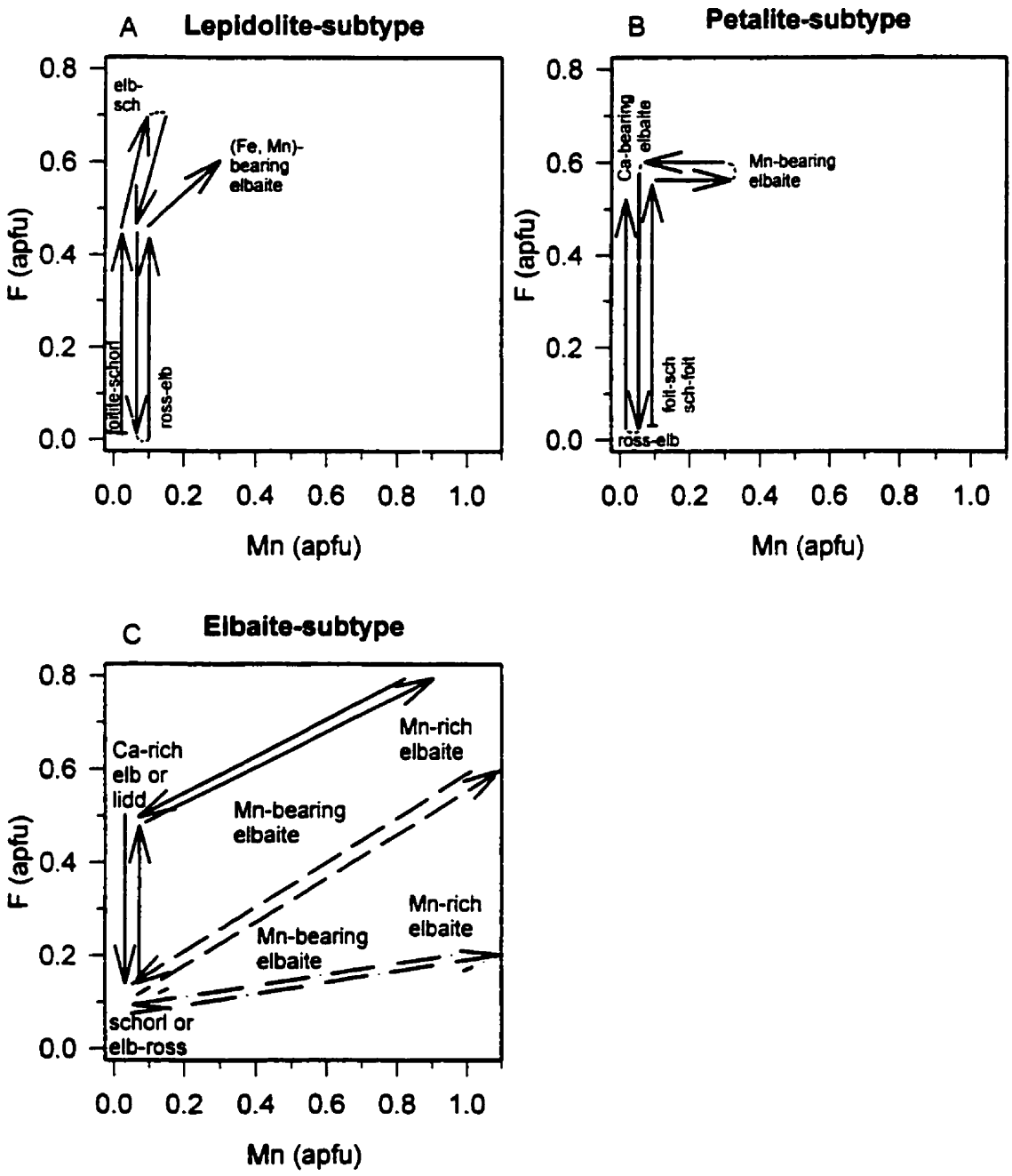

Figure 8.5. Idealized tourmaline compositional trends plotted in F vs. Mn graphs. (C) any combination of the three trends for Mn-rich elbaite is possible within an individual pegmatite.

- In petalite-subtype pegmatites, the abundance of blocky microcline-perthite indicates a general trend of high salinity (μKF). Petalite-bearing zones contain abundant to rare lepidolite, indicating intermediate acidity. Very rare topaz associated with amblygonite in the petalite-bearing zones may indicate a brief period of high acidity.
- In elbaite-subtype pegmatites, the presence of abundant K-feldspar and rare lepidolite and topaz in the pockets indicates that pocket minerals crystallized from an aqueous fluid with high acidity and high salinity. The presence of B-rich minerals, other than tourmaline, the presence of rare polylithionite and the absence of muscovite indicate a relative increase in alkalinity of the pegmatite melt.

Late-stage tourmaline in each pegmatite subtype is enriched in (Fe + Mn) or (Ca + F).

- In lepidolite-subtype pegmatites, late Fe-enrichment in tourmaline is likely due to infiltration of country-rock fluids after thermal equilibration of the pegmatites with their host rocks, whereas the Mn-enrichment is due to fractionation of the pegmatite melt and increased acidity of the pegmatite melt.
- In the petalite- and elbaite-subtype pegmatites, late Ca-enrichment in tourmaline is due to conservation of Ca through consolidation of the pegmatite by sequestering Ca in the melt as fluoride complexes. In petalite-subtype pegmatites, evidence of fluoride complexes is suggested by the association of Ca-bearing elbaite-rossmanite with fluorapatite and F-rich microlite. In elbaite-subtype pegmatites, evidence of fluoride complexes is suggested by the positive correlation of Ca and F in liddicoatite-elbaite and the presence of rare fluorapatite and fluorite in pockets.

8.4. Late-stage Fe-rich tourmaline

Influx of Fe-rich fluids from an Fe-rich host rock produces rare Fe-rich rims or terminations on late-stage tourmaline in lepidolite- and petalite-subtype pegmatites. The Fe-rich rims and terminations may be Fe-bearing elbaite or rarely foitite. For example, the sequence of crystallization of zoned tourmaline in late pockets in the lepidolite-subtype Dobrá Voda pegmatite is as follows: pink to colourless elbaite-rossmanite, pale-green to violet Fe-bearing elbaite and dark-violet to black foitite. In the quartz core of the petalite-subtype Urubu pegmatite, zoned tourmaline grains have colourless elbaite-rossmanite cores and green Fe-bearing elbaite rims.

In elbaite-subtype pegmatites, pocket rupture results in an influx of Fe-rich fluids into pockets. The source of these fluids may be (a) alteration of Fe-rich minerals within the pegmatite, or (b) the host rock. The Fe-rich fluids produce rims, terminations or zones which interrupt the crystallization sequence. This late-stage tourmaline may be elbaite-schorl, Fe-rich elbaite, Fe-bearing elbaite or foitite. For example, the pockets in the Elba pegmatite contain multicoloured elbaite which is capped by overgrowths of fibrous black foitite.

8.5. Late-stage cookeite, micas and zeolites

In lepidolite-subtype pegmatites, cookeite occurs as an alteration product of F-rich lepidolite in the lepidolite zones, and as a coating on pocket walls. In the petalite-bearing zone of the petalite-subtype Tanco pegmatite, pink rossmanite-elbaite is commonly

altered along rims and cracks or completely pseudomorphed by pink (Rb, Cs)-bearing mica or fine-grained green mica. Most tourmaline throughout the petalite-subtype Utö pegmatite is cross-cut by cookeite veinlets. Cookeite is one of the last minerals to crystallize in lepidolite- and petalite-subtype pegmatites, and its presence indicates decreasing salinity and low F-activity in the late low- temperature hydrothermal fluids.

In elbaite-subtype pegmatites, primary pocket minerals may be coated by "snow-on-the-roof" which consists of K-feldspar, boromuscovite, muscovite and/or stilbite. The presence of K-feldspar indicates conditions of high salinity, whereas boromuscovite indicates high alkalinity. The K may come from release of K following albitization of K-feldspar. Pocket minerals may also be coated or replaced by hydrothermal Ca- and Na-rich zeolites; the source of Ca- and Na-rich alkaline fluids is probably the host rock.

8.6. Application of conclusions

Extensive substitution in the crystal structure of tourmaline makes it an excellent petrological and geochemical indicator mineral. Changes in the composition of tourmaline within a zoned crystal and from the outermost to innermost pegmatite zone can be used to determine the crystallization sequence. Elemental trends within the crystallization sequence are affected by fractional crystallization, partition coefficients between tourmaline and other minerals, and crystal-chemical constraints within the tourmaline structure. Each pegmatite subtype has a characteristic compositional evolution for tourmaline due to the subtype's unique conditions of melt crystallization.

Each pegmatite subtype may contain economic quantities of rare-elements:

lepidolite-subtype pegmatites may contain lepidolite (Li, Rb), Ta-oxides and pollucite; petalite-subtype pegmatites may contain Ta-oxides, pollucite (Cs) and ceramic grade petalite or spodumene (Li); elbaite-subtype pegmatites contain multicoloured gem-quality elbaite. Deciphering the compositional evolution of tourmaline will contribute to our understanding of processes leading to the formation of the above commodities. If one fully understands how a pegmatite subtype forms, then a model can be developed and used in exploration for rare-element deposits.

References Cited

Althaus, E. (1979):Wassermelonen und Mohrenköpfe. *Lapis* **4**, 8-11.

Appleman, D.E. & Evans, H.T.Jr. (1973): Job 9214: Indexing and least-squares refinement of powder diffraction data. U.S. National Technical Information Service, Document PB 216 188.

Aurisicchio, C., Ottolini, L., Pezzotta, F. (1999): Electron- and ion-microprobe analyses, and genetic inferences of tourmaline of the foitite-schorl solid solution, Elba Island (Italy). *Eur. J. Mineral.* **11**, 217-225.

Aurisicchio, C., Ottolini, L., Pezzotta, F. (1997): Electron and ion microprobe analyses, paragenesis, and genetic inferences of foitite of Elba Island (Italy). *in* "Tourmaline 1997 International Symposium on Tourmaline, Abstract volume", Nové Město na Moravě, Czech Republic, 117.

Aurisicchio, C. & Pezzotta, F. (1997): Tourmaline-group minerals of the LCT miarolitic pegmatites of the Elba Island, (Italy): chemical composition and genetic and paragenetic inferences. *Tourmaline 1997, International Symposium on Tourmaline, Abstract volume*, Nové Město na Moravě, Czech Republic, 1-2.

Barton, R. (1969): Refinement of the crystal structure of buergerite and the absolute orientation of tourmalines. *Acta Crystallogr.* **B25**, 1524-1533.

Beakhouse, G.P., Stott, G.M., Blackburn, C.E., Breaks, F.W., Ayer, J., Stone, D., Farrow, C. & Corfu, F. (1996): Western Superior province - Field Trip Guidebook A5/B6. *Geol. Assoc. Can./Mineral. Assoc. Can. Ann. Meet.*, Winnipeg, Manitoba, May

27-29, 1996.

Bloomfield, M.J. (1997): *Gem tourmaline pegmatite deposits.* M.Sc. thesis, Leicester University, Leicester, England.

Brown, I.D. (1981): The bond-valence method: an empirical approach to chemical structure and bonding. *In* Structure and Bonding in Crystals II (M. O'Keeffe & A. Navrosky, eds.) Academic Press, New York.

Burnham, C.W. & Nekvasil, H. (1986): Equilibrium properties of granite pegmatite magmas. *Am. Mineral.* **71**, 239-263.

Burns, P.C., MacDonald, D.J., & Hawthorne, F.C. (1994): The crystal chemistry of manganese-bearing elbaite. *Can. Mineral.* **32**, 31-41.

Burt, P.C. (1989): Vector representation of tourmaline compositions. *Am. Mineral.* **74**, 826-839.

Campbell, J.L., Maxwell, J.A., Teesdale, W.J., Wang, J.-X. & Cabri, L.J. (1990): Micro-PIXE as a complement to electron probe microanalysis. *Nucl. Instrum. Methods Phys. Res.* **B44**, 347-356.

Cassedanne, J. & Cassedanne J. (1981): The Urubu pegmatite and vicinity. *Mineral. Rec.*, **12(2)**, 73-77.

Čech, F. (1957): About bertrandite from Ctidružice near Moravské Budějovice (western Moravia). *Acta Univ. Carol., Geol.* **6**, 255-261 (in Czech).

Černý, P. (1982): The Tanco pegmatite at Bernic Lake, southeastern Manitoba. *In* Mineral. Assoc. Can. Short Course Handbook, **8**: Granitic pegmatites in science and industry. (P. Černý, ed.) 527-543.

Černý, P. (1991a): Rare-element granitic pegmatites. Part I: anatomy and internal evolution of pegmatite deposits. *Geosci. Canada* **18**, 49-67.

Černý, P. (1991b): Fertile granites of Precambrian rare-element pegmatite fields: is geochemistry controlled by tectonic setting or source lithologies? *Precambrian Research* **51**, 429-468.

Černý, P. (1991c): Rare-element granitic pegmatites. Part II: Regional to global environments and petrogenesis. *Geosci. Canada* **18**, 68-81.

Černý, P. (1992): Geochemical and petrogenetic features of mineralization in rare-element granitic pegmatites in the light of current research. *Applied Geochemistry* **7**, 393-416.

Černý, P., Ercit, T.S. & Vanstone, P.J. (1998): *Mineralogy and petrology of the Tanco rare-element pegmatite deposit, southeastern Manitoba.* International Mineralogical Association, 17th General meeting, Toronto, Field Trip Guidebook B6.

Černý, P. & Lenton, P.G. (1995): The Buck and Pegli Lithium Deposits, Southeastern Manitoba: The problem of updip fractionation in subhorizontal pegmatite sheets. *Econ. Geol.* **90**, 658-675.

Černý, P., Povondra, P., Staněk, J. (1971): Two cookeites from Czechoslovakia: a boron-rich variety and a II*b* polytype. *Lithos*, **4**, 7-15.

Černý, P., Rieder, M., & Povondra, P. (1970): Three polytypes of lepidolite from Czechoslovakia. *Lithos* **3**, 319-325.

Černý, P., Staněk, J., Novák, M., Baadsgaard, H., Rieder, M., Ottolini, L., Kavalová, M.,

and Chapman, R. (1995): Geochemical and structural evolution of micas in the Rožná and Dobrá Voda pegmatites, Czech Republic. *Mineral. Petrol.* **55**, 177-201.

Černý, P., Teertstra, D.K., Chapman, R., Fryer, B.J., Longstaffe, F.J., Wang, X.-J., Chackowsky, L.E. & Meintzer, R.E. (1994): Mineralogy of extreme fractionation in rare-element granitic pegmatites at Red Cross Lake, Manitoba, Canada. *Internat. Mineral. Assoc. 16th General Meeting Pisa, Abstracts* 67.

Chackowsky, L.E., Wang X., Eby, R. & Černý, P. (1985): Pegmatitic granites, pegmatites and other felsic plutonic rocks at Gods Lake and Red Cross Lake, Manitoba. *Manitoba Energy and Mines Report of Field Activities 1985*, 209-211.

Cooper, D.G. (1964): The geology of the Bikita pegmatite. *In* The geology of some ore deposits in Southern Africa **II**, 441-462.

Dietrich, R.V. (1985a): The tourmaline group: a résumé. *Mineral. Rec.* **16**, 339-351.

Dietrich, R.V. (1985b): *The Tourmaline Group*. Van Nostrand Reinhold Co, New York.

Donnay, G. & Barton, R. Jr. (1972): Refinement of the crystal structure of elbaite and the mechanism of tourmaline solid solution. *Tschermaks. Mineral. Petrogr. Mitt.* **18**, 273-286.

Dunn, P.J., Appleman, D.E. & Nelen, J.E. (1977): Liddicoatite, a new calcium end-member of the tourmaline group. *Am. Mineral.* **62**, 1121-1124.

Eby, R.K. (1986): *A Structural & Petrofabric Study of Sheared Pegmatites, Red Cross Lake, Manitoba*. B.Sc. thesis, University of Manitoba, Winnipeg, Manitoba.

Epprecht, W. (1953): Die Gitterkonstanten der turmalin. *Schweiz. Min. Petr. Mitt.* **33**,

481-505.

Ercit, T.S. (1986): The simpsonite paragenesis; the crystal chemistry and geochemistry of extreme Ta fractionation. Ph.D. thesis, University of Manitoba, Winnipeg, Manitoba, 468 p.

Faure, G. (1991): *Principles and Application of Inorganic Geochemistry*. Collier MacMillan Canada, Toronto.

Foit, F.F. Jr. (1989): Crystal chemistry of alkali-deficient schorl and tourmaline structural relationships. *Am. Mineral.* **74**, 422-431.

Foit, F.F.Jr. & Rosenberg, P.E. (1977): Coupled substitutions in the tourmaline group. *Contrib. Mineral. Petrol.* **62**, 109-127.

Foit, F.F.Jr. & Rosenberg, P.E. (1979): The structure of vanadium-bearing tourmaline and its implications regarding tourmaline solid solution. *Am. Mineral.* **64**, 788-798.

Foord, E.E., Spaulding, L.B. Jr., Mason, R.A. & Martin, R.F. (1989): Mineralogy and paragenesis of the Little Three mine pegmatites Ramona District, San Diego County, California. *Mineral. Rec.* **20**, 101-127.

Foord, E.E., Starkey, H.C. & Taggart, J.E., Jr. (1986): Mineralogy and paragenesis of "pocket" clays and associated minerals in complex granitic pegmatites, San Diego County, California. *Am. Mineral.* **71**, 428-439.

Fuge, R. & Power G.M. (1969): Chlorine in tourmaline from SW. England. *Mineral. Mag.* **37**, 293-294.

Gallagher, V. (1988): Coupled substitutions in schorl-dravite tourmaline: a new evidence from SE Ireland. *Mineral. Mag.* **52**, 637-650.

Gebert, W. von & Zemann, J. (1965): Messung des Ultrarot-Pleochroismus von Mineralen. II Der Pleochroismus der OH-Streckfrequenz in Turmalin. *N. Jb. Mineral. Mh.*, **8**, 232-236.

Ginsburg, A.I., Timofeyev, I.N. & Feldman, L.G. (1979): Principles of geology of the granitic pegmatites. Nedra, Moscow, 296 pp. (in Russian)

Gordiyenko, V.V. & Ponomareva, N.I. (1988): Physico-chemical stability conditions of lithian micas of the lepidolite series. *Zapiski Vses Mineral Obsh*, **117**, 193-196 (in Russian).

Gorskaya, M.G., Frank-Kamenetskaya, O.V., Rozhdestvenskaya, I.V. & Frank-Kamenetskii, V.A. (1982): Refinement of the crystal structure of Al-rich elbaite, and some aspects of the crystal chemistry of tourmalines. *Soviet Phys. Cryst.* **27**, 63-66.

Grice, J.D. & Ercit, T.S. (1993): Ordering of Fe and Mg in tourmaline: The correct formula. *N. Jahrb. Mineral. Abh.* **165**, 245-266.

Grice, J.D., Ercit, T.S. & Hawthorne, F.C. (1993): Povondraite, a redefinition of the tourmaline ferridravite. *Am. Mineral.* **78**, 433-436.

Grice, J.D. & Robinson, G.W. (1989): Feruvite, a new mineral of the tourmaline group, and its crystal structure. *Can. Mineral.* **27**, 199-203.

Hawthorne, F.C. (1996): Structural mechanisms for light-element variations in tourmaline. *Can. Mineral.* **34**, 123-132.

Hawthorne, F.C., Burns. P.C. & Grice, J.D. (1996): The Crystal Chemistry of Boron. *In* Boron Mineralogy, Petrology and Geochemistry (E.S. Grew & L.M. Anovitz,

eds.) *Rev. Mineral.*, **33**, ch. 2 Mineralogical Society of America, Washington, D.C.

Hawthorne, F.C. & Henry, D.J. (1999): Classification of the minerals in the tourmaline group. *Eur. J. Mineral.* **11**, 201-215.

Hawthorne, F.C., MacDonald, D.J. & Burns, P.C. (1993): Reassignment of cation site occupancies in tourmaline: Al-Mg disorder in the crystal structure of dravite. *Am. Mineral.* **78**, 265-270.

Hawthorne, F.C., Selway, J.B., Kato, A., Matsubara, S., Shimizu, M., Grice, J.D. & Vajdak, J.: Magnesiofoitite, □ (Mg_2Al) Al_6 (Si_6O_{18}) $(BO_3)_3$ $(OH)_4$, a new alkali-deficient tourmaline. *Am. Mineral.* (in press).

Henry, D.J. & Dutrow, B.L. (1992): Tourmaline in a low grade clastic metasedimentary rock: an example of the petrogenetic potential of tourmaline. *Contrib. Mineral. Petrol.* **112**, 203-218.

Henry, D.J. & Dutrow, B.L. (1996): Metamorphic tourmaline and its petrologic applications. *In* Boron mineralogy, Petrology and geochemistry (E.S. Grew & L.M. Anovitz, eds.). *Reviews in Mineralogy* **33**, 503-558.

Henry, D.J. & Guidotti, C.V. (1985): Tourmaline as a petrogenetic indicator mineral: an example from the staurolite-grade metapelites of NW Maine. *Am. Mineral.* **70**, 1-15.

Jahns, R.H. (1979): Gem-bearing pegmatites in San Diego County, California: The Stewart mine, Pala district, and the Himalaya mine, Mesa Grande district. *In* Mesozoic Crystalline rocks: Peninsular ranges batholith and pegmatites Point Sal

Ophiolite (P.L. Abbott & V.R. Todd, eds.) Department of Geological Sciences, San Diego State University, San Diego, California, p. 3-38.

Jahns R.H. (1982): Internal evolution of pegmatites bodies. *In* Granitic pegmatites in science and industry (P. Černý, ed.) *Mineral. Assoc. Can., Short-Course Handbook* **8**, 293-327.

Jahns R.H. & Burnham, C.W. (1969): Eperimental studies of pegmatites genesis: I. A model for the derivation and crystallization of granitic pegmatites. *Econ. Geol.* **64**, 843-864.

Jahns, R.H. & Wright, L.A. (1951): Gem- and lithium-bearing pegmatites of the Pala district, San Diego County, California. *California Division of Mines Special Report* **7-A**, 1-72.

Jambor, J.L. & Potter, R.R. (1967): Rubidium-bearing dykes, Gods River area, Manitoba. *Geol. Surv. Can. Pap.* **67-15**, 1-7.

Jolliff, B.L., Papike, J.J. & Shearer, C.K. (1986): Tourmaline as a recorder of pegmatite evolution: Bob Ingersoll pegmatite, Black Hills, South Dakota. *Am. Mineral.* **71**, 472-500.

Laurs, B.M., Dilles, J.H., Wairrach, Y., Kausar, A.B. & Snee, L.W. (1998): Geological setting and petrogenesis of symmetrically zoned, miarolitic granitic pegmatites at Stak Nala, Nanga Parbat - Haramosh massif, northern Pakistan. *Can. Mineral.* **36**, 1-47.

Leeman W.P. & Sisson, V.B. (1996): Geochemistry of boron and its implications for crustal and mantle processes. *In* Boron Mineralogy, Petrology and Geochemistry

(E.S. Grew & L.M. Anovitz, eds.) *Rev. Mineral.*, **33**, ch. 12 Mineralogical Society of America, Washington, D.C.

Linnen, R.L. & William-Jones, A.E. (1993): Mineralogical constraints on magmatic and hydrothermal Sn-W-Ta-Nb mineralization at the Nong Sua aplite-pegmatite, Thailand. *Eur. J. Mineral.*, **5**, 721-736.

London, D. (1982): Stability of spodumene in acidic and saline fluorine-rich environments. *Carnegie Institution of Washington, Geophysical Laboratory Annual Report*, **81**, 331-334.

London, D. (1984): Experimental phase equilibria in the system $LiAlSiO_4$ - SiO_2 - H_2O: a petrogenetic grid for lithium-rich pegmatites. *Am. Mineral.* **69**, 995-1004.

London, D. (1986a): Magmatic-hydrothermal transition in the Tanco rare-element pegmatite: evidence from fluid inclusions and phase equilibrium experiments. *Am. Mineral.* **71**, 376-395.

London, D. (1986b): Formation of tourmaline-rich gem pockets in miarolitic pegmatites. *Am. Mineral.* **71**, 396-405.

London, D. (1987): Internal differentiation of rare-element pegmatites: effects of boron, phosphorus, and fluorine. *Geochim. Cosmochim. Acta* **51**, 403-420.

London, D. (1990): Internal differentiation of rare-element pegmatites: a synthesis of recent research. *In* Ore-bearing granite systems; petrogenesis and mineralizating processes (H.J. Stein & J.L. Hannah, eds.) *Geol. Soc. Am., Abstr. Programs* **22**, A346.

London, D. (1992): The application of experimental petrology to the genesis and

crystallization of granitic pegmatites. *Can. Mineral.* **30**, 499-540.

London, D., Hervig, R.L. & Morgan, G.B., VI (1988): Melt-vapor solubilities and element partitioning in peraluminous granite-pegmatite systems: experimental results with Macusani glass at 200 MPa. *Contrib. Mineral. Petrol.* **99**, 360-373.

London, D., Morgan, G.B., VI & Hervig, R.L. (1989): Vapor-undersaturated experiments with Macusani glass + H_2O at 200 Mpa, and the internal differentiation of granitic pegmatites. *Contrib. Mineral. Petrol.* **102**, 1-17.

London, D., Morgan, G.B. VI & Wolf, M.B. (1996): Boron in granitic rocks and their contact aureoles. *In* Boron Mineralogy, Petrology and Geochemistry (E.S. Grew & L.M. Anovitz, eds.) *Rev. Mineral.*, **33**, ch. 7 Mineralogical Society of America, Washington, D.C.

MacDonald, D.J. & Hawthorne, F.C. (1995): The crystal chemistry of Si ▫ Al substitution in tourmaline. *Can. Mineral.* **33**, 849-858.

MacDonald, D.J., Hawthorne, F.C. & Grice J.D. (1993): Foitite, ▫$[Fe^{2+}_2(Al,Fe^{3+})]$ Al_6 $Si_6O_{18}(BO_3)_3$ $(OH)_4$, a new alkali-deficient tourmaline: description and crystal structure. *Am. Mineral.* **78**, 1299-1303.

Manning, D.A.C. (1982): Chemical and morphological variation in tourmaline from the Hub Kapong batholith of pennisular Thailand. *Mineral. Mag.* **45**, 139-147.

Marchetti, A. (1997): *Relazioni composizionali in tourmaline di genesi pegmatitica: La pegmatite di Urubu, MG (Brasile).* Thesis, Università Degli Studi di Roma "La Sapienza", Rome, Italy (in Italian).

Maxwell, J.L., Campbell, J.L. & Teesdale, W.J. (1989): The Guelph PIXE software

package. *Nucl. Instrum. Methods Phys. Res.* **B43**, 218-230.

Morgan, G.B., VI & London, D. (1987): Alteration of amphibolitic wallrocks around the Tanco rare-element pegmatite, Bernic Lake, Manitoba. *Am. Mineral.* **72**, 1097-1121.

Morgan, G.B., VI & London, D. (1989): Experimental reactions of amphibolite with boron-bearing aqueous fluids at 200 MPa: implications for tourmaline stability and partial melting in mafic rocks. *Contrib. Mineral. Petrol.* **102**, 281-297.

Morgan, G.B. VI & London, D. (1999): Crystallization of the Little Three layered pegmatite-aplite dike, Ramona district, California. *Contrib. Mineral. Petrol.* (in press).

Němec, D. (1969): Fluorine in tourmalines. *Contrib. Mineral. Petrol.* **20**, 235-243.

Němec, D. (1981): Ein Pegmatit mit Li-Mineralisierung von Dolní Bory in Westmähren (ČSSR). *Chem. Erde*, **40**, 146-177 (in German with English abstract).

Němec, D. (1983): Masutomilite in lithium pegmatites of West-Moravia, Czechoslovakia. *N. Jb. Miner. Mh.* **1983, H.12**, 537-540.

Novák, M. (1992): Rožná near Bystřice nad Pernštejnem, a large pegmatite dike of the lepidolite subtype. type locality of lepidolite. *in* "Field trip guidebook, Lepidolite 200 Symposium", M. Novák & P. Černý, ed. Nové Město na Moravě, Czechoslovakia, 21-26.

Novák, M. (1996): Compositional variation in tourmaline from complex pegmatites in the Moldanubicum, Czech Republic. *Geol. Assoc. Can./Mineral. Assoc. Can. annual meeting, Winnipeg '96*, **21**, A-70.

Novák, M. & Černý, P. (1998): Niobium-tantalum oxide minerals from complex granitic pegmatites in the Moldanbicum, Czech Republic: primary *versus* secondary compositional trends. *Can. Mineral.* **36**, 659-672.

Novák, M., Černý, P., Cooper, M., Hawthorne, F.C., Ottolini, L, Xu, Z., Liang, J.-J. (1999b): Boron-bearing $2M_1$ polylithionite and $2M_1$ + 1M boromuscovite from an elbaite pegmatite at Řečice, western Moravia, Czech Republic. *Eur. J. Mineral.* **11**, 669-678.

Novák, M., Burns, P.C. & Morgan, G.B. VI (1998): Fluorine variation in hambergite from granitic pegmatites. *Can. Mineral.* **36**, 441-446.

Novák, M. & Hyršl, J. (1992): Locality No. 3: Vlastějovice near Zruč nad Sázavou, pegmatites with fluorite penetrating skarn. *In* Lepidolite 200, International Symposium on the mineralogy, petrology and geochemistry of granitic pegmatites (M. Novák & P. Černý, eds.) Nové Město na Moravě, Czech Republic, 11-20.

Novák, M. & Povondra, P. (1995): Elbaite pegmatites in the Moldanubicum: a new subtype of the rare-element class. *Mineral. Petrol.* **55**, 159-176.

Novák, M. & Selway, J.B. (1997): Rožná near Bystřice nad Pernštejnem, Hradisko hill. *in* "Field trip guidebook, Tourmaline 1997 Symposium", M. Novák & J.B. Selway, eds. Nové Město na Moravě, Czech Republic, 23-38.

Novák, M., Selway, J.B., Černý, P., Hawthorne, F.C. & Ottolini, L. (1999a): Tourmaline of the elbaite-dravite series from an elbaite-subtype pegmatite at Bližná, southern Bohemia, Czech Republic. *Eur. J. Mineral.* **11**, 557-568.

Novák, M., Selway, J.B., Korbel P. & Šarbach M. (1997): Locality No.4 Bližná near

Černá v Pošumaví, elbaite subtype pegmatite penetrating marble with exomorphic tourmaline. *In* Field trip guidebook Tourmaline '97 (M. Novák & J.B. Selway, eds.). Nové Město na Moravě, Czech Republic, 55-70.

Novák, M. & Taylor, M.C. (1996): New occurrences of foitite and its position in pegmatite evolution. *Geol. Assoc. Can./Mineral. Assoc. Can., Program Abstr.*, **21**, A-70.

Nuber, B. & Schmetzer, K. (1981): Strukturverfeinerung von Liddicoatit. *N. Jahrb. Mineral. Mon.* **5**, 215-219.

Pan, Y. & Breaks, F.W. (1997): Rare-earth elements in fluorapatite, Separation Lake area, Ontario: evidence for S-type granite - rare-element pegmatite linkage. *Can. Mineral.* **35**, 659-671.

Pan, Y., Breaks, F.W. & Therens, C. (1996): Granulites of the English River subprovince: metamorphic petrology and geochemistry. *Lithoprobe Rep.* **53**, 56-64.

Pezzotta, F. Hawthorne, F.C., Cooper, M.A. & Teertstra, D.K. (1996): Fibrous foitite from San Piero in Campo, Elba, Italy. *Can. Mineral.* **34**, 741-744.

Potter R.R. (1962): Gods River Map Area, Manitoba 53N. *Geol. Surv. Can. Pap.* **62-8**.

Pouchou, J.L. & Pichoir, F. (1984): A new model for quantitative analysis. I. Application to the analysis of homogeneous samples. *La Recherche Aerosp.* **3**, 13-38.

Pouchou, J.L. & Pichoir, F. (1985): "PAP" $\varphi(\rho Z)$ procedure for improved quantitative microanalysis. p. 104-106 *Microbeam Anal.- 1985*. San Francisco Press, San Francisco, California.

Povondra, P. (1981): The crystal chemistry of tourmalines of the schorl-dravite series.

Acta Universitatis Carolinae-Geologica., **3**, 223-264.

Povondra, P., Čech, F., Staněk, J. (1985): Crystal chemistry of elbaites from some lithium pegmatites of the Czech Massif. *Acta Universitatis Carolinae-Geologica.*, **1**, 1-24.

Power, G.M. (1968): Chemical variation in tourmalines from south-west England. *Mineral. Mag.* **36**, 1078-1089.

Quéméneur, J., Lagache, M. & Correia Neves, J.M. (1993): The Urubu pegmatite, Araçuai, Minas Gerais (Brazil), an example of complex petalite-subtype pegmatite: mineralogical zonation and geochemistry of micas and tourmalines. *Comptes Rendus de l'Académie des Sciences, Série II, Mécanique - Physique - Chimie, Sciences de la Terre et de l'univers* **317**,1425-1431 (in French).

Robert, J.-L., Beny, J.-M., Della Ventura, G., Hardy, M. (1993): Fluorine in micas: crystal-chemical control of the OH-F distribution between trioctahedral and dioctahedral sites. *Eur. J. Mineral.*, **5**, 7-18.

Robert, J.-L., Gourdant, J.-P., Linnen, R.L., Rouer, O., Benoist, P. (1997): Crystal-chemical relationships between OH, F and Na in tourmaline. *Tourmaline 1997 International Symposium on Tourmaline, Abstract volume.* Nové Město na Moravě, Czech Republic, 84-85.

Robert, J.L., Linnen, R., Rouer, O. (1993): The OH-F substitution in natural and synthetic tourmalines. *Terra Abstr.* **5**, 498.

Ruggieri, G. & Lattanzi, P. (1992): Fluid inclusion studies on Mt. Capanne pegmatites, Isola d'Elba, Tuscany, Italy. *Eur. J. Mineral.* **4**, 1085-1096.

Rumantseva. E.V. (1983): Chromdravite, a new mineral. *Zap. Vses. Mineral. Obsh.* **112**,

222-226 (English summary in *Am. Mineral.* **69**, 210).

Sekanina, J. (1946): Minerály a horniny v území mezi Nedvědicí a Rožnou. Sbor. Klubu příod. Brno, **26**, 99-113 (in Czech).

Selway, J.B., Černý, P. & Hawthorne, F.C. (1998b): Feruvite from lithium pegmatites at Red Cross Lake, Manitoba. *Can. Mineral.* **36**, 433-439.

Selway, J.B., Hawthorne, F.C.,Černý, P., Ottolini, L., Novák, M. & Kyser, T.K. (1998a): Rossmanite,$\square LiAl_2Al_6Si_6O_{18}(BO_3)_3(OH)_4$, a new alkali-deficient tourmaline: description and crystal structure. *Am. Mineral.* **83**, 896-900.

Selway, J.B. & Novák, M. (1997): Experimental conditions, normalization procedures and used nomenclature for tourmaline. *In* Tourmaline 1997 International Symposium on Tourmaline Field Trip Guidebook (M. Novák & J.B. Selway, eds.) Nové Město na Moravě, Czech Republic, 19-21.

Selway, J.B., Novák, M., Černý, P. & Hawthorne, F.C. (1999): Compositional evolution of tourmaline in lepidolite-subtype pegmatites. *Eur. J. Mineral.* **11**, 569-584.

Shannon, R.D. (1976): Revised effective ionic radii and systematic studies of interatomic distances in halides and chalcogenides. *Acta Crystallogr.* **A32**, 751-767.

Shigley, J.E. & Brown, G.E., Jr. (1985): Occurrence and alteration of phosphate minerals at the Stewart Pegmatite, Pala District, San Diego County, California. *Am. Mineral.* **70**, 395-408.

Shigley, J.E., Kampf, A.R., Foord, E.E. & London, D. (1986): *Field trip guide book to Gem Pegmatites of Southern California.* 14th General Meeting of the IMA, July 1986, Stanford University. Stanford, California. 39 p.

Sjögren, H. (1916): The chemical composition of tourmaline from Utö. *Bulletin of the Geological Institute of the University of Upsala* **15**, 317-324.

Smeds, S.-A. & Černý, P. (1989): Pollucite from the Proterozoic petalite-bearing pegmatites of Utö, Stockholm archipelago, Sweden. *Geologiska Föreningens i Stockholms Förhandlingar* **111(4)**, 361-372.

Smeds, S.-A. & Černý, P. & Chapman, R. (1999): Niobian calciotantite and plumboan-stannoan cesstibtantite from Utö, Sweden. *Can. Mineral.* (submitted).

Staatz, M.H., Murata, K.J. & Glass, J.J. (1955): Variation of composition and physical properties of tourmaline with its position in the pegmatite. *Am. Mineral.* **40**, 789-804.

Staněk, J. (1963): Turmalíny z pegmatitu od Dobré Vody u Velkého Meziříčí. *Folia Fac. Sci. Nat. Univ. Purkynianae*, **4-5**, 13-26 (in Czech).

Staněk, J. (1965): Pegmatit od Dobré Vody u Velkého Meziříčí. *Folia Fac. Sci. Nat. Univ. Purkynianae*, **6-8**, 1-39 (in Czech).

Staněk, J. (1973): Mineral paragenesis of the new lithium bearing pegmatite at Laštovičky, western Moravia, Czechoslovakia. *Scr. Univ. Purkyn. brun., Geol.*, **3**, 1-14.

Staněk, J. (1981a): Nov lithn pegmatit na západní Moravě (A new lithium pegmatite in western Moravia). *Čas. Mineral. Geol.* **26**, 175-178 (in Czech with german summary).

Staněk, J. (1981b): Pegmatity Moravy (Moravian pegmatites). *In* Mineralogie Československa, J.H. Bernard, ed., Academia Praha, 132-174 (in Czech).

Staněk, J. & Povondra, P. (1987): Elbaites from Řečice, western Moravia. *Acta Musei Moraviae, Scientiae naturales* **72**, 35-42.

Stern, L.A., Brown, G.E. Jr., Bird, D.K., Jahns, R.H., Foord, E.E., Shigley, J.E. & Spaulding, L.B. Jr. (1986): Mineralogy and geochemical evolution of the Little Three pegmatite-aplite layered intrusive, Ramona, California. *Am. Mineral.* **71**, 406-427.

Stilling, A. (1998): *The bulk composition of the Tanco pegmatite at Bernic Lake, Manitoba, Canada*. M.Sc. thesis, University of Manitoba, Winnipeg, Manitoba.

Taylor, M.C. (1997): Mineralogy, geochronology, and petrogenesis of an elbaite subtype of complex rare-element pegmatite, Peninsular Ranges Batholith, southern California. *First International Workshop on petrology, rare minerals and gemstones of shallow-depth pegmatites, Milan, Italy.*

Taylor, M.C., Cooper, M.A. & Hawthorne, F.C. (1995): Local charge-compensation in hydroxy-deficient uvite. *Can. Mineral.* **33**, 1215-1221.

Teertstra, D.K., Černý, P. & Ottolini, L. (1999): Stranger in paradise: liddicoatite from the High Grade Dike pegmatite, southeastern Manitoba, Canada. *Eur. J. Mineral.* **11**, 227-235.

Tennyson, C. (1979): Schörl vom Hörlberg. *Lapis* **4**, 12-13.

Thomas, A.V., Bray, C.J. & Spooner, E.T.C. (1988): A discussion of the Jahns-Burnham proposal for the formation of zoned granitic pegmatites using solid-liquid-vapour inclusions from the Tanco pegmatite, S.E. Manitoba, Canada. *Transactions of the Royal Society of Edinburgh: Earth Sciences* **79**, 299-315.

Thomas, A.V., Pasteris, J.D., Bray, C.J. & Spooner, E.T.C. (1990): H_2O-CH_4-NaCl-CO_2

inclusions from the footwall contact of the Tanco granitic pegmatite: estimates of internal pressure and composition from microthermometry, laser Raman spectroscopy, and gas chromatography. *Geochimica et Cosmochimica Acta* **54**, 559-573.

Thomas, A.V. & Spooner, E.T.C. (1988a): Fluid inclusions in the system H_2O-CH_4-NaCl-CO_2 from metasomatic tourmaline within the border unit of Tanco zoned granitic pegmatite, S.E. Manitoba. *Geochimica et Cosmochimica Acta* **52**, 1065-1073.

Thomas, A.V. & Spooner, E.T.C. (1988b): Occurrence, petrology and fluid inclusion characteristics of tantalum mineralisation in the Tanco granitic pegmatite, S.E. Manitoba. *In* CIM Special Volume **39**. Granite-related mineral deposits. (R.P. Taylor & D.F. Strong, eds.) 208-222.

Tonarini, S., Dini, A., Pezzotta, F. & Leeman, W.P. (1998): Boron isotopic composition of zoned (schorl-elbaite) tourmalines, Mt. Capanne Li-Cs pegmatites, Elba (Italy). *Eur. J. Mineral.* **10**, 941-951.

Trueman, D.L. (1982): A report on the Red Cross Lake pegmatite locality. *Internal Report, Tantalum Mining Corporation of Canada, Ltd.*

Webber, K.L., Falster, A.U., Simmons, W.B. & Foord, E.E. (1997): The role of diffusion-controlled oscillatory nucleation in the formation of line rock in pegmatite-aplite dikes. *J. Petrol.* **38**, 1777-1791.

Weidner, J.R. & Martin, R.F. (1987): Phase equilibria of a fluoride-rich leucogranite from the St. Austell pluton, Cornwall. *Geochim. Cosmochim. Acta* **51**, 1591-1597.